WILEY-VCH

Matthias Findeisen, Stefan Berger

50 and More Essential NMR Experiments

A Detailed Guide

Matthias Findeisen
Stefan Berger

50 and More Essential NMR Experiments

Related Titles

Zerbe, O., Jurt, S.

Applied NMR Spectroscopy for Chemists and Life Scientists

2013
Print ISBN: 978-3-527-32774-4 (Hardcover)
Print ISBN: 978-3-527-32775-1 (Softcover)
Also available in digital formats

Berger, Stefan/Sicker, Dieter

Classics in Spectroscopy

Isolation and Structure Elucidation of Natural Products

2009
ISBN: 978-3-527-32617-4 (Hardcover)
ISBN: 978-3-527-32516-0 (Softcover)

Günther, H.

NMR Spectroscopy

Basic Principles, Concepts and Applications in Chemistry

Third Edition

2013
Print ISBN: 978-3-527-33000-3 (Hardcover)
Print ISBN: 978-3-527-33004-1 (Softover)
Also available in digital formats

Berger, Stefan/Braun, Siegmar

200 and More NMR Experiments

A Practical Course

ISBN: 978-3-527-31067-8

Friebolin, H.

Basic One- and Two-Dimensional NMR Spectroscopy

Fifth Edition

2011
Print ISBN: 978-3-527-32782-9

Matthias Findeisen
Stefan Berger

50 and More Essential NMR Experiments

A Detailed Guide

WILEY-VCH
Verlag GmbH & Co. KGaA

Authors

Matthias Findeisen
University of Leipzig
Dept. of Analytical Chemistry
Johannisallee 29
04103 Leipzig
Germany

Stefan Berger
Dept. of Analytical Chemistry
University of Leipzig
Johannisallee 29
04103 Leipzig
Germany

Cover
The cover shows *Strychnos nux vomica*, the tree from which semen strychnine, one of the model compounds used in many of the experiments in this book, is extracted. The picture was taken by the senior author in the botanical garden of Cape town. In addition, the 3D structure of strychnine and the HSQC pulse diagram to observe 2D (^{1}H,^{13}C)-correlation NMR spectra is given.

Library of Congress Card No.:
applied for

British Library Cataloguing-in-Publication Data
A catalogue record for this book is available from the British Library.

Bibliographic information published by the Deutsche Nationalbibliothek
The Deutsche Nationalbibliothek lists this publication in the Deutsche Nationalbibliografie; detailed bibliographic data are available on the Internet at <http://dnb.d-nb.de>.

Print ISBN: 978-3-527-33483-4
ePDF ISBN: 978-3-527-33696-8
ePub ISBN: 978-3-527-33694-4
Mobi ISBN: 978-3-527-33697-5

Cover Design Adam-Design, Weinheim
Printing and Binding **Markono, Singapore**

Printed on acid-free paper

Preface

Many of our readers know the earlier books in this series, "*100 and more Basic NMR Experiments*" (**1996**), "*150 and more Basic NMR Experiments*" (**1998**) and "*200 and more NMR Experiments*" (**2004**). Since all books of this highly successful series have been sold out, we have asked ourselves whether it would be worthwhile to further increase the number of NMR experiments in a next edition. This could easily have been done, because NMR is still a very vivid field of science with a steady urge of innovation.

However, in daily discussions with our own co-workers we had to realize that even these people were not able to recall all or even the more important experiments from "*200 and more*". Thus we finally decided on a "*downsizing*" and present in this volume "*50 and more Essential NMR Experiments*", a much smaller collection. We feel that at least these should be known to the experimental NMR operator in a chemical environment. A severe cut concerns solid state NMR and NMR in structural biology, where we provide only 4 examples in this volume, knowing that especially these two fields of NMR are currently the most active ones. However, since this volume is mainly intended for organic and inorganic chemists we feel that this community is better served with a more targetted selection.

By implementing the experiments on your spectrometer, please keep in mind that some of the parameters are strongly machine dependent (e.g. power levels, spectral widths in Hz) and must be modified according to your situation. We reflect the values here as we used them to record the spectra pictured in the book.

Compared with the previous editions there are several changes to note.

(1) Dr. Matthias Findeisen, a physicist, replaces Siegmar Braun who retired several years ago.

(2) Nearly all experiments shown in this volume have been recorded anew, and the cited literature goes to mid 2012. There are a few entirely new experiments not present in the previous volumes. All experiments have been regrouped from a more chemical perspective.

(3) There is a new section **Variants** in which modifications of the actual experiments are mentioned.

(4) There is a new **Question** section at the end of each experiment. We hope that answering these questions will give the reader much more insight. Short answers are provided in the Appendix.

(5) The biggest change is certainly in the layout. Whereas our previous books were solid but rather dry scholarly textbooks, we have this time tried to compose a more modern book with accompanying graphics and photographs, with some historic text clips from celebrities of NMR and theire pictures. We hope that this change will help to raise interest, especially for the young people entering this fascinating field.

From the number of sold copies of our previous books we know that this information is at hand alongside numerous NMR spectrometers in the world, not counting the Chinese edition of "*200 and more*". We certainly hope that the "*50 Essentials*" will be equally successful. We are fairly certain that every experiment works as described, but if not, please complain by email to

Prof. Dr. Stefan Berger
Institut für Analytische Chemie der Universität Leipzig
Linnéstr. 3, D-04103 Leipzig
e-mail: stberger@rz.uni-leipzig.de
Fax: + 49 341-9736115
Internet: http://www.uni-leipzig.de/~nmr/STB

Finally, we have to thank many colleagues for helpful discussions and in particular Mrs. U. Zeller, who provided all the layout ideas and who was responsible for getting all this together. In addition, we thank Dr. P. Tzetkova for recording the data of experiment 3.9 and Dipl. Biochem. A. Beil for recording the data of experiment 6.7.

Leipzig, April 2013

Matthias Findeisen Stefan Berger

Quo innumerabiles libros et bibliothecas, quarum dominus vix tota vita indices perlegit? Onerat discentem turba, non instruit, multoque satius est paucis te auctoribus tradere quam errare per multos.

Lucius Annaeus Seneca (4 bc - 65 ad, De tranquillitate animi, IX, 4.)

What is the use of having countless books and libraries whose titles their owners can scarcely read through in a whole lifetime? The learner is not instructed but burdened by the mass of them, and it is much better to surrender yourself to a few authors than to wander through many.

Translated by J. W. Basore

Contents

Preface

Chapter 1 The Organic Set of NMR Spectra 1

1.1 The ^{1}H NMR Experiment 3
1.2 APT-^{13}C NMR 7
1.3 COSY 11
1.4 NOESY 17
1.5 HSQC 23
1.6 HMBC 29

Chapter 2 Advanced Organic NMR Spectroscopy 35

2.1 2D *J*-Resolved ^{1}H NMR Spectroscopy 37
2.2 ROESY 41
2.3 TOCSY 45
2.4 HSQC-TOCSY 49
2.5 HOESY 53
2.6 INADEQUATE 57
2.7 ADEQUATE 61
2.8 *J*-HMBC 65
2.9 Gated Decoupling 71

Chapter 3 Selective Methods 75

3.1 Water suppression by Presaturation 77
3.2 Solvent Suppression by 1D-NOESY 81
3.3 Water Suppression by SOGGY Excitation Sculpting 85
3.4 Solvent Suppression using WET 89
3.5 SELTOCSY 93
3.6 SELNOESY 97
3.7 SELINCOR 101
3.8 SELINQUATE 105
3.9 Band Selective HMBC 109

Chapter 4 Heteronuclear NMR 113

4.1 ^{11}B NMR Spectroscopy 119
4.2 ^{15}N NMR Spectroscopy 123
4.3 ^{17}O NMR Spectroscopy 127
4.4 ^{19}F NMR Spectroscopy 131
4.5 ^{29}Si NMR Spectroscopy 135
4.6 ^{57}Fe NMR Spectroscopy 139
4.7 ^{195}Pt NMR Spectroscopy 145

Chapter 5 Experiments in Physical Organic Chemistry 149

5.1 Measurement of the Spin–Lattice Relaxation Time T_1 151
5.2 Measurement of the Spin–Spin Relaxation Time T_2 155
5.3 Dynamic ^{1}H NMR Spectroscopy 159
5.4 Diffusion Measurement with DOSY 163
5.5 Residual Dipolar Couplings (RDC) 167

Chapter 6 Organic Chemistry Applications 173

6.1 ASIS 175
6.2 Chirality Determination 179
6.3 Advanced Mosher Method 183
6.4 Quantitative NMR and Relaxation Reagents 187
6.5 Determination of Association Constants K_a 193
6.6 STD NMR 199
6.7 A Kinetic Experiment 203

Chapter 7 An Excursion to the Solid State and to Structural Biology 209

7.1 The CP/MAS Experiment 211
7.2 High-Resolution Magic-Angle Spinning 215
7.3 HN-HSQC 219
7.4 HNCA 225

Chapter 8 Maintenance and Calibration 233

8.1 Calibration of Pulse Duration in the Transmitter Channel 235
8.2 Calibration of the Pulse Duration in the Indirect Channel 241
8.3 Shaped Pulses 247
8.4 Adiabatic pulses 253
8.5 Temperature Calibration in NMR 257
8.6 Calibration of Pulsed Field Gradients 265

Appendix

Answers 273

Pulse Programs 295

Elementary Product Operator Formalism Rules 296

Chemical Shift and Spin-Coupling Data for Strychnine 298

Picture Credits 300

Index 301

Chapter 1

The Organic Set of NMR Spectra

There are six NMR spectral methods, which are usually first measured on a routine basis if an organic chemist has produced a new compound. Usually, this organic set is sufficient for a complete structural elucidation, especially if additional support comes from mass spectrometry and IR- or UV-spectroscopy.

These six methods are:

1.1	^{1}H-NMR		3
1.2	APT-^{13}C-NMR	[**A**ttached **P**roton **T**est]	7
1.3	COSY	[**CO**rrelation **S**pectroscop**Y**]	11
1.4	NOESY	[**N**uclear **O**verhauser **E**ffect Spectroscop**Y**]	17
1.5	HSQC	[**H**eteronuclear **S**ingle **Q**uantum **C**oherence]	23
1.6	HMBC	[**H**eteronuclear **M**ultiple **B**ond **C**orrelation]	29

We describe therefore in this first chapter these six methods in some detail using strychnine as an example. Strychnine with its rather complicated molecular structure provides all the typical problems encountered during spectral assignments in organic chemistry. With concurrent instrumentation and about 20 mg of substance having a molecular weight around 500 Da, the total recording time of these techniques will be about 5 h.

Of course, this book offers much more, but this organic set comprises the most essential of all our essentials.

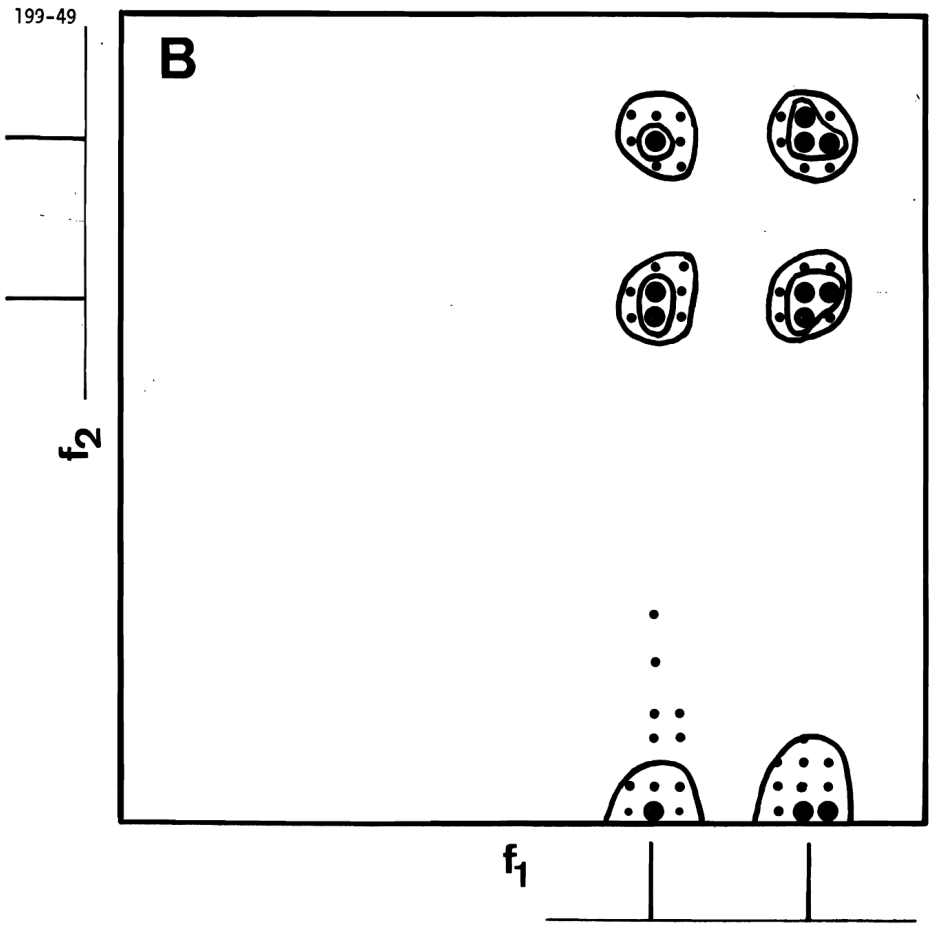

These spectra are preliminary in several respects. First of all, resolution is severely limited by the available computer memory. A 64x64 data matrix was used. Secondly, the absolute value of the 2D spectrum is plotted disregarding phase information which may be of particular interest. This experiment has several further interesting aspects which we presently are investigating.

Sincerely yours

Richard

Richard R. Ernst

taken from *TAMU NMR Letters*, **1975,** *199*, 49.

Experiment 1.1

^1H NMR Experiment

1. Purpose

The aim of the standard ^1H NMR experiment is to record a routine proton NMR spectrum in order to get structure-related information for the protons of the sample, i. e. chemical shifts, spin–spin couplings, and intensities. Here we apply this standard procedure to strychnine and discuss different weighting functions and problems of integration.

2. Variants

Variants of this form of NMR spectroscopy include first of all excitation with different pulse angles.

However, since recent NMR instruments are sensitive enough, usually one 90° scan is sufficient to obtain a spectrum. Therefore no considerations about reduced pulse angles are necessary. Second, if a strong solvent signal is present, different forms of signal suppression are available. These are discussed in chapter 3.

3. Pulse Scheme and Phase Cycle

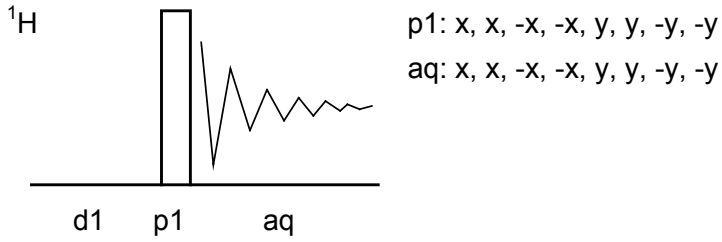

Scheme 1.1-1

4. Acquisition

Special values used for the spectrum shown:

Sample: 3% strychnine in $CDCl_3$.
Time requirement: 1 min
Spectrometer: Bruker DRX-600 with 5-mm-TBI-probe

td:	64K
sw:	15 ppm
aq:	3.6 s
o1:	middle of ^1H NMR spectrum
d1:	2 s
ns:	1

These data will lead to an FID digital resolution of 0.28 Hz/point for the real or imaginary part of the FID.

The prospect of measuring very rapid reaction rates by NMR provided the inspiration for getting an affirmative response from Linus Pauling [then chairman of the division of Chemistry and Chemical Engineering at California Institute of Technology] that "with NMR, we could investigate the borderline between resonance and tautomerism". For example, investigating the NMR spectrum of cycloheptatriene with temperature to see if it existed as a rapidly equilibrating mixture of cycloheptatriene and norcaradiene, or was what later would be called a "monohomobenzene". The argument was persuasive and we soon ordered a 30-MHz Varian proton and fluorine spectrometer.

J. D. Roberts, * 1918 "A Personal NMR Odyssey" *Enyclopedia of NMR*, **1996**, *1*, 590–598.

Common values:

p1: 90° ^1H transmitter pulse
d1: relaxation delay

The appearance of an unsplit methyl signal in a CH_3CH moiety, where the chemical shift difference was large compared to the vicinal coupling constant, expected to be about 7 Hz, subsequently impressed on me the importance of MR spectral analysis. When I understood what was going on, I wrote a paper which was published in 1961 on the nature of the signals of C-methyl groups, and this explained many anomalous "coupling constants" involving methyl groups in steroids and other compounds; it anticipated later research by others on virtual coupling. Although spectral analysis is becoming almost a lost art in the midst of so-called "modern NMR", it is in fact just as useful and necessary as it has ever been, in my own experience.

F. A. L. Anet, * 1926 "A lapsed organic chemist in the wonderland of NMR" *Enyclopedia of NMR*, **1996**, *1*, 187–190.

5. Processing

Use zero filling to si = 64K and exponential weighting with lb = 0.1 Hz, phase correction and referencing to internal TMS, which is the only acceptable reference scheme. The digital resolution of the spectrum will be with these data sw/si = 0.14 Hz/point. Before integration, perform phase and baseline correction on the spectrum accurately. A comparison of the spectra in Fig. 1.1-3 and 1.1-4 shows how a Gaussian weighting function with lb = –1 Hz and gb = 0.3 makes additional small spin couplings visible.

6. Result

The figures show two expansions of the 600 MHz ^{1}H NMR spectrum of strychnine.

A closer inspection of the integrals reveals that the integral of H-4 is too small as compared to all other integrals of the compound. Although the spectrum was recorded with only one scan, the waiting time after the receiver gain adjust command before and the actual measurement was appartently too short (see Question A).

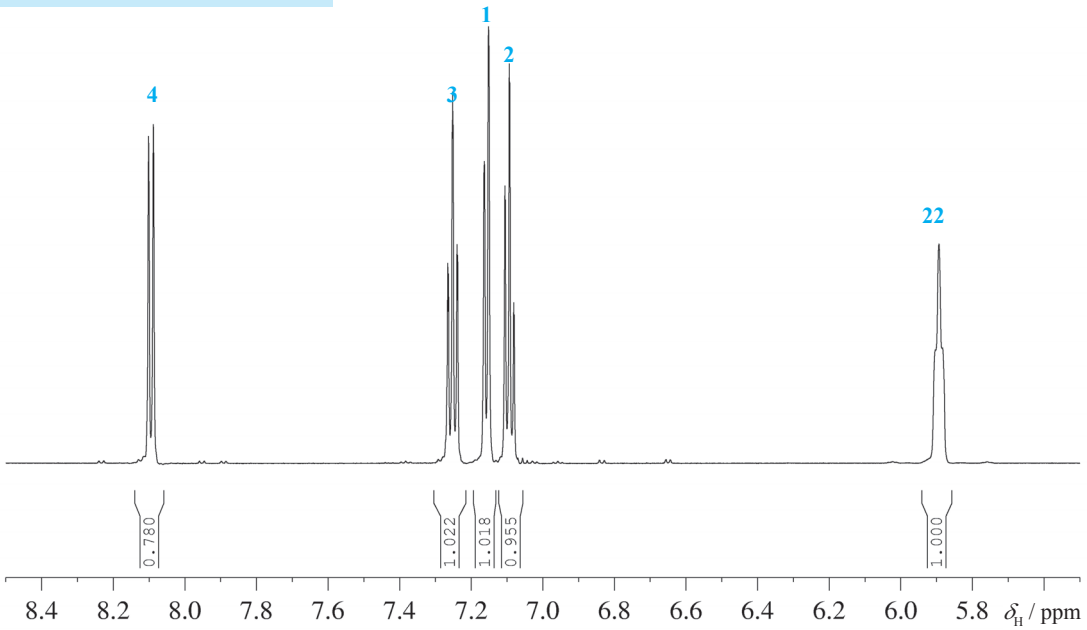

Fig. 1.1-1 Expansion of the ^{1}H-NMR spectrum in the aromatic region

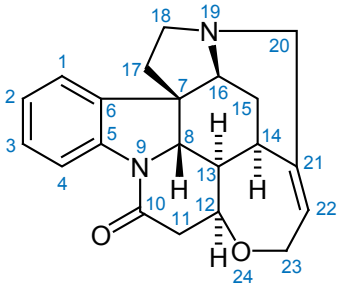

Scheme 1.1-2

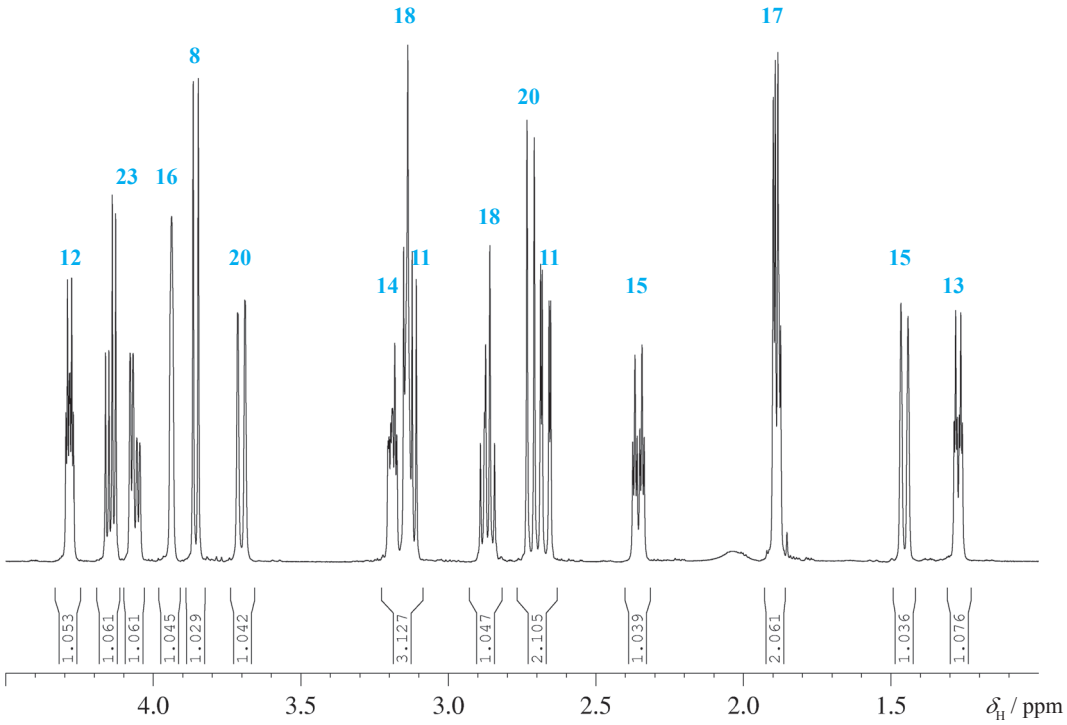

Fig. 1.1-2 Expansion of the ^{1}H-NMR spectrum in the aliphatic region

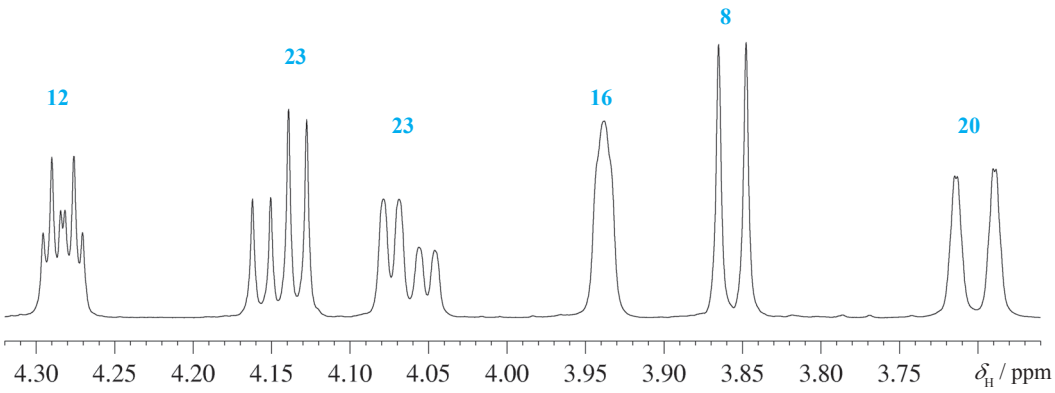

Fig. 1.1-3 Edited with lb = 0.1 Hz (zoom of Fig. 1.1-2)

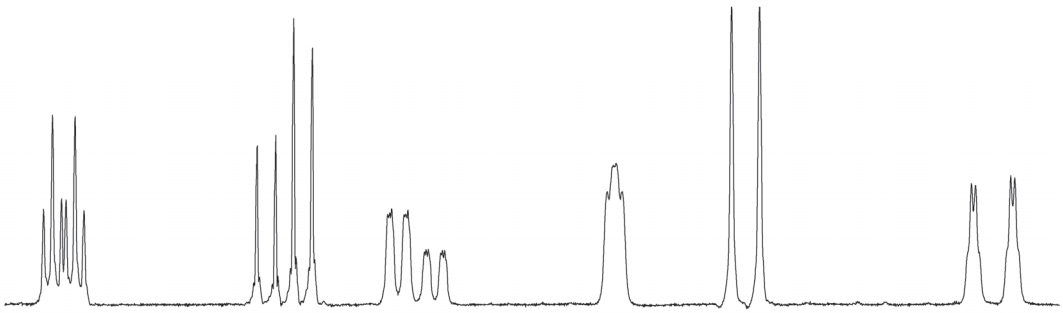

Fig. 1.1-4 Edited with gb = 0.3, lb = –1

7. Comments

The excitation pulse p1 converts the equilibrium magnetization of the ^1H nuclei into a transverse magnetization as shown in Equation (1). During the acquisition time chemical shifts and spin–spin couplings develop in the *x,y* plane, as shown separately in Equations (2) and (3), and are detected by the receiver in the *x,y* plane in quadrature mode.

(1)

$$I_{H_z} \xrightarrow{90^\circ I_x} -I_{H_y}$$

(2)

$$-I_{H_y} \xrightarrow{\Omega I_z t} -I_{H_y}\cos\Omega t + I_{H_x}\sin\Omega t$$

(3)

$$-I_{H_y} \xrightarrow{\pi J 2I_{1z}I_{2z} t} -I_{H_y}\cos\pi Jt + 2I_{H_x}I_{H_z}\sin\pi J t$$

[1] T. D. W. Claridge, "High-resolution NMR techniques in organic chemistry", Pergamon, Oxford, **1999**.

[2] I. K. M. Sanders, B. K. Hunter, "Modern NMR spectroscopy", 2nd Edition, Oxford University Press, Oxford, **1993**.

[3] H. Friebolin, "Basic one- and two-dimensional NMR spectroscopy", 3rd Edition, Wiley-VCH, Weinheim, **1998**.

[4] H. Günther, "NMR Spectroscopy", 2nd Edition, Wiley, Chichester, **1995**.

8. Questions

A. Suggest a reason why the integral of H-4 is considerable smaller than the others.

B. How would one classify the aromatic spin system?

C. The intensity pattern of the signals between 4.2 and 4.0 ppm has a special name?

D. The signals at 2.35 and 1.27 ppm both belong to the methylene group of C-15 and are spin coupled to each other; however, only one has an additional spin coupling. Why?

9. Own Observations

Experiment 1.2

ATP-^{13}C NMR

1. Purpose

The aim of a routine ^{13}C NMR experiment is to record a ^{13}C NMR spectrum with proton broad-band decoupling and data accumulation in order to get chemical shift information for structure determination. At the same time one wants to have multiplicity information. From the many schemes proposed we feel the APT (**A**ttached **P**roton **T**est) technique is the most useful and convenient method available, especially if carried out with a chirp 180° pulse on the carbon channel to avoid phase problems at high field spectrometers.

2. Variants

Alternative methods that give information about the multiplicities are INEPT, DEPT, DEPTQ, and PENDANT, and the historic off-resonance ^{1}H-decoupling technique. Unlike INEPT or DEPT, the APT method yields ^{13}C NMR spectra that are only enhanced by the NOE. However, APT also gives information about quaternary carbon atoms. Improved modifications of APT are known [2-4].

3. Pulse Scheme and Phase Cycle

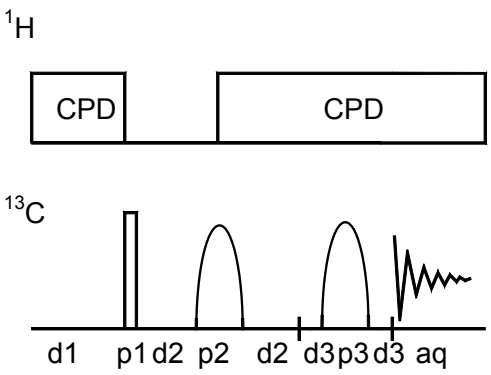

p1: $(x)_4$, $(y)_4$, $(-x)_4$, $(-y)_4$

p2: x, y, -x, -y, y, -x, -y, x, -x, -y, x, y, -y, x, y, -x

p3: x, y, y, x, $(y, x, x, y)_2$, x, y, y, x

aq: x, x, -x, -x, y, y, -y, -y

Scheme 1.2-1

4. Acquisition

Special values used for the spectrum shown:

Sample:	3 % strychnine in $CDCl_3$.
Time requirement:	1 h
Spectrometer:	Bruker DRX-600 with 5-mm TBI probe

Fig. 1.2-1 P. J. Lauterbur (1929-2007)

Common values:

p1: 45° ^{13}C transmitter pulse
p2: 180° ^{13}C CHIRP pulse
d1: relaxation delay
d2: $1/J_{CH}$
d3: switching delay
CPD composite pulse decoupling

Fig. 1.2-2 J. D. Roberts (*1918)

Natural-abundance ^{13}C NMR was not really routine until the introduction of broadband noise proton decoupling. Such decoupling removes the proton splittings from the ^{13}C resonances and, in addition, gives a favorable nuclear Overhauser effect (NOE). Thus, a proton-coupled doublet ^{13}C resonance, such as exhibited by trichloromethane, with broadband decoupling produces a singlet peak with a sixfold increase over the intensity of each of the individual doublets. There is hardly a better early example of the utility of broadband proton decoupling for ^{13}C spectra than for cholesterol. Weigert had found it impossible to make sense out of the 15-MHz coupled spectrum of cholesterol, because of the jumble of resonances and the generally poor signal-to-noise ratio, even after hours of signal averaging. In contrast, with broadband proton decoupling, 25 rather well-separated resonances were observed. A challenge was thus presented of spectral assignments and was met by H. Reich and M. Jautelat in about six months. An important element in the unraveling of the resonances was D. M. Grant's work on the steric influence of axial methyl groups on ^{13}C shifts in cyclohexane rings.

J. D. Roberts, * 1918 "A personal NMR odyssey" *Enyclopedia of NMR*, **1996**, *1*, 590-598.

td: 64K
sw: 200 ppm
aq: 1.0 s
p1: 45° ^{13}C transmitter pulse 6 µs
o1: middle of ^{13}C NMR spectrum
o2: middle of ^{1}H NMR spectrum
p2: adiabatic chirped 180° ^{13}C pulse [crp 60, 0.5, 20.1; 500 µs, 5.5 dB]
d1: 2 s
d2: 6.9 ms corresponding to a J_{CH} = 145 Hz
d3: 100 µs
CPD: WALTZ16 sequence, individual 90° ^{1}H pulse:100 µs at 12 dB
ns = 1024

5. Processing

Use zero filling to si = 64K and exponential weighting with lb = 2 Hz, phase correction and referencing to either internal TMS or via the Ξ scale using the proton spectrum of the same sample.

6. Result

The figure shows the ^{1}H broad-band decoupled APT ^{13}C NMR spectrum of strychnine as obtained on an DRX-600 spectrometer using a TBI probe head. Because of the inverse probe a certain number of scans had to be accumulated. Note that as usual no integration is performed, since under routine conditions the signal areas are not necessarily proportional to the number of ^{13}C nuclei giving rise to that signal. Furthermore, since the d2 delay hits exactly one $J_{C,H}$ value, the others will be scaled in intensity.

The signal of the solvent $CDCl_3$ was adjusted to be negative like the other signals of carbon atoms carrying no protons. Signals of CH and CH_3 groups are positive and signals of CH_2 groups negative.

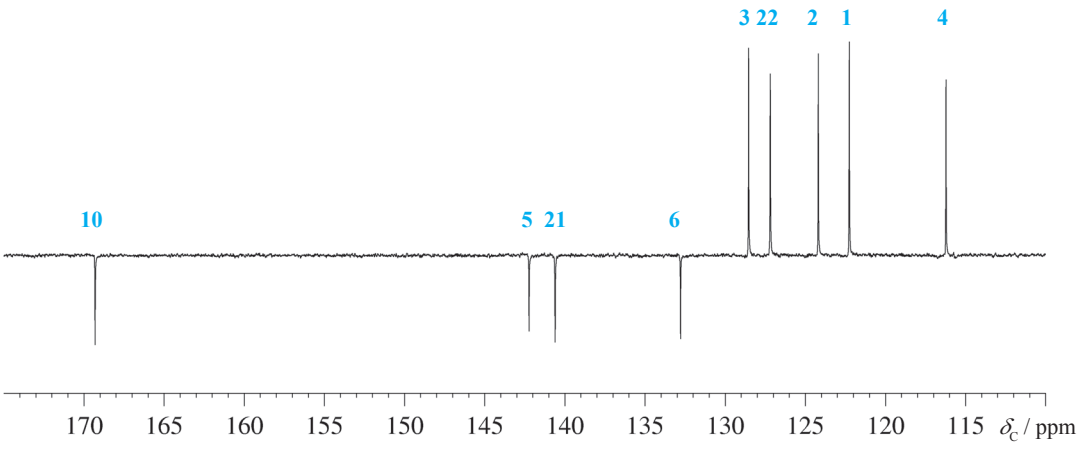

Fig. 1.2-3 Expansion of the ^{13}C NMR spectrum in the aromatic and carbonyl region

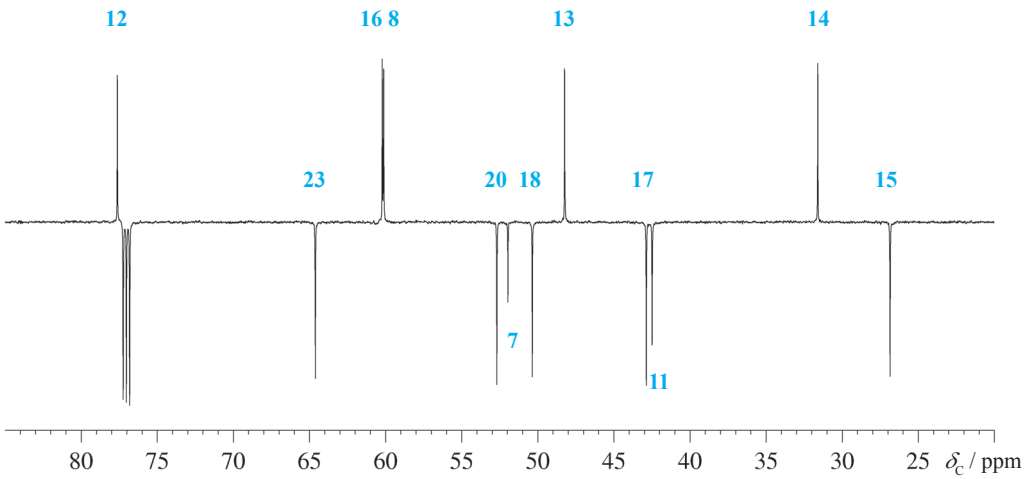

Fig. 1.2-4 Expansion of the ^{13}C NMR spectrum in the aliphatic region

7. Comments

The APT sequence is in principle a double spin-echo experiment. In the first echo period d2 the evolution of *J*-coupling modulates the phases of the signals according to C_q or CH_2 groups respective CH and CH_3 groups. By using a 45° or shorter excitation pulse a part of the initial magnetization remains in the *z*-direction and is inverted to $-z$ by the first 180° pulse. This could lead to a canceling of signals with long spin-lattice relaxation times, but in the second spin-echo period the 180° pulse reinverts the *z*-magnetization, thus eliminating this problem. In comparison with all other editing techniques APT still seems to be the most simple and efficient method, since it gives in one experiment all the necessary information on *all* sorts of carbon atoms. The lower sensitivity compared with polarization transfer methods such as DEPT is in practice not important for the C,H spin pair. See, however, the new DEPTQ experiment where the shortcomings of the traditional DEPT are overcome.

Scheme 1.2-2

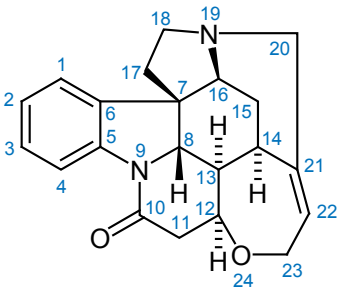

It was the time of the Korean War, however, and my deferments ran out. I was drafted and eventually ended up at the Army Chemical Center. where my 'experience' with NMR got me a transfer and assignment to help set up the Varian NMR machine (40 MHz proton and ^{19}F, 17 MHz ^{31}P) which they purchased to support chemical warfare research. There I actually learned something about NMR and even published a few papers. After Army service two options developed: go to Illinois as a graduate student with Gutowsky, or persuade the Mellon Institute to buy an NMR spectrometer. The institute itself declined, but the Dow Corning group took the plunge, at least partly because I claimed that useful ^{29}Si spectra would be possible. I chose that option, visited Varian, and confirmed that ^{29}Si spectra could be seen (with an 8.5 Mc s^{-1} rf unit) and immediately decided that ^{13}C would be even more interesting. I soon published the first paper on ^{13}C NMR spectra. The rest is another branch of personal and scientific history, except that ^{13}C led to interest in spin decoupling and biological polymers, which were both to become essential links in the chain of events leading to 'zeugmatography', as I originally called magnetic resonance imaging.

Paul Lauterbur (1929-2007)
"One Path out of Many – How MRI actually began" *Enyclopedia of NMR*, **1996**, *1*, 445–449.

[1] H.-O. Kalinowski, S. Berger, S. Braun, "Carbon-13 NMR spectroscopy", Wiley, Chichester, **1988**.

[2] T. D. W. Claridge, "High-resolution NMR techniques in organic chemistry", Pergamon, Oxford, **1999**.

[3] K. M. Sanders, B. K. Hunter, "Modern NMR spectroscopy", 2nd Edition, Oxford University Press, Oxford, **1993**.

[4] S. L. Patt, J. N. Shoolery "Attached proton test for carbon-13 NMR" *J. Magn. Reson*. **1982**, *46*, 535–539.

[5] J. C. Madsen, H. Bildsøe, H. J. Jakobsen, O. W. Sørensen "ESCORT editing. An update of the APT experiment" *J. Magn. Reson*. **1986**, *67*, 243–257.

[6] A. M. Torres, T. T. Nakashima, R. E. D. McClung "Improved *J*-compensated APT experiments" *J. Magn. Reson*. Ser. A **1993**, *101*, 285–294.

[7] U. Beckmann, W. Dietrich, R. Radeglia "ORSAT and modifications of SEFT and APT" *J. Magn. Reson.* **1999**, *137*, 132–137.

8. Questions

A. What is understood by the "Ernst angle"?

B. Which parameter controls the correct phases obtained in this experiment?

C. What is meant with a WALTZ16 sequence?

D. The signals of $CDCl_3$ show a 1:1:1 triplet with a spin coupling of 31.7 Hz. Explain and calculate from this the spin coupling found in $CHCl_3$.

E. Looking at the spectrum and the chemical formula of strychnine, you should be able to assign at once at least two carbon atoms. Which ones?

9. Own Observations

Experiment 1.3

COSY

1. Purpose

The COSY (**CO**rrelation **S**pectroscop**Y**) pulse sequence generates a 2D NMR spectrum in which the signals of a normal ^{1}H NMR spectrum are correlated with each other. Cross-peaks appear if homonuclear spin coupling is present; thus the COSY sequence detects coupled pairs of protons (or pairs of other nuclei such as ^{19}F, ^{31}P or even ^{13}C in the case of labelled proteins). Since coupled protons are usually separated by two or three bonds, the connectivity and very often a chemical structure can be derived from the COSY spectrum; however, one must be also aware of long-range spin couplings. The COSY sequence is the most important and most frequently used 2D NMR experiment.

2. Variants

Due to the importance of the COSY technique an impressive number of variants has been developed in the last 40 years. The current Bruker pulse sequence library, for example, contains more than 30 different applications, and it is impossible to discuss them all in this book. We show here a COSY sequence which includes a gradient-selected double quantum filter and the echo-antiecho scheme for the phase sensitive frequency generation in the indirect dimension. The reason for this selection is that in COSY one usually wants to see and interpret the interaction of two protons with each other. The double quantum filter suppresses singlets and reduces multiplets to AX patterns; the echo-antiecho scheme provides phase sensitive spectra.

Other important variants of COSY which should be mentionend are:

(1) The long-range COSY, which emphasizes connectivities caused by small spin-coupling constants. This is important in the case of allylic or W-spin couplings < 2 Hz.

(2) The COSY-45 or the E.COSY methods, which lead to slim diagonals and allow the determination of the sign of spin-coupling constants.

(3) All COSY variants may be combined with different schemes of water suppression.

(4) The phase-sensitive COSY variants can be recorded in high resolution in both dimensions which enables the extraction of digital correct spin-coupling values in the direct dimension.

Fig. 1.3-1 J. Jeener *1931

Almost in despair, I started investigating this latter problem with the help of Gerit Alewaelers, initially on the simple case of the standard AB spectrum in liquids. This soon led to the general proposal of 2D FT NMR spectroscopy in the simple case of homonuclear COSY without phase cycling. We tried to observe the effect experimentally on ethylbenzene, spending weekends working with the rather primitive FT spectrometer available in organic chemistry at our university. Due to the bad phase stability of this spectrometer and to our total lack of practice of high-resolution NMR, Gerit Alewaeters could only observe some of the strongest cross peaks of the 2D spectrum with a signal-to-noise ratio high enough to confirm that our quantum mechanical predictions were correct (not really a surprise.....), but too low to make the new technique look very usable. Formal publication was deferred until cleaner experimental confirmation would be available, but I kept spreading the idea by personal contacts, lectures (probably for the first time at the AMPERE Summer School in Basko Polje in 1971) and by circulating 'unpublished' notes written in November 1971. Soon, Richard Ernst let me know that his co-worker Baumann had brought the 2D FT idea back from Basko Polje to Zürich, and that the Zürich group intended to work on it. As it turned out, one of our recurrent delights in Brussels for a number of years has been receiving news from Zürich about the progress of 2D NMR, both experimental and theoretical. It was also a pleasure to learn about the new 2D FT ideas developing in many other groups.

Jean Jeener, *1931, "Reminiscences about the early days of 2D NMR" *Enyclopedia of NMR*, **1996**, *1*, 409–410.

3. Pulse Scheme and Phase Cycle

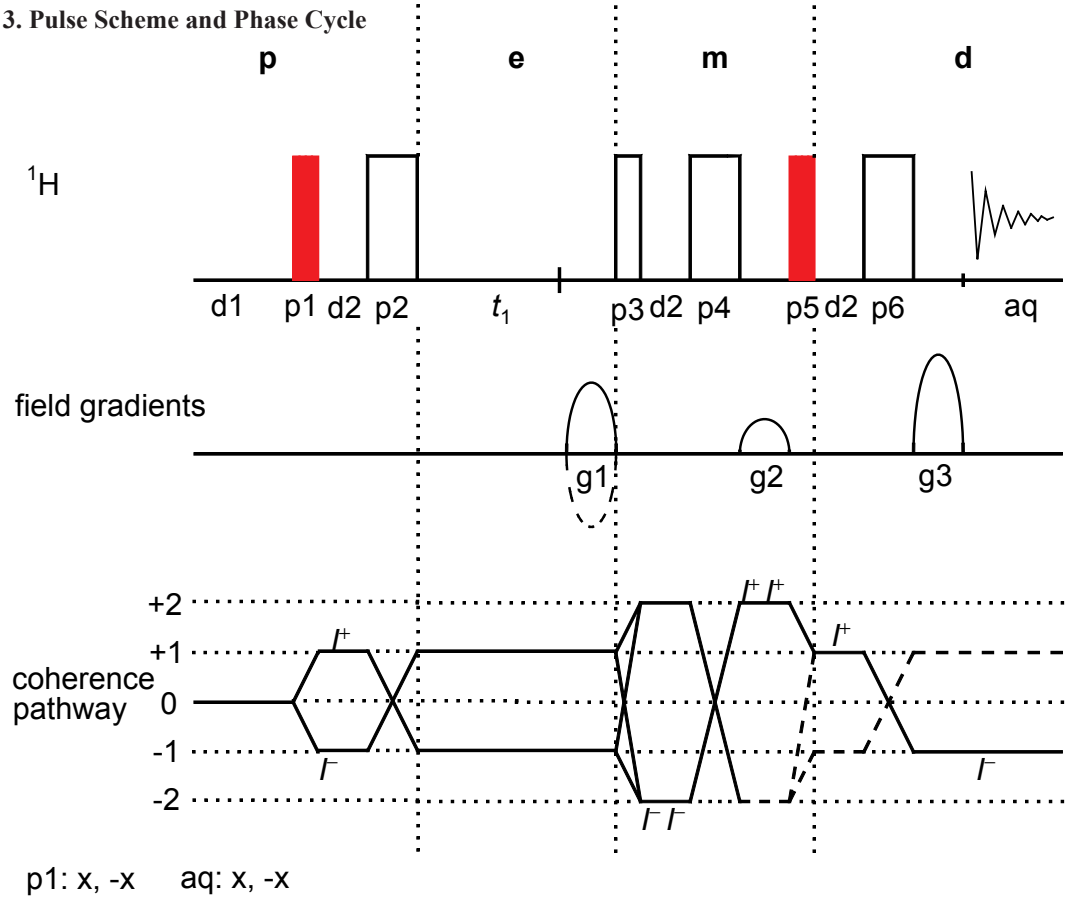

Scheme 1.3-1

Common values:

p1, p3, p5: 90° ^{1}H transmitter pulse
p2, p4, p6: 180° ^{1}H transmitter pulse
d1: relaxation delay
d2: effective length of gradient
t1: evolution increment
g1, g3: gradients for Echo/Antiecho selection
g2: gradient for double quantum selection

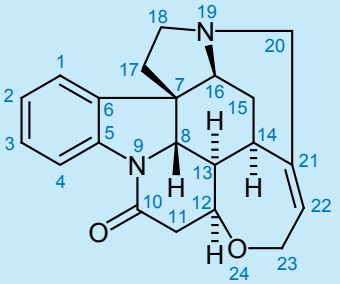

Scheme 1.3-2

4. Acquisition

Special values used for the spectrum shown:

Sample: 3% strychnine in $CDCl_3$.
Time requirement: 20 min
Spectrometer: Bruker DRX-600 with 5-mm-TBI probe

td2:	2K data points in F_2
td1:	256 data points in F_1
sw2:	10 ppm
sw1:	10 ppm
aq1:	0.023 s
aq2:	0.19 s
o1:	middle of ^{1}H NMR spectrum
d1:	2 s
d2:	equal to effective duration of gradient used, here 1.05 ms
g1, g2, g3:	sinusoidal-shaped field gradients, 1 ms duration gradient ratio 30:10:50 with 0.56 T/m = 100%
rg:	One must be very careful in setting the receiver gain for this experiment. The gradient filter allows only the

desired coherences to pass into the receiver; however, the double-quantum coherences develop only at higher t_1 increments because of modulation with sin ($\pi J t_1$), cf. Equ. 2 see Question C. The receiver gain must therefore be set using a high t_1 increment to avoid overloading.

ds: 2
ns: 2

5. Processing

Apply zero-filling in F_1 to 1K words in order to have a symmetrical matrix of 1024×1024 data points. Use an exponential window with lb = 3 Hz in the F_2 dimension and a squared π/2 shifted sinusoidal window in the indirect dimension. Apply complex Fourier transformation in both dimensions. Phase correction in both dimensions can be performed after the 2D transformation in order to get clean up/down patterns of the cross-peaks. Zero order phase correction of 90° is a good starting point for the F_1 dimension.

6. Result

The overview spectrum displays all relevant connectivities for strychnine. In the aliphatic expansion clearly the AX pattern can be observed, even though more complicated multipletts are coupled to each other. In the aromatic expansion this is also demonstrated.

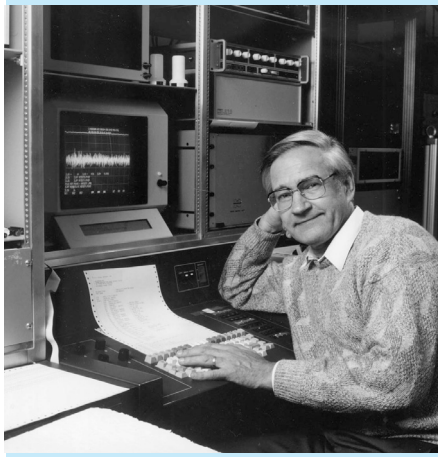

Fig. 1.3-2 R. R. Ernst *1933

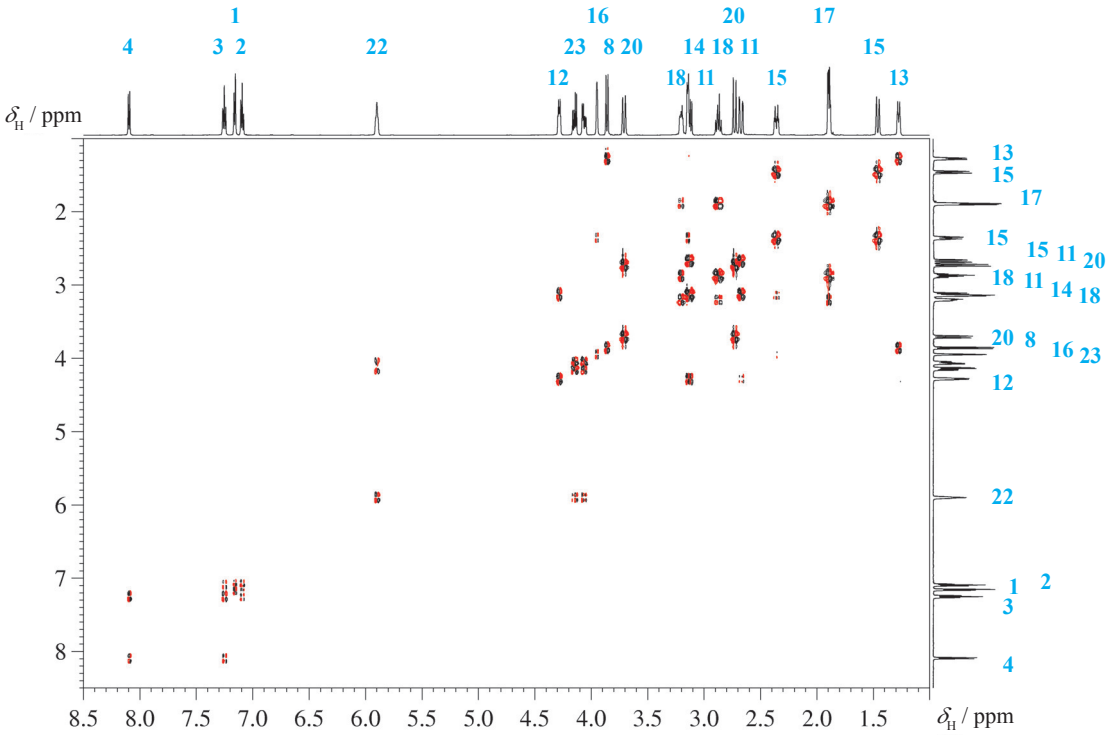

Fig. 1.3-3 COSY spectrum of strychnine

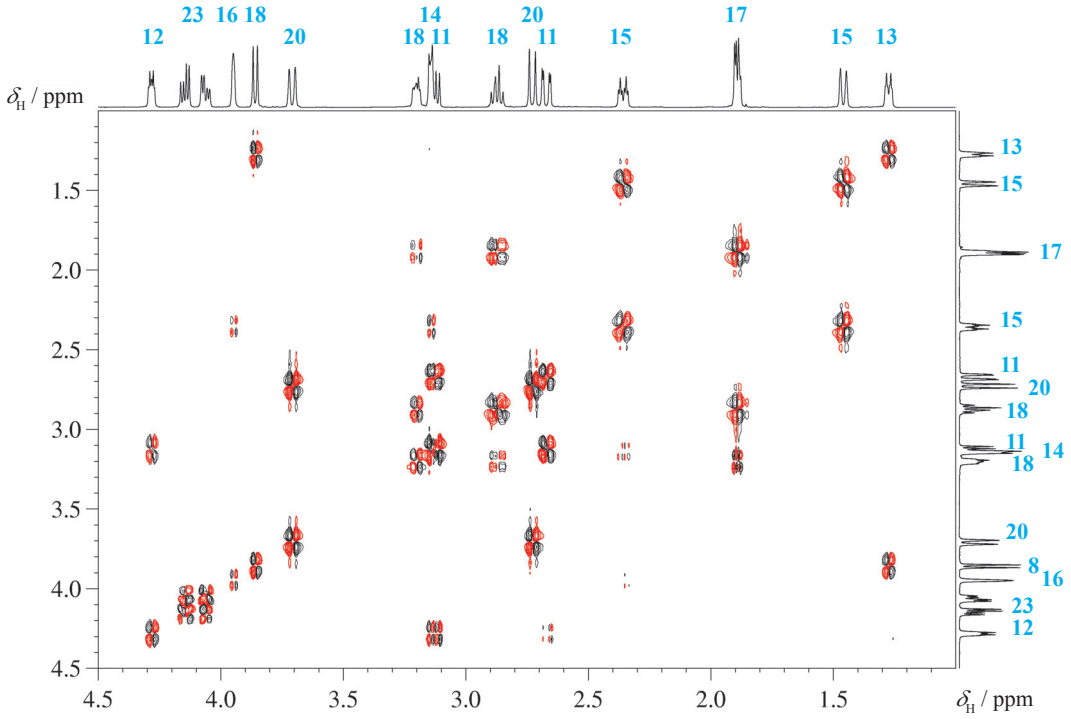

Fig.1.3-4 Expansion of the COSY spectrum in the aliphatic region

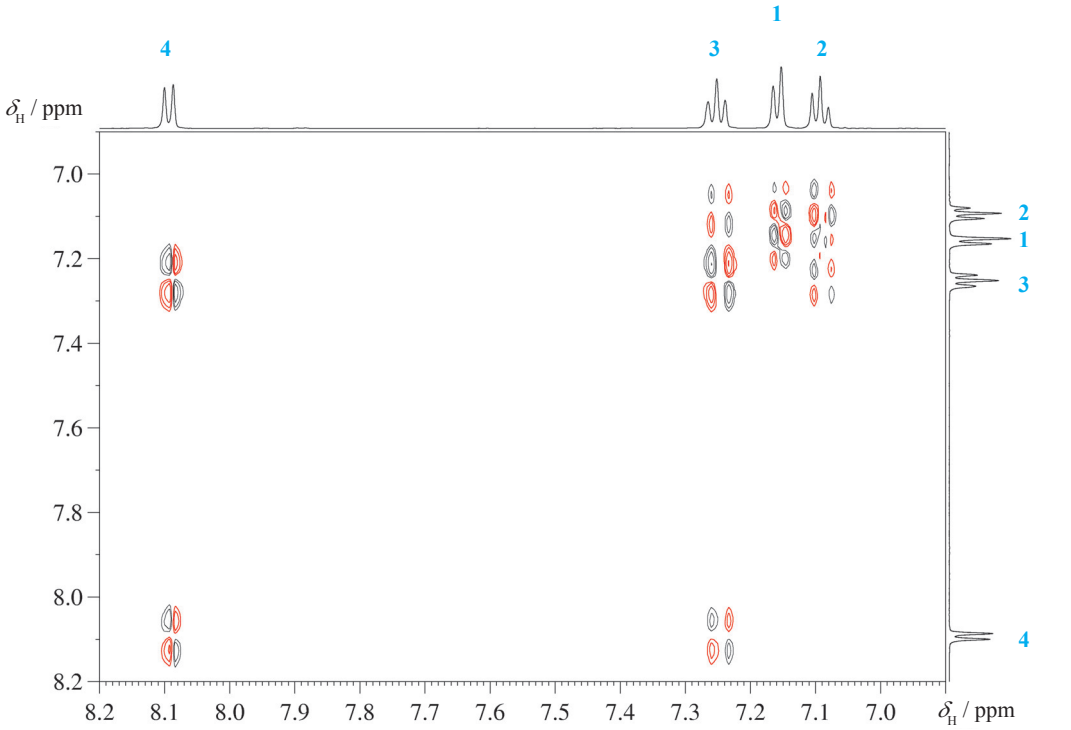

Fig. 1.3-5 Expansion of the COSY spectrum in the aromatic region

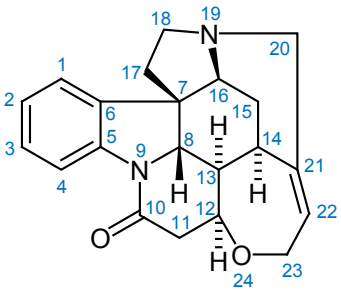

Scheme 1.3-3 Strychnine

The participation of Thomas W. Bauman at the AMPERE summer School in Basko Polje, Yugoslavia, in September 1971 was an extremely fortunate event. Being a meticulous scientist, he brought home a careful script of the lectures, among them one by Jean Jeener that attracted my attention immediately: a simple two-pulse experiment that produced revealing 2D spectra by 2D Fourier transformation of a 2D set of response signals. This was exactly the technique I had been waiting for. I had been thinking for some time about systematic computer-controlled double resonance experiments, but appreciated the complexity of the resulting 2D spectra should they follow the shape of the famous Anderson-Freeman plots.

R.R. Ernst "The success story of fourier transformation in NMR" *Enyclopedia of NMR*, **1996**, *1*, 297.

7. Comments

The two pulses given in red color are the essential COSY pulses used in the original pulse sequence. The additional pulses are used for the double-quantum filter (p3) and for phase correction due to the finite length of the gradient pulses (p2, p4, p6)

In the *preparation period* **p** of the pulse sequence we find the relaxation delay d1 and the first r.f. pulse p1 which transforms *z*-magnetization into transverse magnetization. The delay d2 and the 180° pulse p2 only serve to alleviate the finite length of the gradient pulse g1, which would otherwise cause a problem in phasing the 2D spectrum. Then the chemical shift develops in the *evolution period* **e** during t_1, which is written here only for proton 1, giving Equation (1). In addition, spin–spin coupling develops; thus each of the two terms with a modulation by the chemical shift will create two more terms including the spin–spin coupling.

$$I_{1_z} + I_{2_z} \xrightarrow{I_x} -I_{1_y} - I_{2_y} \xrightarrow{\Omega_1 t_1 I_{1_z}} -I_{1_y}\cos\Omega_1 t_1 + I_{1_x}\sin\Omega_1 t_1 \qquad (1)$$

$$\xrightarrow{\pi J t_1 2I_{1_z} I_{2_z}} -I_{1_y}\cos\Omega_1 t_1\cos\pi J t_1 + 2I_{1_x} I_{2_z}\cos\Omega_1 t_1\sin\pi J t_1$$
$$+ I_{1_x}\sin\Omega_1 t_1\cos\pi J t_1 + 2I_{1_y} I_{2_z}\sin\Omega_1 t_1\sin\pi J t_1 \qquad (2)$$

In the *mixing period* **m** of the pulse sequence the r.f. pulse p3 creates double-quantum magnetization $-2I_{1_x} I_{2_y}$, as in Equation (3). Again the delay d2 and the 180° pulse p4 are only for phase correction and correct for the finite length of the gradient pulse g2, which encodes the double-quantum magnetization.

$$2I_{1_x} I_{2_z}\cos\Omega_1 t_1\sin\pi J t_1 \xrightarrow{I_x} -2I_{1_x} I_{2_y}\cos\Omega_1 t_1\sin\pi J t_1 \qquad (3)$$

The 90° pulse p5 creates antiphase magnetization from the double-quantum term as given in eq. (4)

(4)

$$-2I_{1_x}I_{2_y}\cos\Omega_1 t_1 \sin\pi J t_1 \xrightarrow{I_x} -2I_{1_x}I_{2_z}\cos\Omega_1 t_1 \sin\pi J t_1$$

In the *detection period* **d** chemical shift and spin–spin coupling develop once again during the acquisition time t_2, giving Equation (5).

(5)

$$\xrightarrow{\Omega_2 t_2 I_{1_z}} \xrightarrow{\pi J t_2 2I_{1_z}I_{2_z}} I_{2_y}\cos\Omega_1 t_1 \sin\pi J t_1 \sin\Omega_2 t_2 \sin\pi J t_2$$

The last expression describes a cross-peak in the COSY matrix.

With the pulse sequence and the echo-antiecho scheme of the gradients used, the sign of the frequencies in F_1 is determined by keeping the sine and cosine terms separate, and thus allows phase-sensitive processing.

As can be seen from the coherence pathway diagram above, the first gradient g1 acts during a period when single-quantum magnetization I^+ is present (coherence level +1), whereas the second acts during a period when double-quantum coherence I^+I^+ is present. The final gradient pulse acts on I^-. Therefore the gradient ratios 30:10:50 and -30:10:50 will be successful to obtain the desired signals. All other coherences are further dephased and are not observable.

[1] J. Jeener, *Ampère International Summer School*, Basko Polje, **1971** (proposal).

[2] W. P. Aue, E. Bartholdi, R. R. Ernst "Two-dimensional spectroscopy. Application to nuclear magnetic resonance" *J. Chem. Phys.* **1975**, *64*, 2229–2246.

[3] T. D. W. Claridge, "High-Resolution NMR techniques in organic chemistry", Pergamon, Oxford, **1999**, 155–159.

[4] J. Keeler, "Understanding NMR spectroscopy", Wiley, Chichester, 2nd Ed. 2010.

8. Questions

A. Why does the standard COSY not reveal strong cross peaks for long-range spin couplings and what is the trick, whereby the long-range COSY is functioning?

B. In which dimension one would extract spin coupling values from a high-resolution COSY and why?

C. Why are double quantum coherences only developing at higher t_1 increments?

D. In the aromatic expansion of the strychnine spectrum one observes only an AX pattern from the triplet. Why?

E. Only one of the protons H-15 displays a cross peak to H-16. Why?

9. Own Observations

Experiment 1.4

NOESY

1. Purpose

The NOESY (**N**uclear **O**verhauser **E**nhancement **S**pectroscop**Y**) experiment is the two-dimensional equivalent of the NOE difference experiment (see chapter 3.6) and yields correlation signals that are caused by dipolar cross-relaxation between nuclei in a close spatial relationship.

The intensities of the cross-peaks under certain conditions are proportional to the sixth power of the proton–proton distances. Quantitatively, the results differ from 1D NOE difference spectroscopy, since the latter is a steady-state experiment obtained from a saturation of the energy levels, whereas NOESY is a transient experiment obtained after population inversion of the energy levels. In a qualitative way, the NOESY technique gives answers to many stereochemical problems such as *exo/endo*, *E/Z* and similar assignment questions. In NMR studies of peptides and proteins NOESY is the essential method for determining peptide conformations or tertiary structure of proteins. We show here a phase-sensitive version with two spoiling gradients during the mixing time.

Fig. 1.4-1 A. W. Overhauser (1925-2011)

2. Variants

The gradient pulses during the mixing time destroy most of the COSY artefacts present in NOESY, however, not the zero-quantum coherences. Further improvements of a gradient-supported NOESY technique have been described recently [4]. The NOESY technique has been combined with different schemes of water suppression, if biological samples have to be measured. Also, in protein NMR a 3D version with ^{15}N editing is the standard technique. Selective 1D NOESY sequences are known if only the answer of a particular spin is needed. An echo-antiecho method as shown in chapter 1.3 for COSY is not advisable because of diffusion effects during the mixing time (encoding gradients before and after the mixing time).

A considerable drawback of the NOESY technique is the dependence of the NOE effect on molar mass and viscosity, which can change its sign and may cause it to disappear for certain conditions. The ROESY technique as described in Experiment 2.2 may be more effective in this case.

In both, chemical exchange of nuclei may yield cross peaks, too.

Fig. 1.4-2 R. R. Ernst *1933

3. Pulse Scheme and Phase Cycle

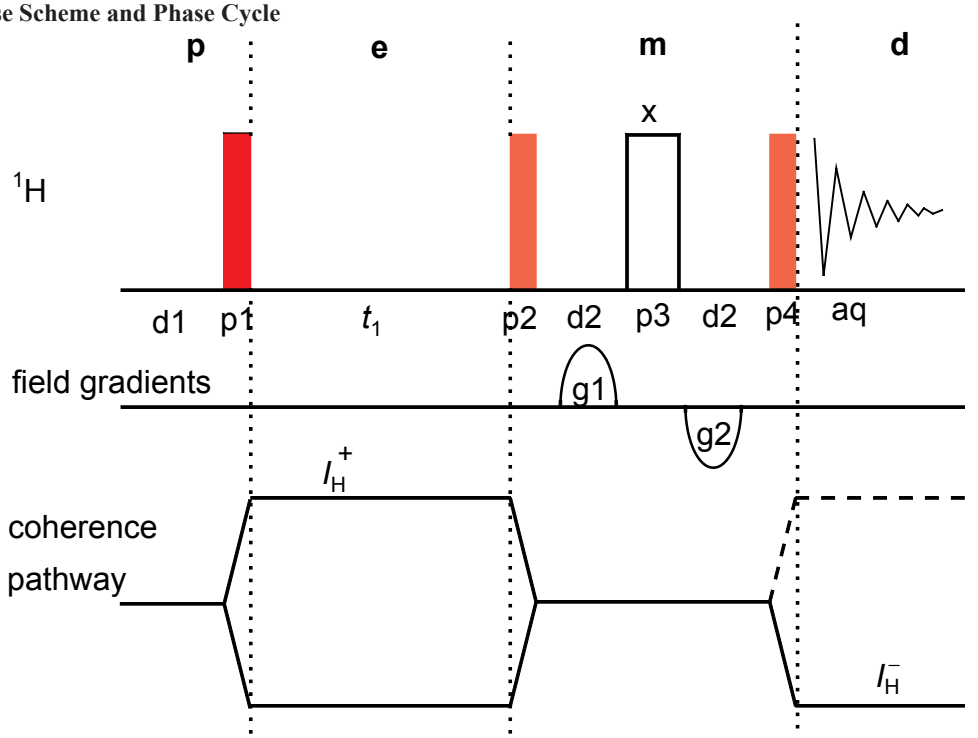

p1: x, -x p2: $(x)_8$, $(-x)_8$ p4: x, x, -x, -x, -y, -y, y, y

aq: x, -x, -x, x, y, -y, -y, y, -x, x, x, -x, -y, y, y, -y

phase cycle for p1 incremented according to States-TPPI

Scheme 1.4-1

Common values:

p1, p2, p4: 90° ^{1}H transmitter pulse
p3: 180° ^{1}H transmitter pulse
d1: relaxation delay
d2: mixing time 2, in the order of ^{1}H relaxation time
t1: evolution increment
g1, g2: gradients for artifact suppression

4. Acquisition

Special values used for the spectrum shown:

Sample: 3% strychnine in $CDCl_3$.
Time requirement: 5 h
Spectrometer: Bruker DRX-600 with 5-mm-TBI-probe

td2:	2K data points in F_2
td1:	256 data points in F_1
sw2:	10 ppm
sw1:	10 ppm
aq2:	0.17 s
aq1:	0.021 s
o1:	middle of ^{1}H NMR spectrum
d1:	2 s
d2:	1 s
ds:	4
ns:	8
g1, g2:	40 : (-40) with 0.6 T/m = 100 %

5. Processing

Apply zero-filling in F_1 to 1K real data points to obtain a symmetrical matrix of 1K×1K real data points. Use an exponential window in F_2 with lb = 5 Hz and a π/2-shifted squared sine bell in F_1.

Apply complex Fourier transformation corresponding to the States-TPPI mode of data acquisition in F_1. Adjust the phase of the diagonal signals so that they are negative. The NOESY correlation signals will then be positive if the compound has a molar mass below 1000 (positive NOE effect). Correlation signals caused by chemical exchange will have the same phase as the diagonal signals.

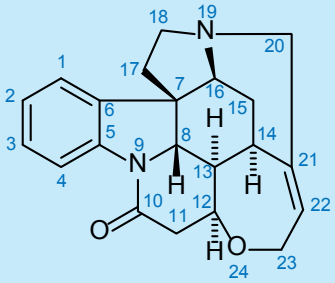

Scheme 1.4-2

6. Result

The figures show the result obtained on a DRX-600 spectrometer. Note that the phase of the diagonal signals is opposite to that of the cross-peaks as can be seen from the dotted contours. There is a wealth of information to be taken from the spectrum, which can best be studied using a molecular model or an electronic 3D file. Notice, for instance, that only one of the H-20 protons has an NOE contact with one of the H-15 protons, from which a relative assignment of the protons in these methylene groups can be derived.

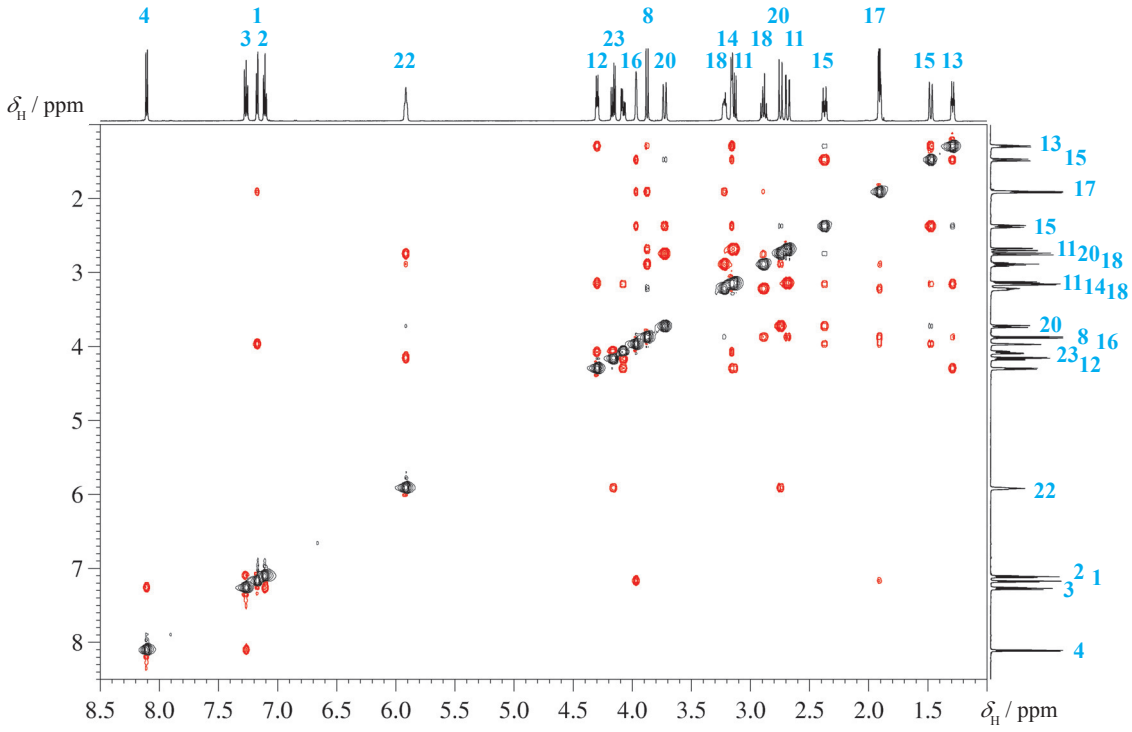

Fig. 1.4-3 NOESY spectrum of strychnine

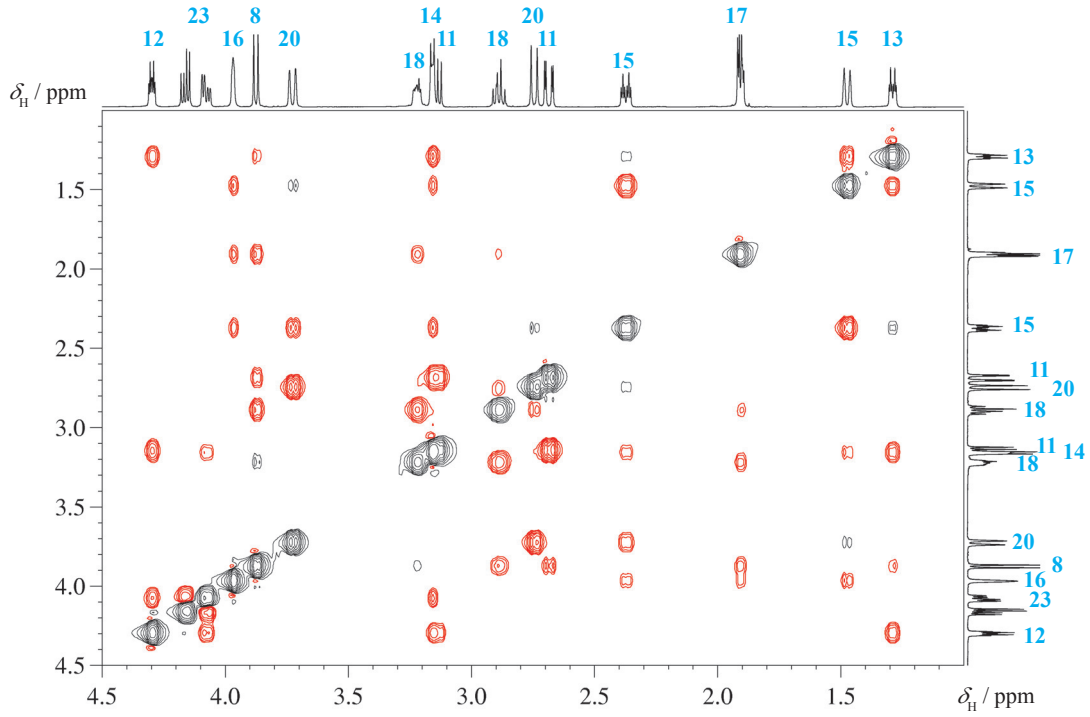

Fig. 1.4-4 Expansion of the spectrum in the aliphatic region

Albert Overhauser, a young theoretician from the University of Illinois, had made the following prediction: in a metal, where the conduction electrons are known to be responsible for the nuclear relaxation, the saturation of the ESR resonance of these electrons should lead to an enormous increase in the nuclear polarization. [...] Secondly, that Overhauser's audience at the meeting of the American Physical Society − where he had (in ten minutes) presented the calculations which had led to his amazing conclusion − was immediately split into two parts, which, however, overlapped: those who did not understand a single word of his demonstration, and those who did not believe a single word of his conclusions. In the first row of the sceptics who did not believe his conclusions shone all the stars of magnetic resonance: Bloch and Purcell, Rabi and Ramsey. Bloembergen was of two minds and so was I. As for the presentation itself, 1 will repeat what Van de

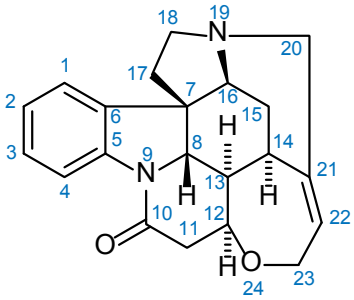

Scheme 1.4-3

7. Comments

The NOESY sequence can be understood from the vector model. We consider two protons with different chemical shifts and without spin–spin coupling.

The *preparation period* **p** starts with the relaxation delay d1. The first pulse p1 of the NOESY sequence shown in red aligns all proton magnetization into the *x,y*-plane which is the end of the time slot **p**.

In the *evolution period* **e**, chemical shift and spin−spin coupling evolve during t_1. In the *mixing period* **m** the second red pulse p2 aligns the *y* components of the two vectors, which are by now labelled with their individual chemical shifts into the negative *z*-direction. This situation is called a chemical shift-encoded *z*-magnetization. In the second scan of the phase cycle pulse p2 aligns the *y* components to the positive *z* direction to get a FID without NOE effect. Both scans are subtracted by receiver phase to yield the difference spectrum. During the mixing time (2×d2) both protons are allowed to relax and show cross relaxation.

This pathway is shown in the coherence diagram. In addition, however, the pulse p2 can generate zero-, double-quantum- and antiphase coherences, since H,H spin coupling is also evolved during t_1. The positive and negative gradient pulses in the mixing time, which embrace the 180° pulse p3, dephase all these components except the zero-quantum coherences. Furthermore, they dephase axial signals of those protons that have relaxed during t_1 and are excited again by p2. The final pulse p4 reads the situation at the end of the mixing time and realigns the vectors into the *x,y* plane, where the FID is recorded.

Graaff had told me of de Broglie‘s defensc of his thesis in Paris in 1924. „Never had so much gone over the heads of so many“.

The real question was of course: „Was Overhauser right?“ He was: the proof of the pudding was given the same year by Charles Slichter, a physicist from Illinois, and his student, Carver. They saturated the resonance of conduction electrons in metallic lithium and saw the enhancement of the nuclear polarization predicted by Overhauser.

A. Abragam, (1914-2011) "Time reversal, an autobiography", Oxford University Press **1989**

[1] J. Jeener, B. H. Meier, P. Bachmann, R. R. Ernst "Investigation of exchange processes by two-dimensional NMR spectroscopy" *J. Chem. Phys*. **1979**, *71*, 4546–4553.

[2] D. J. States, R. A. Haberkorn, D. J. Ruben "A two-dimensional nuclear Overhauser experiment with pure absorption phase in four quadrants" *J. Magn. Reson*. **1982**, *48*, 286–292.

[3] G. Bodenhausen, H. Kogler, R. R. Ernst "Selection of coherence-transfer pathways in NMR pulse experiments" *J. Magn. Reson.* **1984**, *58*, 370–388.

[4] R. Wagner, S. Berger "Gradient-selected NOESY—A fourfold reduction of the measurement time for the NOESY experiment" *J. Magn. Reson*. Ser. A **1996**, *123*, 119–121.

[5] T. Parella, F. Sánchez-Ferrando, A. Virgili "Quick recording of pure absorption 2D TOCSY, ROESY, and NOESY spectra using pulsed field gradients" *J. Magn. Reson*. **1997**, *125*, 145–148.

[6] M. J. Thrippleton, J. Keeler "Elimination of zero quantum interference in two-dimensional NMR spectra" *Angew. Chem. Int. Ed*. **2003**, *42*, 3938–3941.

[7] D. Neuhaus, M.P. Williamson, "The nuclear Overhauser effect in structural and conformational analysis", 2nd Ed., Wiley-VCH, Weinheim, **2000**.

8. Questions

A. Explain why the mixing time is best approached by the spin-lattice relaxation time of the spins involved.

B. What is meant by a NOESY build-up curve and how is it obtained?

C. What is the reason that build-up curves have a maximum and decay to zero at long mixing times?

D. If the ROESY technique does not have the sign problem that NOESY has, why does one not use only ROESY in all situations?

E. Which molecular entities are suitable for a distance reference?

9. Own Observations

Experiment 1.5

HSQC

1. Purpose

C,H correlation, as well as other X,H correlations, is now mainly achieved by the HSQC (**H**eteronuclear **S**ingle **Q**uantum **C**oherence) method, because in this sequence the signals are not broadened by homonuclear H,H coupling in F_1. The HSQC scheme is included as a building block in many 3D sequences, especially for structural biology, but has become established as the standard scheme of C,H correlation in organic chemistry. In the experiment shown here (using strychnine as example) we demonstrate a combination of several features which persuade us that it is today the method of choice.

Fig. 1.5-1 G. Bodenhausen (*1951)

2. Variants

Since the introduction of this experiment [1], there has been a permanent development. Today, mostly a gradient-selected variant is used, with the gradients operating in the echo-antiecho method for sensitivity reasons.

Additional sensitivity improvement by a factor of $\sqrt{2}$ is achieved by a double back INEPT transfer; however, this occurs only for CH groups [2-5]. In reference [6], applications for long-range spin couplings are discussed. In most cases it is desirable to obtain an editing of 2D H,X correlation spectra. This can yield a multiplicity determination in case of overlapping ^{13}C signals, or reveal CH moieties in the presence of many CH_2 groups or NH_2 groups in the middle of many NH groups in proteins. This kind of multiplicity determination can be achieved by including an editing period.[7-10]

In contrast to HMQC, the HSQC experiment employs 180° pulses, which causes problems if the 180° pulses become too long (e.g., in a triple-tuned probe) but have to cover a very wide spectral range. This leads to severe phasing problems for instruments with a magnetic field above that corresponding to 500 MHz ^1H frequency. The remedy for this problem is to apply frequency-swept adiabatic 180° ^{13}C pulses (see chapter 8.4), which can cover the large spectral width of ^{13}C [11, 12].

The enhancement in sensitivity possible with this scheme dwarfs the enhancement obtainable with the nuclear Overhauser effect (when observing the low-γ nucleus directly), and therefore it has been referred to as the *Overbodenhausen* experiment.

Ad Bax et al., *J. Magn.Reson*. **1990**, *86*, 304-318.

3. Pulse Scheme and Phase Cycle

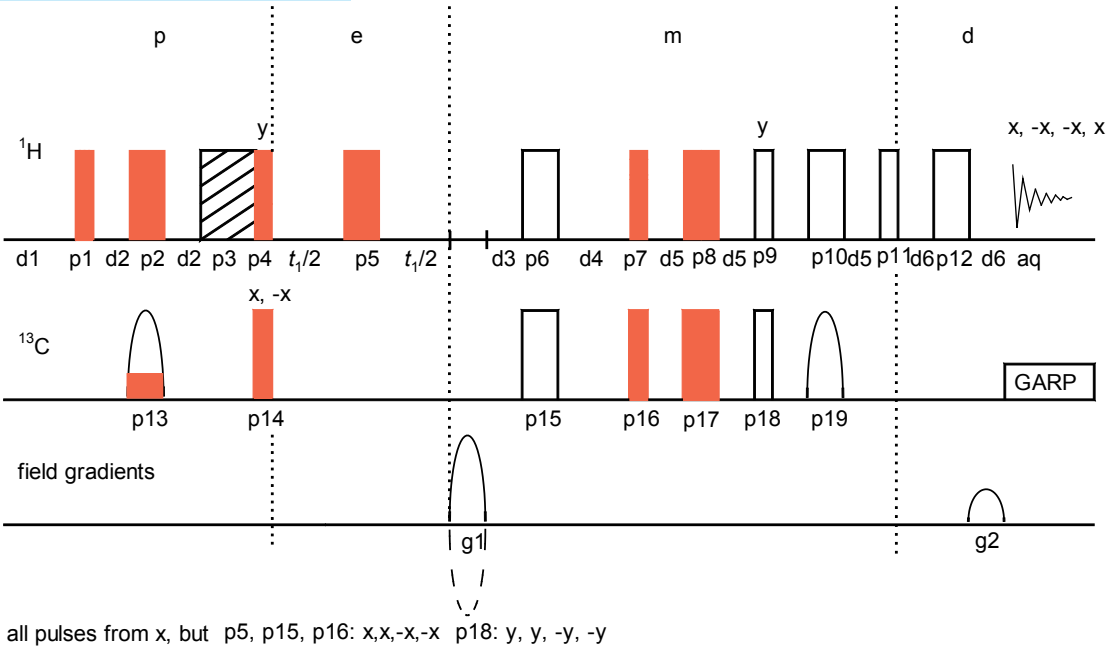

Scheme 1.5-1

Common values:

p1, p4, p7, p9, p11: 90° ^{1}H transmitter pulse
p2, p5, p6, p8, p10, p12: 180° ^{1}H transmitter pulse
p3: trim pulse
p14, p16, p18: 90° ^{13}C transmitter pulse
p15, p17: 180° ^{13}C transmitter pulse
p13, p19 ^{13}C-CHIRP pulse for inversion
d1: relaxation delay
d2, d5: polarization delay during INEPT or back INEPT transfer
d3, d4: editing delay for multiplicity recognition
t_1: evolution increment
g1,g2: gradients for echo/antiecho selection

4. Acquisition

Special values used for the spectrum shown:

Sample: 3% strychnine in $CDCl_3$.
Time requirement: 80 min
Spectrometer: Bruker DRX-600 with 5-mm TBI probe

td2: 2K data points in F_2
td1: 256 data points in F_1
sw2: 9 ppm
sw1: 160 ppm
aq2: 0.13 s
aq1: 0.005 s
offset of ^{1}H frequency: middle of ^{1}H NMR spectrum [4.5 ppm]
offset of ^{13}C frequency: middle of ^{13}C NMR spectrum [80 ppm]
p3: ^{1}H trim pulse [1 ms, 5 dB]
p13, p19: adiabatic chirped 180° ^{13}C pulse [crp 60, 0.5, 20.1; 500 µs, 5.5 dB]
^{13}C decoupler attenuation and 90° pulse for GARP [14.3 dB, 70 µs]
d1: 2 s
d2: 1/[4*J*(C,H)] = 1.72 ms, calculated from ^1J(C,H) ≈ 145 Hz
d3: 1/[2*J*(C,H)] minus effective gradient length g1 (=1.05 ms) = 2.39ms
d4: 1/[2*J*(C,H)] = 3.44 ms calculated from ^1J(C,H) ≈ 145 Hz
d5: 1/[8*J*(C,H)] = 0.862 ms calculated from ^1J(C,H) ≈ 145 Hz
d6: effective length of pulsed field gradients, here 1.05 ms
g1, g2: 80 : 20.1; g1 switched to negative according to echo-antiecho scheme
ds: 8
ns: 8

5. Processing

Apply zero-filling in F_1 to 1K words in order to have a symmetrical matrix of 1024×1024 data points. Use an exponential window with lb = 3 Hz in the F_2 dimension and a squared π/2 shifted sinusoidal window in the indirect dimension. Apply real Fourier transformation in both dimensions. Phase correction in both dimensions can be performed, after the 2D transformation, to positive and negative signals for the CH or CH_3 and the CH_2 groups.

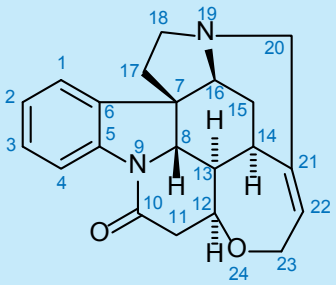

Scheme 1.5-2

6. Result

The figures show the spectrum obtained on an DRX-600 spectrometer with a multinuclear inverse probe equipped with *z*-gradients. The overview spectrum displays all relevant connectivities for strychnine. Since the compound is chiral, all CH_2 groups are diastereotopic, which can be nicely observed for the red signals. Due to the adiabatic 180° pulses on ^{13}C, there are no phase problems.

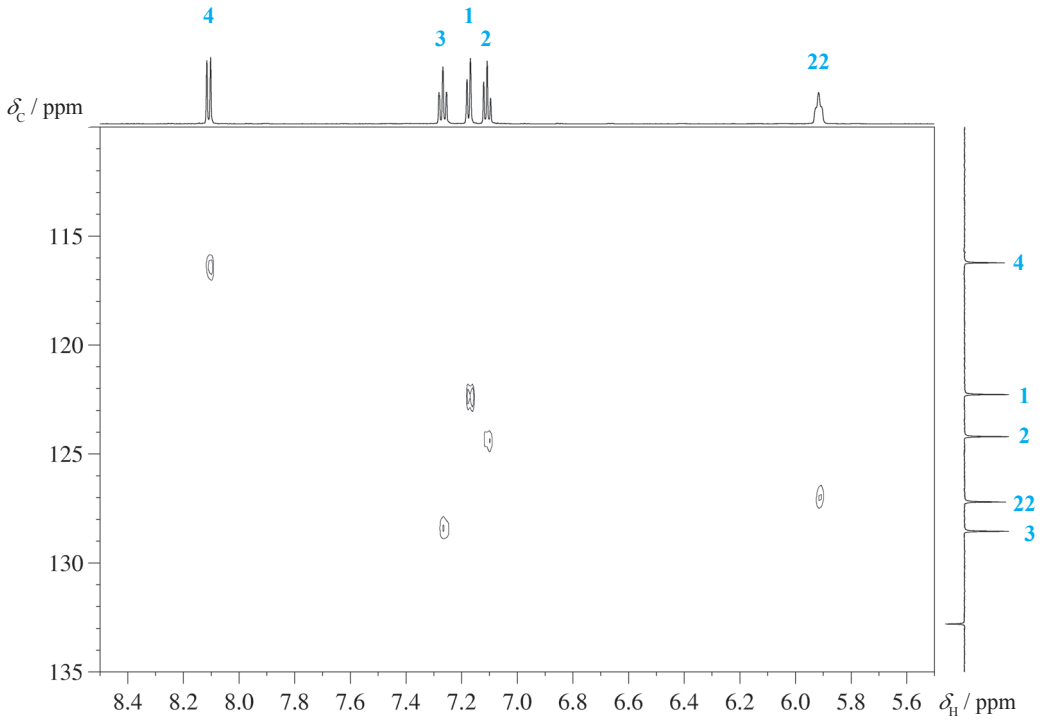

Fig. 1.5-2 Expansion of the HSQC spectrum in the aromatic region

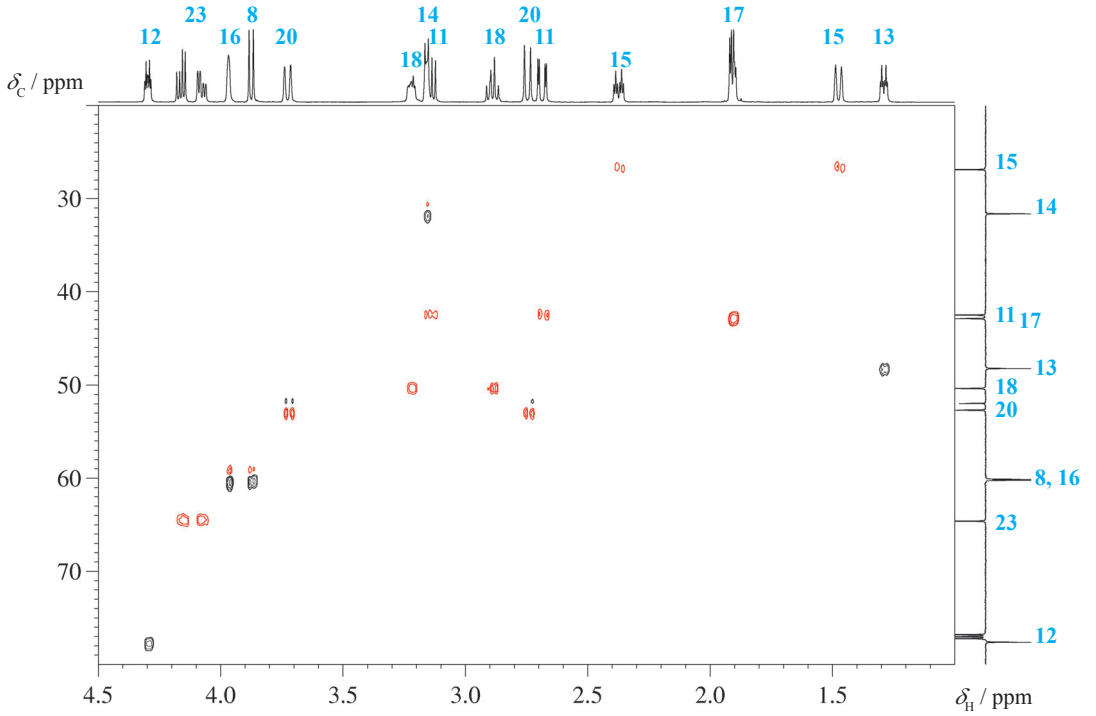

Fig. 1.5-3 Expansion of the HSQC spectrum in the aliphatic region

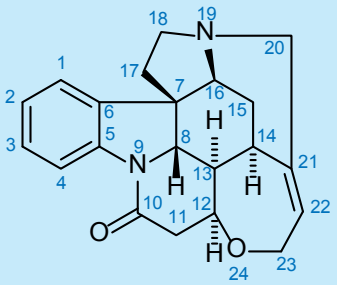

Scheme 1.5-3

7. Comments

The pulses given in red color are the essential HSQC pulses used in the original pulse sequence. p3 acts as a trim pulse during the INEPT transfer, p6 and p15 are refocusing pulses during the editing period, and all others are for the double INEPT back transfer. The 180° pulses p13 and p19 are shaped adiabatic pulse to alleviate phase problems and cover the large ^{13}C chemical shift range.

In the preparation period **p** the sequence starts with an INEPT transfer from proton to ^{13}C. This INEPT transfer results in antiphase magnetization of ^{13}C with respect to proton; thus $-2I_{H_z}I_{C_y}$ single-quantum coherence is present at the end of this section. The trim pulse p3 removes unwanted magnetization.

In the evolution period **e** one t_1 section follows with a 180° pulse on the protons in the middle of t_1. During t_1 the term $-2I_{H_z}I_{C_y}$ develops ^{13}C chemical shift as described by Equation (1). The 180° proton pulse p5 eliminates the J(C,H) couplings in F_1 and for simplicity is not shown in the equations.

(1)

$$-2I_{H_z}I_{C_y} \xrightarrow{\Omega_C t_1 I_{C_z}} -2I_{H_z}I_{C_y}\cos\Omega_C t_1 + 2I_{H_z}I_{C_x}\sin\Omega_C t_1$$

After the chemical shift evolution an editing period in the mixing period **m** serves for different signs of CH and CH_3 or CH_2 signals. The editing period starts with gradient g1, delay d3, consists of the two pulses p6

and p15, and ends with the delay d4. The length of (g1 + d3) is equal to d4. If, for instance, the delays are set to 1/2*J,* the total length of the editing period is 1/*J* as in the APT method (see chapter 1.2), and CH_2 spin vectors will point in the opposite direction compared to those of CH and CH_3 moieties.

After the editing period **e** a double back INEPT transfer occurs from ^{13}C to proton.

The first INEPT back transfer converts the term of equation (1) by the pulses p16 and p7 into ($2I_{H_y}I_{C_z}\cos\Omega_C t_1 - 2I_{H_y}I_{C_x}\sin\Omega_C t$), where the second part is a double-quantum magnetization. In the first spin echo period with the 180° pulses p17 and p8 these terms are therefore converted into ($I_{H_x}\cos\Omega_C t_1 - 2I_{H_y}I_{C_x}\sin\Omega_C t$). The second INEPT back transfer starts with the pulses p18 and p9 and these store I_{H_x} as *z*-magnetization and convert the double-quantum term into antiphase magnetization: ($I_{H_z}\cos\Omega_C t_1 - 2I_{H_y}I_{C_z}\sin\Omega_C t$). The latter develops in the second spin-echo period, interrupted by the pulses p19 and p10 and by the final 90° pulse p11 into ($-I_{H_y}\cos\Omega_C t_1 + I_{H_x}I_{C_z}\sin\Omega_C t$).

Thus both the sin and the cos chemical shift terms contribute to the intensity of the signal, and this is called "sensitivity enhancement (SI)" or "preservation of equivalent pathways (PEP)" or "coherence selective transfer (COS)" by different authors.

The detection period **d** consists of the d6-p12-gradient g2 sandwich and the acqusition with GARP decoupling.

Fig. 1-5.4 "Die zweite Dimension", Harald Jancke, Berlin 1985

[1] G. Bodenhausen, D. J. Ruben "Natural abundance nitrogen ^{15}NMR by enhanced heteronuclear Spectroscopy" *Chem. Phys. Lett.* **1980**, *69*, 185–189.

[2] L. E. Kay, P. Keifer, T. Saarinen"Pure absorption gradient enhanced heteronuclear single quantum correlation spectroscopy with improved sensitivity" *J. Am. Chem. Soc*. **1992**, *114*, 10663–10665.

[3] A. G. Palmer III, J. Cavanagh, P. E. Wright, M. Rance "Sensitivity improvement in proton-detected two-dimensional heteronuclear correlation NMR spectroscopy" *J. Magn. Reson*. **1991**, *93*, 151–170.

[4] G. Kontaxis, J. Stonehouse, E. D. Laue, J. Keeler "The sensitivity of experiments which use gradient pulses for coherence pathway selection" *J. Magn. Reson*. Ser. A **1994**, *111*,70–76.

[5] J. Schleucher, M. Schwendinger, M. Sattler, P. Schmidt, O. Schedletzky, S. J. Glaser, O. W. Sørensen, C. Griesinger "A general enhancement scheme in heteronuclear multidimensional NMR employing pulsed-field gradients" *J. Biomol. NMR* **1994**, *4*, 301–306.

[6] R. Marek, L. Králik, V. Sklenár "Gradient-enhanced HSQC experiments for phase-sensitive detection of multiple bond interactions" *Tetrahedron Lett*. **1997**, *38*, 665–668.

[7] D. G. Davies "Simplification of proton-detected, natural abundance carbon-13 correlation spectra of proteins via multiplet editing" *J. Magn. Reson*. **1990**, *90*, 589–596 "Improved multiplet editing of proton-detected, heteronuclear shift-correlation spectra" *ibid*. **1991**, *91* 665–672.

[8] X. Zhang, C. Wang "^{1}H-detected editable heteronuclear multiple-quantum correlation experiment at natural abundance" *J. Magn. Reson*. **1991**, *91*, 618–623.

[9] W. Willker, D. Leibfritz, R. Kerssebaum, W. Bermel "Gradient selection in inverse heteronuclear correlation spectroscopy" *Magn. Reson. Chem*. **1993**, *31*, 287–292.

[10] T. Parella, J. Belloc, F. Sánchez-Ferrando, A. Virgili "A general building block to introduce carbon multiplicity information into multi-dimensional HSQC-type experiments" *Magn. Reson. Chem*. **1998**, *36*, 715–719.

[11] R. Fu, G. Bodenhausen "Broadband decoupling in NMR with frequency-modulated 'chirp' pulses" *Chem. Phys. Letters* **1995**, *245*, 415–420.

[12] E. Kupce, R. Freeman "Optimized Adiabatic Pulses for Wideband Spin Inversion" *J. Magn. Reson.* Ser. A **1996**, *118*, 299–303.

8. Questions

A. Discuss the difference between the basic HSQC and HMQC sequence. Why is HSQC preferred over HMQC?

B. Why is the PEP mechanism only advantageous for CH groups, but not for CH_2 groups?

9. Own Observations

Experiment 1.6

HMBC

1. Purpose

HMBC [**H**eteronuclear **M**ultiple **B**ond **C**orrelation] is the last experiment within our organic set of essential NMR techniques. It is probably the most important one and typically gives the final answers with respect to a structural problem. The pulse sequence was developed to obtain H,C correlations via ^{2}J(C,H) and ^{3}J(C,H). Sometimes even ^{4}J(C,H) correlations are revealed. An unresolved problem is the incomplete suppression of correlations via ^{1}J(C,H). The experiment is therefore usually performed without broadband ^{13}C decoupling to distinguish long-range correlations from signals originating from ^{1}J(C,H).

Here we describe a recent gradient-selected version [6], which is phase-sensitive using the echo-antiecho mode, but will be with a double low pass filter typically processed in the magnitude mode.

2. Variants

In more than 25 years of development there has been a large variety of proposals concerning how to obtain the long-range CH correlation information most effectively. The main issues are:

(1) The variability of the long-range J parameter in organic molecules which ranges from 1 to 20 Hz. Methods which should cope with this include full 3D techniques, where the J parameter is evolved in an extra dimension, or semi 3D techniques, where the J parameter is incremented at the same time as t_1 like ACCORDION-HMBC [8] and varieties thereof. After extensive experimentation it seems that the recording and co-adding of three different HMBC spectra focused with 2 Hz, 6 Hz and 10 Hz is the most time- and effort - effective solution to this problem.

(2) The variability of the ^{1}J parameter which affects the suppression of ^{1}J break-throughs. Different low-pass filter methods have been proposed and also methods which do not filter at all but separate the two kinds of information (HMSC [9]).

(3) The separation of ^{2}J and ^{3}J correlations, which has been proposed by a sequence called H2BC [10].

(4) The overall sensitivity of the method.

(5) The use of J-HMBC for the digital measurement of the long-range CH spin-coupling constants; the combination with J-resolved spectroscopy and the high resolution band HMBC (see chapter 3.9) are further current developments.

Fig. 1.6-1: A. Bax, *1956

Although the same HMQC pulse schemes, together with a large number of alternative schemes were proposed independently by the Australian group of Bendall, Pegg, and Doddrell, the application of our experiment to a biological macromolecule and to natural abundance peptides was probably the main reason for the surge in popularity of these HMQC experiments. For me it was my first encounter with a biological application of NMR, and I liked it.

Ad Bax, "NMR of Ethanol and Interferon γ", *Enyclopedia of NMR,* **1996**, *1*, 202–207.

3. Pulse Scheme and Phase Cycle

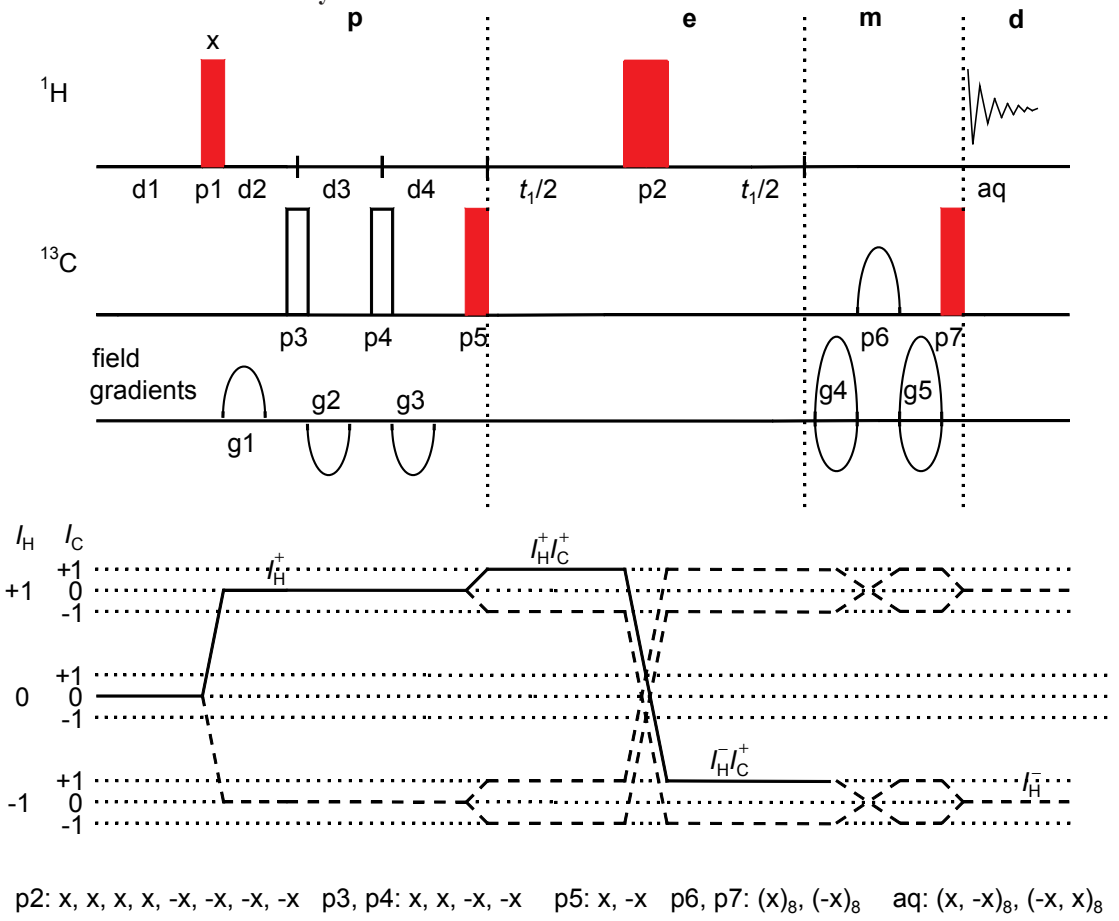

Scheme 1.6-1

Common values:

p1: 90° ^{1}H transmitter pulse
p2: 180° ^{1}H transmitter pulse
p3, p4, p5, p7: 90° ^{13}C transmitter pulse
p6: 180° ^{13}C-CHIRP pulse for refocusing
d1: relaxation delay
d2: 1/[2*J] , minimum ^1J(C,H)
d3: 1/[2*J] , maximum ^1J(C,H)
d4: 1/[2*J] , ^nJ(C,H)
t1: evolution increment
g1,g2,g3: gradients for ^1J-low pass filter
g4,g5: switched to positive/negative according to echo/anti-echo scheme

4. Acquisition

Special values used for the spectrum shown:

Sample: 3 % strychnine in $CDCl_3$
Time requirement: 90 min
Spectrometer: Bruker DRX-600 with 5-mm TBI probe

td2: 2K data points in F_2
td1: 512 [2 ×256] data points in F_1
ns: 4
sw2: 9 ppm
sw1: 180 ppm
aq2: 0.19 s
aq1: 0.009 s
offset of ^{1}H frequency: middle of ^{1}H NMR spectrum
offset of ^{13}C frequency: middle of ^{13}C NMR spectrum
p7: 2 ms composite CHIRP , 60 KHz sweep, "Crp60comp.4"
d1: 2.5 s
d2: 4 ms, calculated from ^1J(C,H) ≈ 125 Hz
d3: 2.94 ms, calculated from ^1J(C,H) ≈ 170 Hz

d4: 62.5 ms, calculated from J(C,H) ≈ 8 Hz
g1 to g5: sine-shaped field gradients, 1 ms, 50µs ring-down delay,
g1: 15%, g2: −10 %, g3: −5 %, g4: 80 % and −42 %, g5: −42 % and 80 % (100 % ≈ 0.56 T/m)

5. Processing

Apply zero-filling in F_1 to 1K data points in order to have a matrix of 1K×1K real data points. Before Fourier transformation use an exponential window in F_2 with lb = 3 Hz and π/2-shifted squared sine window in F_1. Phase correction is unnecessary, since the spectrum is processed in magnitude mode in F_1.

6. Result

The figures show extensions of the 2D spectrum obtained on a DRX-600 spectrometer with an inverse multinuclear z-gradient probe. Note the wealth of information obtainable from ^2J and ^3J couplings in this molecule.

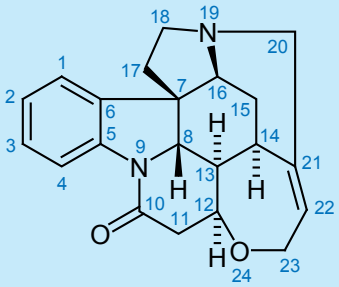

Scheme 1.6-2

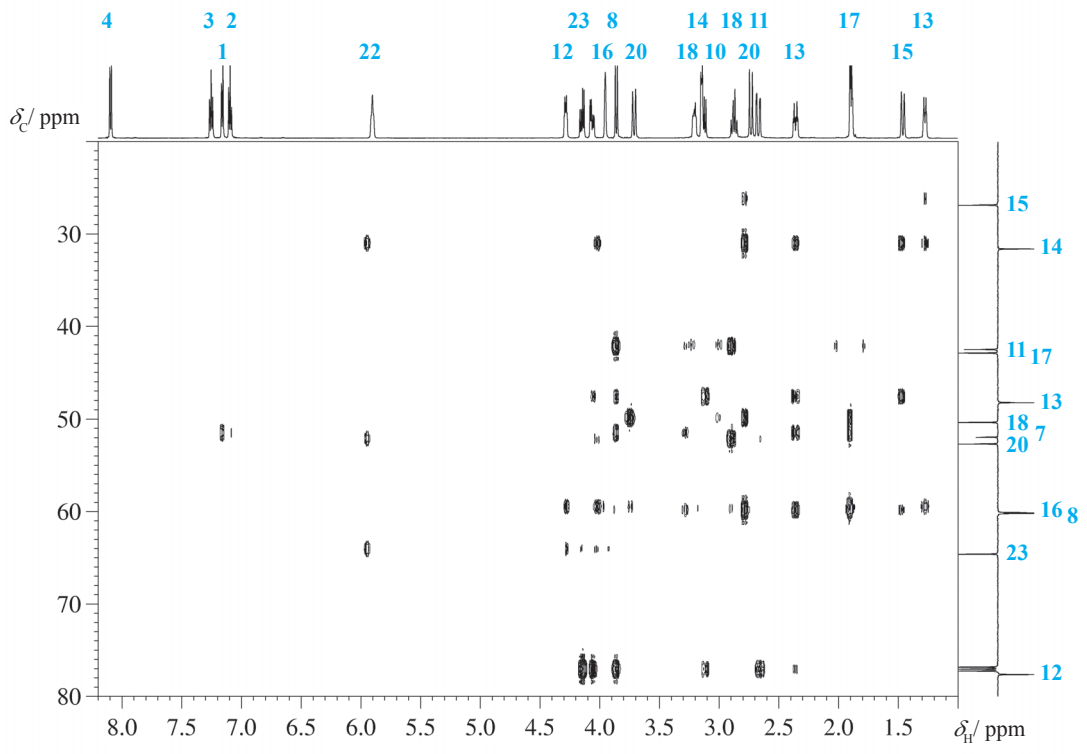

Fig. 1.6-2: HMBC expansion in the aliphatic ^{13}C region

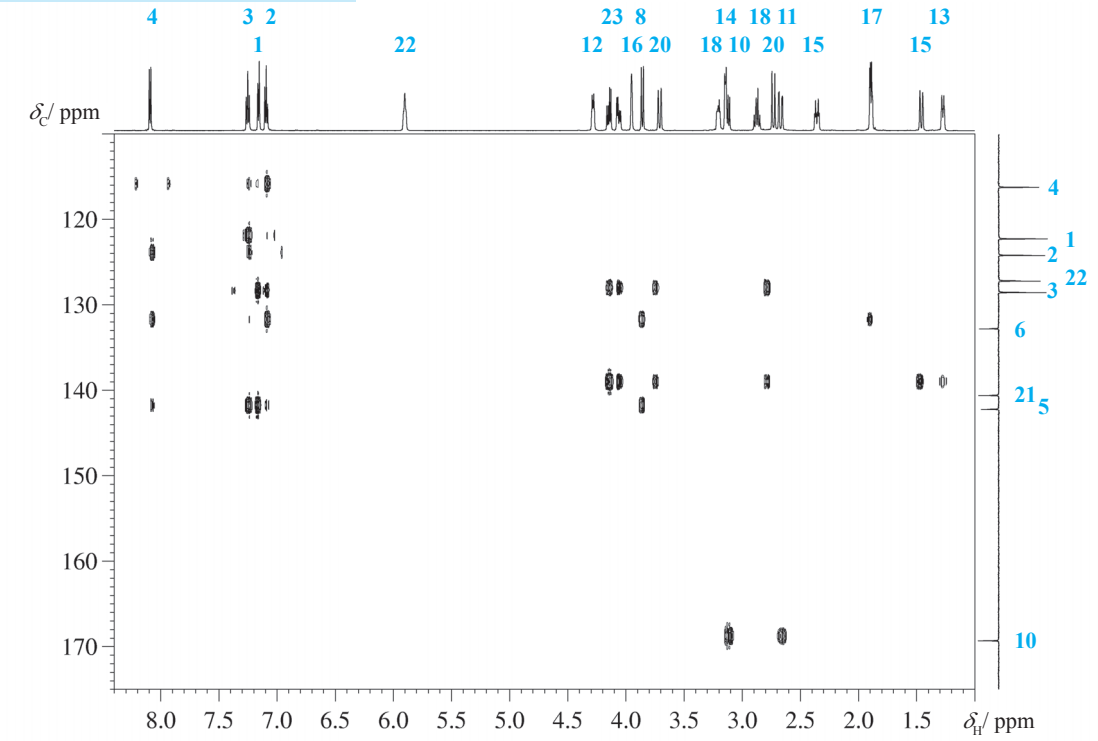

Fig. 1.6-3: HMBC expansion in the aromatic ^{13}C region

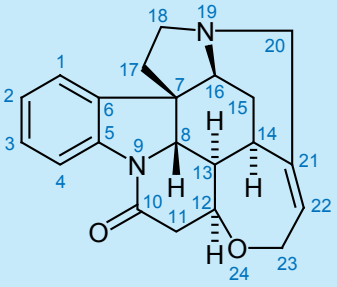

Scheme 1.6-3

8. Comments

HMBC has originally been derived from HMQC by simply increasing the delay after the first pulse before the creation of multiple-quantum coherence. The red-colored pulses in the sequence shown in Scheme 1.6-1 comprise this original experiment [1].

The first 90° proton pulse creates a transverse proton magnetization $-I_{H_y}$ as in Equation (1). During the delay d4 the ^2J and ^3J CH spin couplings develop and create antiphase magnetization $2I_{H_x}I_{C_z}$.

(1)

$$I_{H_z} + I_{C_z} \xrightarrow{I_{H_x}} -I_{H_y} + I_{C_z} \xrightarrow{\pi J \tau I_{H_z} I_{C_z}} 2I_{H_x} I_{C_z}$$

The two ^{13}C pulses p3 and p4 and the three gradient pulses g1 to g3 during the preparation period **p** serve as a dual-stage low-pass filter [7]. They eliminate the signals of protons experiencing a one-bond coupling ^1J(C,H). Therefore the action of these pulses is not considered in the POF description and in the coherence pathway diagram.

The third 90° ^{13}C pulse p5 transforms the antiphase magnetization of ^nJ(C,H) into double-quantum magnetization $2I_{H_x}I_{C_y}$ as in Equation (2).

(2)

$$2I_{H_x}I_{C_z} \xrightarrow{I_{C_x}} -2I_{H_x}I_{C_y}$$

In the evolution period **e** this term develops ^{13}C chemical shift as in Equation (3). Of course, ^{1}H chemical shift and H,H spin coupling also evolve during t_1. The former is removed by the 180° proton pulse p2, which for simplicity is not shown in the equations. Furthermore, this 180° proton pulse interchanges double-quantum and zero-quantum terms.

$$\xrightarrow{\Omega_C t_1 I_{C_z}} -2I_{H_x}I_{C_y}\cos\Omega_C t_1 + 2I_{H_x}I_{C_x}\sin\Omega_C t_1 \qquad (3)$$

In the mixing period **m** the adiabatic 180° refocusing pulse p6 in the ^{13}C channel, together with the pair of gradients g4 and g5 which are working in the echo-antiecho mode, selects for protons bound to ^{13}C only and suppresses all protons bound to ^{12}C. The final pulse p7 transfers the magnetization back to the proton channel as given in equation (4).

$$\xrightarrow{I_{C_x}} -2I_{H_x}I_{C_z}\cos\Omega_C t_1 + 2I_{H_x}I_{C_x}\sin\Omega_C t_1 \qquad (4)$$

In the detection period **d** the proton chemical shifts are sampled without ^{13}C decoupling. This is because despite the low-pass filter, some correlation signals via ^{1}J(C,H) can be seen in any HMBC spectrum. In order to distinguish these signals from the desired correlations it is advisable not to use ^{13}C decoupling, so ^{1}J breakthrough, giving rise to large doublets.

[1] A. Bax, M. F. Summers "^{1}H and ^{13}C assignments from sensitivity-enhanced detection of heteronuclear multiple-bond connectivity by multiple quantum NMR" *J. Am. Chem. Soc.* **1986**, *108*, 2093–2094.

[2] W. Willker, D. Leibfritz, R. Kerssebaum, W. Bermel "Gradient selection in inverse heteronuclear correlation spectroscopy" *Magn. Reson. Chem.* **1993**, *31*, 287–292.

[3] J. Ruiz-Cabello, G. W. Vuister, C. T. W. Moonen, P. van Gelderen, J. S. Cohen, P. C. M. van Zijl "Gradient-enhanced heteronuclear correlation spectroscopy. Theory and experimental aspects" *J. Magn. Reson.* **1992**, *100*, 282–302.

[4] R. Araya-Maturana, T. DelgadoCastro, W. Cardona, B. E. Weiss-Lopez "Use of long-range C-H heteronuclear multiple bond connectivity in the assignment of the ^{13}C NMR spectra of complex organic molecules" *Current Organic Chemistry*, **2001**, *5*, 253–263.

[5] W. F. Reynolds, R. G. Enríquez, "Choosing the best pulse sequences, acquisition parameters, postacquisition processing strategies, and probes for natural product structure elucidation by NMR spectroscopy" *J. Nat. Prod.* **2002**, *65*, 221–244.

[6] D. O. Cicero, G. Barbato, R. Bazzo, "Sensitivity enhancement of a two-dimensional experiment for the measurement of heteronuclear long-range coupling constants, by a new scheme of coherence selection by gradients" *J. Magn. Reson.* **2001**, *148*, 209–213.

[7] A. Meissner, O. W. Sørensen, "Measurement of J(H,H) and long-range *J*(X,H) coupling constants in small molecules, broadband XLOC and *J*-HMBC" *Magn. Reson. Chem.* **2001**, *39*, 49–52.

[8] R. Wagner, S. Berger, "ACCORD-HMBC: A superior technique for structural elucidation" *Magn. Reson. Chem.* **1998**, *36*, S44–S46.

[9] R. Burger, C. Schorn, P. Bigler, "HMSC: Simultaneously detected heteronuclear shift correlation through multiple and single bonds" *J. Magn. Reson.* **2001**, *148*, 88–94.

[10] N. T. Nyberg, J. O. Duus, O. W. Soerensen, "Editing of H2BC NMR spectra" *Magn. Reson. Chem.* **2005**, *43*, 971–974.

[11] T. E. Burrow, P. G. Enriquez, W. F. Reynolds "The signal/noise of an HMBC spectrum can depend dramatically upon the choice of acquisition and processing parameters" *Magn. Reson. Chem.* **2009**, *47*, 1086–1094.

[12] W. Schoefberger, J. Schlagnitweit, N. Müller "Recent developments in heteronuclear multiple-bond correlation experiments" *Ann. Rep. NMR Spectrosc.* **2011**, *72*, 1−60.

8. Questions

A. Why is HMBC intrinsically less sensitive than HSQC?

B. What is the expected range of ^{1}J(C,H) in organic Chemistry?

C. Why does one observe ^{1}J breakthrough especially for C-4 and C-17?

D. Why has the processing of this spectrum to use the magnitude mode, although the phase-sensitive echo-antiecho recording technique is employed?

E. Explain in detail how the gradient supported dual-stage low-pass filter functions.

F. Calculate the gradient strength for g4 and g5 in the case of ^{1}H, ^{15}N HMBC.

G. Why is an adiabatic chirp pulse used for p6?

9. Own Observations

Chapter 2

Advanced Organic NMR Spectroscopy

In rare cases the six NMR spectral methods which are given in Chapter 1 are not sufficient to elucidate the structure of a given compound. Of course there are a lot more techniques which can be employed. The nine methods which we find most promising and helpful are given in this chapter:

2.1 2D *J*-Resolved ^{1}H NMR Spectroscopy 37
2.2 ROESY
[**R**otating Frame Nuclear **O**verhauser **E**ffect **S**pectroscop**Y**] 41
2.3 TOCSY
[**TO**tal **C**orrelation **S**pectroscop**Y**] 45
2.4 HSQC-TOCSY
[**H**eteronuclear **S**ingle **Q**uantum **C**oherence
TOtal **C**orrelation **S**pectroscop**Y**] 49
2.5 HOESY
[**H**eteronuclear **O**verhauser **E**ffect **S**pectroscop**Y**] 53
2.6 INADEQUATE
[**I**ncredible **N**atural **A**bundance **D**oubl**E** **QUA**ntum **T**ransfer **E**xperiment] 57
2.7 ADEQUATE
[**A**dequate **D**oubl**E** **QUA**ntum **T**ransfer **E**xperiment] 61
2.8 *J*-HMBC
[*J*-resolved **H**eteronuclear **M**ultiple **B**ond **C**orrelation] 65
2.9 Gated Decoupling 71

We describe therefore in this second chapter these nine methods in some details using appropriate molecules which demonstrate best the additional virtues of these techniques as an example. Each of the given methods may add some important knowledge about the structural features of the investigated compound.

EIDG. TECHNISCHE HOCHSCHULE
ZÜRICH
Laboratorium
für Physikalische Chemie
Prof. Dr. R. R. Ernst

CH-8006 Zürich, Universitätstrasse 22
Tel. (01) 32 62 11

18 October 1975

Prof. B. L. Shapiro
Department of Chemistry
Texas A+M University

2D RESOLVED ^{13}C - SPECTROSCOPY

Dear Barry,

More and more ^{13}C - fans try to utilize nowadays the additional information contained in undecoupled spectra, very often with bad success due to the numerous overlapping multiplets for medium size or larger molecules. Off-resonance decoupling is one way out but not without considerable loss of information.

We would like to present here an intriguing idea to resolve overlapping multiplets: Apply a 90° pulse to your carbons (Fig.1), wait a bit, turn on the decoupler and record at the same time the FID. Repeat this experiment several times but with different waiting times. Perform a 2D-Fourier transformation on the obtained data set and plot the 2D set of Fourier coefficients in a suitable manner. The result will look like Fig. 2 (if you have done it properly). The 2D spectrum displays all multiplets resolved in two dimensions and the interpretation of the undecoupled spectrum is a matter of seconds. One can see that the decoupled spectrum is just the projection of the 2D plot onto the ω_2-axis and the undecoupled spectrum is the projection onto the ω_1-axis. Resolution is in the moment limited by the available computer memory.

Numerous modifications of the basic experiment are possible, utilizing the Overhauser effect, selecting one specific carbon and mapping its multiplet structure and many more. The computer requirements are not trivial, but instrument manufacturers will be happy to supply you with more memory or with a disk. We are convinced that this technique will find its application in the routine NMR laboratory whenever there is a need for undecoupled ^{13}C spectra. The complete story will be published shortly.

Sincerely yours

Luciano Müller Anil Kumar Richard R. Ernst

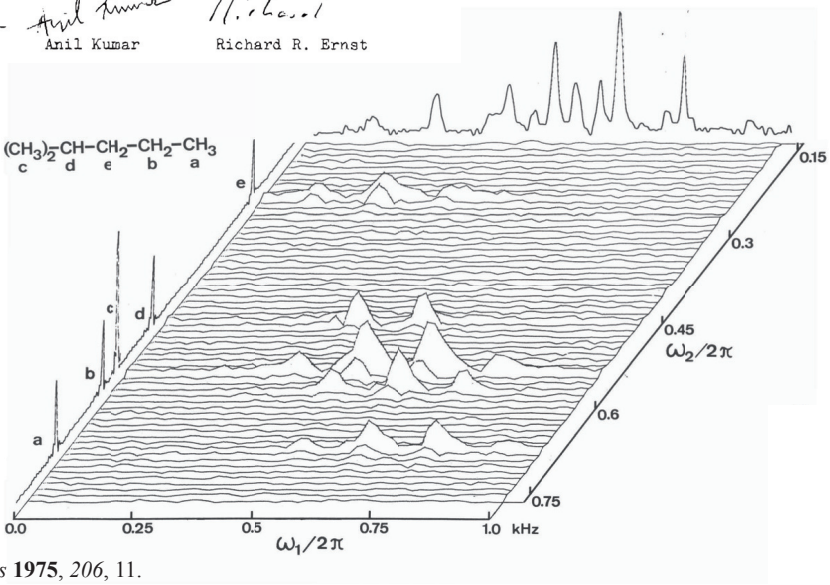

Taken from *TAMU NMR Letters* **1975**, *206*, 11.

Experiment 2.1

2D *J*-Resolved ^{1}H NMR Spectroscopy

1. Purpose

In a normal 1D ^{1}H NMR spectrum, chemical shift and spin–spin coupling information may be obscured by overlapping multiplets. In the 2D *J*-resolved experiment these two parameters are separated and displayed on different axes of the 2D spectrum. On the F_2-axis only chemical shift information is present, and on the F_1-axis only homonuclear spin–spin coupling information. The projection of the 2D spectrum onto the F_2-axis is effectively an "^{1}H broad-band decoupled" proton spectrum. However, in the case of very closely resonating spins and strong coupling the information given by this method will be limited. We demonstrate this technique here, because a very important advantage of the experiment is the separation of homonuclear spin couplings from hetero-nuclear spin couplings (such as couplings to ^{31}P or ^{19}F), since the latter are confined to the F_2-axis. Therefore the method can be employed to elucidate complicated spin patterns. The technique is very much favored in metabolomics research [11].

2. Variants

J-resolved spectroscopy belongs to the oldest 2D NMR methods [1]. One of the big drawbacks is that the 2D spectra are in principle not phase sensitive but have to be processed in the magnitude mode. There have been several trials to overcome this limitation [4, 9, 10]. Another line of development was to change the 2D method into a 1D selective sequence, which was dubbed SERF [5, 6] and applied to aligned samples. Further selective variants followed [7, 8]. A goal which is still not fully achieved is the generation of an artifact-free proton broadband decoupled proton NMR spectrum with correct intensities throughout[12].

3. Pulse Scheme and Phase Cycle

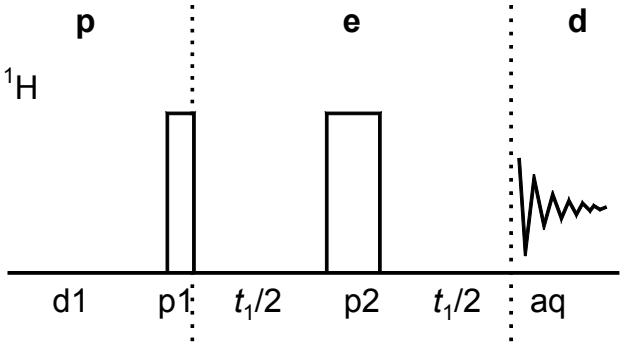

p1: $(x)_4$, $(y)_4$, $(-x)_4$, $(-y)_4$

p2: x, -x, y, -y, $(y, -y, -x, x)_2$, -x, x, -y, y

aq: $(x)_2$, $(-x)_2$, $(y)_2$, $(-y)_2$

Scheme 2.1-1:

At Shell Development Company in Emeryville, CA, the person making an offer said that if I accepted an assistant professor position at the newly created University of South Florida (USF) in Tampa, I would never be heard from again. At USF my attention related to the theory of nuclear spin-spin coupling. It appeared that the conformational dependence of long range H, H coupling constants could also be explained via valence bond (VB) methods. During this period there deve1oped a correspondence with Martin Karplus. which was to continue for several years and was concerned, in part, with the popular misconceptions of the factors affecting *J* couplings. The problems were especially apparent in the often and misunderstood terms 'through space' and 'through bond', which we defined in terms of a VB bond order formulation.

Michael Barfield, *1934 "Thirty-three Years of NMR Parameters" *Enyclopedia of NMR*, **1996**, *1*, 201–202.

Common Values:

p1: 90° ^{1}H transmitter pulse
p2: 180° ^{1}H transmitter pulse
d1: relaxation delay
t_1: evolution increment

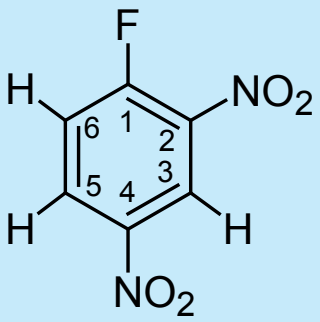

Scheme 2.1-2

4. Acquisition

Special values used for the spectrum shown:

Sample: 0.2 M 1-fluor-2,4-dinitrobenzene in $CDCl_3$.
Time requirement: 25 min
Spectrometer: Bruker DRX-400 with 5-mm TBI probe

td2:	5K data points in F_2
td1:	64 data points in F_1
sw2:	3 ppm
sw1:	20 Hz
aq2:	2 s
aq1:	1.6 s
o1:	middle of ^{1}H NMR spectrum
p1:	9.15 µs, 0 dB
p2:	18.3 µs, 0 dB
d1:	2.5 s

5. Processing

Apply zero-filling in F_2 to 8K and in F_1 to 256 real data points. Use unshifted sinusoidal windows in both dimensions. Apply complex Fourier transformation corresponding to the N-type signal selection using the quadrature-off mode in F_1. Phase correction is not necessary, since the data are processed in magnitude mode. After the Fourier transformation the 2D spectrum is tilted, since the signals are also modulated by J in F_2. This tilt can be eliminated by a software command. Finally the data may be symmetrized with respect to the horizontal through the center of F_1.

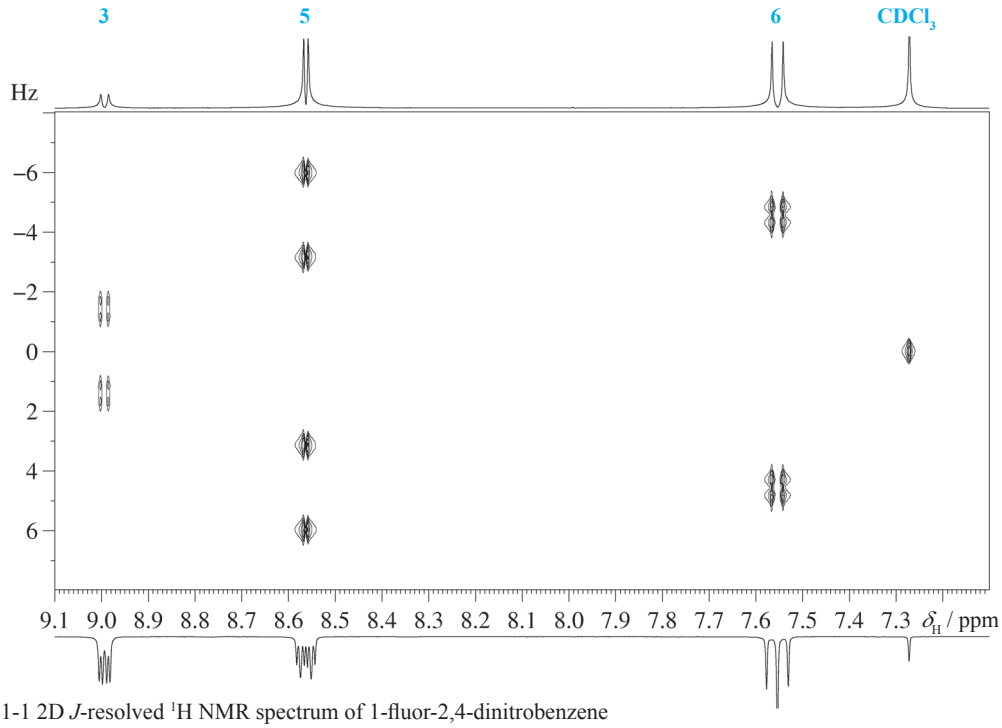

Fig. 2.1-1 2D *J*-resolved ^{1}H NMR spectrum of 1-fluor-2,4-dinitrobenzene
above: 2D projection in F2; below: 1D spectrum for comparison

6. Result

The figure shows the 2D spectrum obtained on a DRX-400 spectrometer after the tilt and symmetrization operations. The high-resolution ^{1}H NMR spectrum is shown below the F_2 axis; the internal projection shown above the 2D spectrum reveals the proton fluorine spin couplings. In F_1 the individual proton multiplets are observed. From these the individual assignment can be obtained. The signal of H-3 at 9 ppm forms on close inspection a doublet of doublet pattern (dd) with 2.8 and 0.5 Hz, the signal of H-5 at 8.56 ppm forms also a "dd" pattern with 9.1 and 2.8 Hz, and the signal of H-6 at 7.55 ppm again displays a doublet of doublets with 9.1 and 0.5 Hz.

All three signals display in the F_2 direction a fluorine spin coupling with 6.6 Hz for H-3, 3.8 Hz for H-5 and 9.6 Hz for H-6. Thus we have an ABCX spin system with the spin couplings and chemical shifts given in the following table:

	F-1	H-3	H-5	H-6
F-1		6.6 Hz	3.8 Hz	9.6 Hz
H-3	6.6 Hz	9.0 ppm	2.8 Hz	0.5 Hz
H-5	3.8 Hz	2.8 Hz	8.56 ppm	9.1 Hz
H-6	9.6 Hz	0.5 Hz	9.1 Hz	7.55 ppm

Table 2.1-1 Chemical shifts and spin coupling constants of 1-fluor-2,4-dinitrobenzene

7. Comments

The pulse sequence is, in principle, identical to the spin–echo technique described in Chapter 5.2, but differs in that the spin–echo delay is now incremented, with $\tau = t_1$, thus creating the second dimension. In the preparation period **p** the spin system relaxes and is excited by the pulse p1. During the evolution period **e** chemical shifts and spin–spin couplings evolve. At the end of t_1 the chemical shift information is refocused. However, the echo is modulated by the homonuclear spin–spin coupling that evolved during t_1, and thus a 2D Fourier transformation will separate these two signal components after the tilt operation. There is no distinct mixing period in this sequence. Well-resolved multiplets are obtained in F_1, because line broadening due to field inhomogeneity is refocused. Artifacts due to higher-order spin systems may occur [4]. The 2D spectrum cannot be recorded in the phase-sensitive mode [5]. For a high spectral resolution in F_1 it would be desireable to have a high number of increments. But then, because of the large time increment (in order of some ten milliseconds due to small spectral width), the maximal t_1 time may extend to the order of seconds. This leads to relaxation losses. Nevertheless, for sampling reasons the condition $t_{1max} > 1/J$ should be kept.

In this experiment phase cycling is not necessary for frequency detection in F_1. For the sample used here, one scan would in principle be sufficient.

E. J. Corey, who was at that time an assistant professor at Illinois and later became a colleague at Harvard, was one of the people with whom I had dinner on a fairly regular basis at the Tea Garden, a passable restaurant in Champaign-Urbana. We often discussed recent work that we thought might be of mutual interest and one day I described the studies that I had made of vicinal coupling constants. Corey immediately recognized the possibility of using the results for structure determination and shortly published what is probably the first application in organic chemistry. Shortly after, the theory appeared in a comprehensive review of the use of nuclear magnetic resonance in organic structure determination. Someone introduced the name 'Karplus equation' for the relationship I had developed – a mixed blessing which was to haunt me for many years. Many people attempted to apply the equation to determine dihedral angles in organic structures and, of course, since it was a qualitative relationship, found deviations of the measured coupling from the predicted dihedral angle dependence for known structures.

Martin Karplus, *1930 "Theory of Vicinal Coupling Constants" *Encyclopedia of NMR*, **1996**, *1*, 420–422.

[1] W. P. Aue, J. Karhan, R. R. Ernst, "Homonuclear broad band decoupling and two-dimensional J-resolved NMR spectroscopy" *J. Chem. Phys*. **1976**, *64*, 4226–4227.

[2] T. D. W. Claridge, "High-resolution NMR techniques in organic chemistry", Pergamon, Oxford, **1999**, 267–273.

[3] D. D. Traficante, M. D. Meadows, "Strong coupling effects in 2D J spectra: An application for the determination of the conformational isomers of some 1,4 disubstituted dioxanes" *Concepts Magn. Reson*. **1997**, *9*, 359–384.

[4] P. Mutzenhardt, F. Guenneau, D. Canet, "A Procedure for Obtaining Pure Absorption 2D *J*-spectra: Application to quantitative fully *J*-decoupled homonuclear NMR spectra" *J. Magn. Reson*. **1999**, *141*, 312–321.

[5] T. Fäcke, S. Berger, "SERF, A new method to measure H,H spin coupling constants in organic chemistry" *J. Magn. Reson*. Ser. A **1995**, *113*, 114–116.

[6] J. Farjon, D. Merlet, P. Lesot, J. Courtieu, "Enantiomeric excess measurements in weakly oriented chiral liquid crystal solvents through 2D ^{1}H selective refocusing experiments" *J. Magn. Reson*. **2002**, *158*, 169–172.

[7] M. Findeisen, S. Berger, "A selective pulse sequence for determination of long-range C,H spin coupling constants", *Magn.Reson.Chem*. **2003**, *41*, 431–434.

[8] F. Rastrelli, A. Bagno "Selective J-resolved spectra: A double pulsed field gradient spin-echo approach" *J. Magn. Reson*. **2006**, *182*, 29–37.

[9] A. J. Pell, J. Keeler, "Two-dimensional J-spectra with absorption mode lineshapes", *J. Magn. Reson*. **2007**, *189*, 293–299

[10] B. Luy, "Adiabatic z-filtered J-spectroscopy for absorptive homonuclear decoupled spectra", *J. Magn. Reson*. **2009**, *201*, 18–24.

[11] C. Ludwig, M. R. Viant, "Two-dimensional J-resolved NMR spectroscopy: Review of a key methodology in the metabolomics toolbox", *Phytochemical Analysis*, **2010**, *1*, 22–32.

[12] K. Zangger, H. Sterk, "Homonuclear broadband-decoupled NMR spectra", *J. Magn. Reson*. **1997**, *124*, 486–489.

[13] A. Martinez, F. Bourdreux, E. Rigueta, J.-M. Nuzillard "High-resolution and high-sensitivity 2D homonuclear *J*-resolved NMR spectroscopy" *Magn. Reson. Chem*. **2012**, *50*, 28–32.

8. Questions

A. The residual proton in DMSO-d_6 shows a distinct multiplet pattern in the ^{1}H NMR spectrum. Construct this pattern and calculate the relative intensities. How would this look in a 2D *J*-resolved spectrum?

B. Can you explain why the pulse sequence shown must be processed in magnitude mode?

C. What is the reason for the phase cycle used?

D. The resolution of the multiplets obtained in the F_1 direction is usually much better than those of the corresponding multiplets in F_2. Why?

9. Own Observations

Experiment 2.2

ROESY

1. Purpose

The NOESY technique (see Exp. 1.4) has the disadvantage that for molecules with a molar mass in the order of 1000 to 3000 the cross-signals may disappear, since the NOE effect changes its sign depending on the molecular correlation time. However, the nuclear Overhauser effect in the rotating frame under spin-lock conditions is always positive [1,2]. One disadvantage of the ROESY (**R**otating frame **O**verhauser **E**nhancement **S**pectroscop**Y**) experiment is that TOCSY correlations may also break through. This problem has been greatly diminished with a special spin lock [3–5] which is used here. The experiment described gives results similar to those with the NOESY technique, but in a shorter time, due to the shorter mixing period during which the spin lock is used. Because the relaxation of spin-locked transverse magnetization in the rotation frame is observed here, the relaxation times and intensitities of the cross peaks differ from that of the NOE, where the relaxation of inverted z-magnetization is recorded.

2. Variants

Several types of spin locks have been proposed and demonstrated. Despite the earlier use of a continuous-wave spin lock now the scheme of alternating 180° pulses with opposite phases seems to be established. In one recent paper, for 1D application of natural products, an additional weak field gradient during the spin lock is applied [7].

3. Pulse Scheme and Phase Cycle

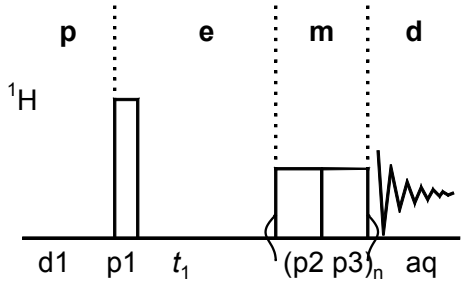

p1: x, $(-x)_2$, x, y, $(-y)_2$, y p2: $(x, -x)_2$, $(y, -y)_2$

p3: $(-x, x)_2$, $(-y, y)_2$ aq: x, $(-x)_2$, x, y, $(-y)_2$, y

phase cycle for p1 incremented according to TPPI

Scheme 2.2-1

4. Acquisition

Special values used for the spectrum shown:

Sample: 3% strychnine in $CDCl_3$.
Time requirement: 5 h
Spectrometer: Bruker DRX-600 with 5-mm-TBI-probe

As spectrometer frequencies have risen and as more attention has centered on larger and more complex molecules, the situation has arisen more frequently where $\omega_0\tau_c$, the product of spectrometer angular frequency and molecular rotational correlation time, is equal to or exceeds unity. When $\omega_0\tau_c \approx 1$, no NOE occurs; when it greatly exceeds 1, as in the case of macromolecules, the NOE approaches –1 and specificity is lost due to spin diffusion. Observation of the NOE at short times, or of transient NOES, overcomes this difficulty in part, but at the price of observing very small effects. We have found that the observation of transient NOES in the rotating frame overcomes these difficulties. (….)
We think a suitable acronym for this type of experiment is CAMELSPIN (cross-relaxation appropriate for minimolecules emulated by locked spins). Ice-skating enthusiasts will have no difficulty with the origin of the term.

Aksel A. Bothner-By, *1921, *J. Am. Chem. Soc*. **1984**, *106*, 811–813.

Common values:

p1: 90° ^{1}H transmitter pulse
p2,p3: 180° ^{1}H transmitter pulse at spin lock power
n: integer loop counter determines the spin lock length
n = length / (p2+p3)
d1: relaxation delay
t_1: evolution increment

Fig. 2.2-1: A. A. Bothner-By interpreting the original name of the sequence CAMELSPIN

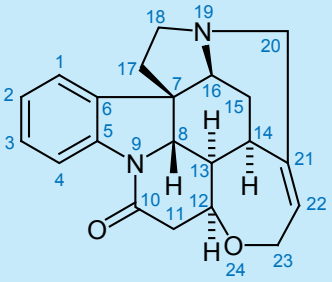

Scheme 2.2-2

td2:	2K data points in F_2
td1:	256 data points in F_1
sw2:	9 ppm
sw1:	9 ppm
aq2:	0.19 s
aq1:	0.023 s
o1:	middle of ^{1}H NMR spectrum
d1:	2 s
p1:	9.5 µs, 5 dB
p2, p3:	180 µs, 24.5 dB
ds:	8
n:	832 (corresponds to spin lock of 300 ms)
ns:	16

5. Processing

Apply zero-filling in F_1 to 1K real data points to obtain a symmetrical matrix of 1K × 1K real data points. Use an exponential window in F_2 and a squared π/2-shifted sinusoidal window in F_1. Apply Fourier transformation corresponding to the TPPI mode of data acquisition in F_1. Phase correction in both dimensions is necessary. Adjust the phase of the diagonal signals negative so that the ROESY correlation signals are positive. TOCSY breakthrough signals would have the same phase as the diagonal peaks.

6. Result

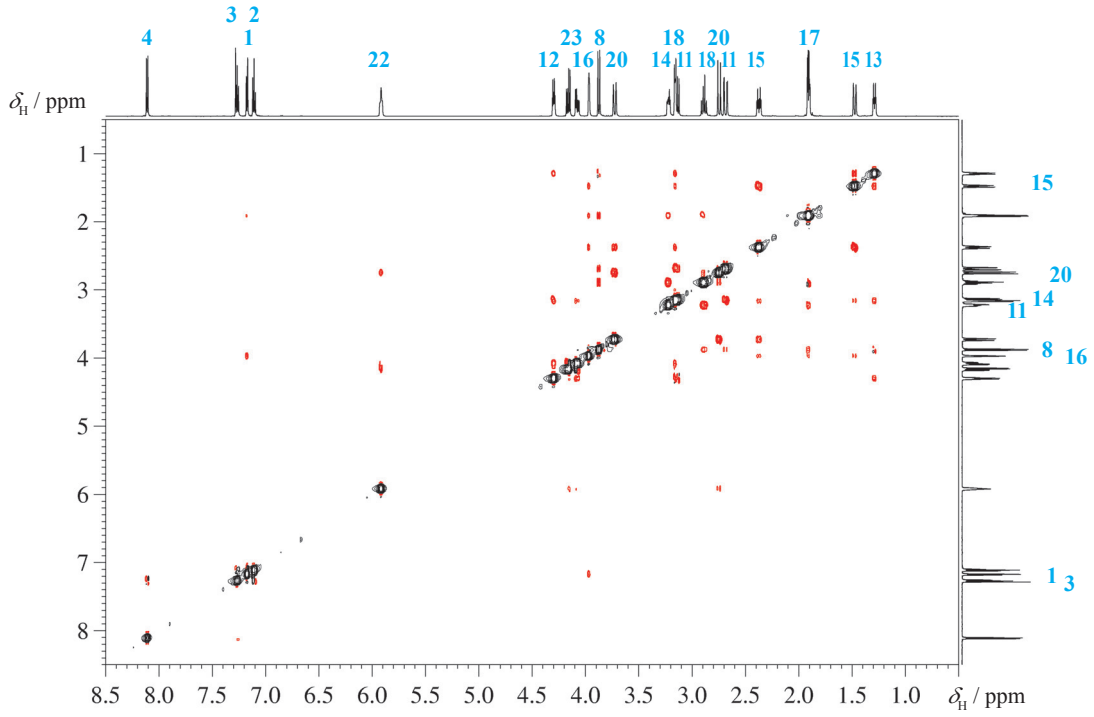

Fig. 2.2-2 ROESY spectrum of strychnine

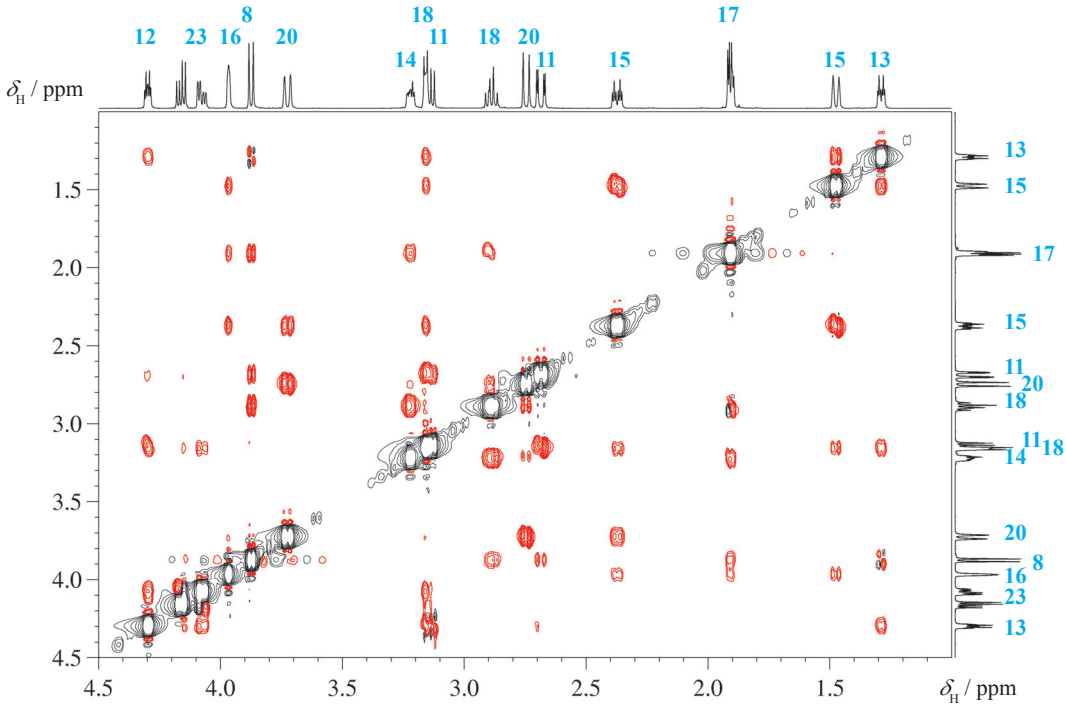

Fig. 2.2-3 Expansion of the ROESY spectrum of strychnine in the aliphatic region

The figures show the result obtained on a DRX-600 spectrometer. Note that the diagonal signals have a negative phase (black contours). Some TOCSY breakthrough signals are observed, e.g., the crosspeak between H-4 and H-3 and the cross peak between H-8 and H-13 where apparently the strong coupling results in a TOCSY pattern. There is a wealth of information to be taken from the spectrum, which can best be studied with a molecular model. Note, for instance, that only one of the H-20 protons is connected with one of the H-15 protons, from which a relative assignment of the diastereotopic protons in these methylene groups can be derived.

7. Comments

The ROESY sequence is, in principle, identical to the TOCSY sequence as described in Experiment 2.3. The preparation period **p** ends with the first pulse p1. After this chemical shifts and spin couplings evolve in the evolution period **e** during t_1. In the mixing period **m** the spins are locked by the spin lock field B_1, which is considerably weaker in ROESY than in TOCSY. The explanation of the suppression of TOCSY correlations due to the special spin lock sequence used here is given in the literature [3,4]. In spectra with sharp signals near the offset (e.g., methoxy groups) artifacts have been observed. The detection period **d** starts directly after the mixing.

[1] A. A. Bothner-By, R. L. Stephens, J.-M. Lee, C. D. Warren, R. W. Jeanloz, "Structure determination of a tetrasaccharide: transient nuclear Overhauser effects in the rotating frame" *J. Am. Chem. Soc.* **1984**, *106*, 811–813.

[2] A. Bax, D. G. Davis, "Practical aspects of two-dimensional transverse NOE spectroscopy" *J. Magn. Reson.* **1985**, *63*, 207–213.

[3] T. L. Hwang, A. J. Shaka, "Cross relaxation without TOCSY: Transverse rotating-frame Overhauser effect spectroscopy" *J. Am. Chem. Soc.* **1992**, *114*, 3157–3159.

[4] T. L. Hwang, M. Kadkhodaei, A. Mohebbi, A. J. Shaka, "Coherent and incoherent magnetization transfer in the rotating frame" *Magn. Reson. Chem.* **1992**, *30*, S24–S34.

[5] T. L. Hwang, A. J. Shaka, "Multiple-pulse mixing sequences that selectively enhance chemical exchange or cross-relaxation peaks in high-resolution NMR spectra" *J. Magn. Reson*. **1998**, *135*, 280–287.

[6] D. Neuhaus, M.P. Williamson, The nuclear Overhauser effect in structural and conformational analysis, 2nd Ed., Wiley-VCH, Weinheim, **2000**.

[7] J. Furrer "One-dimensional ROESY experiments with full sensitivity and reliable cross-peak integration when applied to natural products" *J. Nat. Prod*. **2009**, *72*, 1437–1441.

8. Questions

A. Find a "handwaving" argument for the explanation of the spin lock used.
B. Why should the power of the spin lock pulses be lower than they are in TOCSY?
C. Explain the TOCSY breakthrough for the pair H-8, H-13.
D. People often wonder about the relative assignment of H-1 and H-4. Discuss how the two ROESY crosspeaks of H-1 solve the problem.

9. Own Observations

Experiment 2.3

TOCSY

1. Purpose

The TOCSY (**TO**tal **C**orrelation **S**pectroscop**Y**) method [1,2] can in principle give a total correlation of all protons of a chain with each other. Whereas this would not make sense for a molecule with a single chain of resonances, it is of great value for molecules which have several repeating units, such as peptides or carbohydrates. The technique serves in these cases for the identification of single residues of such molecules. The gradient-selected method shown below requires in principle only one transient and produces a spectrum that is formally phase-sensitive. Since the TOCSY experiment leads to mixed-phase cross-signals, the magnitude spectrum shown here is usually sufficient to quickly provide connectivity information.

2. Variants

Especially in the carbohydrate field the selective TOCSY (see chapter 3.5) has become very popular. Due to the signal separation of the anomeric protons it is possible to excite one anomeric proton signal individually and test in a 1D manner the connectivity within one carbohydrate residue. Some pulse sequences address the phase problem during the TOCSY transfer. There are several combinations known with HSQC, DOSY, or STD sequences, as well as heteronuclear edited versions with and without additional water suppression.

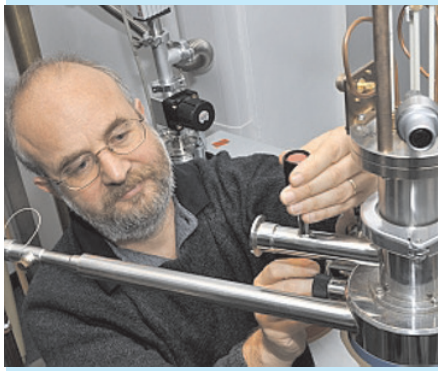

Fig. 2.3-1 Malcom H. Levitt *1957

3. Pulse Scheme and Phase Cycle

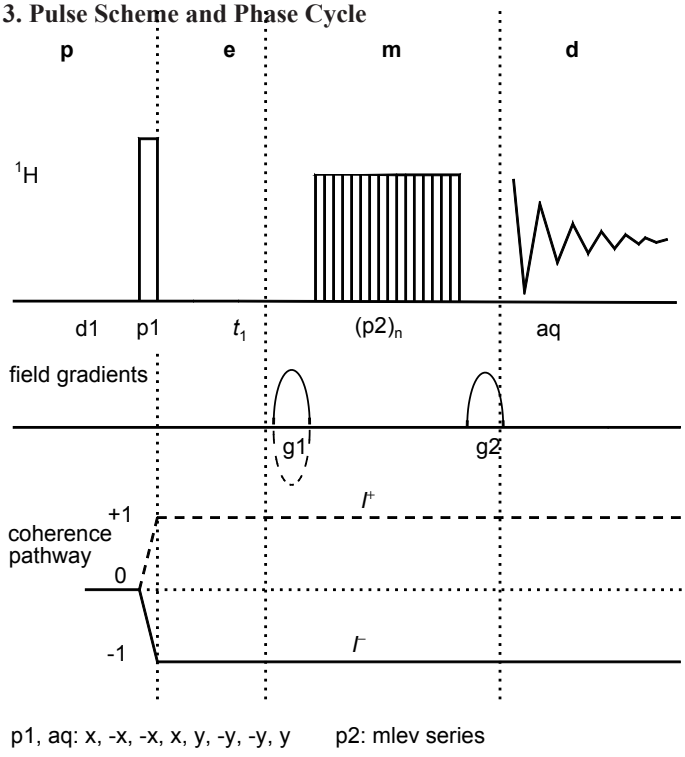

Scheme 2.3-1

Common values:

p1: 90° ^{1}H transmitter pulse
p2: series of pulses at spin lock power following a certain phase cycle
n: integer loop counter, determines the spin lock length
d1: relaxation delay
t_1: evolution increment

4. Acquisition

Special values used for the spectrum shown:

Sample: 3 % sucrose in D_2O
Time requirement: 1.7 h
Spectrometer: Bruker DRX-600 with 5-mm TBI probe

The 90° pulse width and attenuation of the spin lock pulses must be calibrated prior to the experiment. Important is the spectral width covered by the spin lock sequence. Special care has to be taken not to use too much r.f. power on the ^1H transmitter coil of the probe.

td2:	1K data points in F_2
td1:	256 data points in F_1
sw2:	3 ppm
sw1:	3 ppm
aq2:	0.57 s
aq1:	0.07 s
o1:	middle of ^1H NMR spectrum
p1:	9.4 µs, 5 dB
p2:	MLEV series of composite 180° pulses (90°, 180°, 90°) at transmitter attenuation of spin lock; 90° pulse width and transmitter attenuation typically in the order of 40 µs and 16 dB, corresponding to an effective spin lock field of ca. 7000 Hz (magnetic field dependent). Duration of spin lock set to 200 ms by loop parameter of spin lock sequence. The loop parameter must be an even number.
d1:	2 s
g1, g2:	sinusoidal-shaped field gradients, 1 ms duration and 30 % (100 % ≈ 0.56 T/m)
ds:	4
ns:	8

5. Processing

Apply zero-filling in F_1 to 1K real data points to obtain a symmetrical matrix of 1K × 1K real data points. Use unshifted sinusoidal windows in both dimensions. Apply complex Fourier transformation. Since magnitude data are calculated, no phase correction is necessary.

6. Result

The figure shows the result for sucrose as obtained on a DRX-600 spectrometer using a multinuclear *z*-gradient probe. A spin lock of 200 ms was applied. Grossly speaking, there are two separate "carpet patterns" to be seen, one from the glucose part of the molecule and one of the fructose part. The glucose part starts with the anomeric proton H-1' at δ = 5.44 ppm and connects the remaining 5 protons between 3.95 and 3.65 ppm with each other. To follow the fructose resonances one starts best with the proton H-3 at 4.24 ppm. Note that the methylene group of C-1 forms a singlet and therefore has no TOCSY connectivities. By recording the TOCSY spectra with increasing lengths of the spin lock one can easily confirm the individual assignments.

Much of NMR can be interpreted in terms of rotations, so I had hit upon an idea with a bright future. For a long time I was to teach myself chunks of NMR purely by pushing composite pulses into some area. Ray Freeman stressed one particular line. He was intuitively convinced that the unsolved problem of broadband heteronuclear decoupling should eventually yield to the composite pulse, and never ceased pressing me to look into it. The breakthrough was Aue and Ernst's paper on J scaling.: This put the missing theoretical tools into my hands, and with some head scratching the first composite pulse broadband decoupling sequence was a reality. Demonstrating it, however, still required realms of octal machine code.
I could not count beyond seven for weeks. The next step was to generalize the construction principles. I came up with a scheme based on phase shifts and cyclic permutations. This was suggested by my experience as an electric guitarist in a jazz-fusion band, where we were using permutations to generate unusual musical effects.

Malcolm H. Levitt, *1957 "A Cyclic Evolution in Spin State"
Enyclopedia of NMR, **1996**, *1*, 453–454.

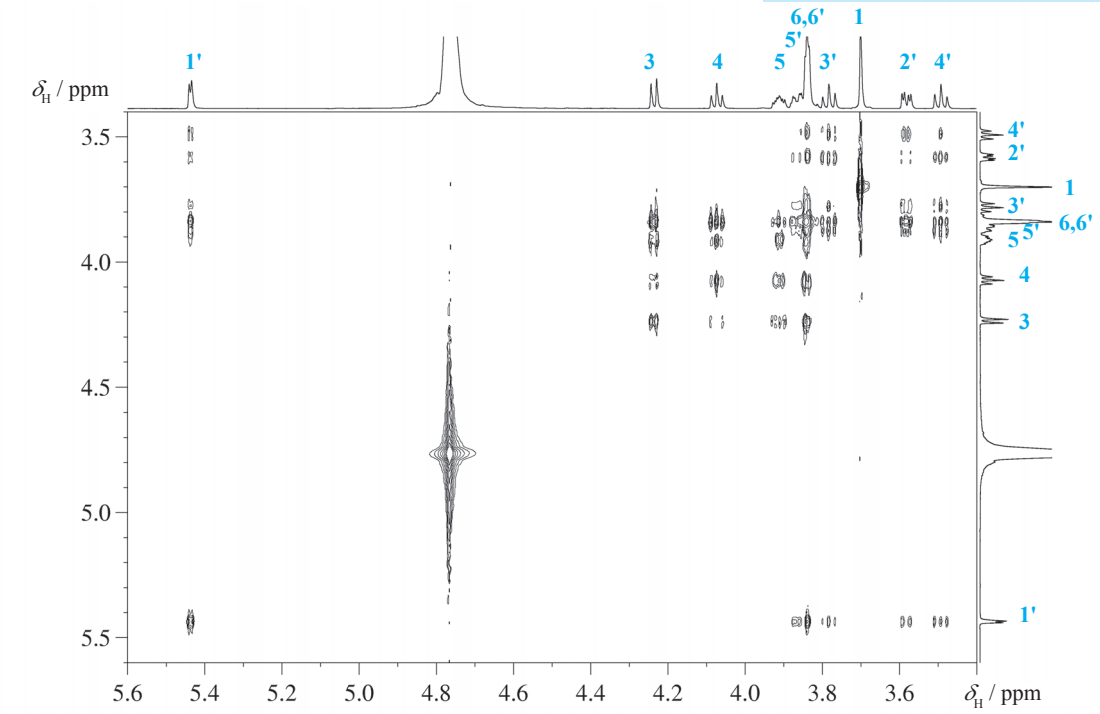

Fig. 2.3-2 TOCSY spectrum of sucrose

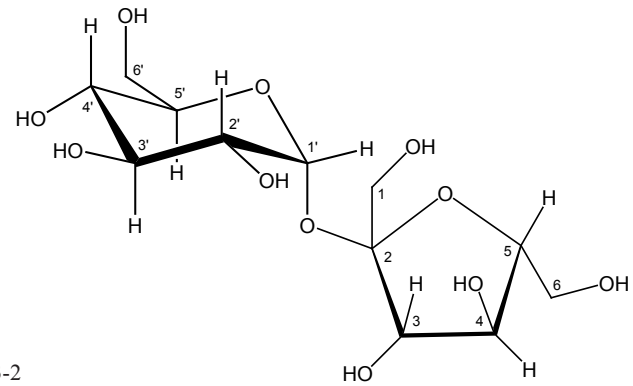

Scheme 2.3-2

7. Comments

During the spin-lock time the spins are affected only by B_1 as the effective field. Therefore their chemical shift differences become negligible and the spin systems are all of higher order, leading to cross signals of all protons with each other along a chain of connected XH_n groups. It is possible to adjust the length of the spin lock for different results. Thus, a rather short spin-lock duration (30 ms) gives roughly the equivalent of a COSY spectrum, intermediate spin-lock times may display results similar to a relayed COSY, and, finally, long spin-lock times result in the desired total correlation. Another adjustable parameter is the individual 90° pulse within the spin lock defined by the transmitter attenuation, which determines the spectral width covered by the spin lock.

The design of spin lock sequences is an active field of research and is well described in Ref. [4].

[1] L. Braunschweiler, R. R. Ernst, "Coherence transfer by isotropic mixing: Application to proton correlation spectroscopy" *J. Magn. Reson.* **1983**, *53*, 521–528.

[2] A. Bax, D. G. Davis, "MLEV-17-based two-dimensional homonuclear magnetization transfer spectroscopy" *J. Magn. Reson.* **1985**, *65*, 355–360.

[3] G. E. Martin, A. S. Zektzer, Two-dimensional NMR methods for establishing molecular connectivity, VCH, Weinheim, **1988**, 303–316.

[4] S. J. Glaser, J. J. Quant, "Homonuclear and heteronuclear Hartmann-Hahn transfer in isotropic liquids" *Adv. Magn. Opt. Reson.* **1996**, *19*, 59–252.

[5] R. E. Hurd, "Gradient-enhanced spectroscopy" *J. Magn. Reson.* **1990**, *87*, 422–428.

[6] K. E. Kövér, D. Uhrín, V. J. Hruby, "Gradient- and sensitivity-enhanced TOCSY experiments" *J. Magn. Reson.* **1998**, *130*, 162–168.

[7] E. Kupce, W. Hiller, "Clean adiabatic TOCSYs" *Magn. Reson. Chem*. **2001**, *39*, 231–235.

[8] A. Kirschstein, C. Herbst, K. Riedel, M. Carella, J. Leppert, O. Ohlenschläge, M. Görlach, R. Ramachandran "Broadband homonuclear TOCSY with amplitude and phase-modulated RF mixing schemes" *J. Biomol. NMR*, **2008**, *40*, 227–237.

8. Questions

A. Calculate the energy in Ws dissipated in the probe head coil for a spin lock lasting 300 ms and an individual 90° pulse of 40 µs at 12 dB using a 100 Watt ^{1}H amplifier. Compare this energy with a 10 µs hard pulse at – 6 dB which corresponds to maximal power.

B. Why is the spectrum shown recorded in a phase-sensitive mode, however processed with magnitude calculation?

C. How is the relationship between the individual 90° pulse length of the spin lock pulses and the spectral width covered of the spin lock?

D. Give the name of some popular spin lock sequences.

9. Own Observations

Experiment 2.4

HSQC-TOCSY

1. Purpose

The combination of the HSQC method with the TOCSY sequence leads, in principle, to a 3D technique. However, if the evolution period of the TOCSY part is omitted, one obtains a 2D sequence which provides a ^{13}C-edited TOCSY spectrum. Starting from each HSQC cross-signal one finds additional signals in the same row of the F_1 carbon frequency which are caused by a TOCSY transfer. This is very helpful for structural elucidation, since normal TOCSY spectra may often be rather crowded. Compared with true 3D sequences, the digital resolution is far better using significantly less recording time. There are many variants; here we show an echo-antiecho gradient selected method.

2. Variants

Originally, this method started as HMQC-TOCSY and rapidly gained interest especially in the field of natural products. Up to now, the most applications can be read in "*Carbohydrate Research*" or in the "*Journal of Natural Products*". Due to the sharpening of the signals in the F_1 dimension, the HMQC part was replaced by HSQC. Combinations with DOSY are also known which separate the signals of mixtures.

3. Pulse Scheme and Phase Cycle

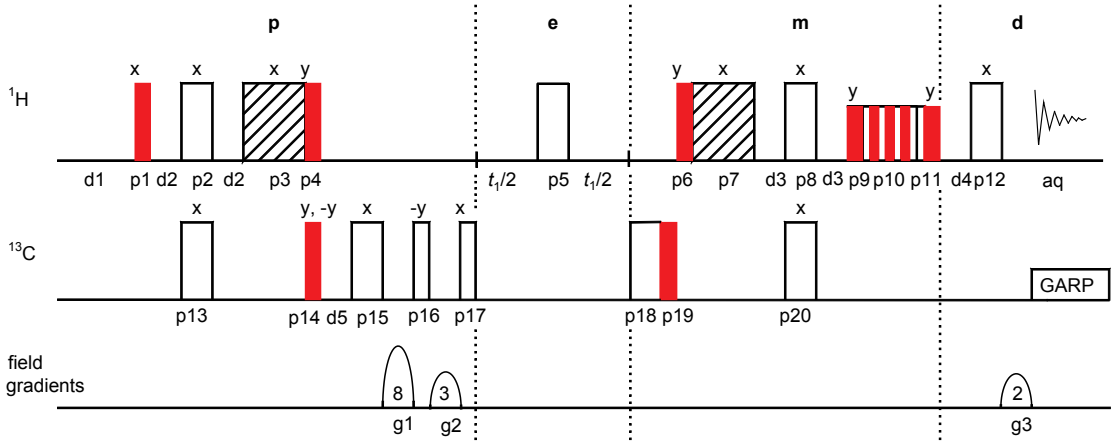

p5: x, x, -x, -x p10: mlev sequence p18, p19: x_4, $-x_4$ aq: $(x, -x)_2$, $(-x, x)_2$

Scheme 2.4-1

4. Acquisition

Special values used for the spectrum shown:

Sample: 3 % sucrose in D_2O
Time requirement: 1.7 h
Spectrometer: Bruker DRX-600 with 5-mm TBI probe

Common values:

p1, p4, p6: 90° ^{1}H transmitter pulse
p2, p5, p8, p12: 180° ^{1}H transmitter pulse
p14, p16, p17, p19: 90° ^{13}C transmitter pulse
p13, p15, p18, p20: 180° ^{13}C transmitter pulse
p3, p7: trim pulse at high power
p9, p11: trim pulse at low power
p10: 90° and 180° pulses according MLEV-17 sequence at low power
d1: relaxation delay
t_1: evolution increment
d1, d2: 1/[2J(C,H)]

Of the possible hybrid 2D sequences, we believe that HMQC-TOCSY and HSQC-TOCSY are the most generally useful. This is particularly true for crowded ^{1}H spectra, where the superior ^{13}C resolution helps in interpreting the TOCSY data. Because of the superior ^{13}C resolution of HSQC over HMQC, we prefer HSQC-TOCSY.

Taken from W. F. Reynolds, R. G. Enríquez "Choosing the Best Pulse Sequences, Acquisition Parameters, Postacquisition Processing Strategies, and Probes for Natural Product Structure Elucidation by NMR Spectroscopy" *J. Nat. Prod.* **2002**, *65*, 221−244.

Fig. 2.4-1 Sugar Beet (*Beta vulgaris*)

Fig. 2.4-2 Sugar Cane (*Saccarum*)

The 90° pulse width and attenuation of the spin-lock pulses must be calibrated prior to the experiment. Important is the spectral width covered by the spin-lock sequence. Special care has to be taken not to use too much r.f. power on the ^{1}H transmitter coil during long mixing times.

td2: 2K data points in F_2
td1: 256 data points in F_1
sw2: 3 ppm
sw1: 60 ppm
aq2: 0.28 s
aq1: 0.014 s
p3, p7: ^{1}H trim pulses, 1 ms
p9,p11: ^{1}H trim pulses at spin lock power, 2.5 ms
p10: MLEV series of composite 180° pulses (90°, 180°, 90°) at transmitter attenuation of spin lock; 90° pulse width and transmitter attenuation typically in the order of 40 µs and 16 dB, corresponding to an effective spin lock field of ca. 7000 Hz (magnetic field dependent).
Duration of spin lock set to 150 ms by loop parameter *n* of the spin lock sequence. The loop parameter *n* must be an even number.
d1: 2 s
d2: $1/[2J(C,H)] = 3.45$ ms, calculated from $^{1}J(C,H) \approx 145$ Hz
d3: $1/[2J(C,H)] = 3.45$ ms, calculated from $^{1}J(C,H) \approx 145$ Hz
d4, d5: effective duration of gradient pulse, 1.05 ms
^{13}C decoupler attenuation and 90° pulse for GARP (19 dB, 70 µs)
g1, g2, g3: sinusoidal-shaped field gradients, 1 ms duration and 80 %, 30 %, 20.1 % strength (100% ≈ 0.56 T/m)
ds: 4
ns: 8

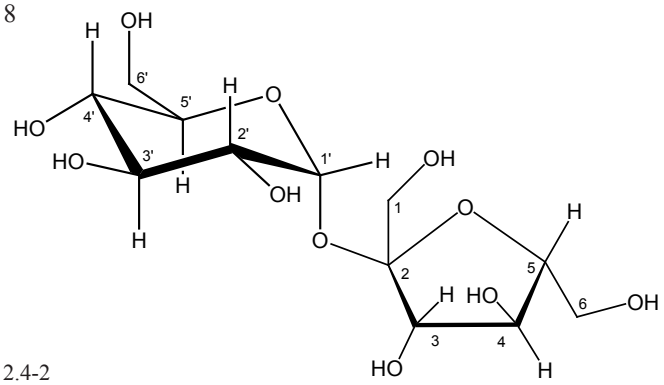

Scheme 2.4-2

5. Processing

Apply zero-filling in F_1 to 1K words in order to have a matrix of 1K × 1K real data points. Before Fourier transformation use π/2 shifted sinusoidal windows in both F_2 and F_1. Phase correction is applied in both dimensions.

6. Result

The figure shows an expansion of the HSQC-TOCSY spectrum obtained on an DRX-600 spectrometer equipped with a TBI *z*-gradient

probe head. The spectrum is very intriguing since we see six times a completely separated TOCSY spectrum of the glucose moiety of sucrose, edited by each carbon atom of this subunit. The lowest trace of these six rows at δ_C = 94.9 ppm contains the diagonal signal of C-1'. Similarily we observe four times a ^{13}C-edited TOCSY spectrum of the fructose subunit. The signal of H-1 stays as a singlet, because it has no vicinal proton partner and the signal of C-2 does not appear, because it bears no proton. By adjustment of the spin lock duration further assignments can be proven.

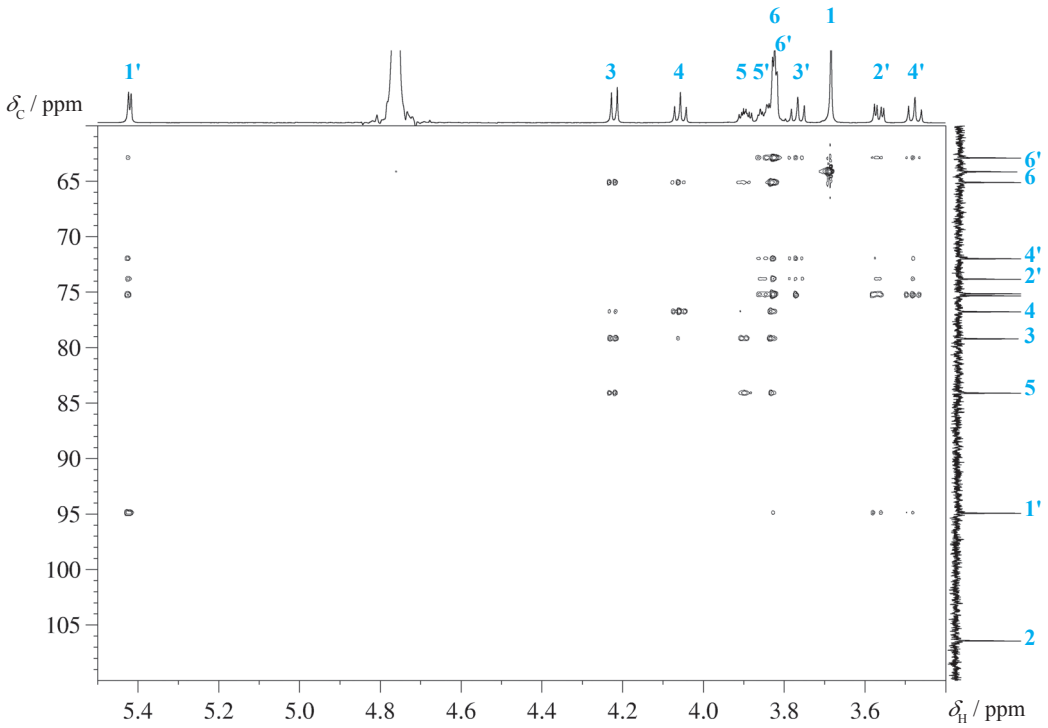

Fig. 2.4-3 HSQC-TOCY spectrum of sucrose

7. Comments

The HSQC and TOCSY parts of the sequence have already been described in Experiments 1.5 and 2.3. After completion of the INEPT transfer during the preparation period **p** we see a [d5, p15, g1] sandwich which encodes the magnetization of the protons bound to ^{13}C to prepare the coherence transfer. The following sandwich [p16, g2, p17] returns the magnetization into the *z*-direction where the gradient g2 destroys all leftover transverse magnetization and the pulse p17 reestablishes the tranverse situation.

After the evolution period **e** the pulse p18 corrects for the initial delay during this time and the finite pulse length of p5, whereas the pulses p19 and p6 establish a back INEPT transfer to protons.

After another trim pulse p7 the sandwich [d3, p8 and p20, d3] transfers the antiphase proton magnetization $2I_{Hx}I_{Cz}$ into in phase magnetization I_{Hy}, ready for the spin lock at the *y* axis in the mixing period **m**. As a

[1] L. Lerner, A. Bax, "Sensitivity-enhanced two-dimensional heteronuclear relayed coherence transfer NMR spectroscopy" *J. Magn. Reson.* **1986**, *69*, 375–380.

[2] T. Domke, "A new method to distinguish between direct and remote signals in proton-relayed X,H correlations" *J. Magn. Reson*. **1991**, *95*, 174–177.

[3] G. E. Martin, T. D. Spitzer, R. C. Crouch, J.-K. Luo, R. N. Castle, "Inverted and suppressed direct response HMQC-TOCSY spectra − a convenient method of spectral editing" *J. Heterocyclic Chem*. **1992**, *29*, 577–582.

[4] B. K. John, D. Plant, S. L. Heald, R. E. Hurd, "Efficient detection of $C_\alpha H$-HN correlations in proteins using gradient-enhanced ^{15}N HMQC-TOCSY" *J. Magn. Reson*. **1991**, *94*, 664–669.

[5] W. Willker, D. Leibfritz, R. Kerssebaum, W. Bermel, "Gradient selection in inverse heteronuclear correlation spectroscopy" *Magn. Reson. Chem.* **1993**, *31*, 287–292.

[6] R. T. Williamson, B. L. Márquez, W. H. Gerwick, "Use of ^{1}H-^{15}N PEP-HSQC-TOCSY at natural abundance to facilitate the structure elucidation of naturally occurring peptides" *Tetrahedron*, **1999**, *55*, 2881–2888.

[7] P. Nolis, M. Perez, T. Parella, "Time-sharing evolution and sensitivity enhancements in two-dimensional HSQC-TOCSY and HSQMBC-experiments" *Magn. Resonance Chem*. **2006**, *44*, 1031–1036.

spin lock the MLEV-17 sequence is used. Note that there is no third dimension attached as in 3D TOCSY sequences.

In the detection period **d** the final gradient pulse g3 decodes those resonances which had been encoded by the gradient pulse g1. The sandwich d4, p12, g3 is the usual gradient-echo block to refocus chemical shift development during the gradient time.

8. Questions

A. Using the product operator formalism, show the transformations achieved in this pulse sequence according to the description in the Comments section.

B. Explain, why the phase of the two trim pulses p3 and p7 is from the *x*-direction.

C. Explain, why the MLEV spin lock has to act from the y-direction

D. In sucrose, as seen in the formula, the fructose is bound axially to the glucose unit, although this is more sterically demanding. Explain and show how one can detect this stereochemistry from the ^{1}H NMR spectrum.

9. Own Observations

Experiment 2.5

HOESY

1. Purpose

HOESY (**H**eteronuclear **O**verhauser **E**ffect **S**pectroscop**Y**) yields information on the spatial relationship between spins in the heteronuclear case. It will mainly be of value in cases where information from spin–spin couplings is unhelpful or unavailable. Since it is usually proton-detected, it has a high inherent sensitivity, and unwanted signals are effectively removed by the gradient selection. It has been applied for the spin pairs $^{1}H/^{31}P$, $^{1}H/^{19}F$ and $^{1}H/^{7}Li$ [1]. The example shown here is taken from the field of organofluorine chemistry. The major applications in current chemistry are in the field of organolithium compounds [5], inorganic complexes [11] and ionic liquids [12].

This new heteronuclear 2D-NOE NMR experiment should be useful for identifying the structures surrounding the metal ion binding sites in complexes with organic and biological ligands. In combination with other 2D-NMR NOE experiments, it could provide the complete solution structure of metal ion complexes. $^{15}N(^{1}H)$ heteronuclear 2D-NOE experiments might provide information on the protons involved in exchange in compounds such as peptides.

Taken from ref. [1]

2. Variants

There exist gradient-selected pulse sequences, which are best if the natural abundance of the heteronucleus is low and therefore suppresses proton signals which do not "see" the heteronucleus. In the case shown here, gradients are not necessary. Selective 1D versions for the $^{1}H,^{13}C$ spin pair have also been reported [7, 10], and recently an improved 2D version with an additional pulse and a modified phase cycle was described [8]. Important are combinations of the DOSY and the HOESY techniques [11], especially for inorganic chemistry.

3. Pulse Scheme and Phase Cycle

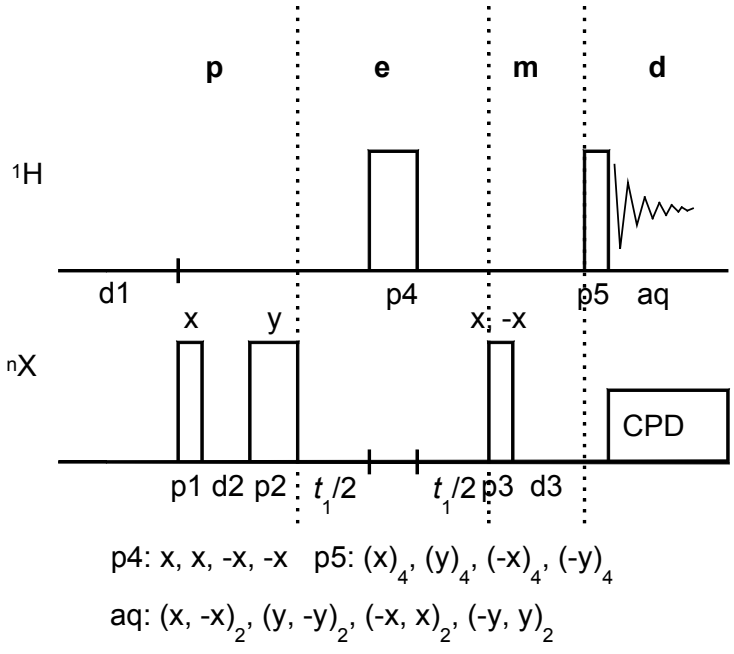

Scheme 2.5-1

Common values:

p1, p3: 90° ^{19}F transmitter pulse
p2: 180° ^{19}F transmitter pulse
p5: 90° ^{1}H transmitter pulse
p4: 180° ^{1}H transmitter pulse
d1: relaxation delay
d3: mixing time
d2: refocusing delay ($2 \cdot t_1/2$ + p4)
CPD composite pulse decoupling

Fluorine takes more and more a leading part as a substituent in organic compounds and especially in biologically active substances. It is known that fluorine atoms form short contacts or weak hydrogen bonds in rare cases. We found with fluorine substituted benzamides a system which is very sensitive concerning hydrogen bond formation and F-H-N short contacts. The ability to measure these interactions by X-ray, NMR, and IR may be important in structure-activity investigations of fluorine substituted active compounds.

Taken from ref. [9]

4. Acqusition

Special Values used for the spectrum shown:

Sample: N-(Diethylcarbamothioyl)-2,4-difluorobenzamide 15 mg in 0.7 ml $CDCl_3$
Time requirement: 18.5 h
Spectrometer: Bruker DRX-600 with H/F probe

td2:	2048 data points in F_2
td1:	128 data points in F_1
sw2:	13 ppm
sw1:	40 ppm
aq2:	0.06 s
aq1:	0.003 s
offset of ^{1}H frequency:	middle of ^{1}H NMR spectrum
offset of ^{19}F frequency:	middle of ^{19}F NMR spectrum
p1, p3:	90° ^{19}F decoupler pulse
p3:	180° ^{19}F decoupler pulse
p4:	180° ^{1}H transmitter pulse
p5:	90° ^{1}H transmitter pulse
d1:	3 s
d3:	1 s mixing time
ds:	4
ns:	128

5. Processing

Apply zero-filling in F_1 to 1024 real data points. Use exponential windows with lb = 5 Hz in F_2 and a π/2-shifted squared sinusoidal window in F_1. Apply complex Fourier transformation corresponding to the States-TPPI mode of data acquisition in F_1.

6. Result

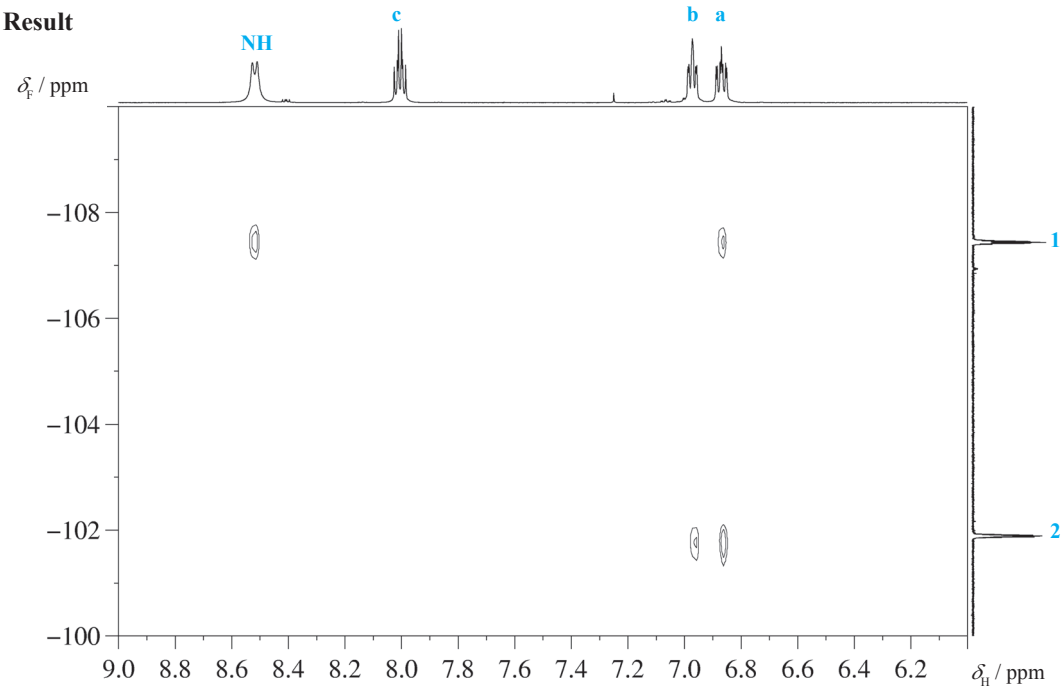

Fig. 2.5-1 HOESY spectrum of N-(Diethylcarbamothioyl)-2,4-difluorobenzamide

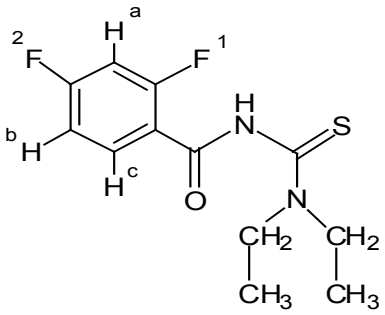

Scheme 2.5-2

The figure shows the result obtained on a DRX-600 spectrometer with a 5 mm dual ^{1}H, ^{19}F probe. The compound used has two aromatic bound fluorine atoms **1** and **2** and three aromatic protons **a**, **b** and **c**. In addition we find one amide proton. The spectrum shows nicely that the proton **a** shows cross-relaxation to fluorine **1**, whereas both protons **a** and **b** show cross relaxation to fluorine **2**. No effect is seen for proton **c**. The important result of this spectrum is that the NH proton also displays an NOE effect to fluorine **1** and this may be discussed in terms of an HF-hydrogen bridge.

7. Comments

The HOESY sequence can be understood from the simple vector analysis. The first pulse on the ^{19}F nucleus creates fluorine magnetization $-I_{Fy}$. The following short delay d2 and the180° ^{19}F pulse p2 are used for refocusing the finite length of the proton 180 pulse p4. During t_1 fluorine chemical shift develops the evolution period **e**. The 180° ^{1}H pulse p4 removes any ^{19}F,^{1}H spin coupling during t_1 and creates $-I_{Hz}$ magnetization. After t_1 the fluorine pulse p3 changes the fluorine transverse magnetization into the negative *z*-direction at the beginning of the mixing period **m**. Now both spins are in the $-z$-direction, and the fluorine signal is modulated with its chemical shift information. The spins undergo cross-relaxation during the mixing time d3. The final read pulse p5 creates transverse magnetization of protons, which is detected during t_2.

The F_2 dimension with the higher digital resolution is used for protons, whereas the lower resolution F_1 dimension contains the ^{n}X signal.

[1] P. L. Rinaldi, "Heteronuclear 2D-NOE spectroscopy" *J. Am. Chem. Soc.* **1983**, *105*, 5167−5168.

[2] C. Yu, G. C. Levy, "Solvent and intramolecular proton dipolar relaxation of the three phosphates of ATP: A heteronuclear 2D NOE study" *J. Am. Chem. Soc.* **1983**, *105*, 6994−6996.

[3] C. Yu, G. C. Levy, "Two-dimensional heteronuclear NOE (HOESY) experiments: Investigation of dipolar interactions between heteronuclei and nearby protons" *J. Am. Chem. Soc.* **1984**, *106*, 6533−6537.

[4] K. E. Kövér, G. Batta, "Theoretical and practical aspects of one- and two-dimensional heteronuclear Overhauser experiments and selective carbon-13 T_1-determinations of heteronuclear distances" *Prog. NMR Spectrosc.* **1987**, *19*, 223−266.

[5] W. Bauer, P. v. R. Schleyer, "Recent results in NMR spectroscopy of organolithium compounds" *Adv. Carbanion Chem.* **1992**, *1*, 89−175.

[6] W. Bauer, "Pulsed field gradient 'inverse' HOESY applied to the isotope pairs ^{1}H, ^{31}P and ^{1}H, ^{7}Li" *Magn. Reson. Chem.* **1996**, *34*, 532−537.

[7] K. Stott, J. Keeler, "Gradient-enhanced one-dimensional heteronuclear NOE experiment with ^{1}H detection" *Magn. Reson. Chem.* **1996**, *34*, 554−558.

[8] T. M. Alam, D. M. Pedrotty, T. J. Boyle, "Modified, pulse field gradient-enhanced inverse-detected HOESY pulse sequence for reduction of *t*1 spectral artifacts" *Magn. Reson. Chem.* **2002**, *40*, 361−365.

[9] L. Hennig, K. Ayala-Leon, J. Angulo-Cornejo, R. Richter, L. Beyer "Fluorine hydrogen short contacts and hydrogen bonds in substituted benzamides" *J. Fluorine Chem.* **2009**, *130*, 453–460.

[10] M. Yemloul, S. Bouguet-Bonnet, L. Aï cha Ba, G. Kirsch, D. Canet "Selective HOESY experiments for stereochemical determinations" *Magn. Reson. Chem.* **2008**, *46*, 939–942.

[11] P. S. Pregosin, P. G. Anil Kumar, I. Fernández "Pulsed gradient spin-echo (PGSE) diffusion and ^{1}H,^{19}F heteronuclear Overhauser spectroscopy (HOESY) NMR methods in inorganic and organometallic chemistry: Something old and something new" *Chem. Rev.* **2005**, *105*, 2977−2998.

[12] P. S. Pregosin "NMR spectroscopy and ion pairing: Measuring and understanding how ions interact" *Pure Appl. Chem.* **2009**, *81*, 615–633.

8. Questions

A. For the pair ^{6}Li,^{1}H this experiment is usually perfomed by observing ^{6}Li and ^{1}H in the indirect dimension, whereas for the pair ^{7}Li,^{1}H the reverse is true. Give a reason.

B. Why is the experiment rather seldom performed for the pair ^{13}C,^{1}H?

C. Calculate the appropriate gradient ratios for the pairs ^{31}P,^{1}H and ^{7}Li,^{1}H.

9. Own Observations

Experiment 2.6

INADEQUATE

1. Purpose

The 2D-INADEQUATE experiment (**I**ncredible **N**atural **A**bundance **D**oubl**E** **QUA**ntum **T**ransfer **E**xperiment) is probably the best NMR can do for a structural question. It provides the ultimate form of structure elucidation of organic compounds in solution, since C,C-connectivities can be obtained unequivocally. The possibility to form a ^{13}C-^{13}C pair at natural abundance is only $(1.1\ 10^{-2}) \times (1.1\ 10^{-2}) = 1.2\ \ 10^{-4}$. Due to its inherent insensitivity, there have been many attempts to improve the experiment [2–4]. From the many versions known we show here a method with a gradient double-quantum filter. We have chosen sucrose as an example, although it has a rather narrow chemical shift range. However, since sucrose is cheap and can be used in high concentration, this sample serves very well as a test even on inferior instruments.

2. Variants

Originally, the sequence started as a 1D experiment, but due to the similarity of C,C spin coupling constants this proved impractible. Methods which display the spectra in a COSY type manner have been proposed, but the technique shown here with a vertical double-quantum frequency axis is most often used in the literature. 1D selective techniques are also known [5]. The two most recent reviews describe the current state of the technique [6,7].

3. Pulse Scheme and Phase Cycle

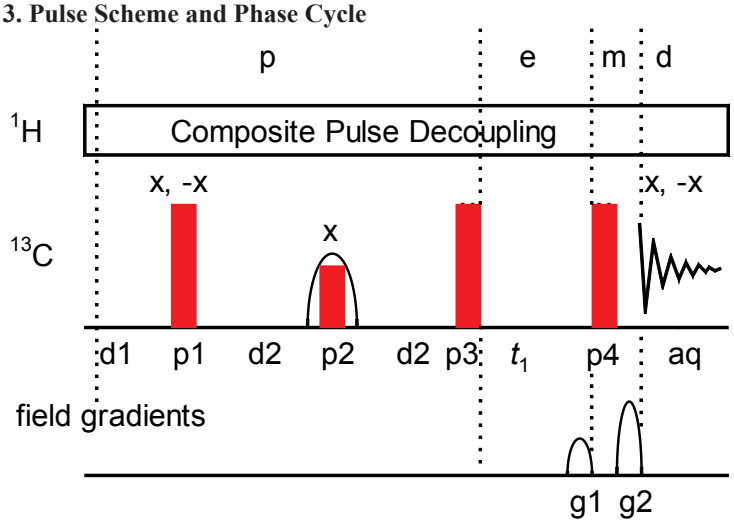

Scheme 2.6-1

4. Acquisition

Special values used for the spectrum shown:

Sample: 2M sucrose in D_2O
Time requirement: 4 h
Spectrometer: Bruker Avance 700 with 5-mm cryo probe

We propose a new method of establishing the connectivity of the carbon skeleton of an organic molecule, the first and most important step in complete structural determination. The technique is based on an earlier NMR experiment for studying carbon-13-carbon-13 spin-spin coupling which uses the momentary creation of double-quantum coherence to suppress the strong signals from isolated carbon-13 spins and reveal the weak carbon-13 satellite spectrum. If the magnitudes of the coupling constants are sufficiently well differentiated, they may be assigned to specific pairs of carbon resonances simply by picking out the repeated splittings. Adjacent carbon sites are thus identified directly. However, in many cases the molecular framework is too complex for this simple method to be applicable-each carbon site can have up to four directly bonded neighbors, and the carbon- carbon splittings may be close in magnitude or not clearly resolved. Consequently an independent method of assignment is needed.

Taken from ref. [1]

Common values:

p1, p3, p4 90° ^{13}C transmitter pulse
p2: 180° ^{13}C transmitter pulse (best as CHIRP pulse)
d1: relaxation delay
t_1: evolution increment
d2: 1/[4J(C,C)]

Tune the probe head to the actual sample, record a normal ^{13}C NMR spectrum, and optimize the spectral width. Determine the ^{13}C and observe pulse length for *this sample*. For this experiment the instrument must be set so as to obtain optimum performance.

td2: 4K data points in F_2
td1: 150 data points in F_1
sw2: 70 ppm
sw1: 140 ppm (double-quantum frequency)
aq2: 0.16 s
aq1: 0.003 s
o1: middle of ^{13}C NMR spectrum
d1: 3 s
d2: $1/[4J(C,C)] = 5.5$ ms, calculated from $^{1}J(C,C) = 45$ Hz
p2: chirped 180° ^{13}C pulse for refocussing (Crp60comp. 4, 2 ms, 2.9 dB)
ns: 32

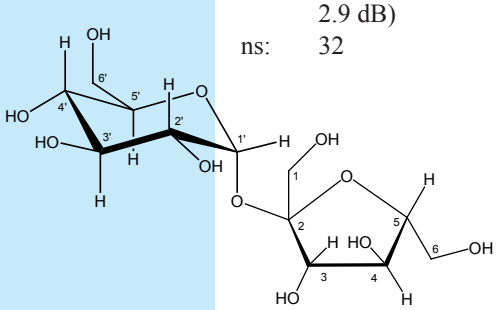

Scheme 2.6-2

5. Processing

Apply zero-filling in F_1 to 1K data points to obtain a matrix of 2K×1K data points. Use an exponential window with lb = 2 Hz in F_2 and a sinusoidal window in F_1. Phase correction is not necessary, since the data are processed in the magnitude mode.

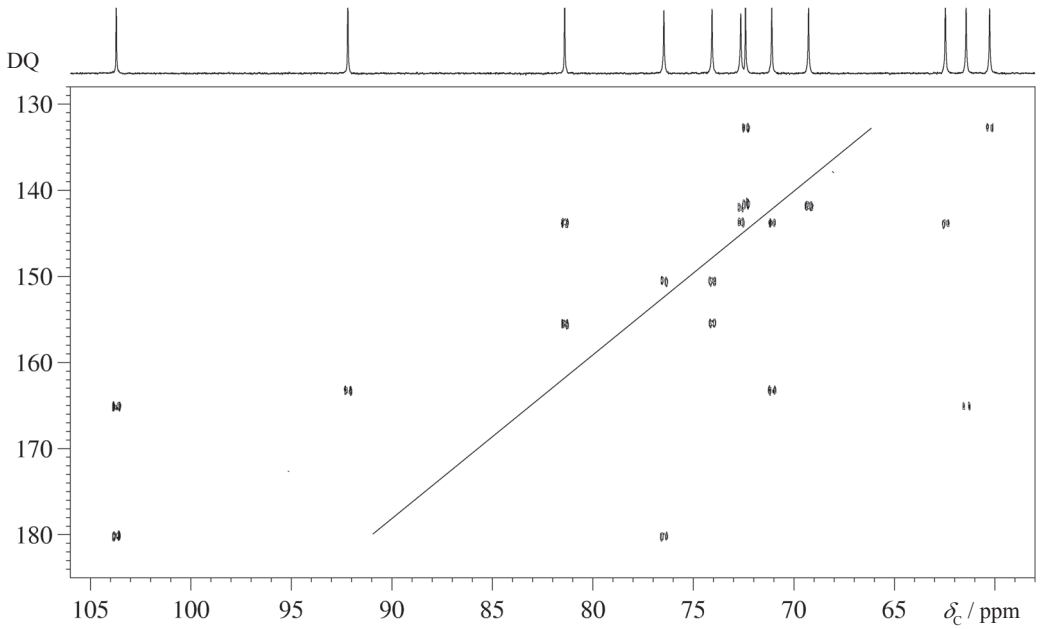

Fig. 2.6-1 2D-INADEQUATE spectrum of sucrose. Straight line: diagonal with a slope of 2.

6. Result

The figure shows the 2D-INADEQUATE spectrum obtained on an Avance-700 spectrometer with a cryo probe. Each pair of connected ^{13}C nuclei forms an AX or AB spin system, which is found in the same row of the data matrix; the pairs of doublets are symmetrical with respect to the diagonal (thin line), and spin coupling constants can be obtained from such a row. If one carbon is connected to more than one other carbon, the corresponding doublets are found at the same chemical shift in F_2, but at another double-quantum frequency in F_1. Thus the molecular carbon skeleton can be obtained by a criss-cross progression through the 2D spectrum.

Fig. 2.6-2 R. Freeman *1932

7. Comments

Using the product operator formalism we consider a C,C spin pair. During the preparation period **p** the first pulse p1 creates transverse magnetization, which develops C,C spin coupling during both delays d2. The 180° pulse refocuses the chemical shifts, and for simplicity is not shown in the equations. Thus, at the end of the spin-echo period we have in-phase and antiphase carbon magnetization multiplied by the respective cosine and sine terms as seen in Equation (1).

$$I_{C_z} \xrightarrow{I_{C_x}} -I_{C_y} \xrightarrow{\pi J\tau 2 I_{C_z} I_{C_z}} -I_{C_y}\cos\pi J\tau + 2I_{C_x} I_{C_z}\sin\pi J\tau \qquad (1)$$

If the delay τ is set equal to 2×d2 = 1/[2J(C,C)] the cosine term becomes zero and the sine term unity. After the pulse p3, which creates double-quantum magnetization $2I_{1_x} I_{2_y}$, chemical shift evolution of $2I_{1_x} I_{2_y}$ during t_1 yields the double-quantum frequencies, of which only one typical term is shown in Equation (2) for simplicity.

$$2I_{1_x} I_{2_y} \xrightarrow{\Omega_1 t_1 I_{1_z}} \xrightarrow{\Omega_2 t_2 I_{2_z}} 2I_{1_x} I_{2_y}\cos\Omega_1 t_1 \cos\Omega_2 t_2 \qquad (2)$$

After the evolution period **e** the magnetization is transformed back into antiphase magnetization by pulse p4. In the mixing period **m** a gradient double-quantum filter consisting of g1 and g2 ensures that only double-quantum coherences reach the receiver. The final pulse p4 transforms the double-quantum magnetization back into single-quantum terms. Evolution of spin coupling between the coupled ^{13}C nuclei creates in-phase magnetization, which is detected during t_2.

During the detection period **d**, C,C spin coupling develops again, forming an observable in-phase ^{13}C magnetization.

The main drawback of the method is its very poor sensitivity; many attempts have therefore been made to improve its performance. Nevertheless, there is a rule of thumb by which you can judge whether a 2D-INADEQUATE experiment will be successful. Record a normal ^{13}C NMR spectrum with one transient using a 90° pulse. If the signal-to-noise ratio is better than 30:1 you might invest the time for the experiment. The 1D ^{13}C-NMR spectrum shown was obtained with ns = 1.

[1] A. Bax, R. Freeman, T. A. Frenkiel, "An NMR technique for tracing out the carbon skeleton of an organic molecule" *J. Am. Chem. Soc*. **1981**, *103*, 2102−2104.

[2] D. L. Mattiello, R. Freeman, "Blood, sweat, and tears. Toward a rehabilitation of the INADEQUATE experiment" *J. Magn. Reson*. **1998**, *135*, 514−521.

[3] M. Bourdonneau, B. Ancian, "Rapid-pulsing artifact-free double-quantum-filtered homonuclear spectroscopy the 2D-INADEQUATE experiment Revisited" *J. Magn. Reson*. **1998**, *132*, 316−327.

[4] J. Bunkenborg, N. C. Nielsen, O. W. Sorensen, "Doubling the sensitivity of natural abundance ^{13}C–^{13}C INADEQUATE with off-resonance compensation", *Magn. Reson. Chem*. **2000**, *38*, 58−61.

[5] S. Berger, "Selective INADEQUATE, a farewell to 2D-NMR?" *Angew. Chem., Int. Ed.* Engl. **1988**, *27*, 1196−1197.

[6] J. Buddrus, J. Lambert, "Connectivities in molecules by INADEQUATE: recent developments" *Magn. Reson. Chem*. **2002**, *40*, 3−23.

[7] D. Uhrin, "Recent developments in liquid-state INADEQUATE studies" *Ann. Rep. NMR Spectrosc*. **2010**, *70*, 2−34.

[8] C. K. Anand, A. D. Bain, S. C. Watson "Use of continuous optimization methods to find carbon links in 2D INADEQUATE spectra" *J. Magn. Reson*. **2011**, *210*, 146–150.

8. Questions

A. What is the exact reason why INADEQUATE is so insensitive?

B. What is the purpose of the chirped 180° pulse p2?

C. Why is the ratio of the gradients g1 and g2 1: 2 and not 2: 1?

D. Draw criss-cross lines in the spectrum to confirm the assignment.

9. Own Observations

Experiment 2.7

ADEQUATE

1. Purpose

The INADEQUATE Experiment described in chapter 2.6 suffers from its inherent low sensitivity. Since the detection of carbon–carbon connectivities is probably the most important task in structure elucidation of natural products [4, 7, 10], where usually only limited material is available, a family of improved pulse sequences has been developed and termed ADEQUATE (**A**dequate sensitivity **D**oubl**E** **QUA**n**T**um sp**E**ctroscopy). In contrast to Experiment 2.6, these experiments detect carbon–carbon connectivities by proton observation. We show here the result of 1,1-ADEQUATE, where the correlation works via ^1J(C,H) and ^1J(C,C), using our 3 % strychnine standard in $CDCl_3$. The method lacks the generality of the normal 2D INADEQUATE since connectivities between two quaternary carbon atoms C_q–C_q cannot be detected; however, it is possible to see a C_q–CH_n moiety.

The major challenge in designing a ^{1}H-detected INADEQUATE experiment is the suppression of signals originating from ^{12}C-bound protons bound to ^{13}C–^{13}C fragments at natural isotopic abundance. It turns out that pulsed field gradients (PFGs), which have been successfully used to suppress the water signal by this order of magnitude (4), are invaluable for this application.

Taken from ref. [1]

2. Variants

The first variant of the basic idea was published under the name INEPT-INADEQUATE, suggesting an INEPT polarization transfer from ^{1}H to ^{13}C, collecting an INADEQUATE in the indirect dimension with a subsequent back transfer [1]. This original pulse sequence was then considerably improved including chirp pulses and was given the name ADEQUATE [2–5]. The standard ADEQUATE works in the [1,1] form, meaning a polarization transfer via $^1J_{CH}$ is being used and the INADEQUATE step also works via $^1J_{CC}$. There have been proposals for extended forms like [1,n] and [n,1] ADEQUATE [3]. Other modifications of the experiment have been developed to accurately measure C,C spin coupling constants, employing a *J* scaling. [9] Further variants include multiplicity editing [8] or the ACCORDION principle [6]. New adiabatic pulses correct for J_{CC} changes due to the finite length of the chirp pulses [11].

Common values:

p1, p3, p5, p7, p9:
90° ^{1}H transmitter pulse
p2, p4, p6, p8, p10:
180° ^{1}H transmitter pulse
p12, p14, p18, p20:
90° ^{13}C transmitter pulse
d1: relaxation delay
t1: evolution increment
p11, p21: 180°-CHIRP pulse for inversion
p13, p15, p17, p19: 180°-CHIRP pulse for refocussing
d2 = 1/[4J(C,H)]
d3 = 1/[4J(C,C)]
d4 = gradient lengths

3. Pulse Scheme and Phase Cycle

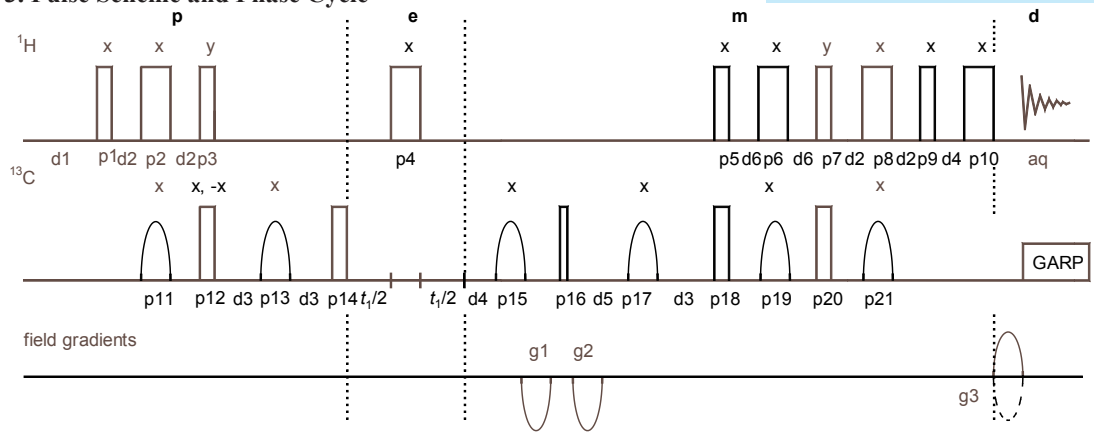

p14: $(x)_4$, $(-x)_4$ p16: $(x)_8$, $(-x)_8$ p18: $(x)_2$, $(-x)_2$ p20: $(y)_2$, $(-y)_2$ aq: x, -x, -x, x, $(-x, x, x, -x)_2$,x, -x, -x, x

Scheme 2.7-1

Fig. 2.7-1 G. Otting *1958

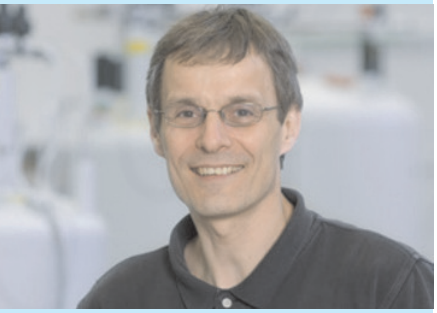

Fig. 2.7-2 C. Griesinger *1960

4. Acquisition

Special values used for the spectrum shown:

Sample: 3 % strychnine in $CDCl_3$
Time requirement: 10 h
Spectrometer: Bruker Avance 700 with 5-mm-cryo probe

td2: 1K data points in F_2
td1: 256 data points in F_1
sw2: 9 ppm
sw1: 310 ppm
aq2: 0.08 s
aq1: 0.0023 s
o1: center of ^{1}H NMR spectrum [4.5 ppm]
o2: center of ^{13}C NMR spectrum [77.5 ppm]
p16: 60° ^{13}C transmitter pulse
p11, p21: chirped 180° ^{13}C transmitter pulse (500 µs, Crp60,0.5,20.1)
p13, p15, p17, p19: chirped 180°^{13}C transmitter pulse (2 ms, Crp60comp.4)
d1: 2 s
d2: $1/[4J(C,H)]$ = 1.72 ms, calculated from $^{1}J(C,H) \approx 145$ Hz
d3: $1/[4J(C,C)]$ = 6.25 ms, calculated from $^{1}J(C,C) \approx 40$ Hz
d4: 1.05 ms = effective gradient duration
d5: d3 minus effective gradient duration
d6: $1/[6J(C,H)]$ = 1.15 ms, calculated from $^{1}J(C,H) \approx 145$ Hz
g1, g2, g3: Gradient strength ratio: (−78.4) : (−77.4) : (±59), sign of g3 varied according to echo-antiecho mode.
Decoupler attenuation and 90° pulse for GARP [70 µs, 14 dB]
ns: 64
ds: 16

5. Processing

Apply zero-filling to obtain a matrix of 2048×1024 real data points. Use an exponential window in F_2 with lb = 3 Hz and a π/2-shifted squared sinusoidal window in F_1. Choose the echo-antiecho FT mode of the software corresponding to the acquisition technique.

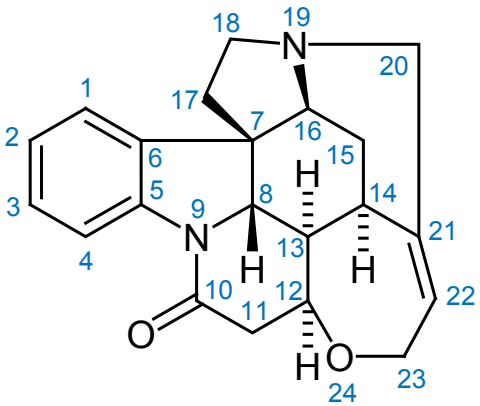

Scheme 2.7-2

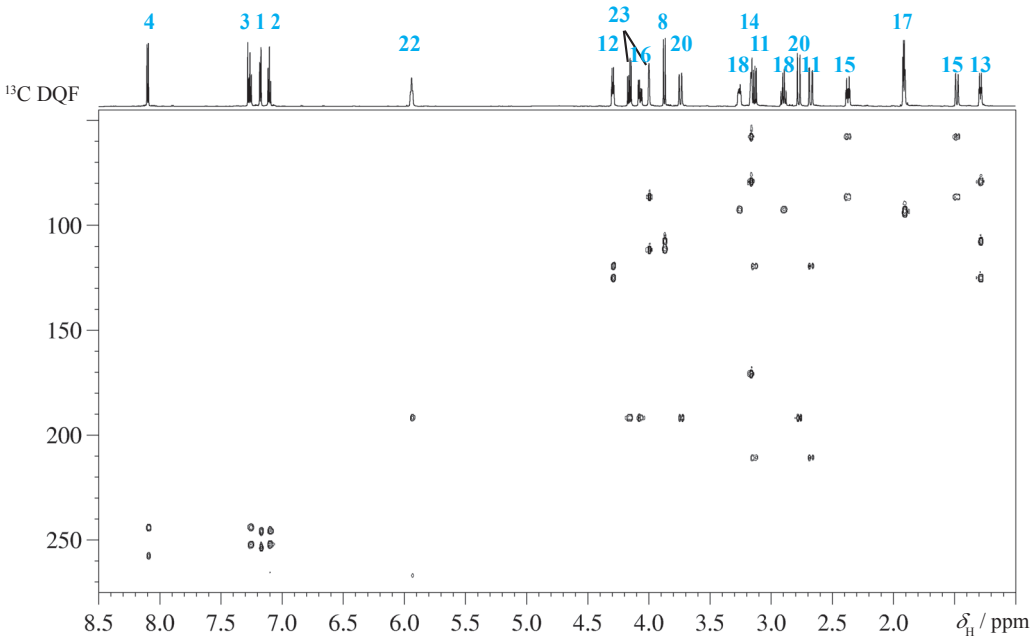

Fig. 2.7-3 2D-ADEQUATE spectrum of strychnine

6. Result

The figure shows the full region of the 1,1-ADEQUATE spectrum obtained on an Avance-700 spectrometer using a cryo probe. We start the interpretation of the figure at the right-hand side. Here we find H-13 at δ_H = 1.27 ppm. In the strychnine structure, C-13 at δ_C = 48.2 ppm is connected to three other carbon atoms, C-8, C-12 and C-14. Therefore we find the three correlation signals at the corresponding double-quantum frequencies 108.3 = 48.2 + 60.1 (=$\delta_{C\text{-}13}$ + $\delta_{C\text{-}8}$), 125.1= 48.2 + 76.9 (=$\delta_{C\text{-}13}$ + $\delta_{C\text{-}12}$) and 79.8 = 48.2 + 31.6 (=$\delta_{C\text{-}13}$ + $\delta_{C\text{-}14}$).

In the middle of the spectrum we find the signal of proton H-12 at δ_H = 4.28 ppm. In the strychnine structure the carbon atom C-12 is bound to C-13 and C-11. We expect therefore two correlation signals at the double-quantum frequencies δ_C = 119.3 and 125.1. This corresponds to $\delta_{C\text{-}12}$ = 76.85 + $\delta_{C\text{-}11}$ (42.48) and $\delta_{C\text{-}12}$ = 76.9 + $\delta_{C\text{-}13}$(48.2) and confirms the binding situation for C-12. Note that the double quantum value of 125.1 was already seen from proton H-13. The protons H-23 (δ_H = 4.0 to 4.2) are situated on a carbon with only one carbon atom neighbor. Therefore their correlation signals are found at $\delta_{C\text{-}23}$ = 64.60 + $\delta_{C\text{-}22}$ (127.34) giving 191.9.

Similarly all the other correlation signals can be assigned using the table of chemical shift data for strychnine in the appendix.

7. Comments

In the preparation period **p** of the sequence we find an INEPT transfer from protons to ^{13}C. The antiphase ^{13}C magnetization $2I_{H_z}I_{C_y}$, present after p12, develops C,C spin coupling to a second ^{13}C nucleus yielding

[1] J. Weigelt, G. Otting, "^{1}H detected INEPT-INADEQUATE at natural ^{13}C abundance" *J. Magn. Reson. Ser. A*. **1995**, *113*, 128−130.

[2] B. Reif, M. Köck, R. Kerssebaum, H. Kang, W. Fenical, C. Griesinger, "ADEQUATE, a new set of experiments to determine the constitution of small molecules at natural abundance" *J. Magn. Reson. Ser. A* **1996**, *118*, 282−285.

[3] B. Reif, M. Köck, R. Kerssebaum, J. Schleucher, C. Griesinger, "Determination of ^{1}J, ^{2}J, and ^{3}J carbon–carbon coupling constants at natural abundance" *J. Magn. Reson. Ser. B* **1996**, *112*, 295−301.

[4] M. Köck, B. Reif, W. Fenical, C. Griesinger, "Differentiation of HMBC two- and three-bond correlations: A method to simplify the structure determination of natural products" *Tetrahedron Letters* **1996**, *37*, 363−366.

[5] M. Köck, R. Kerssebaum, W. Bermel, "A broadband ADEQUATE pulse sequence using chirp pulses" *Magn. Reson. Chem*. **2003**, *41*, 65−69.

[6] R. T. Williamson, B. L. Marquez, W. H. Gerwick F. E. Koehn, "ACCORD-ADEQUATE: an improved technique for the acquisition of inverse-detected INADEQUATE" *Magn. Reson. Chem*. **2001**, *39*, 544–548.

[7] S. W. Meyer and M. Köck, "NMR studies of phakellins and isophakellins" *J. Nat. Prod*. **2008**, *71*, 1524–1529.

[8] K. E. Kövér, and P. Forgó, "*J*-modulated ADEQUATE (JM-ADEQUATE) experiment for accurate measurement of carbon–carbon coupling constants" *J. Magn. Reson*. **2004**, *166*, 47–52.

[9] T. Parella, F. Sanchez-Ferrando, "Improved multiplicity-edited ADEQUATE experiments" *J. Magn. Reson*. **2004**, *166*,123–128.

[10] H. He, J. E. Janso, R. T. Williamson, H. Y. Yang, G. T. Carter, "Cytosporacin, a highly unsaturated polyketide: Application of the ACCORD-ADEQUATE experiment to the structural determination of natural products" *J. Org. Chem*. **2003**, *68*, 6079−6082.

[11] C. M. Thiele, W. Bermel, "*J*-modulated ADEQUATE experiments using different kinds of refocusing pulses" *Magn. Reson. Chem*. **2007**, *45*, 889–894.

[12] G. E. Martin, B. D. Hilton, M. R. Willcott, K. A. Blinov "HSQC-1,n-ADEQUATE: a new approach to long-range $^{13}C–^{13}C$ correlation by covariance processing" *Magn. Reson. Chem*. **2011**, *49*, 641−647.

[13] R. T. Williamson, A. V. Buevich, G. E. Martin "Experimental and theoretical investigation of $^{1}J_{CC}$ and $^{n}J_{CC}$ coupling constants in strychnine" *Org. Lett*. **2012**, *14*, 5098−5101.

a term $4I_{H_z}I_{C_x}I_{C_z}$. This is transformed into double-quantum coherence with respect to carbon by p14 at the end of section **p**. In the evolution period **e** the double-quantum chemical shifts of ^{13}C develop during t_1. The mixing period **m** has two purposes. The double-quantum ^{13}C coherences have to be reconverted to single-quantum coherences, which is achieved by a 60° pulse p16, giving a higher efficiency for this process than in the original experiment. The gradient g1 dephases signals that are in the double-quantum state and gradient g2 further dephases the ^{13}C coherences after reconversion into proton-^{13}C antiphase magnetization. Finally, the situation must be prepared for the back transfer to protons, which is achieved by the refocusing elements [g2, d5, p17, d3]. The back transfer is performed with sensitivity enhancement using the PEP principle as already described in Experiment 1.5.

Note that both ^{1}J(C,H) and ^{1}J(C,C) vary widely in organic compounds and the success of the experiment relies on reasonably well-chosen values. According to Reference [4] it is very advisable to use adiabatic 180° pulses for this sequence. p11 and p21 are adiabatic inversion pulses, whereas p13, p15, p17 and p19 comprise of adiabatic refocussing pulses.

8. Questions

A. Calculate the theoretical improvement of ADEQUATE versus INADEQUATE.

B. How good should the signal suppression for normal proton signals be in order that the desired signals become visible?

C. Correlation signals displayed by H-22, H-23a and H-23b, H-20a and H-20b seem to be all at the same horizontal line at 191.5 ppm. Explain.

9. Own Observations

Experiment 2.8

J-HMBC

1. Purpose

In view of the importance of long-range C,H spin coupling constants [1], developing effective methods for measuring them is currently an active topic of research, and several proposals were published recently. We show here a gs-*J*-Resolved HMBC [3], where each long-range correlation signal will display an additional splitting in F_1 which is proportional to ^nJ(C,H). The method achieves this by disentangling H,H spin couplings from C,H spin couplings and by the use of a scaling scheme by which the small spin couplings are enlarged by a chosen factor to overcome digital resolution problems in F_1. The result is demonstrated with the strychnine sample.

2. Variants

There are several quite different methods [6, 7] which try to achieve the same goal. In addition, some selective methods have been proposed, which yield the information by spin selection [8, 9]. Of particular interest are the application to heteronuclear spin systems [5] and the construction of modified Karplus curves [10].

Common values:

p1: 90° ^{1}H transmitter pulse
p2, p3, p4: 180° ^{1}H transmitter pulse
p5, p7, p8: 90° ^{13}C transmitter pulse
p6: 180° ^{13}C transmitter pulse
d1: relaxation delay
t_1: evolution increment
d2: 1/[2^{1}J(C,H)]
d3 + d4: constant time interval / increment and decrement with scaling factor *m*

3. Pulse Scheme and Phase Cycle

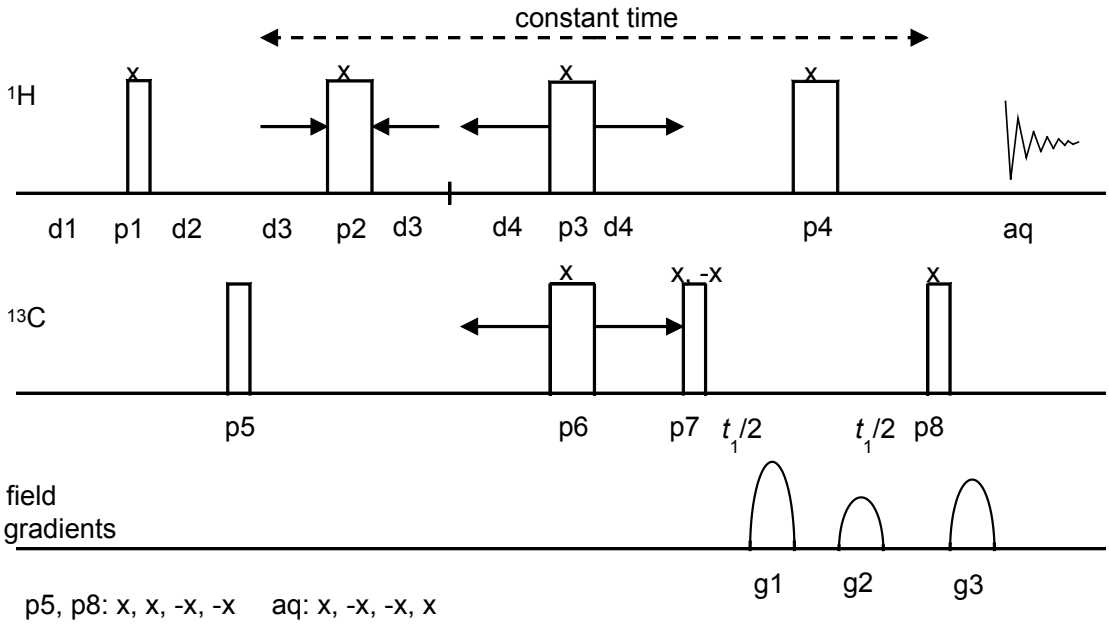

Scheme 2.8-1

The spin-coupling constant is a useful NMR parameter for conformational studies of biomolecules as seen in its application to polypeptides or polynucleotides. In particular, proton-proton vicinal coupling constants ($^3J_{H,H}$) are most frequently used for this purpose because of their dependence on dihedral angles. These coupling constants, including those due to carbon-proton coupling ($^2J_{C,H}$ and $^3J_{C,H}$), possess several advantages over NOE for acyclic systems. In systems with conformational changes, the coupling constants are observed as a weighted average of those due to each conformer, which greatly facilitates the determination of a population ratio among conformers.

Taken from ref. [1]

Fig. 2.8-1 Seeds from *strychnos nux vomica*

4. Acquisition

Special values used for the spectrum shown:

Sample: 3 % strychnine in $CDCl_3$
Time requirement: 4 h
Spectrometer: Bruker Avance 600 with 5-mm TBI probe

td2: 2K data points in F_2
td1: 320 data points in F_1
sw2: 9 ppm
sw1: 180 ppm
aq2: 0.19 s
aq1: 0.009 s
offset of ^{1}H frequency: middle of ^{1}H NMR spectrum [4.5 ppm]
offset of ^{13}C frequency: middle of ^{13}C NMR spectrum [85 ppm]
m: scaling factor = 30
d1: relaxation delay 2.5 s
d2: $1/[2J(C,H)] = 3.5$ ms, calculated from $^1J(C,H) \approx 145$ Hz, delay for low-pass filter
d3: $[m \times t_{1(max)}]/2$, where m is the scaling factor [~ 330 ms with m = 30 and td1 = 320], d3 is decremented during the experiment by $(m+1)/[2 \times sw1]$
d4: $m \times 3\mu s = 90$ µs, incremented during the experiment by $m/[2 \times sw1]$
gradient ratio 50 : 30 : 40.1 % % (100 % ≈ 0.56 T/m)
ds: 16
ns: 16

5. Processing

Apply zero-filling in ind F_1 and F_2 to 2K in order to have a matrix of 2K × 2K real data points. Before Fourier transformation use unshifted sinusoidal windows in both dimensions. Use the quadrature-off scheme for magnitude calculation of the spectrum. Phase correction is therefore not necessary.

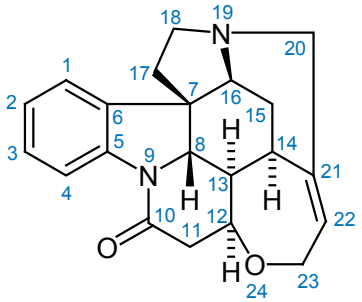

Scheme 2.8-2

6. Result

The carboxyl ^{13}C nucleus C-10 shows long-range correlations over three bonds to H-12 and over two bonds to both the H-11 protons. Whereas the former is not clearly resolved, the correlation signals to the protons 11 show splittings in F_1 of 189.7 and 237.2 Hz, from which spin coupling constants of 6.3 and 7.9 Hz can be calculated. Couplings of the protons H-23 to the ^{13}C nuclei C-21 and C-22 corresponding to 8.1 Hz and 3.3 Hz can also be observed, as well as spin couplings of H-8 to both C-5 and C-6 with 2.7 and 3.4 Hz, and of H-20 at $\delta_H = 3.75$ ppm to C-21 and C-22 with 5.4 and 4.1 Hz.

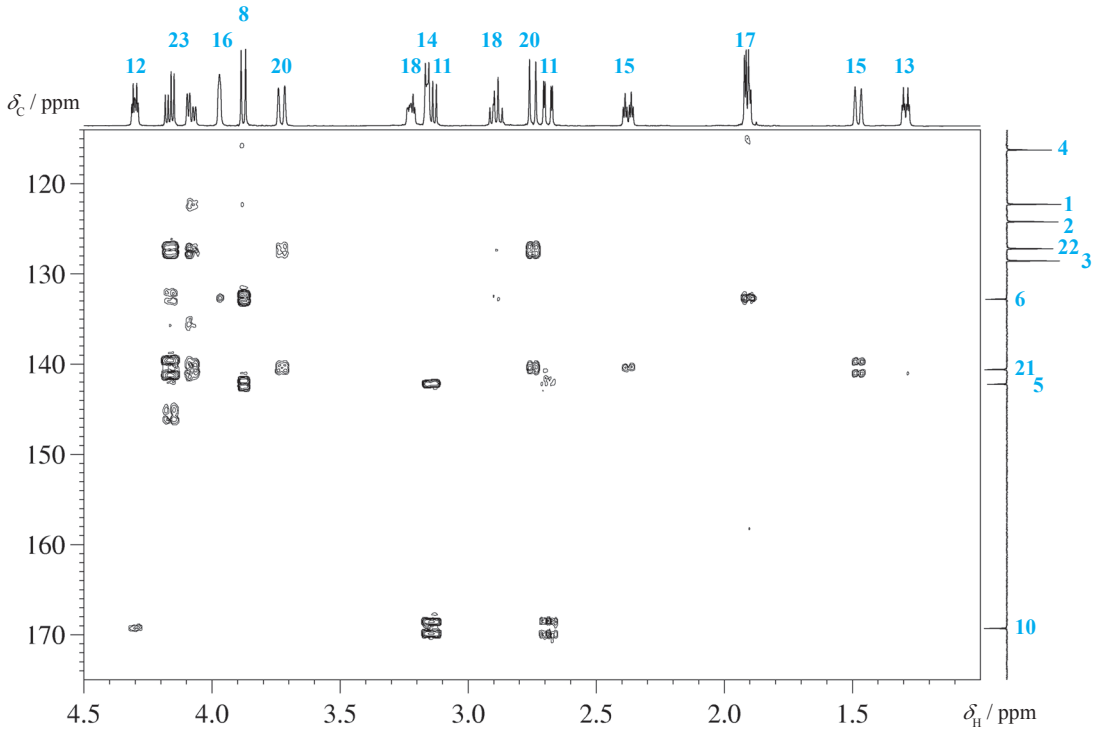

Fig. 2.8-2 Expansion of the *J*-HMBC spectrum for the aliphatic protons and aromatic carbon atoms

The figures show the 2D spectra obtained on an DRX-600 spectrometer with an inverse multinuclear *z*-gradient TBI probe.

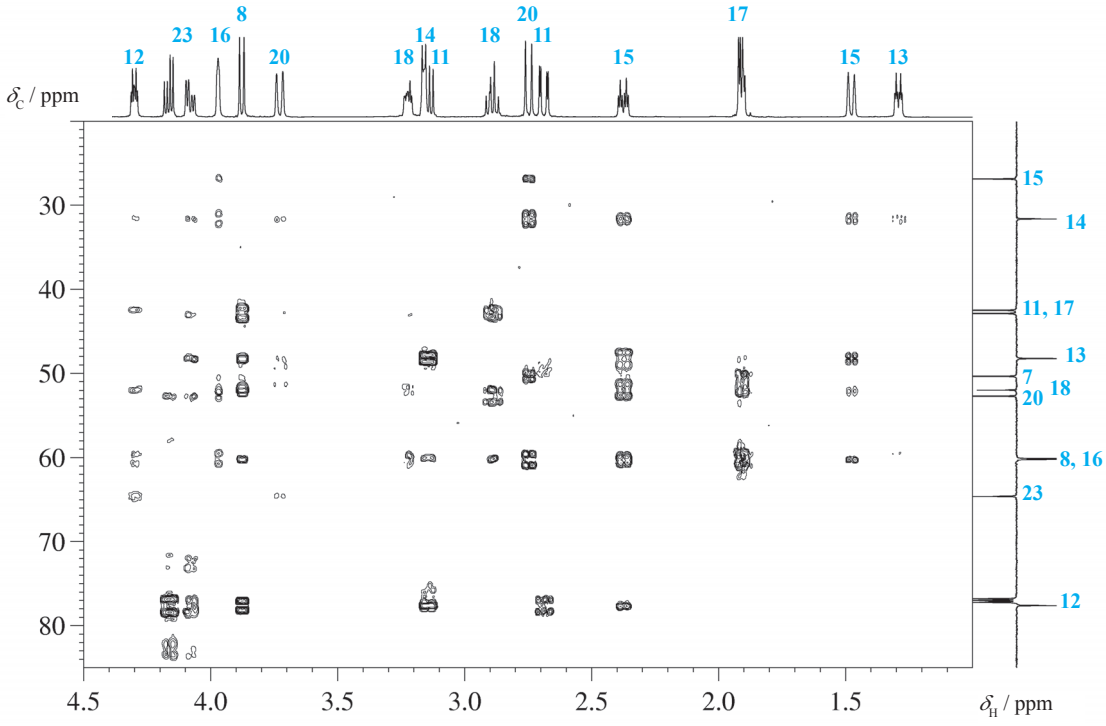

Fig. 2.8-3 Expansion of the *J*-HMBC spectrum for the aliphatic protons and aliphatic carbon atoms

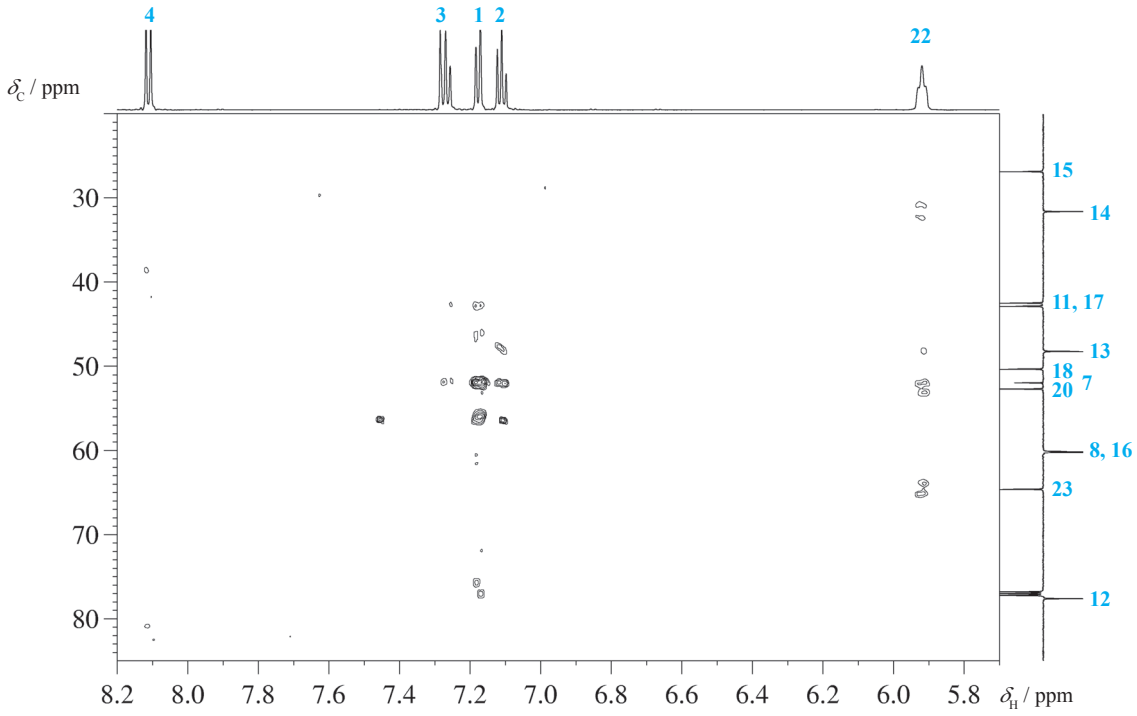

Fig. 2.8-4 Expansion of the *J*-HMBC spectrum for the aromatic protons and aliphatic carbon atoms

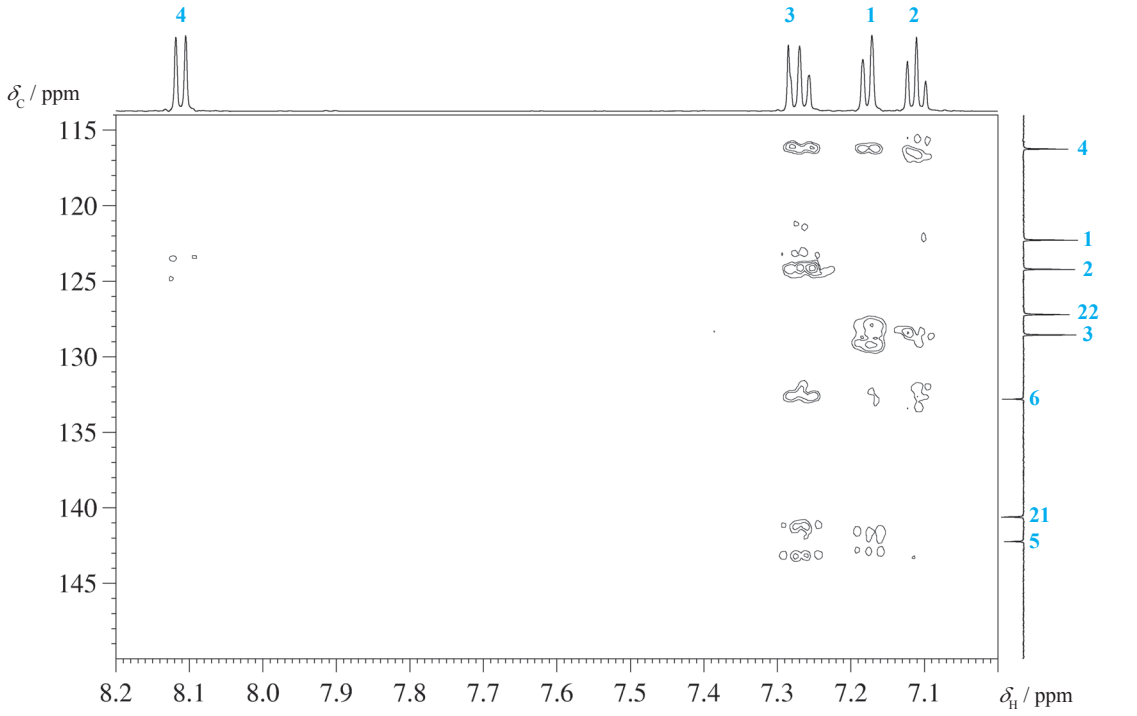

Fig. 2.8-5 Expansion of the *J*-HMBC spectrum for the aromatic protons and aromatic carbon atoms

7. Comments

The sequence is in part a standard gradient-selected HMBC with a low-pass filter; thus the pulses p1, p4, p5, p7, and p8 have the identical meaning that already described in Chapter 1.6; (there: p1, p2, p3, p5, and p7). The delay d2 is the low-pass filter delay.

The sequence employs a constant time period with stepwise shifted 180° pulses, and this constant time period starts after p5 and ends with p8. It consists of three parts: the first part (2×d3), which is decremented during the experiment, the second part (2×d4), and the third part (t_1), both of which are incremented. The total duration of this constant time period should be set to about 500 ms; much more will be problematic due to relaxation, much less will not give very good resolution in F_1.

Homonuclear proton spin couplings will not contribute to a modulation in F_1, since the total time for their evolution is fixed and the 180° pulses p2, p3, and p4 will always lead to a complete refocusing of the proton chemical shift. On the other hand, the C,H spin couplings are decoupled in the first part of the constant time period by pulse p2, but will be effective in the second part, since two 180° pulses p3 and p6 are applied at the same time. During t_1, the C,H spin couplings are again decoupled by pulse p4. The incrementation steps during the first two periods are m×[1/(2×sw1)], where m is a scaling factor usually set to 30; thus the modulation by the C,H spin coupling during the second period will be multiplied by this factor, and this has to be known when recalculating the spin coupling constants from the spectral splittings in F_1. Note that insufficiently suppressed ^1J(C,H) correlations will also be scaled in F_1 by the factor m, and this therefore leads to a splitting of several kHz.

The method is considerably less sensitive than the gradient-selected HETLOC experiment, and a compromise has to be found between the average length of the active HMBC period (2×d4), the total length of the constant time period, the number of t_1 increments, and the chosen scaling factor m for the achievable resolution. As an advantage and in contrast to HETLOC, it also gives spin coupling constants to quaternary carbon nuclei as demonstrated in the figure.

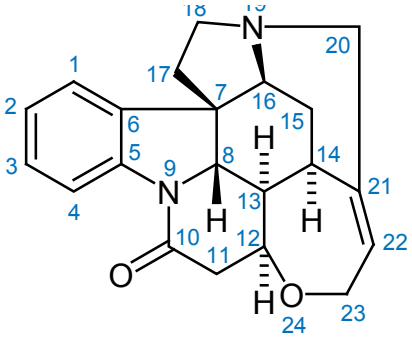

Scheme 2.8-3

[1] N. Matsumori, D. Kaneno, M. Murata, H. Nakamura, K. Tachibana, "Stereo-chemical determination of acyclic structures based on carbon-proton spin-coupling constants. A method of configuration analysis for natural products", *J. Org. Chem.* **1999**, *64*, 866−876.

[2] B. L. Marquez, W. H. Gerwick, R. T. Williamson, "Survey of NMR experiments for the determination of ^nJ(C,H) heteronuclear coupling constants in small molecules" *Magn. Reson. Chem.* **2001**, *39*, 499−530.

[3] K. Furihata, H. Seto, "*J*-Resolved HMBC, a new NMR technique for measuring heteronuclear long-range coupling constants", *Tetrahedron Letters* ***1999***, *40*, 6271−6275.

[4] C. H. Gotfredsen, A. Meissner, J. Ø. Duus and O. W. Sørensen, "New methods for measuring ^{1}H–^{31}P coupling constants in nucleic acids" *Magn. Reson. Chem.* **2000**, *38*, 692−695.

[5] M. Biesemans, J. C. Martins, R. Willem, A. Lycka, A. Ruzicka, J. Holecek "^{1}H,^{117}Sn *J*-HMBC spectroscopy as a tool for the determination of long-range ^nJ(^{1}H,^{117}Sn) coupling constants in the investigation of intramolecular donor–acceptor interaction in [2-(N,N-dimethylaminomethyl)phenyl]stannanes" *Magn. Reson. Chem.* **2002**, *40*, 65–69.

[6] A. Meissner, O. W. Sørensen, "Measurement of *J*(H,H) and long-range *J*(X,H) coupling constants in small molecules. Broadband XLOC and *J*-HMBC" *Magn. Reson. Chem.* **2001**, *39*, 49−52.

[7] R. A. E. Edden and J. Keeler "Development of a method for the measurement of long-range ^{13}C–^{1}H coupling constants from HMBC spectra" *J. Magn. Reson.* **2004**, *166*, 53–68.

[8] M. Findeisen and S. Berger "A selective pulse sequence for the determination of long-range C,H spin coupling constants" *Magn. Reson. Chem*. **2003**, *41*, 431–434.

[9] K. Furihata, M. Tashirob, H. Seto "Selective *J*-resolved HMBC, an efficient method for measuring heteronuclear long-range coupling constants" *Magn. Reson. Chem*. **2009**, *47*, 814–818.

[10] M. Tafazzoli, M. Ghiasi "New Karplus equations for $^2J_{HH}$, $^3J_{HH}$, $^2J_{CH}$, $^3J_{CH}$, $^3J_{COCH}$, $^3J_{CSCH}$, and $^3J_{CCCH}$ in some aldohexopyranoside derivatives as determined using NMR spectroscopy and density functional theory calculations" *Carbohydrate Research* **2007**, *342*, 2086–2096.

8. Questions

A. Give a reason, why the $^2J_{CH}$ spin couplings of the carbonyl group to the two diastereotopic protons H-11 should be different.

B. Give a reason, why the $^3J_{CH}$ spin coupling of the carbonyl group to the proton H-12 is so small.

C. Why are "constant time" pulse sequences inherently less sensitive than "normal" ones?

D. What spectral changes do you expect if the sequence shown here is not performed in the constant time mode?

9. Own Observations

Experiment 2.9

Gated Decoupling

1. Purpose

One of the oldest ^{13}C NMR techniques has been dubbed "Gated Decoupling". This experiment is used for determining C,H spin−spin coupling constants without losing to much of nuclear Overhauser enhancement. It yields proton-coupled ^{13}C NMR spectra, which usually have to be analyzed with the help of spin simulation and iteration, since the carbon atoms may often form the X part of relatively complicated $A_mB_n...X$ spin systems. The digital resolution of such 1D ^{13}C NMR spectra is far better than that of any of the 2D NMR methods. A knowledge of long-range C,H spin coupling constants is very helpful in structural elucidation of organic molecules and nowadays plays an important role in the field of residual dipolar couplings.

It has been noted that when proton decoupling is terminated immediately before a field-sweep passage through the carbon-13 resonance of methyl iodide, ^{13}C-H spin coupling returns immediately, whereas reequilibration of populations of nuclear energy levels is slower, being determined by relaxation times.

From reference [1]

2. Variants

The basic scheme is so straightforward that not many improvements seem to be possible. However, an edited version has been proposed [5] which yields subspectra according to the number of protons attached to a carbon center. There also exists the inverse gated technique, in which the decoupler is off during the relaxation delay but on during the acquisition.This technique yields proton-decoupled ^{13}C NMR spectra but without the NOE effect, which is important for quantitative ^{13}C NMR.

3. Pulse Scheme and Phase Cycle

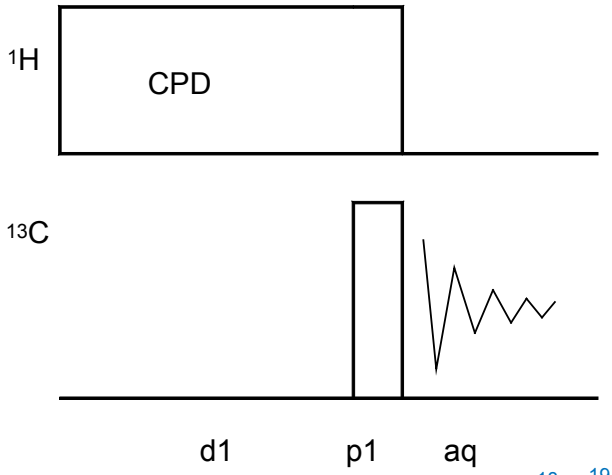

p1: x, x, -x, -x, y, y, -y, -y

aq: x, x, -x, -x, y, y, -y, -y

Scheme 2.9-1

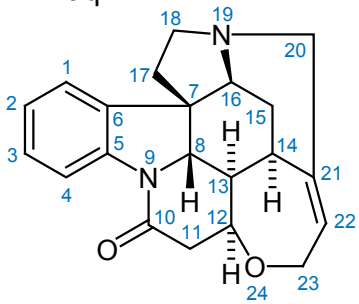

Scheme 2.9-2

Common values:

p1: 70° ^{13}C transmitter pulse
d1: relaxation delay
CPD composite pulse decoupling

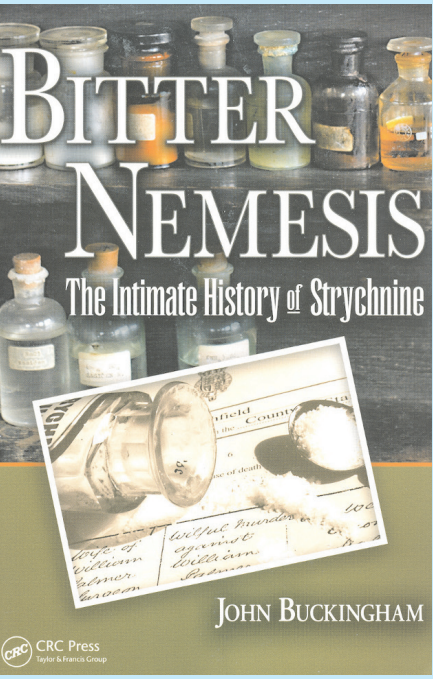

Fig. 2.9-1 Recent book about strychnine

4. Acquisition

Special values used for the spectrum shown:

Sample: 3 % strychnine in $CDCl_3$.
Time requirement: 5 h
Spectrometer: Bruker DRX-700 with 5-mm cryo probe

td: 64K
sw: 200 ppm
o1: middle of ^{13}C NMR spectrum
o2: middle of ^{1}H NMR spectrum
aq: 1 s
d1: 2 s
CPD: Waltz16 sequence, individual 90° ^{1}H pulse:100 µs at 12 dB
ns: 7000

5. Processing

Use standard 1D processing with Gaussian multiplication (gb = 0.25, lb = −1 Hz) si = 64K.

6. Result

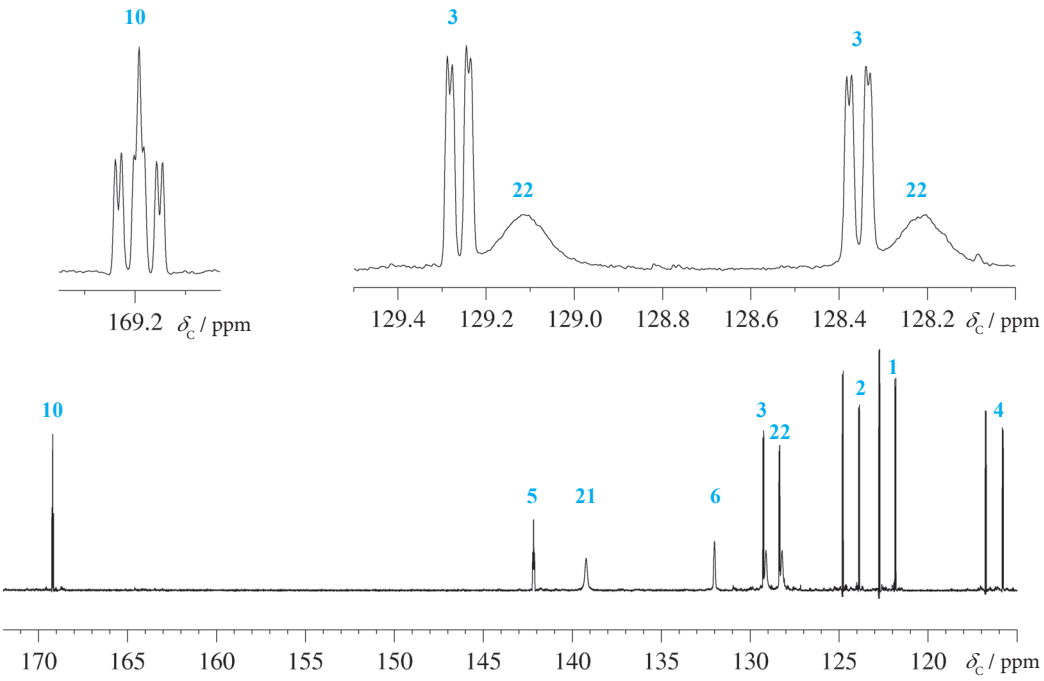

Fig. 2.9-2 Expansion of the gated decoupled ^{13}C NMR spectrum in the aromatic region

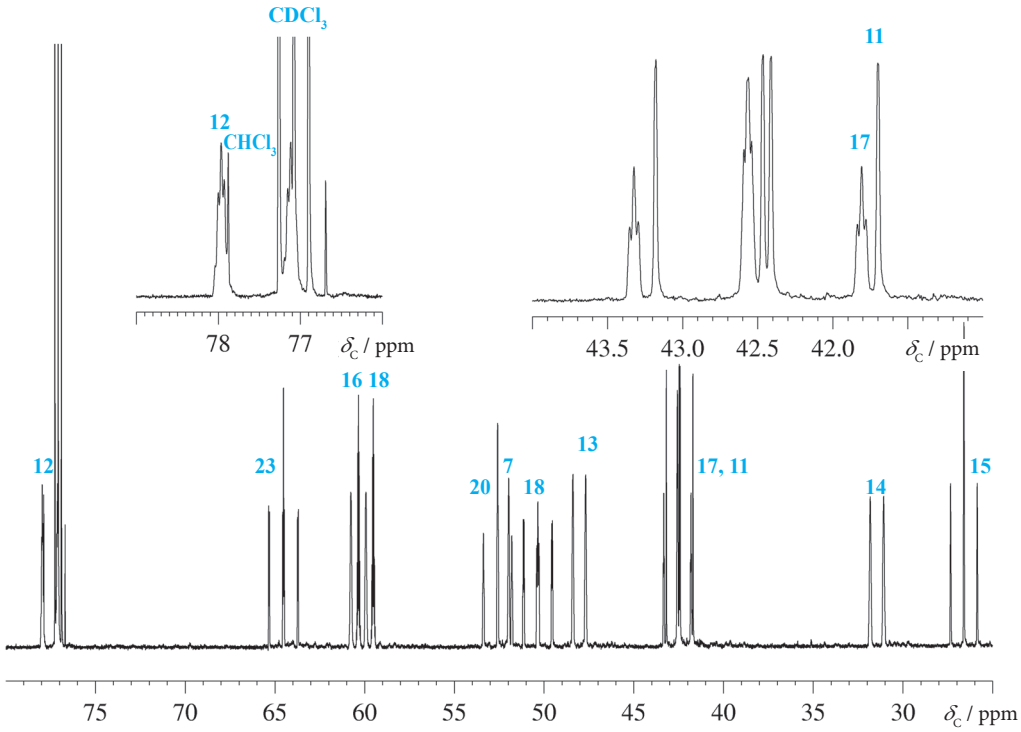

Fig. 2.9-3 Expansion of the gated decoupled ^{13}C NMR spectrum in the aliphatic region

The figures show the ^{1}H-coupled ^{13}C NMR spectrum of strychnine obtained with an Avance-700 spectrometer. Every signal is split into multiplets according to the underlying spin system. The insets expand the carbonyl group, the region of C-3 and C-22, the region at the $CDCl_3$ signal, and the region of C-17 together with C-11. All these regions lead to interesting questions (see below).

7. Comments

In this experiment decoupling is applied during the delay d1 but not during the acquisition time. Coupling information is present immediately after switching off the decoupling field, whereas the populations of the energy levels decay with the spin−lattice relaxation times. During d1 (same order as the acquisition time), favorable ^{13}C energy level populations become established and coupled spectra with NOE can be obtained. One has to be careful about assuming a first-order interpretation of such spectra since higher-order effects can occur. Make sure that the observed splittings are in fact first-order, and use spin simulation programs to analyze the spin systems.

[1] O. A. Gansow, W. Schittenhelm, "Alternately pulsed carbon-13 and proton magnetic resonance, an alternative to nuclear off-resonance decoupling" *J. Am. Chem. Soc*. **1971**, *93*, 4294−4295.

[2] F. W. Wehrli, T. Wirthlin, Interpretation of Carbon-13 NMR Spectra, Heyden, London, **1978**, Ch. 3.

[3] M. L. Martin, J.-J. Delpuech, G. J. Martin, Practical NMR Spectroscopy, Heyden, London, **1980**, Ch. 6.2.

[4] H.-O. Kalinowski, S. Berger, S. Braun, Carbon-13 NMR Spectroscopy, Wiley, Chichester, **1988**, Ch. 2.3.

[5] D. Canet, C. Millot, J. Brondeau "Determination of carbon multiplicities by a double-echo sequence and gated decoupling" *Magn. Reson. Chem*. **1986**, *24*, 951−953.

[6] R. Freeman, H. D. W. Hill, R. Kaptein, "Proton-decoupled NMR spectra of carbon-13 with the nuclear Overhauser effect suppressed" *J. Magn. Reson*. **1972**, *7*, 327–329.

[7] P. Giraudeau, E. Baguet "Improvement of the inverse-gated-decoupling sequence for a faster quantitative analysis of various samples by ^{13}C NMR spectroscopy" *J. Magn. Reson*. **2006**, *180*, 110–117.

8. Questions

A. In the expanded region underneath the $CDCl_3$ signal at 77 ppm exists a rather broad, but split doublet and a very sharp doublet with a considerable larger splitting. Explain.

B. The expanded region at 42 ppm shows the signals of C-17 and C-11: both are CH_2 groups. Why does one show a triplet of triplets, whereas the other is a doublet of doublets?

C. The signals displayed at 129 ppm stem from C-3 and C-22. Why does C-3 give a sharp ddd pattern, whereas C-22 is rather unstructured and broad?

D. Use a spin simulation program to reproduce the signal of the carbonyl group.

E. It is often suggested, to use d1 at least ≈ aq for this pulse sequence. Give a reason.

9. Own Observations

Chapter 3

Selective Methods

In routine NMR so called "hard" pulses are used to excite all spins of a sample. However, there are applications, where it is advantageous to saturate or excite only a specific spin sort. For this purpose so-called "soft" or selective pulses are used. Meanwhile there exists a large zoo of such selective pulses ranging from a simple Gaussian shape to cascades of shaped pulses, see examples in Chapter 8.3.

In this chapter we at first focus on four different forms of water suppression where special pulses are applied. We show then five applications of selective pulses in organic chemistry which may replace the standard 2D NMR techniques:

3.1 Water Suppression by Presaturation 77
3.2 Solvent Suppression by 1D-NOESY 81
3.3 Water Suppression by SOGGY Excitation Sculpting 85
3.4 Solvent Suppression using WET 89
3.5 SELTOCSY
[**SEL**ective **T**otal **C**orrelation **S**pectrosciop**Y**] 93
3.6 SELNOESY
[**SEL**ective **NOE S**pectroscop**Y**] 97
3.7 SELINCOR
[**SEL**ective **IN**verse **COR**relation] 101
3.8 SELINQUATE
[**SEL**ective **IN**ADE**QUATE**] 105
3.9 Band Selective HMBC
[Band Selective **H**eteronuclear **M**ultiple **B**ond **C**orrelation] 109

All these techniques require a bit more thinking, adjustments, and experience of the operator; however, he or she will soon learn the huge gain obtained from these methods.

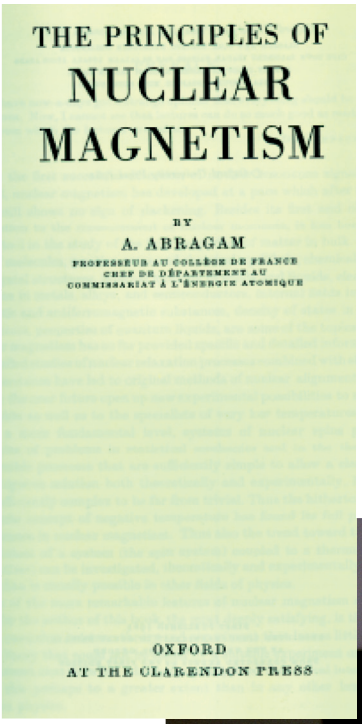

published 1961

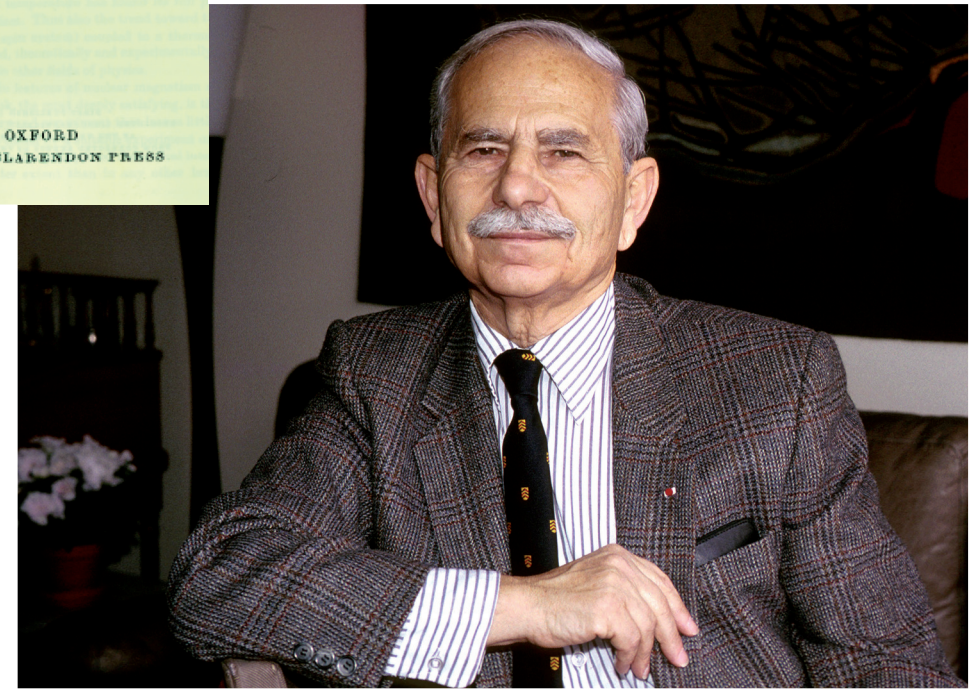

"What I had in mind was to attempt for nuclear magnetism what Van Vleck has done for the theory of electric and magnetic susceptibilities in a book which thirty years after its publication is still *the* book on the subject. A demi-succès in this undertaking wood be good enough.

Fig. 3.0-1 Anatole Abragam (1925-2011)

Experiment 3.1

Water Suppression by Presaturation

1. Purpose

For biological and biochemical applications ^{1}H NMR spectra usually have to be recorded in H_2O, with the addition of only 10 % D_2O to provide the necessary lock signal. Higher D_2O content would cause the signals of the exchangeable NH protons to disappear. Thus, there is a need to suppress the huge solvent signal. For this purpose a multitude of techniques have been proposed of which the simplest is the classical presaturation experiment.

2. Variants

Presaturation can be easily combined with other techniques to give further improvement of the result. A selective 180° pulse between two magnetic field gradients was used [6], or a combination with the DOSY technique was proposed [5]. The PURGE sequence applies the presaturation embedded between gradients [4]. However, all techniques work best if the magnet is well shimmed. A probe head yielding a reasonable line shape is mandatory.

3. Pulse Scheme and Phase Cycle

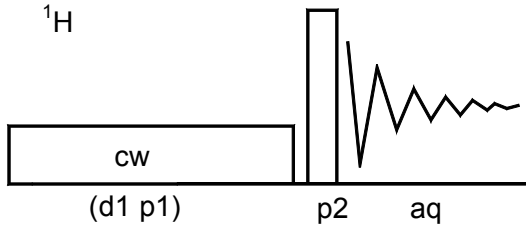

p1: x

p2: x, -x, -x, x, y, -y, -y, y

aq: x, -x, -x, x, y, -y, -y, y

Scheme 3.1-1

Common values:

d1: relaxation delay
p1: cw irradiation signal, on resonance of water, power to be adjusted
p2: 90° excitation pulse

4. Acquisition

Special values used for the spectrum shown:

Sample: 2 mM sucrose in 90 % H_2O / 10 % D_2O + 0.5 mM DSS (2,2-dimethyl-2-silapentane-5-sulfonate, sodium salt) + trace of NaN_3 against bacterial growth.
Time requirement: 5 min
Spectrometer: Bruker Avance-700 with 5-mm TBI probe

The magnet is well shimmed on the water sample. A normal ^{1}H NMR spectrum is recorded and the offset of the transmitter adjusted on the water resonance.

aq: 3.344 s
td: 64K
sw: 14 ppm
aq: 3.3 s
o1: on resonance of water signal
p1 = d1: 2 s, presaturation pulse at transmitter power level corresponding to $\gamma B_1 \approx 25$ Hz; here 0.2 mW has been used
p2: 90° ^{1}H transmitter pulse
rg: receiver gain for correct ADC input
for inverse probe heads: spinner off
ds: 4
ns: 16

5. Processing

Use standard 1D processing as described in Experiment 1.1, an exponential window with lb = 0.1 Hz was used.

6. Result

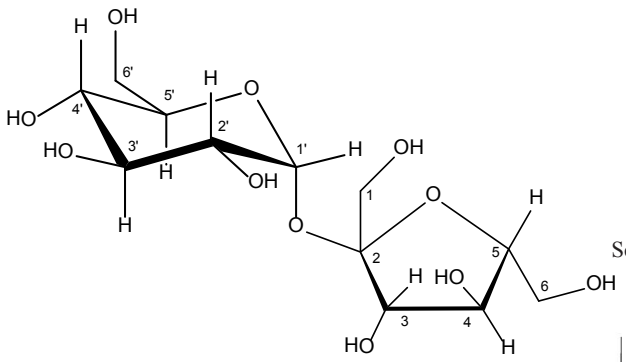

Scheme 3.1-2

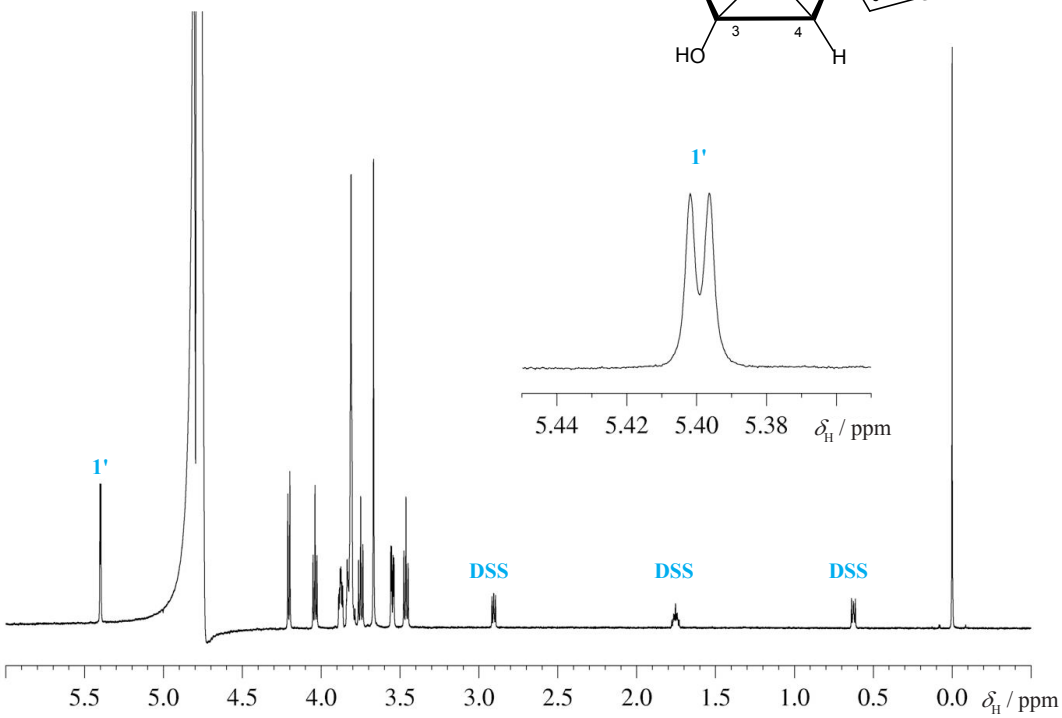

Fig. 3.1-1 Water suppression by presaturation in a 2 mM solution of sucrose

The figure shows the result of the above procedure using an inverse probe on an Avance-700 spectrometer. The quality of the result is checked by two observations: first the line width of the residual water signal at half height of the DSS signal, and second the signal-to-noise ratio and resolution of the doublet of the anomeric proton under these conditions. The residual water line width should be below 100 Hz and the splitting of the anomeric signal at δ_H = 5.41 should be visible at least down to 40 % of the signal height. Note that an even better suppression of the water signal could be obtained, although at the cost of the nearby signal of the anomeric proton.

7. Comments

For NMR probes with a very high Q factor, such as cryo probes, one observes that the best irradiation frequency is not at the apparent water resonance but several Hz off [3]. This is due to radiation damping in these probes which causes a kind of Bloch-Siegert shift. The quality of the water suppression is strongly dependent on the irradiation power and this parameter has to be adjusted for each instrument configuration.

8. Questions

A. In the sample used, what is the theoretical integral-relationship between the anomeric proton and the water signal?

B. Would this technique be appropriate in the case of peptides?

C. Could one use this technique to suppress other solvent signals, e. g., those of ethanol?

D. The three signals between 3 and 0.5 ppm stem from the DSS. Classify the spin system.

Fig. 3.1-2 Falls in Croatia

[1] P. J. Hore, "Solvent suppression" *Methods Enzym*. **1989**, *176*, 64–77.

[2] M. Guéron, P. Plateau, M. Decorps, "Solvent signal suppression in NMR" *Prog. NMR Spectrosc*. **1991**, *23*, 135–209.

[3] S. Y. Huang, C. Anklin, J. D. Walls, Y.-Ya Lin, "Sizable concentration-dependent frequency shifts in solution NMR using sensitive probes" *J. Am. Chem. Soc*. **2004**, *126*, 15936–15937.

[4] A. J. Simpson, S. A. Brown "Purge NMR: Effective and easy solvent suppression" *J. Magn. Reson*. **2005**, *175*, 340–346.

[5] N. Esturau, J. F. Espinosa "Optimization of diffusion-filtered NMR experiments for selective suppression of residual nondeuterated solvent and water signals from ^{1}H NMR Spectra of organic compounds" *J. Org. Chem*. **2006**, *71*, 4103–4110.

[6] H. Mo, D. Raftery "Pre-SAT180, a simple and effective method for residual water suppression" J. Magn. Reson. 2008, 190, 1–6.

[7] R. T. McKay, "Recent advances in solvent suppression for solution NMR: a practical reference" *Ann. Rep. NMR Spectrosc*. **2009**, *66*, 33–76.

[8] G. Zheng, W. S. Price "Solvent signal suppression in NMR" *Progr. NMR Spectrosc*. **2010**, *56*, 267–288.

Provided that the conditions outlined above are adequately fulfilled, the saturation method of solvent peak reduction functions admirably, and is adequate for most situations encountered in biochemical NMR spectroscopy. The most serious criticism of the method is that under conditions of exchange, saturation can be transferred to other spectral lines, and therefore relaxation times and intensity measurements may be in error. The technique has been employed extensively by Campbell and co-workers, who find that at 270 MHz, lines as close as 0.5 ppm to the water peak may be observed satisfactorily, the latter being "saturated" by phase randomization over a period of a second prior to accumulation.

Taken from D. I. Hoult, *J. Magn. Reson*. **1976**, *21*, 337–347.

9. Own Observations

Experiment 3.2

Solvent Suppression by 1D-NOESY

1. Purpose

The method shown here is the most often used technique for solvent suppression in the field of metabolomics, e.g., the measurement of metabolites in urine. It consists of a presaturation as shown in experiment 3.1 combined with a 1D NOESY sequence.

2. Variants

Modifications of the techniques include the FLIPSY method with additional 180° pulses for better volume selection [1]. Pulse field gradients have also been added to the sequence in our hands, however, this yielded no significant improvement.

3. Pulse Scheme and Phase Cycle

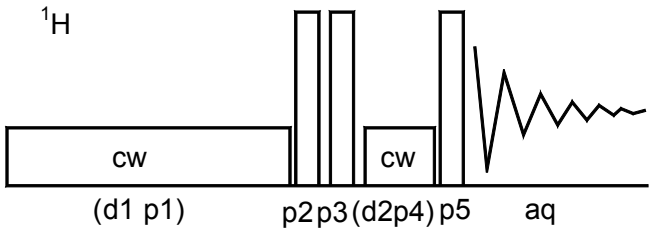

p1, p4: x, p2:x, -x, p3: $(x)_8$, $(-x)_8$, p5: x, x, -x, -x, y, y, -y, -y

aq: x, -x, -x, x, y, -y, -y, y, -x, x, x, -x, -y, y, y, -y

Scheme 3.2-1

Common values:

d1: relaxation delay
d2: short delay
p1, p4: cw irradiation signal, on resonance of water, power to be adjusted
p2, p3, p5: 90° excitation pulse

4. Acquisition

Special values used for the spectrum shown:

Sample: 2 mM sucrose in 90 % H_2O / 10 % D_2O + 0.5 mM DSS (2,2-dimethyl-2-silapentane-5-sulfonate, sodium salt) + trace of NaN_3 against bacterial growth.
Time requirement: 5 min
Spectrometer: Bruker Avance-700 with 5-mm TBI probe

The magnet is well shimmed on the water sample. A normal ^1H NMR spectrum is recorded and the offset of the transmitter adjusted on the water resonance.

td: 64K
sw: 14 ppm
aq: 3.344 s
o1: on resonance of water signal
p1=d1: 2 s, presaturation pulse at transmitter power level corresponding to $\gamma B_1 \approx 25$ Hz; here 0.2 mW has been used
p2, p3, p5: 90° ^{1}H transmitter pulse
d2: 20 µs
rg: receiver gain for correct ADC input
for inverse probe-heads: spinner off
ds: 4
ns: 16

5. Processing

Use standard 1D processing as described in Experiment 3.1, an exponential window with lb = 0.1 Hz was used.

6. Result

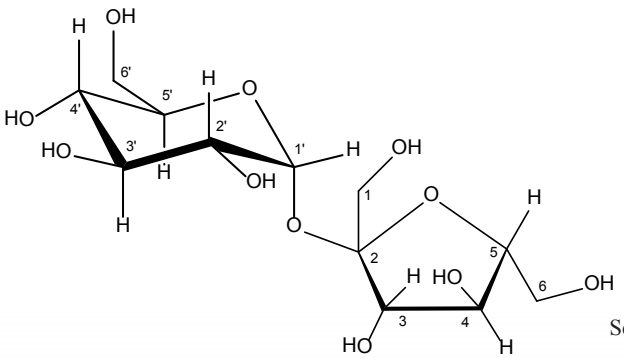

Scheme 3.2-2

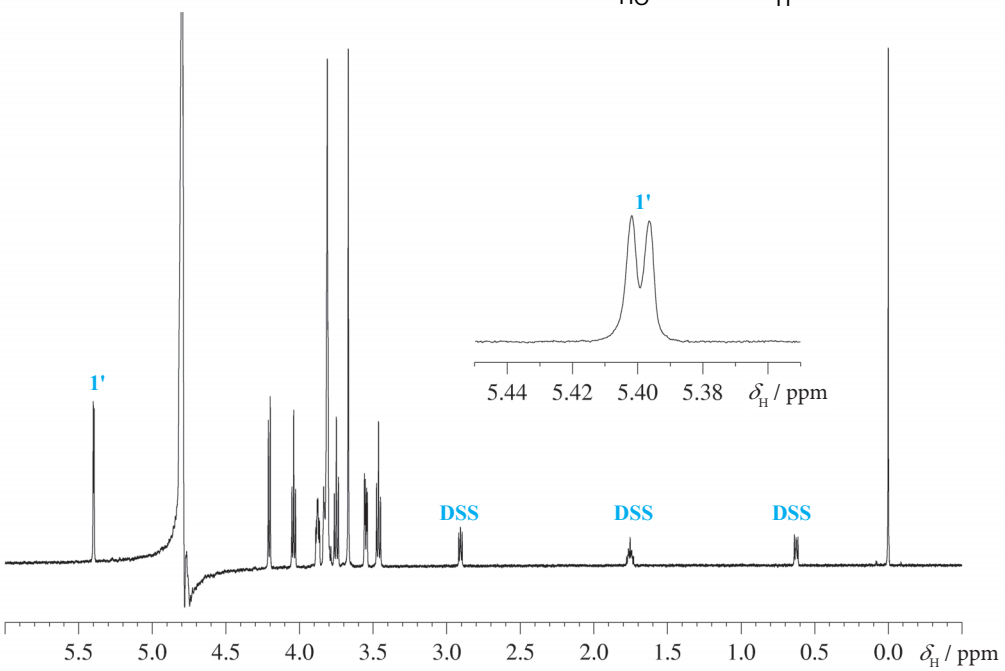

Fig. 3.2-1 Water suppression by 1D-NOESY in a 2 mM solution of sucrose

The figure shows the result of the above procedure using an inverse probe on an Avance-700 spectrometer. The quality of the result is checked by two observations, first the line-width of the residual water signal at half height of the DSS signal, and second the signal-to-noise ratio and resolution of the doublet of the anomeric proton under these conditions. The residual water line-width was here 22 Hz compared in experiment 3.1. The splitting of the anomeric signal at $\delta_H = 5.41$ should be visible at least down to 40 % of the signal height. Note that all sugar signals display their normal intensity.

Fig. 3.2-2 Falls in Croatia

Why the 1D-NOESY?
We have seen in the referred papers and reviews that many methods of solvent suppression exist. These processes can range from the simple to initiate with adequate suppression, to rapid experiments capable of suppressing multiple signals simultaneously, to complex pulse sequences with many associated NMR parameters needing detailed optimization but yielding extraordinary suppression. Despite all the choices, the 1D-NOESY seems to have become the de facto sequence of choice for NMR-based metabonomics studies. The selection of this pulse sequence has been based on several factors. The first reason was the easily obtained quality of water suppression. The second reason was the increasing number of well-established research groups utilizing the sequence (i.e., consistency). While the sequence performance is apparent, the reasons to how solvent is suppressed may not be. As mentioned, the 1D-NOESY often yields adequate solvent suppression with little optimization required. We say 'often' because in particular metabonomics samples, such as extremely dilute urine, this is not the case. A better understanding of the pulse sequence will assist us in improving these results.

Taken from ref. [4]

[1] D. Neuhaus, I. M. Ismail, C.-W. Chung "FLIPSY − A new solvent-suppression sequence for nonexchanging solutes offering improved integral accuracy relative to 1D NOESY" *J. Magn. Reson. Ser. A* **1996**, *118*, 256–263.

[2] R. T. McKay, "Recent advances in solvent suppression for solution NMR: a practical reference" *Ann. Rep. NMR Spectrosc*. **2009**, *66*, 33−76.

[3] G. Zheng, W. S. Price "Solvent signal suppression in NMR" *Progr. NMR Spectrosc*. **2010**, *56*, 267–288.

[4] R. T. McKay "How the 1D-NOESY Suppresses Solvent Signal in Metabonomics NMR Spectroscopy: An Examination of the Pulse Sequence Components and Evolution" *Concepts Magn. Reson*. **2011**, *38A*, 197–220.

7. Comments

After presaturation of the solvent signal the two 90° pulses turn the magnetization into the $-z$ direction. During the short mixing time the presaturation is continued and the final 90° pulse p5 creates transverse magnetization. On closer inspection of the NOESY phase cycle it becomes apparent that the method mainly improves the solvent suppression by a volume selection using the three 90° pulses [4].

8. Questions

A. Discuss the volume selectivity of this sequence.

B. Will a larger difference between the T_1 of the solvent and the T_1 of the solutes be helpful for the suppression of the solvent signals?

C. In gradient-modified pulse sequences one finds a z-gradient of 50% strength before the first and of −10 % before the last 90° pulse. Explain.

9. Own Observations

Experiment 3.3

Water Suppression by SOGGY-Excitation Sculpting

1. Purpose

In 1995 Hwang and Shaka [1] published a general pulse scheme for the suppression of strong solvent signals, especially water, which was termed "excitation sculpting". It consists of an excitation profile **S** embedded between two pulsed field gradients **G**. The main trick to achieve a flat baseline is to apply this scheme twice, using the sequence [$\mathbf{G}_1$ **S** $\mathbf{G}_1$] [$\mathbf{G}_2$ **S** $\mathbf{G}_2$], where the two gradients $\mathbf{G}_1$ and $\mathbf{G}_2$ are not correlated to each other. As an excitation profile Hwang and Shaka used in their original paper the 3-9-19 binomial sequence, which essentially acts as zero excitation at the offset equal of the water resonance and as a 180° pulse for all other signals of the sample. The delay d2 between the 3-9-19 pulses has to be adjusted according to the frequency of the spectrometer used, since there is zero excitation at points at +/− (1/d2).

2. Variants

Although the original excitation sculpting was extremely successful, there have been numerous attempts to further improve the signal suppression and to avoid the suppression of nearby signals. Other binomial sequences such as "W5" have been proposed, or combination of soft and hard pulses such as ($90°_{soft}$, $180°_{hard}$, $90°_{soft}$) or ($180°_{hard}$, $180°_{soft}$), where the soft pulses act only on the water resonance. We show here the SOGGY variant [4] in which one soft 180° pulse is combined with a set of four composite pulses which add together to a hard 180° pulse. According to the authors, this seems currently the most efficient water suppression technique available and has no additional zero excitation points.

3. Pulse Scheme and Phase Cycle

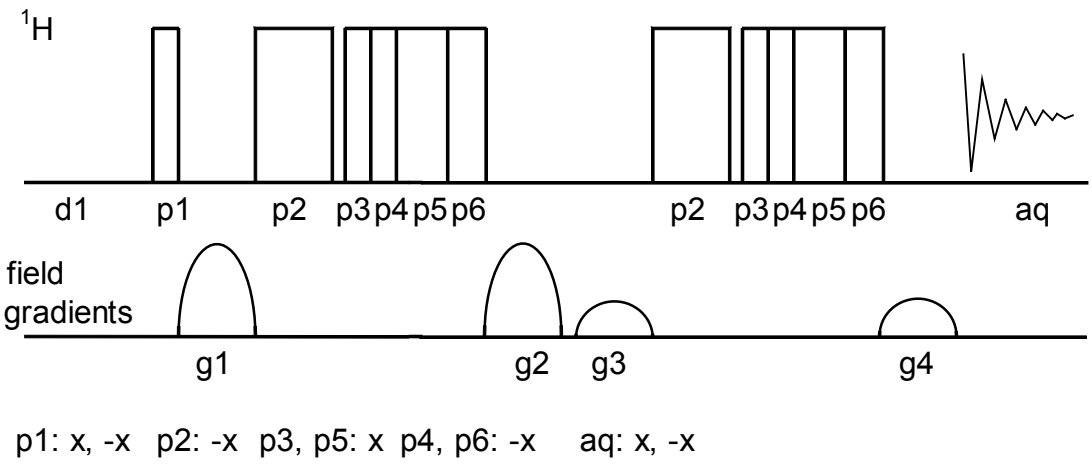

Scheme 3.3-1

Fig. 3.3-1 A. J. Shaka

Common values:

d1: relaxation delay
p1: 90° excitation pulse
p2: 180° selective excitation pulse on water resonance, special value
p3-p6: composite 180° pulse, (81° x, 81° -x, 342° x, 162° -x) at a power level of an 90° pulse with 30 µs length (at 700 MHz) to 40 µs length (at 400 MHz)

4. Acquisition

Special values used for the spectrum shown:

Sample: 2 mM sucrose in 90 % H_2O / 10 % D_2O + 0.5 mM DSS (2,2-dimethyl-2-silapentane-5-sulfonate, sodium salt) + trace of NaN_3 against bacterial growth.
Time requirement: 5 min
Spectrometer: Bruker Avance-700 with 5-mm TBI probe

The probe head must be tuned to the sample used. Record a normal ^1H NMR spectrum and center the offset at the water resonance.

td : 64K
sw: 10 ppm
aq: 4.462 s
o1: on water resonance
p1: 90° ^1H transmitter pulse
p2: 2 ms, 43.5 dB (100W amplifier used), rectangular shape
p3: 27 µs 13.85 dB
p4: 27 µs 13.85 dB
p5: 114 µs, 13.85 dB
p6: 54 µs, 13.85 dB
d1: 2 s
g1, g2, g3, g4: pulsed field gradients, 500 ms length,
ratio 40 % : 40 % : 12 % : 12 %, "sine.100" shape (100 % ≈ 0.56 T/m)
ds: 4
ns: 16

5. Processing

Use standard 1D processing as described in Experiment 1.1 with exponential multiplication (lb = 0.5 Hz) and a baseline correction.

Fig. 3.3-2 Falls in Croatia

The early days of pulsed NMR were an exciting time to be a bright- eyed graduate student – even one studying abroad in a system that could seem at once magical and Kafkaesque. Luck, hard work, the healthy spirit of competition, a helpful hand or two at crucial moments, and a steady hand guiding the entire group were all factors that produced an interesting product. Two-dimensional spectroscopy was one of the most intriguing topics to study, and in the late 1970s, there were only a handful of groups doing it. While adjusting to Oxford took some time and was not painless, the author has no regrets and would do it again in a second.

A. J. Shaka, "Stay in School and You May End Up Flipping…Spins!" *Encyclopedia of Magnetic Resonance* , **2011**

6. Result

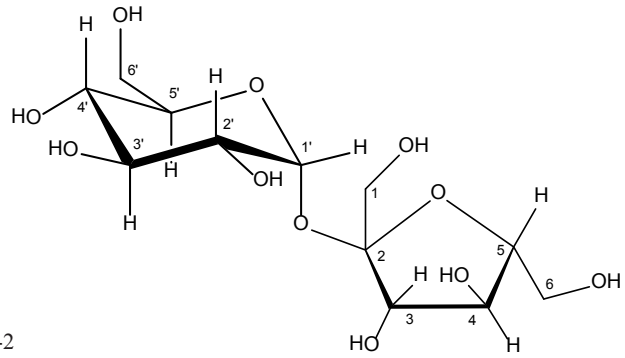

Scheme 3.3-2

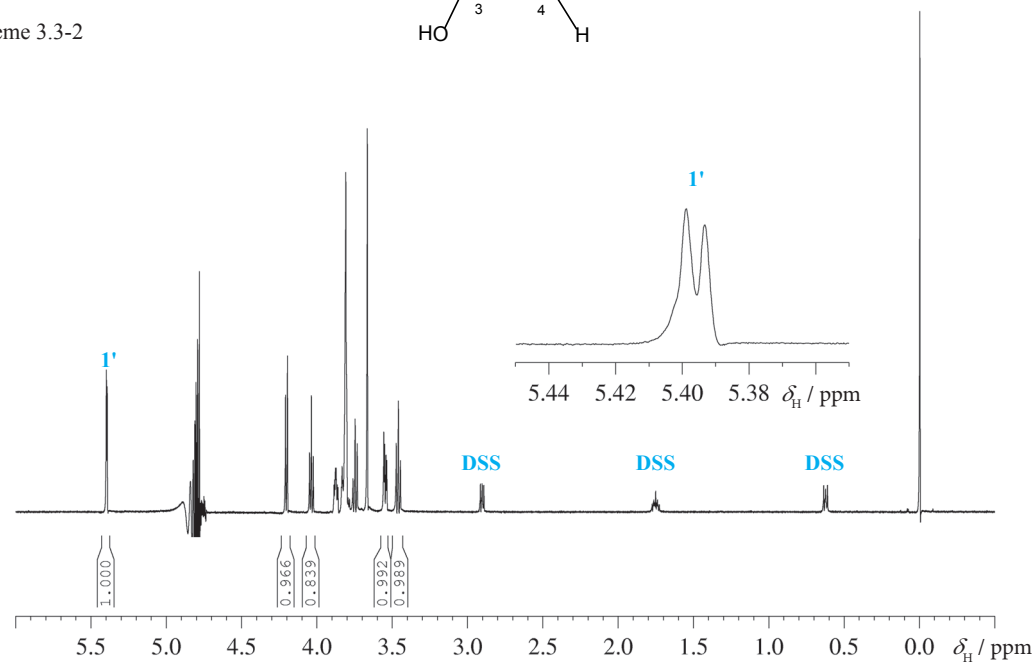

Fig. 3.3-3 Water suppression by SOGGY in a 2 mM solution of sucrose

The figure shows the result obtained on an Avance 700 spectrometer Note the correct integrals of the two protons nearby the water signal.

7. Comments

By an elegant matrix treatment given in [1] it can be shown that on applying the filter sequence twice, all base-line distortions and phasing problems are eliminated as long as g1 and g2 are not correlated to g3 and g4. Fine tuning may be necessary at the specific spectrometer and probe head used. As an additional exercise you may try replacing the ($180°_{soft}$, 180° composite pulse) part of the sequence by other schemes, such as a binomial sequence, e.g., the "W5" sequence [6].

[1] T.-L. Hwang, A. J. Shaka, "Water suppression that works. Excitation sculpting using arbitrary waveforms and pulsed field gradients." *J. Magn. Reson. Ser. A* **1995**, *112*, 275–279.

[2] A. Jerschow, "Unwanted signal leakage in excitation sculpting with single axis gradients" *J. Magn. Reson*. **1999**, *137*, 206–214.

[3] E. Prost, P. Sizun, M. Piotto, J.-M. Nuzillard, "A simple scheme for the design of solvent-suppression pulses" *J. Magn. Reson*. **2002**, *159*, 76–81.

[4] B. D. Nguyen, X. Meng, K. J. Donovan, A.J. Shaka "SOGGY: Solvent-optimized double gradient spectroscopy for water suppression. A comparison with some existing techniques" *J. Magn. Reson*. **2007**, *184*, 263–274.

[5] G. Zheng, A. M. Torres, W. S. Price "Solvent suppression using phase-modulated binomial-like sequences and applications to diffusion measurements." *J. Magn. Reson*. **2008**, *194*, 108–114.

[6] M. Liu, X. Mao, C. He, H. Huang, J. K. Nicholson, J. C. Lindon, "Improved WATERGATE pulse sequence for solvent suppression in NMR sprectroscopy" *J. Magn. Reson*. **1998**, *132*, 125−129.

8. Questions

A. Estimate the excitation bandwidth of a 2 ms 180° pulse

B. Discuss the action of the 81–x, 81 –x, 342 x, 162–x composite pulse

C. What is the main advantage over the original excitation sculpting sequence using the binomial 3-9-19 filter?

9. Own Observations

Experiment 3.4

Solvent Suppression Using WET

1. Purpose

Among the many solvent suppression schemes, the WET (**W**ater suppression **E**nhanced through T_1 effects) sequence has become very popular, especially in the field of hyphenated techniques such as HPLC-NMR, although it was originally introduced for localized *in vivo* spectroscopy. The method uses selective pulses on the solvent resonance, which may contain more than one frequency band in the case of dual solvent systems and pulsed field gradients to dephase the residual solvent magnetization. For comparison with the other water suppression techniques demonstrated in this book (see Exps. 3.1 to 3.3), the performance of the method is again shown for the 2 mM sucrose sample. A special composite excitation pulse is used at the end of the sequence.

2. Variants

Several different schemes for the sequence of the selective pulses followed by pulse field gradients have been discussed in the literature [2,3] For the suppression of organic solvents like acetonitrile used in LC applications it is advisable to apply ^{13}C decoupling in order to remove also the ^{13}C satellites of the solvent signals. Combinations with NOESY are known, as well as with other 2D methods (COSY, TOCSY).

Common values:

d1: relaxation delay
p1: 81.4° selective pulse
p2: 101.4° selective pulse
p3: 69.3° selective pulse
p4: 161.0° selective pulse
p5, p6, p7, p8: 90° ^1H transmitter pulse
d2: gradient ring down delay
d3: relaxation delay for solvent signal

3. Pulse Scheme and Phase Cycle

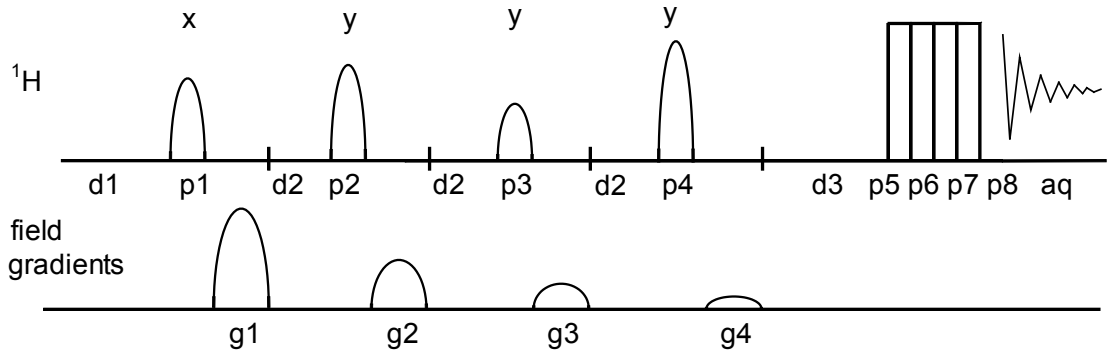

p5: y, -y, -y, y, -x, x, x, -x
p6: -x, x, -x, x, -y, y, -y, y
aq: x, -x, x, -x, y, -y, y, -y
p7: -y, y, y, -y, x, -x, -x, x
p8: x, -x, x, -x, y, -y, y, -y

Scheme 3.4-1

4. Acquisition

Special values used for the spectrum shown:

Sample: 2 mM sucrose in 90 % H_2O / 10 % D_2O + 0.5 mM DSS (2,2-dimethyl-2-silapentane-5-sulfonate, sodium salt) + trace of NaN_3 against bacterial growth.
Time requirement: 5 min
Spectrometer: Bruker Avance-700 with 5-mm TBI probe

The probe head must be tuned to the sample used; the temperature should be regulated and controlled to 298 K. Record a normal ^{1}H NMR spectrum and center the offset at the water resonance. Determine the attenuation for a 90° selective square pulse of 2 ms (see Exp.8.1) [here 42 dB was used].

td : 64K
sw: 14 ppm
aq: 3.33 s
o1: on water resonance
d1: 2 s
d2: 2 ms
d3: 10 ms
p1: square shape, 2 ms, (42 + 0.87) dB = 42.87 dB
p2: square shape, 2 ms, (42 − 1.04) dB = 40.96 dB
p3: square shape, 2 ms, (42 + 2.27) dB = 44.27 dB
p4: square shape, 2 ms, (42 − 5.05) dB = 36.95 dB
p5, p6, p7, p8: 8.75 µs, + 4 dB
g1−g4: sinusoidal-shaped field gradients, 2 ms duration, Gradient strength ratio: 80 % : 40 % : 20 % : 10 % (100 % ≈ 0.56 T/m).
ds: 8
ns: 16

5. Processing

Use standard 1D processing as described in Experiment 1.1 with exponential multiplication (lb = 0.1 Hz) and a base line correction.

6. Result

The figure shows the result obtained on an Avance-700 spectrometer with a 5 mm inverse multinuclear gradient probe. Compare the result with those in Exps. 5.1 to 5.3 and observe the integration of the sugar resonances.

Fig. 3.4-2 Falls in Croatia

One of the major impediments to the wider growth of the field is the difficulty of observing analyte resonances in the presence of the larger resonances from the mobile phase. While this problem appears similar to the well-known problem of water suppression in normal liquid-phase biomolecular NMR samples it is exacerbated by three additional characteristics: (1) in typical reversed-phase HPLC mobile phases, there is more than one protonated solvent resonance (and all corresponding 13C satellites); (2) the sample in the detector coil is typically flowing, and this replenishment of fresh spins complicates many solvent suppression techniques, such as presaturation; (3) the solvent resonances change during the course of the solvent gradients (the chromatography "method") thus presenting the spectroscopist with moving targets.

Taken from ref. [2]

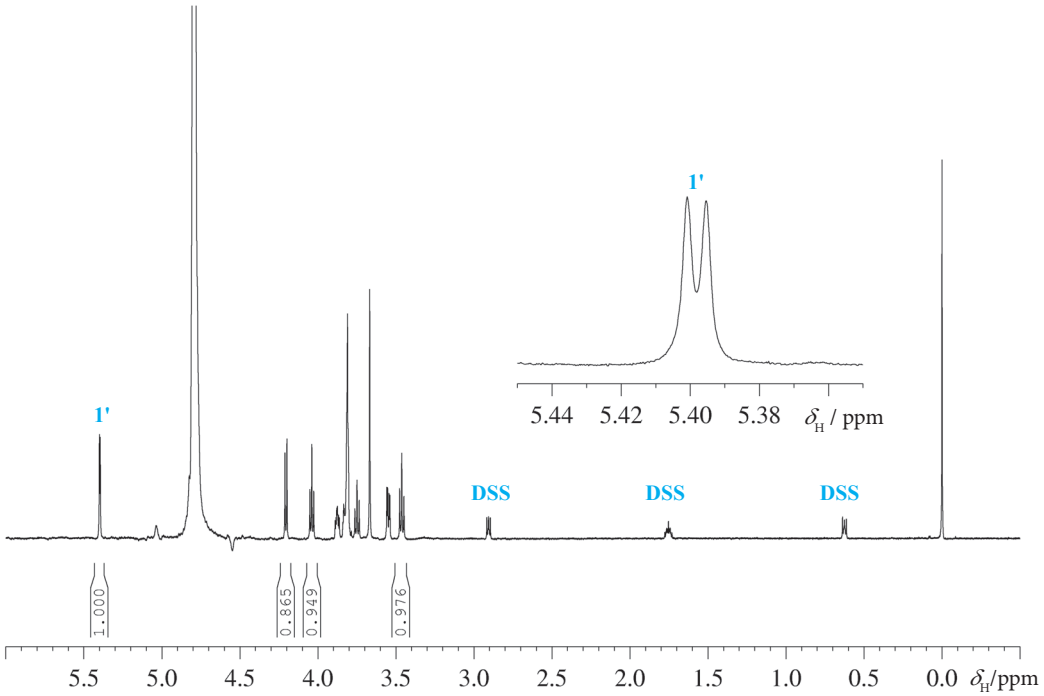

Fig. 3.4-2 Water suppression by WET in a 2 mM solution of sucrose

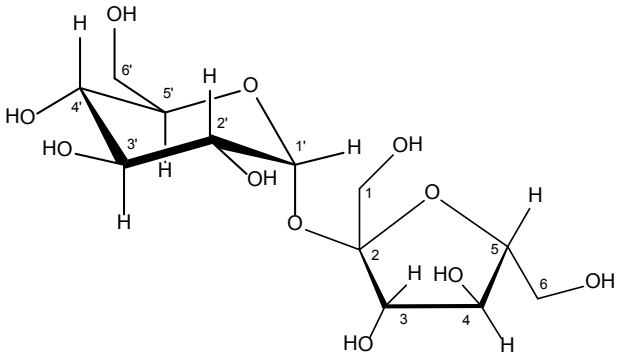

Scheme 3.4-2

7. Comments

The basic idea of this solvent suppression method is first to excite only the solvent signal by a selective pulse and to dephase this transverse magnetization using a pulsed field gradient. A subsequent hard r.f. pulse will then excite only the resonances of the solutes, because no longitudinal magnetization of the solvent remains. This scheme has been optimized by a computer simulation [1], leading to a fourfold selective excitation with pulses of different lengths and gradients of different strengths. This results in a very effective suppression of the solvent resonance. The final excitation is performed by a spatially-selective composite pulse [4], which gives better base-line performance at the residual solvent line.

[1] R. J. Ogg, P. B. Kingsley, J. S. Taylor, "WET, a T_1 and B_1 insensitive water suppression method for *in vivo* localized ^{1}H NMR spectroscopy" *J. Magn. Reson. Ser. B* **1994**, *104*, 1–10.

[2] S. H. Smallcombe, S. L. Patt, P. A. Keifer, "WET solvent suppression and its applications to LC NMR and high-resolution NMR spectroscopy" *J. Magn. Reson. Ser. A* **1995**, *117*, 295–303.

[3] S. Zhang, X. Yang, D. G. Gorenstein, "Enhanced suppression of residual water in a "270" WET sequence" *J. Magn. Reson*. **2000**, *143*, 382–386.

[4] A. Bax, "A spatially selective composite 90° radiofrequency pulse" *J. Magn. Reson*. **1985**, *65*, 142–145.

[5] G. Zheng, W. S. Price "Solvent signal suppression in NMR" *Progr. NMR Spectrosc*. **2010**, *56*, 267–288.

The shape of the selective pulses may be varied. The authors of [2] recommend, e.g., a SEDUCE shape, modulated for one or two frequencies (acetonitrile, water). The relaxation delay d3 may be optimized for the sample, 10 ms is an recommended value.

8. Questions

A. In typical HPLC applications a water/acetonitrile mixture is used with a solvent gradient during the run. What are the problems for solvent suppression in such experiments?

B. Inform yourself about the spatial selectivity of the composite pulse used.

C. How would the WET sequence react with exchangeable OH and NH protons?

9. Own Observations

[6] S. J. Kim, S. M. Kim, M. C. Kim, S. W. Kang, B. H. Um "Fast identification of flavonoids in the roots of *Sophora flavescens* by on-flow LC-NMR" *J. Med. Plants Research* **2010**, *4*, 2452–-2459.

Experiment 3.5

SELTOCSY

1. Purpose

This is the 1D variant of the TOCSY experiment (see Chapter 2.3). Instead of recording the full 2D matrix, one can simply measure one "row" by selective excitation, thus looking only for spin couplings that affect the particular proton excited. The gradient-selected method demonstrated here gives clean results without the need for phase cycling, using only one or two scans. A recent variant is shown which uses a 180° selective pulse for the selection of a specific proton resonance. The selective TOCSY experiment finds its main application in the field of carbohydrates as an assignment tool and in metabolomics.

2. Variants

Different spin lock variants have been used for this purpose and different shapes of selective pulses may be used.The sequence shown here, in addition, uses one form of zero-quantum coherence suppression.

3. Pulse Scheme and Phase Cycle

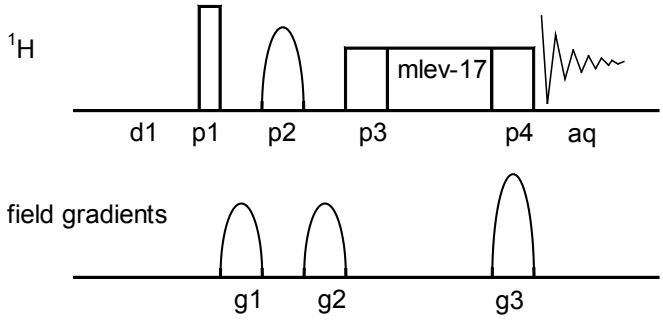

p1: x, -x p2: x, x, y, y, -x, -x, -y, -y p3, p4: y aq: x, -x, -x, x

Fig. 3.5-1

4. Acquisition

Special values used for the spectrum shown:

Sample: 20 mg sucrose in 0.7 ml D_2O
Time requirement: 5 min
Spectrometer: Bruker Avance-700 with 5-mm TBI probe

The probe must be tuned to the sample used; the temperature should be regulated and controlled to 298 K. Record a normal ^1H NMR spectrum and center the offset at the water resonance. Determine the attenuation for a 180° Gaussian pulse of 50 ms (see Exp. 8.3) [here 64 dB was used].

In this paper we describe how two-dimensional NMR experiments can be converted to analogous one-dimensional experiments with the aid of Gaussian pulses. These 1D techniques have distinct advantages over 2D experiments when a limited amount of information is desired. This is often the case for medium-sized molecules. The requirements in storage capacity and acquisition as well as data manipulation time for these 1D experiments are drastically reduced compared to corresponding 2D techniques.
In addition, some of the 1D techniques proposed here have unique properties for which no practical equivalent in 2D NMR exists.

Taken from ref.[1]

Common values:

d1: relaxation delay
p1: 90° transmitter pulse
p2: selective 180°Gaussian pulse
p3, p4: trim pulses

td: 32K
sw: 5 ppm
aq: 4.68 s
o1: on resonance of water signal.
p1: 90° ^{1}H transmitter pulse
p2: 180° Gaussian shape ^{1}H transmitter pulse, 50 ms length, transmitter attenuation corresponding to 180° excitation [64 dB]
p3, p4: trim pulses 2.5 ms at 17.1 dB
MLEV-17 series of composite pulses at 17.1 dB corresponding to a 90° pulse of 40 µs, total spin lock time [p3 + p4 + (MELV-17)] to be varied from 20 to 140 ms
d1: 2s
g1−g3: sinusoidal-shaped field gradients
Gradient strength ratio: 15 : 15 : 40
ns: 2
ds: 4

5. Processing

Use standard ^{1}H processing with exponential line broadening using lb = 0.3 Hz.

6. Result

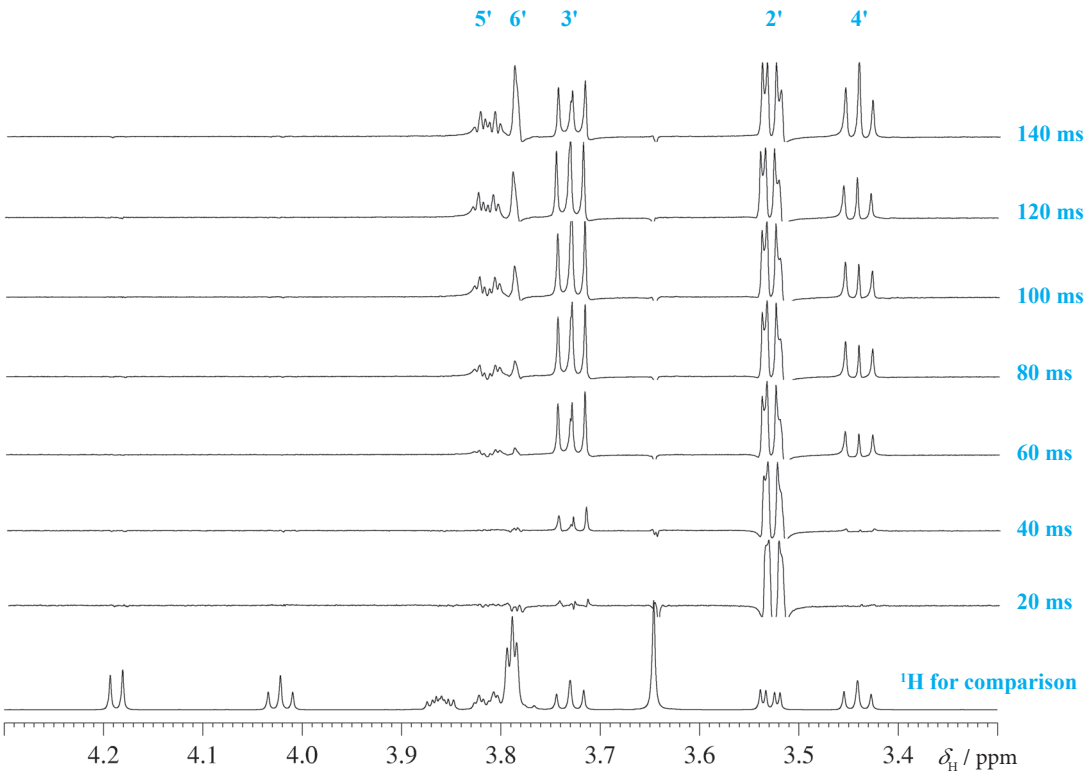

Fig. 3.5-2 Series of SELTOCSY spectra for sucrose, irradiation of H-1'

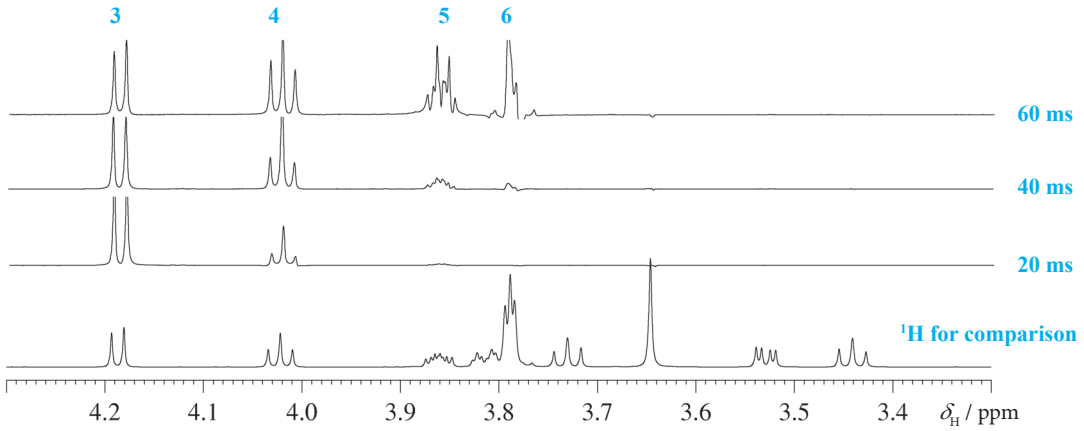

Fig. 3.5-3 Series of SELTOCSY spectra for sucrose, irradiation of H-3

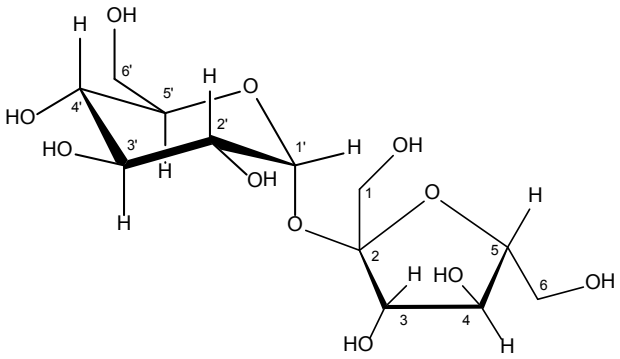

Fig. 3.5-4 Sucrose

The figures show the result for a 3 % solution of sucrose in D_2O. In the first series the anomeric proton at $\delta_H = 5.384$ ppm was irradiated by the selective pulse. When the mixing time was increased from 20 to 140 ms all protons of the glucose unit emerged subsequentially. Similarly, in the second series the proton H-3 at $\delta_H = 4.19$ ppm of the fructose unit was irradiated. Note that there is no spill-over by the TOCSY transfer between glucose and fructose within the sucrose. Compare the result with the 2D spectrum in experiment 2.3.

7. Comments

The first 90° ^{1}H transmitter pulse excites all proton resonances. In the following [gradient pulse, selective 180° pulse, gradient pulse] sandwich, all these resonances are dephased and only the one chosen by the selective 180° pulse is retained. Since a selective 180° pulse is applied, its relative phase with respect to the "hard" pulses does not need to be determined. During the last trim pulse p4 of the spin-lock sequence a strong pulsed field gradient is applied. This diminishes contribution and thus phasing errors introduced by zero-quantum coherences.

Since the experiment requires only a few minutes, it is ideal for studying the influence of the spin-lock length on the number of signal responses as well as their relative intensities and signal shapes.

[1] H. Kessler, H. Oschkinat, C. Griesinger, W. Bermel, "Transformation of homonuclear two-dimensional NMR techniques into one-dimensional techniques using Gaussian pulses" *J. Magn. Reson*. **1986**, *70*, 106−133.

[2] T. Fäcke, S. Berger, "Application of pulsed field gradients in an improved selective TOCSY experiment" *J. Magn. Reson. Ser. A* **1995**, *113*, 257−259.

[3] C. Dalvit, S. Y. Ko, J. M. Böhlen, "Single and multiple-selective excitation combined with pulsed field gradients" *J. Magn. Reson. Ser. B* **1996**, *110*, 124−131.

[4] M. J. Thrippleton, J. Keeler, "Elimination of zero-quantum interference in two-dimensional NMR spectra" *Angew. Chem. Int. Ed*. **2003**, *42*, 3938−3941.

[5] P. W. A. Howe "Removal of zero-quantum peaks from 1D selective TOCSY and NOESY spectra" *J. Magn. Reson*. **2006**, *179*, 217–222.

[6] P. Sandusky, E. A. Amponsah, D. Raftery "Use of optimized 1D TOCSY NMR for improved quantitation and metabolomic analysis of biofluids" *J. Biomol NMR* **2011** *49*, 281–290.

8. Questions

A. Find a "handwaving" argument to explain why the TOCSY transfer works.

B. Why do we need 140 ms as a mixing time for the glucose unit to show the full pattern; in the fructose, however, only 60 ms?

C. Why is there no spill-over of the magnetization between the glucose and fructose units?

9. Own Observations

Experiment 3.6

SELNOESY

1. Purpose

The 1D NOE difference technique can suffer from artifacts caused by insufficient spectrometer stability. Very weak NOE effects are often obscured by residual signals. By using pulsed field gradients, unwanted signals can be better suppressed and, with a selective excitation pulse tailored to the multiplet under consideration, the desired NOE effects can be recorded without interference from other signals. This is achieved by combination of the gradient spin echo method and NOE spectroscopy and results in spectra without phase distortion. This technique has become the standard of nuclear Overhauser difference spectroscopy.

2. Variants

There are variants with a double spin echo, but in our hands already the single spin echo has seemed to be sufficient. The choice of the best selective pulse shape is quite debatable; here we used a REBURP shape, but a 50 ms Gaussian pulse is probably easier to use. There are also methods which include zero-quantum filtering.

3. Pulse Scheme and Phase Cycle

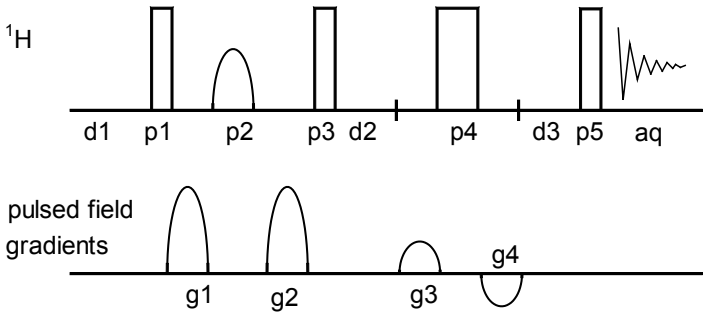

p1: x, -x p2: $(x)_2$, $(y)_2$, $(-x)_2$, $(-y)_2$ p3, p4, p5: x aq: x, -x, -x, x

Scheme. 3.6-1

4. Acquisition

Special values used for the spectrum shown:

Sample: 3 % strychnine in $CDCl_3$
Time requirement: 10 min
Spectrometer: Bruker Avance-700 with 5-mm TBI probe

The probe head must be tuned to the sample used; the temperature should be regulated and controlled to 298 K.

td: 50K data points
sw: 12 ppm
aq: 3.0 s
o1: middle of ^{1}H NMR spectrum

Common values:

d1: relaxation delay
p1, p3: 90° transmitter pulse
p2: selective 180° pulse
p4: 180° transmitter pulse
d2 + d3: NOE mixing time

p1, p3: 90° ^{1}H transmitter pulse, 9.1 µs, 4 dB
p2: selective 180° ^{1}H transmitter pulse, REBURP shape, 116.3 ms length, modulated with the difference Δ between o1 and the off set of the signal to be irradiated, transmitter attenuation corresponding to 180° [58.2 dB]
p4: 180° ^{1}H transmitter pulse, 18.2 µs, 4 dB
d1: 3 s
d2, d3: 0.5 s; i.e. mixing time 1.0 s
g1−g4: sinusoidal-shaped field gradients, 1 ms duration. Ratio 15 % : 15 % : 40 % : −40 % (100 % ≈ 0.56 T/m)
ds: 4
ns: 32

5. Processing

Use standard 1D processing with exponential multiplication (lb = 0.3 Hz which may be extended to 0.5 ... 1.0 Hz to reduce difference artifacts). Adjust a negative phase for the irradiated multiplet.

6. Result

The figure shows the result obtained on an Avance-700 spectrometer in a 5 mm inverse gradient probe head. **a** is the normal ^{1}H NMR spectrum. In **b** the selective pulse was adjusted on the signal of H-8 at δ_H = 3.86; strong NOE effects are observed for H-18β (δ_H = 2.88), H-11β (δ_H = 2.67), both H-17 (δ_H = 1.90), and H-13 (δ_H = 1.28). Note the very small NOE effect for H-12 (δ_H = 4.29) and the small negative effect for H-18α (δ_H = 3.22).

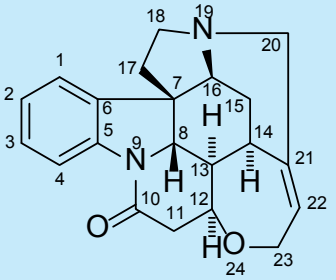

Scheme. 3.6-2

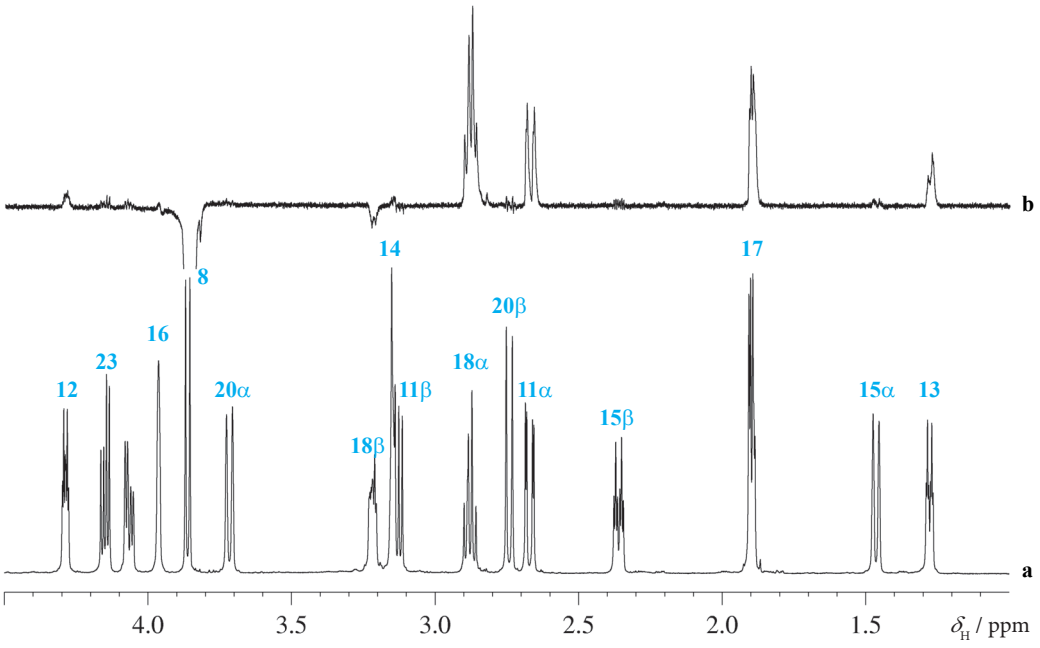

Fig 3.6-1 Selective NOESY spectrum of strychnine, irradiation of H-8

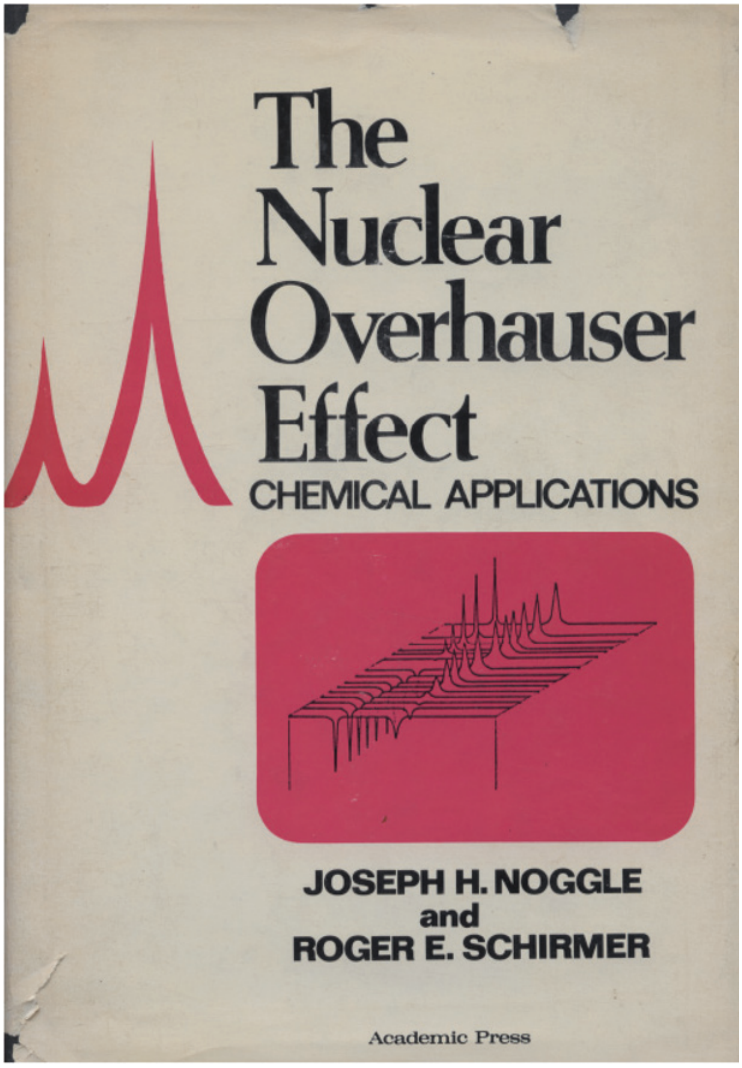

Fig. 3.6-2 The earliest book on NOE, 1971

7. Comments

After the first r.f. pulse all spins are dephased by the pulsed field gradient g1. The coherence order is changed only for the signal selected by the shaped r.f. pulse p2; thus only this is rephased by the gradient pulse g2, whereas all other signals are further dephased. The selected magnetization is moved into the negative *z*-direction by the r.f. pulse p4. During the mixing time [d2 + d3] cross-relaxation occurs, and the NOE result is transformed into observable magnetization by the read pulse p5. In the mixing time a 180° pulse p4 inverts the *z*-magnetization caused by relaxation; the gradient pulses g3 and g4 remove any *x,y* components caused by an imperfect 180° pulse. The phase cycle provides a difference mode.

Note that, like the NOESY experiment 1.4, this experiment belongs to the transient methods.

The nuclear Overhauser effect (NOE), which is the change in the integrated intensity of the NMR absorption of a nuclear spin as a result of the concurrent saturation of another NMR resonance, has found limited use over the past two decades in the study of chemical kinetics and, somewhat more recently, in the assignment of NMR spectra. Lately, interest in the NOE has grown enormously following the realization that detailed qualitative and quantitative information on molecular configuration and conformation can be obtained from it. The uniqueness of this approach to problems in molecular structure, together with the increasing availability of NMR spectrometers sufficiently sophisticated for NOE studies and sufficiently simple in operation to be used on a routine basis, have increased and will continue to increase the applications of the method manyfold.

Taken from the preface of the book shown above.

[1] J. Stonehouse, P. Adell, J. Keeler, A. J. Shaka, "Ultrahigh-Quality NOE Spectra" *J. Am. Chem. Soc*. **1994**, *116*, 6037−6038.

[2] K. Stott, J. Stonehouse, J. Keeler, T.-L. Hwang, A. J. Shaka, "Excitation sculpting in high-resolution nuclear magnetic resonance spectroscopy: Application to selective NOE experiments" *J. Am. Chem. Soc*. **1995**, *117*, 4199−4200.

[3] K. Stott, J. Keeler, Q. N. Van, A. J. Shaka, "One-dimensional NOE experiments using pulsed field gradients" *J. Magn. Reson*. **1997**, *125*, 302−324.

[4] A. Bagno, F. Rastrelli, G. Scorrano "Detecting intermolecular NOEs by means of a novel DPFGSE pulse sequence. Application to the solvation of carbohydrates in binary mixtures" *J. Magn. Reson*. **2004**, *167*, 31–33.

[5] H. Hu, K. Krishnamurthy "Revisiting the initial rate approximation in kinetic NOE measurements" *J. Magn. Reson*. **2006**, *182*, 173–177.

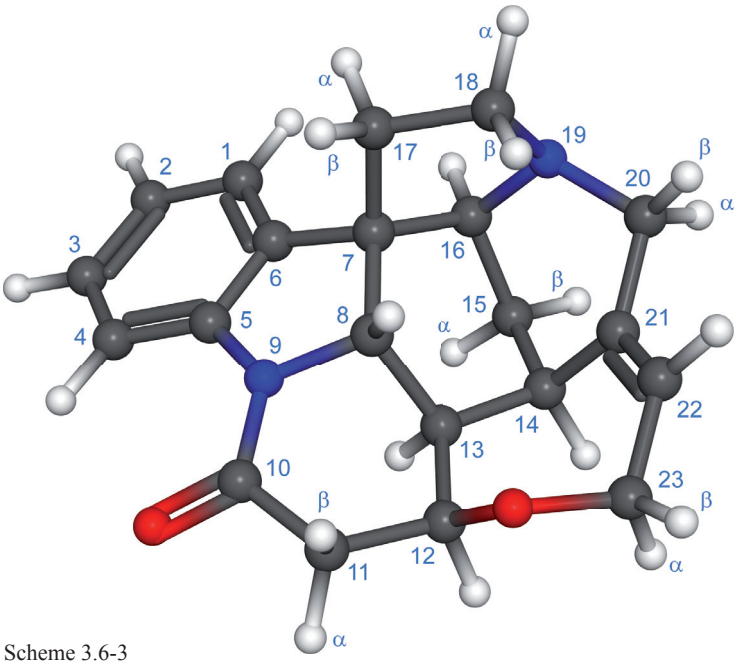

Scheme 3.6-3

8. Questions

A. Why can one observe negative NOE effects, such as the signal for H18α?

B. Can one obtain NOE build-up curves with this method?

C. Why is the signal of H-13 significantly smaller than those of H-18β and H-11β?

9. Own Observations

Experiment 3.7

SELINCOR

1. Purpose

This experiment yields 1D proton spectra in which the desired proton signal is selected via a selective pulse on the directly bonded ^{13}C nucleus using the $^{1}J(C,H)$ spin coupling in an HSQC manner. The elimination of the signals of protons bonded to ^{12}C is achieved by pulsed field gradients. Here we show a recent gradient-selected SELINCOR version [5] which uses a 180° selective pulse on carbon, and is applied to strychnine as an example. The sequence will be chosen to identify protons in a crowded region due to the higher dispersion of the corresponding carbon signals.

2. Variants

The pulse scheme can serve as an initial building block for a variety of further sequences such as SELINCOR-COSY [2], SELINCOR-TOCSY [3], or 2D *J*-resolved spectroscopy [6] and for the measurement of CH spin coupling constants [4, 7].

3. Pulse Scheme and Phase Cycle

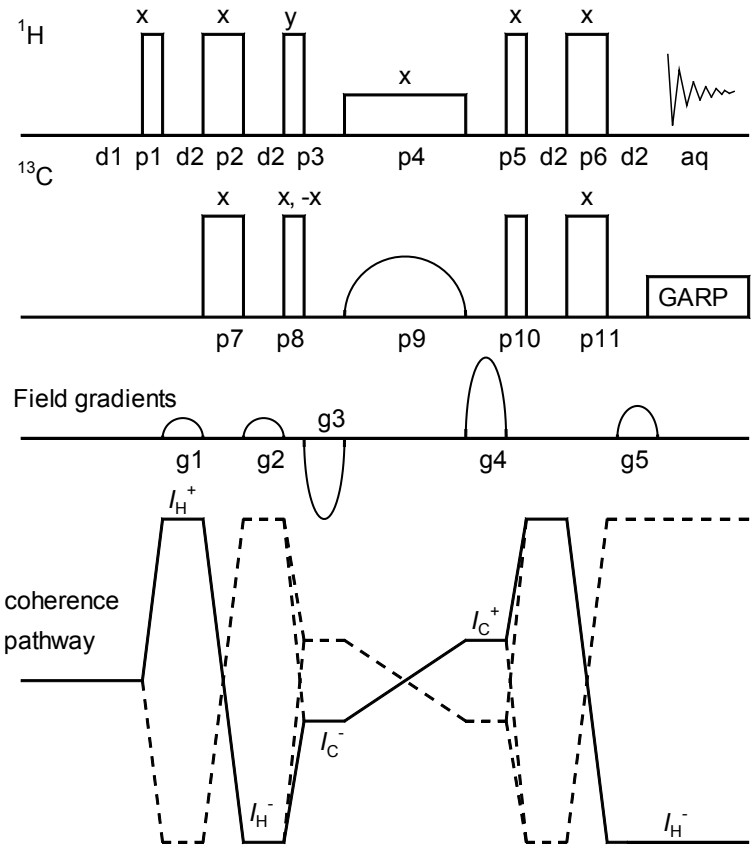

Scheme 3.7-1

Common values:

d1: relaxation delay
d2: $1/[4J_{CH}]$
p1, p3; p5: 90° ^{1}H transmitter pulse
p2, p6: ^{1}H 180° transmitter pulse
p8, p10: 90° ^{13}C transmitter pulse
p7, p11: 180° ^{13}C transmitter pulse
p4: ^{1}H spin lock pulse for decoupling
p9: selective 180° Gaussian pulse on carbon

p9: x, x, y, y, -x. -x, -y, -y
p10: x, x, -x, -x
aq: x, -x, -x, x

4. Acquisition

Special values used for the spectrum shown:

Sample: 3 % strychnine in $CDCl_3$
Time requirement: 5 min for each selected carbon atom
Spectrometer: Bruker Avance-700 with 5-mm TBI probe

The probe must be tuned to the sample used; the temperature should be regulated and controlled to 298 K.

td:	4K
sw:	10 ppm
aq:	293 ms, reduced due to GARP decoupling during acquisition,
o1:	middle of ^{1}H NMR spectrum
o2:	middle of ^{13}C NMR spectrum
p1, p3, p5:	90° ^{1}H transmitter pulse [9.75 µs at 4 dB]
p2, p6:	180° ^{1}H transmitter pulse [19.5 µs at 4 dB]
p8, p10:	90° ^{13}C decoupler pulse [13.4 µs at 3 dB]
p7, p11:	180° ^{13}C decoupler pulse [26.8 µs at 3 dB]
p4:	^{1}H spin lock pulse, same length as p9 [50 ms, 16 dB]
p9:	selective 180° ^{13}C decoupler pulse, Gaussian shape, 50 ms [61 dB]
d1:	2 s
d2:	$1/[4J(C,H)] = 1.8$ ms, calculated from $^{1}J(C,H) \approx 140$ Hz, adjusted the signal in question.
g1−g5:	sinusoidal-shaped field gradients, 1 ms duration. Gradient strength ratio: 5 % : 5 % : −40 % : 40 % : 20.1 % (100 % ≈ 0.56 T/m)
^{13}C decoupler attenuation and 90° pulse for GARP (18 dB, 70 µs)	
ns:	32

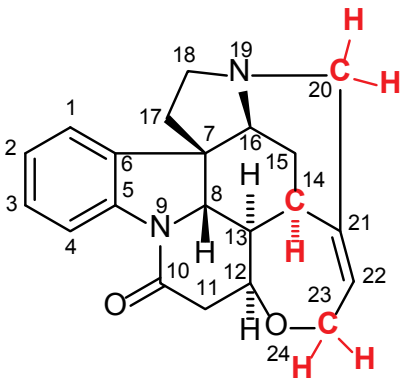

Scheme 3.7-2

[1] S. Berger "Selective inverse correlation of ^{13}C and ^{1}H NMR signals, an alternative to 2D NMR" *J. Magn. Reson*. **1989**, *81*, 561−564.

[2] T. Fäcke, S. Berger, "Gradient-enhanced SELINCOR for selective excitation in a ^{13}C-resolved COSY experiment" *Magn. Reson. Chem*. **1995**, *33*, 144−148.

[3] T. Fäcke, S. Berger, "Complete proton assignment in acetylcholesterol using ge-SELINCOR" *Tetrahedron* **1995**, *51*, 3521−3524.

[4] T. Fäcke, S. Berger "α/β-ge-SELINCOR-TOCSY, a new method for the determination of H,C coupling constants" *J. Magn. Reson. Ser. A* **1996**, *119*, 260–263.

[5] R. Wagner, S. Berger, "A significant improvement of the gradient selected SELINCOR technique" *Fresenius Z. Anal. Chem*. **1997**, *357*, 470−472.

[6] M. Findeisen, S. Berger, "A selective pulse sequence for determination of long-range C,H spin coupling constants2, *Magn. Reson. Chem*. **2003**, *41*, 431−434.

[7] J. F. Espinosa, P. Vidal, T. Parella S. Gil "Measurement of long-range proton–carbon coupling constants from pure in-phase 1D multiplets" *Magn. Reson. Chem*. **2011**, *49*, 502–507.

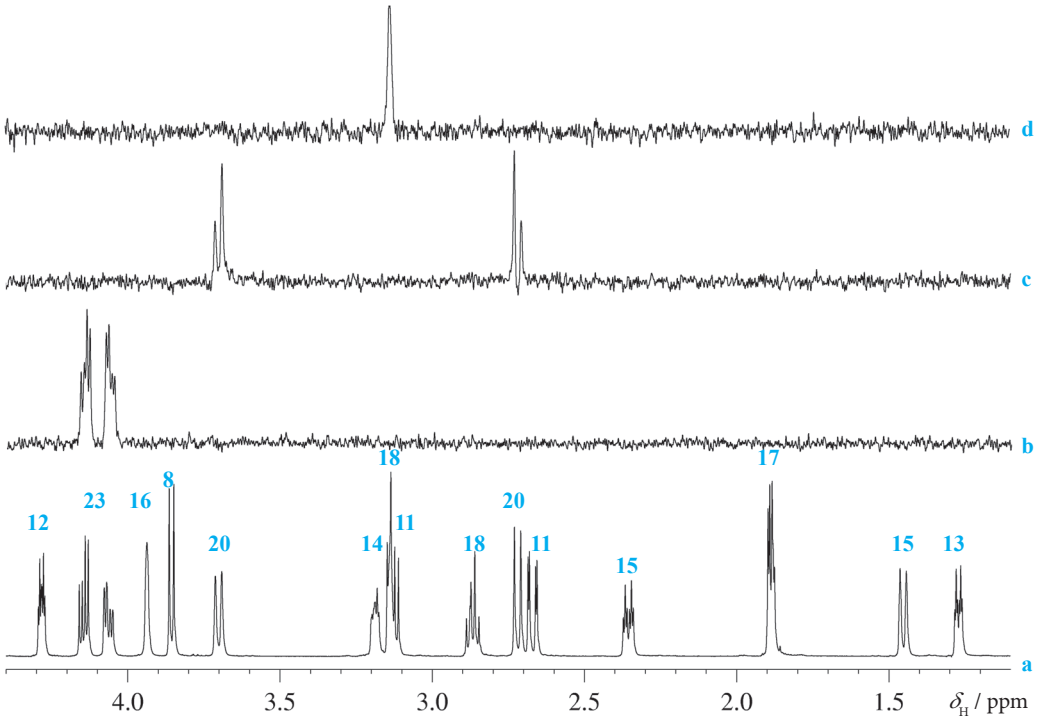

Fig. 3.7-1 SELINCOR spectra of strychnine, irradiation of C-23, C-20 and C-14 from **b** to **d**

5. Processing

Use standard 1D processing as described in Experiment 1.1, use an exponential window with lb = 1 Hz.

6. Result

The figure shows the SELINCOR spectra obtained on an Avance 700 spectrometer using a TBI probe. **a** is the normal ^{1}H NMR spectrum. In **b** the selective ^{13}C pulse was adjusted to C-23, in **c** to C-20, and in **d** to C-14. Note that the spectra show correct phases and relative intensities within the multiplets. There are no other signals besides the selected ones.

7. Comments

The sequence starts with an INEPT transfer from protons to carbons as in any HSQC sequence. A proton spin-lock pulse p4 decouples the carbon nuclei for the duration of the selective pulse p9. All carbon coherences are dephased by gradients g3 and g4 and only the selected ^{13}C magnetization is retained by the 180° selective pulse. Gradients g1 and g2 only control pulse imperfections. The usual reverse INEPT part of the sequence (see Exp. 1.5) transfers the magnetization back to protons, while the gradient pulse g5 rephases only the desired coherence.

Following our experience with a selective version of INADEQUATE we propose in this paper a new and selective pulse sequence dubbed SELINCOR, which yields essentially the same information as the 2D inverse correlation experiment, however, in a shorter time and in high digital resolution. We have simply replaced the magnetization transfer pulse of the inverse 2D experiment with a frequency-selective Gaussian-shaped pulse which only transfers the magnetization of a specific carbon atom into the proton spectrum.

Taken from ref [1]

8. Questions

A. Looking at the coherence pathway diagram given below the pulse sequence, can you confirm the ratio shown for the pulsed field gradients g3, g4 and g5?

B. Why is in this sequence a significant shorter acquisition time used than for normal ^{1}H NMR spectra?

C. In this sequence the protons are selected via their respective bound carbon atom. Discuss the drawback of this approach.

9. Own Observations

Experiment 3.8

SELINQUATE

1. Purpose

The SELINQUATE method [2] is the selective version of the INADEQUATE [3] sequence. Whereas with 1D-INADEQUATE the $^{13}C,^{13}C$ spin coupling constants can yield partially overlapping signals, the 2D version (see Exp. 2.4) is very time-consuming and has limited digital resolution [3]. With SELINQUATE it is possible to measure specific $^{13}C,^{13}C$ coupling constants over one or more bonds selectively with the high digital resolution of a 1D method [5]. Thus, the experiment yields connectivity information for the irradiated carbon nucleus and $^{13}C,^{13}C$ spin coupling constants with high accuracy. Here we show the result on a 3 % strychnine solution using a cryo probe which demonstrates the feasibity of the method even on samples with no high concentrations.

2. Variants

There have been several variants reported with respect to the placement of the selective pulse. The choices of the pulse shape is also debatable and we recommend an EBURP shape. For large spectral widths on high field instruments it is advisable to replace the 180° pulse by a chirped adiabatic refocussing pulse.

Common values:

d1: relaxation delay
d2: $1/[4J_{CC}]$
p1, p3: 90° ^{13}C transmitter pulse
p2: ^{13}C 180° transmitter pulse or chirped refocussing pulse
p4: 90° selective ^{13}C transmitter pulse, EBURP shape

3. Pulse Scheme and Phase Cycle

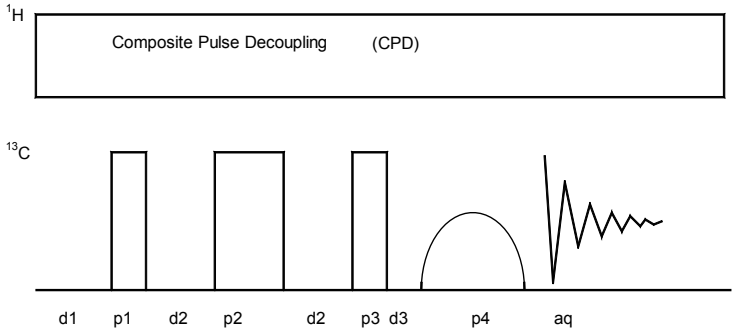

p1, p3: $(x)_8$, $(y)_8$, $(-x)_8$, $(-y)_8$
p2: $(x, -x)_4$, $(y, -y)_4$
p4: $(x)_2$, $(y)_2$, $(-x)_2$, $(-y)_2$, $(y)_2$, $(-x)_2$, $(-y)_2$, $(x)_2$, $(-x)_2$, $(-y)_2$, $(x)_2$, $(y)_2$, $(-y)_2$, $(x)_2$, $(y)_2$, $(-x)_2$
aq: $(x)_2$, $(-y)_2$, $(-x)_2$, $(y)_2$, $(y)_2$, $(x)_2$, $(-y)_2$, $(-x)_2$, $(-x_2)$, $(y)_2$, $(x)_2$, $(-y)_2$, $(-y)_2$, $(-x)_2$, $(y)_2$, $(x)_2$

Scheme 3.8-1

4. Acquisition

Special values used for the spectrum shown:

Sample: 3 % strychnine in $CDCl_3$
Time requirement: 26 h for each selected carbon atom
Spectrometer: Bruker Avance-700 with cryo probe head

Because of the low sensitivity of this experiment the probe head should be tuned to the sample in use accurately. The temperature should be regulated and controlled to 298 K.

td: 113.5 K
aq: 1.326 s
sw: 250 ppm (to keep the selective pulse on resonance)
o1: 51.96 ppm (δ_{C7})
o2: middle of ^{1}H NMR spectrum
p1, p3: 90° ^{13}C transmitter pulse [13.0 µs at 4 dB]
p2: chirped 180° ^{13}C refocusing pulse "Crp60comp.4", 2 ms
p4: selective 90° ^{13}C transmitter pulse, EBURP1 shape, 70 Hz, 64.49 ms, 50.4 dB
d1: 4 s
d2: should be reduced by half of p2, $1/[4J(C,C)] = 5.25$ ms, calculated from $^1J(C,C) \approx 40$ Hz
^{1}H decoupler attenuation and 90° pulse for CPD (WALTZ16), [80 µs, 11.8 dB]
ns: 17.120

5. Processing

Use standard ^{13}C NMR processing. Note that the experiment typically yields ^{13}C satellites in antiphase. The residual signals of the molecules containing only one ^{13}C atom should not be used for phasing.

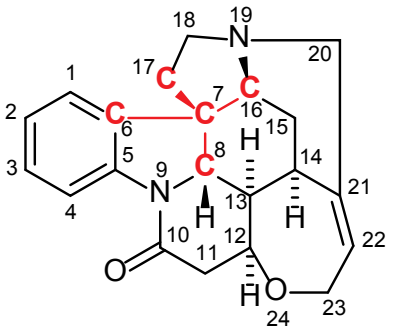

Scheme 3.8-2

[1] D. Canet, J. Brondeau, J. C. Boubel, A. Retournard "A one-dimensional selective version of the INADEQUATE experiment for determining carbon-carbon connectivities. Analysis of multi-pulse experiments by a vectorial representation" *Magn. Reson. Chem*. **1987**, *25*, 798–803.

[2] S. Berger, "Selective INADEQUATE, a farewell to 2D-NMR?" *Angew. Chem. Int. Ed. Engl*. **1988**, *27*, 1196–1197.

[3] A. Bax, R. Freeman, S. P. Kempsell, "Natural abundance ^{13}C-^{13}C coupling observed via double-quantum coherence" *J. Am. Chem. Soc*. **1980**, *102*, 4849–4851.

[4] A. Bax, R. Freeman, T. A. Frenkiel, M. H. Levitt, "Assignment of carbon-13 NMR spectra via double-quantum coherence" *J. Magn. Reson*. **1981**, *43*, 478–483.

[5] A. Y. Denisov, A. V. Tkachev, V. I. Mamatyuk "Vicinal ^{13}C-^{13}C coupling constants in bicyclic monoterpenes" *Magn. Reson. Chem*. **1992**, *30*, 95–100.

[6] K. E. Kövér, D. Uhrin, T. Liptaj, G. Batta "Easy implementation of selective INADEQUATE and H-C-C relay experiments using heteronuclear chemical shift filtering" *Magn. Reson. Chem*. **1992**, *30*, 68–72.

6. Result

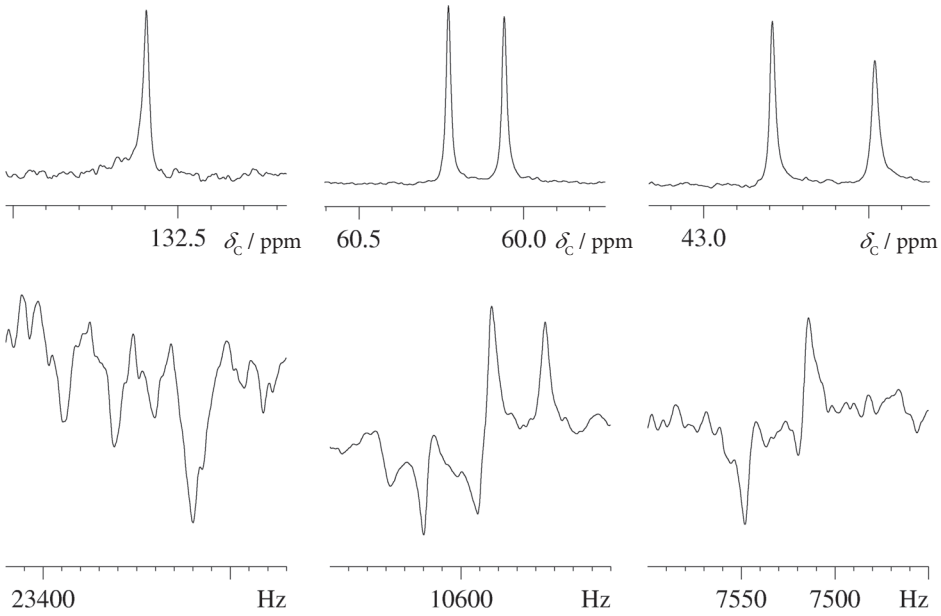

Fig. 3.8-1 upper trace: ^{13}C spectrum, lower trace: SELINQUATE

For this experiment C-7 of strychnine was chosen for the frequency of the selective pulse. Therefore four responses are expected, those of C-6 at δ_C = 132.7, C-8 at δ_C = 60.1, C-16 at δ_C = 60.3, and C-17 at δ_C = 42.8. In the upper row of the figure are the normal expansions of the ^{13}C NMR spectrum in these regions given. In the lower row, we measure for C-6 42 Hz, for C-8 36 Hz, for C-16 36.1, and for C-17: 34.1 Hz. Thus the method reveals unequivocally the four binding partners of C-7.

7. Comments

The theory of the experiment is the same as that for the 1D-INADEQUATE experiment. In SELINQUATE only the double-quantum coherence of the selectively irradiated carbon atom is transformed back into an observable magnetization. Note that the excitation bandwidth of the selective pulse used must be broad enough to excite both satellites of the carbon signal.

There has been no lack of attempts in recent years to make INADEQUATE more sensitive, but none of the improvements put forward so far can be considered as of general utility. Kessler and Freeman have recently indicated how 2D-methods by frequency-selective excitation can be reduced to the recording of a few 1D-NMR spectra. Some 2D-INADEQUATE experiments of limited application have also been reported. In continuation of our INADEQUATE studies we present here a generally applicable frequency-selective version of INADEQUATE which makes 2D-recordings superfluous.

Taken from ref. [2]

8. Questions

A. Would a gradient-selected double-quantum filter improve the sequence?

B. Which d2 value would you recommend to observe spin couplings within the aromatic ring?

C. Will it be possible to observe all three binding partners of C-21 in one measurement?

9. Own Observations

Experiment 3.9

Band Selective HMBC

1. Purpose

The standard HMBC [**H**eteronuclear **M**ultiple **B**ond **C**orrelation] technique as described in Experiment 1.6 has a problem of resolution in the indirect dimension, since typically 200 ppm of ^{13}C frequencies are distributed on 256 time domain points leading (e.g., on a 400 MHz spectrometer) to about 80 Hz/point. If several carbon atoms resonate close to each other, one has difficulties in making a correct assignment since the cross peaks correlate with more than one signal. Therefore the band-selective version was developed, which reduces the spectral width in the indirect dimension and hence increases the desired resolution significantly.

2. Variants

During the time of development of this modification every pulse of the original HMBC sequence was probed for replacement by a band selective pulse. Furhermore, many different shapes of the soft pulses used have been proposed. The sequence applied here [6] seems to be most often used currently and is very easy to handle.

Common values:

p1: 90° ^{1}H transmitter pulse
p2: 180° ^{1}H transmitter pulse
p3, p4, p5, p7: 90° ^{13}C transmitter pulse
p6: 180° ^{13}C pulse for refocussing, band selective
d1: relaxation delay
d2: 1/[2**J*(C,H)] , minimum ^{1}J(C,H)
d3: 1/[2**J*(C,H)] , maximum ^{1}J(C,H)
d4: 1/[2**J*(C,H)] , ^{n}J(C,H)
g1, g2, g3: gradients for ^{1}J-low pass filter
g4, g5, g6: encoding and refocussing gradients

3. Pulse Scheme and Phase Cycle

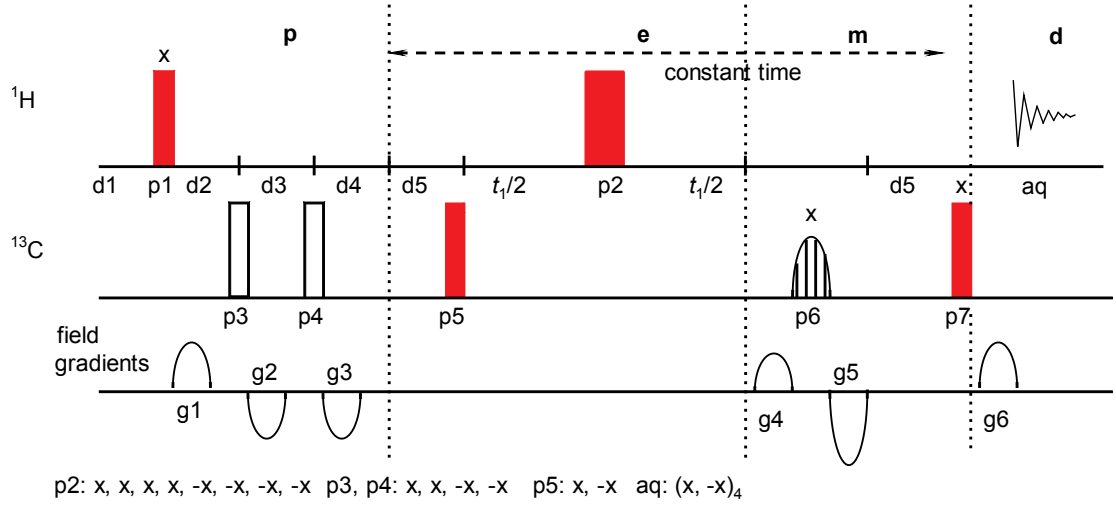

Scheme 3.9-1

4. Acquisition

Special values used for the spectrum shown:

Sample: 14 mg Cyclosporin A, 1M LiCl in 0.5 ml THF-d_8
Time requirement: 5 h
Spectrometer: Bruker DRX-600 with 5-mm TBI probe

For peptides the connectivities of protons and carbonyl carbons are of special interest since they provide the peptide sequence. In addition, C,H long-range couplings contain information about the peptide angles φ and χ. The spectral dispersion of carbonyl resonances in peptides is very small (6 ppm) compared to total ^{13}C spectral width, usually 180 ppm. Since analog filtering is not feasible in the ω_1 dimension, with the conventional technique, the whole spectral width of the carbon spectrum must be recorded in ω_1, which leads to poor resolution in ω_1. By use of a selective carbon pulse the carbonyl carbons alone can be excited and thus exclusively recorded with high digital resolution and a small number of t_1 increments.

Taken from ref. 1

[1] W. Bermel, K. Wagner and C. Griesinger "Proton-detected C,H correlation via long-range couplings with soft pulses; Determination of coupling constants" *J. Magn. Res*. **1989**, *83*, 223−232.

[2] R. C. Crouch, T. D. Spitzer, G. E. Martin " Region-selective inverse-detected long-range heteronuclear chemical shift correlation using shaped pulses" *Magn. Reson. Chem*. **1992**, *30*, 595−605.

[3] J.-M-Bernassau, J.-M. Nuzillard "Selective HMBC experiments using soft inversion pulses" *J. Magn. Res. Ser. B* **1994**, *103*, 71−81.

[4] A. Bax, K. A. Farley, G. S. Walker "Increased HMBC sensitivity for correlating poorly resolved proton multiplets to carbon-13 using selective or semi-selective pulses" *J. Magn. Res. Ser. A* **1996**, *119*, 134−138.

[5] C. Gaillet, C. Lequart, P. Debeire, J.-M. Nuzillard "Band-selective HSQC and HMBC experiments using excitation sculpting and PFGSE" *J. Magn. Reson*. **1999**, *139*, 454–459.

td2: 2K data points in F_2
td1: 512 [2×256] data points in F_1
aq: 155 ms
ns: 32
sw2: 11 ppm
sw1: 15 ppm
offset of ^1H frequency: middle of ^1H NMR spectrum
offset of ^{13}C frequency: middle of the CO region of the ^{13}C NMR spectrum, 173 ppm
p6: 1 ms IBURP, 13 dB, corresponds to 30 ppm bandwidth
d1: 2 s
d2: 4 ms, calculated from $^1J(C,H) \approx 125$ Hz
d3: 2.94 ms, calculated from $^1J(C,H) \approx 170$ Hz
d4: 62.5 ms, calculated from $^nJ(C,H) \approx 8$ Hz
d5: 0.5*(t_1 increment*256) = 0.056 s
start increment for t_1 evolution: 3 µs
increment for t_1 evolution: 1/2*sw1
g1 to g6: sine shaped field gradients, 1 ms, 50µs ring down delay,
g1: 15 %, g2: –10 %, g3: –5 %, g4: 30 % , g5: –50 %, g6: 40.1 % (100 % ≈ 0.56 T/m)

5. Processing

Apply zero-filling in F_1 to 1K data points in order to have a matrix of 1K×1K real data points. Before Fourier transformation use an exponential window in F_2 with lb = 4 Hz and π/2-shifted squared sine window in F_1. Phase correction is unnecessary, since the spectrum is processed in magnitude mode in F_1.

6. Result

The figure shows the 2D spectrum obtained on a DRX-600 spectrometer with an inverse multinuclear *z*-gradient probe. Note that for each carbonyl atom a clear correlation can be found.

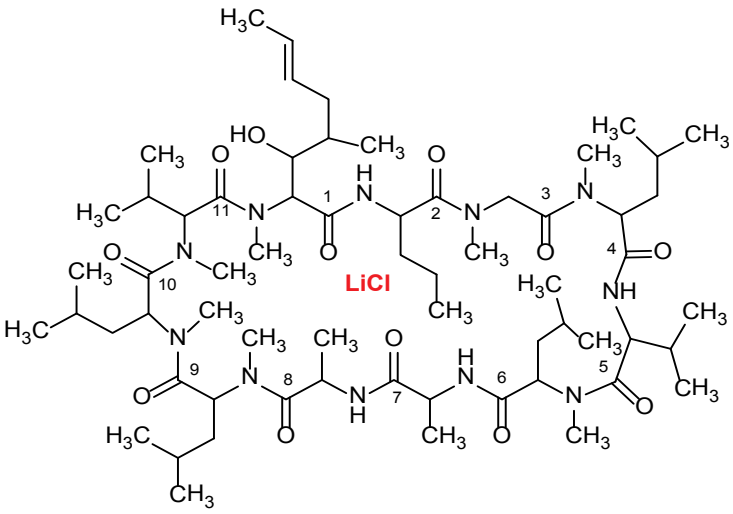

Scheme 3.9-2

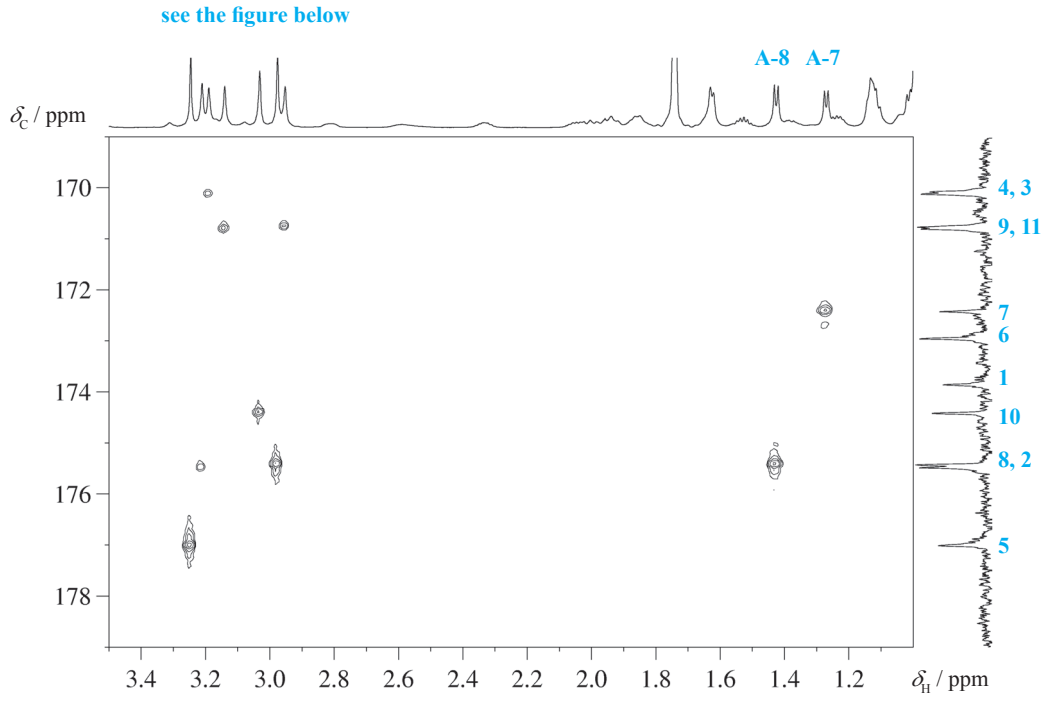

Fig. 3.9-1 Band selective HMBC spectrum of cyclosporin

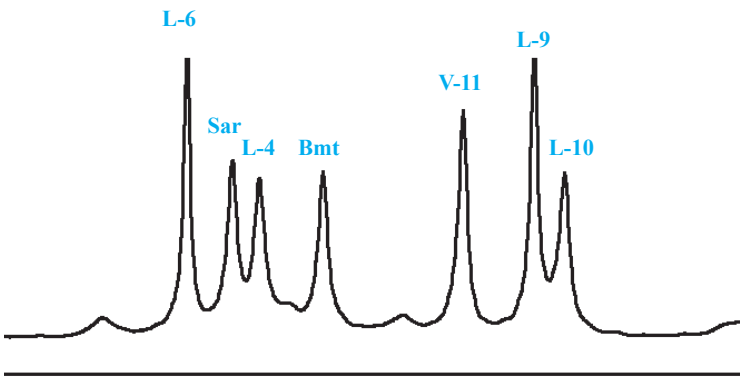

7. Comments

The difference from the HMBC sequence shown in chapter 1.6 is that the sequence shown here is not phase sensitive. In addition, the constant-time principle is used. Thus the values of d5 are decremented at the same time, as d0 is incremented, keeping the sum of evolution and mixing time constant. The pulse p6 has only a narrow spectral range corresponding to the spectral width used. In combination with the pulsed field gradients therefore only these resonance will give a HMBC signal which is flipped by this 180° pulse.

Fig. 3.9-2 Dr. Wolfgang Bermel (Bruker Biospin) *1956

8. Questions

A. Why is here an IBURP pulse used and not an EBURP shape?

B. Why is the sequence especially valuable for peptides?

C. Would the dual low pass filter shown in the sequence be necessary for the demonstrated example?

9. Own Observations

[6] T. D. W. Claridge, I. Pérez-Victoria "Enhanced ^{13}C resolution in semi-selective HMBC: a band-selective, constant-time HMBC for complex organic structure elucidation by NMR" *Org. Biomol. Chem*. **2003**, *1*, 3632−3634.

[7] P. G. Williams, W. Y. Yoshida, M. K. Quon, R. E. Moore, V. J. Paul "The structure of Palau'amide, a potent cytotoxin from a species of the marine yanobacterium Lyngbya" *J. Nat. Prod*. **2003**, *66*, 1545−1549.

[8] S. Hajdok, J. Conrad, H. Leutbecher, S. Strobel, T. Schleid, U. Beifuss "The Laccase-catalyzed domino reaction between catechols and heterocyclic 1,3-dicarbonyls and the unambiguous structure elucidation of the products by NMR spectroscopy and X-ray crystal structure analysis" *J. Org. Chem*. **2009**, *74*, 7230–7237.

[9] M. Köck, H. Kessler, D. Seebach, A. Thalert "Novel backbone conformation of cyclosporin A: The complex with lithium chloride" *J. Am. Chem. Soc* **1992**, *114*, 2676-2686.

Chapter 4

Heteronuclear NMR

Although NMR in Chemistry deals mainly with the nuclei ^{1}H and ^{13}C, there are very interesting applications with all the spins throughout the periodic system, and especially Inorganic Chemistry will focus on these. Of course we cannot show one example for each nucleus; however, we restrict ourselves in this chapter to some selected cases: nuclei with very low abundance such as ^{15}N, quadrupolar nuclei such as ^{17}O and ^{11}B, nuclei with interest both in Organic and Inorganic Chemistry (^{19}F, ^{29}Si), and metal nuclei with a very low frequency (^{57}Fe) or a very wide spectral range, such as ^{195}Pt.

4.1 ^{11}B NMR Spectroscopy 119

4.2 ^{15}N NMR Spectroscopy 123

4.3 ^{17}O NMR Spectroscopy 127

4.4 ^{19}F NMR Spectroscopy 131

4.5 ^{29}Si NMR Spectroscopy 135

4.6 ^{57}Fe NMR Spectroscopy 141

4.7 ^{195}Pt NMR Spectroscopy 145

The relevant data of all nuclei are given in the initial tables of this chapter accompanied by the explanation of the Ξ scale for referencing.

Referencing in Hetereonuclear NMR

Referencing was a frequently discussed problem in heteronuclear NMR spectroscopy. This has now ended with a "regulation" issued by the IUPAC committee as published in 2001 [6]. The idea of the concept is that only one valid primary reference compound is recognized, namely tetramethylsilane (TMS). Its proton frequency is used to calculate the frequencies of all heteronuclear secondary reference compounds, which are defined and tabulated by IUPAC; these tables are reproduced here.

The method is known as the Ξ-scale ("xsi", greek capital letter). The Ξ-value is the ratio between the absolute frequency ν_x of an X nucleus reference substance, recommended and measured by the authors of the IUPAC paper [6], and the absolute ^{1}H frequency ν_{TMS} of TMS on the identical B_0 field and sample:

(1)

$$\Xi_X = \frac{\nu_x}{\nu_{TMS}} \cdot 100$$

Once you have measured the frequency of TMS in your sample, you can calculate the absolute frequency of the (virtual) X nucleus reference signal without the need to have the X reference substances in the sample, from

(2)

$$\nu_x = \Xi_X \cdot \nu_{TMS}$$

Using the Ξ value in % (as given in the tables), one may figure that the Ξ values would be the frequencies of the reference substances scaled to the TMS frequency of 100.000 000 MHz.

For example: assume that you have detected on a 400 MHz spectrometer the ^{17}O frequency of some compound at ν_O = 54.250 399 MHz. You have measured (at the same field strength using the same lock solvent, preferably in the same tube) the frequency of the ^{1}H TMS signal at ν_{TMS}= 400.130 021 MHz. The Ξ-value of the ^{17}O reference compound D_2O is listed in Table 4.2 as Ξ = 13.556 457 %. Using Equation (2) you first calculate the virtual ^{17}O frequency ν_{D2O} under these conditions, which will be

$\nu_{D2O} = (\Xi_X/100)\ \nu_{TMS} = 0.135\ 564\ 57 \times 400.130\ 021 = 54.243\ 454$ MHz.

Therefore, the difference between the frequency ν_O of your compound of interest and D_2O is 6945 Hz, which yields 128.03 ppm through division by ν_{D2O}.

Note that for this procedure you never needed to measure an actual sample of the reference D_2O. Moreover, for the purpose of global standardization, this should not be done; instead, the recommended values should be used worldwide. On Bruker spectrometers the calculation procedure given above simplifies to multiplying the SF-value of the proton spectrum by the appropriate Ξ-value and inserting this as SF in the heteronuclear spectrum. Even easier is the use of a macro with the name "xsi.mf", which is available from one of the authors of this book on request.

A distinguishing feature of nuclear magnetic resonance (NMR) is that signals are isotope-specific. In other words, each signal can be firmly linked to a particular element and nuclide. Two features follow: Firstly, there is a close connection with chemistry and, in particular, with the periodic table, since almost all elements can be studied; secondly, the spin properties of each isotope need to be clearly tabulated and firmly understood. It is a principal purpose of this document to provide such information.

Taken from ref [6]

Table 4.1: Nuclides with $I = 1/2$

Nuclide	Natural abundance N [%]	Gyromagnetic ratio γ [10^7 rad $T^{-1}s^{-1}$]	frequency ratio[a] Ξ [%]	Standard[c]	Receptivity D[b]
^{1}H	99.9885	26.752 212 8	100.000 000	Me_4Si	5.87×10^{3}
^{3}H	-	28.534 977 9	106.663 974	Me_4Si-t_1	-
^{3}He	1.37×10^{-4}	−20.380 158 7	76.179 437	He / gas	3.56×10^{-3}
^{13}C	1.07	6.728 284	25.145 020	Me_4Si	1.00
^{15}N	0.368	−2.712 618 04	10.136 767	$MeNO_2$ / neat	2.25×10^{-2}
^{19}F	100.0	25.181 48	94.094 011	CCl_3F	4.90×10^{3}
^{29}Si	4.6832	−5.319 0	19.867 187	Me_4Si	2.16
^{31}P	100.0	10.839 4	40.480 742	H_3PO_4 85 %	3.91×10^{2}
^{57}Fe	2.119	0.868 062 4	3.237 778	$Fe(CO)_5$	4.25×10^{-3}
^{77}Se	7.63	5.125 385 7	19.071 513	Me_2Se	3.15
^{89}Y	100.0	−1.316 279 1	4.900 198	$Y(NO_3)_3$ / aq.	0.70
^{103}Rh	100.0	−0.846 8	3.186 447	$Rh(acac)_3$	0.186
^{109}Ag	48.161	−1.251 863 4	4.653 533	$AgNO_3$ / aq.	0.290
^{113}Cd	12.22	−5.960 915 5	22.193 175	Me_2Cd	7.94
^{115}Sn	0.34	−8.801 3	32.718 749	Me_4Sn	0.711
^{117}Sn	7.68	−9.588 79	35.632 259	Me_4Sn	20.8
^{119}Sn	8.59	−10.031 7	37.290 632	Me_4Sn	26.6
^{125}Te	7.07	−8.510 840 4	31.549 769	Me_2Te	13.4
^{129}Xe	26.44	−7.452 103	27.810 186	$XeOF_4$	33.6
^{169}Tm	100.0	−2.218	8.29		3.35
^{171}Yb	14.28	4.728 8	17.499 306	$Yb(\eta\text{-}C_5Me_5)_2$	4.63
^{183}W	14.31	1.128 240 3	4.166 387	Na_2WO_4	6.31×10^{-2}
^{187}Os	1.96	0.619 289 5	2.282 331	OsO_4	1.43×10^{-3}
^{195}Pt	33.832	5.838 5	21.496 784	Na_2PtCl_6	20.7
^{199}Hg	16.87	4.845 791 6	17.910 822	Me_2Hg / neat[d]	5.89
^{205}Tl	70.476	15.692 180 8	57.683 838	$Tl(NO_3)_3$	8.36×10^{2}
^{207}Pb	22.1	5.580 46	20.920 599	Me_4Pb	11.8

a) values given in 6 digits after the point as measured for the standard compounds, other data calculated from the γ-values in column 3.

b) receptivity relative to ^{13}C

c) Me = Methyl

d) This compound is extremely dangerous. Do not use it, but apply the recommended Ξ-value.

Table 4.2: Selected Quadrupolar Nuclei ($I > 1/2$)

Nuclide	Spin I	Quadrupole moment Q [$10^{-30}m^2$]	Natural abundance N [%]	Gyromagnetic ratio γ [10^7 rad $T^{-1}s^{-1}$]	frequency ratio[a] Ξ [%]	Reference	Receptivity D[b]
^{2}H	1	0.2860	0.0115	4.106 627 91	15.350 609	$(CD_3)_4Si$	6.52×10^{-3}
^{6}Li	1	−0.0808	7.59	3.937 170 9	14.716 086	LiCl / aq.	3.79
^{7}Li	3/2	−4.01	92.41	10.397 701 3	38.863 797	LiCl / aq.	1.59×10^{3}
^{9}Be	3/2	5.288	100	−3.759 666	14.051 813	$BeSO_4$ / aq.	81.5
^{11}B	3/2	4.059	80.1	8.584 704 4	32.083 974	BF_3Et_2O	7.77×10^{2}
^{14}N	1	2.044	99.632	1.933 779 2	7.226 317	CH_3NO_2	5.90
^{17}O	5/2	−2.558	0.038	−3.628 08	13.556 457	D_2O	6.50×10^{-2}
^{23}Na	3/2	10.4	100	7.080 849 3	26.451 900	NaCl / aq.	5.45×10^{2}
^{25}Mg	5/2	19.94	10.00	−1.638 87	6.121 635	$MgCl_2$ / aq.	1.58
^{27}Al	5/2	14.66	100	6.976 271 5	26.056 859	$Al(NO_3)_3$	1.22×10^{3}
^{33}S	3/2	−6.78	0.76	2.055 685	7.676 000	$(NH_4)_2SO_4$ / aq.	0.101
^{35}Cl	3/2	−8.165	75.78	2.624 198	9.797 909	NaCl / aq.	21.0
^{37}Cl	3/2	−6.435	24.22	2.184 368	8.155 725	NaCl / aq.	3.87
^{39}K	3/2	5.85	93.2581	1.250 060 8	4.666 373	KCl / aq.	2.79
^{41}K	3/2	7.11	6.7302	0.686 068 08	2.561 305	KCl / aq.	3.33×10^{-2}
^{43}Ca	7/2	−4.08	0.135	−1.803 069	6.730 029	$CaCl_2$ / aq.	5.10×10^{-2}
^{45}Sc	7/2	−22.0	100	6.508 797 3	24.291 747	$Sc(NO_3)_3$ / aq.	1.78×10^{3}
^{47}Ti	5/2	30.2	7.44	−1.510 5	5.637 534	$TiCl_4$ / neat	0.918
^{49}Ti	7/2	24.7	5.41	−1.510 95	5.639 037	$TiCl_4$ / neat	1.20
^{51}V	7/2	−5.2	99.750	7.045 511 7	26.302 948	$VOCl_3$ / neat	2.25×10^{3}
^{53}Cr	3/2	−15.0	9.501	−1.515 2	5.652 496	K_2CrO_4 / aq.	0.507
^{55}Mn	5/2	33.0	100	6.645 254 6	24.789 218	$KMnO_4$ / aq.	1.05×10^{3}
^{59}Co	7/2	42.0	100	6.332	23.727 074	$K_3[Co(CN)_6]$	1.64×10^{3}
^{63}Cu	3/2	−22.0	69.17	7.111 789 0	26.515 473	$[Cu(CH_3CN)_4][ClO_4]$	3.82×10^{2}
^{65}Cu	3/2	−20.4	30.83	7.604 35	28.403 693	$[Cu(CH_3CN)_4][ClO_4]$	2.08×10^{2}
^{67}Zn	5/2	15.0	4.10	1.676 688	6.256 803	$Zn(NO_3)_2$ / aq.	0.692
^{71}Ga	3/2	10.7	39.892	8.181 171	30.496 704	$Ga(NO_3)_3$ / aq.	3.35×10^{2}
^{73}Ge	9/2	−19.6	7.73	−0.936 030 3	3.488 315	$(CH_3)_4Ge$	0.642

Nuclide	Spin I	Quadrupole moment Q [$10^{-30}m^2$]	Natural abundance N [%]	Gyromagnetic ratio γ[10^7 rad $T^{-1}s^{-1}$]	frequency ratio[a] Ξ [%]	Reference	Receptivity D[b]
^{75}As	3/2	31.4	100	4.596 163	17.122 614	$NaAsF_6$ / aq.	1.49×10^2
^{79}Br	3/2	31.3	50.69	6.725 616	25.053 980	NaBr / aq.	2.37×10^2
^{81}Br	3/2	26.2	49.31	7.249 776	27.006 518	NaBr / aq.	2.88×10^2
^{83}Kr	9/2	25.9	11.49	−1.033 10	3.847 600	Kr / gas	1.28
^{87}Rb	3/2	13.35	27.83	8.786 400	32.720 454	RbCl / aq.	2.90×10^2
^{87}Sr	9/2	33.5	7.00	−1.163 937 6	4.333 822	$SrCl_2$ / aq.	1.12
^{93}Nb	9/2	−32.0	100	6.567 4	24.476 170	$K[NbCl_6]$	2.87×10^3
^{95}Mo	5/2	−2.2	15.92	−1.751	6.516 926	Na_2MoO_4 / aq.	3.06
^{115}In	9/2	81.0	95.71	5.897 2	21.912 629	$In(NO_3)_3$	1.98×10^3
^{121}Sb	5/2	−36.0	57.21	6.443 5	23.930 577	$KSbCl_6$	5.48×10^2
^{127}I	5/2	−71.0	100	5.389 573	20.007 486	KI / aq.	5.60×10^2
^{131}Xe	3/2	−11.4	21.18	2.209 076	8.243 921	$XeOF_4$	3.50
^{133}Cs	7/2	−0.343	100	3.533 253 9	13.116 142	$CsNO_3$ / aq.	2.84×10^2
^{137}Ba	3/2	24.5	11.232	2.992 95	11.112 928	$BaCl_2$ / aq.	4.62
^{139}La	7/2	20.0	99.910	3.808 331 8	14.125 641	$LaCl_3$	3.56×10^2
^{181}Ta	7/2	317.0	99.988	3.243 8	11.989 600	$KTaCl_6$	2.20×10^2
^{187}Re	5/2	207.0	62.60	6.168 2	22.751 600	$KReO_4$	$5.26.10^2$
^{189}Os	3/2	85.6	16.15	2.107 13	7.765 400	OsO_4	2.32
^{201}Hg	3/2	38.6	13.18	−1.788 769	6.611 583	$(CH_3)_2Hg$[c]	1.16
^{209}Bi	9/2	−51.6	100	4.375 0	16.069 288	$Bi(NO_3)_2$	8.48×10^2

a) values given in 6 digits after the point as measured for the standard compounds; other data calculated from the γ-values in column 5.

b) receptivity relative to ^{13}C

c) This compound is extremely dangerous. Do not use it, but apply the recommended Ξ-value.

This procedure is especially common in structural biology, where the ^{15}N chemical shifts of proteins are referenced and calculated using the proton signal of DSS (2,2-dimethyl-2-silapentane-5-sulfonate, sodium salt) [5]. The ratio of the frequency of the common reference compound liquid ammonia (note that in contrast to the common usage of nitromethane as a reference compound structural biologists prefer NH_3) and the DSS frequency was determined to be 0.101329118. Multiplying this value by the actual DSS frequency of the sample immediately gives the frequency of liquid ammonia, which is set to $\delta_N = 0$ by the spectrometer software. Correspondingly, ^{13}C is referenced to DSS using the factor 0.25144953.

Fig. 4.0-1 Warning signs at the door of a spectrometer laboratory

[1] R. K. Harris, B. E. Mann (eds.), *NMR and the Periodic Table*, Academic Press, London, **1978**.

[2] C. Brevard, P. Granger, *Handbook of High Resolution Multinuclear NMR*, Wiley, Chichester, **1981**.

[3] J. Mason (ed.), *Multinuclear NMR*, 2nd Edition, Plenum Press, London, **1989**.

[4] S. Berger, S. Braun, H.-O. Kalinowski, *NMR Spectroscopy of the Non-Metallic Elements*, Wiley, Chichester, **1997**.

[5] D. S. Wishart, C. G. Bigam, J. Yao, F. Abildgaard, H. J. Dyson, E. Oldfield, J. L. Markley, B. D. Sykes, "^{1}H, ^{13}C, and ^{15}N chemical shift referencing in biomolecular NMR" *J. Biomol. NMR* **1995**, *6*, 135−140.

[6] R. K. Harris, E. D. Becker, S. M. Cabral de Menezes, R. Goodfellow, P. Granger, "NMR Nomenclature. Nuclear spin properties and conventions for chemical shifts" *Pure Appl. Chem*. **2001**, *73*, 1795−1818.

Experiment 4.1

^{11}B NMR Spectroscopy

1. Purpose

This experiment demonstrates the technique used to obtain NMR spectra of ^{11}B (I = 3/2, natural abundance 80.1%). As an example we have chosen the commercially available 1,7-dicarba-*closo*-dodecaborane, since this compound gives a spectrum containing four different signals with rather low line width. Furthermore, the spectrum can be recorded with or without proton decoupling; thus a spin–spin coupling ^{1}J(B,H) can be observed.

2. Variants

There are no relevant variants of ^{11}B NMR spectroscopy. Being a quadrupolar nucleus with a line width often exceeding 500 Hz, all modern schemes of multiple pulse NMR involving delays governed by the coupling constant will be fruitless. Very recently, ^{10}B NMR was proposed as a background-free technique. [6]

3. Pulse Scheme and Phase Cycle

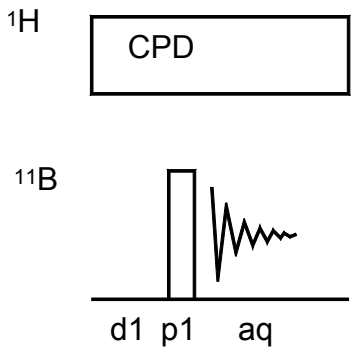

Scheme 4.1-1

4. Acquisition

Special values used for the spectrum shown:

Sample: 100 mg 1,7-dicarba-*closo*-dodecaborane in 0.7 mL $CDCl_3$
Time requirement: 5 min
Spectrometer: Bruker AC-300 with 5-mm BBO probe

A multinuclear probe is required for the measurement of ^{11}B spectra. There are special ^{11}B probes available which don't have a glass insert, thereby reducing the background signal. After tuning the multinuclear probe to ^{11}B on the observe channel and to ^{1}H on the decoupler channel, use a sample of $BF_3 \cdot O(C_2H_5)_2$ to detect the ^{11}B resonance and to determine the 90° pulse. The δ_B value of this standard can be referenced to 0, but better is the use of TMS and the Ξ-value (32.083974) of this compound as described in the introduction to this chapter. To obtain the spectrum displayed below you have to set:

Fig. 4.1-1
Colemanite ($CaB_3O_4(OH)_3 \cdot H_2O$) is a borate mineral and a source of boron. It was first described in 1884 for an occurrence near Furnace Creek in Death Valley and was named after William Tell Coleman (1824–1893), owner of the mine Harmony Borax Works where it was first found. Photograph by courtesy of Dr. H.-J. Höbler, Mineralogical and petrographical collection, University of Leipzig

Common values:

p1: 90° ^{11}B transmitter pulse
d1: relaxation delay

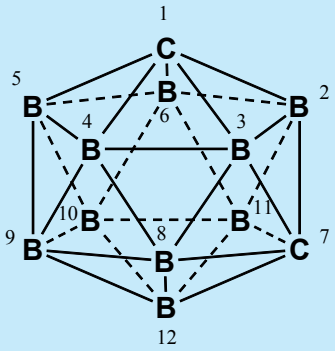

Scheme 4.1-2

Briefly, boron neutron capture therapy (BNCT) can be classified as a binary cancer treatment, wherein two components, each administered at sub-toxic levels, are combined (ideally within cancer cells) to produce the desired cell-killing effect. The two components of the binary system are 10B nuclei and low-energy (thermal or epithermal) neutrons. The reaction between these components releases linear energy transfer (LET) alpha particles with a spatial range of approximately 10 mm.

Taken from ref. [5]

td : 4K
sw: 36 ppm
aq: 0.4 s
o1: middle of ^{11}B NMR spectrum
o2: middle of ^{1}H NMR spectrum
d1: 100 ms
p1: 90° ^{11}B transmitter pulse
decoupler attenuation and 90° pulse for CPD
ns: 8

5. Processing

Use standard 1D processing with exponential multiplication (lb = 2 Hz) and a baseline correction.

6. Result

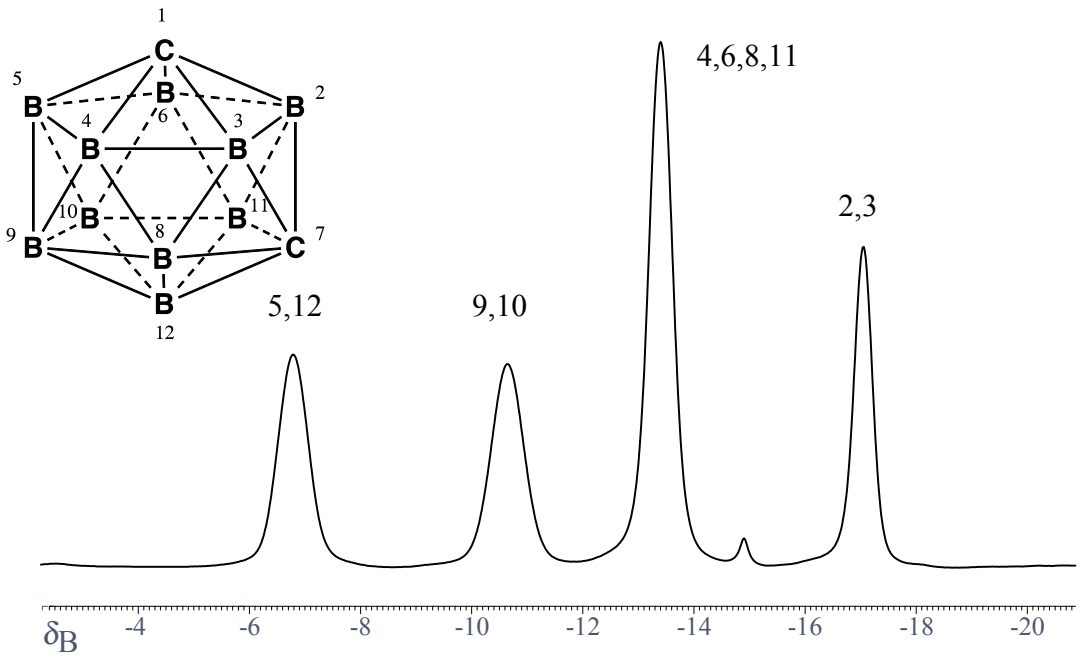

Fig. 4.1-2 ^{11}B NMR spectrum of 1,7-dicarba-*closo*-dodecaborane

The figure shows the 96.23 MHz ^{11}B NMR spectrum obtained on an AC-300 spectrometer with a special 5 mm boron probe-head.

7. Comments

The pulse repetition time of the experiment can be selected according to the sample used, so that much faster pulsing than used here is often possible.

To obtain ^{11}B spectra without any background signal, both the insert of the probe-head and the NMR sample tube must be made from boron-free material, such as quartz or teflon.

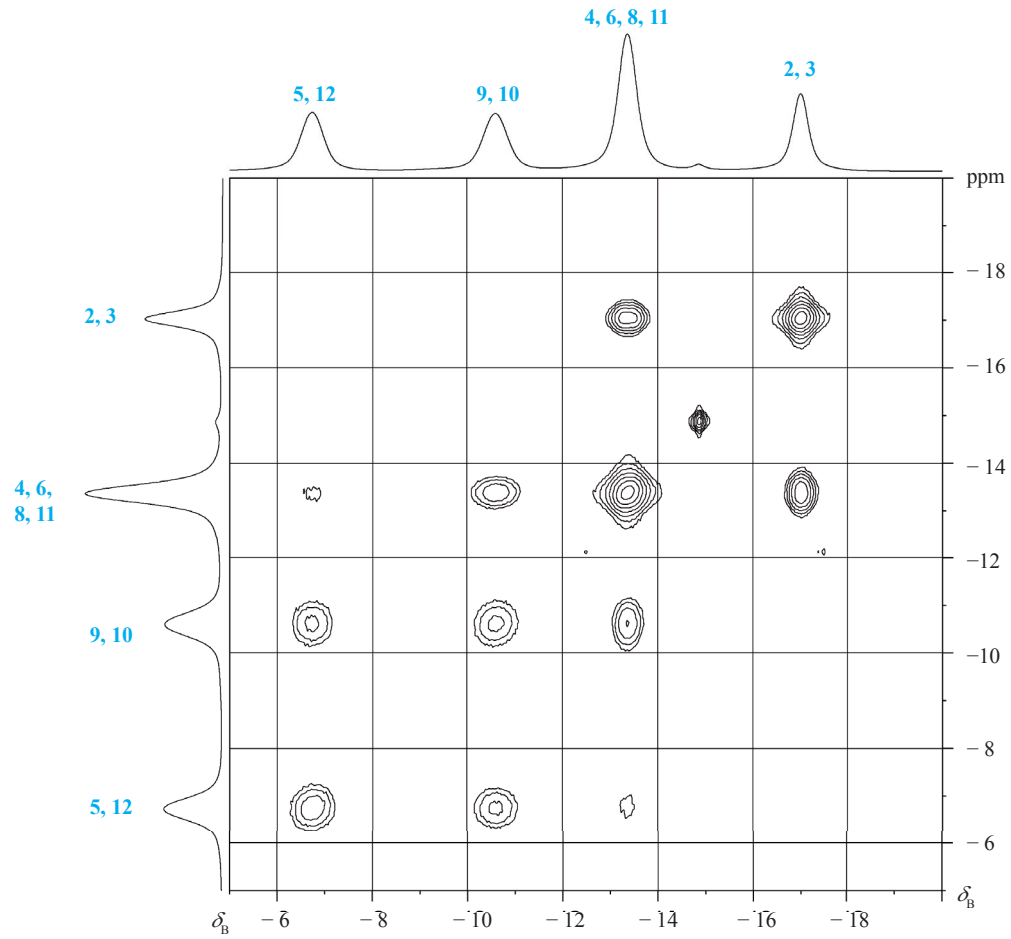

Fig. 4.1-3 ^{11}B NMR COSY spectrum of 1,7-dicarba-*closo*-dodecaborane

In principle, it is possible to adopt NMR methods used in H,H correlations or H,C correlations in similar way to X nuclei. In some cases the fast relaxation of nuclei with spin number > 1/2 may be a pitfall and may limit the choice of tools.

In the second figure we provide an impressive example of an homonuclear correlation spectrum, an ^{11}B,^{11}B-COSY with ^{1}H decoupling and gradient selection, on the above mentioned sample at a 400 MHz spectrometer.

The acquisition conditions are similar to the 1D spectrum (cf. paragraph 4), but the number data points *td* reduced to 2 K and recording 256 increments. If the number of scans *ns* is reduced to 1, the total experiment time is below 2 min.

[1] D. Reed, "The role of NMR in boron chemistry" *Chem. Soc. Rev*. **1993**, 109−116.

[2] B. Wrackmeyer, "Nuclear magnetic resonance spectroscopy of boron compounds containing two-, three- and four-coordinate boron" *Annu. Rep. NMR Spectrosc*. **1988**, *20*, 61−203.

[3] A. R. Siedle, "Boron-11 NMR spectroscopy" *Annu. Rep. NMR Spectrosc*. **1988**, *20*, 205−314.

[4] S. Hermánek "NMR as a tool for elucidation of structures and estimation of electron distribution in boranes and their derivatives" *Inorg. Chim. Acta* **1999**, *289*, 20–44.

[5] P. Bendel, "Biomedical applications of ^{10}B and ^{11}B NMR" *NMR Biomed*. **2005**, *18*, 74–82.

[6] P. Király "Background-free solution boron NMR spectroscopy" *Magn. Reson. Chem*. **2012**, *50*, 620−626.

8. Questions

A. The line width in this sample is about 100 Hz, which is relatively sharp for boron NMR. What could be the reason?

B. If one wants to detect ^{13}C signals of carbon atoms bound directly to boron one often has severe difficulties because the ^{13}C signal is also broadened. Suggest a remedy.

C. Surprisingly, the ^{11}B signal of $BF_3 \cdot O(C_2H_5)_2$ appears as a sharp singlet. Why is this not a quadruplet by spin coupling to ^{19}F?

9. Own Observations

Experiment 4.2

^{15}N NMR Spectroscopy

1. Purpose

For the observation of nitrogen, ^{15}N with $I = 1/2$ is the isotope of choice, despite its low natural abundance (0.37 %) and low NMR sensitivity; its receptivity as compared to ^{13}C is only 0.022. Additionally one has to take into account that under the conditions of ^{1}H broad-band decoupling a decrease in intensity may occur due to a negative NOE effect resulting from the negative gyromagnetic ratio of ^{15}N. This problem may be circumvented, however, using the inverse gated ^{1}H decoupling technique.

Fig. 4.2-1 Big liquid nitrogen tank of the Physics department, University Leipzig

2. Variants

The preferred methods for direct observation are those with polarization transfer, such as the INEPT [1] or DEPT sequences, which may be performed with or without ^{1}H broad-band decoupling in "refocused" versions of pulse schemes and can be tuned either to ^{1}J(N,H) or to ^{2}J(N,H)/ ^{3}J(N,H). Currently, nitrogen will be observed in the inverse mode with gradient selection as described as well below. Here we start with the forward DEPT experiment on formamide with ^{1}H broad-band decoupling, followed by the proton-coupled spectrum and finally show the current HSQC technique.

3. Pulse Scheme and Phase Cycle

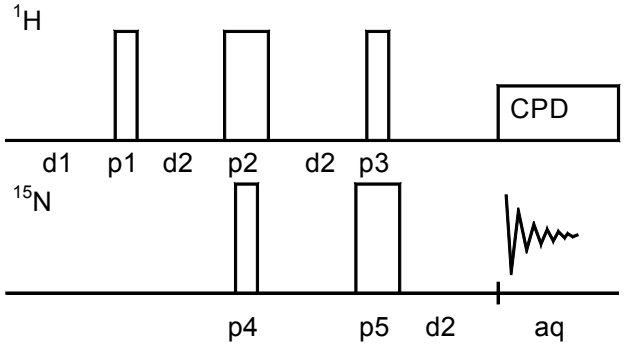

Scheme 4.2-1 DEPT

p1: x

p2: x, -x, y, -y

p3: $(y)_4$, $(-y)_4$

p4: $(x)_8$, $(y)_8$, $(-x)_8$, $(-y)_8$

p5: $(x, -x)_4$, $(y, -y)_4$

aq: $(y)_2$, $(-y)_4$, $(y)_2$, $(-x)_2$, $(x)_4$, $(-x)_2$,
$(y)_2$, $(y)_4$, $(-y)_2$, $(x)_2$, $(-x)_4$, $(x)_2$

4. Acquisition

Special values used for the spectrum shown:

Sample: 90% formamide in [D_6]dimethylsulfoxide.
Time requirement: 5 min
Spectrometer: Bruker ARX-300 with 5-mm-BBO-probe

Set up your spectrometer to ^{15}N, find the signal, and determine the 90° transmitter pulse-length. The reference compound is CH_3NO_2, (Ξ-scale), and formamide has $\delta_N = -268$.

Common values:

p1: 90° ^{1}H transmitter pulse
p2: 180° ^{1}H transmitter pulse
p3: 45° ^{1}H transmitter pulse
p4: 90° ^{15}N transmitter pulse
p5: 180° ^{15}N transmitter pulse
d1: relaxation delay
d2: 1/(2J)

Fig. 4.2-2 Nitratine ($NaNO_3$) − a nitrogen − containing mineral which can be found in the Atacama desert, Chile. Photograph as a courtesy of Dr. H.-J. Höbler, Mineralogical Collection University of Leipzig.

You have to set:

td: 32K
aq: 1.5 s
sw: 350 ppm (chemical shift range of NH-groups)
o1: − 220 ppm
(middle of NH region)
o2: middle of ^{1}H NMR spectrum
d1: 2s
d2: $1/[2\cdot J(N,H)] = 5.6$ ms, calculated from $^1J(N,H) = 90$ Hz
decoupler attenuation and 90° pulse for CPD
ns: 4

5. Processing

Use standard 1D processing as described in Experiment 1.2.

6. Result

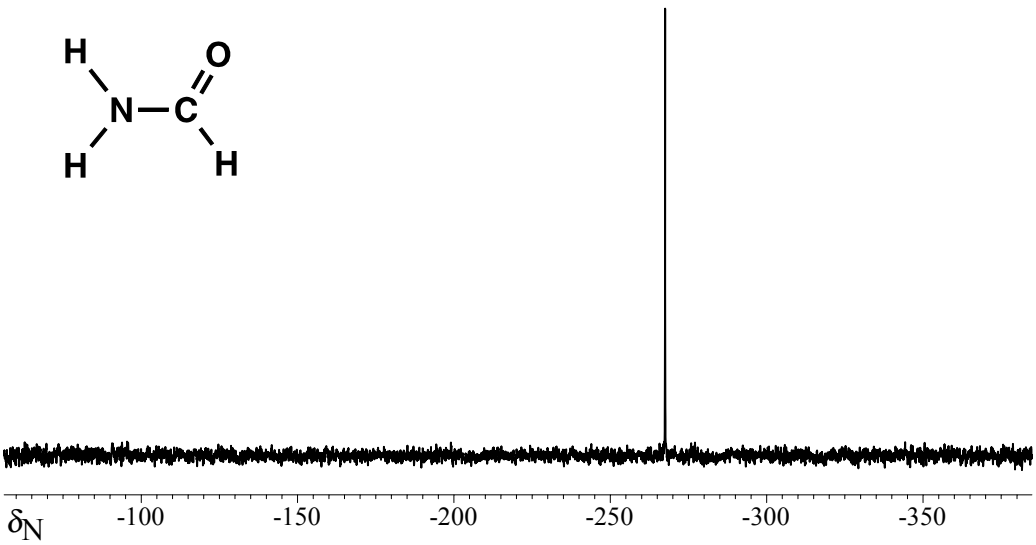

Fig. 4.2-3 DEPT NMR spectrum of formamide

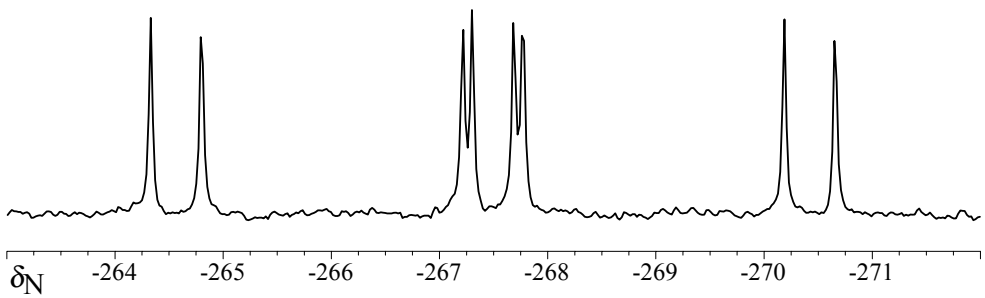

Fig. 4.2-4 Spectrum without ^{1}H decoupling, zoomed in

The figures show the 30.4 MHz ^{15}N NMR DEPT spectrum obtained on an ARX-300 spectrometer with a 5 mm multinuclear probe. As an exercise you may perform an inverse gated experiment (without NOE) and one with the normal procedure; theoretically, the gain in intensity using DEPT instead of the inverse gated method is given by $|\gamma(^1H)/\gamma(^{15}N)| = -9.87$. Note the probable sign change of the signal. After this, turn the decoupler off and run the spectrum again:

From the pattern, which represents a doublet of doublets of doublets, the following coupling constants can be deduced: $^1J(^{15}N,H^{syn}) = 87.9$ Hz, $^1J(^{15}N,H^{anti}) = 90.3$ Hz, and $^2J(^{15}N,H) = 14.0$ Hz.

Today, inverse detection is the method of choice, particularly if the unwanted signals can be effectively suppressed with pulsed field gradients. In the experiment described here we demonstrate the efficiency of this approach with the strychnine sample, tuned, of course, to long-range N,H couplings. HMQC or HSQC techniqes without ^{15}N decoupling can be used.

[1] G. A. Morris, "Sensitivity enhancement in ^{15}N NMR: Polarization transfer using the INEPT pulse sequence" *J. Am. Chem. Soc*. **1980**, *102*, 428−429.

[2] O. W. Sørensen, R. R. Ernst, "Elimination of spectral distortion in polarization transfer experiments. Improvements and comparison of techniques" *J. Magn. Reson*. **1983**, *51*, 477−489.

[3] W. Witanowski, L. Stefaniak, G. A. Webb, "Nitrogen NMR spectroscopy" *Annu. Rep. NMR Spectrosc*. **1993**, *25*, 1−480.

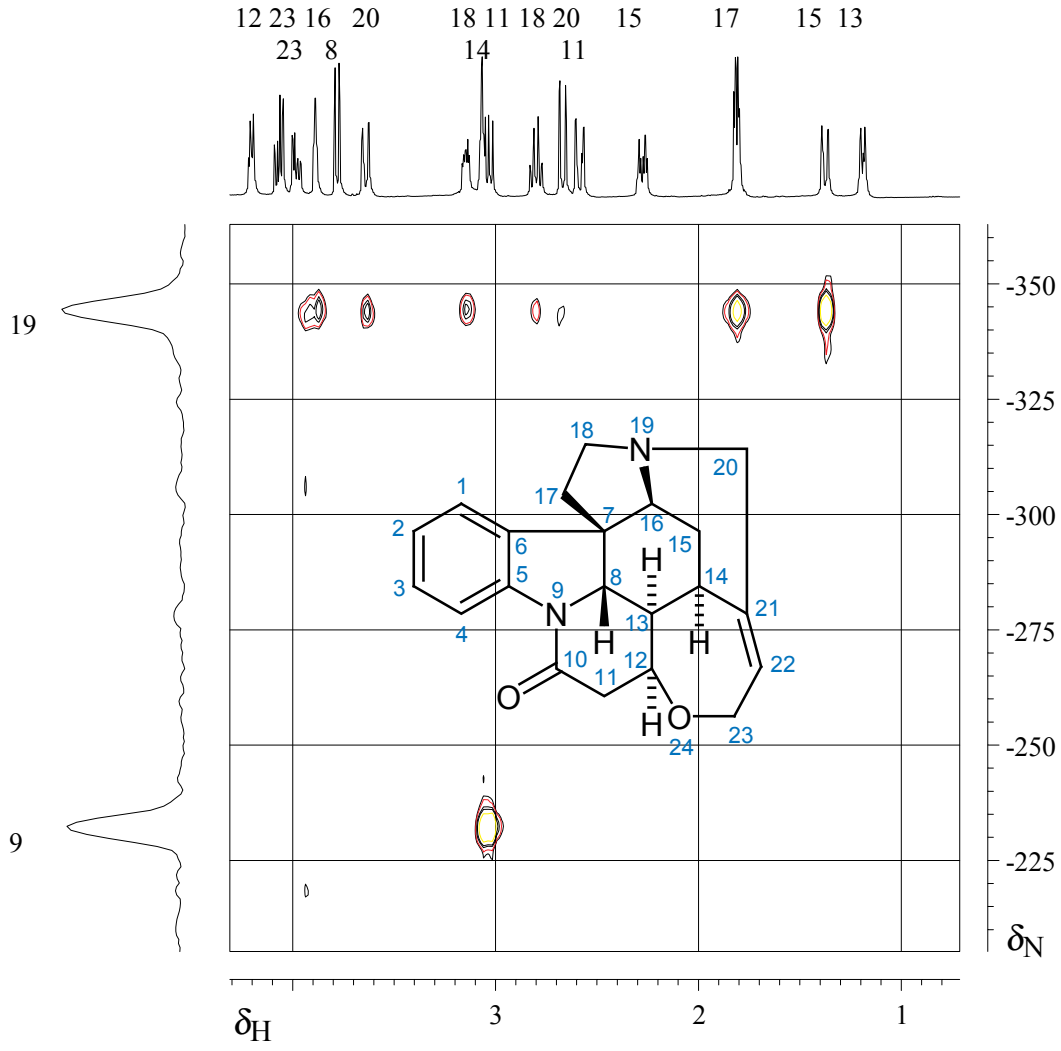

Fig. 4.2-5 $^1H,^{15}N$ HMQC spectrum of strychnine

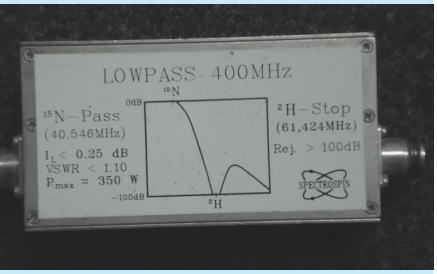

Fig. 4.2-6 Typical ^{15}N low pass filter with lock stop

[4] S. Berger, S. Braun, H.-O. Kalinowski, "NMR Spectroscopy of the Non-Metallic Elements" Wiley, Chichester, **1997**, Chapter 4, 111−318.

[5] J. Mason, L. F. Larkworthy, E. A. Moore, "Nitrogen NMR spectroscopy of metal nitrosyls and related compounds" *Chem. Rev*. **2002**, *102*, 913−934.

[6] G. E. Martin, A. J. Williams, "Long-range ^{1}H-^{15}N heteronuclear shift correlation" *Annu. Rep. NMR Spectrosc*. **2005**, *55*, 1−119.

[7] R. Marek, A. Lycka, "^{15}N NMR spectroscopy in structural analysis" *Curr. Org. Chem*. **2002**, *6*, 35−66; **2007**, *11*,1154−1205.

[8] G. E. Martin, M. Solntseva, A. J. Williams, "Applications of ^{15}N NMR spectroscopy in alkaloid chemistry" in *Modern Alkaloids*, Chapter 14, Wiley, **2008**, 409−471.

The amide ^{15}N nucleus N-9 ($\delta_N = -233$) couples with one of the protons 11, whereas the other one, presumably because of the small coupling constant (Karplus relationship), does not give a correlation signal. The tertiary amine nitrogen ($\delta_N = -345$) does show correlation signals to all protons that are separated by two bonds (16, 18, and 20) and furthermore a correlation signal over three bonds to one of the protons 15.

7. Comments

Note that the gradient ratios are quite different, compared with a $^{1}H,^{13}C$ correlation, since the ratio of the gyromagnetic ratios of ^{15}N and ^{1}H is about 1 : 10. It is advantageous to use the exact gradient ratios as extracted from the carrier frequencies in both channels of the instrument. Gradients should not only select the desired coherences but also most efficiently deselect the undesired ones, and there are computer programs which perform this task.

Also keep in mind that for ^{15}N two different shift scales are common. The organic reference compound is CH_3NO_2, whereas for biological samples NH_3 is used. The difference between them is 380 ppm. Accordingly, two different Ξ values are defined.

8. Questions

A. What is the main disadvantage of ^{14}N, although its natural abundance is near to 100 %?

B. How would the INEPT spectrum of ^{1}H-coupled formamide look?

C. If a compound contains an NH nitrogen and a nitrogen without a hydrogen atom, is it possible to perform an inverse detection of both nitrogens in one setting?

9. Own Observations

Experiment 4.3

^{17}O NMR Spectroscopy

1. Purpose

This experiment demonstrates the technique used to obtain NMR spectra of ^{17}O (I = 5/2, natural abundance 0.037%). ^{17}O is a quadrupolar nucleus with a relatively low γ value. Probe-head ringing poses an experimental problem for these types of nuclei, resulting in considerable baseline roll.

2. Variants

There are several techniques to remove the base line roll caused by the probe ringing.The easiest method is to lengthen the preacquisition delay from the typical value of 4 µs used for spin ½ nuclei such as ^{13}C to about 50 µs. However, this may already induce a significant loss of signal to noise and introduces large phase distortions of first order. Special pulse sequences have been developed to alleviate the ring down problem such as RIDE [1] (**RI**ng **D**own **E**limination) or ARING from the Bruker company. 2D NMR applications involving ^{17}O are – though not impossible – rather rare due to the quadrupolar properties of the nucleus.

3. Pulse Scheme and Phase Cycle

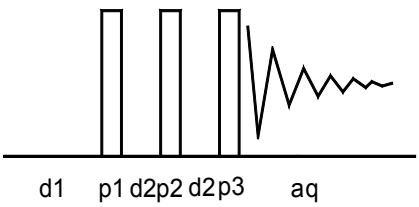

p1: x
p2: -x, x
p3: x, x, -x, -x, y, y, -y
aq: x, -x, -x, x, y, -y, -y

Scheme 4.3-1

4. Acquisition

Special values used for the spectrum shown:

Sample: neat ethylcrotonate in a 10 mm NMR tube
Time requirement: 15 min
Spectrometer: Bruker DRX-600 with 10-mm BBO probe

Set up your spectrometer to ^{17}O, find the signal using a sample of D_2O, since the ^{17}O content of D_2O is a little bit higher than that of normal water, and determine the 90° transmitter pulse length. The reference compound is D_2O, (Ξ-scale). Be sure to remove any ^{2}H stop filter from the transmitter line, since ^{17}O and ^{2}H NMR frequencies are rather similar at lower field strengths.

td : 64K
sw: 1200 ppm
aq: 0.08 s
o1: 100 ppm above the frequency of the ^{17}O water signal
d1: 1s
d2: 3 µs

Fig. 4.3-1 Liquid oxygen in a transparent dewar with its typical pale blue color

Common values:

p1, p2, p3: 90° ^{17}O transmitter pulse
d1: relaxation delay
d2: short switching delay

preacquisition delay: 6 μs
ns: 820

5. Processing

Use standard 1D processing with exponential multiplication (lb = 200 Hz).

6. Result

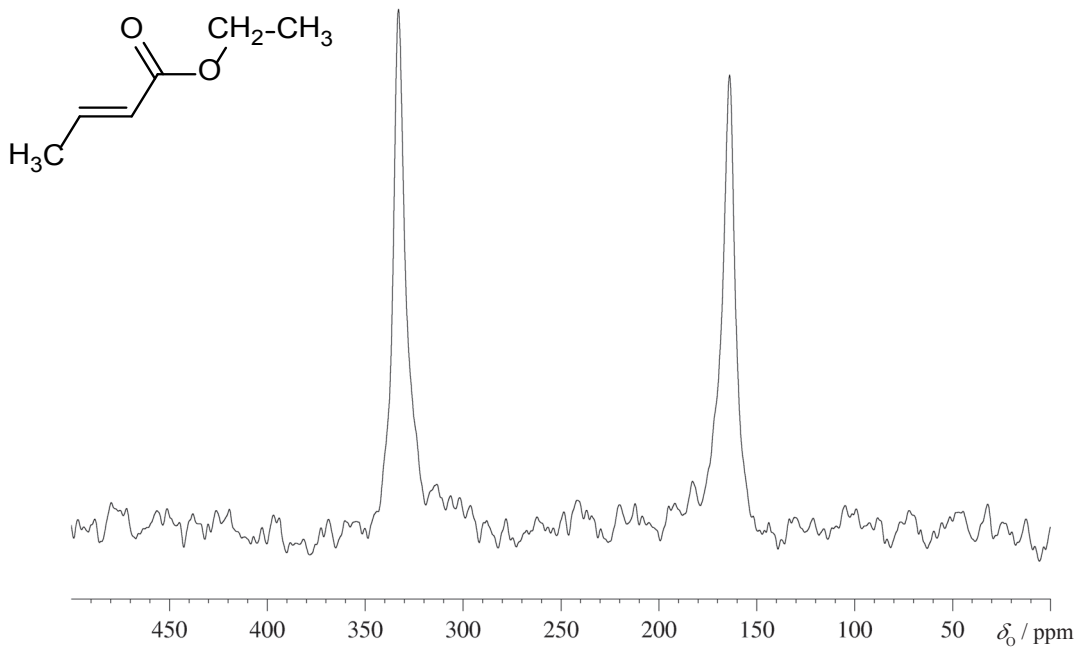

Fig.4.3-2 ^{17}O NMR spectrum of ethylcrotonate

The figure shows the 54.24 MHz ^{17}O NMR spectrum obtained on a DRX-600 spectrometer with a 10 mm multinuclear probe-head. A carboxylic ester gives two signals, one for the C=O oxygen (here at $\delta_O = 333$) and one for the C−O oxygen (here at $\delta_O = 164$). As an exercise record a normal ^{17}O NMR spectrum and compare the baseline roll.

7. Comments

The reasoning behind the ARING sequence shown here is that probe-head ring-down is dependent on the phase of the r.f. pulses, but independent of any previous pulses.Thus, using the phase cycling of the pulse program shown above we can deduce the following result after the three pulses, where **R** stands for ringing and **S** for the signal:

p1	x	x	x	x
p2	−x	x	−x	x
p3	x	x	−x	−x
	+R	+3R	−R	+R
	−S	+S	+S	−S

Since the receiver has the phases

Rec:	x	−x	−x	x
	+R	−3R	+R	+R
	−S	−S	−S	−S

we end up with no ringing contribution, but with four times the desired signal.

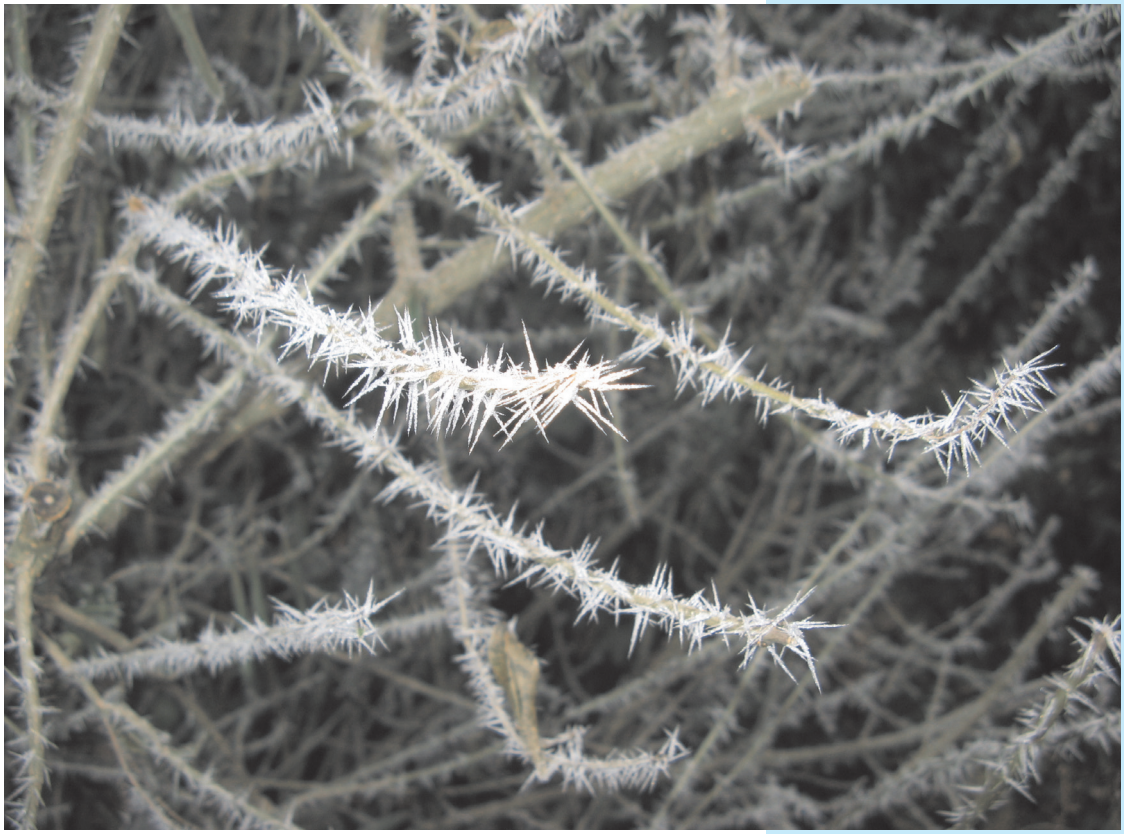

Fig. 4.3-3 As H_2O is the chemical compound with the highest oxygen content we show a picture of ice crystals forming dendrites. Photograph by courtesy of Dr. H.-J. Höbler, Mineralogical and Petrographical Collection, University of Leipzig.

The ^{17}O isotope is therefore one of the more difficult nuclei to observe by NMR spectroscopy. It is however of great interest to use a nucleus, such as oxygen, that is located at strategic molecular sites and is directly involved in inter- and intra-molecular interactions. The ^{17}O NMR parameters, i.e., isotropic shielding, principal elements of the ^{17}O shielding and electric field gradient tensors and transverse and longitudinal relaxation times can be considered as excellent means for probing structure, bonding and dynamics of oxygen containing compounds. Further, recent advances in instrumentation, the extremely large chemical shift scale (which aids in, several cases, in the resolution of quadrupole broadened resonances) and the availability of ^{17}O enriched compounds have alleviated some of the experimental difficulties; thus, an increased use of the ^{17}O NMR technique can be foreseen.

Taken from ref. [4]

[1] P. S. Belton, I. J. Cox, R. K. Harris, *J. Chem. Soc. Faraday Trans. 2* **1985**, *81*, 63−75.

[2] D. W. Boykin (ed.), *^{17}O NMR in Organic Chemistry*, CRC Press, Boca Raton, Florida, **1991**, 1−325.

[3] S. Berger, S. Braun, H.-O. Kalinowski, *NMR Spectroscopy of the Non-Metallic Elements*, Wiley, Chichester, **1997**, 19−397.

[4] I. P. Gerothanassis "Oxygen-17 NMR spectroscopy: Basic principles and applications" *Prog. NMR Spectrosc*. **2010**, *56*, 95−197.

8. Questions

A. Why can the ^{17}O content in D_2O be higher than that in H_2O?

B. Why are ^{17}O chemical shifts reported without a decimal point?

C. What is the chemical explanation of the fact that the carbonyl oxygen is deshielded versus the ether oxygen in ethyl crotonate?

9. Own Observations

Experiment 4.4

^{19}F NMR Spectroscopy

1. Purpose

The ^{19}F nucleus (I = 1/2, natural abundance 100 %) has nearly the same NMR sensitivity as the proton and may occupy equivalent positions in an organic molecule. However, fluorine is much less widely distributed than hydrogen and hardly occurs at all in natural compounds, and therefore it does not have the same importance for NMR spectroscopy, although it has been investigated since the very beginning of NMR. On the other hand, it is exactly for this reason that the nuclide is very well suited for biochemical and medical applications, so that ^{19}F NMR spectroscopy plays an increasing role in these areas [3,7].

2. Variants

Because of the proximity of the resonance frequencies of ^{1}H and ^{19}F it may be possible to tune a proton probe to the ^{19}F frequency, so that no special equipment, other than an ^{19}F preamplifier, is needed for the standard experiment described here. However, often one wants to measure fluorine under proton decoupling, and for this special equipment is necessary. Since fluorine behaves in many respects just like the proton, nearly all proton-based 1D and 2D NMR experiments, e.g., COSY, can be performed using fluorine as well. In addition, there exist ^{1}H,^{19}F correlation techniques using the spin coupling or the dipolar relaxation (HOESY) as the parameter [5]. 2D ^{13}C^{19}F correlation techniques are also known [8].

3. Pulse Scheme and Phase Cycle

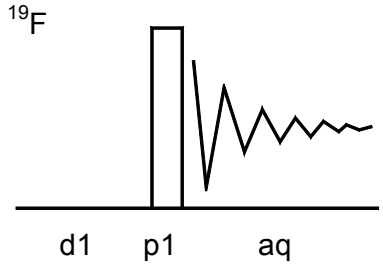

p1: x, x, -x, -x, y, y, -y, -y

aq: x, x, -x, -x, y, y, -y, -y

Scheme 4.4-1

Common values:

p1: 90° ^{19}F transmitter pulse
d1: relaxation delay

4. Acquisition

Special values used for the spectrum shown:

Sample: 1 % CCl_3F (one drop) in $CDCl_3$
Time requirement: 5 min
Spectrometer: Bruker ARX-300 with 5-mm-^{1}H/^{13}C dual probe, detuned for ^{19}F

Set up your spectrometer to ^{19}F, find the signal, and determine the 90° transmitter pulse-length. CCl_3F serves as the reference compound for ^{19}F NMR, its Ξ value = 94.094011. If your sample contains TMS, you may use this for Ξ-referencing.

td: 64K
sw: 300 ppm (typical range for fluorine bonded to carbon)
aq 0.387 s
o1: about 100 ppm below the frequency of CCl_3F (center of that range)
p1: 30° ^{19}F transmitter pulse
d1: 1 s
ns: 1

5. Processing

Use standard 1D processing.

6. Result

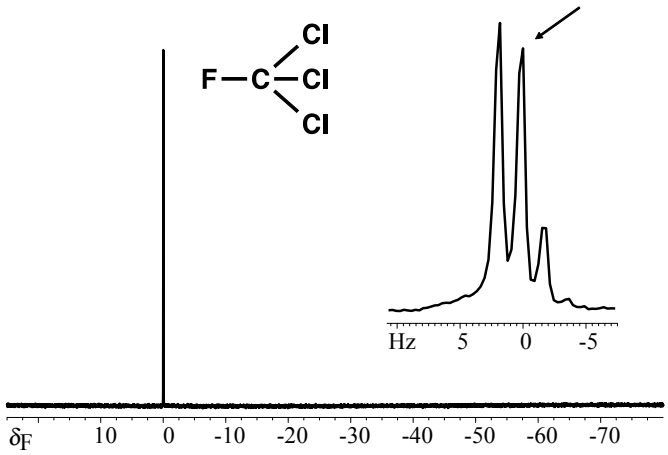

Fig. 4.4-1 ^{19}F NMR spectrum of CCl_3F

The figure shows the 282.1 MHz ^{19}F NMR spectrum obtained on an ARX-300 spectrometer with a 5 mm $^{1}H/^{13}C$ dual probe tuned to the ^{19}F resonance frequency and using an ^{19}F preamplifier for that frequency. In order to achieve better resolution the experiment was repeated with improved digital resolution (see inset). As an exercise you may record an $^{19}F,^{19}F$-COSY spectrum on a mixture of *cis/trans* perfluorodecalin (commercially available) or a 2D *J*-resolved ^{19}F NMR spectrum on 2,4,5-trifluoroaniline. Both experiments may be performed in the above configuration, since they don't need an ^{1}H channel.

7. Comments

The fine structure of the ^{19}F signal of CCl_3F results from the different chlorine isotopomers; $C^{35}Cl_2{}^{37}ClF$ is used for the calibration of high-precision ^{19}F NMR spectra. Although isotopes have the same electronic properties within the Born–Oppenheimer approximation, they cause slightly different chemical shifts for a nearby nucleus. This is due to a different ground state vibrational energy, which alters the average bond lengths; the heavier isotope usually causes the lower resonance frequency.

Although fluorine is the most abundant halogen in the earth's crust, it plays a very minor role in biology; fluorinated compounds, biosynthesised *de novo*, are rare in nature. This reflects the properties of the fluoride ion, such as its high redox potential and its propensity to become hydrated, but also the predominantly insoluble character of fluorine containing minerals, such as fluorspar (CaF_2), which renders fluorine biologically unavailable compared with the other halogens. Nevertheless, the uniqueness of fluorine has resulted in this element being increasingly important in the area that is broadly defined as 'chemical biology'.
The fluorine atom is isosteric with hydroxyl and its Van der Waal's radius (1.47Å) is close to that of hydrogen (1.20Å), thus its substitution in organic compounds results in a sterically unchanged product. However, these substitutions have profound effects on the electronic properties of the compound, since fluorine's electronegativity (4.0 on the Pauling scale) is the greatest of all the elements, and the bond dissociation energy of C-F (110 kcal mol^{-1} in CH_3F) is greater than that of C-H (99 kcal mol^{-1}). Thus fluorinated derivatives of naturally occurring compounds, such as metabolic intermediates, have proved extremely useful in medicine and agriculture, and the numbers of fluorinated compounds used in these areas are ever increasing

Taken from ref. [7]

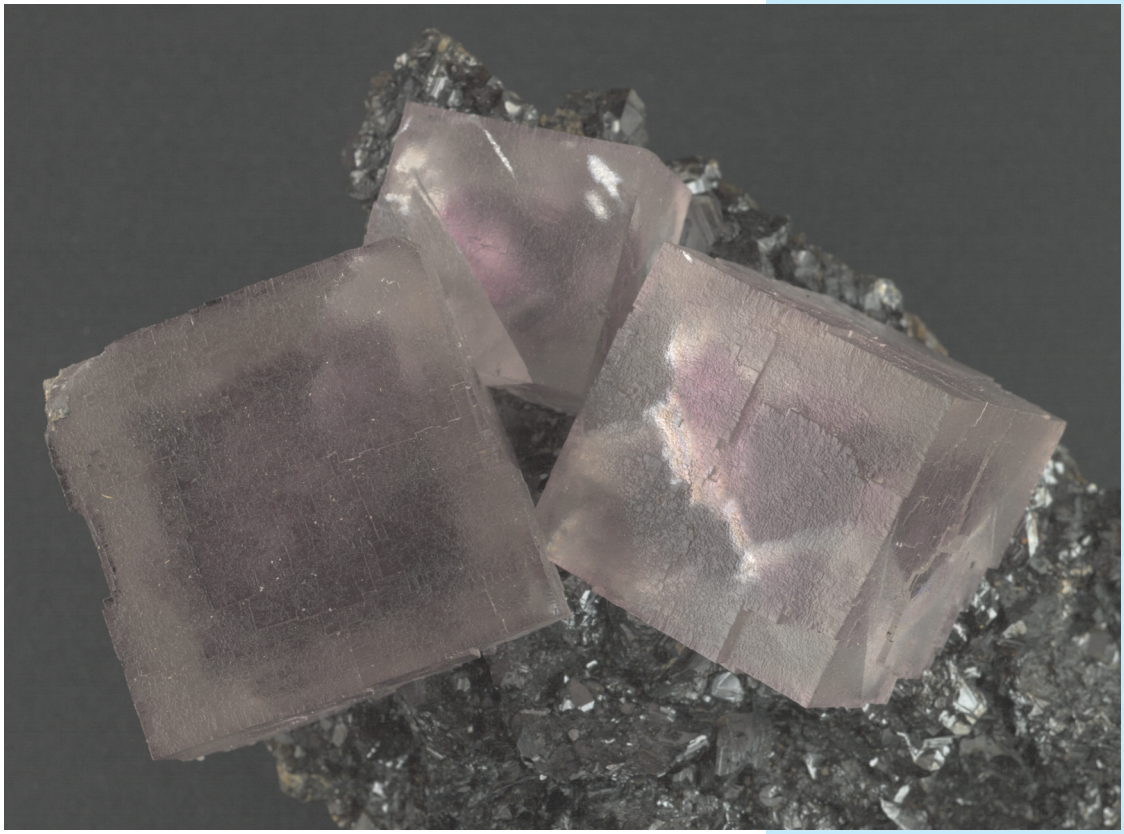

Fig. 4.4-2 Fluorite mineral, composed of calcium fluoride, CaF_2. It is an isometric mineral with a cubic habit .The word fluorite is derived from the Latin root fluo, meaning "to flow" because the mineral is used in iron smelting to decrease the viscosity of slags at a given temperature.
In 1852 fluorite gave its name to the phenomenon of fluorescence, which is prominent in fluorites from certain locations, due to certain impurities in the crystal. Fluorite also gave the name to its constitutive element fluorine. Photograph by courtesy of Dr. H.-J. Höbler, Mineralogical and petrographical collection, University of Leipzig.

[1] J. T. Gerig, "Fluorine NMR of Proteins", *Prog. NMR Spectrosc*. **1994**, *26*, 293−370.

[2] S. Berger, S. Braun, H.-O. Kalinowski, *NMR Spectroscopy of the Non-Metallic Elements*, Wiley, Chichester, **1997**, Chapter 6, 398−699.

[3] P. Bachert, "Phamacokinetics using Fluorine in vivo", *Prog. NMR Spectrosc*. **1998**, *33*, 1−56.

[4] J. M. Seco, E. Quinoa, R. Riguera, "The assignment of absolute configuration by NMR" *Chem. Rev*. **2004**, *104*, 17−117.

[5] J. Battiste, R. A. Newmark, "Applications of ^{19}F multidimensional NMR" *Progr. NMR Spectrosc*. **2006**, *48*, 1−23.

[6] P. Espinet, A. C. Albeniz, J. A. Casares, J. M. Martinez-Ilarduya, "^{19}F NMR in organometallic chemistry", *Coord. Chem. Rev*. **2008**, *252*, 2180−2208.

[7] S. L. Cobb, C. D. Murphy, "^{19}F NMR applications in chemical biology" *J. Fluor. Chem*. **2009**, *130*, 132−143.

[8] S. Berger, "2D ^{13}C,^{19}F Correlation Spectroscopy", *J. Fluorine Chem*. **1995**, *72*, 117−119.

8. Questions

A. There exist dual ^{1}H^{19}F probes. For all experiments employing these two nuclei at the same time, one needs, however, special frequency filters. Why?

B. Compared to ^{1}H, the frequency range of ^{19}F is very large and comprises only for organic compounds about 300 ppm. Give a reason for this behavior.

C. ^{19}F NMR has been widely used for detecting isotope effects of deuterium. Give a reason.

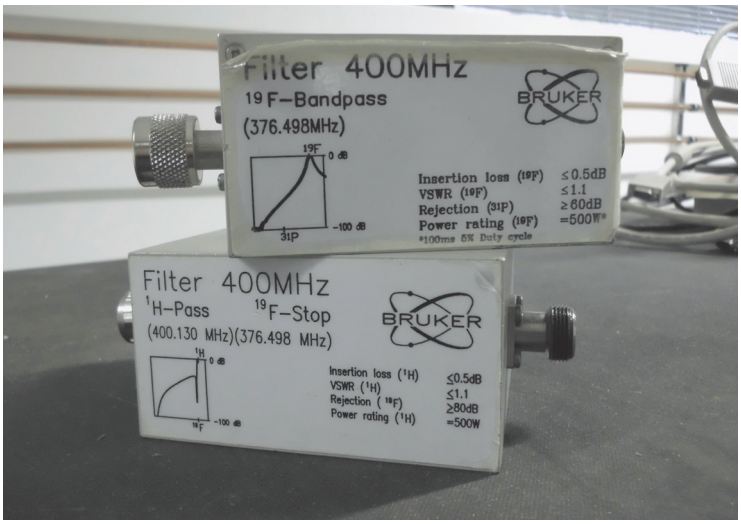

Fig. 4.4-3 Typical HF-filter units for 1H/19F double resonance experiments

9. Own Observations

Experiment 4.5

^{29}Si NMR Spectroscopy

1. Purpose

^{29}Si (I = 1/2, natural abundance 4.7 %) is a nucleus with a small negative gyromagnetic ratio. This means that under normal ^{1}H broadband decoupling conditions the nuclear Overhauser effect can lead to a reduction in signal intensity or even a cancellation of the signal. It is therefore better to use one of the polarization transfer methods such as DEPT, which can result in a sensitivity enhancement up to a factor of 5, caused by the the protons that are responsible for the polarization transfer [1]. In addition the signal of the glassware surrounding the receiver coil is suppressed since DEPT will not pass the signals of silicon atoms without protons.

2. Variants

In addition to INEPT or DEPT, also cross-polarization techniques with spin-locking can be used [3]. Of course, indirect detection of ^{29}Si by 2D HMQC or HSQC is an appropriate technique. In a 1D version, this indirect detection is popular to detect the synthetic outcome for silicon-containing protection groups [4].

3. Pulse Scheme and Phase Cycle

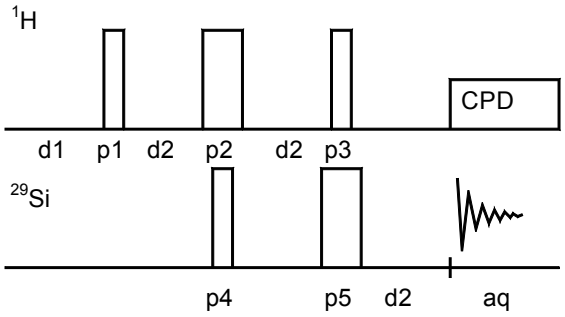

p1: x p3: $(y)_4$, $(-y)_4$ p5: $(x, -x)_4$, $(y, -y)_4$

p2: x, -x, y, -y p4: $(x)_8$, $(y)_8$, $(-x)_8$, $(-y)_8$

aq: $(y)_2$, $(-y)_4$, $(y)_2$, $(-x)_2$, $(x)_4$, $(-x)_2$, $(-y)_2$, $(y)_4$, $(-y)_2$, $(x)_2$, $(-x)_4$, $(x)_2$

Scheme 4.5-1 DEPT

4. Acquisition

Special values used for the spectrum shown:

Sample: 50 % TMS in $CDCl_3$.
Time requirement: 15 min
Spectrometer: Bruker AM-400

A wave of NMR applications began when it was realized in 1972 that the precision of hydroxyl and carboxyl group quantitation can be increased by a nine-fold amplification of the ^{1}H NMR signal through the conversion of a OH into a $Si(CH_3)_3$ group. Applications in ^{1}H NMR spectroscopy of polyols, coal liquefaction oils, and other coal products were soon followed by ^{13}C NMR spectroscopy of similarly important samples. The first systematic investigations of the analytical potential of trimethylsilylation combined with ^{29}Si NMR spectroscopy (TMS ^{29}Si NMR tagging) were undertaken independently by the group of Harris and in our laboratory in 1975. Progress was slow until 1979, when a great impetus came from the invention of INEPT by Morris and Freeman. With a manifold increase in the sensitivity of ^{29}Si NMR measurement, the pace of progress quickened and practical applications have became feasible.

Taken from ref. [2]

Common values:

p1: 90° ^{1}H transmitter pulse
p2: 180° ^{1}H transmitter pulse
p3: 90° ^{1}H transmitter pulse
- see "7. Comments"
p4: 90° ^{29}Si transmitter pulse
p5: 180° ^{29}Si transmitter pulse
d1: relaxation delay
d2: 1/[2J(Si,H)]

td: 64K
sw: 250 ppm
aq: 1.65 s
o1: 70 ppm below the frequency of the ^{29}Si signal of TMS
o2: middle of ^{1}H NMR spectrum
d1: 1 s
d2: 1/[2J(Si,H)] = 71 ms, calculated from ^{2}J (^{29}Si,^{1}H) = 7 Hz
ds: 2
ns: 32

5. Processing

Use standard 1D processing as described in Experiment 1.2.

6. Result

The figure shows the 79.44 MHz ^{29}Si NMR spectrum obtained for TMS with an AM-400 spectrometer. Spectrum **a** is a normal spectrum, which shows in addition to the TMS signal a broad signal at approximately −110 ppm. This signal is due to the glass NMR tube and the quartz insert surrounding the receiver coil. Spectrum **b** was taken with the DEPT sequence under otherwise identical conditions. Note the improvement in the signal-to-noise ratio. The broad signal of the glass is suppressed.

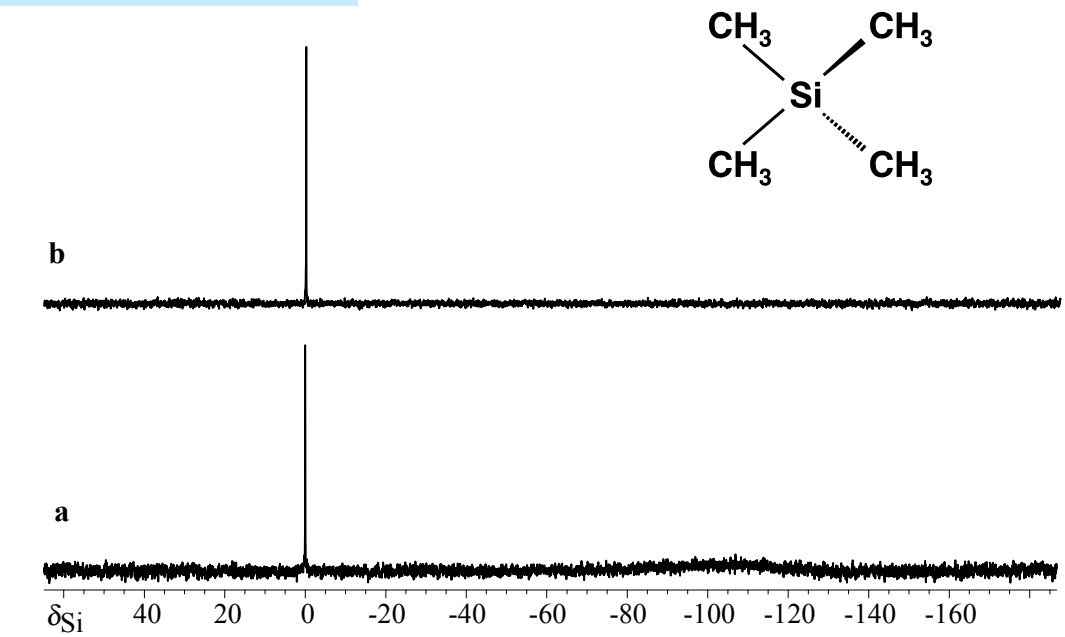

Fig. 4.5-1 **a**: Spectrum inverse gated decoupled, **b**: DEPT spectrum

7. Comments

In the DEPT experiment the optimal polarization transfer is controlled by the angle α of the last pulse p3. The optimum pulse angle α_{opt} is independent of J, but depends on the number of coupled nuclei n of the polarization source, usually protons, as given in Equation (1):

$$\alpha_{opt} = \arcsin (n)^{-1/2} \text{ radians} \quad (1)$$

Number of protons n	1	2	3	6	9	12
Pulse angle α_{opt} (in degrees)	90	45	35	24.1	19.5	16.8

For silicon compounds n is usually larger than for carbon atoms. The NOE enhancement is independent of the number of protons and has a theoretical limit of $\eta = 1 + \gamma_H / 2\gamma_{Si} = -1.5$ for ^{29}Si.

Fig. 4.5-2 Quartz (SiO_2) is the main source of pure silicon, forming a large variety of crystals and precious gemstones. Photograph by courtesy of Dr. H.-J. Höbler, Mineralogical and petrographical collection, University of Leipzig.

[1] T. A. Blinka, B. J. Helmer, R. West, "Polarization transfer NMR spectroscopy for silicon-29: The INEPT and DEPT techniques" *Adv. Organomet. Chem*. **1984**, *23*, 193−218.

[2] J. Schraml, "Silicon-29 NMR spectroscopy of trimethylsilyl tags" *Prog. NMR Spectrosc*. **1990**, *22*, 289−348.

[3] R. Wagner, S. Berger, "Spin lock versus INEPT and DEPT polarization transfer for ^{29}Si NMR spectroscopy" *Phosphorus, Sulfur, Silicon, and Rel. Elements* **1994**, *91*, 213−218.

[4] G. Aagaard, N. R. Andersen, K. Schaumburg "Determination of protection group position in silylated vitamin D analogs by proton-detected one-dimensional ^{1}H-^{29}Si correlation" *Magn. Reson. Chem*. **1996**, *34*, 945−947.

[5] Y. Takeuchi, T. Takayama, "^{29}Si NMR spectroscopy of organosilicon compounds" *Chem. Org. Silicon Compds*. **1998**, *2*, 267−354.

[6] J. Schraml, "^{29}Si NMR experiments in solutions of organosilicon compounds" *Chem. Org. Silicon Compds*. **2001**, *3*, 223−339.

[7] B. Wrackmeyer, "Applications of ^{29}Si NMR parameters" *Annu. Rep. NMR Spectrosc*. **2006**, *57*, 1−49.

8. Questions

A. What kind of multiplet do you expect, running a proton coupled ^{29}Si NMR spectrum of TMS? What are the intensities of the outer lines?

B. How large with respect to the main signal will be the ^{13}C satellites of a ^{29}Si NMR spectrum of TMS?

C. Is it possible to record a ^{29}Si,^{13}C 2D NMR correlation spectrum?

D. What do you expect from a ^{29}Si-NMR spectrum of silicone oil?

9. Own Observations

Experiment 4.6

^{57}Fe NMR Spectroscopy

1. Purpose

^{57}Fe (I = 1/2, natural abundance 2.12 %) is a nucleus with a very low gyromagnetic ratio and, together with its low abundance, a nucleus very difficult to measure. The accepted reference standard is $Fe(CO)_5$, better to be used as neat liquid, and this is the compound which defines the Ξ-value of ^{57}Fe, 3.237778 MHz. The difficulty to observe ^{57}Fe NMR signals is mainly due to the sensitivity and long relaxation time. Hydrogen atoms are usually not directly bonded to iron, and therefore the relaxation times can be longer than a minute. The large chemical shift range of up to several thousand ppm causes, however, no problems due to the low gyromagnetic ratio. The frequency range is well below the frequencies encountered with ^{13}C. An issue may occur by the probe in use which must be capable of measuring low frequencies. Furthermore, in metalorganic compounds often dynamic equilibria are occurring which may broaden the signals. We show here as an example the standard NMR spectrum of $Fe(CO)_5$ and show a two-dimensional detection by ^{13}C both for the pentacarbonyl and for ferrocene.

2. Variants

Besides the normal single-pulse experiment with and without proton decoupling, INEPT polarization transfer from a distant proton has been reported. Inverse detection (HMQC) via carbon or phosphorus has also been used.

3. Pulse Scheme and Phase Cycle

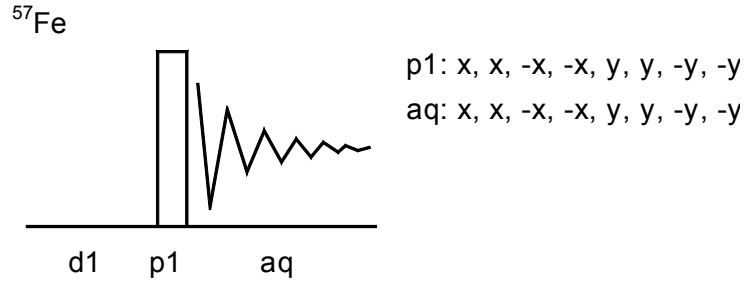

Scheme 4.6-1

4. Acquisition

Special values used for the spectrum shown:

When tuning and matching the first time for ^{57}Fe NMR it is advisable to start from a nearby nucleus, the parameters of which are given by the manufacturer, such as ^{109}Ag in this case. Go down to the iron frequency in small steps.

Sample: neat liquid $Fe(CO)_5$ with a few drops of benzene-d_6 for locking
Time requirement: 7 h
Spectrometer: Bruker DRX-600, 5 mm TBI probe

[1] T. Jenny, W. von Philipsborn, J. Kronenbitter, A. Schwenk "Direct observation of ^{57}Fe Chemical Shifts in diamagnetic organoiron complexes" *J. Organomet. Chem*. **1981**, *205*, 211–222.

[2] E. Haslinger, K. Koci, W. Robien, K. Schlögl "Ferrocene derivatives, Part 67, ^{57}Fe-NMR spectroscopy of ferrocenes" *Monatsh. Chem.* **1983**, *114*, 495–499.

[3] A. Hafner, W. von Philipsborn "Mechanisms for the longitudinal and transverse relaxation of iron-57" *J. Magn. Reson*. **1987**, *74*, 433–449.

[4] R. Benn, A. Rufinska, M. S. Kralik, R. D. Ernst "Structural characterization of open, half-open, and closed ferrocenes in solution by ^{57}Fe and ^{13}C NMR spectroscopy" *J. Organomet. Chem*., **1989**, *375*, 115–121.

Common values: (1D experiment)

p1: 90° ^{57}Fe transmitter pulse
d1: relaxation delay

[5] A. Houlton, P. T. Bishop, R. M. G. Roberts, J. Silver, M. Herberhold "Mössbauer studies on ferrocene complexes XVII. Ferrocenylamines and ferrocenylphosphines" *J. Organomet. Chem* **1989**, *364*, 381–389.

[6] A. Houlton, R. M. G. Roberts, J. Silver, J. Zakrzewski "Mössbauer studies on ferrocene complexes XVIII. A comparative study of azaferrocenes and phosphaferrocenes and their derivatives by ^{57}Fe Mössbauer and ^{13}C NMR spectroscopy" *J. Organomet. Chem* **1993**, *45*, 107–111.

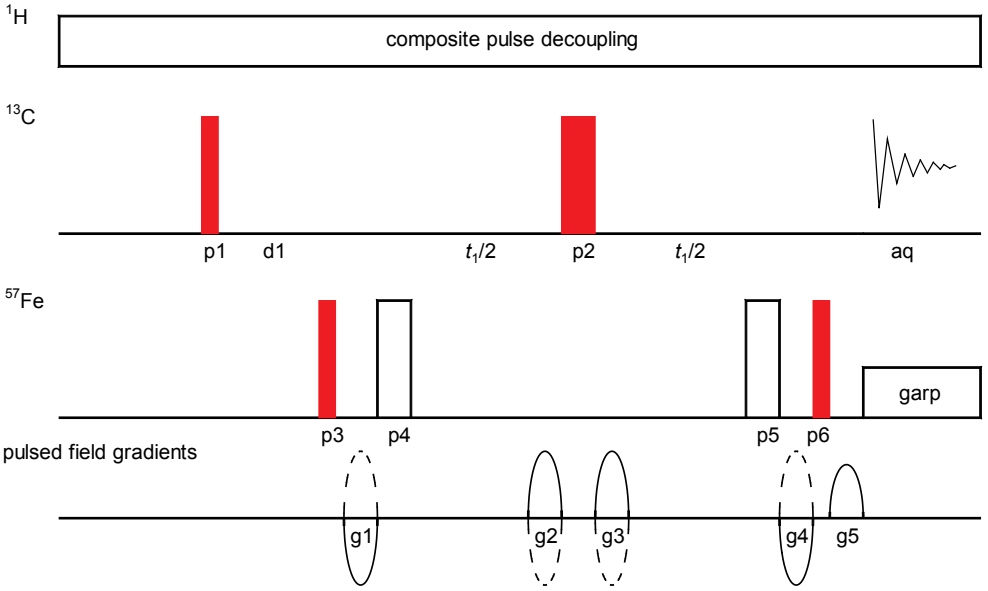

p1: x p2: x, x, -x, -x p3, p4: x, -x p5, p6: $(x)_4$, $(-x)_4$ aq: x, -x, x, -x, -x, x, -x, x

Scheme 4.6-2 HMQC, echo-antiecho mode

[7] G. Schreckenbach "The ^{57}Fe nuclear magnetic resonance shielding in ferrocene revisited. A density-functional study of orbital energies, shielding mechanisms, and the influence of the exchange-correlation functional" *J. Chem. Phys.* **1999**, *110*, 11936–11949.

[8] B. Wrackmeyer, O. L. Tok, M. Herberhold "^{57}Fe NMR of ferrocenes by ^{1}H-^{57}Fe INEPT techniques" *Organometallics* **2001**, *20*, 5774–5776.

[9] B. Wrackmeyer, O. L. Tok, A. Ayazi, H. E. Maisel, M. Herberhold "^{57}Fe NMR spectroscopy of ferrocenes bearing π-acceptor substituents" *Magn. Reson. Chem.* **2004**, *42*, 827–830.

[10] C. López, R. Bosque, S. Pérez, A. Roig, E. Molins, X. Solans, M. Font-Bardía "Relationships between ^{57}Fe NMR, Mössbauer parameters, electrochemical properties and the structures of ferrocenylketimines" *J. Organomet. Chem.* **2006**, *691*, 475–484.

td: 4866
sw: 25 ppm
aq: 5.0 s
o1: 10 ppm to higher frequency from the reported Ξ-value
d1: 90 s
ns: 256

5. Processing

Use standard 1D processing with a lb value of 5 Hz. Use the ^{1}H NMR spectrum of the benzene solution with TMS for Ξ-referencing.

6. Result

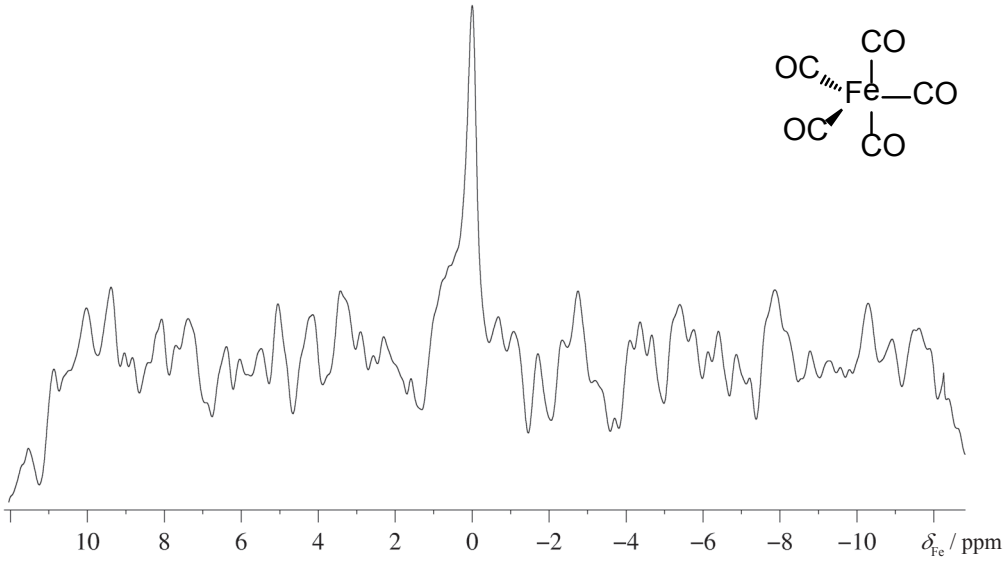

Fig. 4.6-1 ^{57}Fe NMR spectrum of $Fe(CO)_5$

The figure shows the 19.43 MHz ^{57}Fe NMR spectrum obtained from iron pentacarbonyl with a DRX-600 spectrometer.

Special values used for the 2D spectrum shown below:

Time requirement: 6 h
Spectrometer: Bruker DRX-600, 5 mm TBI probe head

td2: 2K
td1: 128
sw2: 25 ppm
sw1: 25 ppm
aq2: 0.27 s
aq1: 0.128 s
o1: 208 ppm
o2: 10 ppm
d1: 20 s
d2: 0.02 s
g1:g2:g3:g4:g5 = 80 % : 80 % : 80 % : 80 % : 41.3 %
(100 % ≈ 0.56 T/m)
ns: 8

Common values (2D experiment)

p1: 90° pulse on ^{13}C
p2: 180° pulse on ^{13}C
p3, p6: 90° pulse on ^{57}Fe
p4, p5: 180° pulse on ^{57}Fe
d1: $1/[2\times J_{Fe,C}]$

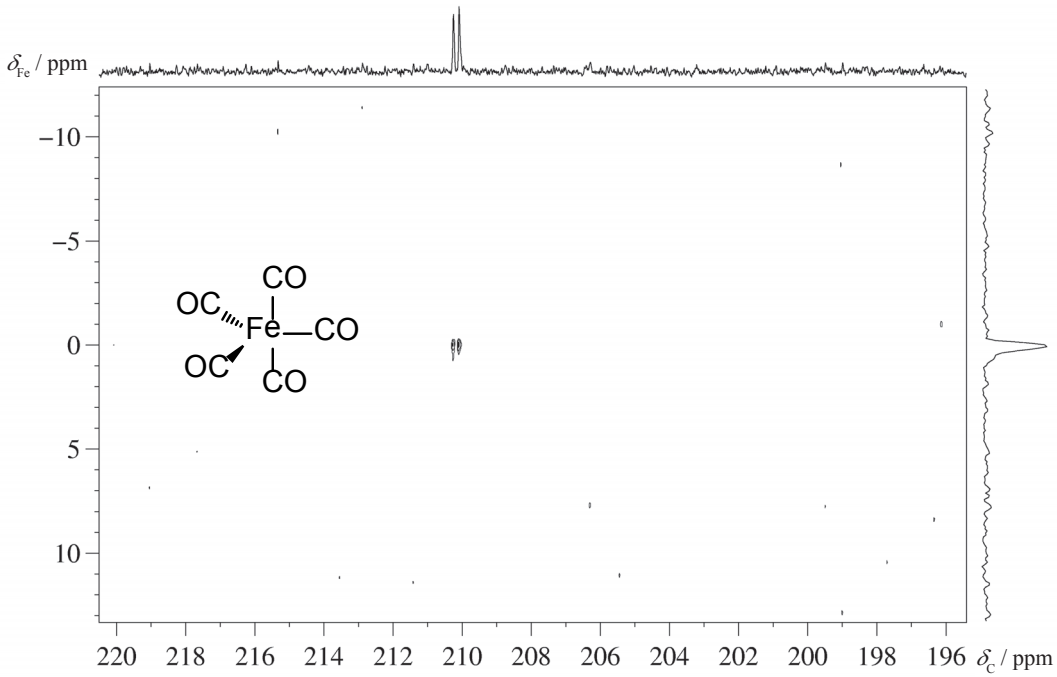

Fig. 4.6-2 ^{57}Fe, ^{13}C-HMQC of $Fe(CO)_5$

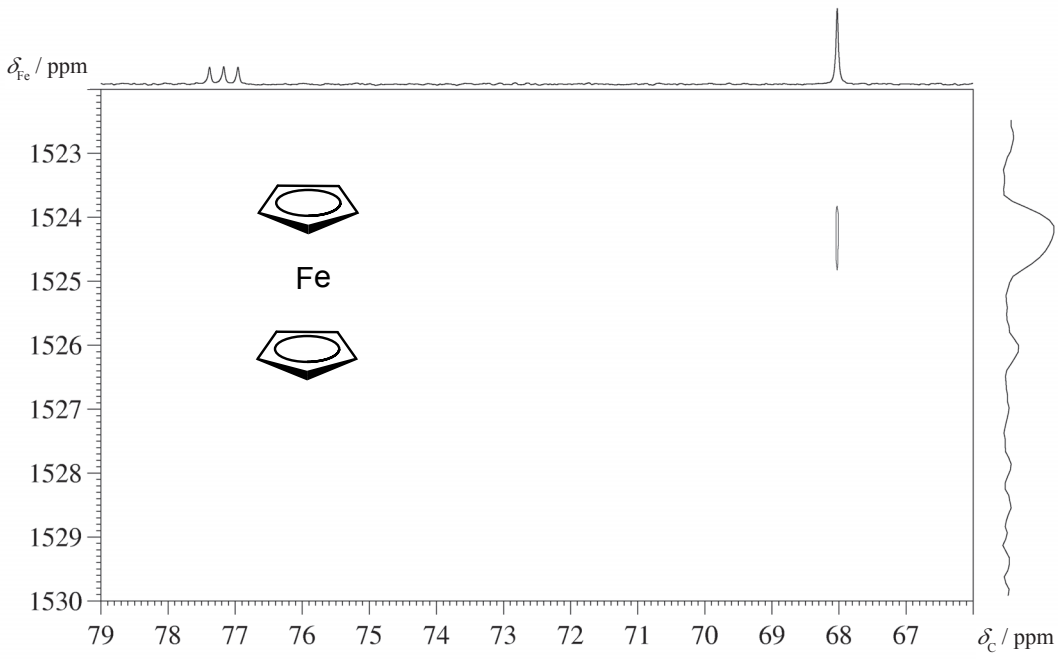

Fig. 4.6-3 ^{57}Fe, ^{13}C-HMQC of ferrocene

In Fig. 4.6-2 the 2D gradient selected echo-antiecho HMQC of $Fe(CO)_5$ spectrum without proton and without iron decoupling is represented to display the $^1J_{Fe,C}$ spin coupling constant of 24 Hz.

As the final example, we show in Fig. 4.6-3 the 2D spectrum of ferrocene in a saturated $CDCl_3$ solution, one of the magic compounds of iron chemistry. Similar parameters to those above have been used, but different offsets, and d2 was set for 5 Hz to 0.1 s. This time both ^{1}H and ^{57}Fe decoupling was used.

Fig. 4.6-4 Hematite (blood ore) Fe_2O_3, from Cumbria (UK), photograph by courtesy of Dr. H.-J. Höbler, Mineralogical and Petrographical collection, University of Leipzig.

7. Comments

The pulse sequence shown for echo-antiecho gradient selected 2D HMQC method on three spectrometer channels deserves some comments. The typical set-up on Bruker instruments would be ^{13}C on the first spectrometer r.f. cannel, ^{1}H on the second, and ^{57}Fe on the third. Using a TBI probe head, the r.f. frequency of ^{13}C is connected to the selective ^{13}C coil, the iron frequency to the BBO coil. The pulses drawn in red in the diagram are the classical four HMQC pulses and the two black 180° iron pulses are only to support the gradient action (see question A). Proton decoupling is working throughout and iron decoupling is used during acquisition.

8. Questions

A. Draw a coherence pathway diagram for the 2D sequence and confirm the used gradient strength ratio.

B. Why is it justified to use for ferrocene both ^{1}H and ^{57}Fe decoupling, but not for iron pentacarbonyl?

9. Own Observations

Experiment 4.7

^{195}Pt NMR Spectroscopy

1. Purpose

^{195}Pt (I = 1/2, natural abundance 33.8 %) is a nucleus with a medium gyromagnetic ratio and comparable to ^{13}C. The accepted reference standard is $Na_2[PtCl_6]$ in D_2O, and this is the compound which is used to define the Ξ-value of ^{195}Pt (21.496784 MHz). The difficulty to observe ^{195}Pt NMR signals is not due to the sensitivity, but due to the extremely large chemical shift range of up to 15000 ppm, which amounts on a 400 MHz spectrometer to about 1.3 MHz. This exceeds by far the maximum spectral width on most spectrometers, and one has carefully to search for the correct signal position. Furthermore, in metalorganic compounds, often dynamic equilibria are occurring which may broaden the signals. We show here as an example *trans* $Pt(NH_3)_2Cl_2$ [1], where the signal of Pt is also severely broadened by the quadrupolar interaction with the nitrogen ^{14}N ligands.

The metal platinum, of which you see some very fine specimens on the table, has been known to us about a hundred years. It has been wrought in a beautiful way in this country, in France, and elsewhere, and supplied to the consumer in ingots of this kind, or in plates, such as we have here, or in masses, that by their very fall upon the table indicate the great weight of the substance, which is, indeed, nearly at the head of all substances in that respect. This substance has been given to us hitherto mainly through the philosophy of Dr. Wollaston, whom many of us know, and it is obtained in great purity and beauty. It is a very remarkable metal in many points, besides its known special uses. It usually comes to us in grains. Here is a very fine specimen of native platinum in grains.

Michael Faraday
Lecture on Platinum, 1861

2. Variants

Besides the normal single-pulse experiment with and without proton decoupling, inverse detection (HSQC or HMQC) via protons has often been used. Also ^{31}P as the detecting nucleus can be employed in special cases of P ligands.

3. Pulse Scheme and Phase Cycle

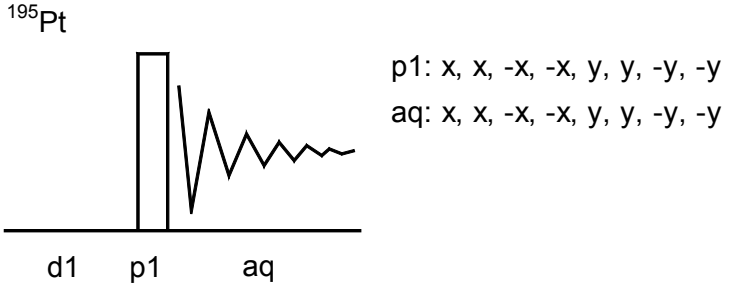

Scheme 4.7-1

Common values:

p1: 90° ^{195}Pt transmitter pulse
d1: relaxation delay

4. Acquisition

Special values used for the spectrum shown:

Sample: ca. 100 mg. *trans* $Pt(NH_3)_2Cl_2$ (commercially available) in dimethylformamide-d_7 (saturated solution)
Time requirement: 10 min
Spectrometer: Bruker DRX-600, 5 mm TBI probe

td:	20K
sw:	776 ppm
aq:	0.1 s
o1:	2100 ppm below the frequency of $Na_2[PtCl_6]$
d1:	0.5 s
ns:	1000

5. Processing

Use standard 1D processing but with a lb value of 100 Hz.

6. Result

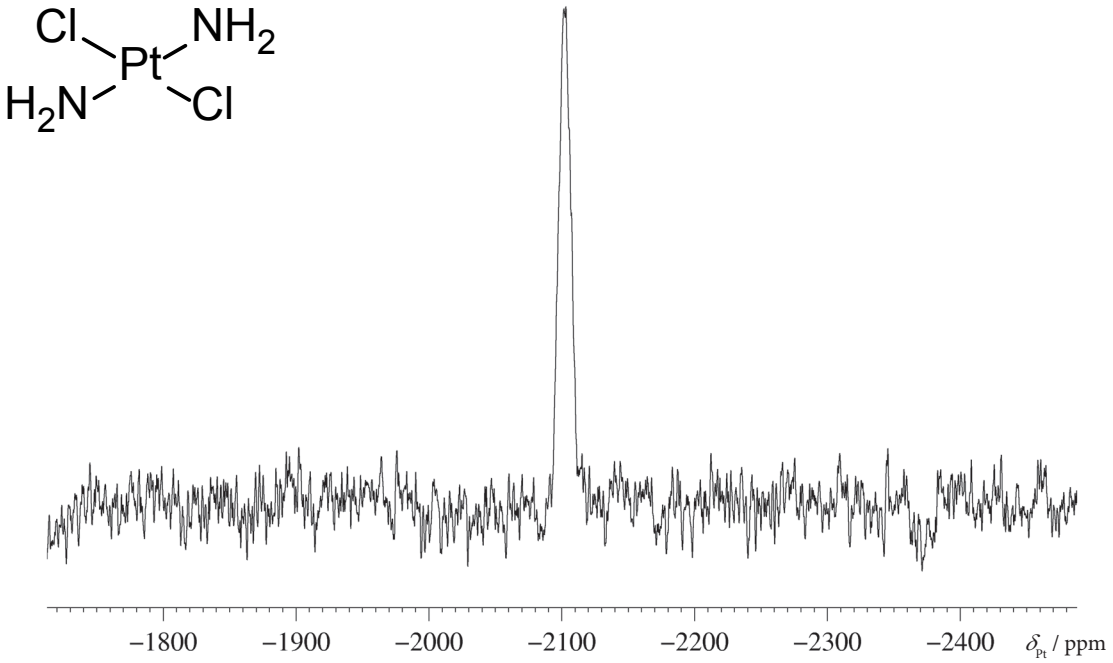

Fig. 4.7-1 ^{195}Pt NMR spectrum of trans $Pt(NH_3)_2Cl_2$

The figure shows the 129 MHz ^{195}Pt NMR spectrum obtained for *trans* $Pt(NH_3)_2Cl_2$ with a DRX-600 spectrometer. Note that the *cis*-compound is an important anti cancer drug. The line width obtained was 1428 Hz and is due to quadrupolar interaction with the amine ligands.

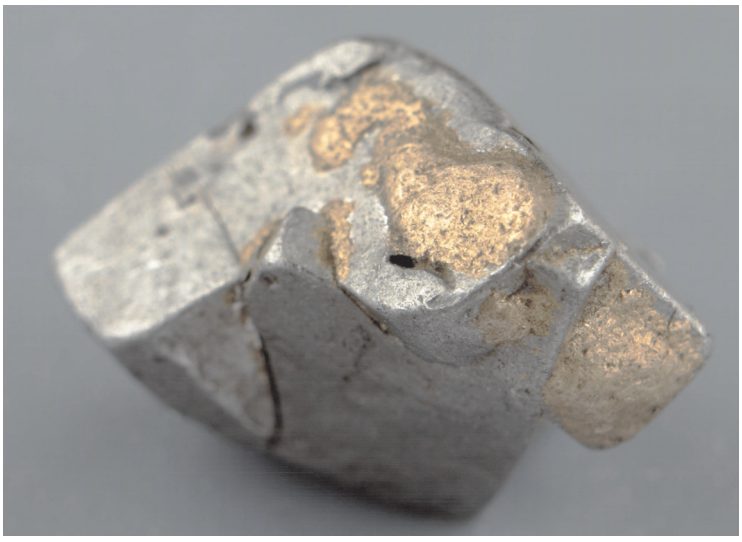

Fig. 4.7-2 Neat platinum covered with gold, Konder mine Yakutia, Russia. Photograph by courtesy of Dr. H.-J. Höbler, Mineralogical and Petrographical collection, University of Leipzig.

7. Comments

The ^{15}N-labeled compound is reported to give very sharp lines [1]; thus the observed linewidth must be due to the presence of ^{14}N. The extremely large chemical shifts of platinum arise from the very large number of electrons around this nucleus and their polarizability. Furthermore, platinum can exist in different oxidation states. As the chemical shifts, also the spin coupling constants to other nuclei, show extraordinarily large values, thus ^{1}J(Pt,H) and ^{1}J(Pt,P), spin coupling constants larger than 1 or 2 kHz and ^{1}J(Pt, Sn) over 20 kHz have been measured..

^{195}Pt is an excellent spin-1/2 nucleus to study because its generally short relaxation times allow for rapid accumulation of spectra with little waiting time between pulses. First-time users of the technique should be aware, however, that the large possible range of chemical shifts means that some time is necessary to initially find the signal. Once the correct parameters are in hand, ^{195}Pt spectra are quick to obtain. ^{195}Pt chemical shifts and ^{195}Pt–^{15}N coupling constants are sensitive to the geometry of the complex, and are useful tools in evaluating the nature of the coordinated ligands. The preparation of platinum coordination complexes illustrates the synthetic utility of the trans effect in the synthesis of inorganic complexes.

Taken from ref. [1]

[1] G. M. Arvanitis, K. L. Wilk "Geometric isomers of platinum coordination compounds: An NMR experiment for the undergraduate inorganic chemistry laboratory" *The Chemical Educators* **1997**, 2, electronic publication, no pp given.

[2] K. R. Koch, M. R. Burger, J. Kramer, A. N. Westra "^{195}Pt NMR and DFT computational methods as tools towards the understanding of speciation and hydration/solvation of $[PtX_6]^{2-}$ ($X = Cl^-$, Br^-) anions in solution" *Dalton Trans*. **2006**, 3277–3284.

[3] E. Gabano, E. Marengo, M. Bobba, E. Robotti, C. Cassino, M. Botta, D. Osella "^{195}Pt NMR spectroscopy: A chemometric approach" *Coord. Chem. Rev*. **2006**, *250*, 2158–2174.

[4] J. R. L. Priqueler, I. S. Butler, F. D. Rochon "An overview of ^{195}Pt nuclear magnetic resonance spectroscopy" *Appl. Spectrosc. Rev*. **2006**, *41*, 185–226.

[5] B. M. Still, P. G. Anil Kumar, J. R. Aldrich-Wright, W. S. Price "^{195}Pt NMR—theory and application" *Chem. Soc. Rev*. **2007**, *36*, 665–686.

[6] A. N. Egorochkin, O. V. Kuznetsova, N. M. Khamaletdinova, Y. A. Kurskii, L. G. Domratchev, L. and G. A. Domracheva "Transition metal NMR chemical shifts and polarizability effect in organometallic complexes" *Magn. Reson. Chem*. **2009**, *47*, 782–790.

8. Questions

A. Why would it not be possible to observe the ^{195}Pt NMR chemical shift of this compound by indirect detection?

B. The $^{1}J(^{195}\mathrm{Pt},^{15}\mathrm{N})$ spin coupling constant in *trans* $Pt(NH_3)_2Cl_2$ was determined to be 280 Hz [1]. How large should be the $^{1}J(^{195}\mathrm{Pt},^{14}\mathrm{N})$ spin coupling constant?

9. Own Observations

Chapter 5

Experiments in Physical Organic Chemistry

Here we describe some methods which are not mainly aimed at structure elucidation, but use NMR to determine certain properties of spins or molecules. These are:

5.1 Measurement of the Spin-Lattice Relaxation Time T_1 151
5.2 Measurement of the Spin-Spin Relaxation Time T_2 155
5.3 Dynamic ^{1}H NMR Spectroscopy 159
5.4 Diffusion Measurement with DOSY 163
5.5 Residual Dipolar Couplings (RDC) 167

All the described methods contribute to the basic understanding of NMR and are in part mandatory to find the correct parameters to run routine 1D and 2D experiments. Especially the last two experiments, however, open the field of traditional NMR into a wide range of new applications.

Dear Barry:

"Zeugmatographic Spectroscopy"

It seems not unlikely that knowledge of the locations within complex objects of various chemical species may at times be of some interest and utility. If their chemical shifts may be distinguished in any NMR experiment in a homogeneous applied magnetic field, their individual distributions within the object may be discovered by combining zeugmatographic spatial discrimination with spectroscopic frequency discrimination. One of the several possible schemes for achieving such a combination may be described with the aid of the diagram below.

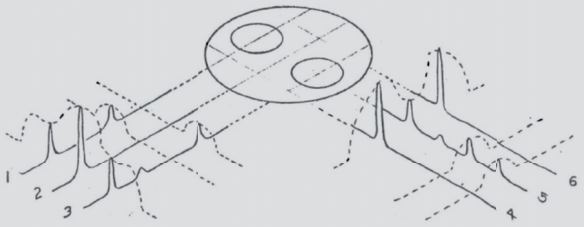

It represents a view along the axis of a set of tubes containing three different compounds in three compartments. In the presence of a field gradient, a long rf pulse may excite only a thin slice of the sample. If the gradient is then switched off, the free induction decay of this selectively excited signal may be observed in a homogeneous field, as in a normal high resolution pulsed NMR experiment. The Fourier transform of the FID is composed only of the peaks of those compounds in the excited region, as sketched, for example, along line 1 in the diagram. Excitation in another plane with the same gradient direction may give the spectrum shown as 2, and so on. Separate projections of the intensities of each observable line may be constructed, as shown by the dashed lines. Repetition of the whole procedure for other gradient directions can give other projections, as shown on the right of the diagram.

Finally, by the image reconstruction techniques used in earlier zeugmatographic experiments, the separate distributions of the three compounds may be found. The actual test sample used by Dave Kramer in these experiments had sulfuric acid in the outer tube, water in one of the inner tubes, and $(CH_3)_3C$–C$_6$H$_4$–NO_2 in the other. The images are shown below, and clearly demonstrate that the objective has been achieved.

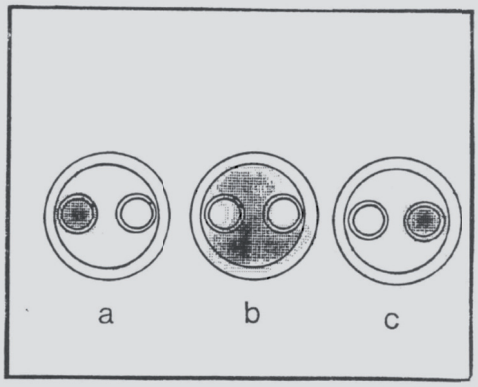

Until we get the whole process under computer control, such an experiment, which required special modifications and additions to our Seimec pulsed NMR system by Waylon House, and computer programming and processing by Ching-Nien Chen, is tedious in the extreme. Nevertheless, it may eventually find use with various objects of technological or biological significance from which narrow liquid lines may be obtained, or whose solid resonances may be narrowed by multiple pulse or double resonance methods.

Yours truly,

Paul

Paul C. Lauterbur
Professor of Chemistry

Fig. 5.0-1 Taken from *TAMU Letters* **1975**, *204*, 24–25.

Experiment 5.1

Measurement of the Spin–Lattice Relaxation Time T_1

1. Purpose

The longitudinal or spin–lattice relaxation time T_1 is the time constant for re-establishing thermal equilibrium of the z-magnetization after an r.f. pulse, and must be clearly distinguished from the transverse or spin–spin relaxation time T_2, which describes the decay of the x,y-magnetization (see Exp. 5.2). As far as structure determination is concerned, T_1 is not as important a parameter as the chemical shift or the spin–spin coupling. But even for routine work at least a qualitative knowledge of this parameter is essential, e.g., for choosing a reasonable pulse repetition time. Furthermore, T_1 values are important for setting up NOE experiments and for studying molecular motions, e.g., diffusion measurements. Here we describe the inversion recovery experiment as applied to the determination of the ^{1}H NMR T_1-values of strychnine.

2. Variants

T_1 measurements have been performed since the beginning of NMR, and a multitude of techniques have been proposed. Besides the inversion recovery technique shown here, other methods are based on the progressive saturation or saturation recovery experiments. Although all these techniques are in principle 1D methods they are usually recorded in a pseudo 2D file, rendering their evaluation much easier.

3. Pulse Scheme and Phase Cycle

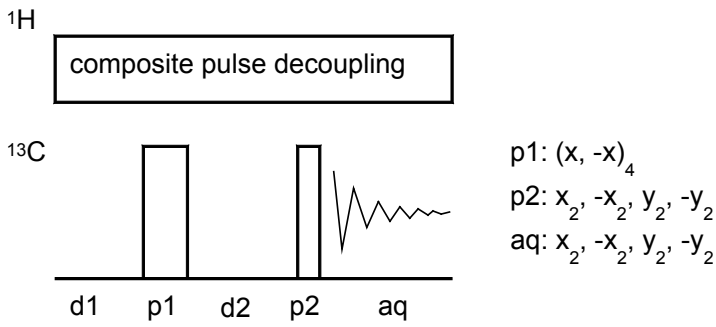

Scheme 5.1-1

4. Acquisition

Special values used for the spectrum shown:

Sample: 3% strychnine in $CDCl_3$ (degassed and sealed)
Time requirement: 3 h
Spectrometer: Bruker DRX-600 with 5-mm TBI probe

Current T_1 program versions handle the data as 2D data: for example, the results of 16 experiments with different delays d2 are stored as rows in a 2D matrix. So you have to create a 2D file and to set:

Fig. 5.1-1 Felix Bloch (1905-1983)

Common values:

p1: 180° ^{1}H transmitter pulse
p2: 90° ^{1}H transmitter pulse
d1: relaxation delay
d2: variable recovery delay

The time of establishment or "relaxation time" can be expected to vary anywhere between fractions of a second and many hours, depending in the most delicate manner upon the nuclear moments, the electronic structure of the atoms in the sample, their distance, and their motion. To study experimentally and theoretically this interesting relationship between nuclear relaxation time and atomic features seems to us, in fact, to be one of the fruitful fields of investigation which have now opened.

Taken from F. Bloch "Nuclear induction" *Phys. Rev.* **1946**, *70*, 460–474.

td1: 16
td2: 46K
aq: 4 s
sw: 10 ppm
o1: middle of ^{1}H NMR spectrum
d1: 70 s (> 5 T_1 in order to achieve the equilibrium *z*-magnetization)
d2: create a list with the following values [ms]: 1, 5, 10, 20, 50, 70, 100, 200, 500, 700, 1000, 2000, 5000, 10 000, 20 000, and 30 000.
ns: 8

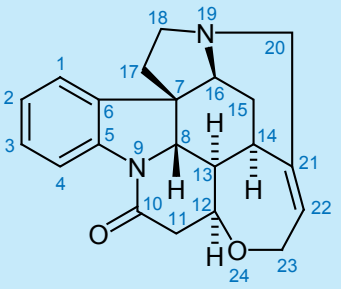

Scheme 5.1-2

5. Processing

If a 2D file has been created, Fourier transformation has to be performed in F_2, using a line-broadening factor lb = 2 Hz. In order to adjust the phase, read spectrum number 16 in which all signals have a positive phase, and transfer this phase correction to all other spectra.

6. Results

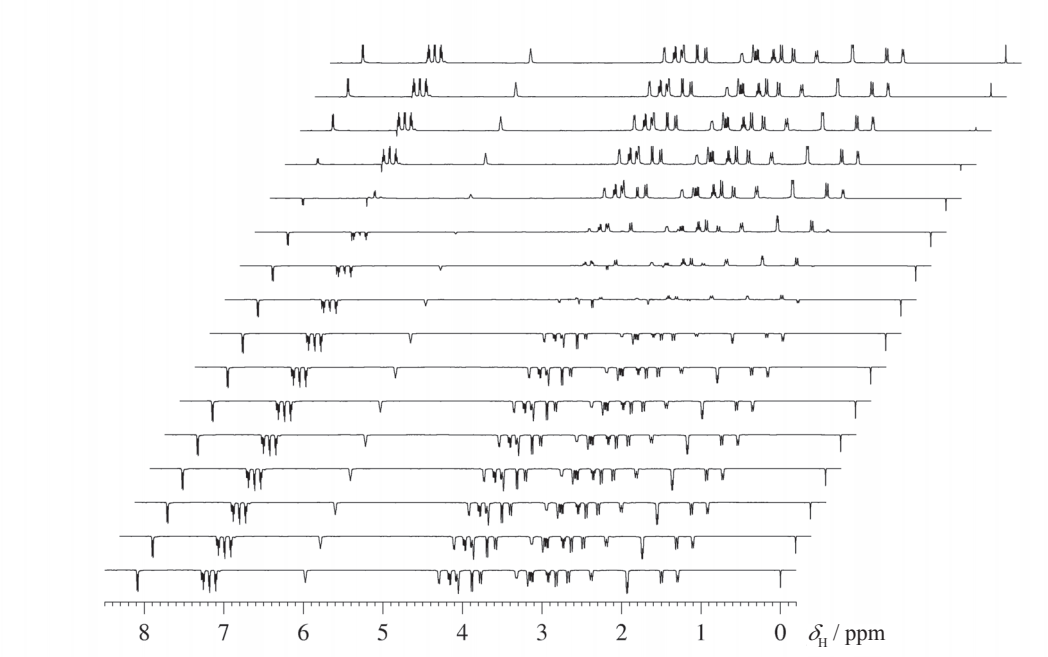

Figure 5.1-2 Stacked plot from a ^{1}H NMR T_1 measurement of strychnine

In the figure the results of a degassed strychnine sample at 600 MHz are presented as a stacked plot for qualitative inspection. In the first eight spectra all signals have a negative intensity, since after the first 180° pulse and the short delays of 1 ... 200 ms all spin vectors are still in the −*z* direction. After a delay d2 of 500 ms the spin−lattice relaxation has reduced the intensity of most signals between 4 and 1 ppm to zero, whereas the aromatic signals are still negative. For a rough estimation of the T_1-values from these spectra you may use Equation (1), where τ_{null} is the (interpolated) delay d2 at which the intensity of a signal is zero. This results from Equ. (2) for $M_z(\tau_{null}) = 0$.

$$T_1 = \tau_{null} / \ln 2 \approx 1.44 * \tau_{null} \quad (1)$$

For quantitative analysis, apply the T_1/T_2 analysis software of your instrument, which uses either the integrals or the peak heights. The basis for the evaluation is Equation (2) with M_0 = equilibrium z-magnetization and M_z = z-magnetization after delay τ (corresponds to parameter d2). Replacing M by I (integral or peak height) yields Equation (3) to be fitted in which A and B are constants.

$$M_z = M_0(1 - 2e^{-\tau/T_1}) \quad (2)$$

$$I(\tau) = A + Be^{-\tau / T_1} \quad (3)$$

The recommended procedure is an iterative exponential fitting according to Equation (3). This yields for H-4 the T_1-value of 5.2 s, based on peak integrals, and the corresponding plot is shown below (relative standard deviation of $6 \cdot 3\ 10^{-3}$). A detailed discussion of the different parameters (length of d1, number and lengths of d2, etc.) is given in Refs. [3, 4].

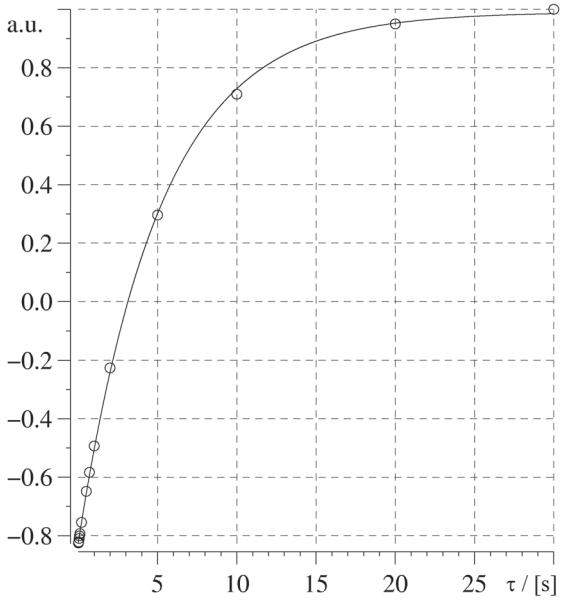

Figure 5.1-3 Exponential build up of the magnetization

7. Comments

The 180° pulse inverts the magnetization so that it lies along the $-z$-direction; relaxation then takes place during the delay d2. At the end of d2, the actual magnetization is measured by the 90° read-pulse, which transfers z-magnetization into measurable y-magnetization. Note that T_1-values are very dependent on concentration, temperature, oxygen content, and magnetic field strength. In this experiment the sample was degassed, so as to give somewhat longer relaxation times. In scientific applications T_1 measurements should only be performed with carefully degassed samples.

[1] R. L. Vold, J. S. Waugh, M. P. Klein, D. E. Phelps, "Measurement of spin relaxation in complex systems" *J. Chem. Phys.* **1968**, *48*, 3831–3832.

[2] J. L Sudmeier, S E. Anderson, J. S. Frye, "Calculation of nuclear spin relaxation times" *Concepts Magn. Reson.* **1990**, *2*, 197–212. J. S. Frye, *Concepts Magn. Reson.* **1989**, *1*, 27–33.

[3] D. J. Craik, G. C. Levy, "Factors affecting accuracy in carbon-13 spin-lattice relaxation measurements" *Top. Carbon-13 NMR Spectrosc.* **1984**, *4*, 239–275.

[4] J. Kowalewski, G. C. Levy, L. F. Johnson, L. Palmer, "Three-parameter non-linear procedure for fitting inversion-recovery measurements of spin-lattice relaxation times" *J. Magn. Reson.* **1977**, *26*, 533–536.

[5] W. R. Carper, "Direct determination of quadrupolar and dipolar NMR correlation times from spin-lattice and spin-spin relaxation rates" *Concepts Magn. Reson.* **1999**, *11*, 51–60.

Note that within the framework of the Bloch equations T_1 is only defined for a single transition, but not for multiplets as in the sample used here. Nevertheless the apparent relaxation times of such multiplets can be used for other purposes. It is of high interest that in this example H-4 has the longest T_1 and the variety of these proton T_1 times explains why in routine measurements the integration often badly fails.

For H-17, e.g., the measurements yields only T_1 = 0.65 s.

8. Questions

A. What is the typical number for the relaxation time of protons in an organic compound of MW = 500?

B. What is the typical relaxation time of ^{13}C in a carbonyl group of an organic compound of MW = 500?

C. What is the typical relaxation time of protons in a protein of 10 KDa?

D. What might be the main source of error in an inversion recovery experiment?

[6] P. B. Kingsley, "Methods of measuring spin-lattice (T_1) relaxation times: An annotated bibliography" *Concepts Magn. Reson*. **1999**, *11*, 243−276.

9. Own Observations

Experiment 5.2

Measurement of the Spin–Spin Relaxation Time T_2

1. Purpose

The transverse or spin–spin relaxation time T_2 determines the decay of the x,y magnetization and is related to the line-width. It must be clearly distinguished from the longitudinal or spin–lattice relaxation time T_1 (Exp. 3.1) and can be measured separately. Although there is hardly a direct relationship between the spin–spin relaxation time and the structure of molecules, a knowledge of its value is important for planning dynamic NMR experiments, investigations on spin diffusion, and generally for devising new pulse sequences, because their evolution periods must not significantly exceed T_2. In the extreme narrowing limit the relationship $T_1 = T_2$ usually holds. The spin echo method for measuring T_2 is described here using $CHCl_3$ as an example. Note that the resolution test sample used here has extremely long T_1 and T_2 relaxation times.

2. Variants

To our knowledge, there are no valid variants of the CPMG (Carr Purcell Meiboom Gill) method to measure relaxation T_2 times. Because homonuclear *J-coupling* is not refocussed by the echo sequence below, the echo signals are modulated by *J-coupling*. To prevent this at least for AX spin systems, it is suggested to insert a 90° pulse between two 180° pulses, see Ref [6]. Although CPMG is in principle a 1D technique, this is usually handled in a formal 2D file with increasing n repetitions in the indirect dimension.

3. Pulse Scheme and Phase Cycle

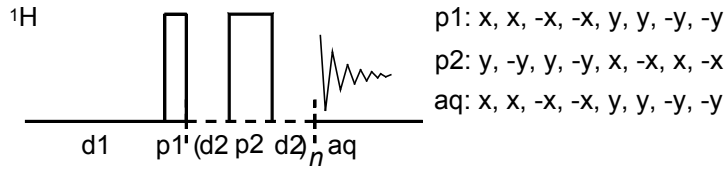

Scheme 5.2-1

4. Acquisition

Special values used for the spectrum shown:

Sample: 1 % $CHCl_3$ in [D_6]acetone, *degassed and sealed*. (NMR reference sample "lineshape")
Time requirement: 4 h
Spectrometer: Bruker DRX-600 with 5-mm TBI-probe

td:	12K
sw:	1200 Hz
aq:	5 s
o1:	on ^{1}H resonance
p1:	90° ^{1}H transmitter pulse
p2:	180° ^{1}H transmitter pulse
d1:	1000 s

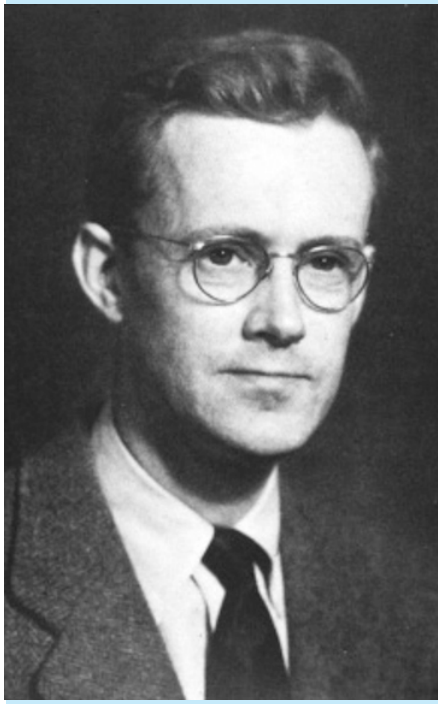

Fig. 5.2-1 Edward M. Purcell (1912–1997)

Common values:

p1: 90° ^{1}H transmitter pulse
p2: 180° ^{1}H transmitter pulse
d1: relaxation delay
d2: spin echo delay
n: number of spin echo repetitions

d2: 10 ms
preacquisition delay as short as possible
ns: 1

n-values of 2, 20, 50, 100, 200, 300, 400, 500, 750, 1000, 2000, 3000 were used here, leading to delays between the first 90° pulse and start of the acquisition of 0.04, 0.4, 1, 2, 4, 6, 8, 10, 15, 20, 40 and 60 s.

5. Processing

Current software treats this experiment as a 2D file; however, Fourier transformation is only performed in the F_2 direction. Use an exponential line broadening of lb = 2 Hz and adjust the phase of the rows. After this, a normal T_1/T_2 software package measures peak integrals or heights from all rows and calculates the T_2 value from the given delays, which the user must provide in a corresponding delay list.

6. Result

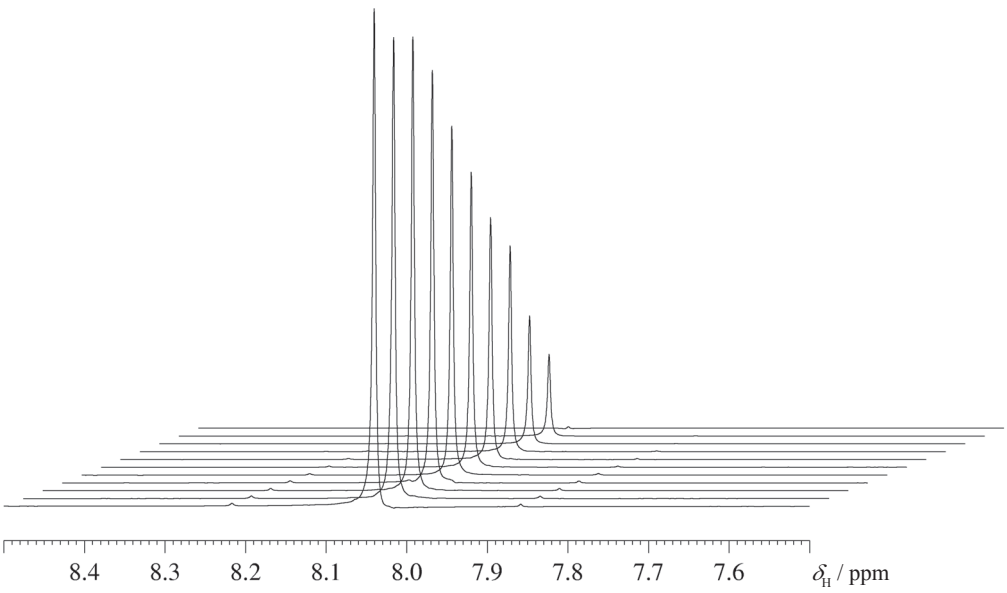

Figure 5.2-2 Stacked plot from a ^{1}H NMR T_2 measurement of $CHCl_3$

We shall show that another process, occurring in many substances, provides a 'local field spectrum' intense enough to account for the observed relaxation times. Every nucleus experiences not only the constant field H_0, and the applied radio-frequency signal H_1 perpendicular to H_0, but also the local field produced by neighbouring nuclear moments and sometimes by small moments caused by molecular rotation, or in paramagnetic substances by large electronic moments. In liquids and gases, at least, the carriers of these neighbouring moments are not stationary but execute Brownian motion, changing position relative to the nucleus under consideration.

Taken from N. Bloembergen, E. M. Purcell, R. V. Pound "Nuclear Magnetic Relaxation" *Nature* **1947**, *4066*, 475−476.

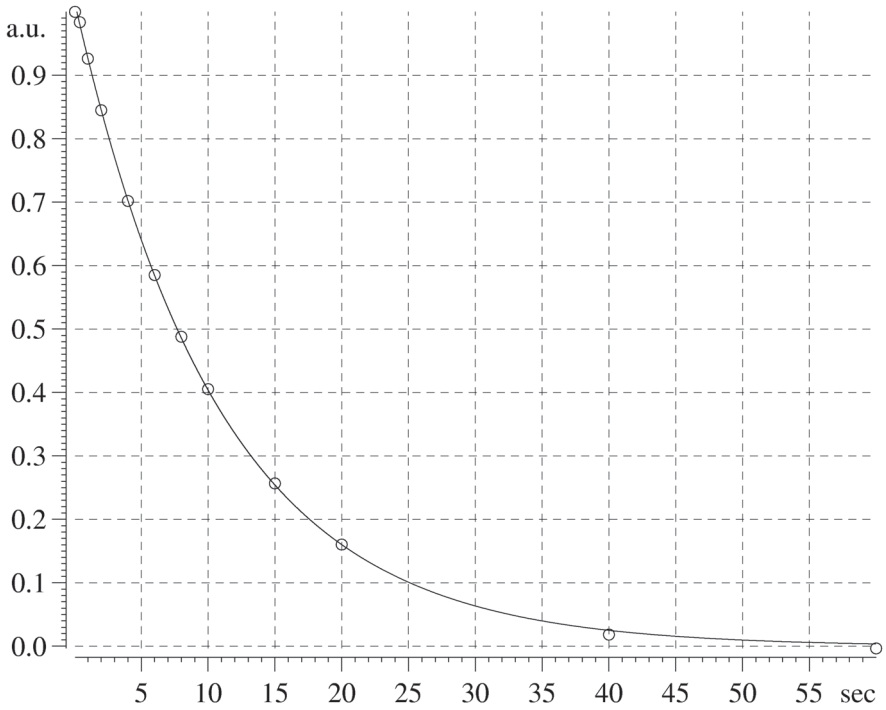

Figure 5.2-3 Exponential decay of the magnetization

The figure shows the exponential decay curve obtained on a DRX-600 spectrometer using the above given parameters. The calculated value of T_2 was 10.83 s, a value exceeding by far the T_2^*value calculated from 0.5 Hz, the apparent line width of the sample, using equation (2) below.

7. Comments

In this experiment the intrinsic value of T_2 is measured. This is related to the composite transverse relaxation time T_2^* by Equation (1).

$$\frac{1}{T_2^*} = \frac{1}{T_2} + \frac{1}{T_2^{\text{inhom}}} \qquad \textbf{(1)}$$

The second term on the right-hand side describes the effect of the magnetic field inhomogeneity. T_2^* is the effective decay time constant of the FID and can also be approximated from the line width using Equation (2), which is based on assuming a Lorentz type lineshape.

$$\Delta\nu_{1/2} = \frac{1}{\pi \cdot T_2^*} \qquad \textbf{(2)}$$

For example, if the observed line width at half height is 0.5 Hz, T_2^*can be calculated as 0.64 s; thus the inhomogeneity of the magnet is predominant for this example.

[1] S. Meiboom, D. Gill, "Modified spin-echo method for measuring nuclear relaxation times" *Rev. Sci. Instrum.* **1958**, *29*, 688−691.

[2] M. L. Martin, J.-J. Delpuech, G. J. Martin, *Practical NMR Spectroscopy*, Heyden, London, **1980**, 280−287.

[3] R. Freeman, *A Handbook of Nuclear Magnetic Resonance*, Longman Scientific Technical, Harlow, **1987**, *48*, 116−117.

[4] S. W. Homans, *A Dictionary of Concepts in NMR*, Revised Edition, Clarendon Press, Oxford, **1993**, 310−314.

[5] W. R. Carper, "Direct determination of quadrupolar and dipolar NMR correlation times from spin-lattice and spin-spin relaxation rates" *Concepts Magn. Reson*. **1999**, *11*, 51−60.

[6] J. A. Aguilar, M. Nilsson, G. Bodenhausen, G. A. Morris, "Spin echo NMR spectra without *J* modulation" *Chem. Commun.* **2012**, *48*, 811−813.

8. Questions

A. Calculate the natural line width from the obtained relaxation time $T_2 = 10.83$ s.

B. Misadjust the homogeneity of the magnet to obtain a line width of 5 Hz and perform the experiment again. Does T_2 change?

C. Quadrupolar nuclei such as ^{14}N or ^{11}B have often a line width in the order of kHz. Why?

D. Besides field inhomogeneity and paramagnetism there is another important phenomenon which broadens NMR lines. Which one?

9. Own Observations

Experiment 5.3

Dynamic ^{1}H NMR Spectroscopy

1. Purpose

The measurement and evaluation of dynamic equilibria and the determination of activation enthalpies and entropies are important tasks which can be performed by high-resolution NMR spectroscopy [1-3]. Dimethylformamide (DMF) was one of the earliest molecules investigated when the methodology of dynamic NMR measurements was being developed [4-6]. In the time of high-field NMR instruments, however, its coalescence point lies at too high temperatures to allow the full series of dynamic NMR measurements with standard probe heads. We therefore chose the chloro derivative, which has a lower rotational barrier and, in addition, has no spin coupling to an amide proton [7,8]. This sample provides an easy starting point to learn the procedures involved in performing measurements at different temperatures and evaluating the results for a simple, non-coupled two-site exchange. The spectra were calculated using the program *SpinWorks* [11], which contains an implementation of the original DNMR3 program [2].

2. Variants

In addition to the 1D method shown here, the two-dimensional variant EXSY exists, which essentially is the NOESY pulse sequence applied to dynamic systems. As a 2D method, EXSY has considerable advantage in complex cases. The 1D line shape technique shown here may be extended toward the region of slow exchange by the saturation transfer experiment. Toward the region of fast exchange the measurement of $T_{1\rho}$ helps if the line shape is not more altered by fast dynamic processes. For accurate values of the activation entropy a large temperature range is mandatory.

3. Pulse scheme and Phase Cycle

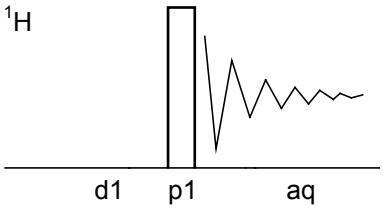

p1: x, -x, -x, x, y, -y, -y, y

aq: x, -x, -x, x, y, -y, -y, y

Scheme 5.3-1

4. Acquisition

Connect your instrument for high-temperature measurements, adjust a reasonable nitrogen gas flow, set the control to room temperature, and let the sample equilibrate for at least 5 min. Change the temperature in 5 K steps until the signals of the methyl groups coalesce and the line sharpens again.

Check the actual sample temperature with the calibrated ethylene glycol sample (see chapter 8.5). Perform these experiments in reverse order

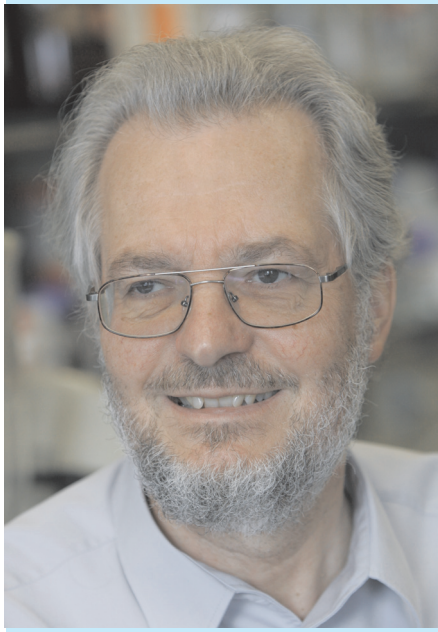

Fig. 5.3-1 H. Kessler *1940

Common values:

p1: 90° ^{1}H transmitter pulse
d1: relaxation delay

Fig. 5.3-2 H. Günther *1935

[1] G. Binsch, "Study of intramolecular rate processes by dynamic nuclear magnetic resonance" *Top. Stereochemistry*, **1968**, *3*, 97−192.

[2] G. Binsch, H. Kessler, "Kinetic and mechanistic evaluation of NMR spectra" *Angew. Chem. Int. Ed. Engl*. **1980**, *19*, 411−429.

[3] H. Günther, *NMR Spectroscopy*, 2nd Ed. Chapter 9, Wiley, Chichester, **1995**.

[4] K. Rabinowitz, A. Pines, "Hindered internal rotation and dimerization of N,N-dimethylformamide in carbon tetrachloride" *J. Am. Chem. Soc*. **1969**, *91*, 1585−1589.

[5] T. Drakenberg, K. I. Dahlqvist, S. Forsén, "The barrier to internal rotation in amides. IV. N,N-dimethylamides; substituent and solvent effects" *J. Phys. Chem*. **1972**, *76*, 2178−2183.

[6] G. J. Martin, M. Berry, D. Le Botlan, B. Mechin, "The varytemp NMR: A dynamic pulse experiment in programmed temperature for lineshape study" *J. Magn. Reson*. **1976**, *23*, 523−526.

and check for reproducibility. Important for all temperature-dependent measurements is to wait at least 5 min after the temperature control unit has reached the target temperature to equilibrate the sample.

Special values used for the spectrum shown:

Sample: 5 % chlorodimethylformamide in $C_2D_2Cl_4$.
Time requirement: ca. 3 h (depending on temperature equilibration)
Spectrometer: Bruker *Fourier 300* with a 5-mm $^1H/^{13}C$ probe

td: 32K
sw: 10 ppm
aq: 5.4 s
o1: middle of ^1H NMR spectrum
p1: 6 µs at −10.8 dBW (corresponding 12 W), 30° excitation
d1: 3 s
ns: 1

5. Processing

Use standard processing as described in Experiment 1.1, and for each temperature run an expanded plot of the signals of the methyl groups. The comparison of theoretically calculated line shapes with the experimental ones can be performed by simulation programs, such as DNMR3 or MEXICO, which are implemented in the *SpinWorks* PC software [11]. Note for each temperature the line width of the residual proton signal of the solvent and use this value as a T_2 reference.

6. Result

Displayed on the next page are seven typical spectra taken on a *Fourier*-300 spectrometer at 296 to 362 K. From the complete series the result $\Delta G^{\#}(298)$ = 73.4 kJ/mol was obtained; $\Delta H^{\#}$ was 799 kJ/mol and $\Delta S^{\#}$ was 23.7 J/mol, but is believed to be essentially zero.

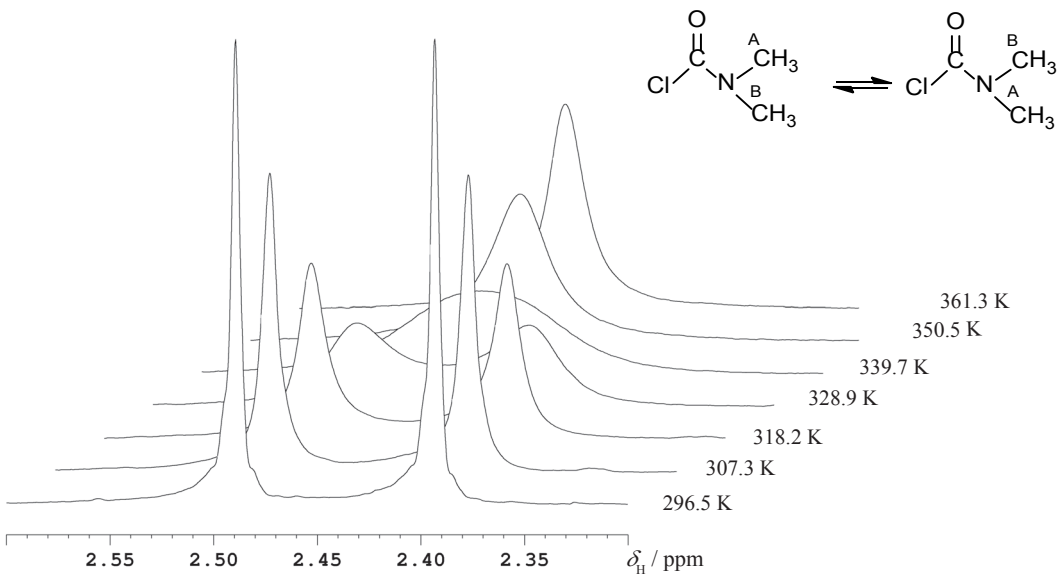

Figure 5.3-3 Temperature dependent lineshapes for chlorodimethylformamide

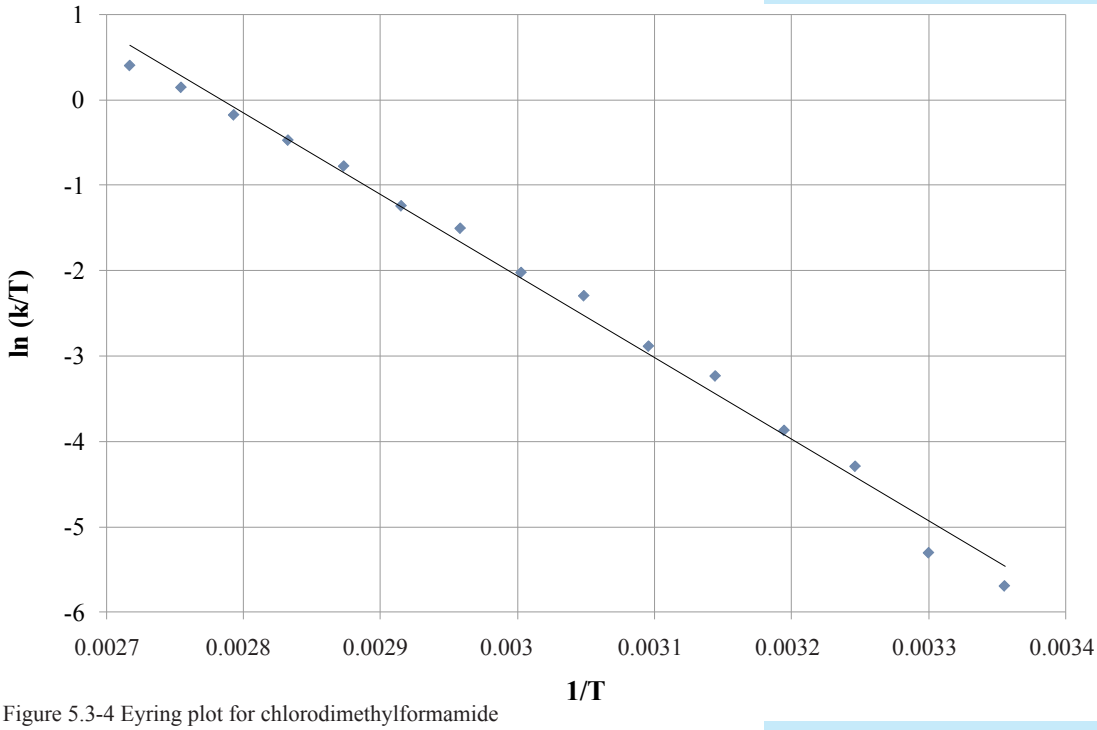

Figure 5.3-4 Eyring plot for chlorodimethylformamide

7. Comments

It would be beyond the scope of this book to describe the theory of line shape investigations in NMR spectroscopy. The interested reader is therefore referred to the fundamental review articles [1, 2, 9, 10]. For our purpose here it is sufficient to know that two exchanging sets of nuclei can only be separately observed if the rate constant of the exchange is considerably smaller than their chemical shift difference in Hz (NMR time scale). Therefore, the coalescence temperature increases with increasing spectrometer frequency. The goal of the experiment is to derive a table of rate constant vs temperature.

From such a table, using the Eyring equation (1), one can calculate values of $\Delta G^{\#}$. By plotting $\Delta G^{\#}$ as a function of temperature one can derive $\Delta H^{\#}$ and $\Delta S^{\#}$ for the observed exchange process.

$$k = \frac{k_B T}{h} e^{-\frac{\Delta G^{\#}}{RT}} \qquad (1)$$

There are many PC-based programs that are able to calculate the theoretical line shape. These require as input the line separation $\Delta\nu$ in the low-temperature limit, the ratio of populations of the two sites, the line width for non-exchanging protons at each temperature, and an estimated rate constant. From this they calculate a line shape that has to be compared with the experimental result at the corresponding temperature. The rate constant at the temperature of coalescence T_c is given for the simple degenerate two-site exchange by Equation (2).

[7] W. M. M. J. Bovée, "The determination of chemical exchange rates by N.M.R. over a large temperature range by a combination of complete line shape analysis and relaxation time (T_1 and T_2) measurements" *Mol. Phys*. **1979**, *37*, 1975−1980.

(2)

$$k_c = \frac{\pi \Delta \nu}{\sqrt{2}}$$

Using Equation (2) the formula (3) was derived, by which the $\Delta G^{\#}$ value at the coalescence temperature T_c can be obtained [3].

(3)

$$\Delta G^{\#}(T_c) = RT_c\,[22.96 + \ln(T_c / \Delta \nu)]$$

[8] M. Minagawa, H. Shirai, T. Morita, Y. Fujikura, Y. Kameda, "Dynamic nuclear magnetic resonance and Raman spectroscopic measurements of five kinds of N,N-dimethylformamide derivatives in relation to the dissolution mechanism of polyacrylonitrile" *Polymer* **1996**, *37* 2353−2358.

[9] A. D. Bain, "Chemical exchange in NMR" *Prog. NMR Spectrosc*. **2003**, *43*, 63–103.

[10] D. Casarini, L. Lunazzi, A. Mazzanti, "Recent Advances in Stereodynamics and Conformational Analysis by Dynamic NMR and Theoretical Calculations" *Eur. J. Org. Chem*. **2010**, 2035–2056.

[11] K. Marat, SpinWorks version 3.0, 2010, University of Manitoba, ftp://davinci.chem.umanitoba.ca/pub/marat/SpinWorks/

8. Questions

A. A simpler evaluation of the data uses an Arrhenius plot. What is the advantage and the disadvantage?

B. Explain the use of diethylene glycol as a temperature reference.

C. Compare the time scale of NMR with that of IR-spectroscopy.

D. Why is the barrier in chlorodimethylformamide lower than the one in dimethylformamide?

9. Own Observations

Experiment 5.4

Diffusion Measurement with DOSY

1. Purpose

Diffusion **O**rdered **S**pectroscop**Y** is the "two-dimensional" version of the pulsed field gradient spin echo experiment for measuring diffusion constants. With DOSY it is possible to obtain the signals of individual compounds from a mixture, separated in different rows of a pseudo 2D data matrix. Thus the result resembles that from a chromatographic separation, but one virtually performed in the NMR tube. Of the many different variants now in use [5, 11, 13], we show in this experiment the stimulated echo version with bipolar gradients and an eddy delay, using a D_2O / methanol / butanol / triethylene-glycol mixture as an example.

Fig. 5.4-1 A drop of ink diffusing in water

2. Variants

One problem of the standard DOSY-technique is the possible overlap of the NMR signals belonging to different molecules, which renders the extraction of reliable multiple diffusion constants difficult. Therefore the INEPT-DOSY experiment was developed, which can be considered as a ^{13}C-detected proton-DOSY experiment. Thus, the diffusion part of the experiment works at the proton frequency and the pulsed field gradients act on the proton gyromagnetic ratio. After the diffusion part, however, a polarization transfer to ^{13}C is achieved, and the result is detected with the higher chemical shift dispersion of ^{13}C to remove signal overlap.

A further extension leads to a "3D" DOSY technique, where the DOSY approach is combined with the HMQC technique, which is in principle more sensitive than the INEPT-DOSY method. One obtains a cuboid of diffusion-ordered HMQC planes, each of which should ideally contain the H,C correlation signals of only one component of the mixture. Also known are combinations of DOSY with COSY or NOESY.

3. Pulse Scheme and Phase Cycle

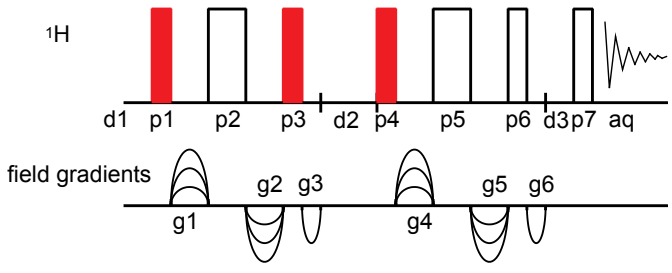

p1, p2, p5: x p3: x, x, -x, -x p4, p7: $(x)_4$, $(-x)_4$, $(y)_4$, $(-y)_4$
p6: $(x, -x)_2$, $(-x, x)_2$, $(y, -y)_2$, $(-y, y)_2$
aq: x, -x, -x, x, -x, x, x, -x, -y, y, y, -y, y, -y, -y, y
gradients g1, g2, g4 and g5 incremented during the experiment

Scheme 5.4-1

Common values:

p1, p3, p4, p6, p7: 90° ^1H transmitter pulse
p2, p5: 180° ^1H transmitter pulse
d1: relaxation delay
d2: diffusion delay
d3: eddy current delay
g1, g2: bipolar encoding gradients (ramp), g1= −g2
g4, g5: bipolar decoding gradients (ramp), g4= −g5
g3, g6: spoiling gradients

[1] K. F. Morris, C. S. Johnson, "Diffusion-ordered two-dimensional nuclear magnetic resonance spectroscopy" *J. Am. Chem. Soc*. **1992**, *114*, 3139−3141.

[2] K. F. Morris, C. S. Johnson, "Resolution of discrete and continuous molecular size distributions by means of diffusion-ordered 2D NMR spectroscopy" *J. Am. Chem. Soc*. **1993**, *115*, 4291−4299.

[3] H. Barjat, G. A. Morris, S. Smart, A. G. Swanson, S. C. R. Williams, "High-resolution diffusion-ordered 2D spectroscopy (HR-DOSY) - A new tool for the analysis of complex mixtures"*J. Magn. Reson.* Ser. B, **1995**, *108*, 170−172.

[4] M. D. Pelta, H. Barjat, G. A. Morris, A. L. Davis, S. J. Hammond, "Pulse sequences for high-resolution diffusion-ordered spectroscopy (HR-DOSY)" *Magn. Reson. Chem*. **1998**, *36*, 706−714.

[5] C. S. Johnson, "Diffusion ordered nuclear magnetic resonance spectroscopy: Principles and applications" *Prog. NMR Spectrosc*. **1999**, *34*, 203−256.

[6] D. Wu, A. Chen, C. S. Johnson, "Heteronuclear-detected diffusion-ordered NMR spectroscopy through coherence transfer" *J. Magn. Reson*. Ser. A **1996**, *123*, 215−218.

[7] N. Gonnella, M. Lin, M. J. Shapiro, J. R. Wareing, X. Zhang, "Isotope-filtered affinity NMR" *J. Magn. Reson*. **1998**, *131*, 336−338.

4. Acquisition

Special values used for the spectrum shown:

Sample: D_2O with 15 vol. % Methanol, 5 vol. % n-Butanol and 5 vol. % Triethyleneglycol.
Time requirement: 1 h 10 min
Spectrometer: Bruker AVANCE-700 with 5-mm cryo probe

Record a normal 1D ^{1}H NMR spectrum and optimize the spectral width. *Set and control* the temperature to 300 K. Use a high air flow rate to avoid convections in the sample. [Other authors recommend no air flow at all if measuring at ambient temperature]. Switch to the 2D mode of the spectrometer software, and load the DOSY pulse program. First record a minimal ^{1}H NMR DOSY spectrum (ns = 1) with a gradient ramp of 8 gradient strengths in order to observe complete signal decay for a given diffusion delay and gradient length, and readjust the gradients or the diffusion delay accordingly. The result is best viewed in the "oblique mode" of the 2D data set.

td2: 25.166 data points in F_2
td1: 30 data points in F_1 (gradient ramp)
aq2: 3 s
sw2: 6.0 ppm
o1: middle of selected ^{1}H NMR region
d1: 30 s
d2: diffusion delay 60 ms
d3: eddy current delay 5 ms
g1, g2, g4, g5: linear gradient ramp of 30 values from 0 to 100 %, shape "smoothed rectangular", length 2 ms, 100 % corresponding 0.56 Tesla/m
g3, g6: −17.14 % and − 13.17 %, resp., length 1 ms, sinusoidal shape
ns: 4

5. Processing

Apply zero-filling to 32K real data points in F_2 and use an exponential window with lb = 1 Hz line-broadening in F_2. Transform only in the F_2 direction. Each signal will now display a decay curve in F_1 as the gradient strength increases. The extraction of decay constants and their transformation into a 2D plot requires special mathematics (e.g. multiexponential fitting, Laplace transformation), the handling of which is very dependent on the software version provided by the instrument manufacturer. You can also transfer the data to an external exponential fitting program.

6. Result

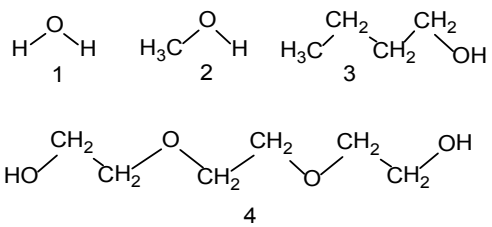

The figure shows the DOSY spectrum obtained on a DRX-600 spectrometer. As can be seen, the signals of the four different compounds are roughly ordered in F_1 by their molecular weight.

Scheme 5.4-2

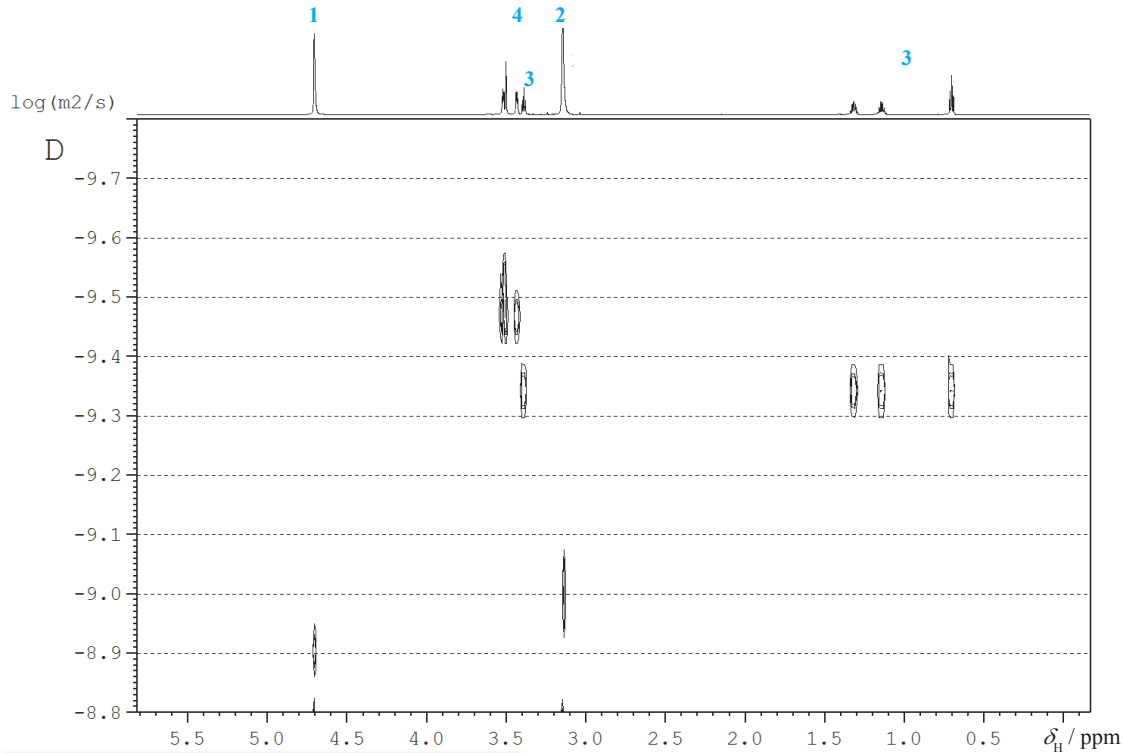

Fig. 5.4-2 DOSY NMR spectrum

7. Comments

The signal decay due to diffusion measured by the sequence shown can be described by the equation:

$$I(g) = I_0 \exp(-\gamma^2 g^2 D \delta^2 (\Delta - \frac{\delta}{3})) \quad \textbf{(1)}$$

Where γ is the gyromagnetic ratio, g the gradient strength, D the diffusion coefficient, δ the length of the gradient pulses and Δ the separation between them (diffusion time d2 in Scheme 5.4-1).

The basic stimulated echo sequence consists of the pulses p1, p3 and p4. Thus the 180° pulse as seen in the spin echo sequence of Experiment 5.2 is here split into two 90° pulses, which has the advantage that the stimulated echo sequence is less prone to T_2 artifacts, because during the diffusion time the magnetization is in the z-direction. The gradient pulse pairs g1 and g2, as well as g4 and g5, are applied as bipolar gradients of opposite sign and are therefore separated by 180° r.f. pulses. This feature reduces gradient artifacts, especially to the lock channel, and allows stronger overall gradients. Since, after the second 90° pulse p3, the spins are in the z-direction, as well as after p6, two additional short gradient pulses g3 and g6 can be applied to destroy transverse magnetization due to pulse imperfections. In order to obtain correct quantitative results of diffusion constants the strength of the gradient pulses has to be calibrated. This is possible either by using a water sample with the known diffusion constant or by using an NMR tube with a slice of plane Teflon of known thickness.

[8] H. Barjat, G. A. Morris, A. G. Swanson, "A Three-Dimensional DOSY–HMQC Experiment for the High-Resolution Analysis of Complex Mixtures" *J. Magn. Reson.* **1998**, *131*, 131–138.

[9] R. Huo, R. Wehrens, J. Van Duynhoven, L. M. C Buydens, "Assessment of techniques for DOSY NMR data processing" *Anal. Chim. Acta* **2003**, *490*, 231–251.

[10] J. C. Cobas, P. Groves, M. Martin-Pastor, A. De Capua, "New applications, process methods, and pulse sequences using diffusion NMR" *Curr. Anal. Chem.* **2005**, *1*, 289–305.

[11] T. Brand, E. J. Cabrita, S. Berger "Intermolecular interaction as investigated by NOE and diffusion studies" *Prog. Nucl. Magn. Reson. Spectrosc*. **2005**, *46*, 159–196.

[12] D. Li, I. Keresztes, R. Hopson, P. G. Williard, "Characterization of reactive intermediates by multinuclear diffusion-ordered NMR spectroscopy (DOSY)" *Acc. Chem. Res*. **2009**, *42*, 270−280.

[13] P. S. Pregosin, "NMR spectroscopy and ion pairing: measuring and understanding how ions interact" *Pure Appl. Chem*. **2009**, *81*, 615−633.

[14] G. A. Morris, "Diffusion-ordered spectroscopy" in: Multidimensional NMR Methods for the Solution State **2010**, 515−532.

For measuring diffusion effects it is very important to suppress any convection due to a temperature gradient within the sample. Keep the filling height of the tube as low as possible. It may be helpful to spin the sample (rotation about long axis). Furthermore, tubes of small diameter diminish the convection possibility appreciably.

In the same way, the linearity of the field gradients is important. Gradient artifacts may also be reduced by using small sample volumes.

8. Questions

A. Why would one, in a ^{13}C detected DOSY, keep the diffusion part of the sequence on the proton channel?

B. Why have the gradients g3 and g6 such strange values?

C. In comparative physical organic studies, should one use a "diffusion standard" and which one would be suitable?

D. With *z*-gradients the diffusion with respect to only one dimension can be measured. For which chemical applications would an *x*,*y*,*z*-gradient probe head be helpful?

9. Own Observations

Experiment 5.5

Residual Dipolar Couplings (RDC)

1. Purpose

Since about the mid-nineties a new field of NMR research emerged aiming to provide an additional tool for structural elucidation. One tries to align molecules in an anisotropic medium very slightly, and this enables the observation of small residual dipolar couplings. These contain information about internuclear distances and angles and therefore provide valuable insights. In contrast to NOEs they are more far-reaching due to their r^{-3} dependence and have therefore been applied first to biomacromolecules [1]. Since these are usually measured in water, the first alignment media were also based on water and comprise liquid crystals, bicelles, micelles, bacteria phages, and paramagnetic lanthanide tags. Because these media are not compatible with small organic molecules, ongoing research is looking for media which will perform the task in this field. In addition to liquid crystals from poly-γ-benzyl-L-glutamate (PBLG) and similar, the most successful systems are currently from stretched polymer gels, but others, like liquid crystals from polyisocyanides and polyacetylenes, are being investigated. In this experiment we show as an example RDCs measured for strychnine in stretched polystyrene.

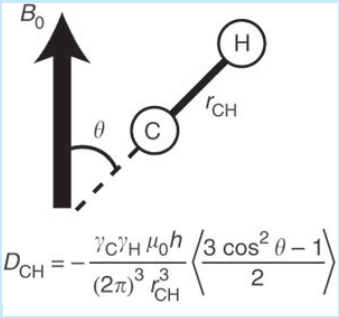

Fig. 5.5-1 Vector diagram for dipolar coupling

2. Variants

The spectroscopic task is to measure ^1J(C,H), the isotropic scalar spin coupling constants, first as a reference in an isotropic medium (such as $CDCl_3$) and then in the presence of an alignment medium which gives the total coupling $T = |J + 2D|$. Finally, the values of the residual dipolar coupling constant D can be extracted by comparing the two measurements.

The classical method to measure ^1J(C,H) spin couplings is the gated decoupling technique (see Exp. 2.9). This is still the most reliable one because of its digital accuracy. However, it can only be applied if the sensitivity of the investigated system is sufficient.

^1J(C,H) spin couplings can also be measured with proton sensitivity using the HSQC method (see Exp. 1.5) by two different approaches. Simply leaving the ^{13}C decoupler off, one obtains the CH doublets in the F_2 dimension. Their extraction can, however, cause difficulties in crowded proton spectra, and the proton-proton spin couplings may have changed due to the alignment.

A modification of the HSQC pulse sequence, which is shown here, omits the middle 180° pulse in the proton channel and replaces it by a BIRD train [3]. This causes the observation of CH doublets in the F_1 dimension, which are usually easier to extract than those in the F_2 dimension. However, the digital resolution in this dimension is another problem.

3. Pulse Scheme and Phase Cycle

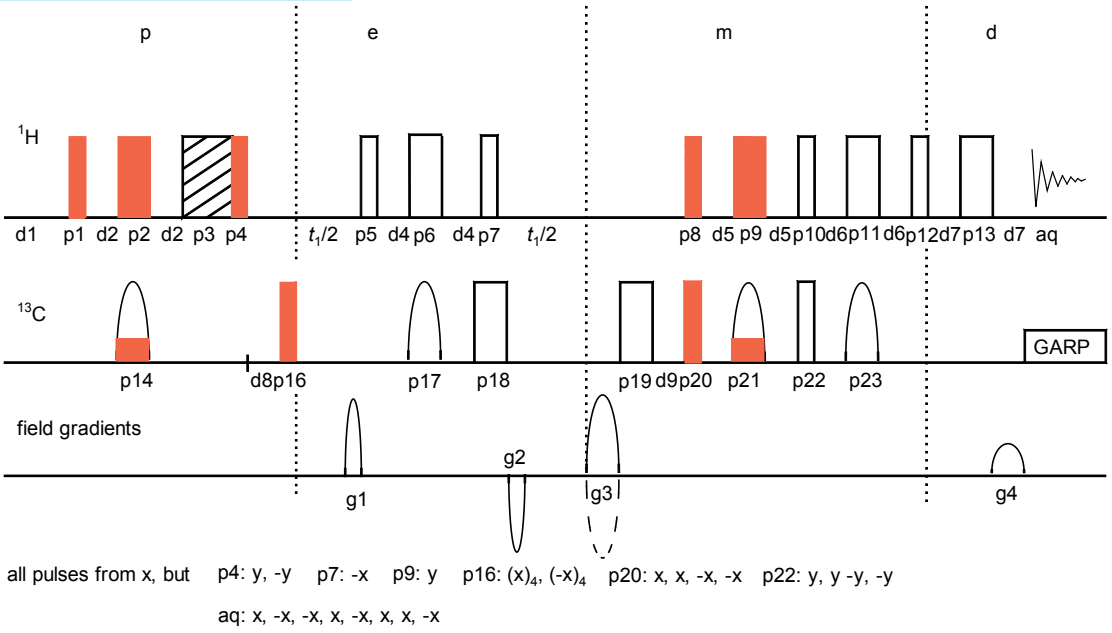

Scheme 5.5-1

Common values:

d1: relaxation delay
d2, d5, d6: INEPT delay for polarization transfer and back transfers
d4: BIRD delay, d4 = $1/(2J_{CH})$
d7, d9: delays adjusted to gradient lengths
d8: delay for zz-filter
p1, p4, p5, p7, p8, p10, p12: 90° ^{1}H transmitter pulses
p2, p6, p9, p11, p13: 180° ^{1}H transmitter pulses
p3: ^{1}H spin lock pulse
p16, p20, p22: 90° ^{13}C transmitter pulses
p18, p19; 180° ^{13}C transmitter pulses
p14, p17, p21, p23: 180° chirped adiabatic ^{13}C transmitter pulses
g1,g2: gradients for BIRD$^{(r)}$ sandwich
g3,g4: gradients for echo-antiecho mode

4. Acquisition

Sample preparation [5]

One-side closed glass tubes (15 cm long, inner diameter 3 mm) were treated with a 1:1 mixture of dimethyldichlorosilane and trimethylsilyl chloride overnight, then washed with dichloromethane and dried at 50° C.

The reagents styrene and divinylbenzene (DVB) were distilled under reduced pressure at ambient temperature to minimize the content of stabilizers.

A mixture of styrene, 0.3 % (v/v) DVB and 0.25 % (m/v) *N*,*N*-azoisobutyronitrile was sonicated for 15 min and then filled into the glass tubes. The tubes were sealed with a gas torch and fixed in an upright position. Polymerization was carried out at 60 °C for 3 days.

The tubes were carefully cracked with a small hammer. The glassy polymer sticks were washed with water to remove small pieces of glass and cut into parts of ca. 1.2 cm length, which should contain no bubbles or cracks. A solution of 50 mg strychnine was prepared in 0.55 ml $CDCl_3$.

After filling a 5 mm NMR tube with 0.25 mL of this solution the stick was added. It was pre-swollen for 5 min to be fixed at its position, and then additional 0.3 mL strychnine/$CDCl_3$ solution was added. Swelling took about 2 weeks and was monitored by measuring the quadrupolar splitting of deuterium.

Special values used for the spectrum shown:

Time requirement: 9 h

Spectrometer: Bruker Avance-700 with cryo probe

td2: 1200
td1: 1000
sw2: 9 ppm
sw1: 140 ppm
aq2: 0.16 s
aq1: 0.024 s
o1: 4.3 ppm
o2: 80 ppm
d1: 2 s
d2: $1/[4J_{CH}–p14/2]$ = (1.724 – 0.5) ms ; ($J_{C,H}$=145 Hz)
d4: 3.448 ms
d5: $1/(8J_{CH})$ = 862 µs
d6: $1/(4J_{CH})$
d7, d9: 1ms
d8: 400 ms
p1, p4, p5, p7, p8, p10, p12: 90° 9.7 µs at –6 dB
p2, p6, p9, p11, p13: 180° 19.4 µs at – 6 dB
p3: ^{1}H spin-lock pulse 1 ms at – 6 dB
p16, p20, p22: 90° 14.5 µs at – 4 dB
p18, p19; 180° 29 µs at – 4 dB
p14, p17, p21, p23: 500 µs at +2.9 dB
g1,g2: gradients 20 %
g3,g4: 80 and 20.1 % (100 % ≈ 0.56 T/m)
ns: 16
ds: 4

5. Processing

Apply zero-filling in F_1 to 2K words in order to have a sufficient digital resolution in this dimension. Use an exponential window with lb = 3 Hz in the F_2 dimension and a squared π/2 shifted sinusoidal window in the indirect dimension.

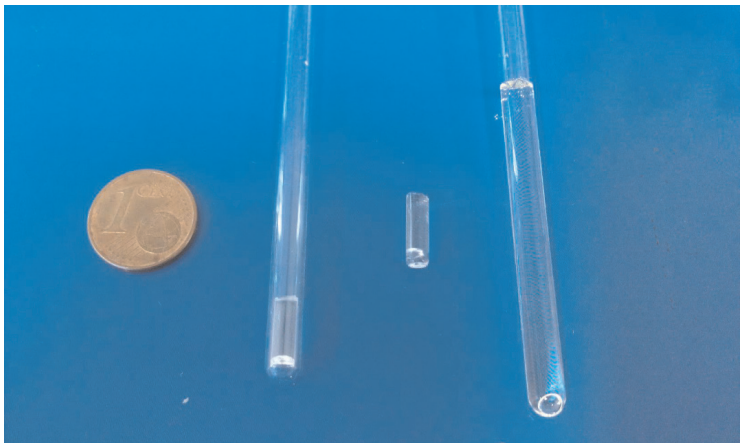

Fig. 5.5-2 from right to left: swollen polystyrene stick in NMR tube, piece of poylstyrene, polystyrene piece in NMR tube without solvent

[1] N. Tjandra, A. Bax "Direct measurement of distances and angles in biomolecules by NMR in a dilute liquid crystalline medium" *Science* **1997**, *278*, 2011–2014.

[2] C. M. Thiele, S. Berger "Probing the diastereotopicity of methylene protons in strychnine using residual dipolar couplings" *Org. Lett*. **2003**, *5*, 705–708.

[3] K. Fehér, S. Berger, K. E. Kövér "Accurate determination of small one-bond heteronuclear residual dipolar couplings by F1 coupled HSQC modified with a G-BIRDr module" *J. Magn. Reson*. **2003**, *163*, 340–346.

[4] J. Yan, E. R. Zartler "Application of residual dipolar couplings in organic compounds" *Magn. Reson. Chem*. **2005**, *43*, 53–64.

[5] B. Luy, K. Kobzar, S. Knör, J. Furrer, D. Heckmann, H. Kessler "Orientational properties of stretched polystyrene gels in organic solvents and the suppression of their residual ^{1}H NMR Signals" *J. Amer. Chem. Soc*. **2005**, *127*, 6459–6465.

[6] G. Pintacuda, M. John, X.-C. Su, G. Otting "NMR structure determination of protein-ligand complexes by lanthanide labeling" *Acc. Chem. Res*. **2007**, *40*, 206–212.

6. Result

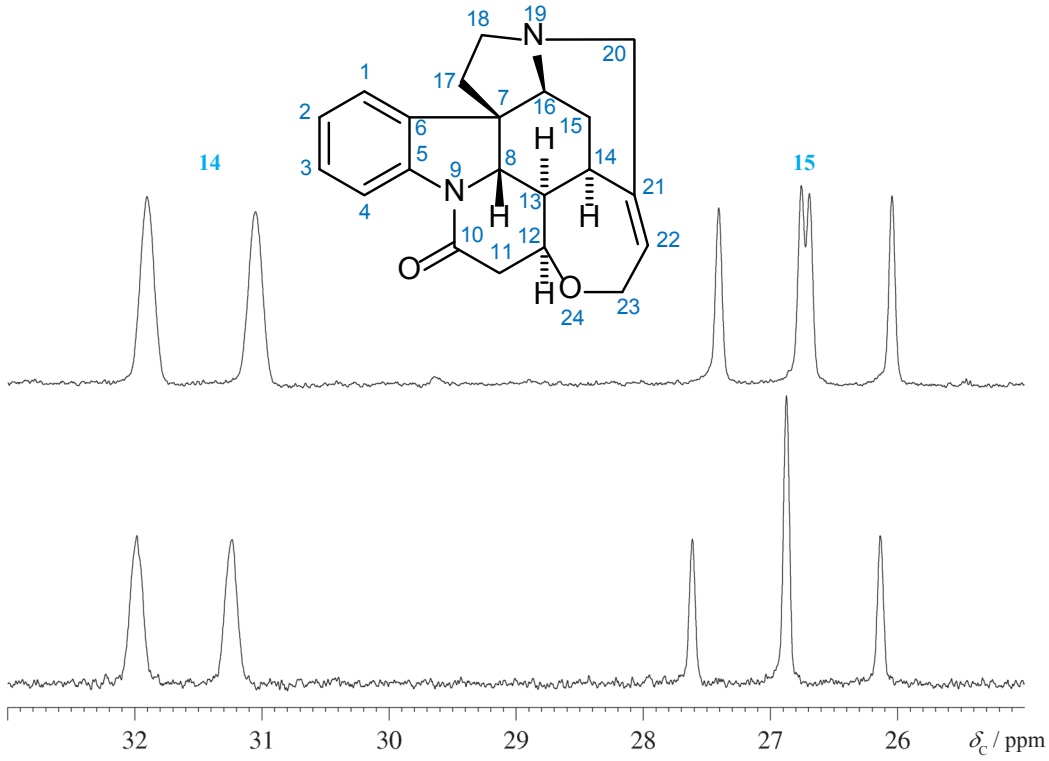

Fig. 5.5-3 Gated decoupled ^{13}C NMR spectra of strychnine in isotropic (bottom) and anisotropic (top) situation.

Shown are first two expansions from the gated decoupled ^{13}C NMR spectra for C-15 at δ_C =27 and for C-14 at δ_C =31.5; the lower row is the normal spectrum in $CDCl_3$, the upper the spectrum within the stretched polystyrene stick. As can be seen, the CH spin coupling for C-15 is diminished; however, the one for C-14 is enlarged.

The figures below show two 2D expansions of the HSQC–BIRD spectrum discussed in this chapter. In black is the normal spectrum in $CDCl_3$, in red the spectrum in the swollen polymer stick, slightly shifted deliberately. Note that for the CH_2 groups the centerline of the triplet is missing in the F_1 dimension of the isotropic spectrum. In the aligned case, the two diastereotopic protons show different spin couplings, and therefore two doublets emerge.

[7] C. M. Thiele "Residual dipolar couplings (RDCs) in organic structure determination" *Eur. J. Org. Chem*. **2008**, 5673–5685.

[8] M. Zweckstetter "NMR: prediction of molecular alignment from structure using the PALES software" *Nature Protocols* **2008**, *3*, 679–690.

[9] M. Ringkjøbing Jensen, J.-L. Ortega-Roldan, L. Salmon, N. v. Nuland, M. Blackledge "Characterizing weak protein–protein complexes by NMR residual dipolar couplings" *Eur. Biophys. J.* **2011**, *40*, 1371–1381.

[10] J. Koehler, J. Meiler "Expanding the utility of NMR restraints with paramagnetic compounds: Background and practical aspects" *Prog. NMR Spectrosc*. **2011**, *59*, 360–389.

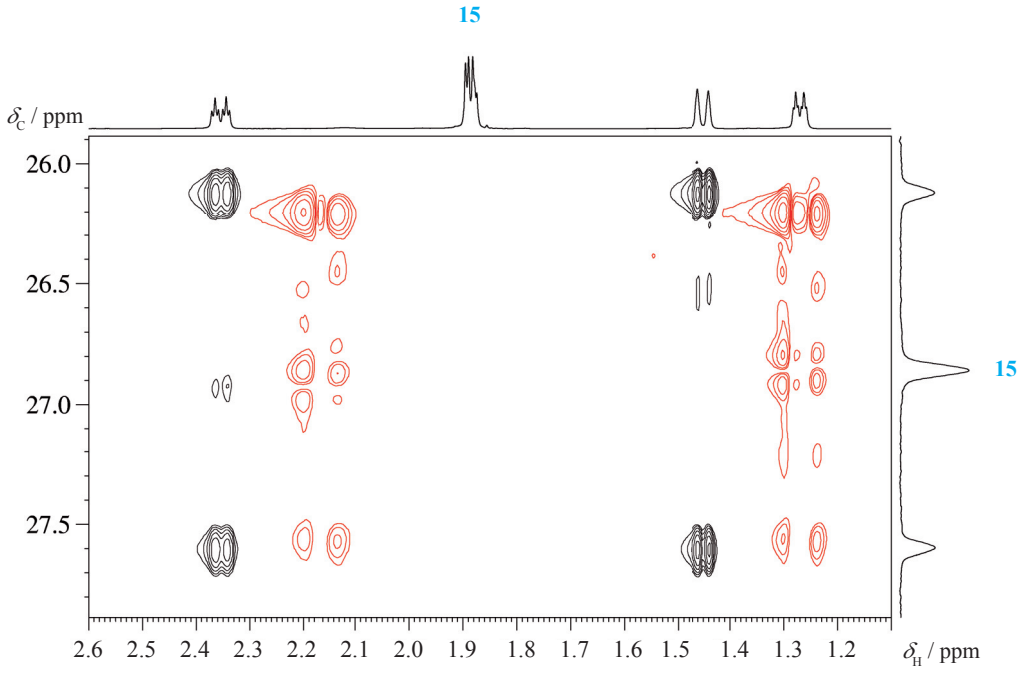

Fig. 5.5-4 HSQC-BIRD spectrum of strychnine, black in isotropic media, red (shifted graphically) in oriented media

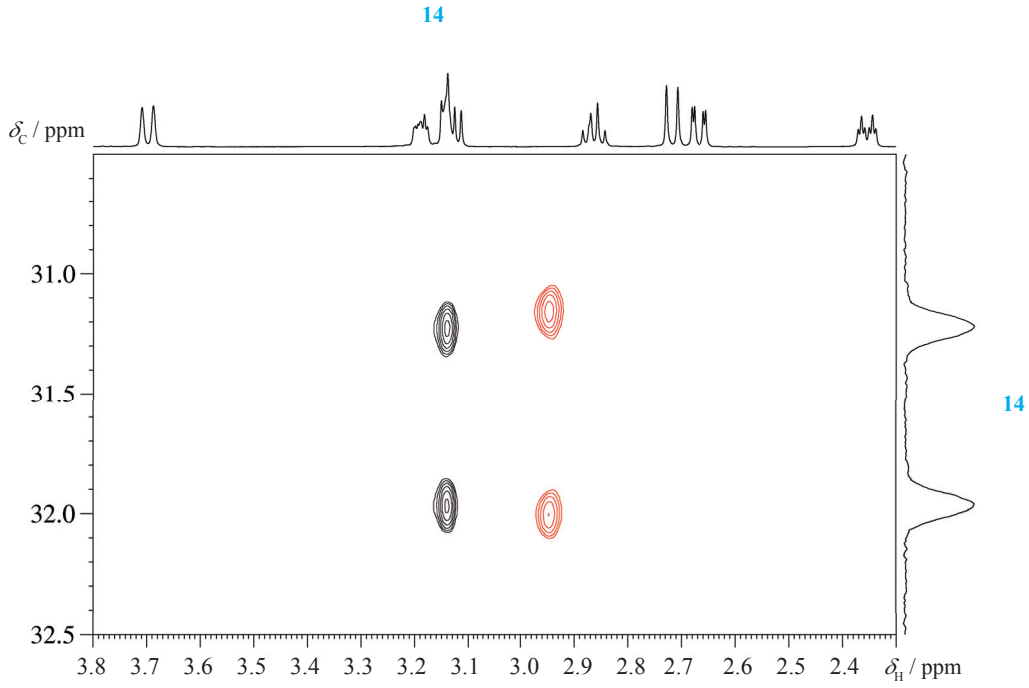

Fig. 5.5-5 HSQC-BIRD spectrum of strychnine, black in isotropic media, red (shifted graphically) in oriented media

7. Comments

The pulse sequence is to a large extent identical to the HSQC method described in chapter 1.5, but has two significant modifications. First, the delay d8 is inserted between the two pulses p4 and p16. It acts as a *zz*-filter and suppresses to some extent the polymer signals.

Second, the 180° proton pulse in the middle of the sequence is replaced by a G-BIRD$^{(r)}$ sandwich. With the value of d4 adjusted to $1/(2^1J_{CH})$ the three pulses on the proton channel and the two pulses on the carbon channel act in sum essentially as 360° pulses, or, in other words, are essentially without action. This is equivalent to the desired removal of the 180° proton pulse. Note that the two gradients g1 and g2 of opposite signs cancel out the fraction of magnetization that does not experience perfect rotation by the BIRD$^{(r)}$ pulse.

For the long-range CH spin couplings the delay d4 is far too short, and therefore these contributions are 180° inverted by the BIRD sandwich, leading to sharp $^1J_{CH}$ doublets in the indirect dimension.

8. Questions

A. Why does one speak of "residual" dipolar couplings?

B. Why can the progress of alignment be checked by ^{2}H NMR?

C. Explain why the center line of the triplets is missing in the indirect dimension of the HSQC method without a 180° proton pulse.

9. Own Observations

Chapter 6

Organic Chemistry Applications

NMR provides tremendous possibilities to organic and inorganic chemistry. Even to mention only the names of available techniques would fill pages. In this chapter we have restricted ourselves to some more basic and very often used applications, and have selected those which can be performed with commercially available material. The selection given should only inspire the reader to look for further extensions.

6.1 ASIS [**A**romatic **S**olvent **I**nduced **S**hifts] 175
6.2 Chirality Determination 179
6.3 Advanced Mosher Methods 183
6.4 Quantitative NMR and Relaxation Reagent 187
6.5 Determination of Association Constants K_a 193
6.6 STD NMR [**S**aturation **T**ransfer **D**ifference NMR] 199
6.7 A Kinetic Experiment 203

Fig. 6.0-1 Varian A60 NMR spectrometer

The Varian A-60 NMR spectrometer was in the sixties of the last century probably the most successful instrument in the hands of organic chemists, and was used by the senior author to perform the measurements for his diploma work. Today, there exists also a small instrument (Bruker Fourier-300) with which nearly all experiments demonstrated in this book can be performed.

Fig. 6.0-2 Bruker Fourier-300 NMR spectrometer

Experiment 6.1

ASIS

1. Purpose

Even in these days of high-field NMR spectroscopy, it often happens that proton spectra show either overlap of signals or higher-order effects because of small chemical shift differences. In these cases a simple change of solvent, especially from chloroform to aromatic solvents, most often benzene, can cause a dramatic simplification of the spectrum due to a better separation of the signals. This effect is called aromatic solvent-induced shift (ASIS). The effect is usually strong in ^{1}H NMR spectroscopy but only weak in ^{13}C NMR. Although the technique is very old, it is by no means outdated. In this experiment we demonstrate ASIS with ethyl anthranilate.

2. Variants

Instead of benzene one can use toluene or in several cases pyridine. All solvents should be fully deuterated.

3. Pulse Scheme and Phase Cycle

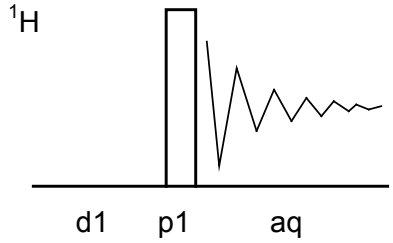

p1: x, x, -x, -x, y, y, -y, -y

aq: x, x, -x, -x, y, y, -y, -y

Scheme 6.1-1

Common values:

d1: relaxation delay
p1: 90° ^{1}H transmitter pulse

4. Acquisition

Special values used for the spectrum shown:

Sample: 3 % ethyl anthranilate, **(a)** in $CDCl_3$ and **(b)** in [D_6] benzene with 0.01 % TMS.
Time requirement: 5 min
Spectrometer: Bruker Avance-700 with 5-mm TBI probe

p1: 8 µs at −4 dB
d1: 2s
td: 64K
aq: 3.3 s
sw: 14 ppm

5. Processing

Use standard 1D processing for ^{1}H NMR spectra, reference both spectra to TMS $\delta_H = 0$ and inspect the aromatic region.

6. Result

The figure shows an expansion of the aromatic region obtained on an Avance-700 spectrometer. Spectrum **a** was obtained in $CDCl_3$, whereas spectrum **b** was recorded in [D_6]benzene. In **a** the signals of H-3 and H-5 are overlapping; however, in **b** all signals of the aromatic ABCD pattern can be individually analyzed. The singlet at δ_H = 7.16 arises from the residual protons of [D_6]benzene.

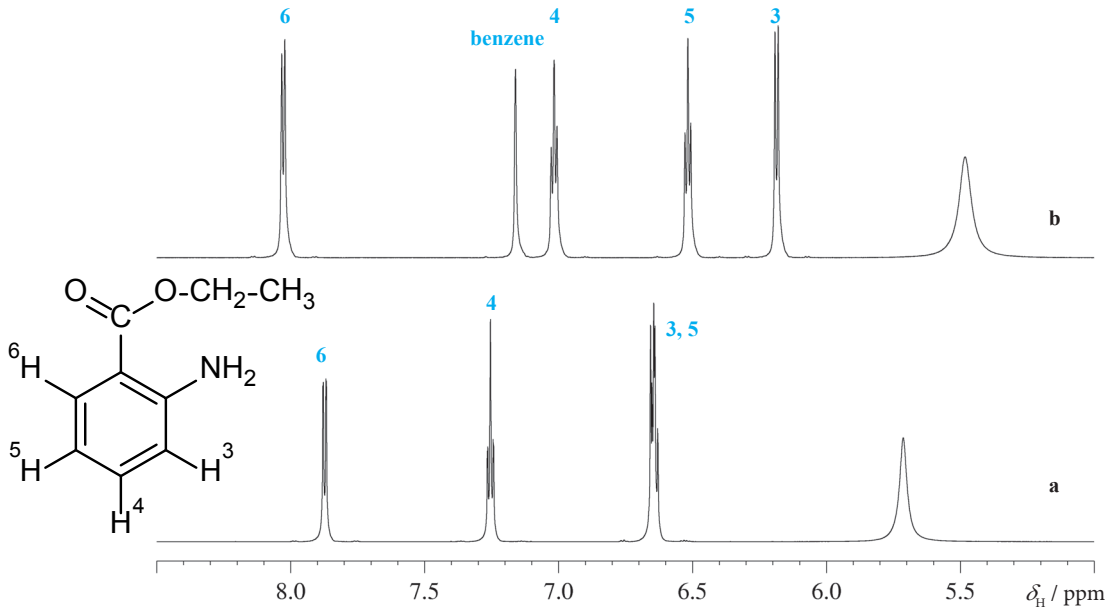

Fig. 6.1-1 ^{1}H NMR spectrum of ethyl anthranilate in (a) $CDCl_3$ and (b) benzene-d 6

7. Comments

The ASIS technique is the most straightforward approach to simplifying proton NMR spectra and should be tested before other means such as lanthanide shift reagents are employed. According to the theory [2], the total shielding σ_t of a proton is composed as described by Equation (1):

(1) $$\sigma_t = \sigma_g + \sigma_b + \sigma_w + \sigma_a + \sigma_e + \sigma_c$$

Here, σ_g refers to the shielding in the gas phase, and the other contributions arise from the bulk susceptibility of the solvent (σ_b), van der Waals interactions (σ_w), anisotropy effects (σ_a), electric field effects (σ_e), and specific solute–solvent interactions (σ_c). All of these effects together are associated with an interaction energy of about 1 kcal/mole. Quantification of the ASIS, however, seems to be difficult and depends critically on the reference system used [3]. ASIS works best with molecules containing polar groups; sometimes pyridine gives superior results.

[1] P. Laszlo, "Solvent effects and nuclear magnetic resonance" *Prog. NMR Spectrosc*. **1967**, *3*, 231−402.

[2] J. Ronayne, D. H. Williams, "Solvent effects in proton magnetic resonance spectroscopy" *Annu. Rep. NMR Spectrosc*. **1969**, *2*, 83−124.

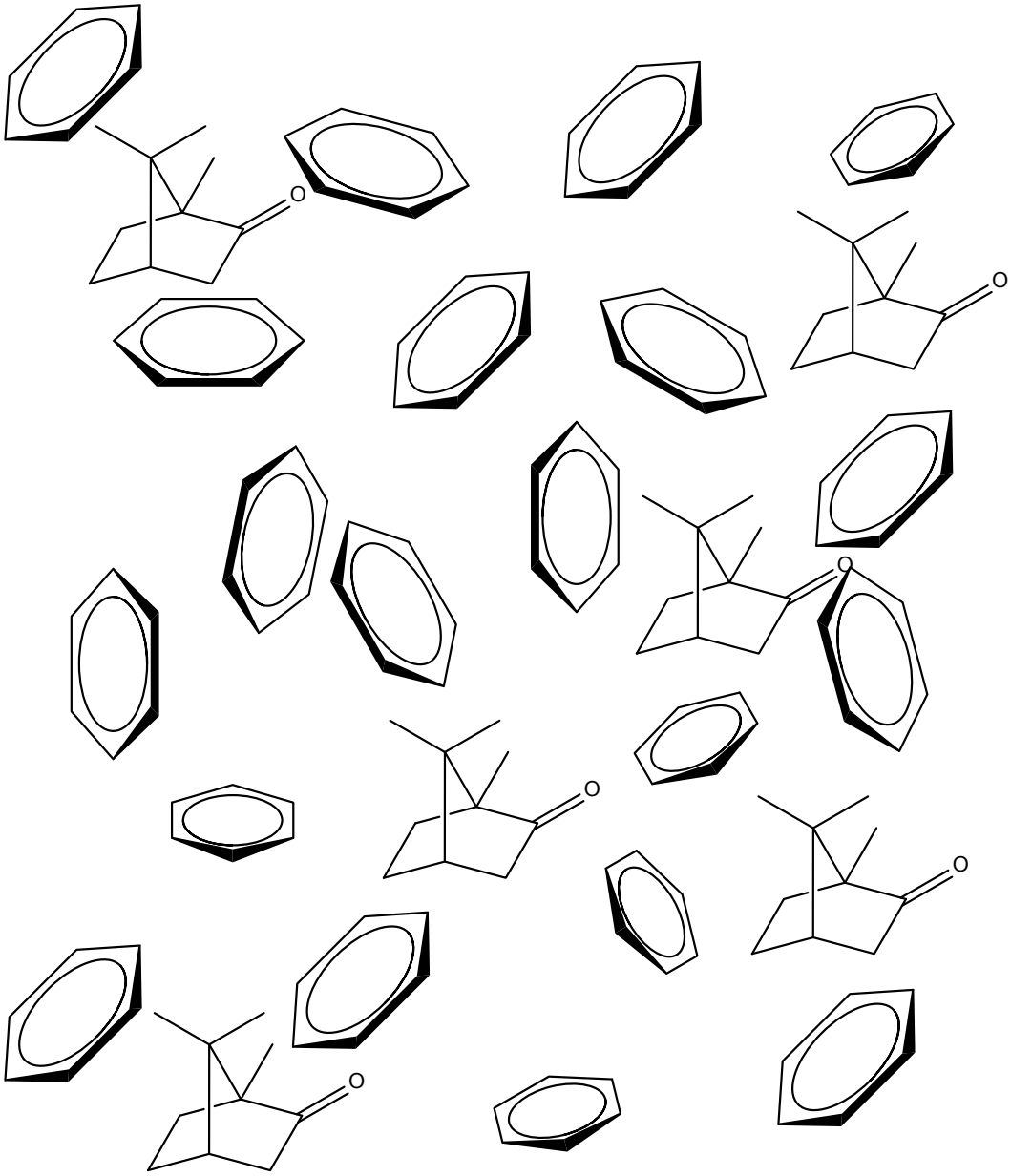

Scheme 6.1-2 Sketch of camphor in benzene

[3] F. H. A. Rummens, R. H. Krystynak, "Intermolecular interactions in nuclear magnetic resonance. VII. The role of the internal reference in aromatic solvent induced shifts" *J. Am. Chem. Soc*. **1972**, *94*, 6914−6921.

[4] H. Stamm, H. Jäckel, "Relative ring-current effects based on a new model for aromatic-solvent-induced shift" *J. Am. Chem. Soc*. **1989**, *111*, 6544−6550.

[5] K. Nikki, "^{1}H and ^{13}C NMR aromatic solvent-induced shifts of *n*-alkanes" *Magn. Reson. Chem*. **1990**, *28*, 385−388.

8. Questions

A. Discuss the effects for the chemical shift of the OH protons in *p*-cresol **I** and salicylaldehyde **II** of changing the solvent from chloroform to (a) benzene and (b) pyridine.

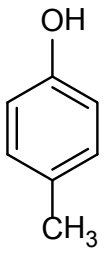

I

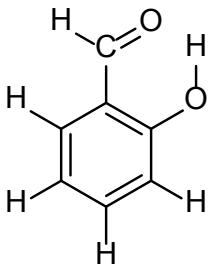

II

B. Measure the temperature-dependent ASIS effects for the three methyl groups of camphor in toluene-d_8 from 273 K to 373 K and discuss.

9. Own Observations

Experiment 6.2

Chirality Determination

1. Purpose

This ^{1}H NMR experiment is used to prove the presence of enantiomers or to determine the enantiomeric purity of a compound. A chiral solvating agent, *R*-(−)-α-acetoxy-phenylacetic acid [*R*-(−)-*O*-acetyl-mandelic acid], which is commercially available in pure enantiomeric form, is employed. The main point of such chiral solvating agents is that no chemical derivatization is required, but the reagent is just added to the NMR tube.

2. Variants

Besides the reagent used here there are many others currently employed in organic chemistry, such as Pirkle's reagent, cyclodextrins, paramagnetic lanthanide complexes, diamagnetic rhodium complexes, zinc porphyrins, and many others. Their choice is dependent on the chemical structure of the analyte.

3. Pulse Scheme and Phase Cycle

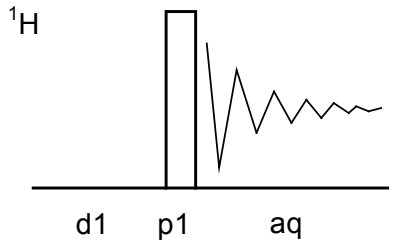

p1: x, x, -x, -x, y, y, -y, -y

aq: x, x, -x, -x, y, y, -y, -y

Scheme 6.2-1

Common values:

d1: relaxation delay
p1: 90° ^{1}H transmitter pulse

4. Acquisition

Special values used for the spectrum shown:

Sample: 10 mg *S*-(−)-1-phenylethylamine and 20 mg *R*-(+)-1-phenylethylamine in 0.7 mL $CDCl_3$, a spatula tip of solid *R*-(−)-*O*-acetyl-mandelic acid.
Time requirement: 5 min
Spectrometer: Bruker Avance-700 with 5-mm TBI probe

p1: 8 µs at −4 dB
d1: 2s
td: 64K
aq: 3.3 s
sw: 14 ppm

Record a spectrum of 1-phenylethylamine; to achieve best resolution use spinning of the sample. Add about 10 mg of *R*-(−)-*O*-acetyl-mandelic acid and record the spectrum again. Increase the amount of the chiral solvating agent until the separation of the two doublets of the methyl group at δ_H = 1.2 ppm is sufficient for integration.

Fig. 6.2-1 Wisteria tree in front of the house of the senior author forming a left turning-helix.

5. Processing

Using standard 1D processing for ^{1}H NMR spectra, the final spectrum shown here was processed with 64K data points and Gaussian windowing using lb = −0.5 Hz and gb = 0.1.

6. Result

The figure shows the ^{1}H-NMR spectrum of the 2:1 enantiomeric mixture of 1-phenylethylamine obtained on an Avance-700 spectrometer **(a)** without and **(b)** in the presence of the chiral solvating agent *R*-(−)-*O*-acetyl-mandelic acid. The signals at δ_H = 1.4 (CH_3) and at δ_H = 4.1 (CH) are doubled, and the signals are just separated for integration. The ^{1}H NMR signals of *S*-(−)-phenylethylamine are at slightly higher frequencies than those of the *R*-(+) enantiomer within the methyl group, but opposite in the methine quadruplet. Both are slightly shielded with respect to the pure compound.

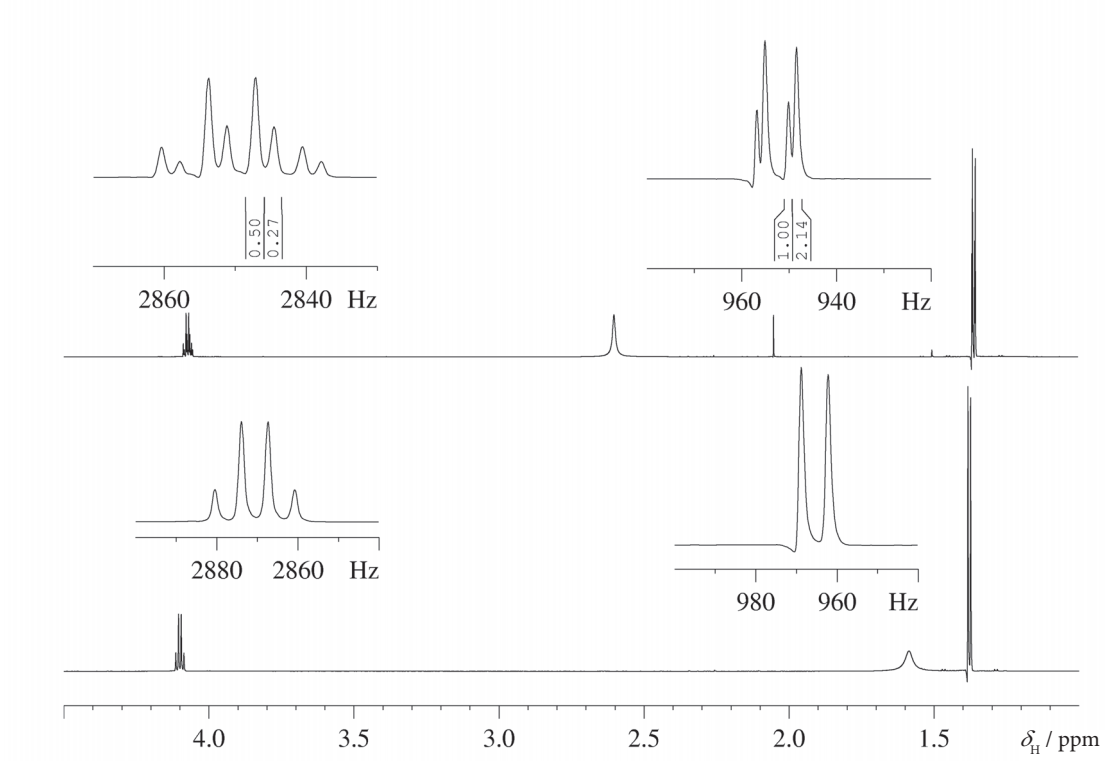

Fig. 6.2-2 ^{1}H NMR spectra from a mixture of R- and S-1-phenylethylamine in $CDCl_3$ (bottom) and after addition of *R*-(−)-*O*-acetylmandelic acid (top)

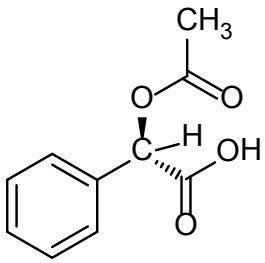

Scheme 6.2-2

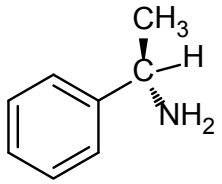

Scheme 6.2-3

7. Comments

Chiral solvating agents form diastereomeric solvation complexes, which are in rapid equilibrium with the uncomplexed species. Solvents with low solvating ability should therefore be used, such as $CDCl_3$ or C_6D_6. In the example presented here the chiral auxiliary may form a salt with the basic phenylethylamine. The salt is still in rapid equilibrium with the base and the acid, so this is not a derivatizing agent like, for example, Mosher esters.

For quantitative determinations use stock solutions of the substrate and the chiral solvating agent to make up a series of solutions of constant volume containing a fixed amount of substrate solution and varying amounts of the chiral agent solution.

The enantiomeric excess *ee* can be calculated from the following equation:

$$ee = \frac{(I_1 - I_2)}{(I_1 + I_2)} \qquad (1)$$

where I_1 and I_2 are the integrals of the corresponding signals. The *ee*-value was determined from the methyl group integrals to be 0.36 for the example given.

[1] W. H. Pirkle, D. J. Hoover, "NMR chiral solvating agents" *Top. Stereochem*. **1982**, *13*, 263−331.

[2] D. Parker, "NMR determination of enantiomeric purity" *Chem. Rev*. **1991**, *91*, 1441−1457.

[3] R. Rothchild, "NMR methods for determination of enantiomeric excess" *Enantiomer* **2000**, *5*, 457−471.

[4] B. Luy, "Distinction of enantiomers by NMR spectroscopy using chiral orienting media" *J. Indian Institute Science* **2010**, *90*, 119−132.

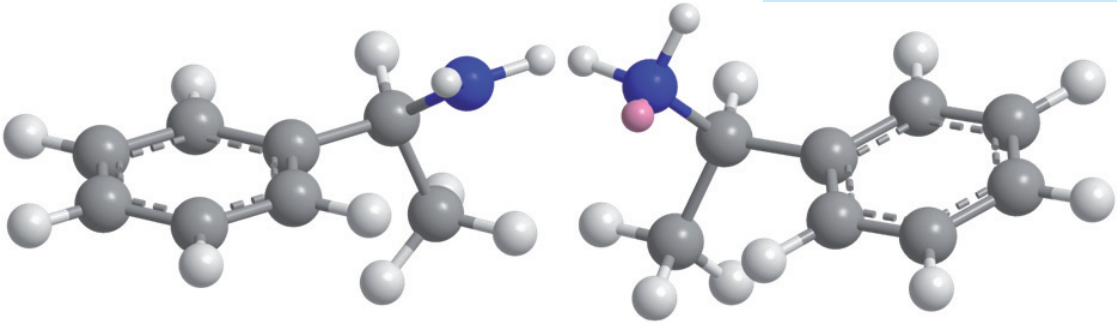

Fig. 6.2-3 The two enantiomers of phenylethylamine

[5] T. J. Wenzel, C. D. Chisholm, "Using NMR spectroscopic methods to determine enantiomeric purity and assign absolute stereochemistry" *Progr. NMR Spectrosc.* **2011**, *59*, 1–63.

8. Questions

A. What is the *ee*-value of a 10:1 mixture? Which ratio of enantiomers do you have synthetically to achieve to report an *ee*-value of 0.9?

B. The shift difference observed here for the methyl group signals was 1.77 Hz. How large would this be on a 300 MHz instrument?

C. Compare the result using different chiral solvating reagents.

9. Own Observations

Experiment 6.3

Advanced Mosher Method

1. Purpose

The determination of absolute stereochemistry is a most important goal in natural product chemistry. Using high-field instruments, this can be performed by NMR if certain rules are obeyed. An enantiomerically pure alcohol is esterified with both (*S*)-(+)-2-methoxy-2-(trifluoromethyl)-2-phenylacetic acid chloride (MTPA-Cl) and (*R*)-(−)-MTPA-Cl. One measures the chemical shift differences ($\delta_S - \delta_R$) of *all* protons between the two diastereoisomers obtained. By assuming an idealized conformation, which can be corroborated by a molecular mechanics calculation and for some derivatives by NOESY measurements [5], these chemical shift differences can be evaluated to determine the absolute configuration. Recently, the additional use of barium salts has been proposed [7]. In this experiment we demonstrate the method using enantiomerically pure menthol of unknown configuration as a substrate.

Fig. 6.3-1 H. S. Mosher (1915-2001)

2. Variants

A multitude of chiral compounds have been proposed throughout the years to contribute to a solution of this task [11]. These compounds range from simple organics via phosphonates, cyclodextrins and calixarenes to transition metal complexes. All these compounds have special advantages for specific analytes such as the MTPA esters shown here for secondary alcohols.

3. Pulse Scheme and Phase Cycle

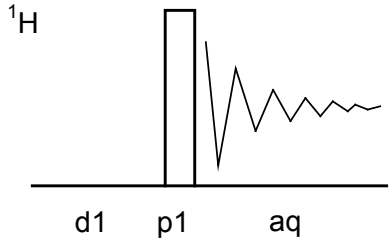

p1: x, x, -x, -x, y, y, -y, -y

aq: x, x, -x, -x, y, y, -y, -y

Scheme 6.3-1

4. Acquisition

Time requirement: 5 min

Samples: (*S*)-MTPA- and (*R*)-MTPA-esters of one enantiomer of menthol in 0.7 mL $CDCl_3$, prepared as below. With addition of 100 mg barium perchlorate use CD_3CN as a solvent.

Preparation: Dissolve 61.8 mg (0.39 mmol) of one enantiomer of menthol in 0.5 mL dry pyridine, dissolve (**a**) 50 mg (0.2 mmol) (*R*)-(−)- and (**b**) (*S*)-(+)-2-methoxy-2- (trifluoromethyl)-2-phenyl acetic acid chloride each in 0.25 mL dry pyridine. Mix each of the acid chloride

[1] J. A. Dale, H. S. Mosher, "Nuclear magnetic resonance enantiomer reagents. Configurational correlations via nuclear magnetic resonance chemical shifts of diastereomeric mandelate, O-methylmandelate, and α-methoxy-α-trifluoromethylphenylacetate (MTPA) esters" *J. Am. Chem. Soc*. **1973**, *95*, 512−519.

[2] I. Ohtani, T. Kusumi, Y. Kashman, H. Kakisawa, "High-Field FT NMR Application of Mosher's method. The absolute configurations of marine terpenoids" *J. Am. Chem. Soc*. **1991**, *113*, 4092−4096.

solutions with 0.25 mL of the menthol solution and let it stand for two days with occasional shaking. Add 20 mL H_2O and a few drops of conc. HCl and extract the solutions with three portions of 20 mL Et_2O. After drying over $MgSO_4$ the solvent is evaporated and the residue purified by preparative TLC (PE/Et_2O 40:1).

Load standard ^{1}H NMR acquisition parameters and record the spectra of both solutions **a** and **b**.

5. Processing

Use standard 1D processing for ^{1}H NMR spectra. The dual display mode is most convenient to extract the chemical shift differences of the two spectra.

6. Result

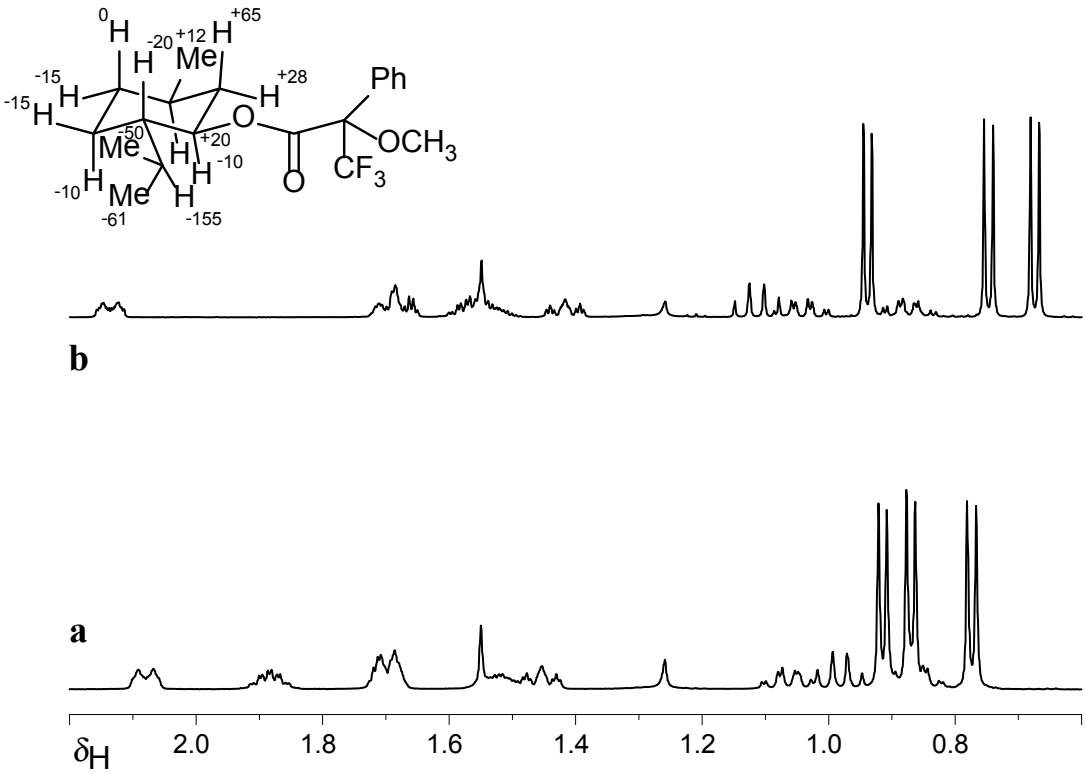

Fig. 6.3-2 ^{1}H NMR spectra of (a) R-MPTA ester and (b) S-MPTA ester of menthol

The Figure shows an expansion of the ^{1}H NMR spectra obtained on an AMX-500 NMR spectrometer. In Fig. **a** the result of the (*R*)-MTPA ester is given, in Fig. **b** the result of the (*S*)-MTPA ester. The chemical shift differences ($\delta_S - \delta_R$) in Hz are shown in the formula. The assignment of the various protons in the menthol moiety must be performed independently using the standard 2D experiments discussed in this book. The further evaluation proceeds as follows: Put the protons with positive $\Delta\delta$ on the right side of the model structure, and those with a negative $\Delta\delta$ on the left side. Construct a molecular model, and con-

firm that *all* assigned protons with positive and negative $\Delta\delta$ are actually found on the right and left sides of the MTPA plane. The absolute values of $\Delta\delta$ must be proportional to the distance from the MTPA moiety. When *all* these conditions are satisfied (do NOT use [D_6]benzene as solvent), the correct configuration can be extracted. For the example shown, the menthol used proved to be (1*R*,2*S*,5*R*)-(−)-menthol.

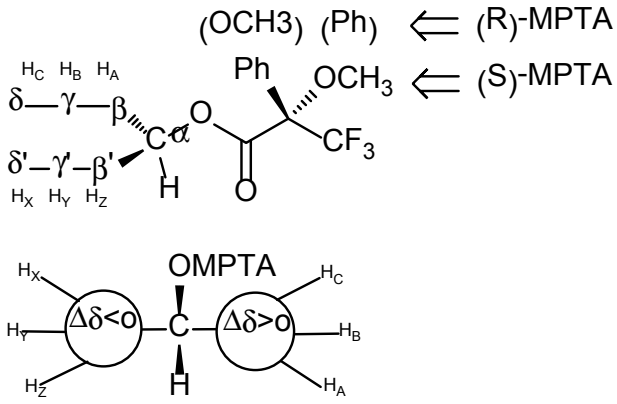

Scheme 6.3-2

7. Comments

The Mosher method is well known among organic chemists as a method of determining the *relative ee*-values in mixtures of enantiomers, mostly using the large chemical shift differences obtained with ^{19}F NMR, by preparing only one MTPA ester. The advantage of the technique shown in this experiment relies mainly on the fact that $\Delta\delta$ values of *all* protons that show a chemical shift difference are evaluated. Recently, many other reagents have been proposed [3−11], which, in principle, use the same effect, namely the aromatic-ring-induced chemical shift differences. The addition of $BaClO_4$ in CD_3CN stabilizes the conformation of the ester as shown:

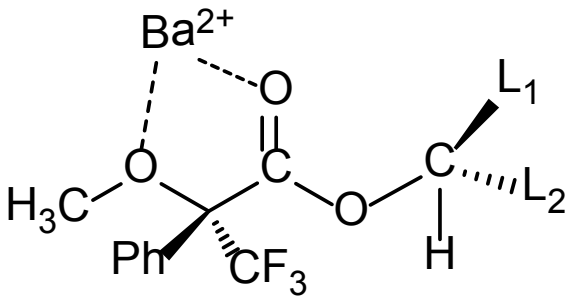

Scheme 6.3-3

[3] G. Uray "Determination of Enantiomeric purity: NMR methods" in Houben-Weyl, *Methods in Organic Chemistry*, *Stereoselective Synthesis*, G. Helmchen, R. W. Hoffmann, J. Mulzer, E. Schaumann (eds.),Thieme, Stuttgart, **1995**, *E21a*, 253−292.

[4] R. Chinchilla, L. R. Falvello, C. Najera, "Determination of the absolute configuration of amines and α-amino acids by ^1H NMR of (*R*)-*O*-aryllactic acid amides" *J. Org. Chem*. **1996**, *61*, 7285−7290.

[5] A. Heumann, J. M. Brunel, R. Faure, H. Kolshorn, "Nuclear Overhauser effects in diastereoisomeric vinyl ethers for the precise structure determination of chiral alcohols" *J.C.S. Chem. Comm*. **1996**, 1159−1160.

[6] J. M. Seco, E. Quinta, R. Riguera, "A practical guide for the assignment of the absolute configuration of alcohols, amines and carboxylic acids by NMR" *Tetrahedron: Asymmetry*. **2001**, *12*, 2915−2925.

[7] R. Garcia, J. M. Seco, S. A. Vázquez, E. Quinoá, R. Riguera, "Absolute configuration of secondary alcohols by ^1H NMR: *In situ* complexation of α-methoxyphenylacetic acid esters with barium(II)" *J. Org. Chem*. **2002**, *67*, 4579−4589.

[8] H. Duddeck "$Rh_2[MTPA]_4$, a dirhodium complex as NMR auxiliary for chiral recognition" *The Chemical Record*, **2005**, *5*, 396–409.

[9] N. Harada "Determination of absolute configurations by X-ray crystallography and ^1H NMR anisotropy" *Chirality* **2008**, *20*, 691–723.

[10] T. J. Wenzel, C. D. Chisholm, "Using NMR spectroscopic methods to determine enantiomeric purity and assign absolute stereochemistry" *Progr. NMR Spectrosc*. **2011**, *59*, 1–63.

8. Questions

A. Would the two compounds (–)-menthol-(S)-MPTA ester and (+)-menthol-(*R*)-MPTA ester give different NMR spectra?

B. Why are the $\Delta\delta$-values dependent on the distance to the MPTA residue?

C. Will the method work with primary and secondary amines?

9. Own Observations

Experiment 6.4

Quantitative NMR and Relaxation Reagents

1. Purpose

In ^{1}H NMR spectroscopy the signal area is normally proportional to the number of nuclei contributing to the signal, provided that saturation and radiation damping are avoided. It is therefore possible to use the integrals of ^{1}H NMR for quantitative determinations in chemistry. For ^{13}C NMR the situation is more complex due to large differences in relaxation times and NOE effects. Here the addition of a relaxation reagent and the inverse gated technique is recommended. For all nuclei with natural abundance lower than 100 %, the precondition is the equal natural abundance at all positions of which NMR signals are inspected for quantification.

2. Variants

In most cases of quantification a reference substance **R** of known mass is added to the sample. The mixture should be homogeneous, and the signals should not overlap. Then the mass of the analyte **A** can be calculated by

$$m_A = m_R \frac{N_R}{N_A} \frac{I_A}{I_R} \frac{M_A}{M_R} \qquad (1)$$

N -number of nuclei that cause the signal
I - intensity (area) of the signal
M- molar mass

To avoid the addition of a reference substance the electronic generation of an external r.f. signal can be used (*ERETIC - **E**lectronic **Re**ference **To** Access **I**n vivo **C**oncentration*), which initially required additional hardware. [6] Under certain measuring conditions one can compare two different spectra directly for quantitative calculations. This is based on the PULCON procedure (***PU**lse **L**ength based **CON**centration determination*) [10] which relates the sensitivity of an r.f. coil to the 90°/360° pulse lengths.

Fig. 6.4-1 Grappa, for quantitative NMR only ...

3. Pulse Scheme and Phase Cycle

Common values:

d1: relaxation delay
p1: 30° ^{1}H transmitter pulse

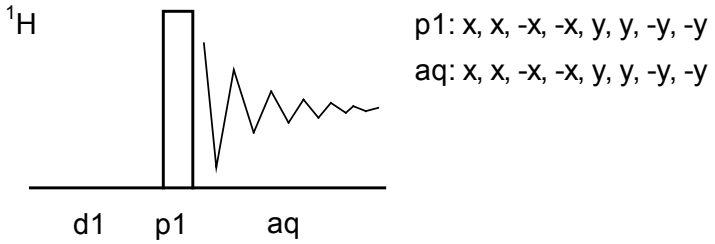

Scheme 6.4-1

and inverse gated for ^{13}C:

Common values:

d1: relaxation delay
p1: 30° ^{13}C transmitter pulse

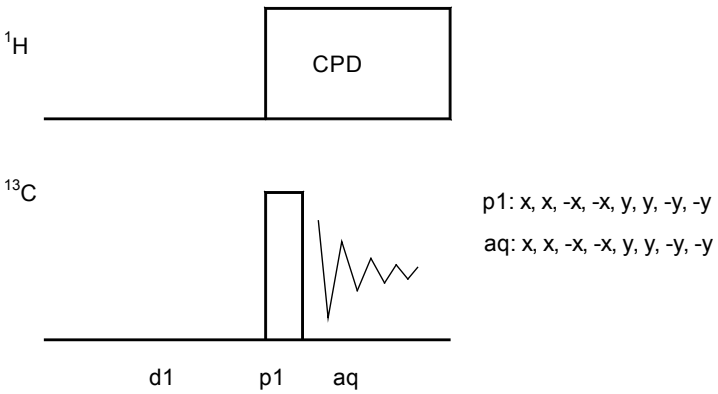

Scheme 6.4-2

4. Acquisition (a) ^{1}H-NMR

Special values used for the spectrum shown:

Sample: 0.7 mL Grappa or similar containing a few drops of D_2O.
Time requirement: 5 min
Spectrometer: Bruker DRX-400 with 5-mm TBI probe

Record a standard ^{1}H NMR spectrum with a large number of data points (10 points/Hz digital resolution). The spectral width should be large enough so that the signals at both ends are not affected by any filter of the spectrometer. Be sure to obtain a good signal-to-noise ratio, at least 35:1. The pulse repetition time must be long enough for complete relaxation ($5T_1$, where T_1 is the longest spin−lattice relaxation time). It is advisable to repeat the experiment with different spectrometer settings and calculate an average of the results. You have to set:

td: 32K
sw: 5 ppm
aq: 7.54 s
o1: middle of ^{1}H NMR spectrum, 3 ppm
p1: 30° ^{1}H transmitter pulse
d1: 10 s
ns: 8
ds: 4

(b) ^{13}C-NMR

Special values used for the spectrum shown:

Sample: 156.4 mg naphthalene and 70.0 mg phenanthrene in 1 mL $CDCl_3$. Add 35 mg $Cr(acac)_3$, which corresponds to a 0.1 M solution.
Time requirement: 30 min
Spectrometer: Bruker DRX-400 with 5-mm BBO probe

Record a ^{13}C NMR spectrum with the inverse gated decoupling sequence. The spectral width should be large enough such that the signals at both ends are not affected by any filter of the spectrometer. Be sure to obtain a good signal-to-noise ratio, at least 35:1. You have to set:

td: 2K
aq: 0.5 s (short aq to avoid NOE build-up during acquisition)
sw: 20 ppm
o1: middle of aromatic region of the ^{13}C NMR spectrum
o2: middle of aromatic region of the ^{1}H NMR spectrum
p1: 90° ^{13}C transmitter pulse
d1: 10 s
decoupler attenuation and 90° pulse for CPD
ns: 40

5. Processing

Use standard 1D processing with additional zero-filling to 64 K data points. Perform a baseline correction on the FID before the Fourier transformation. Phase-adjust the spectrum accurately and perform a baseline correction on the spectrum, then integrate the signals. Ensure that the integral limits are far enough apart to give a complete integration including the ^{13}C satellites in case of ^{1}H NMR. Adjust slope and bias of the individual integrals. This is especially important for the integration of broad signals. In the ^{1}H NMR case there are three signals (H_2O + OH, CH_2 and CH_3 of ethanol), for ^{13}C NMR nine signals can be evaluated.

[1] R. Freeman, H. D. W. Hill, R. Kaptein, "Proton-decoupled NMR spectra of carbon-13 with the nuclear Overhauser effect suppressed" *J. Magn. Reson*. **1972**, *7*, 327−329.

[2] G. C. Levy, U. Edlund, "Quantitative carbon-13 Fourier transform nuclear magnetic resonance. Limitations of spin relaxation reagents" *J. Am. Chem. Soc*. **1975**, *97*, 4482−4485.

[3] D. D. Traficante, "Optimum tip angle and relaxation delay for quantitative analysis" *Concepts Magn. Reson*. **1992**, *4*, 153−160.

[4] J. Peterson, "^{1}H NMR analysis of mixtures using internal standards" *J. Chem. Educ*. **1992**, *69*, 843−845.

[5] D. D. Traficante, L. R. Steward, "The relationship between sensitivity and integral accuracy. Further comments on optimum tip angle and relaxation delay for quantitative analysis" *Concepts Magn. Reson*. **1994**, *6*, 131−135.

[6] S. Akoka, L. Barantin, M. Trierweiler "Concentration measurement by proton NMR using the ERETIC method" *Anal. Chem*. **1999**, *71*, 2554–2557.

[7] G. F. Pauli "qNMR — A versatile concept for the validation of natural product reference compounds" *Phytochem. Anal*. **2001**, *12*, 28–42.

[8] G. Vlahhov, C. Schiavone, N. Simone, "Quantitative ^{13}C NMR method using the DEPT pulse sequence for the determination of the geographical origin (DOP) of olive oils" *Magn. Reson. Chem*. **2001**, *39*, 689−695.

[9] J. Tian, Y. Yin, H. Sun, X. Luo, "Magnesium chloride: an efficient ^{13}C NMR relaxation agent for amino acids and some carboxylic acids" *J. Magn. Reson*. **2002**, *159*, 137−144.

[10] G. Wider, L. Dreier, "Measuring protein concentrations by NMR spectroscopy" *J. Am. Chem. Soc*., **2006**, *128*, 2571−2576.

[11] G. A. Barding Jr., R. Salditos, C. K. Larive "Quantitative NMR for bioanalysis and metabolomics" *Anal. Bioanal. Chem.* **2012**, ahead of print

[12] S. K. Bharti, R. Roy, "Quantitative ^{1}H NMR spectroscopy" *Trends Anal. Chem.* **2012**, *35*, 5–26.

6. Result (a) ^{1}H-NMR

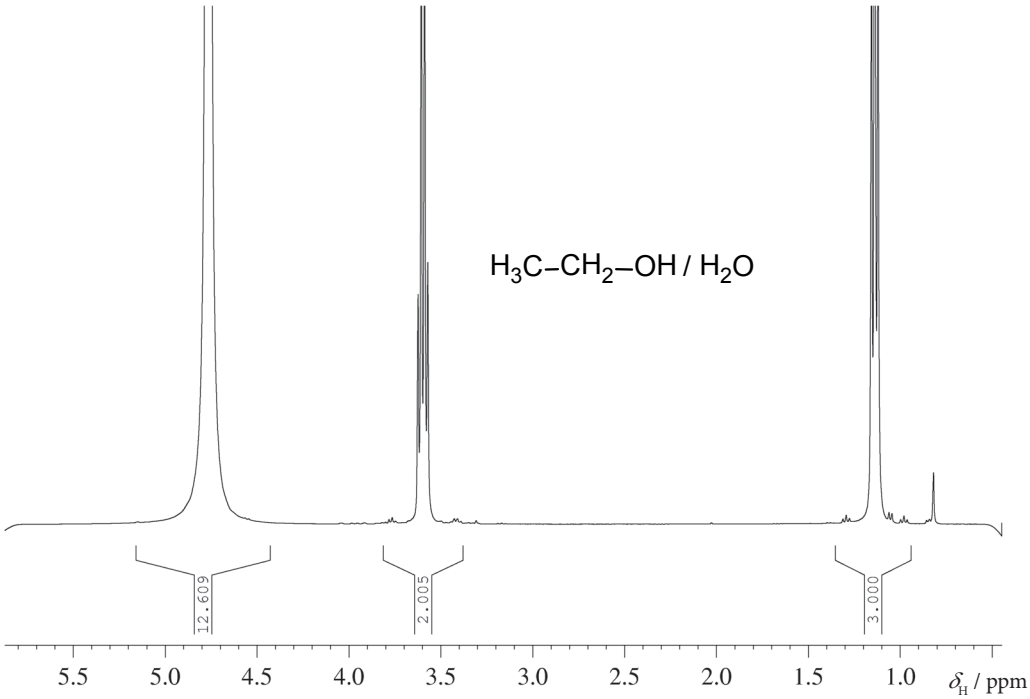

Fig. 6.4-2 Quantitative ^{1}H NMR of a Grappa beverage

The figure shows the ^{1}H NMR spectrum of a Grappa obtained with a DRX-400 spectrometer. The water/alcohol ratio is calculated neglecting the residual protons of the small amount of D_2O.

The methyl group integral is set to 3.0 units; thus, one proton has the integral 1 and this value is subtracted from the water signal to adjust for the OH group of ethanol.

This yields the molar relationship between water and ethanol of 11.609 : 2.0, which transforms into a mass relationship of 208.962 : 92. Hence the mass percentage of this spirit is 30.56 %. For obvious reasons, producers declare only the volume percentage on the label of their bottles. In 100 g of this spirit are 30.56 g ethanol, which is 38.71 mL according to the ethanol density of 0.7893 g/mL. Having measured the density of the spirit in the bottle with a pyknometer to 0.963 g/mL, 100 g will be 103.84 mL and the v/v % is therefore 37.3 %, a value which nicely corresponds to the data of the manufacturer.

(b) ^{13}C-NMR

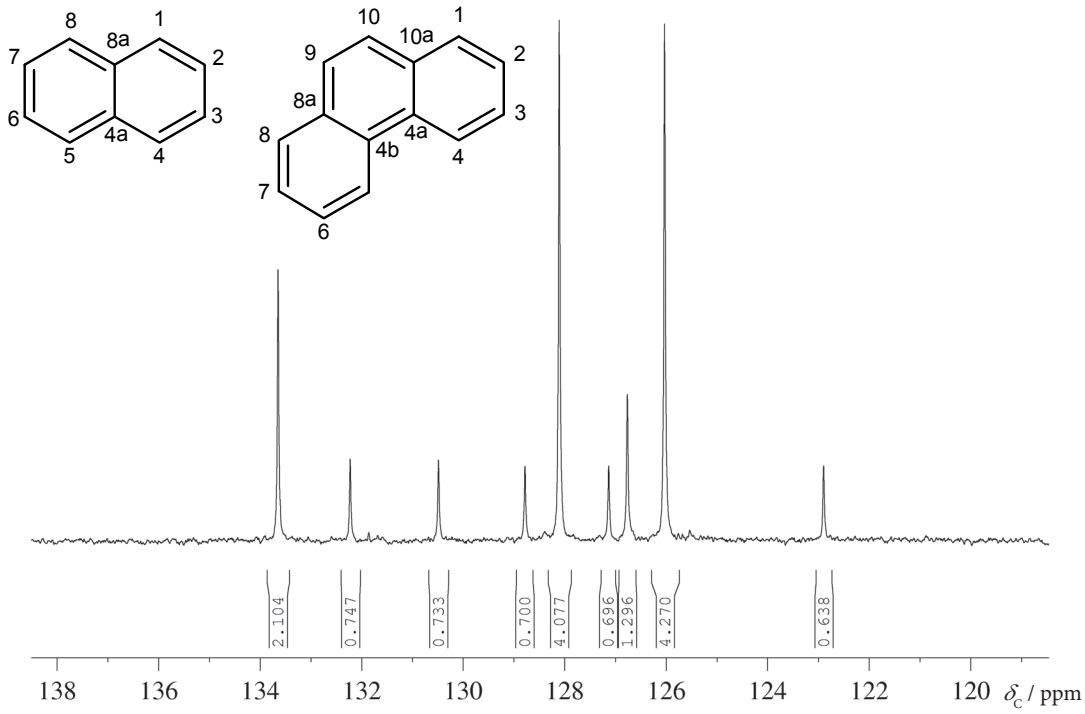

Fig. 6.4-3 Quantitative ^{13}C NMR from a mixture of phenanthrene and naphthaline

The figure shows the aromatic region of the ^{13}C NMR spectrum obtained on a DRX-400 spectrometer. The ratio of the components by weight is calculated as follows:

The three naphthalene signals which are about in the ratio 2 : 4 : 4 average to 1.045 per carbon atom. The six phenanthrene signals in their ratio 2 :2 : 2 : 2 : 4 : 2 average to 0.344 per carbon atom. Multiplication by the respective molecular weights of 128.16 and 178.23 yields a mass ratio of 2.19 : 1, whereas a mass ratio of 2.23 : 1 was weighed in. Thus, the error with less than 2% is quite acceptable.

7. Comments

In the ^{13}C experiment composite pulse decoupling is applied only during the short acquisition time and not during the delay d1. Coupling information that is present after the delay is immediately eliminated by the decoupling field, whereas the populations of the energy levels and hence NOE enhancements require a build-up time in the order of the spin−lattice relaxation times. If the delay d1 is at least 10 times the acquisition time, decoupled spectra without NOE effect can be recorded. To eliminate effects of spin-lattice relaxation, addition of a relaxation agent such as $Cr(acac)_3$ is needed.

Routine ^{13}C NMR spectra are recorded under conditions that maximize sensitivity, such as using the Ernst angle and ^{1}H broad-band decoupling. This results in reduced intensities for signals of quaternary carbon nuclei, which usually have long relaxation times T_1 and smaller NOE

values. The addition of paramagnetic compounds such as $Cr(acac)_3$, $Mn(acac)_2$, $Cu(acac)_2$, or $Gd(acac)_3$ reduces T_1 to less than 1 s for all types of carbon nuclei. Because of the large gyromagnetic ratio of the unpaired electrons, the mechanism of the relaxation is an (electron dipole)−(^{13}C nucleus dipole) interaction. Now, for excitation one can use 90° pulses and higher pulse repetition rates.

The integrals of NMR signals are relative measures of the numbers of resonating nuclei. If one component is present at much lower concentration than another, the percentage error in measurement of the quantity of this minor component could be quite high. For quantitative determinations, deconvolution and curve-fitting methods have been proposed in the literature, especially for cases where peaks are not fully resolved.

8. Questions

A. Why should one not adjust the integral of the methylene group of ethanol to two protons?

B. Calculate the possible error introduced by 0.1 mL D_2O of 99.9 at % enrichment.

C. Addition of $Cr(acac)_3$ usually reduces the signal intensities. Why?

D. Phenanthrene should have 7 distinguishable ^{13}C NMR signals. Why are two peaks overlapping?

9. Own Observations

Experiment 6.5

Determination of Association Constants K_a

1. Purpose

Intermolecular recognition is an expanding field of research in recent bioorganic and biophysical chemistry. "Host–guest chemistry" and "protein–ligand interaction" are only two of many keywords. The association constant K_a as defined in Equation (1) can be reliably determined by NMR, provided that several precautions are taken. In (1) [HG] is the concentration of the host–guest complex and [H] and [G] are the host and guest concentrations in equilibrium.

$$K_a = \frac{[HG]}{[H]} \cdot [G] \qquad (1)$$

When the reaction is fast on the NMR time scale, the observed chemical shift δ_{obs} can be expressed by Equation (2), where x_G and x_{HG} are the molar fractions of the free and complexed species.

$$\delta_{obs} = x_G \cdot \delta_G + x_{HG} \cdot \delta_{HG} \qquad (2)$$

In the case of a 1:1 complex Equations (3) and (4) hold;

$$[G] + [HG] = [G_0] \qquad (3)$$
$$[H] + [HG] = [H_0] \qquad (4)$$

however, only the initial concentrations $[H_0]$ and $[G_0]$ are known. Thus, the problem has to be solved by measuring a concentration dependence of the chemical shifts followed by an iterative computer simulation or a graphical evaluation. In this experiment we show the details of the procedure for a system with a medium K_a value in the region of 10^3 M^{-1}.

2. Variants

Different equations have to be applied in case of 2:1, 1:2 or even more complex stoichiometry, see ref. [5] for these cases.

Fig. 6.5-1 Guests are welcome

Common values

d1: relaxation delay
p1: 90° ^{1}H transmitter pulse

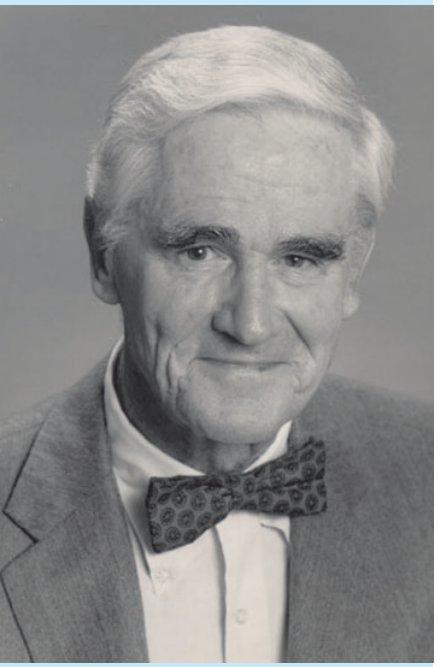

Fig. 6.5-2 Professor Donald J. Cram (1919-2001), Nobel Price 1987 for Host-Guest Chemistry

3. Pulse Scheme and Phase Cycle

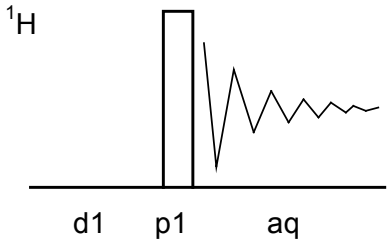

p1: x, x, -x, -x, y, y, -y, -y
aq: x, x, -x, -x, y, y, -y, -y

Scheme 6.5-1

4. Acquisition

Special values used for the spectrum shown:

Sample: Host: β-cyclodextrin hydrate (CD), Guest: 4-*t*-butylpyridine (TBP).
Time requirement: 1.5 h
Spectrometer: Bruker DRX-400 with 5-mm TBI probe

Solvent stock solution

Prepare 20 mL of a 50 mM phosphate-buffered D_2O solvent stock by dissolving 142 mg (1 mmol) Na_2HPO_4. Add 1−3 drops of concentrated H_3PO_4 to adjust the pH to 7.0 using a digital pH meter. *The use of a buffer is absolutely necessary in order not to be deceived by the pH dependence of the chemical shifts*.

10 mM CD stock solution

113.5 mg (0.1 mmol) CD is weighed using an analytical balance and dissolved in 10 mL of the above-described buffered D_2O solution using an analytical volume flask.

10 mM TBP stock solution

7.39 µl TBP (6.76 mg, 0.05 mmol) were syringed into an analytical volume flask containing 5 mL of the above-described buffered D_2O solution. The CD and TBP stock solutions should have equal concentrations as closely as possible. This can be checked by NMR, taking equal amounts and comparing the integrals.

Reference System

Since the different guest and host concentrations may influence the reference signal, prepare a sealed melting-point capillary with acetone and insert this into the sample tubes. On modern digital instruments you may instead use the spectrometer reference value by assuming that the lock signal is not shifted in the different samples.

Sample preparation

Prepare 9 NMR tubes according to the following table. The principle of continuous variation (*Job's method* [1]) is used so that in all samples the condition (5) holds:

(5) $$[H] + [G] = \text{constant}$$

Sample	V_{CD} [µL]	V_{TBP} [µL]	x_{CD}
1	0	600	0
2	75	525	0.125
3	150	450	0.25
4	225	375	0.375
5	300	300	0.5
6	375	225	0.675
7	450	150	0.75
8	525	75	0.875
9	600	0	1

Table 6.5-1 Composition of the measured samples

After all measurements, check whether the condition of constant pH is satisfied.

Load standard ^{1}H NMR acquisition parameters, set and control the temperature to 298 K, and let each sample equilibrate for 10 min. Set the spectral width to 10 ppm, use d1 = 2 s, a 30° excitation pulse, and an acquisition time of 4 s and 8 transients.

5. Processing

Use standard 1D processing for ^{1}H NMR spectra.

6. Result

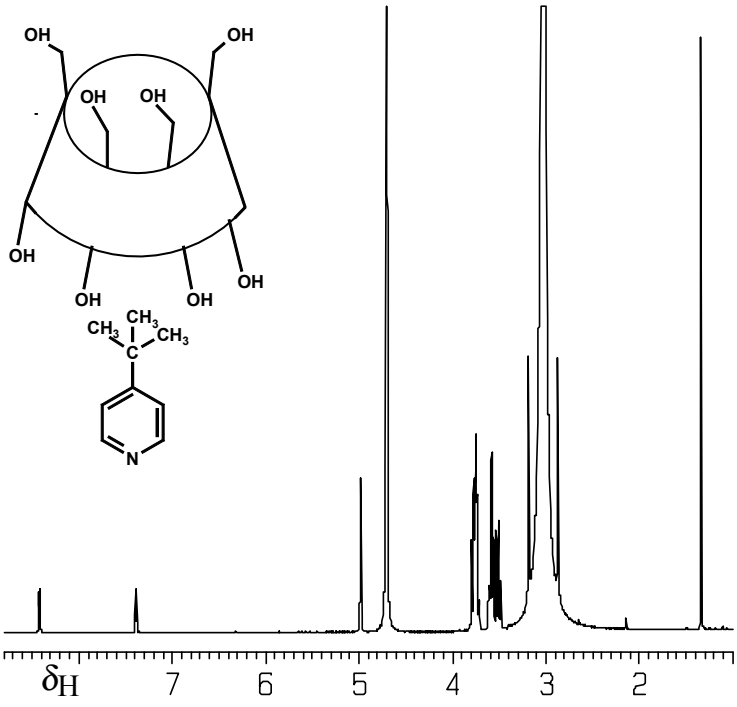

Fig. 6.5-3 ^{1}H NMR spectrum of 4-*t*-butylpyridine in the presence of β-cyclodextrin hydrate

It must be noted, however, that higher-order interactions demand a particularly precise geometrical fit between catalyst and substrate due to the rapid decline of such forces with increasing intermolecular separation r. A close fit is especially difficult to achieve in the stabilization of short-lived transition states. Nature alone has succeeded in meeting this challenge through millions of years of evolution, taking advantage of cooperative interactions of all the various mechanisms. In particular, electrostatic interactions with their extremely long-range character are especially promising in the development of synthetic enzyme-analogous systems, which should also be suitable for more than just one specific substrate.

Taken from ref. [2]

Fig. 6.5-3 shows the spectrum obtained from sample #5 on a DRX-400 spectrometer. Note that the huge signal of the external acetone is not at the usual shift position due to the susceptibility difference. For the evaluation of this series of spectra, either the signals of *t*-butylpyridine or the signal of the protons 3 and 5 of the cyclodextrin may be used.

First, the stoichiometry has to be checked, and this is done with a *Job's* plot as shown in Graph **a**, where the molar fraction x_G of the guest times its chemical shift difference $\Delta\delta_G$ from the pure guest ($x_G \cdot \Delta\delta_G$) for the *t*-butyl group is plotted versus x_G. A symmetrical curve with a maximum at $x_G = 0.5$ indicates a 1:1 complex.

Graph a

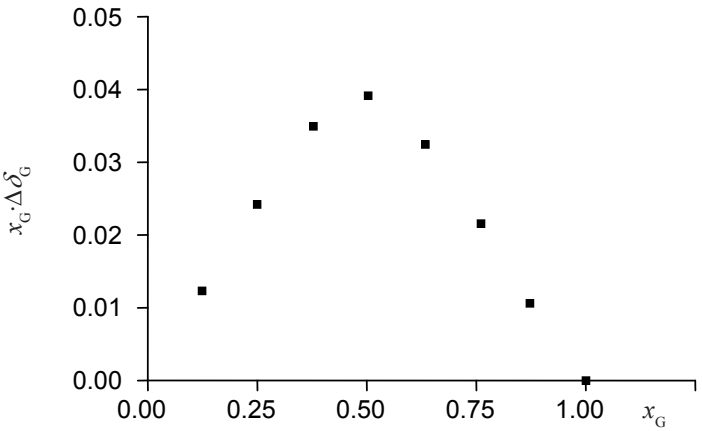

Fig. 6.5-4 *Job*'s plot

Next, one plots the observed chemical shifts (here shown in Graph **b** for the pyridyl protons next to the *t*-butyl group) versus the guest concentration. The sigmoid curve has to be fitted using a computer program to obtain the unknowns [HG] and δ_{HG}. From these an association constant $K_a = 3826\ M^{-1}$ was calculated.

Graph b

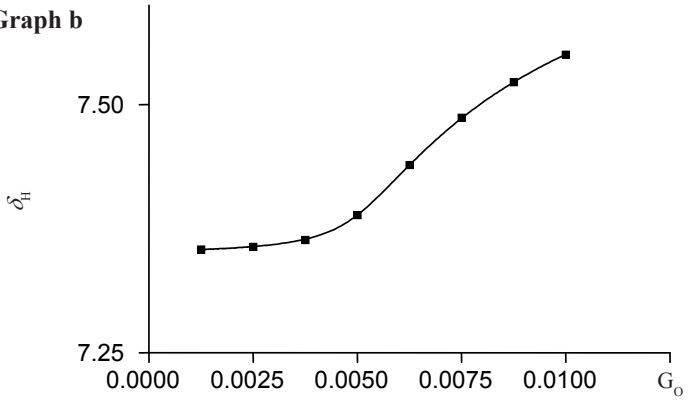

Fig. 6.5-5 Chemical shifts of pyridyl protons vs guest concentration

7. Comments

Besides the iterative computer fitting method there are many other graphical methods available to determine K_a. However, all these require some assumptions or the neglect of approximations and therefore have to be used within restricted concentration ranges of guest and host molecules. Further complications arise if K_a is very small (< 10 M^{-1}) or very large (> 10^5 M^{-1}), and in these cases different methods have to be employed. Association constants can also be determined by diffusion measurements.

From an NMR point of view the most important considerations are the correct choice of a system with large enough chemical shift differences, control of temperature, pH, and correct external referencing. Using more points would increase the reliability of the K_a value.

The equation used for fitting the data had the form

$$Y = \left(1 - \frac{B}{Y}\right) * \delta_G + \left(\frac{B}{X}\right) * \delta_{HG}$$

with

$$B = F - \mathrm{SQRT}(F**2 - X*T + X**2)$$

and

$$F = 0.5 * \left(T + \frac{1}{K_a}\right)$$

Y and X are the observed chemical shifts and the G_o concentration of every sample, δ_G is the chemical shift of the pure guest in sample tube #1, and T is the total concentration.

[1] P. Job "Formation and stability of inorganic complexes in solution", *Annali di Chimica Applicata* **1928**, *9*, 113–203.

[2] H. J. Schneider "Mechanisms of molecular recognition : Investigations of organic host-guest complexes" *Angew. Chem. Int. Ed. Engl*. **1991**, *30*, 1417−1436.

[3] L. Fielding "Determination of Association constants (K_a) from solution NMR data" *Tetrahedron* **2000**, *56*, 6151−6170.

[4] A. Pastor, E. Martínez-Viviente "NMR spectroscopy in coordination supramolecular chemistry: A unique and powerful methodology" *Coord. Chem. Rev*. **2008**, *252*, 2314–2345.

[5] P. Thordarson "Determining association constants from titration experiments in supramolecular chemistry" *Chem. Soc. Rev*. **2011**, *40*, 1305–1323.

8. Questions

A. What other spectroscopic techniques besides NMR are available and often used to measure these association constants?

B. If instead of a chemical shift titration NMR diffusion measurements are performed, how would you judge their accuracy versus the chemical shift titration?

9. Own Observations

Experiment 6.6

STD NMR

1. Purpose

Detection of a specific binding state between a protein and a ligand is an important task in the development of pharmaceuticals and is mandatory for the understanding of biochemical regulation processes. There are many attempts to study protein−ligand interactions by NMR, which include techniques like transferred NOE measurements or DOSY-related methods. Recently, an elegant and very simple experiment called STD (**S**aturation **T**ransfer **D**ifference) was introduced, which relies on the spin diffusion in a protein of high molecular weight (typically > 50000 daltons). If such a protein is irradiated by selective pulses, the magnetization can diffuse towards a ligand residing in a binding pocket for a certain time. This polarization is taken back into the free solution by the ligand and can be detected there. If one records in addition an off-resonance control spectrum, the difference spectrum reveals only the signals of a real ligand and thus confirms the binding ability of this ligand, even in the presence of other small molecules that do not bind. From the many variations known, we show here a STD technique which proved in our hands to be most artifact free.

2. Variants

There are many variants of the basic technique aiming to show no difference artifacts or artifacts of spill-over by left-over magnetization between different scans. Also, the STD experiment was combined with HR-MAS or several 2D techniques like TOCSY and HSQC. More recently, detection by heteronuclei as ^{19}F [8] or ^{13}C [9] was reported.

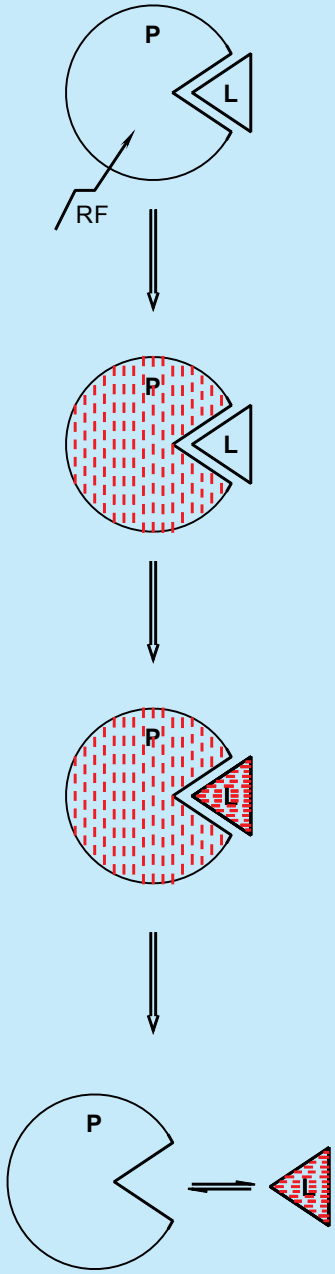

Fig. 6.6-1 Protein−ligand interaction

3. Pulse Scheme and Phase Cycle

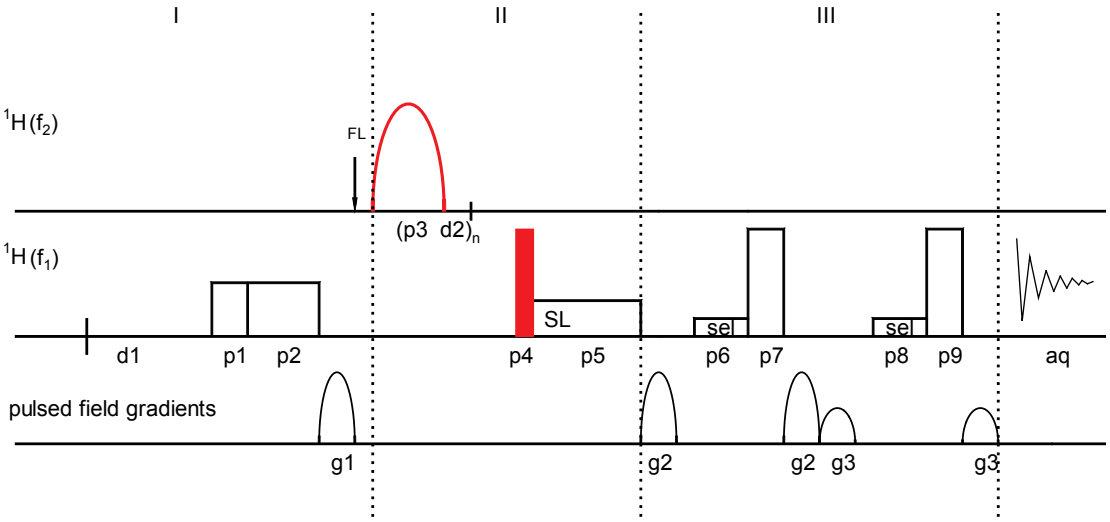

p1, p3: x p2: y p4: x, x, -x, -x, y, y, -y, -y p5: $(y)_4$, $(-y)_4$, $(-x)_4$, $(x)_4$ p6, p8: x, x, -x, -x, y, y, -y, -y

p7, p9: -x, -x, -y, -y, x, x, y, y aq: x, x, -x, -x, y, y, -y, -y

Scheme 6.6-1

Common values:

d1: relaxation delay
d2: interpulse delay
p1, p2, p5: spin lock pulses
p3, p6, p8: selective pulses of different shape and frequency
p4: 90° 1H transmitter pulse
p7, p9: 180° transmitter pulses
n: loop counter determines total length of saturation pulse train (p3 d2)

As can be seen from the diagram, the pulse sequence consists of three principal sections. In the first part **I** any left-over magnetization from previous scans is destroyed by the two orthogonal spin lock pulses p1 and p2 and an additional *z*-gradient g1. The FL-labeled arrow indicates the switching point between on-resonance and off-resonance irradiation. In part **II** the selective irradiation of the protein by the "*n*-fold" pulse train (p3, d2)*n* is followed by the excitation pulse p4. A spin lock pulse p5 will remove the resonances of the of the protein due to their short T_2. The final part **III** is a DPFGSE sequence to suppress the water resonance and is composed of two selective rectangular 180° pulses p6 and p8 on the water and two hard 180° pulses p7 and p9, enclosed by two pairs of gradient pulses g2 and g3. The sequence will be carried out in a pseudo 2D data set and in a interleaved mode, e.g., 128 on-resonance and 128 off-resonance recordings are cycled.

4. Acquisition

Special values used for the spectrum shown:

Sample: Prepare a 25 mM phosphate buffer solution from KH_2PO_4 and Na_2HPO_4 in D_2O. Dissolve in this buffer HSA (Human serum albumin) to obtain a 75 µM solution and add *L*-tryptophane for a final concentration of 4 mM.

The probe-head should be tuned to the sample. Set and control the temperature to 300 K. Adjust the transmitter offset to the residual water signal.

Time requirement: 0.5 h for one loop, 6 loops recorded

Spectrometer: Bruker Avance-700 with cryo probe

td: 32K
sw: 12 ppm
aq: 2 s
o1: on resonance of H_2O signal
p1: 2.5 ms, 8 dB
p2: 5 ms, 8 dB
p3: 50 ms, Gaussian shape, 60 dB, offset switched from 0.8 ppm to 40 ppm
p4: 10.5 µs, –5 dB
p5: 30 ms, 8 dB
p6, p8: 2.2 ms, rectangular shape, 36 dB, offset on water resonance
p7, p9: 21 µs, –5 dB
d1: 3 s
d2: 1 ms, delay within repetition loop for the selective pulses
n: set *n* to 40 which yields a total irradiation time of 2.04 s
fl: provide a frequency list, which switches the selective pulse between 0.8 ppm and 40 ppm
g1: 3 ms, 40 % (100 % ≈ 0.56 T/m)
g2: 1 ms, 70 %
g3: 1 ms, 40 %
ns: 128

5. Processing

The two spectra with on-resonance and off-resonance irradiation will end up as rows 1 and 2 of a pseudo 2D file. Transform the 2D file with phase- and baseline correction. Extract the two rows and form the difference.

[1] M. Mayer, B. Meyer, "Characterization of ligand binding by saturation transfer difference NMR spectroscopy" *Angew. Chem. Int. Ed.* **1999**, *38*, 1784–1788.

[2] J. Klein, R. Meinecke, M. Mayer, B. Meyer, "Detecting binding affinity to immobilized receptor proteins in compound libraries by HR-MAS STD NMR" *J. Am. Chem. Soc.* **1999**, *121*, 5336–5337.

[3] M. Mayer, B. Meyer, "Group epitope mapping by saturation transfer difference NMR to identify segments of a ligand in direct contact with a protein receptor" *J. Am. Chem. Soc.* **2001**, *123*, 6108–6117.

[4] B. Meyer, T. Peters, "NMR spectroscopy techniques for screening and identifyng ligand binding to protein receptors"*Angew. Chem. Int. Ed.* **2003**, *42*, 864–890.

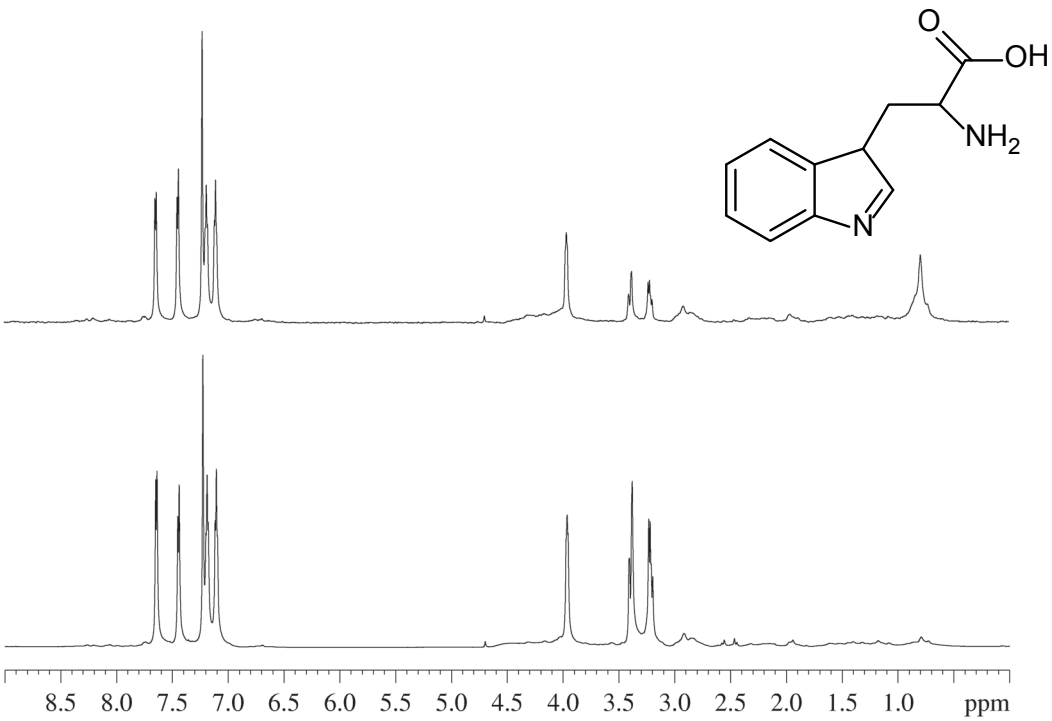

Fig. 6.6-2 below − reference spectrum, above − STD spectrum

[5] N. Rama Krishna, V. Jayalakshmi "Quantitative analysis of STD-NMR spectra of reversibly forming ligand–receptor complexes" *Top. Curr. Chem*. **2008**, *273*, 15–54.

[6] C. Rademacher, T. Peters "Molecular recognition of ligands by native viruses and virus-like particles as studied by NMR experiments" *Top. Curr. Chem*. **2008**, *273*, 183–202.

[7] C. Ludwig, U. L. Guenther "Ligand based NMR methods for drug discovery" *Frontiers in Bioscience* **2009**, *14*, 4565−4574.

[8] T. Diercks, J. P. Ribeiro, F. J. Cañada, S. André. J. J Jiménez-Barbero, H.-J. Gabius "Fluorinated carbohydrates as lectin ligands: Versatile sensors in ^{19}F-detected saturation transfer difference NMR spectroscopy" *Chem. Eur. J*. **2009**, *15*, 5666 –5668.

[9] C. Räuber, S. Berger "^{13}C-NMR detection of STD spectra" *Magn. Reson. Chem*. **2010**, *48*, 91–93.

6. Result

In the lower trace the off-resonance spectrum is shown. The water signal is fully, and the protein resonances are partly suppressed. As required, the aromatic and side-chain resonances of tryptophan have about the same integrals. In the upper trace the STD spectrum is shown, indicating that the saturation transfer from the protein mainly affects the aromatic signals of tryptophan, because these are fully present in the difference spectrum.

7. Comments

The selective pulses are applied in a loop with n = 40. For every 128 scans the frequency of the pre-irradiation is changed from 0.8 to +40 ppm (interleave mode). The band-width of the 50 ms Gaussian pulses is approximately 20 Hz. This results in a narrow-band irradiation of the protein for the first 128 scans and, as a control, in no irradiation for the next 128 scans. The two spectra are stored separately.

By careful titration of the protein with a selected ligand and changing the offset of the irradiation point, more detailed investigations are possible, e.g., determination of the binding constant or epitope mapping, i.e. recognition of the binding pocket.

8. Questions

A. What is the best control to detect whether an STD effect is true?

B. If the ligand investigated has methyl groups or similar, the irradiation of the protein at 0.8 ppm becomes problematic. What do you suggest?

C. What will be the influence of the length of the irradiation time?

9. Own Observations

Experiment 6.7

A Kinetic Experiment

1. Purpose

NMR is one of the best methods to follow chemical reactions, not only in a qualitative but also in a quantitative way, and to extract kinetic parameters. This is due to the fact that temperatures can be controlled in a relatively wide range. Modern spectrometers have enough sensitivity to follow chemical reactions even in dilute solutions, and different nuclei such as ^{1}H, ^{13}C, ^{19}F, or ^{31}P can be chosen. The starting point of a kinetic NMR experiment can be reasonably well defined. Here we show a simple enzymatic biochemical reaction followed by 1D ^{1}H NMR. α-Lactose is cleaved by α-lactase to produce galactose and glucose. The anomeric proton 1' of the galactose unit of α-lactose is monitored.

2. Variants

In addition to the simple time-dependent measurement shown here, more advanced kinetic methods such as the EXSY pulse sequence or relaxation techniques are available. A special method called Rapid Injection NMR [8] extends the time scale to rather short values. Also stopped flow or concentration-jumps in NMR have been employed to obtain kinetic data [7, 10]

3. Pulse Scheme and Phase Cycle

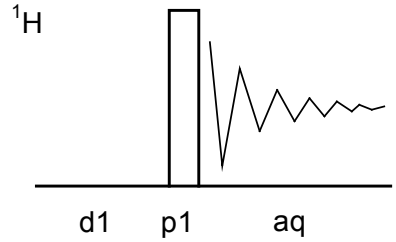

p1: x, x, -x, -x, y, y, -y, -y

aq: x, x, -x, -x, y, y, -y, -y

Scheme 6.7-1

Common values:

p1: 90° ^{1}H transmitter pulse
d1: relaxation delay

4. Acquisition

Special values used for the spectrum shown:

Sample: 40 mM α-lactose in D_2O with 20 mM deuterated tris-(hydroxymethyl)aminomethane buffer, 1 mM mercaptoethanol as antioxidant, and DSS as reference.The temperature was kept at 293 K. After instrument set-up the reaction was started by addition of 6 units of lactase [E.*coli*; units with respect to hydrolysis of o-nitrophenyl β-D-galactoside].

Time requirement: 4 h

Spectrometer: Bruker Avance-700 with cryo probe

td: 25K
sw: 7 ppm
aq: 2.5 s
o1: middle of ^{1}H NMR spectrum
p1: 8 µs at −5 dB
d1: 32 s
ns = 1

5. Processing

Use zero filling to si = 16 K and exponential weighting with lb = 1 Hz, phase correction and referencing to internal DSS.

6. Result

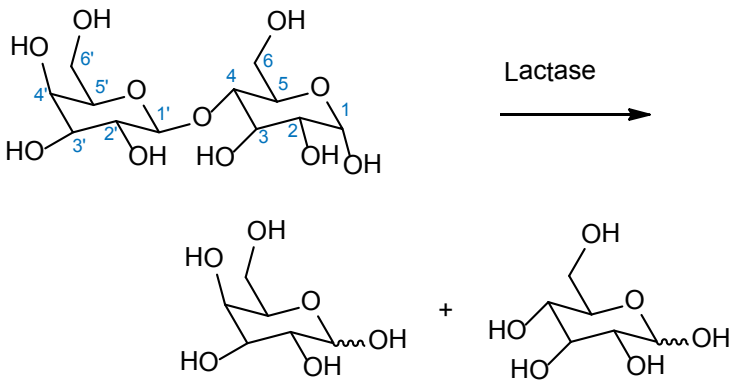

Scheme 6.7-2

Shown are the starting spectrum and the end spectrum obtained at an Avance-700 instrument equipped with a cryo probe. In the former, α-lactose displays two anomeric protons, one from the glucose (H-1) and one from the galactose unit (H-1'). A tiny amount of the β-glucose unit can already be seen. The decay curve monitors the disappearance of the anomeric proton of the galactose unit H-1'. In the end spectrum we see four anomeric signals of the two subunits of lactose which has been cleaved by the enzyme. Finally a Michaelis−Menten plot is given, from which the Michaelis−Menten constant can be extracted.

[1] R. Strom, D. Gandini Attardis, S. Forsén, P. Turini, F. Celada, E. Antonini "The activation of P-galactosidase by divalent and monovalent cations. Transient- and steady-state studies" *Eur. J. Biochem*. **1971**, *23*, 118−124.

[2] S.-T. Yang, M. R. Okos "A new graphical method for determining parameters in Michaelis-Menten-type kinetics for enzymatic lactose hydrolysis" *Biotech. Bioeng*. **1989**, *34*, 763−773.

[3] E. Jurado, F. Camacho, G. Luzón, J. M. Vicaria "Kinetic models of activity for β-galactosidases: influence of pH, ionic concentration and temperature" *Enzyme and Microbial Technology* **2004**, *34*, 33–40.

[4] M. Abdollahi, M. Sharifpour "A new simple procedure to calculate monomer reactivity ratios by using on-line ^{1}H NMR kinetic experiments: Copolymerization system with greater difference between the monomer reactivity ratios" *Polymer* **2007** *48*, 25−30.

[5] R. Johnsson, D. Olsson, U. Ellervik "Reductive openings of acetals: Explanation of regioselectivity in borane reductions by mechanistic studies" *J. Org. Chem*. **2008**, *73*, 5226–5232.

[6] E. Simon, K. Cook, M. R. Pritchard, W. Stripe, M. Bruch, K. Bendinskas "Glycosidation of methanol with ribose: An interdisciplinary undergraduate laboratory experiment" *J. Chem. Educ*. **2010**, *87*, 739−741.

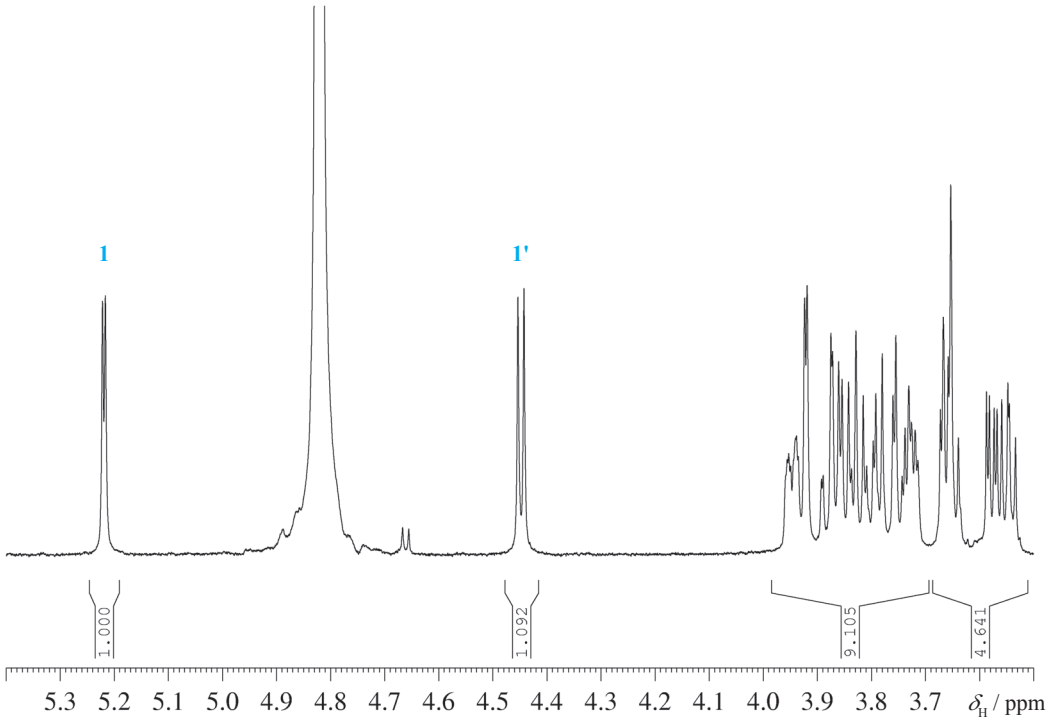

Fig. 6.7-1 Starting ^{1}H NMR spectrum of commercial α-lactose (without buffer)

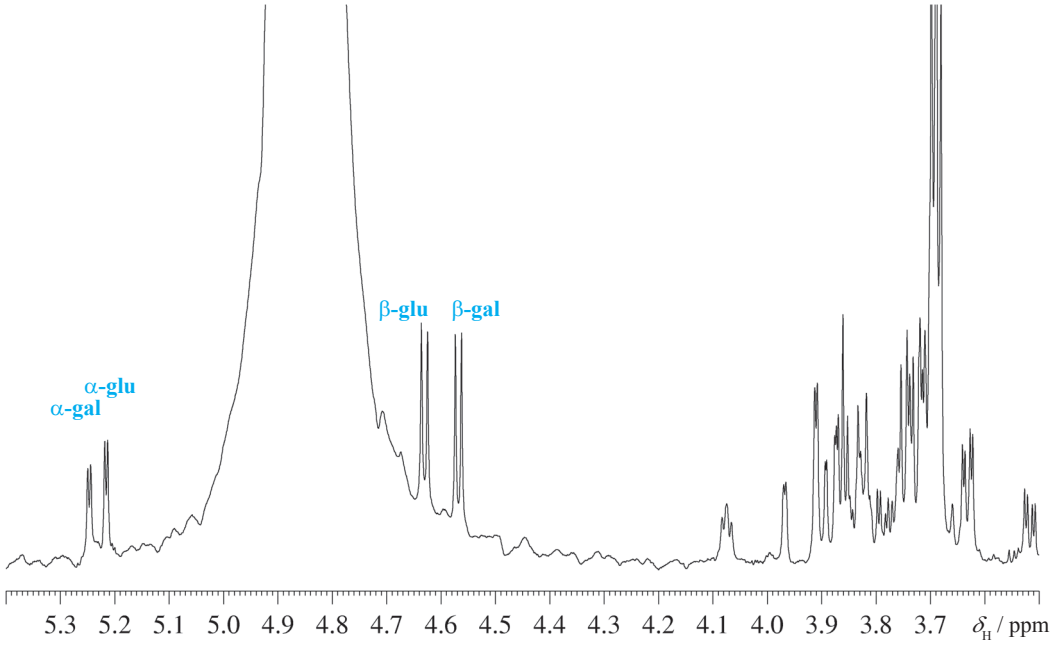

Fig. 6.7-2 ^{1}H NMR spectrum at the end of the reaction

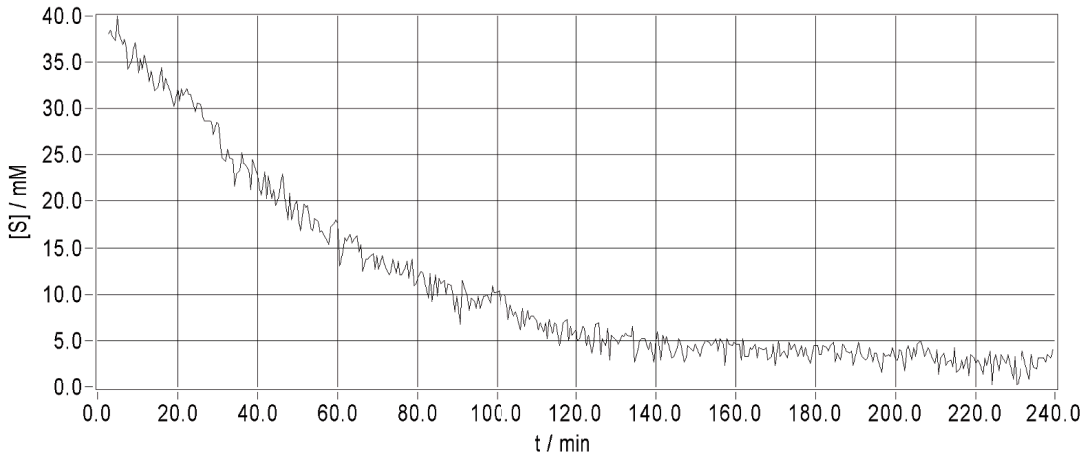

Fig. 6.7-3 The exponential decay of the anomeric signal at $\delta_H = 4.45$ of lactose

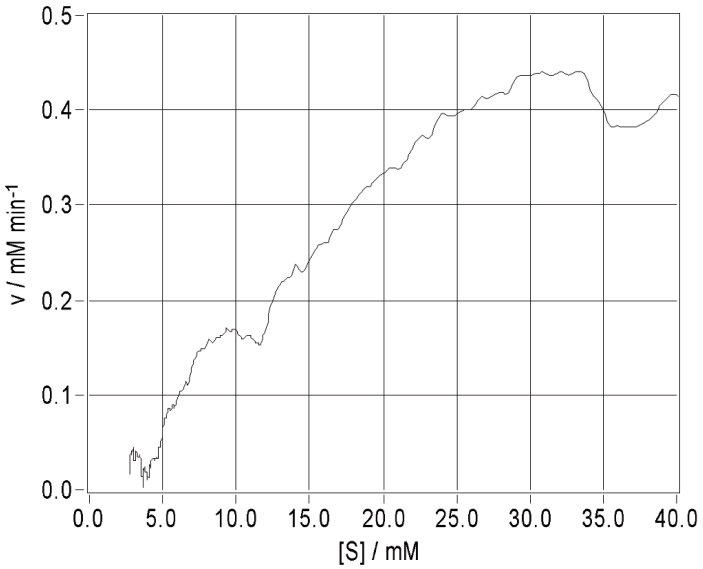

Fig. 6.7-4 Michaelis−Menten plot of the reaction rate vs the substrate concentration

7. Comments

The reaction discussed here is the basis for the production of lactose-free milk or other food to help people with lactose intolerance. Addition of the enzyme lactase cleaves lactose into glucose and galactose; the milk becomes a little sweeter, but causes no harm to people with lactose intolerance.

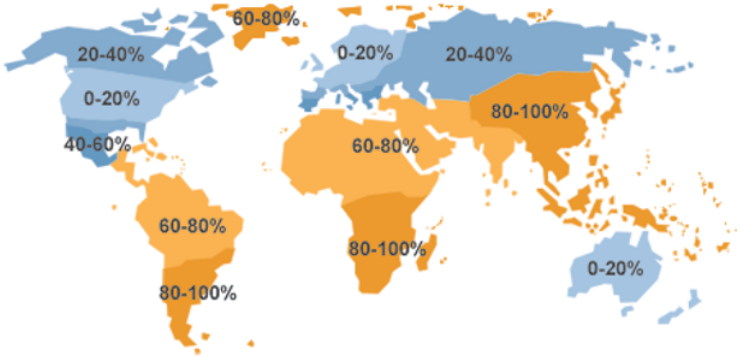

Fig. 6.7-5 World map of lactose intolerance

Fig. 6.7-6 Dietary yogurt

Fig. 6.7-7 Dietary chocolate

[7] M. D. Christianson, E. H. P. Tan, C. R. Landis "Stopped-flow NMR: Determining the kinetics of [*rac*-(C_2H_4(1-indenyl)$_2$)ZrMe][MeB(C_6F_5)$_3$]-catalyzed polymerization of 1-hexene by direct observation" *J. Am. Chem. Soc*. **2010**, *132*, 11461–11463.

[8] S. E. Denmark, B. J. Williams, B. M. Eklov, S. M. Pham, G. L. Beutner "Design, validation, and implementation of a rapid-injection NMR system" *J. Org. Chem*. **2010**, *75*, 5558–5572.

[10] C. R. Pudney, D. J. Heyes, B. Khara, S. Hay, S. E. J. Rigby, N. S. Scrutton "Kinetic and spectroscopic probes of motions and catalysis in the cytochrome P450 reductase family of enzymes" *FEBS Journal* **2012**, *279*, 1534–1544.

[11] C. Kunz, G. Jahreis, R. Günther, S. Berger, G. Fischer, H.-J. Hofmann "Influence of lithium cations on prolyl peptide bonds" *J. Pept. Sci*. **2012**, *18*, 400–404.

[12] R. H. Evjenth, A. K. Brenner, P. R. Thompson, T. Arnesen, N. Å. Frøystein, J. R. Lillehaug "Human protein N-terminal acetyltransferase hNaa50p (hNAT5/hSAN) follows ordered sequential catalytic mechanism. Combined kinetic and NMR study" *J. Biol Chem*. **2012**, *287*, 10081−10088.

8. Questions

A. Enzyme kinetics are described with the Michaelis−Menten equation. Give the equation and the boundary conditions.

B. The repetition time of such kinetic experiments must be at least five times T_1. Why?

C. Why is it advantegeous to run such experiments in a pseudo-2D file?

9. Own Observations

Chapter 7

An Excursion to the Solid State and to Structural Biology

Both fields, **solid-state NMR** and **NMR in structural biology**, have made tremendous progress in the last 10 years. It would be impossible to cover the main developments in this book in an adequate way. Both fields would require their own volumes to enable a reader to perform the most important experiments. Instead, we will give only four examples to show the possibilities and to raise interest for those who possess the necessary equipment.

7.1 The CP/MAS Experiment
Cross-**P**olarization/**M**agic **A**ngle **S**pinning 211
7.2 High-Resolution Magic Angle Spinning 215
7.3 HN-HSQC 219
7.4 HNCA 225

Especially the NMR experiments in structural biology gain tremendously from the sensitivity increase provided since the last decade by cryo probes such as the one pictured below. With these probes one can measure dilute protein samples in and below the one millimolar concentration. The price to pay is the large financial investment and the maintenance costs.

Fig. 7.0-1 Cryo Probe at a 700 MHz spectrometer

Experiment 7.1

The CP/MAS Experiment

1. Purpose

The CP/MAS (**C**ross-**P**olarization/**M**agic-**A**ngle **S**pinning) method provides high-resolution NMR spectra of materials in the solid state and is mostly performed on ^{13}C (or other spin-½ nuclei) with cross polarization from ^{1}H. The signal intensity is thereby increased according to the ratio of the gyromagnetic ratios, and the pulse repetition time is governed by the proton relaxation. Magic-angle spinning narrows the lines by folding first-order quadrupolar couplings, chemical shift anisotropies, and dipolar couplings into spinning sidebands. High-power proton decoupling during acquisition finally provides ^{13}C NMR spectra nearly as well resolved as solution spectra. Originally the cross-polarization method was called *proton-enhanced nuclear-induction spectroscopy* [1]; however, the corresponding acronym was not accepted in the literature. In the experiment described here we demonstrate the CP/MAS technique using a sample of glycine and show the effects of different spinning rates.

Fig. 7.1-1 John S. Waugh *1929

2. Variants

There are many variants of the basic CP/MAS technique. First the question of the spin lock is addressed and one can decide to use a ramped spin lock, by which the spin lock power is changed during the spin lock time. Then there exist different decoupling schemes to provide most efficient decoupling, such as the TPPM (*two pulse phase modulation*) or the SPINAL sequences. The CP/MAS pulse sequence can be modified to introduce sideband suppression (TOSS, SELTICS) or combined with an editing scheme (NQS).

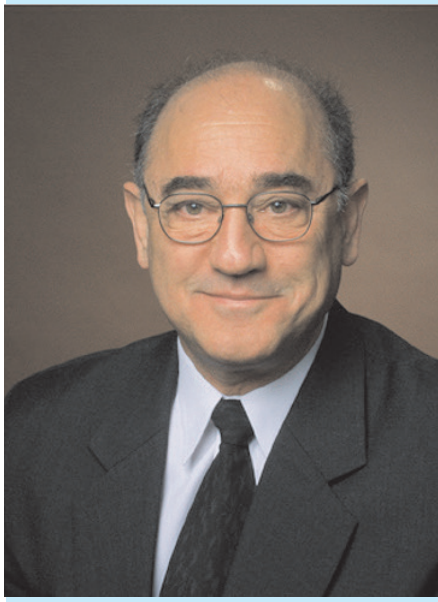

Fig. 7.1-2 Alex Pines (*1945)

3. Pulse Scheme and Phase Cycle

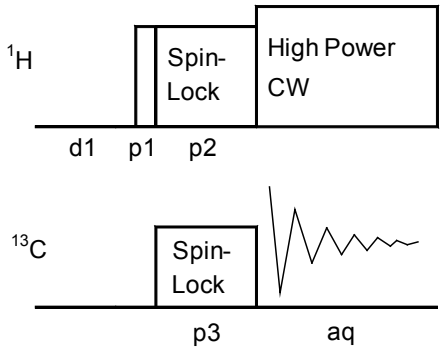

p1: y, y, -y, -y
p2: x
p3: $(x)_4$, $(y)_4$, $(-x)_4$, $(-y)_4$
aq: $(x)_2$, $(-x)_2$, $(y)_2$, $(-y)_2$, $(-x)_2$, $(x)_2$, $(-y)_2$, $(y)_2$

Scheme 7.1-1

4. Acquisition

Special values used for the spectrum shown:

Time requirement: 30 min
Sample: Fill a solid-state rotor with finely powdered glycine.

Common values

d1: relaxation delay
p1: 90° ^{1}H transmitter pulse
p2: ^{1}H spin lock decoupler pulse (Hartmann–Hahn matched)
p3: ^{13}C spin lock transmitter pulse (Hartmann–Hahn matched)

[1] A. Pines, M. G. Gibby, J. S. Waugh, "Proton enhanced nuclear induction spectroscopy. A method for high resolution NMR of dilute spins in solids" *J. Chem. Phys*. **1972**, *56*, 1776–1777; ibid. **1973**, *59*, 569–590.

[2] J. Schaefer, E. O. Stejskal, "Carbon-13 nuclear magnetic resonance of polymers spinning at the magic angle" *J. Am. Chem. Soc*. **1976**, *98*, 1031–1032.

[3] E. O. Stejskal, J. Schaefer, R. A. McKay, "High-resolution, slow-spinning magic-angle carbon-13 NMR" *J. Magn. Reson*. **1977**, *25*, 569–573.

[4] J. Herzfeld, A. E. Berger, "Sideband intensities in NMR spectra of samples spinning at the magic angle" *J. Chem. Phys*. **1980**, *73*, 6021–6030.

[5] R. E. Taylor "Setting up ^{13}C CP/MAS experiments" *Concepts Magn. Reson*. **2004**, *22A*, 37–49.

[6] I. Wawer "Solid-state measurements of drugs and drug formulations" *NMR Spectrosc. Pharm. Anal*. (Ed. U. Holzgrabe, I. Wawer, B. Diehl), **2008**, 201–231.

[7] J. Blümel "Linkers and catalysts immobilized on oxide supports: New insights by solid-state NMR spectroscopy" *Coord. Chem. Rev*. **2008**, *252*, 2410–2423.

[8] K. K. Kumashiro "Solid-state NMR studies of elastin and elastin peptides" *Modern Magnetic Resonance, G. A. Webb (ed.)*, **2008**, 93–99.

[9] M. J. Potrzebowski, S. Kaźmierski, H. Kassassir, B. Miksa "Phosphorus-31 NMR spectroscopy of condensed matter" *Ann. Rep. NMR Spectrosc*. **2010**, *70*, 35–114.

[10] H. Knicker "Solid state CPMAS ^{13}C and ^{15}N NMR spectroscopy in organic geochemistry and how spin dynamics can either aggravate or improve spectra interpretation" *Organic Geochemistry* **2011**, *42*, 867–890.

The probe must have been adjusted to be at the magic angle (which is usually done with a KBr sample) and the Hartmann–Hahn condition

$$\gamma_1 B_1 = \gamma_2 B_2$$

must have been established in order to have the maximum polarization transfer in the spin-lock period.

td: 4K
sw: 500 ppm
aq: 41 ms
o1: middle of ^{13}C NMR spectrum
o2: middle of ^{1}H NMR spectrum
d1: 3 s
p1: 90° ^{1}H decoupler pulse 5 µs at −6 dB
p2: 5 ms ^{1}H spin lock
p3: 5 ms ^{13}C spin lock
decoupler attenuation for cross-polarization
decoupler attenuation for high-power cw decoupling, damping typically 2 dB less than for cross-polarization
spinning rate ν_R **a**: 5000 Hz, **b**: 4000 Hz, **c**: 3000 Hz, **d**: 2000 Hz, **e**: 1000 Hz, **f**: 500 Hz, **g**: 0 Hz
ns: 16 in Experiments Fig. 7.1-4 **a** to **c**, 64 in **d** to **f**, and 256 in **g**

5. Processing

Use standard 1D processing for ^{13}C NMR with zero-filling to 4K and different exponential multiplication corresponding to the line width, ranging from lb = 25 Hz in **a** to lb = 100 Hz in **g**.

6. Result

The figure shows the spectra of glycine obtained using a multinuclear solid-state probe with a 7 mm rotor on an AM-400 spectrometer with wide-bore magnet. As can be seen from the figure, signals of nuclei with large chemical shift anisotropy such as the signal from the carboxyl ^{13}C nucleus, generate spinning sidebands; at low spinning speed the signal of the methylene ^{13}C nucleus also yields sidebands. The spinning rate can be measured from the distance of the spinning sidebands, and the sideband pattern can be analyzed to obtain the chemical shift tensor [4].

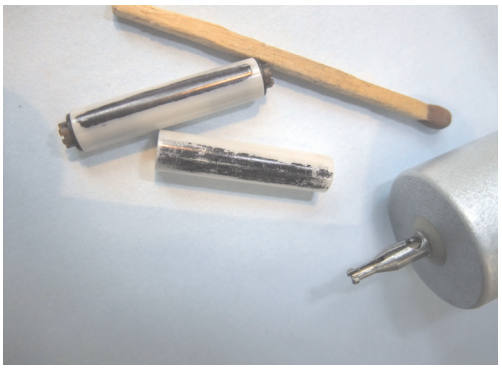

a

Fig. 7.1-3 5-mm-DOTY ceramic rotors XC5 with and without caps and the DOTY cap extraction tool

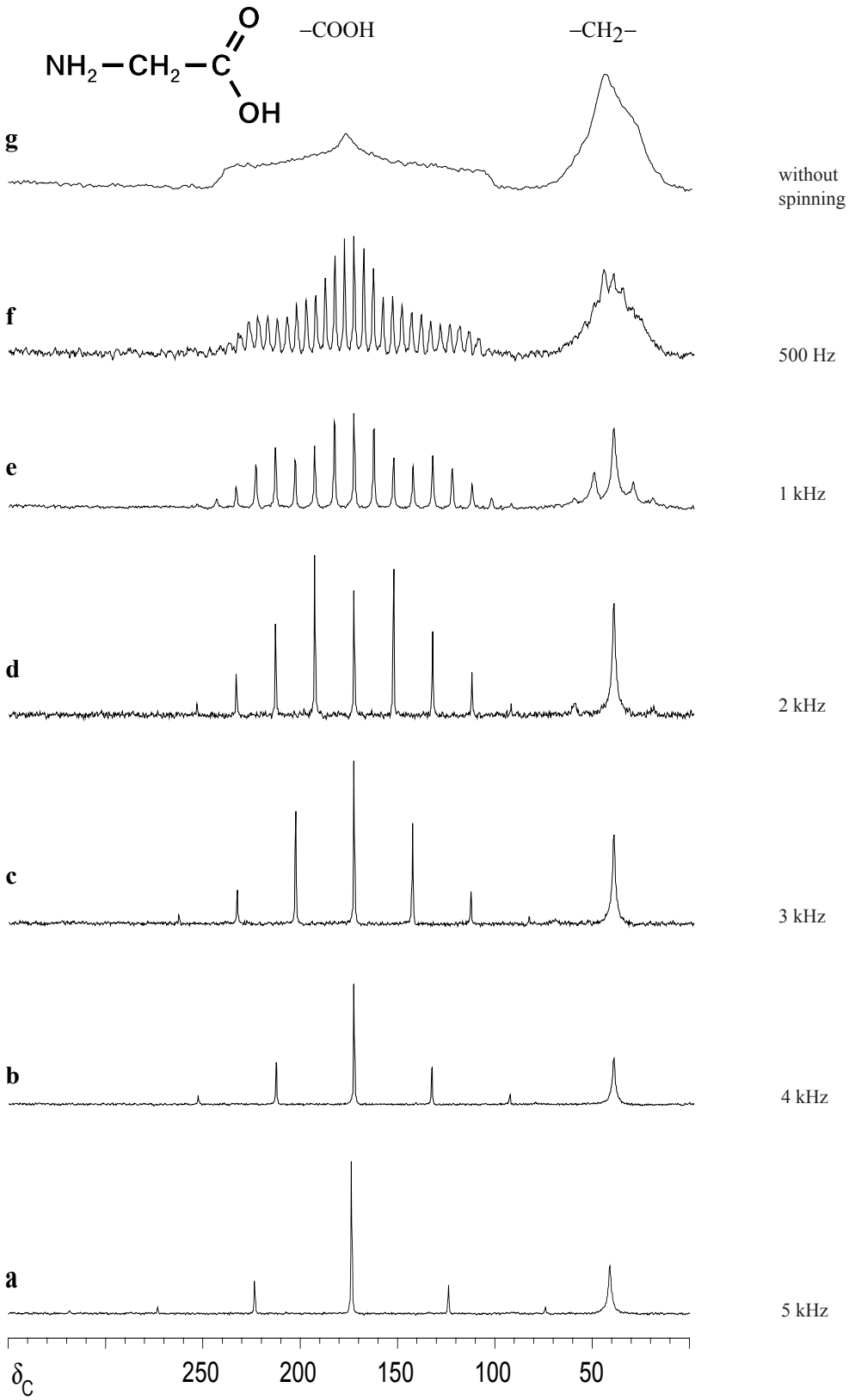

Fig. 7.1-4 CP/MAS of glycine at different spinning rates

Fig. 7.1-5 Stator of DOTY MAS 5-mm probe XC-5

We report preliminary results of a general technique for high resolution NMR of isotopically rare (13C, 15N, 2H, etc.) or chemically dilute spins in solids. The method combines established ideas of double resonance and spin decoupling3 in a novel way. It exploits abundant spins ***I***, of abundance N_I and magnetic moment $\gamma_I h/2\pi$ (usually protons), present in the sample, as a reservoir of polarization for the rare spins S, to permit the accumulation of an adequately intense ***S***-spin spectrum after a single polarization of the ***I*** spins to equilibrium. The general procedure is as follows: (1) Polarize ***I*** in high field. (2) Cool ***I*** to a low spin temperature in the rotating frame. (3) Establish ***I-S*** contact for a time *T*. (4) Record the ***S*** free induction decay while decoupling ***I***.

Taken from ref. [1]

7. Comments

After the first proton pulse, which aligns the magnetization along the $+x$ axis, a proton spin lock pulse p2 with phase x locks this magnetization in the radiofrequency field. A simultaneous ^{13}C spin lock pulse p3 assures the same precession frequency for the ^{13}C spins if the Hartmann–Hahn condition is satisfied. In this situation the ^{13}C and proton spins can exchange energy, which leads to a polarization of the ^{13}C spins in the large energy bath of the abundant protons. High-power proton decoupling removes all dipolar couplings to the protons, and magic-angle spinning removes the chemical shift anisotropy, but also creates spinning side-bands. These often render the analysis of the CP/MAS spectra very difficult. The repetition time of the pulse sequence is determined by the proton relaxation.

With the CP/MAS method an extremely large variety of chemical problems can be investigated, ranging from physical organic questions such as the structure of carbocations to applications in materials science, e.g., the composition of rubber used for car tires. Many examples are given in the review literature cited at the beginning of this chapter.

8. Questions

A. How do you adjust the magic angle with a KBr sample?

B. How do you find the parameters for the Hartmann–Hahn condition?

C. In spectrum **a**, the signal of the CO group shows spinning sidebands, however not the signal of the methylene group. Why?

9. Own Observations

Experiment 7.2

High-Resolution Magic-Angle Spinning

1. Purpose

There exists a class of materials that cannot be dissolved without losing considerable structural information, but which cannot be considered to be solid in the sense of normal organic or inorganic crystalline compounds. These semi-solids include, for example, biological tissues or artificial membranes, lipids, cartilage, polymer-bound monomers, polymer gels, plant materials, and food samples. In order to obtain informative NMR spectra from such materials a new kind of probe head and recording technique has been developed, called HR-MAS (**H**igh-**R**esolution **M**agic-**A**ngle **S**pinning). These probes combine the advantages of a high-resolution probe (such as the lock channel for shimming purposes, and gradient capabilities) with the magic angle spinning technique used in solid-state probes. In this experiment we demonstrate the principal virtues of this technology using commercial butter as an example.

2. Variants

All classical standard 1D and 2D measurement techniques can be performed in such a probe under MAS conditions. However, care has to be taken in case the soft material disintegrates under the centrifugal forces of a high speed rotor. If in doubt one should spin the rotor with moderate rates of 1 to 2 kHz. Very recently, a new sample for determination of the magic angle in this kind of probe was proposed [11].

3. Pulse Scheme and Phase Cycle

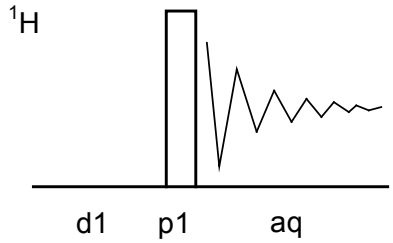

p1: x, x, -x, -x, y, y, -y, -y

aq: x, x, -x, -x, y, y, -y, -y

Scheme 7.2-1

Common values

d1: relaxation delay
p1: 90° ^{1}H transmitter pulse

4. Acquisition

Special values used for the spectrum shown:

Sample: Butter + D_2O.
Time requirement: 5 min
Spectrometer: Bruker DRX-600 with 5-mm HR-MAS probe

Sample preparation:

Mix thoroughly with a spatula half a teaspoon of common butter with 10 drops of D_2O. Transfer this smear into the rotor of the HR-MAS probe and spin the sample at 8 kHz. Control the temperature of the probe by passing room-temperature air through it. Before the experiment, the

[1] R. C. Anderson, J. P. Stokes, M. J. Shapiro "Structure determination in combinatorial chemistry: Utilization of magic angle spinning HMQC and TOCSY NMR spectra in the structure determination of Wang bound lysine" *Tetrahedron Lett*. **1995**, *36*, 5311–5314.

[2] F. Engelke, W. E. Maas, *HR-MAS Manual*, Bruker Instruments, Inc., **1997**.

[3] F. D. Doty, G. Entzminger, Y. A. Yang "Magnetism in high-resolution NMR probe design. II: HR MAS" *Concepts in Magn. Reson*. **1998**, *10*, 239–260.

[4] M. J. Shapiro, J. S. Gounarides "NMR methods utilized in combinatorial chemistry research" *Prog. NMR Spectrosc*. **1999**, *35*, 153–200.

[5] R. Warrass, G. Lippens "Quantitative monitoring of solid phase organic reactions by high-resolution magic angle spinning NMR spectroscopy" *J. Org. Chem*. **2000**, *65*, 2946–2950.

[6] D. Huster, K. Kuhn, D. Kadereit, H. Waldmann, K. Arnold "^{1}H high-resolution magic angle spinning NMR spectroscopy for the investigation of a Ras lipopeptide in a lipid membrane" *Angew. Chem. Int. Ed*. **2001**, *40*, 1056–1058.

[7] I. Schnell "Merging concepts from liquid-state and solid-State NMR spectroscopy for the investigation of supra- and biomolecular systems" *Curr. Anal. Chem*. **2005**, *1*, 3–27.

[8] B. Sitter, T. F. Bathen, M.-Britt Tessem, I. S. Gribbestad "High-resolution magic angle spinning (HR MAS) MR spectroscopy in metabolic characterization of human cancer" *Prog. NMR Spectrosc*. **2009**, *54*, 239–254.

[9] M. Valentini, M. Ritota, C. Cafiero, S. Cozzolino, L. Leita, P. Sequi "The HRMAS–NMR tool in foodstuff characterisation" *Magn. Reson. Chem*. **2011**, *49*, S121–S125.

[10] W. P. Power "High-resolution magic angle spinning-enabling applications of NMR spectroscopy to semi-solid phases" *Ann. Rep. NMR Spectrosc*. **2011**, *72*, 111–156.

[11] M. Leutzsch, M. Findeisen, S. Berger, "Aligned deuterochloroform in cross linked polystyrene as a new sample for adjusting the magic angle in HR-MAS" *Magn. Reson. Chem*. **2012**, *50*, 5–6.

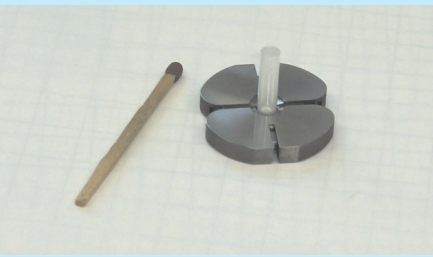

Fig. 7.2-1 Ceramic rotor with cap extraction tool

magic-angle adjustment of the probe should have been checked using a swollen polystyrene stick or KBr. Tune the probe and then lock and shim the sample on D_2O.

td: 32K
sw: 20 ppm
aq: 1.3 s
o1: middle of ^{1}H NMR spectrum [5 ppm]
p1: 90° ^{1}H transmitter pulse [10 µs, 5 dB]
d1: 1s
ns: 1

5. Processing

Use standard 1D processing for ^{1}H NMR spectra

6. Result

The figure shows spectra obtained on a DRX-600 spectrometer equipped with an HR-MAS probe using a standard 4 mm zirconia rotor. In **a** the static spectrum is shown, with the typical broad lines of such semi-solids, whereas in **b** the result with spinning at 8 kHz is given. Under these conditions the typical line width obtained in this sample was 4 Hz, which is a remarkable difference compared with the spectrum shown in **Fig. a.**

7. Comments

Shimming of these probes is not very straightforward. Due to the magic angle of the rotor the usual z shim gradients transform into other directions. Instead of z, z^2 and z^3, you have to use mainly x, xz and xz^2, provided that the axis of the stator within the probe is aligned parallel to the x axis of the shim system. Note that these probes are not built to accept high r.f. power as typically used for other solid-state applications described in experiment 7.1. Only standard high-resolution r.f. techniques can be used, or, for example, no cross-polarization technique should be tried.

Also record for comparison one ^{13}C NMR spectrum in the static mode and with 8 kHz spinning. For ^{13}C NMR the difference will not be as dramatic, because in natural abundance the dipolar interactions between the ^{13}C spins are not predominant.

Combinatorial chemistry using solid phase synthesis is a rapidly developing technology that can result in significant reductions in the time required to find lead compounds and to optimize leads into drug candidates. The application of this approach to "traditional" organic synthesis has led to the construction of libraries of non-peptidic, small organic molecules. However, a major deficiency in the development of combinatorial reactions is the lack of methodology for structure determination of compounds directly attached to polymer supports. This is problematic since it requires the need to remove the compound from the resin for analysis; a time consuming process which may also structurally alter the reaction product. A few non-destructive analytical methods of on-resin-compound analysis have been presented such as Gel-phase ^{13}C NMR and on-resin FTIR to monitor functional group interconversions. However, the total structural and NMR assignment of a compound on-resin has not been reported.

Taken from ref [1]

Fig. 7.2-2 Base of HR-MAS probe (Bruker) with r.f. and air connectors

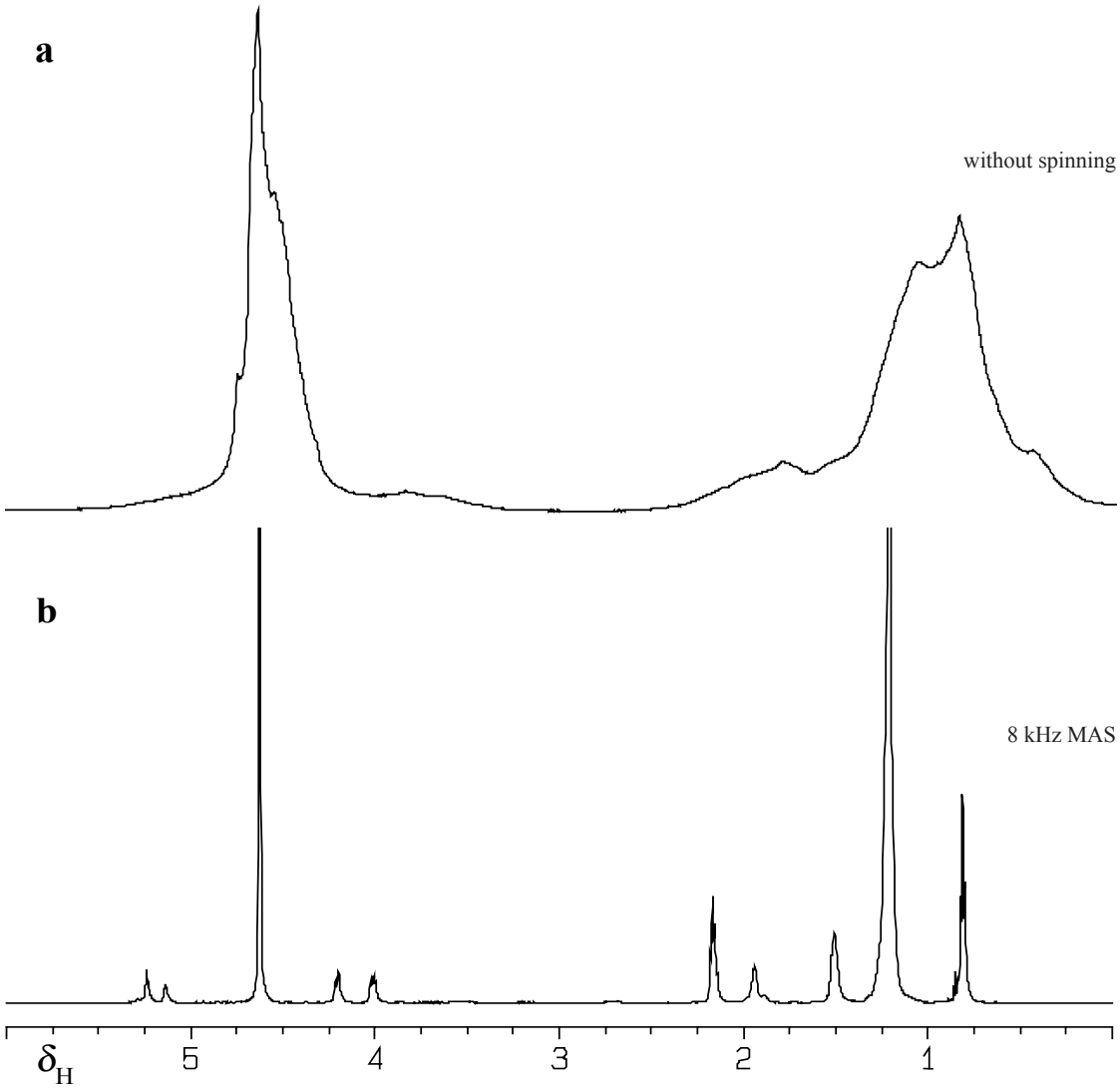

Fig. 7.2-4 ^{1}H-NMR of butter

8. Questions

A. Calculate the centrifugal forces (in units of g) acting on the material in a 4 mm rotor at 8 kHz rotation.

B. Fast rotation may change the temperature within the rotor. Why?

C. There have been concerns about the reliability of NOESY integrals under high-speed rotation. Discuss.

9. Own Observations

HN-HSQC

1. Purpose

This 2D experiment is always the first that will be performed for the structure determination of a new protein. One obtains an H,N chemical shift correlation map, and the number of correlation signals should to some extent correspond to the number of amino acid residues. Proline residues, however, cannot give a signal (because of a missing amide proton within peptide bond), and some amide nuclei might not give a signal due to fast exchange; correlations from nitrogen-bearing side-chains are usually not observed for the same reason. This experiment tells (1) whether the instrument is correctly set up for further protein spectroscopy and, (2) for the protein in question, whether it is folded, and if it is amenable to further investigation by NMR methods.

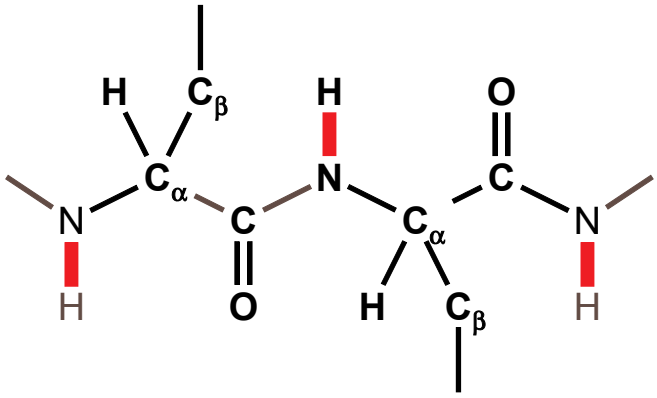

Scheme 7.3-1

2. Variants

There exist a multitude of variants for performing this task. The particular sequence shown here uses a spin lock pulse and a *z*-gradient during the first INEPT step, a chirped ^{13}C 180° pulse for decoupling during the evolution time, and a double INEPT back transfer (PEP = preservation of equivalent pathways) for enhanced sensitivity. The 2D data acquisition is performed with the gradient-selected echo-antiecho scheme. In addition to various modifications of how this sequence can be performed, it can also be combined with an additional TOCSY or NOESY step. The time required for this sequence follows the traditional scheme; however, there are also much faster approaches [6, 8]. For high-molecular−weight proteins the TROSY principle [10] should be used; another of the new features is known as non-uniform data sampling NUS. [9]

This letter describes a two dimensional experiment which initially generates proton magnetization, transfers the coherence to the nitrogen transitions and, after an interval designed to probe the nitrogen chemical shift, transfers the coherence back to the proton transitions to provide the advantage of the detection at high frequencies The pulse sequence indicates the double transfer of coherence symbolically by the sinusoidal pattern representing the precession of the transverse magnetization. The τ delays are approximately adjusted to $(4J_{NH})^{-1}$ and the nitrogen precession is monitored by incrementing the evolution period t_1 in regular increments. The proton decoupling of the nitrogen spectrum, which is achieved by the 180° proton pulse in the middle of the evolution period, may be omitted, the nitrogen decoupling of the proton spectrum during the acquisition period is also optional.

Taken from ref. [1]

3. Pulse Scheme and Phase Cycle

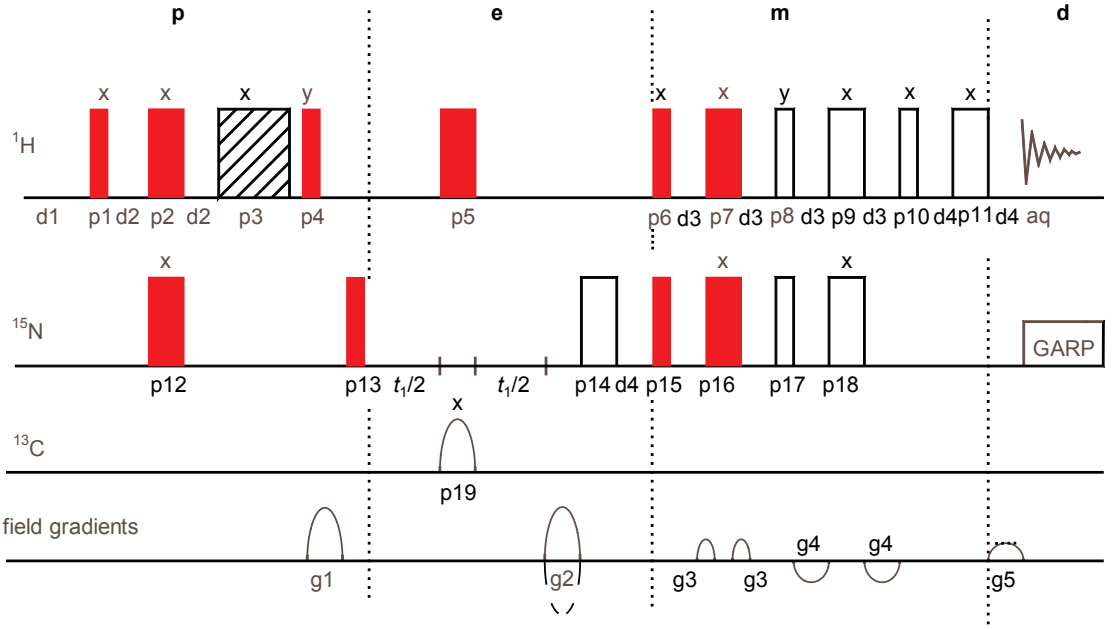

p13: x, -x p5, p14, p15: x, x, -x, -x p17: y, y, -y, -y aq: x, -x, -x, x

Scheme 7.3-2

Common values

d1: relaxation delay
d2, d3 = $1/[4J_{NH}]$
p1,p4, p6, p8, p10: 90° ^{1}H transmitter pulse
p2, p5, p7, p9, p11: 180° ^{1}H transmitter pulse
p3: ^{1}H trim pulse
p13, p15, p17: 90° ^{15}N transmitter pulse
p12, p14, p16, p18; 180° ^{15}N transmitter pulse
p19: chirped 180° ^{13}C transmitter pulse
g1 to g5: pulsed field gradients
d4: equal to gradient length

4. Acquisition

Special values used for the spectrum shown:

Sample: 10 mg fully 13C- and ^{15}N-labeled human ubiquitin in 600 µL 90 % H_2O/ 10 % D_2O, 50 mM phosphate (potassium salt), pH 5.8, 0.5 mM DSS

Time requirement: 2.5 h

Spectrometer: Bruker Avance-700 with 5-mm cryo probe

Set *and control* the temperature to 298 K. The cryo probe with *z*-gradients must be tuned to the sample on all three channels. ^{15}N is assigned to the third hardware channel and ^{13}C to the second. Note that the software uses different numbering; here, protons are not in the first dimension, but in F_2, and the frequency domain for nitrogen is F_1. Be sure to attach the appropriate filter for each r.f. channel to avoid cross talk.

td2: 3072 data points in F_2 (^{1}H)
td1: 512 data points in F_1 (^{15}N)
sw2: 12 ppm
sw1: 40 ppm
aq2: 0.18 s
aq1: 0.09 s
o1: exactly on the water resonance
o2: middle of ^{13}C NMR spectrum for CH_x groups [73 ppm]
o3: middle of ^{15}N NMR spectrum (amide region) [117 ppm]
d1: 2s

d2, d3 = 2.77 ms, calculated from ^{1}J(N,H) = 90 Hz
d4: effective gradient duration, 1.05 ms
p1,p4, p6, p8, p10: 90° ^{1}H transmitter pulse [9.7 µs, –6 dB]
p2, p5, 7, p9, p11: 180° ^{1}H transmitter pulse [19.4 µs, –6 dB]
p3: ^{1}H trim pulse [1 ms, –6 dB]
p13, p15, p17: 90° ^{15}N transmitter pulse [35 µs, –3 dB]
p12, p14, p16, p18: 180° ^{15}N transmitter pulse [70 µs, –3 dB]
p19: chirped 180° ^{13}C transmitter pulse [500 µs, 2.33 dB]
90° ^{15}N transmitter pulse and attenuation for GARP sequence [170 µs, 9.8 dB]
g1 to g5: pulsed field gradients
d1: 2 s
d2, d3: 1/[4J(N,H)] = 2.77 ms, calculated from ^{1}J(N,H) = 90 Hz
d4: effective gradient duration, 1.05 ms
g1–g5: Gradient duration and strength according to the table (100 % ≈ 0.56 T/m):

gradient	g1	g2	g3	g4	g5
duration [ms]	1	1	0.5	1	1
strength [%]	50	80	5	−2	8.1

ds: 4
ns: 8

5. Processing

Apply zero-filling to 4K real data points in F_2 and to 1K data points in F_1 to obtain a matrix of 2K × 512 real data points. Use Gaussian multiplication [gb = 0.1, lb = −2 Hz] in F_2 and π /3-shifted squared sinusoidal window in F_1. Phase correction and base-line correction are necessary for both dimensions. Reference the ^{15}N dimension using the Ξ-scale procedure described in the introduction to chapter 4 using the DSS signal set to $\delta_H = 0$.

6. Result

The figure shows the 2D spectrum obtained on a Avance-700 spectrometer with a triple-resonance cryoprobe with *z*-gradient. Ubiquitin contains 76 amino acid residues; three of these are prolines, which cannot yield an H,N correlation signal. There are six glutamine and two asparagine residues; the side-chain amide NH_2 protons of these each give two signals with an identical nitrogen chemical shift, and they are indicated in the figure by a dotted box or line. Arginine and lysine side-chain NH_x protons often undergo exchange and therefore are not detected, as is also the case for methionine (M-1), the amino end of the protein. Indeed, 86 correlation signals can be counted in the figure, which is close to expectation.

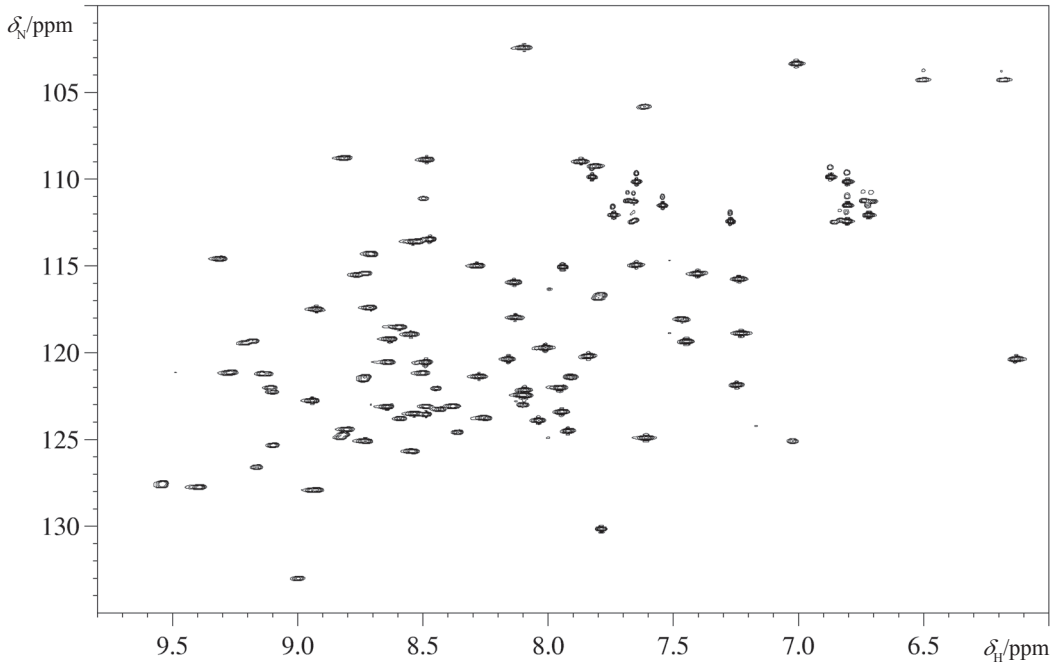

Fig. 7.3-1 $^{1}H,^{15}N$ HSQC spectrum of ubiquitin

7. Comments

In scheme 7.3-2 the pulse sequence is divided into four sections separated by dotted vertical lines. Section **p** consists of an INEPT transfer from proton to ^{15}N yielding the coherence $2I_{H_z}I_{N_x}$ after pulse p13 as described for the standard HSQC experiment in exp. 1.5. A trim pulse removes unwanted proton magnetization from the water and the *z*-gradient between the pulses p4 and p13 destroys all left-over transverse magnetization.

The next section **e** consists of the evolution period. In the middle of this period a chirped adiabatic ^{13}C 180° pulse decouples all proton resonances from ^{13}C. At the end of this period the sandwich of [gradient, 180° ^{15}N pulse p14, delay d4] encodes the magnetization in an echo-antiecho manner.

Having sampled the chemical shifts of ^{15}N, the back-transfer to protons is achieved in section **m** by pulses p15 and p6, and, in addition by p17 and p8 using the PEP scheme yielding $2I_{H_z}I_{N_x}$. The gradient g5 selects those protons bonded to nitrogen, having been encoded by gradients g2. Therefore the gradient ratio g2:g5 is 10:1.

Note that a stripped version of this experiment (with ns = 2 and td1 = 64, lasting about 5 min) immediately tells whether the three channels of the instrument are set up and tuned correctly. Thus, it is advisable to run this and the following Experiment 7.4 in this stripped version before spending a weekend on a more demanding 3D task.

[1] G. Bodenhausen, D. J. Ruben, "Natural abundance nitrogen-15 NMR by enhanced heteronuclear spectroscopy" *Chem. Phys. Lett*. **1980**, *69*, 185–189.

[2] A. G. Palmer III, J. Cavanagh, P. E. Wright, M. Rance, "Sensitivity improvement in proton detected two-dimensional heteronuclear correlation NMR spectroscopy" *J. Magn. Reson*. **1991**, *93*, 151–170.

[3] L. E. Kay, P. Keifer, T. Saarinen, "Pure absorption gradient enhanced heteronuclear single quantum correlation spectroscopy with improved sensitivity" *J. Am. Chem. Soc*. **1992**, *114*, 10663−10665.

[4] W. Willker, D. Leibfritz, R. Kerssebaum, W. Bermel, "Gradient selection in inverse heteronuclear correlation spectroscopy" *Magn. Reson. Chem*. **1993**, *31*, 287–292.

[5] J. Schleucher, M. Schwendinger, M. Sattler, P. Schmidt, O. Schedletzky, S. J. Glaser, O. W. Sorensen, C. Griesinger "A general enhancement scheme in heteronuclear multidimensional NMR employing pulsed field gradients" *J. Biomol. NMR* **1994**, *4*, 301−306.

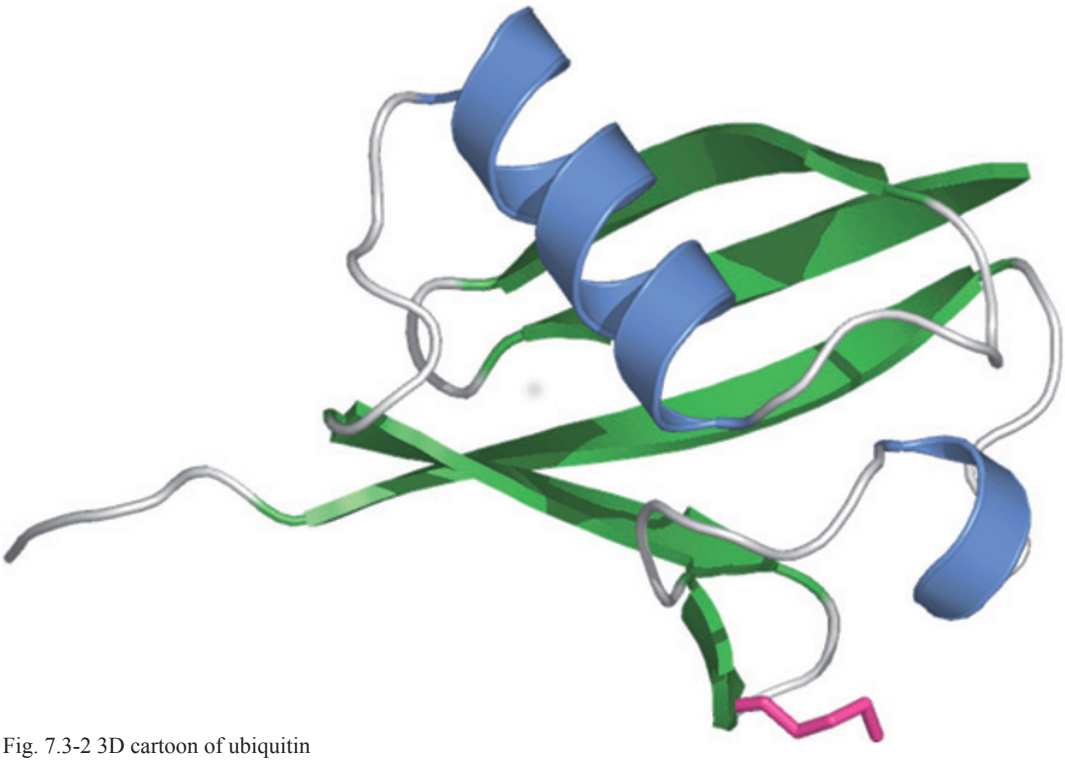

Fig. 7.3-2 3D cartoon of ubiquitin

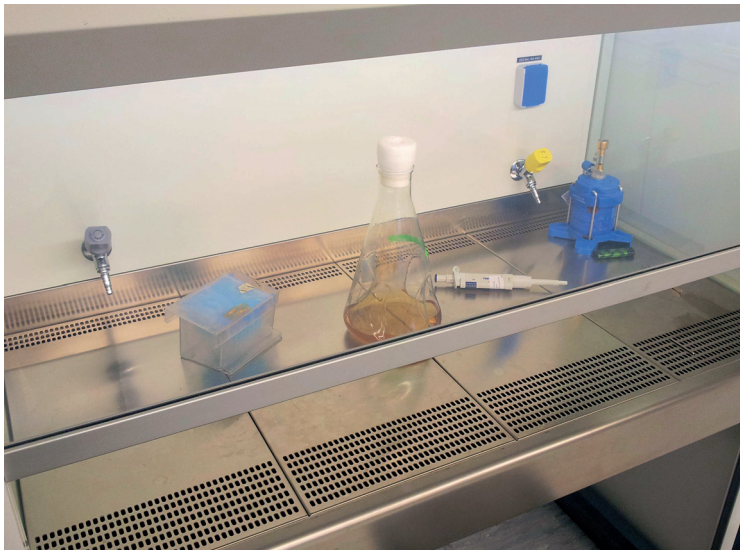

Fig. 7.3-3 Clean bench in a biological safety laboratory

[6] S. Mori, C. Abeygunawardana, M. O'Neil Johnson, P. C. M. van Zijl "Improved sensitivity of HSQC spectra of exchanging protons at short interscan delays using a new fast HSQC (FHSQC) detection scheme that avoids water saturation" *J. Magn. Res. Ser. B* **1995**, *108*, 94−98.

[7] J. Cavanagh, W. J. Fairbrother, A. G. Palmer III, N. J. Skelton, Protein NMR Spectroscopy, *Academic Press*, San Diego, **1996**, 411–435.

[8] T. Diercks, M. Daniels, R. Kaptein "Extended flip-back schemes for sensitivity enhancement in multidimensional HSQC-type out-and-back experiments" *J. Biomol. NMR* **2005**, *33*, 243–259.

[9] D. J. Holland, M. J. Bostock, L. F. Gladden, D. Nietlispach "Fast multidimensional NMR spectroscopy using compressed sensing" *Angew. Chem. Int. Ed.* **2011**, *50*, 6548–6551.

[10] E. R. P. Zuiderweg, A. Rousaki "Gradient-Enhanced TROSY Described with Cartesian Product Operators" *Conc. Magn. Reson.* **2011**, *38A*, 280–288.

8. Questions

A. Describe the idea of the PEP back transfer scheme using the product operator formalism.

B. Confirm the gradient ratio g2 : g5.

C. Would additional ^{13}C decoupling during the acquisition improve the result?

9. Own Observations

HNCA

1. Purpose

The HNCA experiment provides one of the standard assignment methods for fully ^{13}C-and ^{15}N-labelled proteins. In the HNCA experiment, magnetization is transfered from the ^{15}N-bonded protons via ^{15}N to the C_α ^{13}C nuclei of the same and the preceding amino acids. This is due to the fact that $^1J(N,C_\alpha)$ [7−11 Hz] and $^2J(N,C_\alpha)$ (4−9 Hz) are of similar magnitude. The sequence belongs to the "out-and-back" methods, which means that we are detecting the amide proton from which the magnetization transfer started. In the 3D NMR spectrum we find two correlation signals which connect the amide proton with the attached ^{15}N nuclei and the C_α carbon chemical shifts of the same and the previous amino acids.

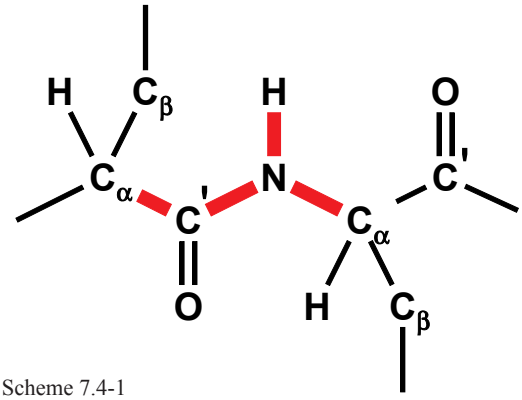

Scheme 7.4-1

2. Variants

Of the many variants known, we show here a gradient-selected sequence using the echo-antiecho scheme [3] and the constant-time feature in the ^{15}N dimension (F_2) [2], but States-TPPI in the ^{13}C dimension (F_1); thus the sequence is phase-sensitive in all three dimensions. The sequence also provides a sensitivity enhancement by the preservation of equivalent pathways (PEP) principle, and a Bloch−Siegert phase shift compensation. The different pulses for the $^{13}C_\alpha$ and ^{13}CO regions are generated by using band-selective pulses working at different offsets. The sequence follows the traditional time requirement. There are now faster sequences available [10,11]; however, for the novice in this field the classical HNCA is still of great value.

Ubiquitin is a stable and well-characterized protein and it is presently the only protein commercially available in a uniformly ^{13}C/^{15}N-enriched form. It is commonly used in a number of laboratories to optimize the performance of multidimensional multinuclear experiments. Therefore, also listed in Table 1 are the ^{1}Hα ^{1}Hβ, ^{13}Cα, ^{13}Cβ and ^{13}C' chemical shifts, obtained from two-scan versions of the HBHA(CO)NH (Grzesiek and Bax, 1993), HBHANH (Wang et al., 1994), CBCA(CO)NH (Grzesiek and Bax, 1992a), CBCANH (Grzesiek and Bax, 1992b), HCACO (Grzesiek and Bax, 1993) and HNCO (Grzesiek and Bax, 1992c) experiments which were optimized on a 1.4 mM ubiquitin sample dissolved in H_2O. In the course of this work, we noticed that several of the ^{15}N, ^{1}HN and ^{1}Hα chemical shifts are quite sensitive to sample concentration, pH and ionic strength.

Taken from ref. [7]

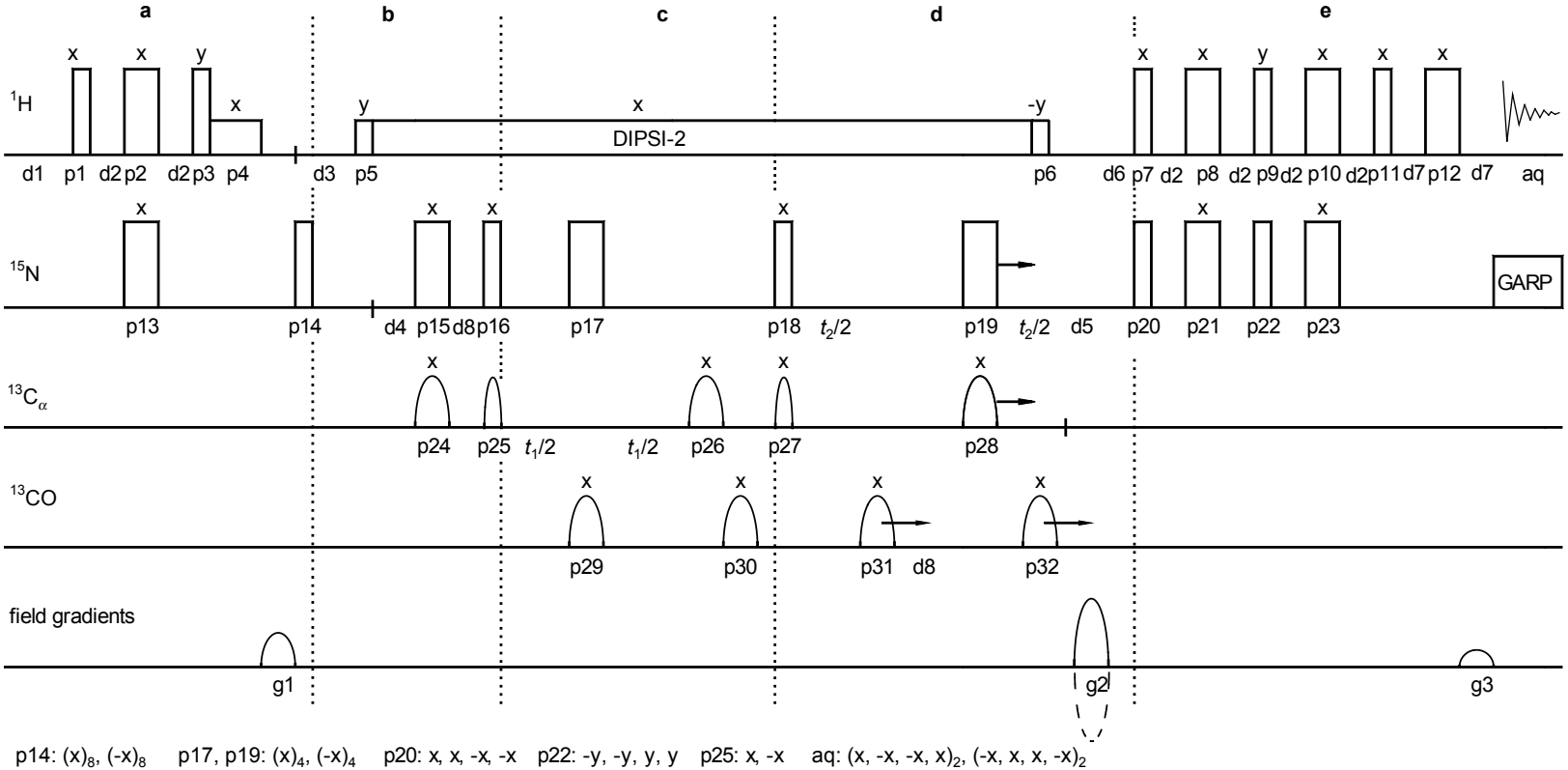

p14: $(x)_8$, $(-x)_8$ p17, p19: $(x)_4$, $(-x)_4$ p20: x, x, -x, -x p22: -y, -y, y, y p25: x, -x aq: $(x, -x, -x, x)_2$, $(-x, x, x, -x)_2$
phase cycle for p22 incremented according to States-TPPI

Scheme 7.4-2

4. Acquisition

Special values used for the spectrum shown:

Sample: 10 mg fully ^{13}C- and ^{15}N-labelled human ubiquitin in 600 µL 90 % H_2O/ 10 % D_2O, 50 mM phosphate (potassium salt), pH 5.8, 0.5 mM DSS

Time requirement: 23 h

Spectrometer: Bruker Avance-700 with 5-mm cryo probe

It is a major task to set up this experiment for the very first time. Set *and control* the temperature to 298 K. A triple resonance cryo probe with *z*-gradients must be tuned to the sample on all three channels. Usually ^{15}N is assigned to the third hardware channel and ^{13}C to the second. Note that the BRUKER software uses different numbering for the frequency dimensions *F*; here protons are not in the first dimension, but in F_3; ^{15}N is in F_2 and ^{13}C is in F_1. This has often led to misunderstandings, i.e. a confusion between frequency dimensions of the spectrum and hardware frequency channels. Record a 1D proton NMR spectrum with water suppression by presaturation for referencing to DSS = 0.

td3: 2048 data points in F_3 (^1H)
td2: 64 data points in F_2 (^{15}N)
td1: 96 data points in F_1 (^{13}C)
sw3: 12 ppm
sw2: 40 ppm
sw1: 32 ppm
aq3: 0.122 s
aq2: 0.011 s
aq1: 0.0085 s
o1: on the water frequency
o2: middle of ^{13}C NMR spectrum (C_α region) [53 ppm]
o3: middle of ^{15}N NMR spectrum (amide region) [117 ppm]
p1, p3, p7, p9, p11: 90° ^1H transmitter pulse [9.7 µs, – 6 dB]
p2, p8, p10, p12: 180° ^1H transmitter pulse [19.4 µs, – 6 dB]
p4: 90° selective rectangular-shaped ^1H transmitter pulse, offset on water frequency [2.2 ms, 40.5 dB]
p5, p6: 90° ^1H transmitter pulse at power level of DIPSI-2 spin lock [80 µs, 12.3 dB]
p14, p16, p18, p20, p22: 90° ^{15}N transmitter pulse [35 µs, – 3 dB]
p13, p15, p17, p19, p21, p23: 180° ^{15}N transmitter pulse [70 µs, – 3 dB]
p24, p26, p28: 180° band selective ^{13}C transmitter pulse, offset on C_α, G3 Gaussian cascade [256 µs, 0 dB]
p25: 90° band selective ^{13}C transmitter pulse, offset on C_α, G4 Gaussian cascade [400 µs, 0 dB]
p27: 90° band selective ^{13}C transmitter pulse, offset on C_α, G4 Gaussian cascade, time reversed shape to p25 [400 µs, 0 dB]
p29, p30, p31, p32: 180° band selective ^{13}C transmitter pulse, offset on CO (176 ppm), G3 Gaussian cascade [256 µs, 0 dB]
d1: 1.5 s
d2: $1/[4J(N,H)]$ = 2.3 ms, calculated from $^1J(N,H)$ with compromise for relaxation
d3: $1/[2J(N,H)]$ = 5.5 ms, calculated from $^1J(N,H)$ = 90 Hz
d4: $1/[4J(N,C_\alpha)] - 1/[2J(N,H)]$ = 9.7 ms

Common values

p1, p3, p7, p9, p11: 90° ^1H transmitter pulse
p2, p8, p10, p12: 180° ^1H transmitter pulse
p4: 90° selective rectangular-shaped ^1H transmitter pulse, offset on water frequency
p5, p6: 90° ^1H transmitter pulse at power level of DIPSI-2 spin lock
p14, p16, p18, p20, p22: 90° ^{15}N transmitter pulse
p13, p15, p17, p19, p21, p23: 180° ^{15}N transmitter pulse
p24, p26, p28: 180° band selective ^{13}C transmitter pulse, offset on C_α,
p25: 90° band selective ^{13}C transmitter pulse, offset on C_α,
p27: 90° band selective ^{13}C transmitter pulse, offset on C_α,
p29, p30, p31, p32: 180° band selective ^{13}C transmitter pulse, offset on CO,
d1: relaxation delay
d2: $1/[4J(N,H)]$
d3: $1/[2J(N,H)]$
d4: $1/[4J(N,C_\alpha)] - 1/[2J(N,H)]$
d5: $1/[4J(N,C_\alpha)] - 1/[2J(N,H)]$
d6: $1/[2J(N,H)]$ minus gradient duration
d7: effective gradient duration
d8: $1/[4J(N,C_\alpha)]$

d5: $1/[4J(N,C_\alpha)] - 1/[2J(N,H)] = 9.7$ ms, decremented in constant time period
d6: $1/[2J(N,H)]$ minus gradient duration = 4.5 ms
d7: effective gradient duration, 1.05 ms
d8: $1/[4J(N,C_\alpha)] = 12.5$ ms
g1, g2, g3: SMQ10 smoothed-square shaped field gradients, 1 ms duration gradient strength ratio: 30 : 80 : 8.1, changed for every other transient in F_2 loop to 30 : −80 : 8.1 (echo-antiecho)
^{1}H transmitter attenuation and 90° pulse for DIPSI-2 spin lock [80 µs, 12.3 dB]
^{15}N decoupler attenuation and 90° pulse for GARP [170 µs, 9.8 dB]
initial value for t_1 evolution: 3 µs
initial value for t_2 evolution: 3 µs
increment for t_1 evolution: 1/[2·sw1]
increment for t_2 evolution: 1/[2·sw2]
decrement for t_2 evolution: 1/[2·sw2], (constant time principle, make sure to set this parameter independently)
ds: 16
ns: 8

5. Processing

Apply zero-filling to 4K real data points in F_3, 128 real data points in F_2 and 128 real data points in F_1 to obtain a matrix of 2K×64×64 real data points. This would result in a huge data set. Therefore use strip FT to display the amide region only. Application of forward linear prediction (ca. 20 coefficients) for both F_2 and F_1 results in somewhat better resolved 3D spectra. Use Gaussian multiplication (lb = –1 Hz, gb = 0.2) in F_3 and a π/3-shifted squared sinusoidal window in the other dimensions. For the data file described, extensive experimentation with different window functions may be worthwhile. Phase correction may be necessary for all dimensions. Reference the indirect dimensions using the Ξ-scale procedure (cf. Chapter 4).

[1] L. E. Kay, M. Ikura, R. Tschudin, A. Bax "Three-dimensional triple-resonance NMR spectroscopy of isotopically enriched proteins" *J. Magn. Reson*. **1990**, *89*, 496−514.

[2] S. Grzesiek, A. Bax "Improved 3D triple-resonance NMR techniques applied to a 31 kDa protein" *J. Magn. Reson*. **1992**, *96*, 432−440.

[3] J. Schleucher, M. Sattler, C. Griesinger "Coherence selection by gradients without signal attenuation: Application to the three-dimensional HNCO experiment" *Angew. Chem. Int. Ed. Engl*. **1993**, *32*, 1489−1491.

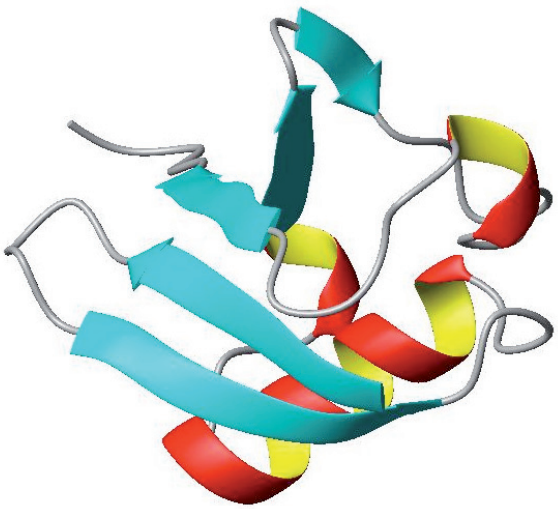

Fig. 7.4-3 Ubiquitin structure model

6. Result

The figures show three planes of the 3D spectrum obtained on a Avance-700 spectrometer with a cryo *z*-gradient triple resonance probe head. As example an H,N plane is chosen in Fig. **a**, which gives, besides others, the signal of the most shielded NH proton at $\delta_H = 6.15$ and $\delta_N = 120.0$. This plane can be easily found from the 3D cuboid. This H/N pair can be identified as arising from the amino acid isoleucine I-36. In Fig. **b** the orthogonal H,C plane for the same proton is shown, which gives two C_α correlation signals, one at $\delta_C = 57.8$ from the same amino acid and one at $\delta_C = 46.0$ from the preceding amino acid glycine G-35. This plane contains many other correlation signals, and nicely displays that for each HN signal there are two C_α correlations. Finally, Fig. **c** shows an N,C plane with the same proton signal at $\delta_H = 6.15$ as parameter.

[4] D. R. Muhandiram, L. E. Kay "Gradient-enhanced triple-resonance three-dimensional experiments with improved sensitivity" *J. Magn. Reson. Ser. B* **1994**, *103*, 203−216.

[5] L. E. Kay, G. Y. Xu, T. Yamazaki "Enhanced-sensitivity triple resonance spectroscopy with minimal H_2O saturation" *J. Magn. Reson. Ser. A* **1994**, *109*, 129−133.

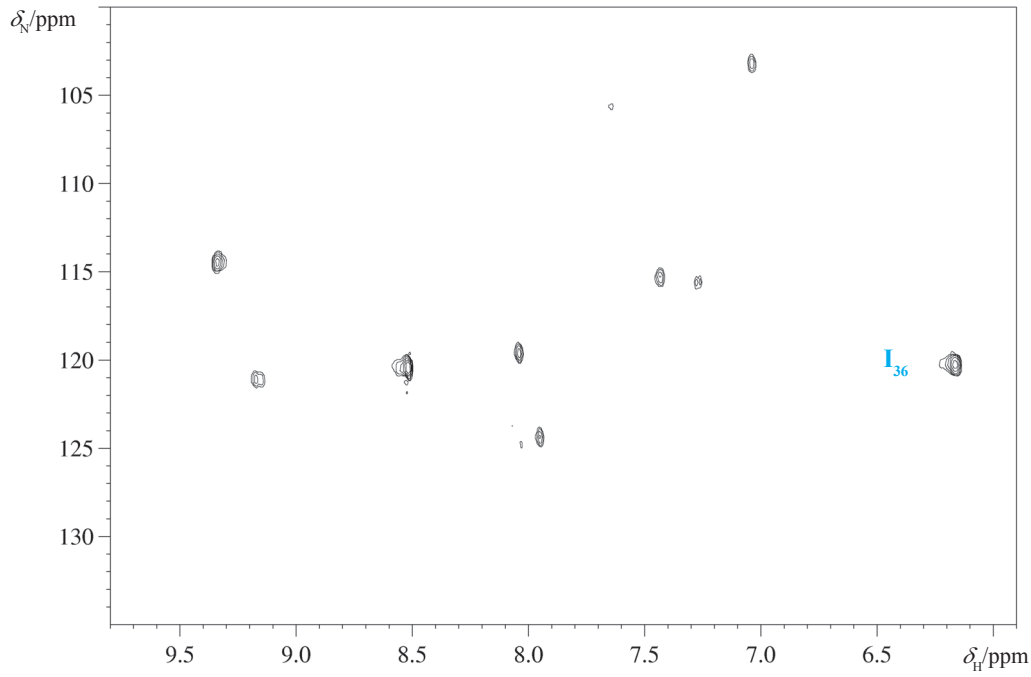

Fig. 7.4-4 **a**: H,N plane at $\delta_C = 55$ ppm

[6] J. Cavanagh, W. J. Fairbrother, A. G. Palmer III, N. J. Skelton, *Protein NMR Spectroscopy*, Academic Press, San Diego, **1996**, 482−491.

[7] A. C. Wang, S. Grzesiek, R. Tschudin, P. J. Lodi, A. Bax "Sequential backbone assignment of isotopically enriched proteins in D_2O by deuterium-decoupled HA(CA)N and HA(CACO)N" *J. Biomol. NMR* **1995**, *5*, 376–382.

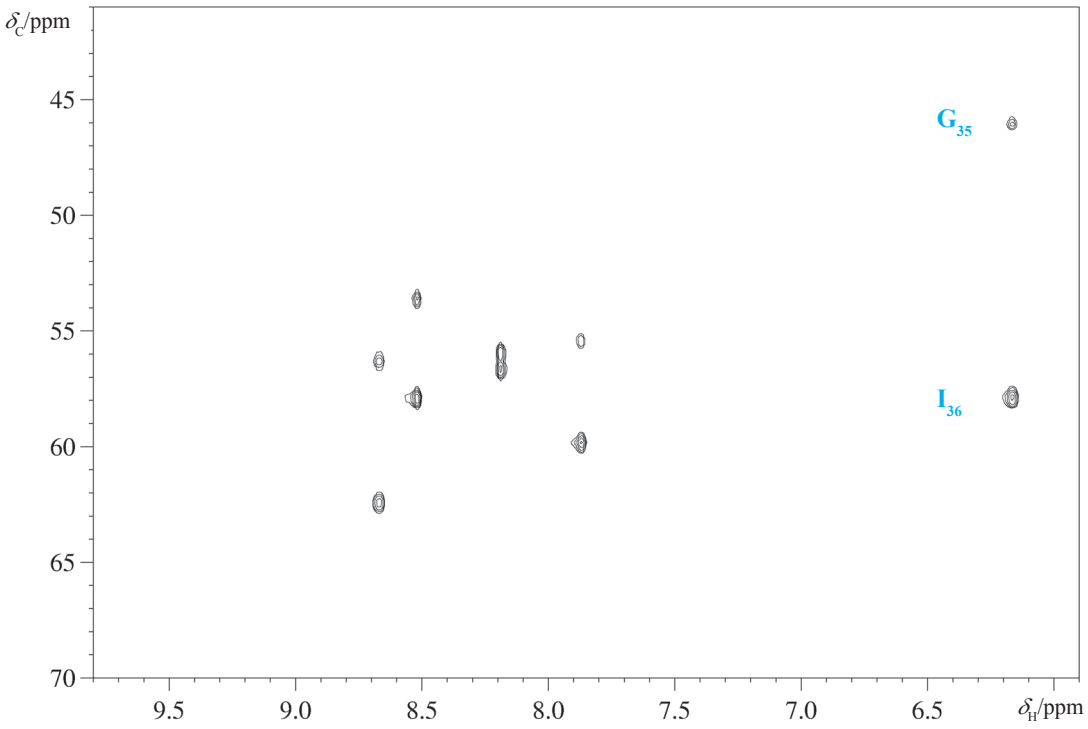

Fig. 7.4-4 **b**: H,C plane at δ_N = 120 ppm

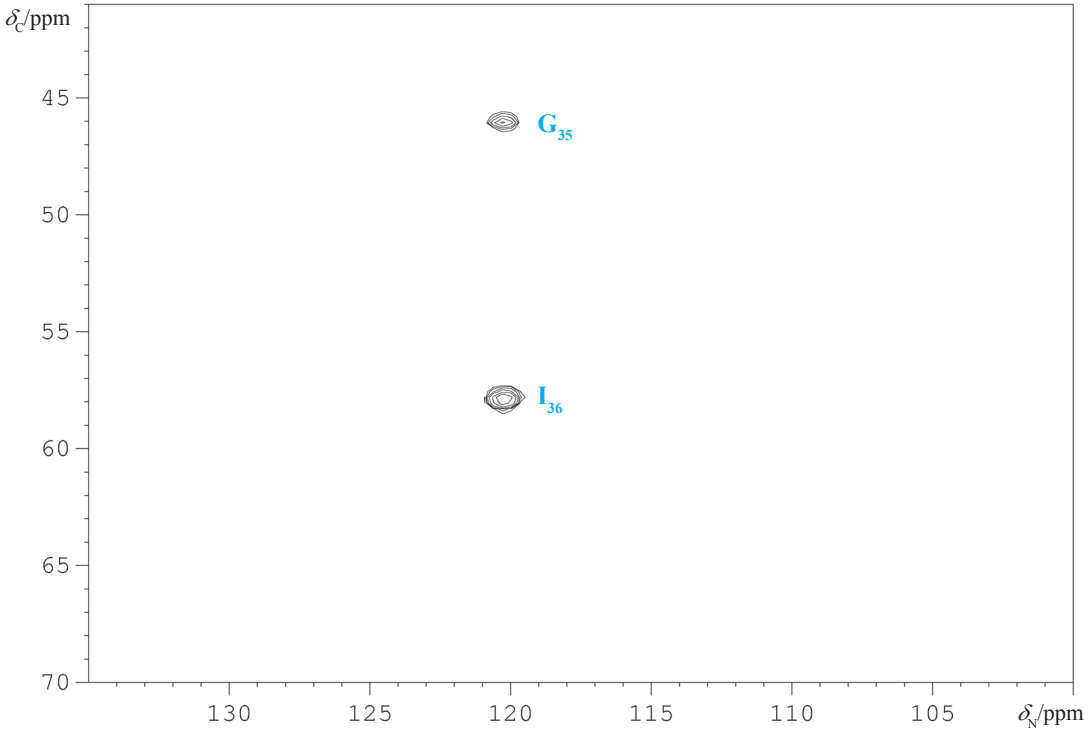

Fig. 7.4-5 **c**: N,C plane at δ_H = 6.17 ppm

7. Comments

The complicated pulse sequence is divided into 5 sections **a**–**e** separated by dotted vertical lines. In section **a** we have the INEPT transfer from proton to ^{15}N, which includes in addition a selective pulse on water (p4) and a dephasing gradient pulse (g1). The water protons and the amide protons are aligned in the −*y*-direction by the first proton pulse p1. Since the water protons develop no spin coupling, they stay in the −*y*-direction and are not affected by p3, but will be flipped back by p4 to the +*z*-direction. This feature leads to a minimum of saturation of the water signal and hence to a better sensitivity for the desired amide proton signals due to less saturation transfer. At this time the amide protons are described by the term $2I_{H_z}I_{N_z}$, and thus the gradient pulse g1 dephases any magnetization caused by pulse imperfections, being not in the *z*-direction. The final pulse p14 on ^{15}N creates $2I_{H_y}I_{N_y}$ for the amide protons.

In section **b** we find a second INEPT transfer, this time from ^{15}N to ^{13}C provided by the pulses p15 and p16 on ^{15}N and the band-selective pulses p24 and p25 working on the C_α region. The total length of this section **b** corresponds to (d3 + d4 + d8) which is set to 1/2[*J*(N,C_α]. After the delay d3 = 1/2[*J*(N,H)], proton decoupling by the DIPSI-2 sequence is started, which ensures that the following sampling of ^{13}C and ^{15}N chemical shifts occurs without interference from proton couplings.

This decoupling is preceded by the 90° pulse p5 which aligns the protons into the *x*-direction, from which point the spin lock sequence acts. This ensures the position of the proton magnetization after decoupling and restoring it into the *z*-direction by p6.

In section **c** the ^{13}C chemical shifts are sampled (t_1), while the 180° pulses p17 on ^{15}N and p29 for the C=O region of carbon decouple the C_α carbon nuclei from these spins. However, applying a band-selective pulse (p29) for the carbonyl region causes Bloch–Siegert phase shifts in the C_α region, and these are remedied by the pair of 180° pulses p26 and p30 at the end of section **c** (see Reference [6], p.137).

Section **d** starts with a back transfer from ^{13}C to ^{15}N, achieved by the 90° pulses p18 and p27, and thereafter this ^{15}N chemical shift evolution is sampled in a constant time manner (t_2). The total constant time period is set to 1/2[*J*(N,C_α]; the pulses p31 and p32 decouple the ^{15}N nuclei from the CO ^{13}C spins. The simultaneous 180° pulses p19 on ^{15}N and p28 on C_α provide a constant modulation of the signal. Toward the end of section **d**, proton decoupling is switched off. In the following delay d6 = 1/2[*J*(N,H)] the gradient pulse g2 is applied, which selects according the correct pathway for the ^{15}N chemical shift evolution to the echo/anti-echo scheme.

The pulse sequence ends in section **e** with a double INEPT transfer back to protons using the PEP principle, and the final gradient g3, with one-tenth of the strength of g2, selects the desired magnetization. ^{15}N GARP decoupling provides singlets for each proton resonance, whereas the splitting due to ^{13}C nuclei disappears in the effective line width due to the digitization in 3D.

[8] E. Kupce, R. Freeman "Projection-reconstruction of three-dimensional NMR spectra" *J. Am. Chem. Soc*. **2003**, *125*, 13958–13959.

[9] L. E. Kay "NMR studies of protein structure and dynamics" *J. Magn. Reson*. **2005**, *173*, 193–207.

[10] E. Lescop, P. Schanda, B. Brutscher "A set of triple-resonance experiments for time- optimized protein resonance assignment" *J. Magn. Reson*. **2007**, *187*, 163–169.

[11] Y. Xu, D. Long, D. Yang "Rapid data collection for protein structure determination by NMR spectroscopy" *J. Am. Chem. Soc*. **2007**, *129*, 7722–7723.

8. Questions

A. What is the advantage or the drawback of a "constant time" evolution period?

B. What is the original Bloch–Siegert shift?

C. Identify the four other pairs of amino acids in Plot **b**.

9. Own Observations

Chapter 8

Maintenance and Calibration

Buying NMR instruments is one thing and probably easier than keeping them alive and in good condition. Especially the maintenance costs are usually underestimated. Trivial maintenance duties are the regular filling with cryogens. We recommend filling with liquid nitrogen once per week on a fixed day to avoid any neglectfulness. Filling with liquid helium is dependent on the magnet's dewar hold time.

Regular checking of the electronics will save you a lot of money, especially if you control the many ventilators sitting deeply hidden in the console of your instrument. An NMR operator should be capable of narrowing down the location of an instrument failure to a specific electronic board, which then can be replaced by mail instead of having the costly service engineer visiting you. The need to keep the magnet laboratory tidy and free from any magnetic material should be self-evident.

Furthermore, an operator should be well-informed about the actual performance of the spectrometer and should be able to carry out some tests.

In this chapter we provide calibration experiments which also should be carried out on a regular basis. Note that meaningful scientific results can only be obtained with calibrated instruments.

8.1 Calibration of Pulse Duration in the Transmitter Channel 235
8.2 Calibration of the Pulse Duration in the Indirect Channel 241
8.3 Shaped Pulses 247
8.4 Adiabatic pulses 253
8.5 Temperature Calibration in NMR 257
8.6 Calibration of Pulsed Field Gradients 265

Fig. 8.0-1 Helium refill on a 600 MHz instrument

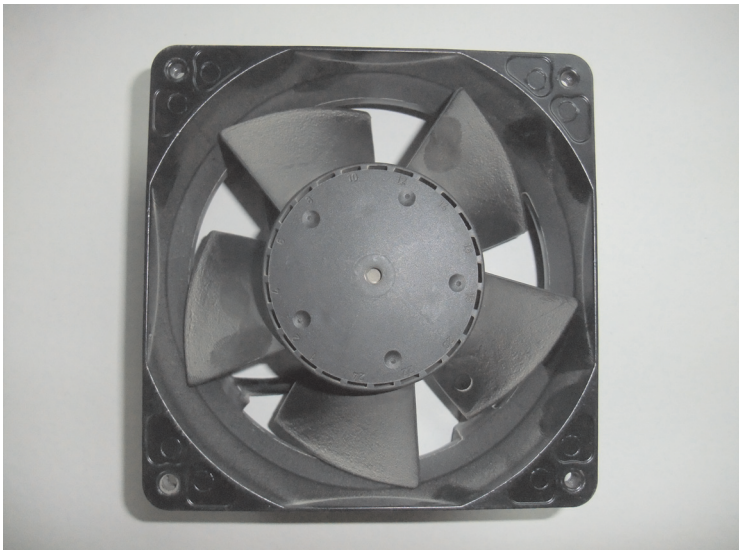

Fig. 8.0-2 Typical fan found in NMR instruments, hold time about 4 years

Experiment 8.1

Calibration of Pulse Duration in the Transmitter Channel

1. Purpose

For any experiment, in particular for multi-pulse experiments, one needs to know the exact flip angle of the magnetization. Therefore, the pulse lengths in all r.f. channels in use have to be calibrated before any experiment. The basic information is the knowledge of the duration of an r.f. pulse which creates a flip angle of 90° at a certain amplifier power level.

The flip angle depends on the r.f. magnetic field strength B_1, the pulse-length *pw*, and the gyromagnetic ratio γ of the nucleus under observation, as expressed in radians and in degrees by Equations (1) and (2) respectively.

$$\theta\,[\mathrm{rad}] = \gamma B_1 \cdot pw \qquad (1)$$

$$\alpha\,[^\circ] = (360/2\pi)\,\gamma B_1 \cdot pw \qquad (2)$$

Often the 90° (or π/2) pulse duration is determined by measuring the 180° (π) or 360° (2π) pulse lengths since these pulses give a minimum signal which is easier to detect than the maximum of intensity.

In principle, the calibration procedure for the transmitter pulse differs from that of the pulses in other channels, because in the transmitter channel the direct observation of the pulse action is possible (the r.f. channel on which the receiver works is denoted as "transmitter channel"), whereas the pulses on the other channels (often denoted as "decoupler channels") have to be evaluated by their indirect actions on a spin system.

In most spectrometers, the special r.f. routings between electronic components differ for various experiments. The r.f. routing may influence the behavior of the channels with respect to lengths and phase of pulses. For that reason one should calibrate the pulse durations in the identical routing mode of the experiment to be performed.

Virtually every modern nuclear magnetic resonance (NMR) experiment requires a user to know, if not calibrate, 90° pulse widths. A 90° pulse width (in the rotating frame) is classically defined to be the time required for the spectrometer to tip the indicated nuclear spins from their equilibrium position (along the z axis) into the xy plane. This "tipping", or "nutation" is usually defined to be a 90° rotation around the +x axis, so that the net magnetization of the spins is tipped from the +z axis onto the −y axis, unless otherwise indicated.

Taken from ref. [2]

2. Variants

In simple cases a few single experiments with different pulse durations are sufficient, especially if one already roughly knows the 90° pulse duration at a given power amplification level. For several reasons one should focus on the 360° flip angle (see below). For special cases, especially in heteronuclear NMR with poor signal-to-noise ratio, the elegant method of Haupt [1] is recommended.

However, the novice should perform a whole set of spectra using increasing pulse durations and a constant increment ("array") over wide range. This should reflect a sine shape intensity course. Thereby some

properties of the probe can be estimated (e.g. r.f. homogeneity) and errors can be detected (arcing /r.f. breakthrough due to high r.f. power, errors due to T_1 relaxation, saturation, or radiation damping).

It is also possible to determine the r.f. field strength by a nutation experiment at weak r.f. field and to recalculate the duration of a 90° pulse at a certain power level assuming linear amplifiers (see [3]). This could be done quickly in one single experiment.

3. Pulse Scheme and Phase Cycle

Common values:

d1 relaxation delay
p1 transmitter pulse, to be varied

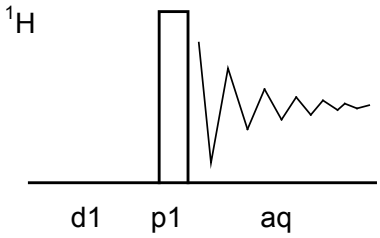

p1: x, x, -x, -x, y, y, -y, -y
aq: x, x, -x, -x, y, y, -y, -y

Scheme 8.1-1

4. Acquisition

Special values used for the spectrum shown:

Sample: pure $CDCl_3$, 99.8 at % enrichment (for probes with lower sensitivity 1 to 5 % $CHCl_3$ may be added), use a non-sealed tube for faster relaxation.
Time requirement: ca. 10 min
Spectrometer: Bruker Avance-700, 5mm TCI Cryoprobe

td:	8388
d1:	5 s
acqu. time:	2.0 s
sw:	3.0 ppm
o1:	7.26 ppm (on resonance of $CHCl_3$)
p1:	initial value 2.0 µs, increment 2.0 µs, 50 single experiments (i.e. p1= 2.0 µs ... 100.0 µs)

5. Processing

Use standard 1D processing with si = 32K and an exponential window with lb = 0.2 Hz.

[1] E. Haupt "A timesaving method to determine the length of a 90° pulse" *J. Magn. Reson*. **1982**, *49*, 358−364.

[2] P. A. Keifer "90° Pulse width calibrations: How to read a pulse width array" *Concepts in Magnetic Resonance*, **1999**, *11*, 165–180.

[3] P. S. C. Wu, G. Otting "Rapid pulse length determination in high-resolution NMR" *J. Magn. Reson*. **2005** *176*, 115–119.

[4] M. P. Augustine, "Transient properties of radiation damping" *Progr. NMR Spectrosc*. **2002**, *40*, 111−150.

6. Result

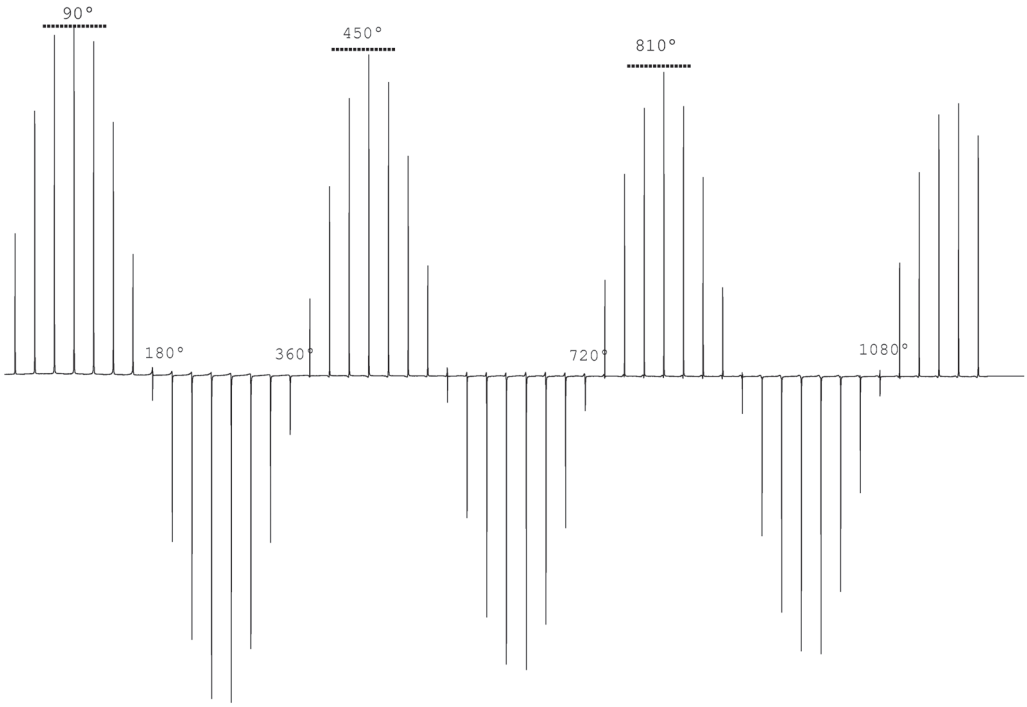

Scheme 8.1-1 Series of pulse responses vs. increasing pulse durations

Fig. 8.1-1 shows a correct sine-shaped intensity course plot against increasing pulse width on a 700 MHz cryoprobe. The reduction in intensity is due to the r.f. field inhomogeneity: the lower the homogeneity of the r.f. coil the faster the decay of the envelope of this curve. According [2] the intensity ratios of I(450°)/I(90°) and I(810°)/I(90°) could be used as a measure of r.f. homogeneity (here 91 % and 85 % , resp.).

When performing this experiment it is important to keep the repetition time between the scans as long as $5T_1$. Otherwise a saturation of the signal could falsify the intensities (see Fig.8.1-3).

On high-sensitivity probe heads and with high concentrated samples (e.g. 90 % H_2O/10 % D_2O samples on cryoprobes) the radiation damping effect may reduce the intensities too and may lead to wrong pulse duration values for the 180° pulse (see Fig 8.1-4).

Because both effects disturb the 360° zero crossing, at least, one can determine with single experiments the 360° pulse duration.

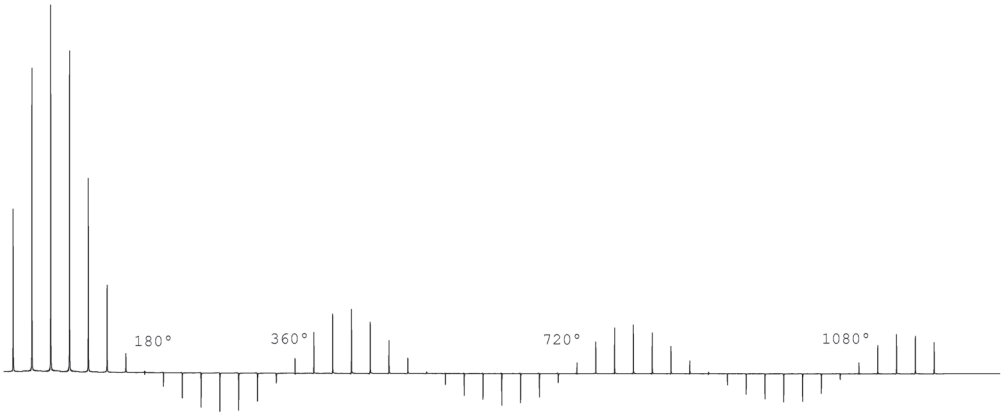

Fig. 8.1-2 Signal intensity vs pulse length, violating the T_1 relaxation condition; same time scale as Fig. 8.1-1 (initial value 2 µs, increment 2 µs, last value 100 µs)

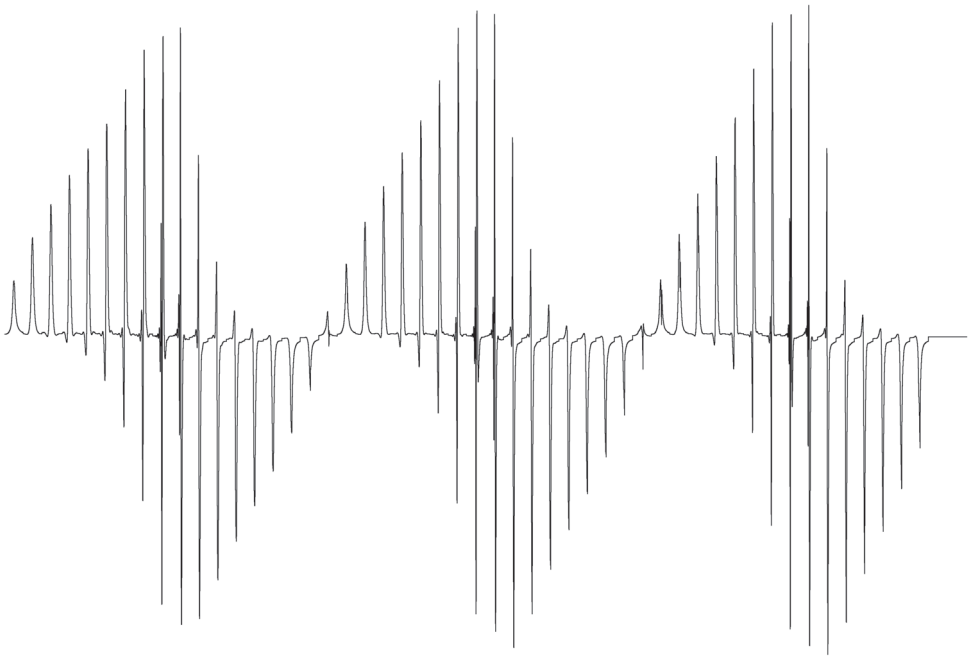

Fig. 8.1-3 Signal intensity vs. pulse length; violation due to radiation damping: the determination of 180° zero crossing is nearly impossible. Same time scale as Fig. 8.1-1 (initial value 2 µs, increment 2 µs, last value 100 µs), sample 54 % H_2O in D_2O

7. Comments

Many modern probe heads, which offer high sensitivity, show a different r.f. behavior for different samples due to magnetic susceptibility characteristics of the samples. Clearly the pulse determination on the actual sample of interest is the best way, but this is not always possible because of low signal intensity. Therefore one should check the 90° (360°, resp.) pulse durations on an example compound in different solvents.

One aim of probe developers is to minimize the sample susceptibility effect sustaining high sensitivity.

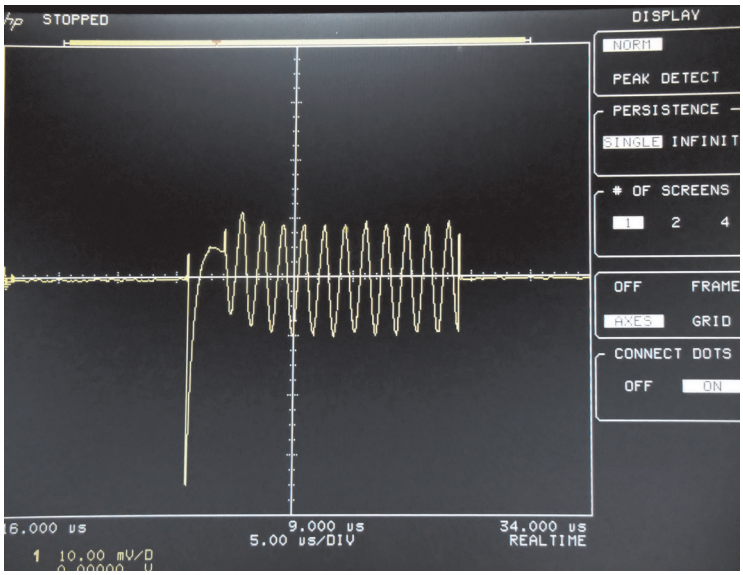

Fig. 8.1-4 A 20 µs r.f. pulse at 19.7 MHz for ^{57}Fe NMR at a 600-MHz spectrometer

8. Questions

A. Why do inverse probes and cryo probes show the strongest radiation damping?

B. There is an additional advantage to determining the 360° pulse instead of the 180° pulse. What it is?

C. Biological samples with dissolved protein in buffer solutions show a large variety of pulse durations. Why?

9. Own Observations

Experiment 8.2

Calibration of the Pulse Duration in the Indirect Channel

1. Purpose

In contrast to the "transmitter channel", to which the receiver is electronically connected, all other r.f. channels used in an experiment have earlier been sometimes called "decoupler channels" and are usually not connected to the receiver. These indirect r.f. channels serve not only for decoupling but also for single pulsing on different nuclei of the spin system. Therefore the influence of these pulses can only be observed indirectly via interaction with the nuclei measured, mainly by the *J*-coupling between both sorts of nuclei.

The indirect pulses should be calibrated in the routing mode of the spectrometer which is identical to the experiment later to be performed, because different routing modes may influence the r.f. behavior and the pulses.

Most decoupling techniques use various schemes of composite pulse decoupling. During the decoupling cycle the power of the decoupler amplifier has to be reduced to minimize thermal effects within the probe head, typically by 12...18 dB, corresponding to factors of 16...63. Therefore one has to calibrate the indirect pulses on different power levels: on high power for single pulsing ("hard pulse") and on low power for composite pulse decoupling ("soft pulse").

Since modern spectrometers show very linear amplifier performance one may recalculate soft and hard pulses by

$$\Delta(\mathrm{dB}) = 20 * \left(\log_{10} \frac{\text{pulse length 1}}{\text{pulse length 2}} \right)$$

but this should be regularly checked experimentally.

The method for determining the decoupler rf field strength described in this paper has already been used in some laboratories for a number of years and has been briefly mentioned in the literature. However, it has appeared to us that most users of the newer-type pulse experiments are unaware of its existence, and are still using the old and, in practice, more cumbersome method of coherent off-resonance decoupling for this purpose.

Taken from ref. [1]

2. Variants

We demonstrate here a procedure which is based upon magnetization transfer via *J* coupling. It can be used for all transmitter power levels and all spectrometer routings.

In the cases of low-abundance nuclei like ^{13}C in the indirect channel, while observing ^{1}H (standard situation in all two-dimensional H,C-correlation spectra) the ^{1}H NMR spectrum is dominated by strong signals without *J* coupling. These signals may be additionally suppressed for better performance, for example by a gradient DQ filter. This assumes knowledge of the approximate value of the 90° decoupler pulse, which is, however, the normal case in routine work.

Manufacturers provide a sample consisting of ^{15}N-labeled urea and ^{13}C-labeled methanol in DMSO-d_6. Since these compounds are labeled, they do not show the center signal of the ^{14}N or ^{12}C species. Therefore this sample can be conveniently used with the standard sequence and we show it with a ^{15}N decoupler pulse example.

3. Pulse Scheme and Phase Cycle

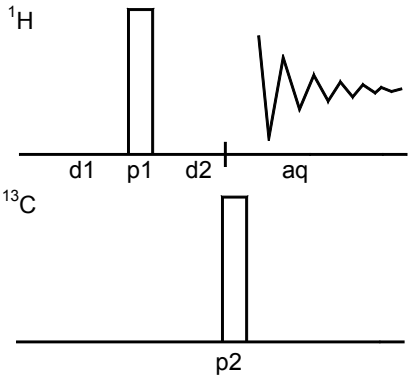

p1: x, -x, -x, x, y, -y, -y, y
p2: x, -x, -x, x, y, -y, -y, y
aq: x, -x, -x, x, y, -y, -y, y

Common values:

p1: 90° transmitter pulse
p2: variable decoupler pulse, 90° length to be determined
d2: $1/(2J_{C,H})$

Scheme 8.2-1 basic pulse scheme (above: transmitter channel, below: indirect channel)

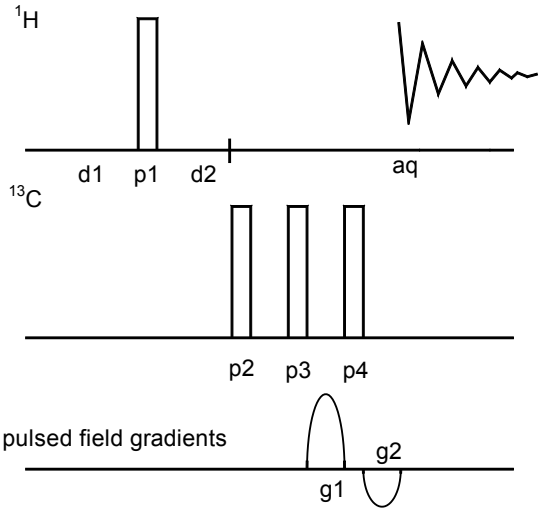

p1, p2, p3, p4, aq: x, -x, -x, x, y, -y, -y, y

Scheme 8.2-2 Pulse scheme with additional gradient DQ filter

for the version with DQ filter:
p3, p4: (approximately) 90° decoupler pulse
g1, g2: gradients for double quantum selection

4. Acquisition

Special values used for the spectrum shown:

Sample: 8 % $CHCl_3$ in $CDCl_3$; for relaxation reasons do not use a degassed and sealed sample.
Time requirement: ca. 10 min
Spectrometer: Bruker DRX-400 with 5-mm-BBO probe

d1: 5 s
d2: 2.381 ms (derived from $J = 210$ Hz)
td: 7182
aq: 3.0 s
sw: 3 ppm
p1: 11.2 µs (−2 dB)
p2: variable (−3 dB)
p3,p4: 7.5 µs (−3 dB)
g1, g2: ratio 40: (−30)
1 ms length + 50 µs recovery delay
sw 3 ppm
o1 7.29 ppm (on resonance on $CHCl_3$)

5. Processing

Use standard ^{1}H NMR processing with exponential weighting and lb = 0.5 Hz.

6. Result

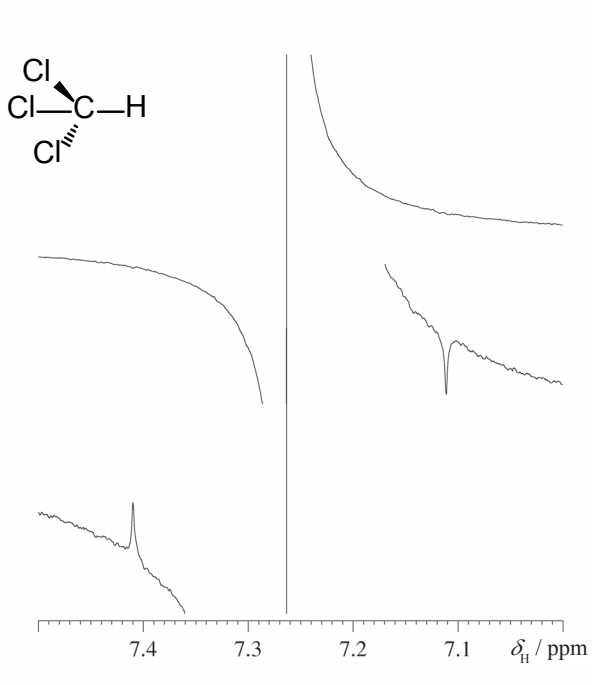

Fig. 8.2-1 Basic pulse sequence. (below p2= 0°, above p2= 90°)

[1] A. Bax "A Simple Method for the Calibration of the Decoupler Radiofrequency Field Strength" *J. Magn. Reson*. **1983**, *52*, 76−80.

[2] N. C. Nielsen, H. Bildsoe, J. Jakobsen, O. W. Sørensen "Pulse Techniques for Calibration of the Decoupler Radiofrequency Field Strength" *J. Magn. Reson*. **1986**, *66*, 456−469.

[3] T. D. W. Claridge, *High-Resolution NMR Techniques in Organic Chemistry*, Pergamon, Oxford, **1999**, 97−99.

[4] G. Esposito, L. Nadalin, G. Verdone, A. Corazza, P. Viglino, M. Fedrigo "Improved method for pulse width calibration in indirectly detected experiments" *Magn. Reson. Chem*. **2001**, *39*, 249–250.

[5] N. Murali "IDEAL–A fast single scan method for X pulse width calibration" *J. Magn. Reson*. **2006**, *183*, 142–144.

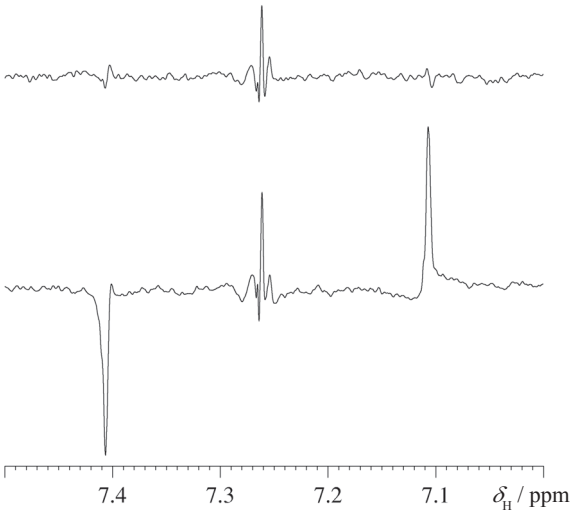

Fig. 8.2-2 pulse sequence with DQ filter. (below p2= 0°, above p2= 90°)

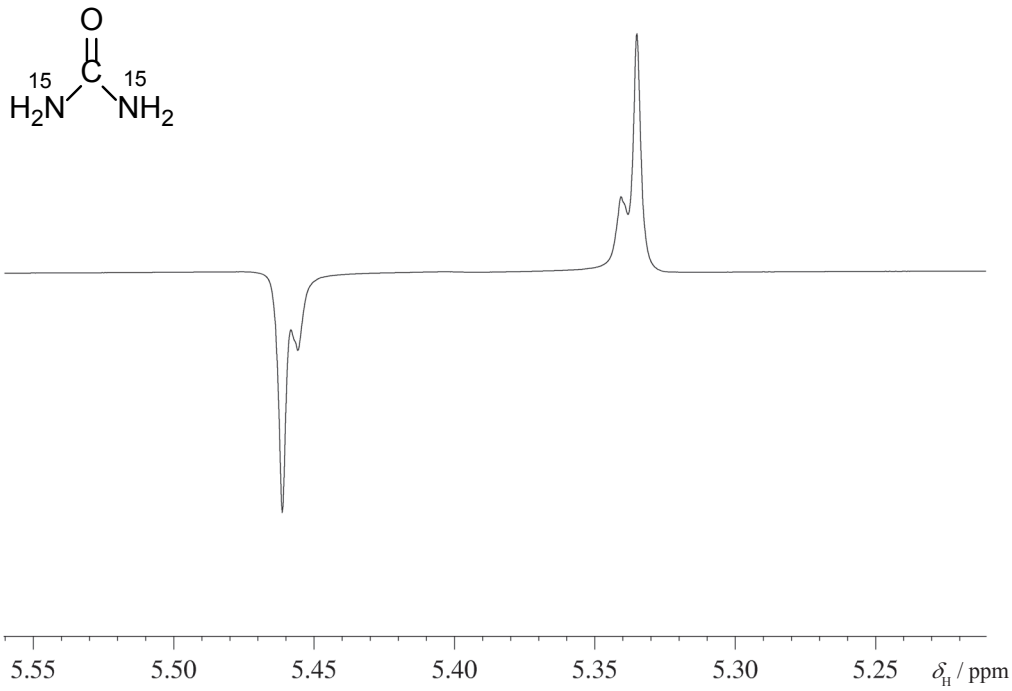

Fig. 8.2-3 The anti-phase ^{1}H NMR spectrum of ^{15}N-labeled urea

7. Comments

We show the principle on a $CHCl_3$ sample with a 400 MHz spectrometer and an X-nucleus optimized probe head, observing ^1H, and with ^{13}C situated on the indirect channel.

This also works in reverse (observe ^{13}C, decouple ^1H – in this case no DQ filter is needed). Of course, the simplest case is samples with 100 % abundance nuclei, as shown with ^{15}N-labeled urea.

We consider a ^{13}C, ^1H spin pair. The equilibrium magnetization is converted by the 90° ^1H pulse into a transverse ^1H magnetization as described by Equation (1).

$$I_{C_z} + I_{H_z} \xrightarrow{90° I_{H_x}} I_{C_z} - I_{H_y} \quad (1)$$

During the period $\tau = d2 = 1/(2J)$ spin–spin coupling between proton and ^{13}C evolves, as in Equation (2).

$$I_{C_z} - I_{H_y} \xrightarrow{\pi J \tau 2 I_{H_z} I_{C_z}} 2 I_{H_x} I_{C_z} \sin\pi J\tau - I_{H_y} \cos\pi J\tau + I_{C_z} \quad (2)$$

Since τ was set to $1/(2J)$, (2) simplifies to (3).

$$= 2 I_{H_x} I_{C_z} + I_{C_z} \quad (3)$$

A 90_x ^{13}C pulse converts $2 I_{H_x} I_{C_z}$ into double quantum magnetization as in Equation (4), from which no observable ^1H signal can be generated. Thus, if the decoupling pulse is exactly 90°, the doublet disappears.

$$2 I_{H_x} I_{C_z} + I_{C_z} \xrightarrow{90° I_{C_x}} -2 I_{H_x} I_{C_y} - I_{C_y} \quad (4)$$

Note that with this method, in contrast to Experiments 8.1, the 90° pulse yields a **minimum** signal, whereas the 180° pulse inverts the initial phases of the doublet.

If to this sequence a gradient double quantum filter is added like in the pulse sequence of Fig. 2, two cases may be discussed. If p2 = 0, only p3 creates $2 I_{H_x} I_{C_y}$ which is present at the time of g1. P4 reconverts this into single quantum magnetization $2 I_{H_x} I_{C_z}$ which gives an antiphase doublet during acquisition as seen in Fig. 4. The center resonance of $CHCl_3$ is eliminated by the action of g1 and g2.

If p2 is close or equal to 90°, $2 I_{H_x} I_{C_y}$ is already present after p2. P3 will reconvert this into single quantum magnetization $2 I_{H_x} I_{C_z}$, but p4 will again create double quantum magnetization, and no signal at all can be observed as seen in the upper trace of Fig. 4.

8. Questions

A. The ^{1}H NMR spectrum of ^{15}N-labeled urea shows more than the expected two lines, which can be further split under very high resolution. Explain.

B. What would be the result of a 360° pulse on the indirect channel?

C. Explain the gradient ratio of g1 and g2 in the pulse sequence with a double quantum filter by drawing a coherence pathway diagram.

9. Own Observations

Experiment 8.3

Shaped Pulses

1. Purpose

In most experiments the transmitter or decoupler amplifier is simply switched *on* for a time *pw*, called *pulse duration*, and afterwards switched *off*. This results in a simple boxed shape (or rectangular) amplitude profile vs time for the r.f. power and B_1 field. The consequence is a *sinc*-shaped excitation profile in the frequency domain with zeros at multiples of +/− (1/pw).

The equipment of present-day spectrometers allows us to create many other time shapes. While the pulse length influences the width of the excitation region in a spectrum, the time shape of a pulse determines its excitation profile. The physical relationship between pulse shape in time domain and excitation profile in frequency domain is dictated by the Fourier transformation, i.e., in principle, time shape and frequency profile are pairs of Fourier functions. This is valid at least for small flip angles α, where the $\sin(\alpha)$ is nearly linear. For the correct frequency profile of a shaped pulse in a spectrum more complex calculations have to be done. In case of isolated spin 1/2 nuclei the Bloch equations can be calculated [3]. Commonly, spectrometer software contains a Bloch simulation module.

By choosing a suitable pulse shape, amplitude, and length it is possible to tailor a specific part of a spectrum. This is the basis for selective excitation experiments and therefore for all 1D variants of 2D procedures.

An ideal selective pulse should have some principal features: first, a good frequency selectivity, i.e. an almost uniform excitation in a limited spectral range and negligible effects on all spins outside this range; second, a uniform phase behaviour of the excited magnetization is often necessary, although small linear phase gradients are tolerable, since they can be compensated easily without spectral deterioration; third, the overall duration of a selective pulse should be as short as possible in order to minimize unwanted effects during the pulse (evolution of chemical shift and couplings, relaxation).

Taken from ref. [1]

2. Variants

There is a huge diversity of pulse shapes for different purposes published [1-4]. The commonly used shapes are: exponential shape or Gaussian shape (even cascades of Gaussian pulses), the families of BURP, SNOB, SEDUCE, VEGA shapes, and many more. Because many shapes are designed for specific cases one has often to differentiate between 90° excitation (i.e. rotation of magnetization from $+z$ to $-y$), 180° inversion (i.e. rotation from $+z$ to $-z$) or 180° refocusing (i.e. rotation from $+x$ to $-x$). The user has to decide which shape is the best one for his experiment by a practical test.

Here we show, as an example, the action of Gaussian-shaped and EBURP-shaped excitation pulses as a function of their lengths.

3. Pulse Scheme and Phase Cycle

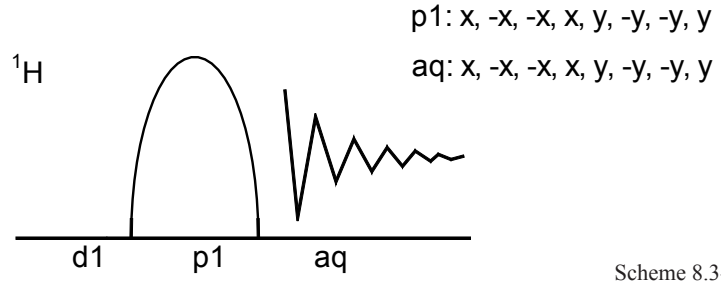

Scheme 8.3-1

Common values:

d1: relaxation delay
p1: 90° pulse length, determines the excitation band width wanted
spname: file name of the pulse shape created with software tool
sp: power amplitude, determines the flip angle of the shaped pulse

4. Acquisition

Special values used for the spectra shown:

Sample: 3 % strychnine in $CDCl_3$.
Time requirement: ca. 15 min
Spectrometer: Bruker AVANCE-700 with 5-mm-TCI cryo-probe

d1:	2s
ns:	1
aq:	3.0 s
td:	50,672
sw:	12 ppm
o1:	3.98 ppm (H-16) and 2.38 ppm (H-15)
spname:	Gauss1.1000 (Gaussian shape on 1.000 digital points), cf. Fig. 1
p1:	20.0 ms, 40.0 ms, and 60.0 ms (corresponds to excitation band widths of 106, 53 and 35 Hz)
sp:	54.14 dB, 60.16 dB, and 63.28 dB (calculated from 90° hard pulse, 8.1 µs at −6 dB)
spname:	EBURP2 (EBURP shape on 1.000 digital points), cf. Fig. 2
p1:	46.7 ms, 93.4 ms, and 141.5 ms (corresponds to excitation band widths of 106, 53, 35 Hz)
sp:	44.93 dB, 50.95 dB, and 54.55 dB (calculated from 90° hard pulse, 8.1 µs at −6 dB)

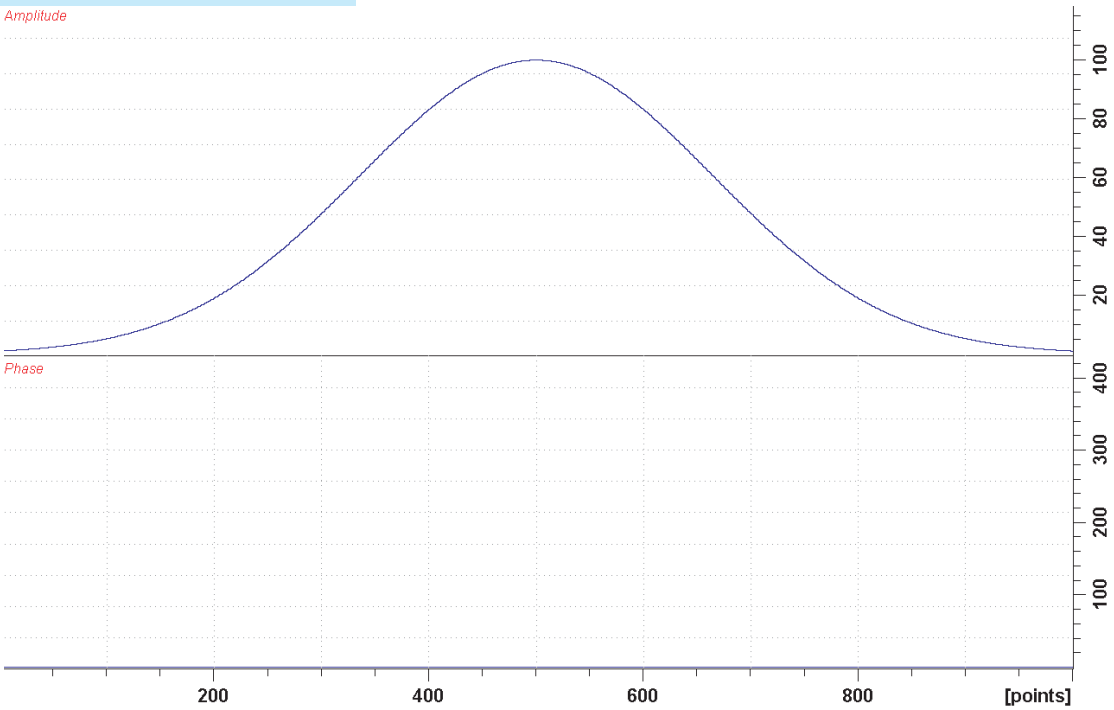

Fig. 8.3-1 Gaussian shape, upper trace amplitude, lower trace phase (picture taken from BRUKER TopSpin Vers. 3.1 software)

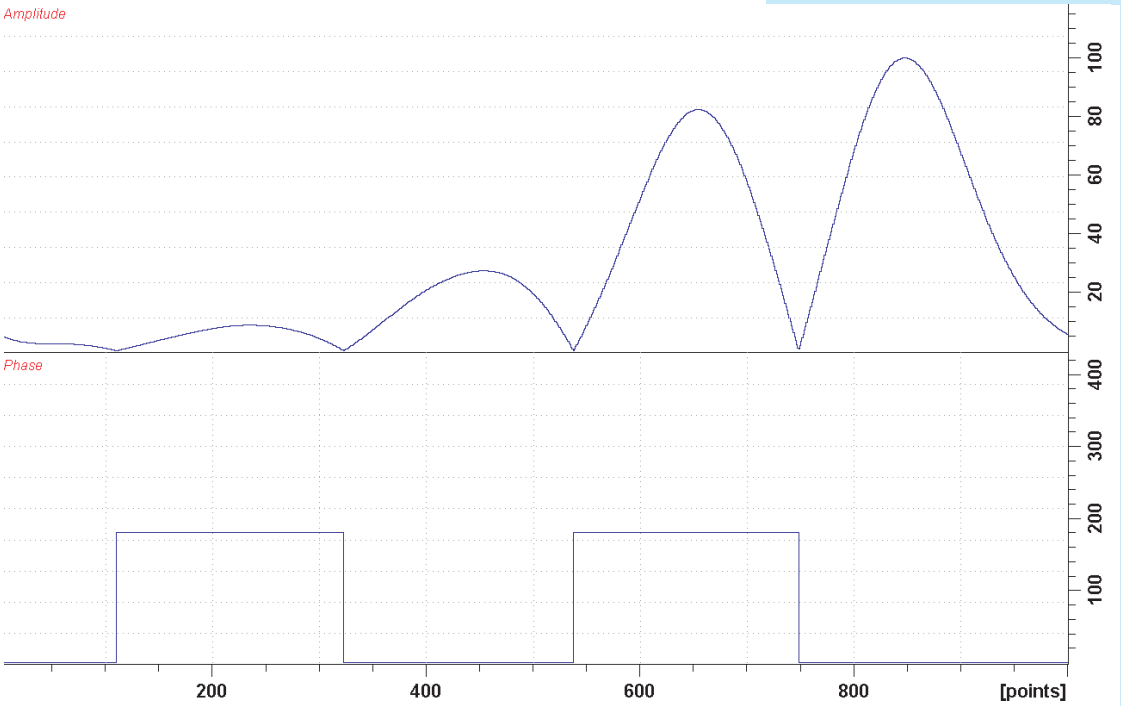

Fig. 8.3-2 EBURP2 shape, upper trace amplitude, lower trace phase (picture taken from BRUKER TopSpin Vers. 3.1 software)

5. Processing

Use standard 1D processing for ^{1}H NMR spectra with si = 64K and lb = 0.3.

6. Result

We show the selective excitation of H-16 in strychnine (Fig. 3 a,b) and of H-15 (Fig. 4 a,b). The different excitation effects of a Gaussian-shaped and an EBURP-shaped pulse, calculated with the same excitation band widths of 35 Hz, 53 Hz and 106 Hz, can be observed.

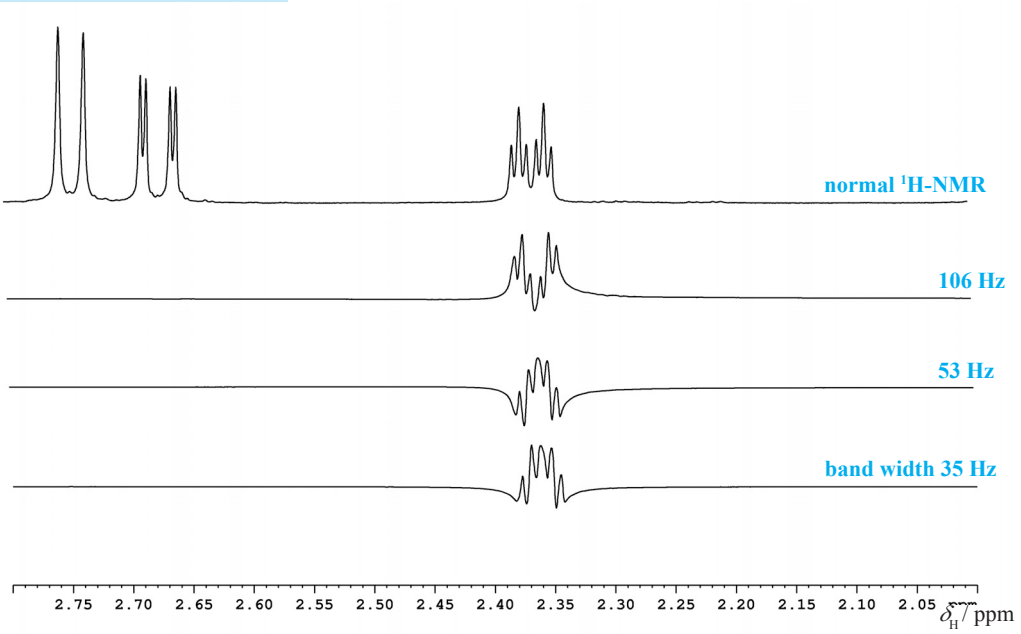

Fig. 8.3-3 Excitation of H-15α with a Gaussian shaped pulse with increasing excitation band widths of 35 Hz, 53 Hz and 106 Hz (bottom to top). Upper trace is the normal ^{1}H NMR spectrum.

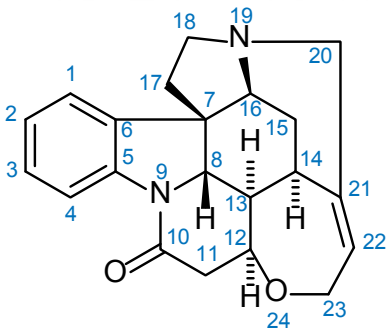

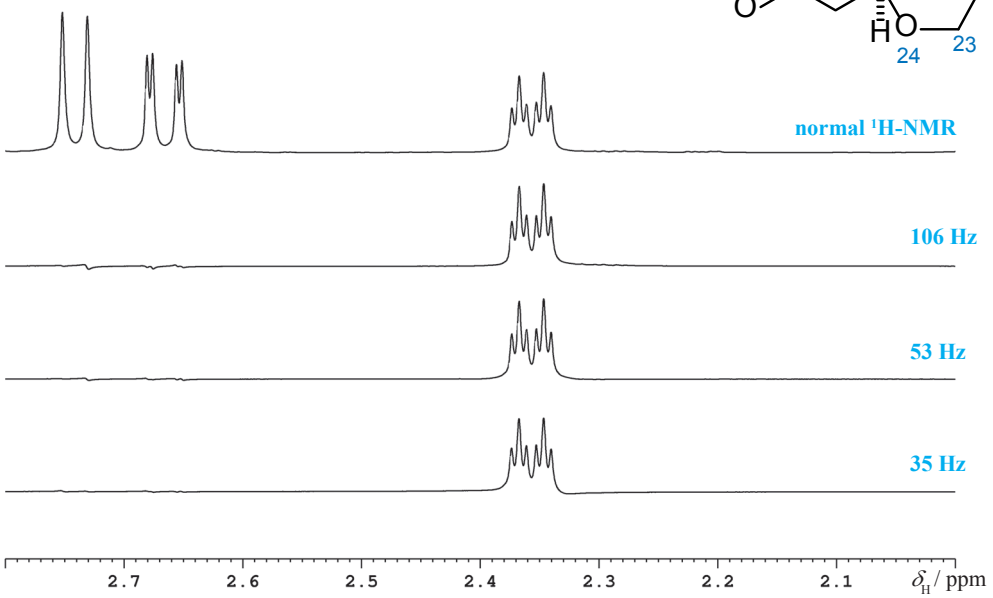

Fig. 8.3-4 Excitation of H-15α with an EBURP-shaped pulse with increasing excitation band widths of 35 Hz, 53 Hz, and 106 Hz (bottom to top). Upper trace is the normal ^{1}H NMR spectrum.

7. Comments

Because the length of the pulses is fixed by the excitation band width, the task is to vary the pulse power amplitude to find the 90° pulse. This can be done within a normal 1D experiment in chapter 8.1. The power variation should be done in small steps, because the dB scale is logarithmic. By a change of 3.01 dB the power is doubled, and, because of the square root dependency, the pulse length is halved by a change of 6.02 dB. On modern spectrometers linearity of the frequency-generating system is provided. If this is the case, the power amplitude of the shaped pulse can be recalculated by the spectrometer's software shape module on the basis of the known 90° hard pulse.

The Gaussian-shaped pulse is not as frequency selective as the EBURP-shaped pulse. This results in much shorter pulse lengths. For the same excitation band width of 35 Hz the Gaussian is 60 ms, but the EBURP 141.4 ms long.

Long selective pulses may have disadvantages because of relaxation problems, possible development of chemical shifts and *J* couplings during this time, and the fact that they are more difficult to fit within an existing multi-pulse sequence. On the other hand, the excitation profile of the EBURP is much better (i.e. box shape profile), which can be seen in Fig. 3 b, whereas a too short Gaussian pulse (i.e too broad excitation band width) introduces intensity and phase problems. These problems are diminished by using Gaussian cascade shapes (GaussQ3 or GaussQ5).

[1] H. Kessler, S. Mronga, G. Gemmecker "Multidimensional NMR experiments using selective pulses" *Magn. Reson. Chem*. **1991**, *29*, 527−557.

[2] J.-M. Bernassau, J.-M. Nuzillard "Clean selective excitation of heteronuclear spin systems" *J. Magn. Reson. Ser. A* **1993**, *104*, 212−221.

[3] R. Freeman *"Spin Choreography"*, Spektrum Academic Publishers, Oxford **1997**, 143−188.

[4] E. Lescop, T. Kern, B. Brutscher "Guidelines for the use of band-selective radiofrequency pulses in hetero-nuclear NMR: Example of longitudinal-relaxation-enhanced BEST-type ^{1}H–^{15}N correlation experiments" *J. Magn. Reson*. **2010**, *203*, 190–198.

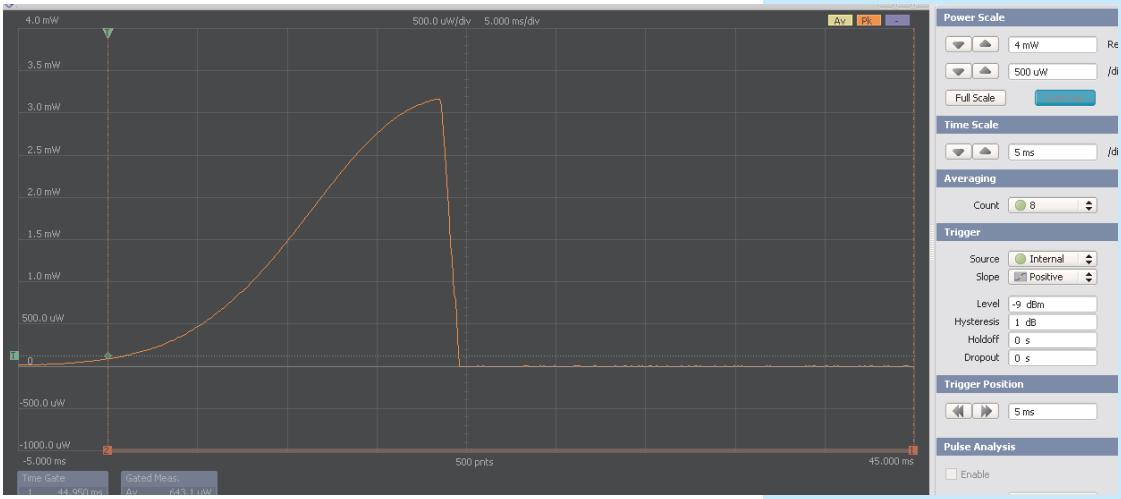

Fig. 8.3-5 Oscillograph photo of 30 ms half gauss pulse (envelope at 400 MHz)

8. Questions

A. Selective pulses can be "transition"-selective (i.e. a single line of a multiplet), "multiplet"-selective or "band"-selective. Give the typical band width in Hz and the typical spectroscopic application.

B. Very roughly one can estimate the excitation band width of a pulse by 1/(4*pw90) neglecting its shape. From this point of view, what is the band width of a 10 µs ^{13}C pulse and of a 2 ms ^{1}H pulse on the water resonance?

C. Shaped selective pulses can also be applied on the indirect channel. How large should a typical excitation band width be for a ^{13}C methyl group at the indirect channel?

9. Own Observations

Experiment 8.4

Adiabatic Pulses

1. Purpose

In contrast to the task of exciting a single resonance line in a small frequency region, there is on the other hand the problem to excite the total spectrum region uniformly. This is not trivial because a usual rectangular pulse yields, in principle, a *sinc* shape frequency profile. This function lowers its intensity to 90 % already at 1/4 of the distance to the next zero point, which is defined by 1/(pulse duration). To avoid this, one needs short pulses with high power, but this is technically limited. The problem arises particularly at high field spectrometers, measuring X nuclei, and using quite long 180° pulses. On a 700 MHz spectrometer, 200 ppm for ^{13}C NMR counts a frequency range of already 35 kHz.

One possibility to overcome the problem is the use of long pulses (in the range of some hundred µs) with their frequency not being constant but swept over a certain range (of some ten kHz) during the pulse time. If the frequency change of the carrier is slow compared to the effective r.f. frequency in the rotating frame (so called "adiabatic condition", [5]) the magnetization vector in the rotating frame follows the effective B_1 field and will be inverted slowly, starting at $+z$, ending at $-z$. This condition holds for a large frequency range. Because the increasing (or decreasing) frequency during the pulse reminds one of a bird's chirp, these pulses are also called "chirp pulses".

Adiabatic fast passage (1-3) is probably the most effective method for inverting nuclear spins over a wide frequency band. It also has the valuable property that the radiofrequency level is not critical, provided that it satisfies the adiabatic condition.

Taken from ref. [2]

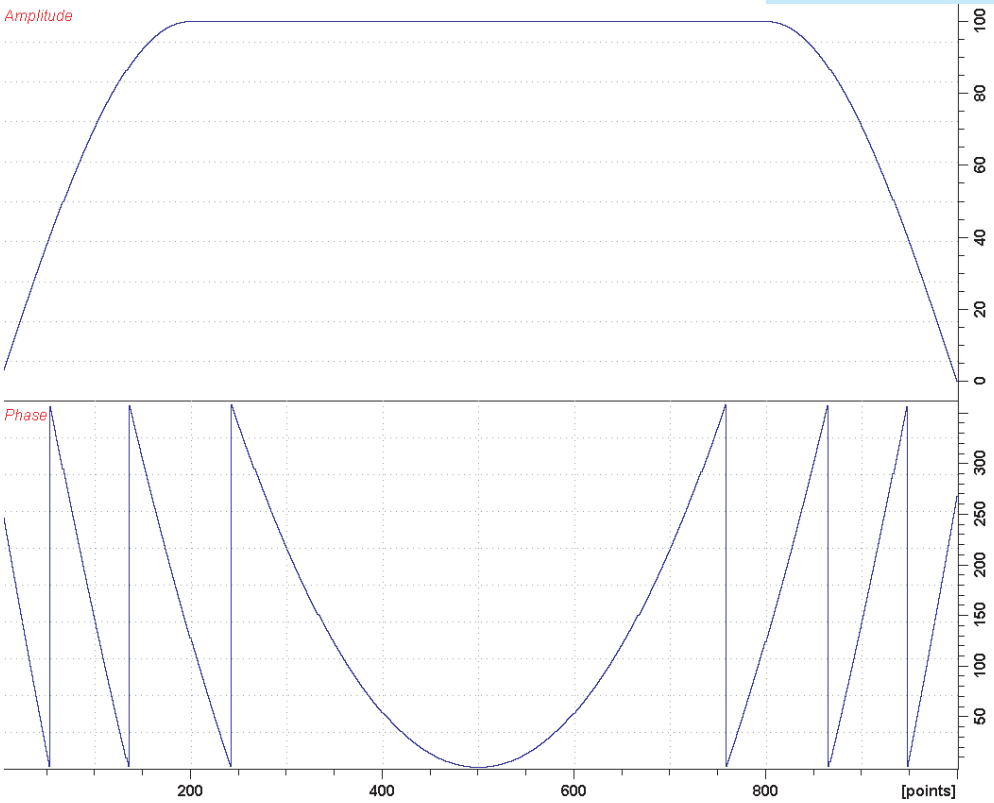

Fig. 8.4.-1 Pulse "Crp60,0.5,20.1" from Software Bruker Topspin 3.1 details see "4. Acquistion"

2. Variants

The amplitude of the adiabatic pulses can be modulated with functions such as *secans hyberbolicus, tangens hyperbolicus* [3], or may be smoothed on the beginning and the end with a modified *sinus* function (WURST shape [5]).

An adiabatic pulse gives a rotation about the *x* (or *y*) axis, starting the magnetization from +*z*, and ending in the *x,y* plane (excitation) or at the –*z* axis (inversion). For refocusing (starting and ending in the *x,y*-plane) one has to construct a special composite adiabatic pulse [4].

We demonstrate here the action of a "smoothed chirp pulse" from Bruker shape library for inversion of magnetization, compared to a usually used rectangular pulse.

3. Pulse Scheme and Phase Cycle

Common values:

d1: relaxations delay
p1: 180° adiabatic inversion pulse
p2: 90° transmitter pulse
spoff: offset of the p1 pulse

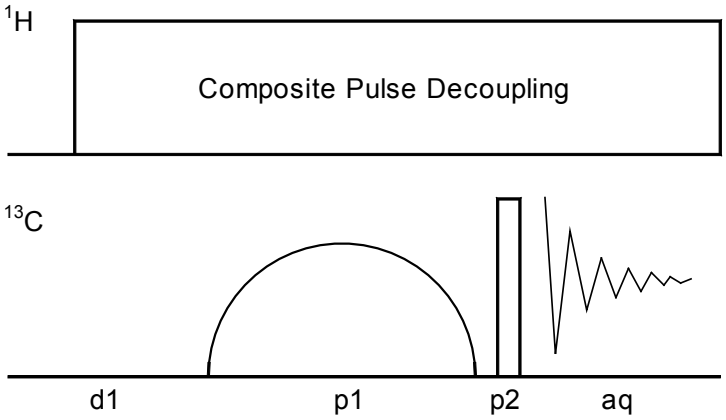

p1, p2, aq: x, -x, -x, x, y, -y, -y, y

Scheme 8.4-1

4. Acquisition

Special values used for the spectrum shown:

Sample: $CHCl_3$/ $CDCl_3$, 90/10 vol %
Time requirement: 2 * 15 min
Spectrometer: Bruker AVANCE-700 with 5-mm-TCI cryo-probe

d1:	20 s
sw:	30 ppm
o1:	77 ppm (on resonance on $CHCl_3$)
td:	10.590
aq:	1 s
p1:	a) rectangular shape, 800 points: 40 µs at 0.66 dB, b) adiabatic pulse: Crp60, 0.5, 20.1 (smoothed chirp, 60 kHz sweep, 20 % smoothing, 1000 points; from Bruker TopsSpin 2.1 shape library) length 500 µs at 2.77 dB
spoff:	offset is varying from +20 kHz to −20 kHz in 1 kHz steps (41 spectra)
p2:	11.7 µs at −4 dB
cpd:	WALTZ16, 80 µs at 11.8 dB

[1] J.-M. Böhlen, G. Bodenhausen "Experimental aspects of chirp NMR spectroscopy" *J. Magn. Reson. A* **1993** , *102*, 293–301.

[2] E. Kupce, R. Freemann "Adiabatic pulses for wideband inversion and broadband decoupling" *J. Magn. Reson. A* **1995**, *115*, 273–276.

[3] D. Rosenfeld, S. L. Panfil, Y. Zur "Design of selective adiabatic inversion pulses using the adiabatic condition" *J. Magn. Reson*. **1997**, *129*, 115–124.

[4] T.-L. Hwang, P. C. M. van Zijl, M. Garwood "Broadband adiabatic refocusing without phase distortion" *J. Magn. Reson*. **1997**, *124*, 250–254.

[5] M. Garwood, L. DelaBarre "The return of the frequency sweep: Designing adiabatic pulses for contemporary NMR", *J. Magn. Reson*. **2001**, *153*, 155–177.

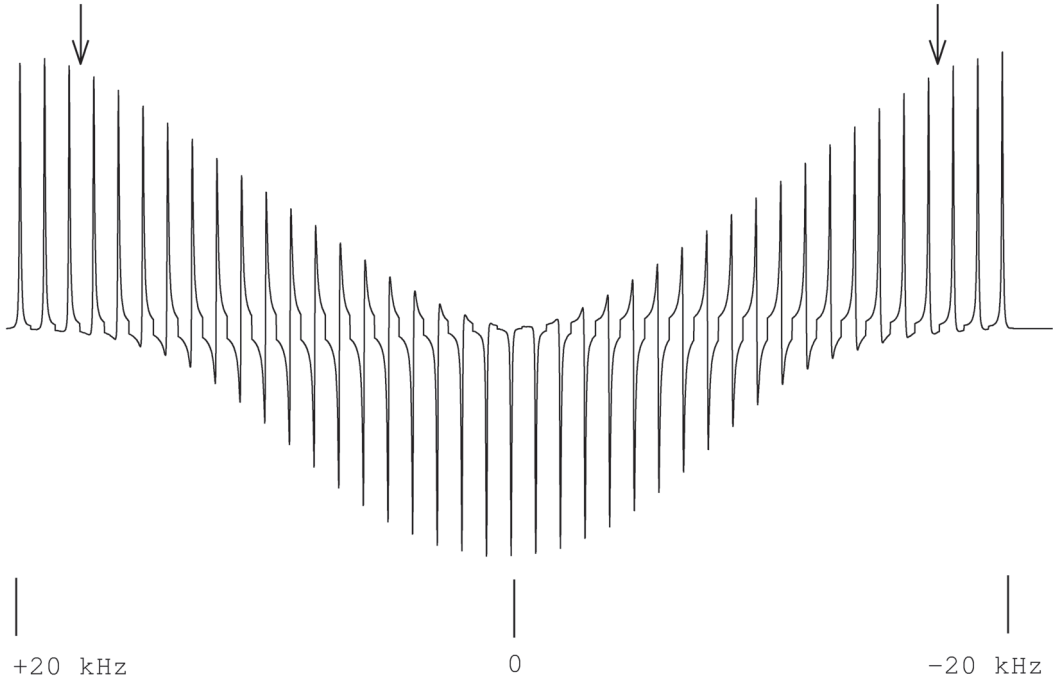

Fig. 8.4-2 Use of a rectangular-shaped 180° inversion pulse of 40 µs length, offset varying from +20 kHz to –20 kHz in 41 steps of 1 kHz. The arrows mark the range of 200 ppm of a ^{13}C NMR spectrum on a 700 MHz spectrometer.

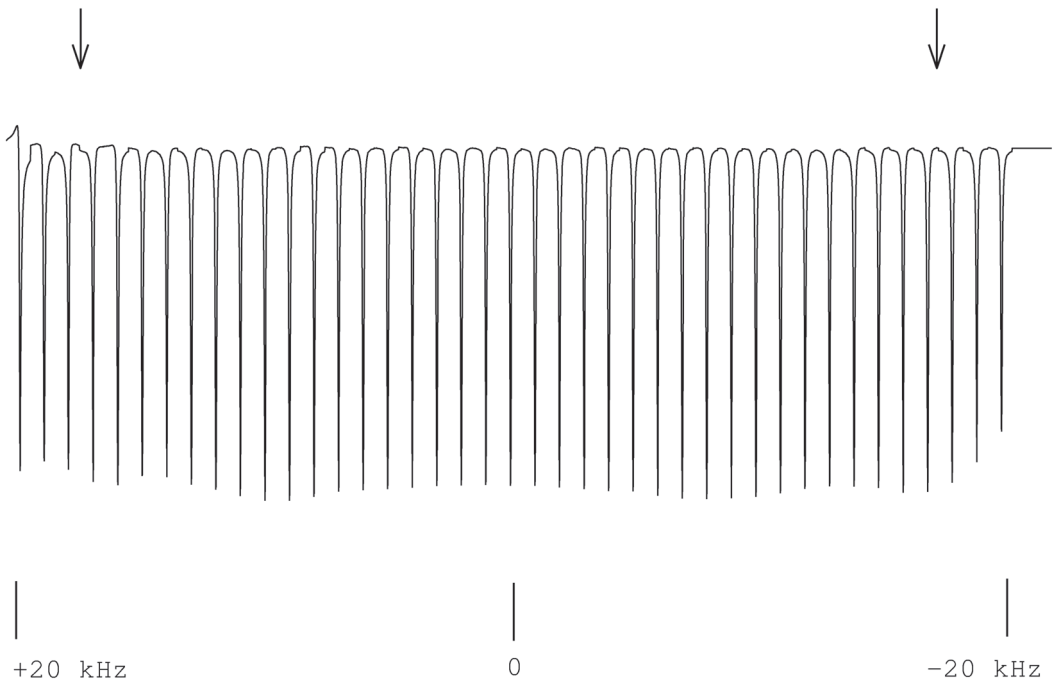

Fig. 8.4-3 Use of an adiabatic chirp 180° inversion pulse, offset varying from +20 kHz to –20 kHz in 41 steps of 1 kHz. The arrows mark the range of 200 ppm of a ^{13}C NMR spectrum on a 700 MHz spectrometer.

[6] E. Kupce "Applications of adiabatic pulses in biomolecular nuclear magnetic resonance" *Methods Enzymology* **2001**, *338*, 82−111.

[7] C. E. Hadden "Adiabatic pulses in ^{1}H–^{15}N direct and long-range heteronuclear correlations" *Magn. Reson. Chem*. **2005**, *43*, 330–333.

[8] H. Koskela, O. Heikkila, I. Kilpelainen, S. Heikkinen "Quantitative two-dimensional HSQC experiment for high magnetic field NMR spectrometers" *J. Magn. Reson*. **2010**, *202*, 24–33.

5. Processing

Use standard ^{13}C NMR processing with si = 8K and exponential weighting with lb = 2 Hz.

6. Result

We show an array of 41 spectra with a 40 µs rectangular 180° pulse and varying offset in 1 kHz steps (Fig. 8.4-2) and the same with an adiabatic Chirp-Pulse (Fig. 8.4-3)

7. Comments

It can be clearly seen that the 40 µs rectangular 180° pulse (i.e. 20 µs for 90°, which may be a realistic value on multiple channel inverse probe heads) inverts the magnetization from $+z$ to $-z$ axis only in a band width of about 14 to 15 kHz, which is too little for ^{13}C NMR even on a 400 MHz routine spectrometer. In contrast, the chirp pulse has a perfect performance over the 40 kHz band width tested here.

Therefore it is advisable to use the adiabatic inversion pulses even on a routine spectrometer, for instance in the APT, INEPT, DEPT, and all HSQC variants.

8. Questions

A. In thermodynamics the term "adiabatic" is very often used. What is its original meaning?

B. Prior to the use of frequency swept adiabatic pulses a different concept was used to remedy phase errors at large offsets. What were these pulses called?

9. Own Observations

Experiment 8.5

Temperature Calibration in NMR

1. Purpose

There are many NMR experiments that are performed at different temperatures or where the emphasis lies on the measurement of a temperature-dependent effect. Hence, it is most important to know whether the temperature controller of the instrument gives a correct reading of the actual temperature within the sample. However, since the electronic temperature measurement and its regulation is not done within the sample, but necessarily at a certain point below the sample tube, there will always be a difference between the temperature reading and the actual temperature of the liquid part within the r.f. coil. Here we restrict the description to the most common low-temperature standard, methanol, and the most common high-temperature standard, 1,2-ethanediol, where the chemical shift difference between the OH proton and those of the methyl group or methylene group is used for the calibration. Since neither sample works for cryoprobes due to radiation damping effects we include a temperature calibration using deuteromethanol.

2. Variants

The problem of temperature measurement and calibration is as old as NMR spectroscopy itself. Many different calibration samples have been proposed throughout the decades, working at different temperature ranges, for different nuclides and specialized for different probe heads. The literature [1-11] recommends different techniques and standards for different nuclides in the solid and liquid states. Recently, the Bruker company introduced temperature measurements via the lock channel.

3. Pulse Scheme and Phase Cycle

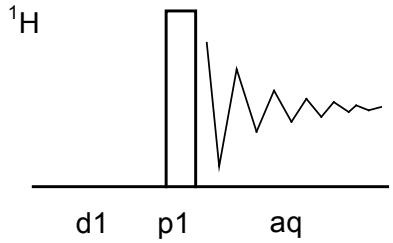

p1: x, x, -x, -x, y, y, -y, -y

aq: x, x, -x, -x, y, y, -y, -y

Scheme 8.5-1

Common values:

d1 relaxation delay
p1 45° ^{1}H transmitter pulse

4. Acquisition

Special values used for the spectrum shown:

Sample below room temperature: 4 % MeOH in [D_4]methanol containing a trace of HCl.
Sample above room temperature: 80 % 1,2-ethanediol in [D_6]DMSO
Time requirement: 1 h for each temperature range
Spectrometer: Bruker AM-400, 5 mm BBO probe

Load standard ^{1}H parameters and connect the low-temperature equipment for your instrument.

Adjust for stable nitrogen gas flow and set the temperature controller in turn to 193, 223, and 273 K. Let each temperature equilibrate for at least 10 min. Measure at each temperature the chemical shift difference $\Delta\delta$ between the two methanol signals.

td: 32K
sw: 8 ppm
aq: 4 s
o1: middle of ^{1}H NMR spectrum
p1: 45° ^{1}H transmitter pulse
d1: 600 s
ns: 1

5. Processing

Use standard 1D processing.

6. Result

a) Low temperature

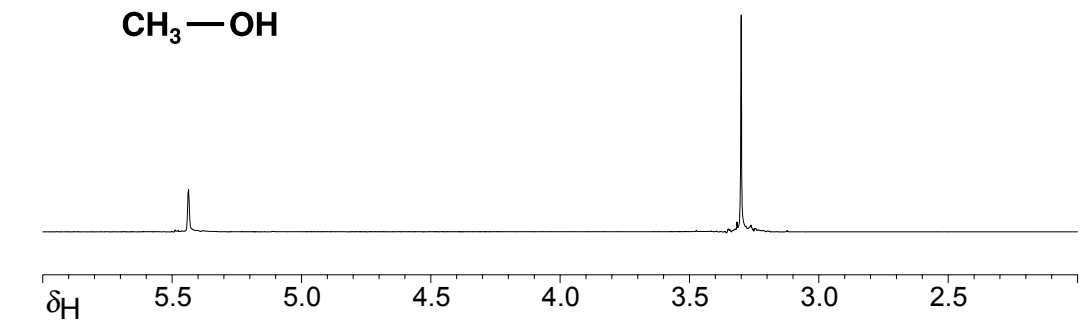

Fig. 8.5-1 ^{1}H NMR spectrum of 4 % methanol in CD_3OD

The Figure shows the result obtained on an AM-400 spectrometer with the temperature unit set to 223 K. A difference of 2.136 ppm between the two signals was measured. Compare the values with those given in the instrument manufacturer's calibration curve or compute the result using the equations given below. Recent instruments provide temperature calculation programs which automatically measure the chemical shift difference $\Delta\delta$ and compute from this difference the sample temperature. The calibration curve shown in the Fig. 8.5-2 1 was drawn using the following equations:

a) For $\Delta\delta$ from 1.4965 to 1.76: $T\,[\mathrm{K}] = -114.83\,\Delta\delta + 471.85$

b) For $\Delta\delta$ from 1.76 to 2.08: $T\,[\mathrm{K}] = -125\,\Delta\delta + 490$

c) For $\Delta\delta$ from 2.08 to 2.43: $T\,[\mathrm{K}] = -140\,\Delta\delta + 521.33$

Below the temperature range covered by methanol one may use a calibrated Pt-100 resistor fixed in a dummy NMR sample, with the r.f. transmitter switched off (see Fig. 8.5-7).

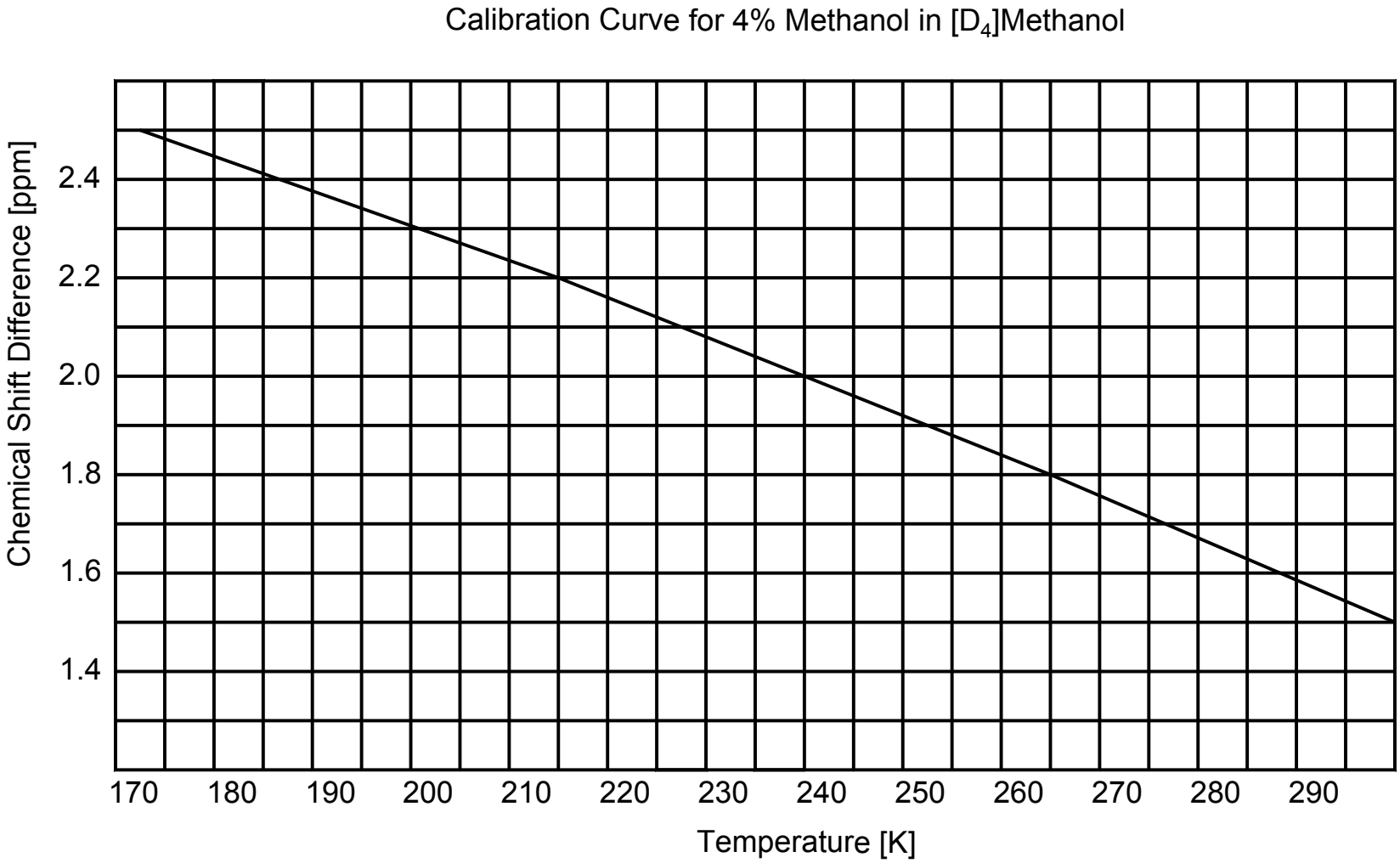

Fig. 8.5-2 Chemical shift differences of methanol vs temperature

b) High temperature

Use the same spectral parameters.

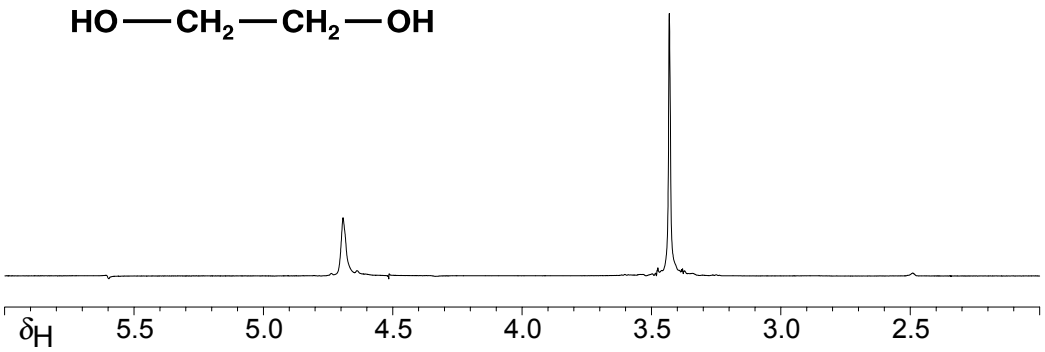

Fig. 8.5-3 ^{1}H NMR spectrum of ethanediol in DMSO-d_6

The figure shows the result obtained on an AM-400 spectrometer with the temperature unit set to 330 K. A difference of 1.262 ppm between the two signals was measured.

Compare the values with those given in the instrument manufacturer's calibration curve or compute the result using the equation given below. The calibration curve shown in Fig. 8.5-5 was drawn using the following equation:

$$T\,[\mathrm{K}] = -108.33\ \Delta\delta + 460.41$$

Fig. 8.5-4 Typical set up for low-temperature NMR measurements

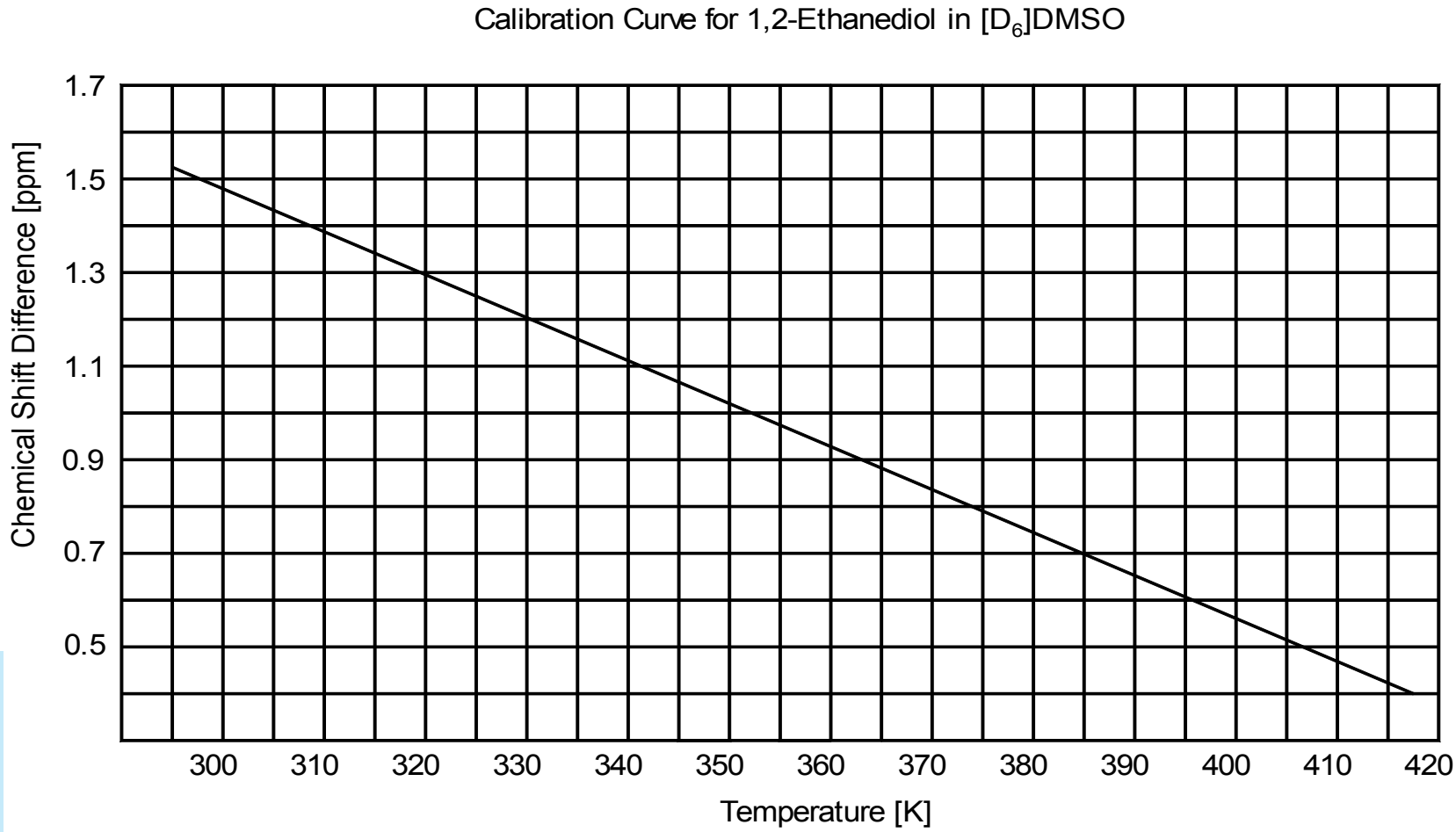

Fig. 8.5-5 Chemical shift differences of ethanediol vs temperature

c) Using a Cryoprobe

Due to the high sensitivity of a cryo probe neither sample used above can be applied, since radiation damping causes severe line broadening and chemical shift deviations. We recommend instead the use of per-deuterated methanol, sealed, but **not** under vacuum to avoid boiling at higher temperatures [10]. The indicator is the chemical-shift difference between the residual OH and CHD_2 signals, which works for such a sample between 282 and 330 K, where the lower temperature limit is dictated by the cryoprobe.

The chemical shift difference is given by the equation

$$T\,[\mathrm{K}] = -16.7467 \times (\Delta\delta)^2 - 52.5130 \times (\Delta\delta) + 419.1381$$

In Figure 8.5-6 a stacked plot is shown for the temperatures between 290 and 330K measured on an Avance-700 spectrometer equipped with a cryoprobe.

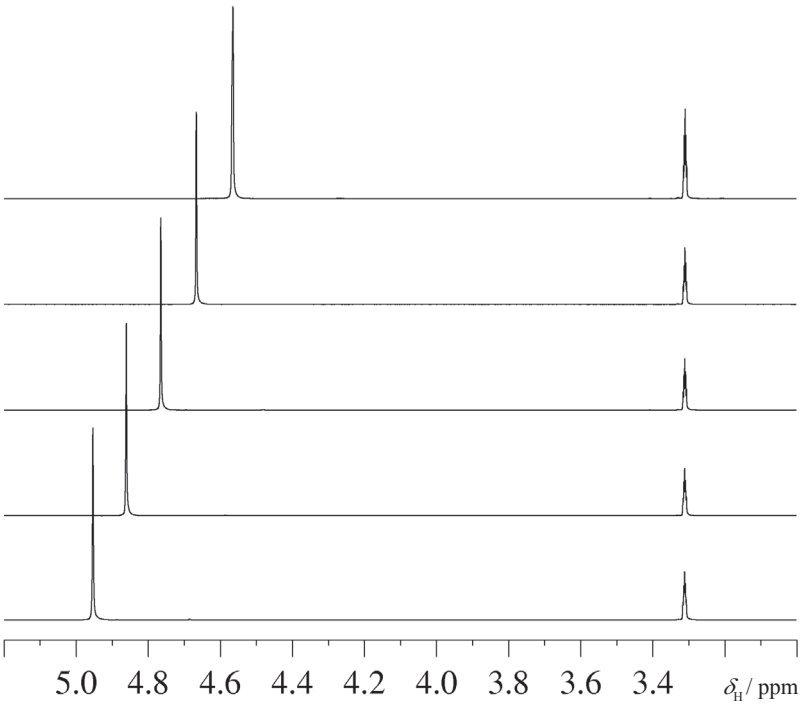

Fig. 8.5-6 ^{1}H NMR spectra of CD_3OD at different temperatures

7. Comments

In principle, a long narrow cylinder, like an NMR sample, surrounded by a gas flow cannot be held at a very accurate and stable temperature compared to the performance of a large temperature water or oil bath as used in chemical kinetics. Temperature gradients in the sample are likely. Nevertheless, modern NMR instrumentation gives reasonably reproducible results if enough time is allowed for temperature equilibration. Your temperature readings should not deviate by more than 1 to 2 K from the calibration curve and should be reproducible in

[1] A. L. van Geet, "Calibration of methanol nuclear magnetic resonance thermometer at low temperature" *Anal. Chem*. **1970**, *42*, 679−680; "Calibration of the methanol and glycol nuclear magnetic resonance thermometers with a static thermistor probe" *ibid*. **1968**, *40*, 2227−2229.

repeated measurements. It is the experience of the authors that around room temperature the agreement between the thermocouple of the NMR spectrometer and the internal measurement with the methanol sample is fairly satisfactory, but deviates considerably when one works at rather low temperatures.

Fig 8.5-7 A Pt-100 resistor in an NMR tube filled with silicon oil for measuring temperature *in situ*

DNMR Spectroscopists Unite!
Dear Barry:
This is a call for action addressed to the subsection of the nmr community interested in variable-temperature work.
It seems hardly necessary to bewail once again the sad state of affairs regarding commercially available variable temperature probes. Whereas the instrument companies have over the years made a commendable effort to keep abreast of engineering developments in magnet design and in electronics, the construction of really satisfactory variable-temperature equipment has received no more than slighting attention. I rather suspect that Leonardo (the inventor of the valve flush toilet, remember?) could have done almost as well. In fact, some of the (supposedly improved) designs I recently had an opportunity to inspect struck me as positively Stone Age.
I happen to believe that this constitutes the only serious bottleneck still remaining in the area and that there can be no genuine progress unless and until it is removed. Those who hold this to be an idiosyncrasy of mine are encouraged to read what the Nestor par excellence of dynamic nmr, Herb Gutowsky, has to say about the situation (cf. the last paragraph of his chapter for the recent Academic Press book, edited by L. M. Jackman and F. A. Cotton).

Gerhard Binsch (1934−1993), taken from *TAMU Letters* **1975**, *203*, 21.

[2] C. Piccinni-Leopardi, O. Fabre, J. Reisse, "Determination of $\Delta H^{\#}$ and $\Delta S^{\#}$ by simultaneous ^{1}H and ^{13}C dynamic n.m.r. studies: Importance of the accuracy of temperature measurement" *Org. Magn. Reson*. **1976**, *8*, 233−236.

[3] J. Bornais, S. Brownstein, "A Low-Temperature thermometer for ^{1}H, ^{19}F, and ^{13}C" *J. Magn. Reson*. **1978**, *29*, 207−211.

[4] H. Friebolin, G. Schilling, L. Pohl, "A new method for the temperature determination in NMR spectrometers" *Org. Magn. Reson*. **1979**, *12*, 569−573.

[5] F. H. Köhler, X. Xie, "Vanadocene as a temperature standard for ^{13}C and ^{1}H MAS NMR and for solution-state NMR spectroscopy" *Magn. Reson. Chem*. **1997**, *35*, 487–492.

[6] H. Quast, M. Heubes, A. Dunger, H. H. Limbach, "A high-precision carbon-13 shift thermometer for the temperature range 100–300 K" *J. Magn. Reson*. **1998**, *134*, 236–244.

[7] W. H. Sikorski, A. W. Saunders, H. J. Reich, "Tris(trimethylsilyl) methane as an internal ^{13}C NMR chemical shift thermometer" *Magn. Reson. Chem*. **1998** *36*, S118–S124.

[8] A. G. Webb, "Temperature measurements using nuclear magnetic resonance" *Ann. Rep. NMR Spectrosc*. **2002**, *45*, 1–67.

[9] N. M. Loening, J. Keeler, "Temperature accuracy and temperature gradients in solution-state NMR spectrometers" *J. Magn. Reson*. **2002**, *159*, 55–61.

[10] M. Findeisen, T. Brand, S. Berger "A ^{1}H-NMR thermometer suitable for cryoprobes" *Magn. Reson. Chem*. **2007**, *45*, 175–178.

[11] X. Guan, R. E. Stark "A general protocol for temperature calibration of MAS NMR probes at arbitrary spinning speeds" *Solid State NMR* **2010**, *38*, 74–76.

8. Questions

A. Consider that from the coalescence point at 340 K a $\Delta G^{\#}$ value is estimated using the usual equation

$$\Delta G^{\#}(T_C) = RT_C\left[22.96 + \ln\left(\frac{T_C}{\Delta\nu}\right)\right]$$

by assuming a $\Delta\nu$ value of 200 Hz. How large is the error in $\Delta G^{\#}$, if the actual temperature of the sample is 5°C off from the indicated temperature?

B. Why are cryo probes usually limited to temperatures above 273 K?

C. Which solvents can be used at temperatures below 173 K?

9. Own Observations

Experiment 8.6

Calibration of Pulsed Field Gradients

1. Purpose

For all experiments working with pulsed field gradients, the gradient strength first has to be known in order to get meaningful results. In particular this holds for diffusion experiments like DOSY, see chapter 5.4. The present experiment describes a calibration routine.

Secondly, in all experiments with coherence selection by pulsed field gradients, Equation (1) must be obeyed. In this equation the terms p_i, the coherence orders present at the instant of the pulsed field gradient, are multiplied by the gyromagnetic ratios γ_i of the corresponding nuclei and the effective field strengths G_i of the gradient pulses.

Common values

p1, p2: 90° and 180° ^{1}H transmitter pulses
d1: relaxation delay
d2: gradient length g1
d3: short delay
g2: length of g1 + d3

$$\sum p_i \gamma_i G_i = 0 \qquad (1)$$

In order to fulfill this equation, the gradient strengths of either sign must be accurate and reproducible. A simple test provided in this experiment checks whether positive and negative gradient pulses have the same effect, and thus detects any imbalance of the hardware.

Finally, pulsed field gradients cause eddy currents in the surrounding conducting material and thus a certain dead time after the gradient pulse is needed. Within this dead time the signal should not be acquired, nor should other r.f. pulses be applied. The length of the gradient dead time is very much dependent on the design of the gradient coils. We show a calibration routine to define a suitable ring down delay.

2. Variants

Instead of working with pulsed field gradients, one can achieve similar results also with r.f. spinlock pulses, formerly called "Poor Man's Gradients" (PMG) [6].

3a. Pulse Scheme and Phase Cycle

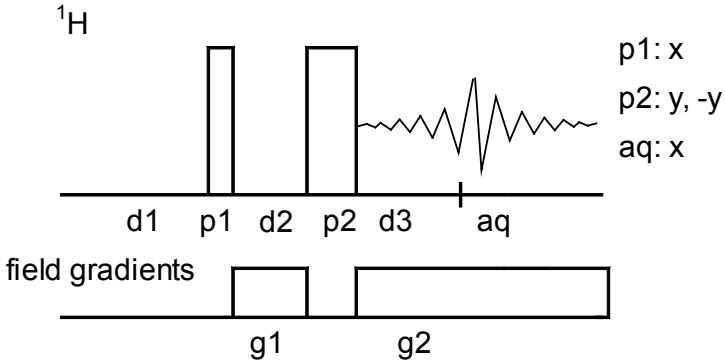

Scheme 8.6-1

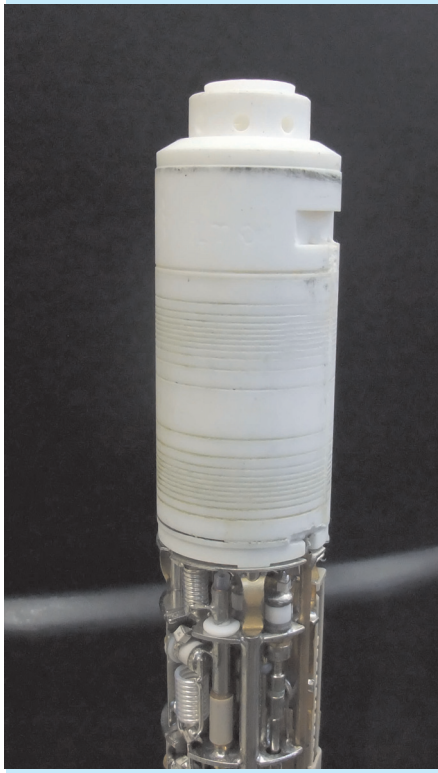

Fig. 8.6-1 Ceramic device supporting the gradient coil

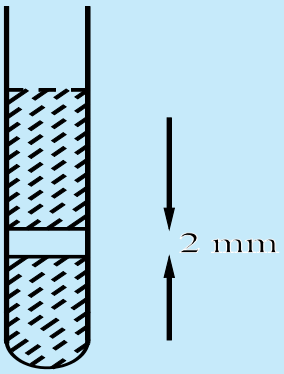

Scheme 8.6-2

4a. Acquisition

Special values used for the spectrum shown:

Sample: Prepare a special calibration sample as shown. In a 5 mm NMR tube, two layers of normal water are separated by a rubber or Teflon disk of 2 mm thickness. The tube should be adjusted in the magnet in such a way that this disk is situated in the center of the r.f. coil. No sample spinning should be applied.

Time requirement: 20 min

Set the instrument to normal ^{1}H NMR operation

td:	2K
sw:	75 kHz
aq:	13.67 ms
o1:	on resonance of water signal
p1:	90° ^{1}H transmitter pulse
p2:	180° ^{1}H transmitter pulse
d1:	1 s
d2:	6.83 ms
d3:	1 ms
g1:	pulsed field gradient, rectangular shape, duration = 6.83 ms, strength to be varied
g2:	pulsed field gradient, rectangular shape, duration = 7.83 ms, same strength as g1.
ns:	1

First record a normal ^{1}H spectrum without gradients, then increase the gradient strength in several steps and observe the dip in the water signal.

5a. Processing

Use standard ^{1}H processing with an exponential window (lb = 20 Hz); however, apply magnitude calculation. Measure the width of the dip [Hz], and calculate the gradient strength G_z according to Equation (2).

$$G_z = \frac{\Delta\omega}{\gamma\,\Delta z} = \Delta\nu \cdot 1.17 \cdot 10^{-5} \qquad (2)$$

where $\Delta\omega$ is 2π times the width of the dip [Hz], γ is the proton gyromagnetic ratio ($26.751 \cdot 107$ $T^{-1}s^{-1}$) and Δz is the thickness of the disk (0.002 m). Equation (2) gives the gradient strength in Tesla/m, which may be converted to Gauss/cm as often used in the literature by multiplying by 100, i.e. 0.1 T/m corresponds to 10 G/cm.

6a. Result

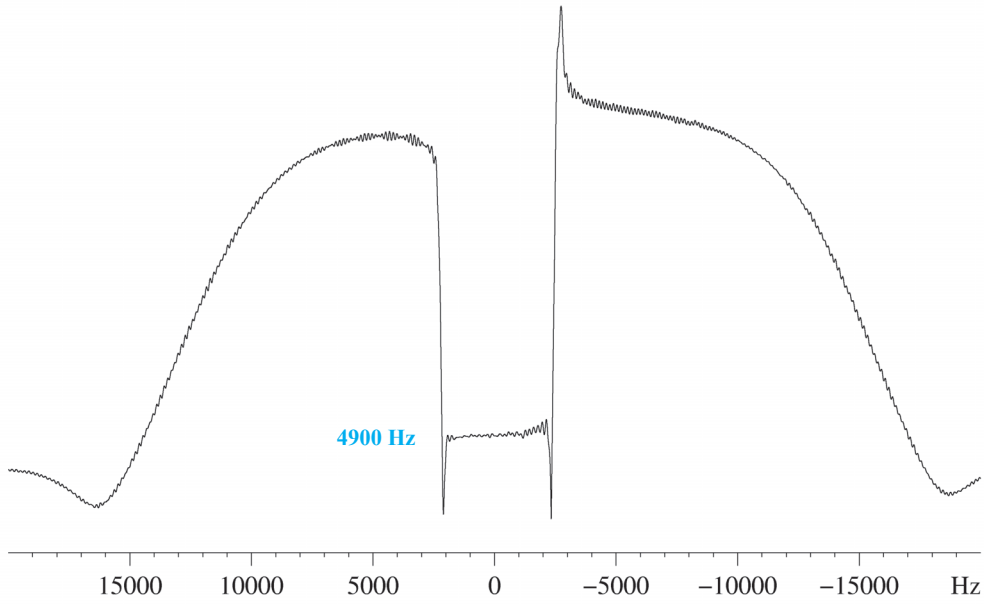

Fig. 8.6-2 ^{1}H NMR spectrum of the phantom sample

The figure shows the result obtained on a DRX-400 spectrometer equipped with a BBO probe. The measurement of the dip is indicated. In this spectrum a gradient of about 0.057 T/m (corresponding to 10 % of maximal value of the gradient system used) was applied.

3b. Pulse Scheme and Phase Cycle

Sign test for the gradient amplifier

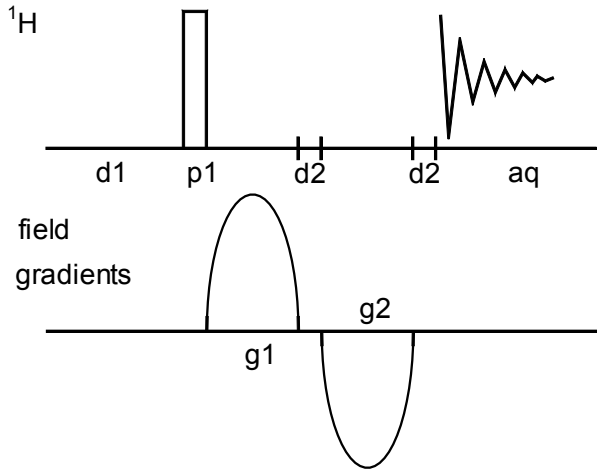

p1: x, x, -x, -x, y, y, -y, -y
aq: x, x, -x, -x, y, y, -y, -y

Scheme 8.6-3

Common values

p1 90° ^{1}H transmitter pulse
d1 relaxation delay
g1, g2 pulsed field gradients
d2: short delay (ring down)

4b. Acquisition

Sample: 10 % $CHCl_3$ in [D_6]acetone with added $Cr(acac)_3$.
Time requirement: 20 min

Set the instrument to normal ^1H NMR operation.

td: 4K
aq: 4.1 s
sw: 500 Hz
o1: on resonance of $CHCl_3$ signal
p1: 30° ^1H transmitter pulse
d1: 5 s
d2: gradient ring-down delay [100 µs]
g1: positive pulsed field gradient, approximately 0.1 T/m, duration 1 ms, sinusoidal shape
g2: negative pulsed field gradient, approximately 0.1 T/m, duration 1 ms, sinusoidal shape, strength to be varied
ns: 1

First record an ^1H NMR spectrum with identical gradients but of opposite sign. Vary the strength of the second gradient within a ± 1 % range in 0.1 % steps of the first and note the signal change. Use other strengths and shapes for both gradients to study the influence of these parameters.

5b. Processing

Use standard ^1H processing.

6b. Result

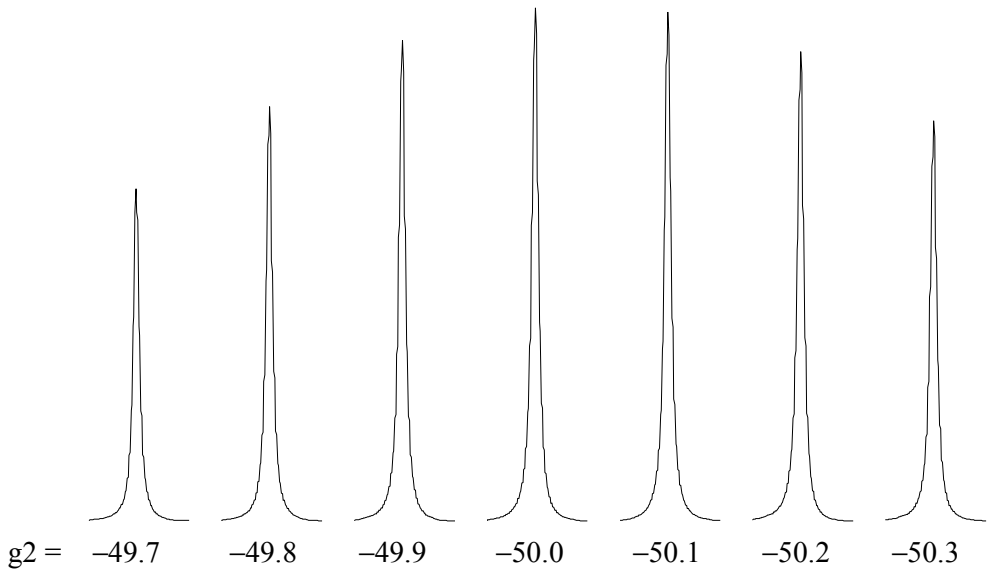

Fig. 8.6-3 Values of g2 amplitude in % of maximum value

The figure shows a series of signals obtained on an AMX-500 spectrometer equipped with an inverse gradient probe with self-shielded gradients. g1 was set to +50.0 (relative units) and g2 was varied in steps of 0.1 from −49.7 to −50.3. Note that the result is slightly asymmetrical and that therefore the zero point of the gradient amplifier has to be more carefully adjusted.

3c. Pulse Scheme and Phase Cycle

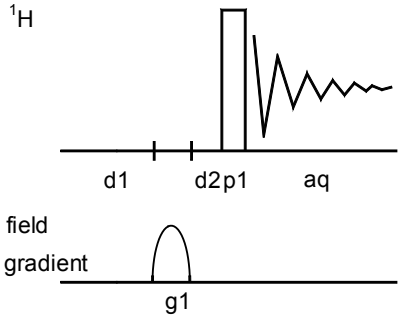

p1: x, x, -x, -x, y, y, -y, -y
aq: x, x, -x, -x, y, y, -y, -y

Scheme 8.6-4

Common values

p1: ^{1}H transmitter pulse
d1: relaxation delay
d2: ring-down delay

4c. Acquisition

Ring-down delay

Sample: 10 % $CHCl_3$ in [D_6]acetone with added $Cr(acac)_3$.
Time requirement: 20 min

Set the instrument to normal ^{1}H NMR operation.

td: 4K
aq: 4.15 s
sw: 500 Hz
o1: on resonance of $CHCl_3$ signal
p1: 30° ^{1}H transmitter pulse
d1: 5 s
d2: 1 s to 1 µs, to be varied
g1: pulsed field gradient, sinusoidal shape on 100 points, duration = 1 ms, strength to be varied
ns: 1

First record a normal ^{1}H NMR spectrum without a gradient, then use a sinusoidal or otherwise shaped gradient with approximately 0.1 T/m field strength using d2 = 1 s. The signal should have identical intensity to that of the normal ^{1}H NMR spectrum. Reduce d2 until the intensity drops significantly. At this point reduce the gradient strength and change the gradient shape to observe the influence of these parameters.

5c. Processing

Use standard ^{1}H processing.

6c. Result

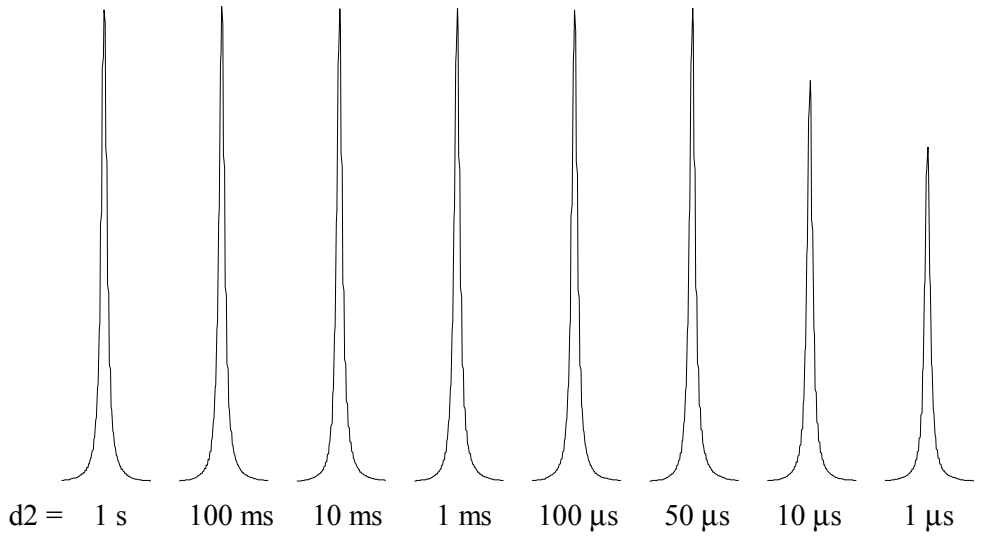

Fig. 8.6-4 ring-down delay d2

The figure shows a series of signals obtained on an AMX-500 spectrometer equipped with an inverse gradient probe with self-shielded gradients. A ring-down delay of 50−100 µs seems to be appropriate for the configuration used. When a rectangular gradient was used, the decrease of the signal was already visible with d2 = 100 µs.

7. Comments

The experiment **a)** as described works only for superconducting magnets since the direction of the magnetic field B_o is vertical, i.e., along the axis of the sample tube, and the field gradient is in the same *z*-direction. Care should be taken for good shimming to avoid overlaying shim gradients.The resonance frequency of a proton in the presence of a *z*-gradient is given by Equation 3.

(3)

$$\omega_z = \gamma B_{\text{eff}} = \gamma \left[B_o + B_z\right]$$

Thus the resonance frequency of the proton is dependent on its *z*-position. A linear field gradient G_z can be defined as in Equation 4.

(4)

$$G_z = \frac{B_{z1} - B_{z2}}{\Delta z} = \frac{\Delta\omega}{\gamma \Delta z}$$

Using a sample such as the one described above with well-defined points z_1 and z_2 determined by the thickness of the Teflon disk, one can measure an image of the water distribution in the tube from a gradient spin-echo experiment and calculate from this image the strength of the gradients.

This experiment can be thought of as a normal spin-echo sequence (see Exp. 5.2), where in addition a gradient is switched on after the first 90° pulse. For technical reasons, however, the gradient pulse is divided into

two, so that the 180° r.f. pulse can be inserted in between. Each spin is spatially labelled by its resonance frequency, thus giving an image of the water distribution within the sample. The 180° pulse refocuses all magnetizations so that the spin-echo builds up to a maximum at a time d2 after the 180° pulse. To avoid oscillations, acquisition is started only after d3. The pulse sequence can be derived from those for automatic *z*-gradient shimming procedure usually delivered within the spectrometer's library.

For most coherence selection experiments such as HMBC the performance shown is quite adequate. For an excellent water suppression using gradients, a more rigorous adjustment would seem to be appropriate.

Pulsed field gradients can be generated by gradient coils that are mounted on the shim system or within the probe head. Recent instruments use self-shielded gradient coils [2], where in the outer part of the assembly a field opposing the one in the inner part is generated. The necessary ring-down delay is very dependent on the gradient shape. If gradients are used within the spin coupling evolution time a rather short ring-down is not necessary, since the spin coupling period is usually longer than the sum of gradient pulse duration and ring-down delay.

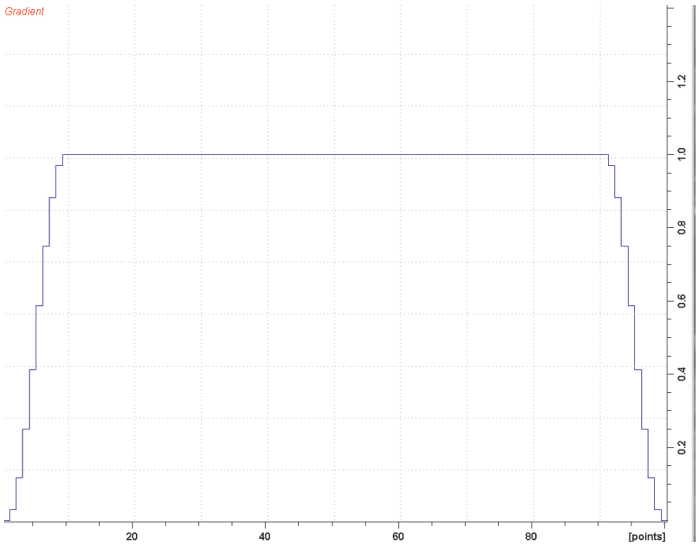

Fig. 8.6-5 Shape of a smoothed square gradient pulse, taken from BRUKER Top Spin Vers. 3.1. software

[1] M. I. Hrovat, C. G. Wade "NMR pulsed-gradient diffusion measurements. I. Spin-echo stability and gradient calibration" *J. Magn. Reson*. **1981**, *44*, 62−75.

[2] P. Mansfield, B. Chapman "Multishield active magnetic screening of coil structures in NMR" *J. Magn. Reson*. **1987**, *72*, 211−223.

[3] M. Holz, H. Weingärtner "Calibration in accurate spin-echo self-diffusion measurements using ^{1}H and less-common nuclei" *J. Magn. Reson*. **1991**, *92*, 115−125.

[4] J. Keeler, R. T. Clowes, A. L. Davis, E. D. Laue "Pulsed-field gradients: Theory and practice" *Methods Enzym*. **1994**, *239*, 145−207.

[5] M. Czisch, A. Ross, C. Cieslar, T. A. Holak "Some practical aspects of B_0 gradient pulses" *J. Biomol. NMR* **1996**, *7*, 121−130.

[6] G. Gasmi, G. Massiot, J. M. Nuzillard "Improvement of HSQC and HMBC experiments by J-modulation, T_1-noise reduction and spectral domain selection. Application to the study of nosiheptide" *Magn. Reson. Chem*. **1996**, *34*, 185−190.

8. Questions

A. The pulse scheme of experiment 8.6a can in principle also be used to generate an image of the excitation pattern of a selective pulse. One would use a normal water sample instead of the sample with a disk used here. Draw the appropriate pulse sequence.

B. Would the experiment 8.6b work with a 180° pulse between the two gradients and both gradients with the same sign?

C. Are very short ring-down delays necessary if a gradient is applied at the beginning of a spin coupling evolution period?

9. Own Observations

Answers Chapter 1

1.1 ^{1}H NMR

A. H-4 has the longest relaxation time

B. ABCD

C. Roof effect

D. This is regulated by the Karplus equation, which predicts a very small vicinal spin coupling in cases where the dihedral angle will be close to 90°.

1.2 APT-^{13}C-NMR

A. R. R. Ernst published a calculation for an optimal pulse angle as a function of repetition time and relaxation time in an FT NMR experiment. This Ernst angle gives the optimum signal-to-noise ratio in a given time under these boundary conditions. See: R. R. Ernst, W. A. Anderson "Application of Fourier Transform Spectroscopy to Magnetic Resonance" *Rev. Sci. Instr*. **1966**, *37*, 93−102.

B. This is the $^{1}J_{CH}$ spin coupling constant. A compromise value of 145 Hz is usually chosen.

C. Composite pulse decoupling means a train of r.f. pulses of different lengths and different phases in a certain "rhythm". One of these schemes has been dubbed WALTZ-16, see A. J. Shaka, J. Keeler, T. Frenkiel, R. Freeman "An improved sequence for broadband secoupling: WALTZ-16" *J. Magn. Reson*. **1983**, *52*, 335−338.

D. Deuterium has the spin I =1, and therefore the carbon signal splits into three lines in accordance with I_z = −1, 0, +1 of the deuterium spin with ratio nearly 1:1:1. One can calculate the J_{CH} spin coupling constant from this value by using the ratio of the γ_D and γ_H values.

E. The carbonyl atom at δ_C = 169.3 ppm and C-12 a δ_C = 77.6 ppm.

1.3 COSY

A. A typical COSY at a 400 MHz instrument has to sample 10 ppm of proton chemical shifts, and this means to sample a 4 kHz frequency range. The corresponding increment for the t_1 evolution is therefore 1/(4000 Hz) = 250 µs. For 256 increments this results in 64 ms for the largest t_1. The best COSY transfer from $2I_{1x}I_{2z}$ to $2I_{1z}I_{2y}$ occurs when the factor sin πJt_1 is equal to 1, i.e. Jt_1 = 0.5. For a coupling constant of 7 Hz we obtain 7 Hz × 0.064 s ≈ 0.45, and this gives an efficient transfer amplitude. For a small spin coupling constant of about 1Hz, however, this is not efficient (1 Hz × ≈ 0.06). The remedy is a fixed delay before and after the mixing pulse to start with a larger $t_1$value.

B. The digital resolution in the indirect dimension F_1 is always very limited. Therefore spin coupling values should only be extracted from the direct dimension F_2.

C. The creation of double-quantum magnetization needs evolved antiphase magnetization $2I_{1x}I_{2z}$ to be transferred into $2I_{1x}I_{2y}$. This pro-

cess is only efficient at higher t_1 values, but not at the beginning (see discussion under A.).

D. The double quantum filter suppresses singlets, and, at the same time reduces more complex spin systems to the AX case. Therefore all cross peaks in a DQF COSY have the AX pattern.

E. The Karplus equation determines the vicinal spin coupling. One of the protons of C-15 has a dihedral angle near 90° with the vector C16-H16.

1.4 NOESY

A. The pulse p3 adjusts the spins into the $-z$-direction of the rotating coordinate frame. After this they relax toward the equilibrium magnetization with the time constant T_1. Depending on the chemical shifts several spins are already in the positive regime and need only one or two T_1 times to reach their equilibrium values. Thus, the best mixing time will be around one T_1 time to allow effective cross relaxation.

B. Build-up curves are measured by running several NOESY spectra with different mixing times. The obtained volume integrals of the NOESY cross peaks are plotted versus the mixing time. A linear fit during the first points is called the initial rate approximation.

C. Only in the linear beginning of the build-up curve does one assume a pair interaction of two spins which is related to their distance. At larger mixing times further spins come into play and spin diffusion might also reduce the integrals. Finally, at very long mixing times most of the spins will have already reached their equilibrium magnetization and do not give cross relaxation values.

D. NOESY cross relaxation starts from $-z$ (inversion of population) and works until the spins have reached $+z$ equilibrium magnetization. ROESY starts from 0 (equal population) and has therefore only half of the dynamic range.

E. Diastereotopic methylene groups or *ortho* situated aromatic protons, where the distance can be easily calculated by geometrical considerations. Care must be taken if other protons are close by.

1.5 HSQC

A. Whereas HMQC works with only four r.f. pulses, HSQC needs ten of such pulses and is therefore rather more sensitive to misadjustments. However, during T_1 in HMQC also H,H spin spin coupling evolves, since the proton spins are also transverse. This leads to a line broadening in F_1 and consequently to a lack of resolution in crowded situations.

B. With an appropriate product operator treatment, one can show that for CH_2 groups the double back transfer leads to a cancellation of the sensitivity gain, which can be observed for CH groups:

A methylene group can be described by three terms, two proton spins I_{H1} and I_{H2} and one carbon spin I_C. For all following calculations the terms containing cos πJ_{CH} d5 = 0 are left off and only those terms containing sin πJ_{CH} d5 = 1 are retained. After the

INEPT transfer we have as relevant terms the expressions $-2I_{H_{1z}}I_{C_y}$ and $-2I_{H_{2z}}I_{C_y}$. Both develop carbon chemical shift during t_1 as given below:

$$-2I_{H_{1z}}I_{C_y}\cos\Omega_C t_1 + 2I_{H_{1z}}I_{C_x}\sin\Omega_C t$$
$$-2I_{H_{2z}}2I_{C_y}\cos\Omega_C t_1 + 2I_{H_{2z}}I_{C_x}\sin\Omega_C t$$

Each of these terms enter the double INEPT back transfer. The first two INEPT pulses p16 and p7 convert these terms into

$$2I_{H_{1y}}I_{C_z}\cos\Omega_C t_1 - 2I_{H_{1y}}I_{C_x}\sin\Omega_C t$$
$$2I_{H_{2y}}I_{C_z}\cos\Omega_C t_1 - 2I_{H_{2y}}I_{C_x}\sin\Omega_C t$$

Evolution of J_{CH} leads now, since we have a three spin system, to more complex terms:

$$I_{H_{1x}}\cos\Omega_C t_1 - 4I_{H_{1y}}I_{H_{2z}}I_{C_y}\sin\Omega_C t$$
$$I_{H_{2x}}\cos\Omega_C t_1 - 4I_{H_{2y}}I_{H_{1z}}I_{C_y}\sin\Omega_C t$$

Pulses p18 and p9 convert these terms into

$$I_{H_{1z}}\cos\Omega_C t_1 - 4I_{H_{1y}}I_{H_{2x}}I_{C_y}\sin\Omega_C t$$
$$I_{H_{2z}}\cos\Omega_C t_1 - 4I_{H_{2y}}I_{H_{1x}}I_{C_y}\sin\Omega_C t$$

The subsequent J_{CH} evolution in the second spin echo period leads to

$$-I_{H_{1z}}\cos\Omega_C t_1 - 4I_{H_{1z}}I_{H_{2z}}I_{C_y}\sin\Omega_C t$$
$$-I_{H_{2z}}\cos\Omega_C t_1 - 4I_{H_{2y}}I_{H_{1x}}I_{C_y}\sin\Omega_C t$$

All observable terms containing a $\sin\Omega_C t$ modulation have also a cos πJ_{CH} d5 = 0 component and therefore cancel. The final pulse p11 creates the observable magnetization:

$$-I_{H_{1z}}\cos\Omega_C t_1 - I_{H_{2z}}\cos\Omega_C t_1$$

This is in contrast to the result for a CH group. Thus, a sensitivity enhancement or a preservation of equivalent pathways will not function in this case. A common remedy is to set the delay d5 not to $1/4J_{CH}$, but to $1/8J_{CH}$, and this compromise will help the methyl and methylene group signals.

C. The best water suppression is usually achieved by using the pathway via the hetero nucleus, and therefore usually no additional water suppression scheme is needed.

D. HSQC stands for **H**eteronuclear **S**ingle **Q**uantum **C**oherence. In this context it means that terms like $-2I_{H_z}I_{C_y}$ are present during t_1 and here only one spin sort, namely ^{13}C is transverse, in contrast to HMQC.

E. 90° pulses have a much better frequency excitation range than the twice-as-long 180° pulses.

F. In principle, if the molecule contains a chiral center, all methylene groups are diastereotopic. However, the amount of diastereotopicity is dependent on the distance to the stereogenic center.

1.6 HMBC

A. The delay between p1 and p5 is much longer than the corresponding delay in HSQC, therefore relaxation effects maybe crucial. Since ^{13}C decoupling is not used, all correlation signals are in principle doublets and not sharp singlets. The transfer from protons to carbons is optimal only for a fraction of the signals.

B. 125 to 170 Hz, *sp* hybridized carbon atoms not taken into account.

C. The spin coupling constant of C-4 is, due to the *ortho* nitrogen substituent, especially large (168 Hz). Similarily, C-17 has a low spin coupling constant (133 Hz) due to its fully aliphatic environment.

D. The final carbon pulse p7 creates anti-phase magnetization, which during the acquisition time develops in-phase magnetization, however with different spin coupling constants. Furthermore, in F_1 there is also modulation by H,H spin coupling. All these factors lead to phase distortions.

E. The first carbon pulse p3 is applied after a delay optimized near the low end of the coupling constant range, and the second carbon pulse p4 follows after a delay optimized near the high end of the coupling constant range. The long-range spin couplings will not be significantly affected by these two pulses.

   The sum of the effects of the gradients g1 to g3 is zero. Thus after g3 we have refocusing of only those signal contributions that maintained their coherence level existing at the onset of g1, and these are the long-range coherences. The ^1J coherences change their coherence level due to the pulses p3 and p4 and will therefore be further dephased by g2 and g3.

F. Before the gradient g4 we have the coherence level $I_H^- I_N^+$ which is changed by p6 into $I_H^- I_N^-$. If we assume the ratio of gyromagnetic ratios of protons vs nitrogen to be = 10 : 1, $I_H^- I_N^+$ corresponds to the number −9 and $I_H^- I_N^-$ to the number −11. Applying a gradient strength of 80 % for g4 will dephase the signal of $I_H^- I_N^+$ by 80 × (−9) = −720 units. Accordingly the strength of g5 has to be −720/−11 = 65.45 %, to pass only $^1H^{15}N$ correlations. To select in the echo anti-echo mode first $I_H^- I_N^-$ and then $I_H^- I_N^+$ g4 must first be set to −65.45 % and g5 to 80 %.

G. On current high-field spectrometers the spectral width for ^{13}C exceeds 20 KHz. A usual hard 180° pulse is not sufficient to refocus the carbon signals on either end of the spectral range. Therefore frequency swept pulses are used (see chapter 8.4 "Chirped Pulses").

Answers Chapter 2

2.1 2D *J*-Resolved ^{1}H NMR Spectroscopy

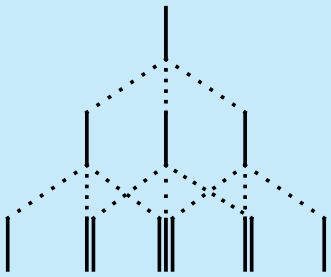

A. Due to the spin coupling with deuterium the proton in $CHD_2CD_3S{=}O$ displays a quintuplet with the intensities 1 : 2: 3: 2: 1 . For deuterium with spin I = 1, each deuterium nucleus holds three magnetic spin numbers $m_z = -1, 0, +1$, which combine in five overall spin numbers of −2, −1, 0, +1, +2. In the 2D *J*-resolved spectrum this signal remains unchanged at the center line in F_1, since this is a heteronuclear spin coupling.

B. Consider two protons with different chemicals shifts and coupled to each other, which form in the normal 1D NMR spectrum an AX spin system. After excitation by p1, chemical shift and spin coupling evolve during t_1. The chemical shifts are refocused by the 180° pulse p2. At the end of t_1 we have in terms of the product operator formalism considering only spin 1:

$$-2I(1x)I(2z)\sin(2\pi{*}J(12){*}t1) + I(1y)\cos(2\pi{*}J(12){*}t1)$$

In the subsequent acquisition all signals will thus be modulated with the *sine* and the *cosine* of the spin coupling constants at the same time, i.e. overlaying absorptive and dispersive line shapes, which yields a twisted shape.

C. This is the usual EXORCYCLE phase scheme, which alleviates pulse imperfections, i.e. too short or too long pulses compared with the nominal ones.

D. The spin echo sequence removes at the point of the spin echo the chemical shift contribution and analogically also the inhomogeneity of the magnetic field causing line broadening. The multiplets in F_1 therefore display their natural line widths.

2.2 ROESY

A. Consider a spin in originally –*y* direction. Pulse p2 will move it to the +*y* axis, whereas pulse p3 will turn it back to the –*y* axis. Thus the phase cycle of the spin lock always reorients the spins in the *xy* plane. This prevents a rapid dephasing and reduces errors of the 180° pulses.

B. In ROESY only the mixing of the weak relaxation terms should occur. TOCSY mixing requires stronger mixing pulses, since spin coupling terms have to be considered.

C. H-8 and H-13 are stereochemically in opposite directions, thus the cross relaxation will be very low, but the spin coupling rather large.

D. The signal of H-1 has a cross relaxation with H-17 and H-16. Only H-1, but not H-4 are within the reach of these spins.

2.3 TOCSY

A. Spin lock: $I_0 = 100$ Watt
$10 \log (I_0/I) = 12;$

$\log (I_0/I) = 1.2$
$I_0/I = 15.84$, $I = 6.31$ W
6.31 W × 0.3 s = 1.893 Ws

Hard Pulse:
100 W × 10×10^{-6} s = 10^{-3} Ws

One spin lock pulse lasting 300 ms dissipates about 2000 times the energy of a single hard pulse.

B. The TOCSY transfer leads to phase distortions in the cross peaks; therefore a magnitude processing is advisable.

C. Different spin lock schemes have different effectivity with respect to the spectral width covered. For the MLEV16 spin lock the factor 1.7 has been reported, meaning that one needs to calculate instead of, e.g., 4000 Hz, 4000 × 1.7 = 6800 Hz. With the equation $p_1 = 1 / (4 \times 6800\ s^{-1}) = 36.8$ µsec is then calculated for the individual 90° pulse length.

D. MLEV: Malcom Levitt
DIPSI: Decoupling in the presence of scalar interactions
GARP: Gobally alternating rectangular pulses

2.4 HSQC-TOCSY

A.

$$I_{H_z} \xrightarrow{I_{H_x}} -I_{H_y} \xrightarrow{2\pi J I_{H_z} I_{C_z} d_2} 2I_{H_x} I_{C_z} \xrightarrow{I_{H_y}, I_{C_y}} 2I_{H_z} I_{C_x} \xrightarrow{I_{C-y}}$$

$$2I_{H_z} I_{C_z} \xrightarrow{I_{C_x}} -2I_{H_z} I_{C_y} \xrightarrow{I_{C_x}, I_{H_y}} -2I_{H_x} I_{C_z} \xrightarrow{2\pi J I_{H_z} I_{C_z} d_3} -I_{H_y}$$

B. Before each of the trim pulses p3 and p6 the proton magnetization is in the *x*-direction, thus the desired magnetization is not affected if the trim pulses act from the same direction.

C. The same argument as for questions B holds. Directly before the onset of the spin lock, the proton magnetization is in the *y*-direction, and therefore the spin lock will catch it.

D. This is due to the well known anomeric effect, an interaction of the lone pairs of the electrons at the oxygen atoms. According to the Karplus equation one expects for this configuration only a small coupling constant, since H-1' and H-2' are in the equatorial/axial position to each other.

2.5 HOESY

A. ^{6}Li has a very long relaxation time: the proton relaxation time is considerable shorter. During the mixing time d3, when the cross relaxation occurs, the protons would probably be fully relaxed before the communication with ^{6}Li is successful.

B. Carbon atoms bearing one or more hydrogen atoms will not need cross relaxation to distant protons, thus the experiment is only of value for quaternary carbon atoms. Structural questions for the former are usually better addressed by HMBC or related methods.

C. The gradient ratios g1: g3 must be as the ratio of the NMR frequencies of these nuclei.

2.6 INADEQUATE

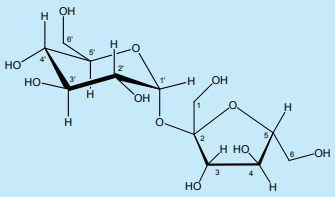

A. In natural abundance, the occurance of ^{13}C,^{13}C pairs in the same molecule is 1.1 % × 1.1 %, thus INADEQUATE can only detect 10^{-4} of the concentration given.

B. Since we are measuring ^{13}C, the spectral distance between spin-coupled carbon atoms can be up to 200 ppm, which, e.g., on a 600 MHz spectrometer corresponds to 30 KHz. A normal hard 180° pulse does not cover this frequency difference. See chapter 8.4.

C. At the time of g1 double-quantum coherence is present, thus the effect of g1 is doubled. At the time of g2 single-quantum coherence is present, thus the strength of g2 must be twice that of g1 to achieve refocusing.

D.

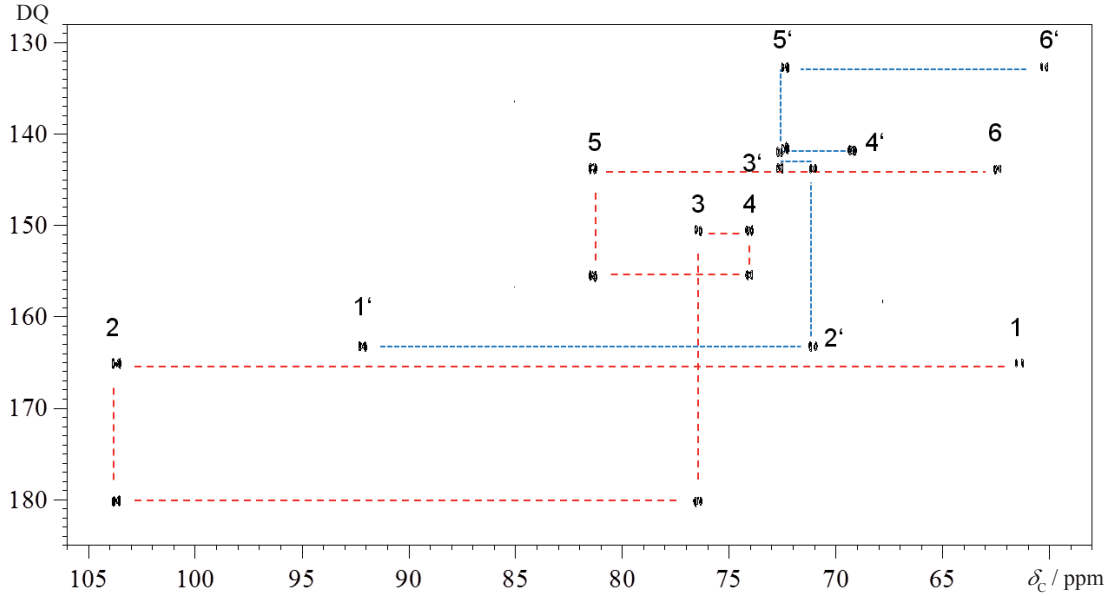

2.7 ADEQUATE

A. INADEQUATE detects 10^{-4} of the concentration with carbon sensitivity. ADEQUATE detects the same number, but with proton sensitivity. According to R. Ernst *et al.* (R. R. Ernst, G. Bodenhausen, A. Wokaun "Principles of NMR in One and Two Dimensions" Clarendon Press Oxford 1987, p. 468) the sensitivity in a 2D experiment follows $\gamma_{exc}\gamma_{obs}^{3/2}$. For INADEQUATE both γ refer to carbon and we have $1 \times 1^{3/2} = 1$. For ADEQUATE both γ refer to proton and we have $4 \times 4^{3/2} = 32$.

B. 10^4, because the possibility of a ^{13}C-^{13}C pair at natural abundance is $(1.1*10^{-2})*(1.1*10^{-2})$ and all other signals must be suppressed.

C. H-23a and H-23b are bound to the same carbon atom with $\delta_C = 64.6$; C-22 resonates at $\delta_C = 127.34$ which gives an ADEQUATE value of 191.94. H-20a and H-20b are bound to a carbon with $\delta_C = 52.68$; C-21 has a $\delta_C = 140.45$ which adds to 193.13. These numbers are not distinguished at this resolution.

2.8 *J*-HMBC

A. Although this is a $^{2}J_{CH}$ spin coupling, a dihedral angle including the oxygen atom with its free electron pairs will become important and influences this spin coupling.

B. According to a molecular model (see http://csi.chemie.tu-darmstadt.de/ak/immel/structures-nmr.html) the dihedral angle between C-10 and H-12 is −113°; therefore the $^{3}J_{CH}$ should be very small according to the Karplus equation.

C. In "constant time" pulse sequences the same delay always exists between the first excitation and the start of detection, whereas in "normal" pulse sequences this delay is incremented from short to long values. Due to relaxation in the constant time one has to face signal loss.

D. In that case there is an additional modulation in F1 by the proton chemical shifts, and the J_{CH} doublets have an offset with respect to each other.

2.9 Gated Decoupling

A. The broad split doublet stems from C-12 which has long range CH spin couplings from H-13, H-11, and H-23, The sharp doublet stems from the residual $CHCl_3$ signal.

B. The protons of C-17 have the same relative chemical shift. The signal of C-17 splits therefore into a triplet with an additional long range triplet caused by the protons of C-18. In contrast, the protons of C-11 display a high degree of diastereotopicity and cause distinctly different $^{1}J_{CH}$ spin coupling with C-11. Therefore we observe a doublet of doublets.

C. C-3 is fixed in the aromatic ring and shows the $^{1}J_{CH}$ to its own proton H-3, a $^{3}J_{CH}$ to H-1 and a further small splitting, probably to H-4. C-22 is surrounded by five protons with a similar $^{3}J_{CH}$; furthermore, this part of the molecule may have some flexibility.

D. From the HMBC spectrum it can be seen that the C=O atom couples with both H-11a/b and H-12.We find the best agreement using the following proton parameters:
$\delta_{H\text{-}11a} = 3.132$, $\delta_{H\text{-}11b} = 2.670$, $\delta_{H\text{-}12} = 4.288$, $^{2}J_{H\text{-}11a,\,H\text{-}11b} = -17.34$ Hz, $^{3}J_{H\text{-}11a,\,H\text{-}12} = 3.34$ Hz and $^{3}J_{H\text{-}11b,\,H\text{-}12} = 8.47$ Hz. With these as proton basis and the chemical shift of the C=O atom at 169.2 we used $^{2}J_{C,H\text{-}11a} = 8$ Hz, $^{2}J_{C,H\text{-}11b} = 6.3$, and $^{3}J_{C,H\text{-}12} = 1.9$ Hz to give perfect agreement.

E. The build-up and the decay of the NOE effect follow the same time constant, and therefore it may be best to keep these two times equal.

Answers Chapter 3

3.1 Water suppression by Presaturation

A. Water, with the molecular weight of 18, is 55.55 molar in itself, and due to the two protons it would yield a relative NMR signal of 111.11 units and, because of the mixture of 90 % H_2O/10 % D_2O, a relative signal of 100 units. A 2 mmol solution of sucrose in this mixture will therefore have a relative integral for 1 proton of $2*10^{-5}$, which is 50000 times less than the integral of the water.

B. No, because of saturation transfer to the NH protons.

C. No, because cw irradiation works only for one frequency. There exist some techniques to cycle through a set of frequencies during the presaturation delay for multiple saturation.

D. AA' BB' CC'

3.2 Solvent Suppression by 1D-NOESY

A. The first acquisition of the 1D-NOESY is essentially a 270° pulse, i.e., 90°x, 90°x, 90°x with delays between pulses. The second step of the acquisition is 90°−x, 90°x, 90°x, and this is identical to the first scheme except for the −x phase of the first pulse. The result, however, is only a 90°x pulse for any resonance experiencing the full intended pulse effects. The receiver subtracts the second from the first scan. Since resonances outside the center of the coil react differently to the first scan and the second, this leads finally to a volume restriction, i.e. the cancellation of signals stemming from the volume ends of the sample with inhomogeneous B_0 field, see ref.[4].

B. Yes, this will help. A long T_1 of the solvent will prohibit its full recovery after p2.

C. At both points in time the magnetization should be in the *z*-direction. *Z*-gradients destroy spurious *xy*-magnetization left over from previous scans ("spoiling gradient").

3.3 Water Suppression by SOGGY Excitation Sculpting

A. A 90° pulse would then be 1 ms long. The intensity of this pulse, expressed in frequency units, is $\gamma B_1/2\pi = 1/(4p_{90}) = 1/0.004 =$ 250 Hz, and this is, roughly speaking, its excitation bandwidth. In the spectrum shown, there is indeed a window of this size not usable.

B. The first two pulses add up to zero, the second two pulses to 180°. The trick of this composite pulse lies in the compensation of B_1 inhomogeneity as described in ref. [4], p. 265.

C. There are no additional zero excitation points of this sequence, thus the NH region or the aliphatic region of the NMR spectra is unaffected.

3.4 Solvent Suppression using WET

A. Due to the solvent gradient the chemical shift of the solvents and the difference of the chemical shifts will be variable. The software must be able to cope with this effect to maintain equally good solvent suppression during the entire run (e.g., with a scout scan, automatic frequency range detection, and following pulse shape calculation).

B. See reference [4]

C. These signals would be also suppressed, since the selective pulses saturate the water resonance and this saturation will be transferred to the exchangeable protons.

3.5 SELTOCSY

A. During the spin lock the spins are precessing in the rotating frame only in the radio frequency field, that is in a very weak magnetic field. They have therefore nearly no chemical shift differences, and all spin systems are of "higher order". The consequence is that every spin is coupling with every other provided that there is an uninterrupted coupling chain. Spin couplings are independent of the magnetic field.

B. There are seven chemical bonds from the anomeric proton H-1' to H-6' and only five chemical bonds from H-3 to H-6.

C. There is no significant spin coupling between H-1' and any of the fructose protons.

3.6 SELNOESY

A. This can be due to a three-spin effect, where one spin acts as a very effective relaxation sink for a spin nearby.

B. Yes, without a problem and – if one is only interested in one sort of protons − in a much shorter time compared to 2D NOESY.

C. H-13 is transoid with respect to H-8.

3.7 SELINCOR

A. After pulse p8 only I_C^- is present which is converted by p9 into I_C^+. The negative value of gradient g3, multiplied by I_C^-, gives a positive contribution which adds to the product $I_C^+ \times$ g4. At the end of the pulse sequence only I_H^- is present. Since hydrogen has a four times higher gyromagnetic ratio than carbon, the equation $(g3 \times I_C^-) + (g4 \times I_C^+) + (g5 \times I_H^-) = 0$ holds.

B. GARP decoupling of carbons needs a power level which causes heating of the probe head and must therefore be reduced to a minimum.

C. Of course the sensitivity of this sequence will be a hundred times less than that for normal proton spectra. However, in crowded proton regions it is often not possible to irradiate single protons, whereas the chemical shift dispersion for carbon atoms is usually larger.

3.8 SELINQUATE

A. No, compared to the phase cycling employed here, a gradient DQF filter is less sensitive by a factor of 2, though this improves the suppression of unwanted signals.

B. The aromatic CC spin coupling is about 60 Hz.

C. Unlikely, since the three-spin couplings range from 35 to 60 Hz.

3.9 Band Selective HMBC

A. The 180° pulse should invert, e.g., from $-y$ to $+y$, but not excite from z t to x, y plane.

B. In oligopeptides the carboxyl groups usually resonate very closely together and are difficult to assign.

C. No, carboxyl groups have no hydrogen attached, and therefore a breakthrough of $^{1}J_{CH}$ is not possible.

Answers Chapter 4

4.1 ^{11}B NMR Spectroscopy

A. This must be connected to the symmetry around the boron nuclei, which is apparently higher than in usual organic boron compounds.

B. ^{13}C NMR signals of such carbon atoms should in principle give a 1:1:1:1 pattern of four multiplet lines, which, however, often coalesce due to the rapid relaxation of boron, and therefore only reveal a broad hump. If one lowers the temperature significantly one could reach a regime where the boron relaxation is slowed down. If one has an appropriate probe head, one can also try to perform boron single frequency decoupling in addition to proton decoupling.

C. The ^{11}B^{19}F spin coupling is smaller than 1 Hz.

4.2 ^{15}N NMR Spectroscopy

A. Very broad lines due to the quadrupolar relaxation.

B. As in the figure given with DEPT, however, the central transitions are missing.

C. Yes, if one uses 10 Hz as the d2-delay, one often also gets correlations for ^{1}J spin couplings of 90 Hz

4.3 ^{17}O NMR Spectroscopy

A. D_2O is prepared by distillation of H_2O, being the heavier isotopes enriched by the distillation process. Depending on the quality of the separation, there could be a higher ^{17}O content in D_2O.

B. In view of the line width of ^{17}O signals a decimal point doesn't make sense.

C. The carbonyl oxygen is sp^2 hybridized and therefore, as in carbon or proton NMR, its signal is deshielded.

4.4 ^{19}F NMR Spectroscopy

A. The frequencies of ^{1}H and ^{19}F are so close that interferences have to be cut off.

B. According to chemical shift theory, the paramagnetic term of the chemical shielding is the dominant one for fluorine in contrast to protons. In addition, the seven outer electrons are much more polarizable than the single one in hydrogen.

C. The reason is the very large chemical shift range of ^{19}F, thus small isotope effects are much better observed than with protons.

4.5 ^{29}Si NMR Spectroscopy

A. In principle 13 lines with the intensities
1 : 13 : 78 : 286 : 715 : 1145 : 1145 : 715 : 286 : 78 : 13 : 1

B. 4 % of the main signal

C. Yes, see S. Berger, "INEPT-HMQC − A new pulse sequence for ^{13}C,^{29}Si correlation", *J. Magn. Reson. Ser. A*, **1993**, *101*, 329−332.

D. A multitude of signals, but less complicated than the corresponding ^{13}C NMR spectrum.

4.6 ^{57}Fe NMR Spectroscopy

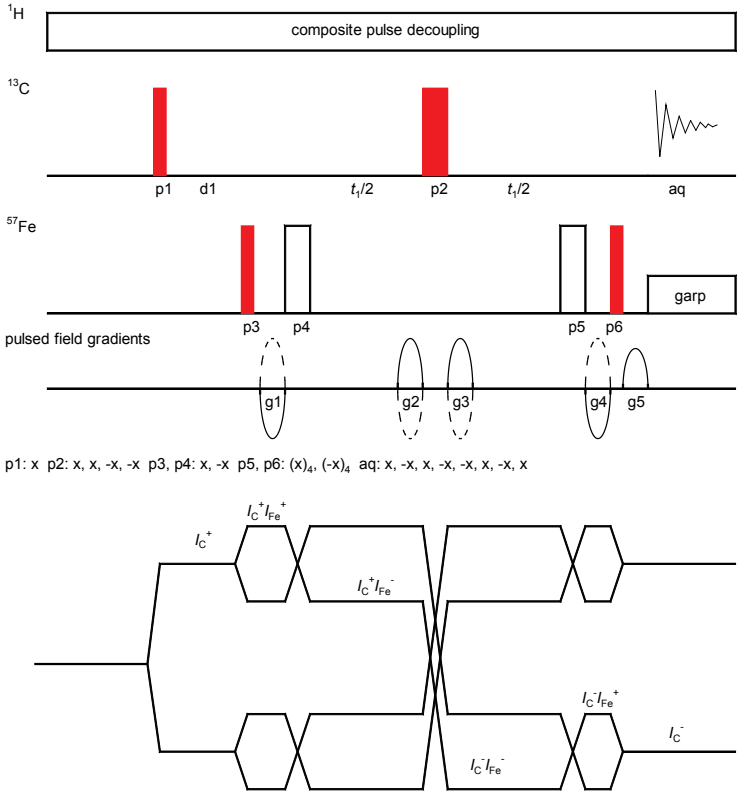

A. On the 600 MHz instrument used, the carbon frequency SFO1 was 150.913 and the iron frequency SFO3 was 19.461 MHz. At the time of the first negative gradient g1 we have therefore the coherence level $I_C^+I_{Fe}^+ = 170.374$; for g2 we find $I_C^+I_{Fe}^- = 131.452$, g3 = $I_C^-I_{Fe}^-$ = –170.374 and g4 = $I_C^-I_{Fe}^+$ = –131.452. If 80 % was chosen for g1-g4, the magnetization is dephased by –80 ×170.374 + 80 ×131.452 + 80 × –170.374 – 80 × –131.452 = 6227.52 units. Since I_C^- is entering the receiver, it has to be rephased by g5 using 6227.52/150.913 = 41.3 %.

B. In ferrocene the carbon atoms are coupled to their respective protons and the NOE will be helpful. The reported Fe,C spin coupling constant with 4.7 Hz would disappear in the 2D line width. Iron pentacarbonyl has no protons, but a nice Fe,C spin coupling of 24 Hz which can only be seen without iron decoupling.

4.7 ^{195}Pt NMR Spectroscopy

A. The line width is too large and hence the transverse relaxation time is much too small to allow the required delay for 1/[2J(Pt,H)] in an HMQC experiment.

B. Spin coupling constants of two isotopes toward the same nucleus are in the ratio of their gyromagnetic ratios. $\gamma^{14}N/\gamma^{15}N = 0.713$, therefore $^1J(^{195}Pt,^{14}N)$ should be 199.6 Hz.

Answers Chapter 5

5.1 Measurement of the Spin–Lattice Relaxation Time T_1

A. Typically 2 to 3 s

B. Typically 15 s

C. Typically 70 ms

D. There are two usual problems:
1) too short waiting time d1 and too short waiting times τ.
2) The inversion property of the 180° pulse is offset-dependent.

5.2 Measurement of the Spin–Spin Relaxation Time T_2

A. Using the equation in the main text one obtains for $\Delta\nu_{1/2}$ the value 0.03 Hz.

B. It should not change.

C. Quadrupolar nuclei relax very fast and the equation $T_1 = T_2$ holds. Their relaxation times are in the order of a few milliseconds.

D. Dynamic exchange of nuclei due to chemical processes.

5.3 Dynamic ^{1}H NMR Spectroscopy

A. There are no unconfirmed assumptions within the Arrhenius scheme. However, the activation energy is assumed to be temperature- independent and the frequency factor is not of much chemical use. Using the Eyring equation, $\Delta G^{\#}$ can be reported for the standard temperature 298 K.

B. The sample works via the temperature dependence of the hydrogen bonds. It must be electronically calibrated versus an external device.

C. The typical frequency difference in NMR for exchanging spins is 10 to 1000 Hz, and from this a dynamic range of 20 to 100 kJ/mol can be calculated for which line shape alterations can be observed. In IR spectroscopy one may see exchange between bands from 10 cm^{-1} to 100 cm^{-1}, which corresponds to a $\Delta\nu$ of 10^5 to 10^4 Hz. Therefore the time scale of IR is two orders of magnitude faster.

D. Chlorine is inductively electron withdrawing, but mesomerically contributing electrons. Due to the latter effect a C=N double bond contribution is less likely, which leads to a lower barrier.

5.4 Diffusion Measurement with DOSY

A. In the diffusion equation, the gyromagnetic ratio γ occurs as a quadratic (i.e. squared) term in the exponent and thus is most important. The standard high resolution NMR spectrometers are not built for diffusion measurements and have only weak gradient pulses. To achieve a good dephasing, one therefore needs the nuclei with the highest gyromagnetic ratio.

B. To avoid any gradient echo during the sequence with increasing gradient strength of g1, g2, g4 and g5.

C. Yes, tetramethylsilane. See: E. J. Cabrita, S. Berger "DOSY studies of hydrogen bond association: TMS as a reference compound for diffusion studies", *Magn. Reson. Chem*. **2001**, *39*, 142−148.

D. In cases of anisotropic diffusion, e.g. rigid molecules with a long carbon chain or stretched gels.

5.5 Residual Dipolar Couplings (RDC)

A. Dipolar coupling constants are much larger than the isotropic values of *J* couplings. By aligning the analyte molecule only very slightly, the dipolar coupling is nearly averaged to zero. In the solid state the dipolar coupling constant is in the order of some kHz (e.g., around 4.5 kHz for a C-H pair within a methylene group); this is reduced to a residual value in the order of a few Hz.

B. In the solid state quadrupolar nuclei will display a Pake doublet with a large dipolar splitting. Thus, a slight anisotropic alignment will also induce a signal splitting, and from this it can easily be judged whether an orientation within the NMR sample tube took place.

C. After the INEPT transfer step the t_1 evolution of a C,H doublet starts with the term $-2I_{H_z}I_{C_y}$, which yields an antiphase doublet in the F_1 domain. The carbon atom of a methylene group originally forms two anti-phase doublets, and the central line of the triplet is composed of the right signal of the left doublet and the left signal of the right doublet. These cancel because they have the opposite phase. The 180° pulse within an HSQC sequence creates in-phase doublets which would show up as a triplet, but since the 180° pulse also reverses the direction of the oscillation, a singlet is finally observed.

Answers Chapter 6

6.1 ASIS

A. The signal of the OH proton in a solution of 10 mg cresol in 0.7 mL $CDCl_3$ appears at δ= 4.76; it is shielded in benzene by 0.82 ppm to δ=3.94, but deshielded by 0.3 ppm to δ= 5.06 in pyridine.

Interestingly, the center of the aromatic AA'XX' system at δ= 6.88 is also shielded in benzene by 0.2 ppm to δ= 6.67, whereas this spin system collapses to a singlet at δ= 7.15 in pyridine. The signal of the methyl group is shielded in benzene by 0.27 ppm to δ= 2.07, whereas in pyridine only a small shielding by 0.04 ppm is observed.

In contrast to the results of cresol, the acidic OH proton of salicylaldhyde is deshielded in benzene by 0.44 ppm to δ= 11.47 and further by another 0.7 ppm in the basic solvent pyridine. The signal of the aldehyde proton is first shielded by 0.75 ppm in benzene, but deshielded by 0.52 ppm in pyridine.

The center of the four aromatic protons is shielded in benzene by 0.6 ppm, but deshielded in pyridine by 0.1 ppm. The ABCD sequence of the chemical shifts in salicylaldehyde obtained in $CDCl_3$ is changed by the aromatic solvents. Apparently, in pyridine two effects are operative, the aromatic solvent and its basic properties.

B. See P. Lazlo and D.H. Williams, "A variable-temperature nuclear magnetic resonance study of toluene-ketone complex" *J. Amer. Chem. Soc* **1966**, *88*, 2799−2802.

6.2 Chirality Determination

A. 0.82 /about 20:1.

B. 0.75 Hz and therefore still observable.

6.3 Advanced Mosher Methods

A. No, these two compounds are a pair of enantiomers and therefore give identical NMR spectra.

B. The chemical shift differences are caused by the anisotropy of the phenyl ring and are therefore dependent on its distance.

C. In principle yes, but secondary amides may display two different rotamers around the amide bond rendering the analysis somewhat more difficult.

6.4 Quantitative NMR and Relaxation Reagent

A. The methylene group of ethanol resonates in the region of sugar and aromatic signals and therefore might give a wrong integration.

B. 0.1 mL 99.9 % D_2O can contain 0.1 % HDO/H_2O, and this corresponds to 0.0001 mL. In 0.7 mL of this Grappa are 0.44 mL H_2O; thus the possible error will be 0.023 %.

C. Due to paramagnetic relaxation $Cr(acac)_3$ introduces line broadening, which affects the signal intensity.

D. The overlapping signals stem from C-2 and C-3. If one draws circles around these carbon atoms, a rather slight environmental difference can only be seen in the third sphere. Line broadening by $Cr(acac)_3$ causes these signals to overlap.

6.5 Determination of Association Constants K_a

A. UV- and fluorescence spectroscopy

B. Diffusion constants are less reliable than frequency-based chemical shifts.

6.6 STD NMR

A. Measure an identical sample under identical conditions, but without any protein.

B. Many proteins have absorption at frequencies lower than the TMS frequency. Otherwise one can irradiate the aromatic residues of a protein if the ligand has no aromatic signals.

C. One obtains a build-up curve (similar to NOE build-up curves) by lengthening the irradiation time.

6.7 A Kinetic Experiment

A. The Michaelis–Menten equation is: $v = v_{max} * [S]/(K_M + [S])$ Boundary conditions: steady-state conditions [Substrate] >> [Enzyme], irreversible reaction from the enzyme–substrate complex to the enzyme–product complex.

B. All signals must have been relaxed before they are excited in the next run, otherwise the kinetics would be in error.

C. A 2D file ensures that all spectra are run identically. Also the processing, e.g., the phase correction, will be identical.

Answers Chapter 7

7.1 The CP/MAS Experiment

A. One observes the FID of ^{79}Br under rapid pulsing. This may work on the ^{13}C channel without detuning, because both NMR frequencies are nearby (e.g., at a 600 MHz spectrometer the ^{79}Br frequency is only 540 kHz below ^{13}C). The FID is modulated by sharp sidebands. One adjusts the magic angle screw until these sidebands last over the entire FID.

B. To set the Hartmann–Hahn condition, the r.f. fields on protons and nuclide X, e.g., ^{13}C, must be the same, which means that the 90-degree pulse widths must be the same. Detect the proton signal of adamantane, spinning at 4 kHz, and set the power level such that the proton 90-degree pulse is 5 to 6 µs. Then observe the adamantane ^{13}C signal with decoupling at this power level, and set the ^{13}C power level to be the same as that for protons. This will give you the power levels to be used as starting values for the Hartmann–Hahn adjustment. Leave the proton power level constant, and vary the ^{13}C power level until a maximum signal is obtained.

C. The CO group has a much larger chemical shift anisotropy.

7.2 High-Resolution Magic-Angle Spinning

A. The centrifugal acceleration of a mass point in circular motion with constant angular velocity is

$$a = \omega^2 \times r$$

With $r = 2*10^{-3}$ m, $\omega = 2\pi*f$, and $f = 8$ kHz one yields $\omega^2 = 2.53*10^9$ 1/s^2 and $a = 5.05*10^6$ m/s^2.

Comparison with the gravity acceleration on earth ($g = 9.81$ m/s^2) results in a factor of around half a million. Including the rotor's wall thickness of 0.5 mm reduces the ratio to around 390000 .

B. The friction of the outer wall of the rotor with air leads to heat dissipation.

C. Through spinning about the magic angle the dipolar interaction between two nuclei is modulated by this rotation, which may cause change in relaxation behavior of the spins in dependence on the spinning speed.
Furthermore, the temperature of the sample may change (cf. question B). Finally, due to the huge g forces (cf. question A), conformational changes of the molecules may be discussed.

7.3 HN HSQC

A. After the evolution period, both $2I_{H_zN_x}$ and $2I_{H_zN_y}$ are present. The pulses p15 and p6 with the phases x convert only $2I_{H_zN_y}$ into $2I_{H_yN_z}$. This develops in the period [d3, p16, p7, d3] into I_{H_y}. The pulse p8 will store this as I_{H_z}. At the same time the pair of pulses p15 and p6 converted $2I_{H_zN_x}$ into double quantum magnetization $2I_{H_yN_x}$, which is reconverted by the pulses p18 and p9 having the phases y into $2I_{H_yN_z}$. This develops in the period [d3, p18, p9, d3] into I_{H_x}. The

final 90° pulse p10 leaves this unchanged but converts the stored magnetization I_{H_z} into I_{H_y}, and therefore both original components are saved.

B. γ_H and γ_N are in the ratio of about 10:1. At the time of gradient g2 a coherence pathway diagram shows only the presence of I_N^+ or I_N^-. At the time of gradient g5 only I_N^- is present. To fulfil the condition that the sum of gradient action $(g2 \times I_N^+) + (g5 \times I_N^-) = 0$ has to be zero, their ratio must also be 10:1.

C. Hardly. The two-bond and three-bond spin couplings of the NH protons to ^{13}C will be in the order of the line width of these protons. There exist, however, pulse sequences which perform this task.

7.4 HNCA

A. In a traditional evolution period, t_1 or t_2 increase throughout the period. As relaxation is time dependant, signals from the beginning of the evolution period have a different weight compared to those which stem from the end. A similar situation is true for spin coupling contributions. When in a constant time evolution scheme the 180° pulses are shifted through the period, all signals have the same weight; however, all have to suffer for the same relaxation losses. Constant time periods are more difficult to program and to set up.

B. The effect is known from homonuclear decoupling. Irradiation of one proton changes the resonance position of nearby protons to higher frequencies. The source is the additional decoupler field which leads to an effective B_0 field in the rotating frame which is larger than without decoupler.

C.

8.66/62.4 and 56.3	T12 and K11
8.52/57.9 and 53.6	K63 and Q62
8.19/56.6 and 55.9	E51 and L50
7.87/59.8 and 55.4	K29 and A28

Answers Chapter 8

8.1 Calibration of Pulse Duration in the Transmitter Channel

A. These probes have the highest proton sensitivity. To get this they are designed with a high quality factor of the resonant circuits to obtain a high induced voltage for response. The drawback is the radiation damping phenomenon if very strong signals are present.

B. Since a pulse near 360° does not create much transverse magnetization, but returns magnetization back to +z, no long waiting times due to T_1 relaxation are necessary between the experiments. Moreover, looking at Fig. 8.1-3, the nulls of the 360° pulse are more reliable than those of the 180° pulse.

C. Biological buffers contain a large variety of inorganic salts, and these strongly affect the susceptibility and may induce eddy currents in the sample due to the ions.

8.2 Calibration of the Pulse Duration in the Indirect Channel

A. The spectrum is inherently of higher order and must be considered as an A_2, A_2', X, X' spin system, see P. Stilbs, S. Forsén "Spin-spin couplings in doubly ^{15}N labeled urea and 1,3-dimethylurea" *Org. Magn. Reson*. **1976**, *8*, 384–386.

B. Same result as with no decoupler pulse: an unchanged anti-phase doublet.

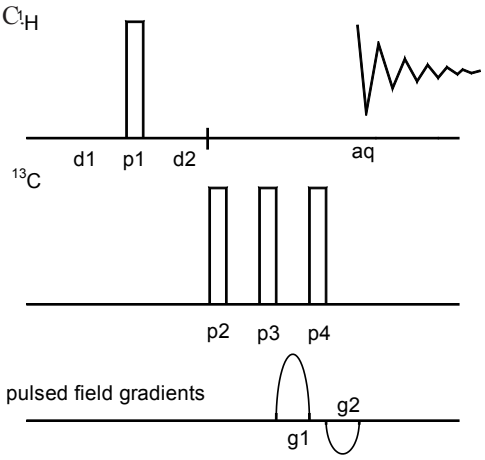

p1, p2, p3, p4, aq: x, -x, -x, x, y, -y, -y, y

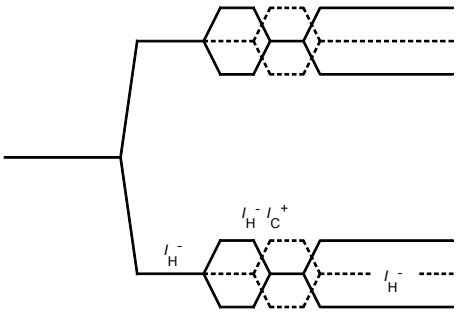

If p2 = 0, only the dashed lines apply. At the time of the first gradient g1, $I_H^- I_C^+$ is present, which has a coherence level of –4 +1 = –3. I_H^- is entering the receiver with a coherence level of –4. Thus g1 and g2 must be in the ratio of 4:(–3) to fulfil the equation:

(g1×level 1) + (g2×level 2) = 0.

If p2 = 90°, the solid lines apply and no single quantum coherence is entering the receiver.

8.3 Shaped Pulses

A. "transition"-selective: 1 to 2 Hz, SPT experiments
"multiplet"-selective: 50 Hz, selective NOE or COSY experiments
"band"-selective: 30 ppm, 3D protein NMR, selective pulses on all C=O or all C_α carbon atoms.

B. $1/[4\times10\times10^{-6}s] = 25$ KHz, i.e. correct at a 400 MHz spectrometer; $1/[4\times2\times10^{-3}s] = 125$ Hz, i.e. sufficient for complete water suppression.

C If the ^{13}C signal is ^{1}H coupled, it has a bandwidth of 3 ×130 Hz = 390 Hz, otherwise 10 Hz should be sufficient.

8.4 Adiabatic pulses

A. From Wikipedia (August 2012, http://en.wikipedia.org): "Adiabatic processes can occur if the container of the system has thermally-insulated walls or the process happens in an extremely short time, so that there is no opportunity for significant heat exchange. The term "adiabatic" literally means impassable, coming from the Greek roots α- ("not"), δια- ("through"), and βαινειν ("to pass"); this etymology corresponds here to an absence of heat transfer."

B. Composite pulses, and these are still being used for decoupling and spin-locks.

8.5 Temperature Calibration in NMR

A. $\Delta G^{\#}(340) = 8.3\times340[22.96 + \ln(340/200)]$
$2822[22.96 + 0.53] = 66290$ J/mol

$\Delta G^{\#}(345) = 8.3\times345[22.96 + \ln(345/200)]$
$2864[22.96 + 0.55] = 67332$ J/mol

The error is in the order of 1 KJ/mol.

B. The required heat insulation between the sample tube and the deep cooled r.f. coil limits the temperature range. Furthermore, cryo probes have been developed, mainly for biological samples as water freezes at 273 K.

C. Most popular in organic chemistry is the Seyfarth mixture of THF and dimethylether, both in the deuterated form.

8.6 Calibration of Pulsed Field Gradients

A.

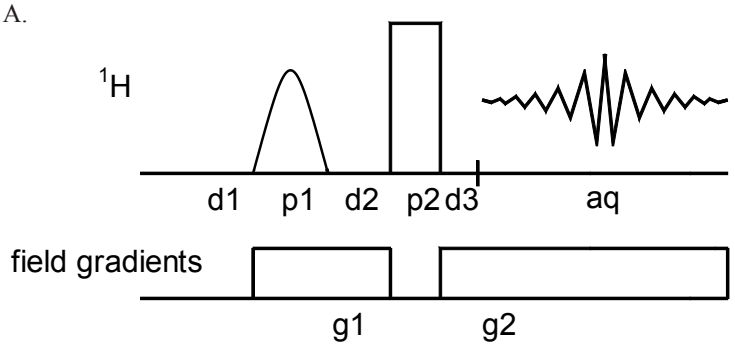

p1, p2: x, x, -x, -x, y, y, -y, -y

aq: x, x, -x, -x, y, y, -y, -y

B. Yes, and it gives the same result and works even for the case when the transmitter offset is not on resonance because chemical shift is refocused by the 180°pulse.

C. Evolution periods are usually much longer than the gradient pulses, and short ring-down times for these are therefore not mandatory.

Pulse Programs

In the following table we provide the names of the standard Bruker pulse programs (Topspin) with which the experiments have been performed, or which are closely related to the ones actually used. Non Bruker programs may be obtained from the authors. **Note, however, that the notation for pulses and delays used in the Bruker pulse programs differs considerably from the notation and numbering used throughout this book.**

Exp.	Pulse program
1.1	zg
1.2	aptsp
1.3	cosydfetgp.2
1.4	noesygpph
1.5	hsqcedetgpsisp
2.6	hmbcetgpl2nd
2.1	jresqf
2.2	roesyph.2
2.3	mlevetgp
2.4	hsqcgpmlph
2.5	hoesyph
2.6	inadgpqfsp
2.7	adeq11etgpsp.fin
2.8	jhmbc2ct.fin
2.9	zggd
3.1	zgpr
3.2	noesypr1d3
3.3	soggy.ber
3.4	wet
3.5	selmlgp.2
3.6	selnogp
3.7	selincor.ber
3.8	selinasp.fin
3.9	bandHMBC2lpqf.fin
4.1	zgdc
4.2	dept

Exp.	Pulse program
4.3	aring
4.4	hoesyph
4.5	dept
4.6	hmqcetf3gpdcber
4.7	zg
5.1	t1ir
5.2	cpmg
5.3	zg30
5.4	ledbpgp2s
5.5	hsqc_F1coupl_2zz.leu
6.1	zg
6.2	zg
6.3	zg
6.4	zg
6.5	zg30
6.6	stdinter180.ber
6.7	zg
7.1	cp
7.2	zg
7.3	hsqcetf3gpsi2
7.4	hncagp3d
8.1	zg
8.2	decp90
8.3	selzg
8.4	zg_180_90.fin
8.5	zg
8.6	calibgp.ber

Elementary Product Operator Formalism Rules

In the **Comments** section of the experiments the product operator formalism is often used to follow the course of the magnetization. This table provides a summary of the various interrelationships for quick reference.

1. 90° Pulses

$$I_{1_z} \xrightarrow{90°I_x} -I_{1_y} \qquad I_{1_x} \xrightarrow{90°I_x} I_{1_x} \qquad I_{1_y} \xrightarrow{90°I_x} I_{1_z}$$

$$I_{1_z} \xrightarrow{90°I_y} I_{1_x} \qquad I_{1_x} \xrightarrow{90°I_y} -I_{1_z} \qquad I_{1_y} \xrightarrow{90°I_y} I_{1_y}$$

$$I_{1_z} \xrightarrow{90°I_{-x}} I_{1_y} \qquad I_{1_x} \xrightarrow{90°I_{-x}} I_{1_x} \qquad I_{1_y} \xrightarrow{90°I_{-x}} -I_{1_z}$$

$$I_{1_z} \xrightarrow{90°I_{-y}} -I_{1_x} \qquad I_{1_x} \xrightarrow{90°I_{-y}} I_{1_z} \qquad I_{1_y} \xrightarrow{90°I_{-y}} I_{1_y}$$

$$2I_{1_x}I_{2_z} \xrightarrow{90°I_y} -2I_{1_z}I_{2_x}$$

$$2I_{1_x}I_{2_z} \xrightarrow{90°I_x} -2I_{1_x}I_{2_y}$$

2. Chemical Shift

$$I_{1_x} \xrightarrow{\Omega I_z t} I_{1_x}\cos\Omega t + I_{1_y}\sin\Omega t \qquad -I_{1_x} \xrightarrow{\Omega I_z t} -I_{1_x}\cos\Omega t - I_{1_y}\sin\Omega t$$

$$I_{1_y} \xrightarrow{\Omega I_z t} I_{1_y}\cos\Omega t - I_{1_x}\sin\Omega t \qquad -I_{1_y} \xrightarrow{\Omega I_z t} -I_{1_y}\cos\Omega t + I_{1_x}\sin\Omega t$$

$$I_{1_z} \xrightarrow{\Omega I_z t} I_{1_z}$$

3. Spin–Spin Coupling

$$I_{1_x} \xrightarrow{\pi J 2 I_{1_z} I_{2_z} t} I_{1_x} \cos \pi J t + 2 I_{1_y} I_{2_z} \sin \pi J t$$

$$-I_{1_x} \xrightarrow{\pi J 2 I_{1_z} I_{2_z} t} -I_{1_x} \cos \pi J t - 2 I_{1_y} I_{2_z} \sin \pi J t$$

$$I_{1_y} \xrightarrow{\pi J 2 I_{1_z} I_{2_z} t} I_{1_y} \cos \pi J t - 2 I_{1_x} I_{2_z} \sin \pi J t$$

$$-I_{1_y} \xrightarrow{\pi J 2 I_{1_z} I_{2_z} t} -I_{1_y} \cos \pi J t + 2 I_{1_x} I_{2_z} \sin \pi J t$$

$$2 I_{1_x} I_{2_z} \xrightarrow{\pi J 2 I_{1_z} I_{2_z} t} 2 I_{1_x} I_{2_z} \cos \pi J t + I_{1_y} \sin \pi J t$$

$$-2 I_{1_x} I_{2_z} \xrightarrow{\pi J 2 I_{1_z} I_{2_z} t} -2 I_{1_x} I_{2_z} \cos \pi J t - I_{1_y} \sin \pi J t$$

$$2 I_{1_y} I_{2_z} \xrightarrow{\pi J 2 I_{1_z} I_{2_z} t} 2 I_{1_y} I_{2_z} \cos \pi J t - I_{1_x} \sin \pi J t$$

$$-2 I_{1_y} I_{2_z} \xrightarrow{\pi J 2 I_{1_z} I_{2_z} t} -2 I_{1_y} I_{2_z} \cos \pi J t + I_{1_x} \sin \pi J t$$

$$I_{1_z} \xrightarrow{\pi J 2 I_{1_z} I_{2_z} t} I_{1_z}$$

4. Shift Operators

$$I^+ = I_x + i I_y \qquad I^+ \xrightarrow{90°_{I_x}} \frac{1}{2}(I^+ + I^-) + i I_z$$

$$I^- = I_x - i I_y \qquad I^- \xrightarrow{90° I_x} \frac{1}{2}(I^+ + I^-) - i I_z$$

$$I_x = \frac{1}{2}(I^+ + I^-) \qquad I^+ \xrightarrow{\Omega I_z t} I^+ e^{-i\Omega t}$$

$$I_y = \frac{1}{2i}(I^+ - I^-) \qquad I^- \xrightarrow{\Omega I_z t} I^- e^{+i\Omega t}$$

$$2 I_{1_x} I_{2_z} = I_{2_z}(I^+ + I^-)$$

5. Literature

[1] O. W. Sørensen, G. W. Eich, M. H. Levitt, G. Bodenhausen, R. R. Ernst, *Prog. NMR Spectrosc*. **1983**, *16*, 163–192.

[2] H. Kessler, M. Gehrke, C. Griesinger, *Angew. Chem. Int. Ed. Engl*. **1988**, *27*, 490–536.

[3] J. Cavanagh, W. J. Fairbrother, A. G. Palmer III, N. J. Skelton, *Protein NMR Spectroscopy*, Academic Press, San Diego, **1996**, Chapter 2.

Chemical Shift and Spin-Coupling Data for Strychnine

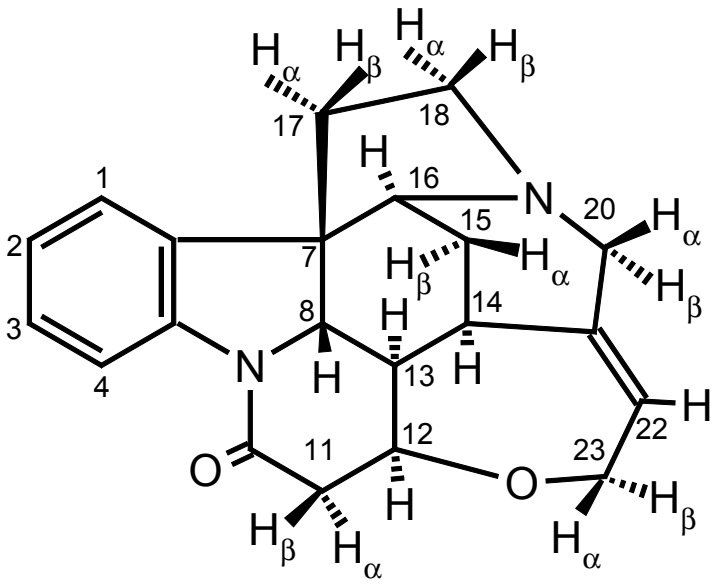

a) Data obtained on a 700 MHz spectrometer from a 3 % solution in $CDCl_3$, chemical shifts vs. int. TMS, chemical shifts and H,H spin coupling constants confirmed by iterative spin simulation, cf. Exp. 3.4;

b) values for ABCD spin system H-17α/β and H-18α/β with larger incertainty.

Nr	δ_C	δ_H	$^1J_{C,H}$	$^nJ_{H,H}$ [Hz]	
1	122.26	7.167	159.0	^3J(H-1,H-2) ^4J(H-1,H-3) ^5J(H-1,H-4)	7.49 1.08 0.23
2	124.20	7.098	160.9	^3J(H-2,H-3) ^4J(H-2,H-4)	7.44 0.98
3	128.56	7.255	159.6	^3J(H-3,H-4)	7.90
4	116.23	8.092	168.0		
5	142.23				
6	132.72				
7	51.96				
8	60.10	3.860	145.4	^3J(H-8,H-13)	10.41
10	169.28				
11α	42.48	3.132	126.3	^2J(H-11α,H-11β) ^3J(H-11α,H-12)	−17.34 3.34
11β		2.670	135.9	^3J(H-11α,H-12)	8.47
12	76.85	4.288	145.4	^3J(H-12,H-13)	3.30
13	48.22	1.276	124.4	^3J(H-13,H-14)	3.29

Nr	δ_C	δ_H	$^1J_{C,H}$	$^nJ_{H,H}$ [Hz]	
14	31.60	3.150	130.1	^3J(H-14,H-15α) ^3J(H-14,H-15β) ^4J(H-14,H-22) ^4J(H-14,H-20α)	4.11 1.96 0.47 1.61
15α	26.84	2.360	131.4	^2J(H-15α,H-15β) ^3J(H-15α,H-16)	−14.35 4.33
15β		1.462	131.4	^3J(H-15β,H-16)	2.42
16	60.28	3.963;	146.2		
17α	42.85	1.89[b]	133.4	^2J(H-17α,H-17β) ^3J(H-17α,H-18α) ^3J(H-17α,H-18β)	−13.9 5.5 7.2
17β		1.89[b]		^3J(H-17β,H-18α) ^3J(H-17β,H-18β)	3.2 10.7
18α	50.35	3.219	136.8	^2J(H-18α,H-18β)	−13.9
18β		2.878			
20α	52.68	2.745	141.0	^2J(H-20α,H-20β) ^4J(H-20α,H-22)	−14.8 1.79
20β		3.716	141.0		
21	140.45				
22	127.34	5.915	157.7	^3J(H-22,H-23α) ^3J(H-22,H-23β)	7.0 6.1
23α	64.60	4.148	144.3	^2J(H-23α,H-23β)	−13.8
23β		4.066	137.2		

Picture Credits

All spectra, schemes and formula have been produced by the authors. The photographs were either recorded by the authors, indicated with "A", or have been obtained from private sources with permission, indicated with "P", or taken from open Internet sources such as Wikipedia, indicated with "I".

Fig. 1.2-1	I	Fig. 4.6-4	P
Fig. 1.2-2	I	Fig. 4.7-2	P
Fig. 1.3-1	I	Fig. 5.1-1	I
Fig. 1.3-2	I	Fig. 5.2-1	I
Fig. 1.4-1	I	Fig. 5.3-1	P
Fig. 1.4-2	I	Fig. 5.3-2	I
Fig. 1.5-1	I	Fig. 5.4-1	A
Fig. 1-5.4	P	Fig. 5.5-1	I
Fig. 1.6-1	I	Fig. 5.5-2	P
Fig. 2.2-1	I	Fig. 6.0-1	I
Fig. 2.3-1	I	Fig. 6.0-2	A
Fig. 2.4-1	I	Fig. 6.2-2	A
Fig. 2.4-2	I	Fig. 6.3-1	I
Fig. 2.6-2	P	Fig. 6.4-1	A
Fig. 2.7-1	P	Fig. 6.5-1	I
Fig. 2.7-2	I	Fig. 6.5-2	I
Fig. 2.8-1	P	Fig. 6.7-5	I
Fig. 2.9-1	I	Fig. 6.7-6	I
Fig. 3.1-2	P	Fig. 6.7-7	I
Fig. 3.2-2	P	Fig. 7.0-1	A
Fig. 3.3-1	I	Fig. 7.1-1	I
Fig. 3.3-2	P	Fig. 7.1-2	I
Fig. 3.4-2	P	Fig. 7.1-3	A
Fig. 3.6-2	I	Fig. 7.1-5	A
Fig. 3.9-2	P	Fig. 7.2-1	A
Fig. 4.1-1	P	Fig. 7.2-2	A
Fig. 4.2-1	A	Fig. 7.3-3	A
Fig. 4.2-2	P	Fig. 8.0-1	A
Fig. 4.2-6	A	Fig. 8.0-2	A
Fig. 4.3-1	A	Fig. 8.1-5	A
Fig. 4.3-3	P	Fig. 8.3-6	A
Fig. 4.4-2	P	Fig. 8.5-4	A
Fig. 4.4-3	A	Fig 8.5-7	A
Fig. 4.5-2	P	Fig. 8.6-1	A

Index

Symbole

1,1-ADEQUATE 61
1,2-ethanediol 257
1,7-dicarba-closo-dodecaborane 119
1D-INADEQUATE 105
1D NOE difference technique 97
1D-NOESY 17, 81
1-fluor-2,4-dinitrobenzene 38
^{1}H,^{19}F correlation 131
^{1}H broad-band decoupled proton spectrum 37
^{1}H broad-band decoupling 191
^{1}H NMR 3, 273
^{1}J breakthrough 33, 34
^{1}J(C,H) 167
2,4,5-trifluoroaniline 132
2D HMQC 135
2D *J*-Resolved ^{1}H NMR Spectroscopy 37, 101, 277
^{2}J(C,H) 29
3-9-19 85
3D DOSY 163
^{3}J(C,H) 29
^{4}J(C,H) 29
4-*t*-butylpyridine 194
^{11}B,^{11}B-COSY 121
^{11}B NMR Spectroscopy 119, 284
^{13}C-and ^{15}N-labelled proteins 225
^{13}C-detected proton-DOSY 163
^{13}C-edited TOCSY 49
^{13}C- labelled methanol 241
^{13}C NMR 7
^{15}N GARP decoupling 231
^{15}N-labelled urea 241
^{15}N NMR Spectroscopy 123, 284
^{17}O NMR Spectroscopy 127, 284
^{19}F NMR Spectroscopy 131, 284
^{29}Si NMR Spectroscopy 135, 284
^{57}Fe NMR Spectroscopy 139, 285
90° read-pulse 153
^{195}Pt NMR Spectroscopy 145, 285
α-acetoxy-phenylacetic acid 179
α-lactose 203
β-cyclodextrin 194Ξ-scale 113, 114, 228
$\Delta G^{\#}$ 161
$\Delta H^{\#}$ 161
$\Delta S^{\#}$ 161
Ξ-scale procedure 221
Ξ-value 119, 131, 139, 145

A

absolute stereochemistry 183
ACCORDION 61
ACCORDION-HMBC 29
acetone 155
acetonitrile 89
activation enthalpies 159
activation entropy 159
actual temperature 257
ADEQUATE (Adequate sensitivity DoublE QUAnTum spEctroscopy) 61, 279
adiabatic 180° refocusing pulse 33
adiabatic chirp 180° inversion pulse 255
adiabatic chirp pulse 34
adiabatic condition 253
adiabatic inversion pulses 256
Adiabatic processes 293
Adiabatic Pulses 253, 293
Advanced Mosher Method 183, 288
Advanced Organic NMR 35
aligned samples 37
alignment medium 167
amino acids 225
amplifier power level 235
anisotropic diffusion 287
anisotropic medium 167
anisotropy 288
anisotropy effects 176
anomeric proton 83, 204
antiphase doublet 245
anti-phase magnetization 59, 273, 276
APT (Attached Proton Test) 7, 256, 273
ARING 127, 128
aromatic ABCD pattern 176
aromatic-ring-induced chemical shift 185
Arrhenius scheme 286
artificial membranes 215
ASIS 175, 288
Association Constants K_a 193
axial signals 21
AX pattern 11, 13

B

bacteria phages 167
Band Selective HMBC 29, 109, 252, 283, 293
band-selective pulse 225, 231
band-width 202
barium perchlorate 183
barium salts 183
base-line distortions 87
BBO probe 267
benzene 175, 288

bicelles 167
binding ability 199
binding constant 202
binding pocket 199, 202
binomial sequence 85
biochemical regulation processes 199
Biological buffers 292
biological safety laboratory 223
biological tissues 215
biomacromolecules 167
bipolar gradients 163
BIRD train 167
Bloch equations 154
Bloch–Siegert phase shift 225, 231
Bloch–Siegert shift 79, 232
Bloch simulation module 247
boron relaxation 284
boxed shape 247
buffer solutions 240
build-up 280
build-up curve 274, 289
build-up time 191
bulk susceptibility 176
BURP 247
Butanol 164
Butter 215

C

Calibration 233
calibration curve 260
calibration experiments 233
Calibration of Pulsed Field Gradients 294
Calibration of Pulse Duration 235
Calibration of Pulse Duration in the Transmitter Channel 292
calibration procedure 235
calibration sample 266
calixarenes 183
carbohydrates 93
carbon–carbon connectivities 61
cartilage 215
cascades of Gaussian pulses 247
CCl_3F 131
CD_3CN 183
centrifugal forces 215, 218
change of solvent 175
$CHCl_3$ 155, 245, 254
C,H correlation 23
chemical derivatization 179
chemical exchange 19
chemical reactions 203
chemical shift anisotropies 211
chemical shift dispersion 163
chemical shift-encoded z-magnetization 21
chiral auxiliary 181
chiral center 275
chiral compounds 183
Chirality Determination 179, 288
chiral solvating agent 179
chirped ^{13}C 180° pulse 219
chirped adiabatic ^{13}C 180° pulse 105, 222
chirp pulses 61, 253
chlorine isotopomers 132
chlorodimethylformamide 160
chromatographic separation 163
C,H spin–spin coupling constants 71
clean bench 223
coalescence T_c 161, 264
coalescence temperature 161
coherence level 276, 293
coherence order 99
coherence pathway diagram 144
coherence selection 265
coherence selection experiments 271
Colemanite 119
composite pulse 85, 241, 293
composite pulse decoupling 191, 241, 273
composite transverse relaxation time 157
computer simulation 91
concentration-jumps 203
connectivity 11
constant time 232
constant time evolution 291
constant time manner 231
constant time period 69
constant time principle 111
continuous-wave spin lock 41
control of temperature 197
convection 166
correct external referencing 197
COSY-45 11
COSY (COrrelation SpectroscopY) 11, 89, 131, 163, 273
COSY transfer 273
CP/MAS (Cross-Polarization/Magic-Angle Spinning) 211
CPMG (Carr Purcell Meiboom Gill) 155
$Cr(acac)_3$ 189, 191, 268, 269, 288, 289
cresol 288
cross-peaks 11
cross-polarization 135, 211
cross-relaxation 55, 99, 274, 277, 278
cryogens 233
cryo probe 59, 63, 79, 105, 210, 220, 227, 240, 254, 257, 262, 264, 293
cryo *z*-gradient triple resonance probe 229

$Cu(acac)_2$ 192
curve-fitting 192
cyclodextrins 179, 183
Cyclosporin A 109

D

D_2O 127, 164
dead time 265
decay 280
decay curve 204
deconvolution 192
degassed samples 153
DEPT 7, 9, 123, 135, 256, 284
DEPTQ 7, 9
detection period 16, 33, 43
Determination of Association Constants K_a 289
deuterium spin 273
deuteromethanol 257
dewar hold time 233
diamagnetic rhodium complexes 179
diastereomeric solvation complexes 181
diastereotopicity 275
diffusion delay 164
diffusion equation 286
diffusion measurements 163, 197
Diffusion Measurement with DOSY 286
Diffusion Ordered SpectroscopY 163
digital resolution 167, 273
dihedral angle 280
dimethyldichlorosilane 168
Dimethylformamide 159
Dipolar coupling constants 287
dipolar couplings 211
DIPSI 278
DIPSI-2 sequence 231
DIPSI-2 spin lock 227
DNMR3 159, 160
DOSY 45, 49, 53, 77, 163, 199, 265
double INEPT back transfer (PEP = preservation of equivalent pathways) 219
double INEPT back transfer 26, 27, 231, 274
double low pass filter 29
double-quantum coherence 59, 64, 107, 279
double-quantum filter 15, 108, 274
double-quantum magnetization 273
double spin-echo experiment 9
DPFGSE 200
DQF filter 283
DSS 203, 227
DSS signal 221
dual $^1H^{19}F$ probes 134
DVB 168
Dynamic ^1H NMR Spectroscopy 159, 286
dynamic equilibria 159
Dynamic exchange 286
dynamic NMR experiments 155
dynamic range 274, 286

E

EBURP 247
EBURP2 shape 249
EBURP shape pulse 105, 112, 250, 251
echo-antiecho gradient selected 49
echo-antiecho manner 222
echo antiecho mode 29, 33, 276
echo-antiecho recording 34
echo-antiecho scheme 11, 219, 225
E.COSY 11
eddy current delay 164
eddy currents 265
eddy delay 163
editing period 23, 26
electric field effects 176
electron withdrawing 286
enantiomeric excess ee 181
enantiomeric purity 179
enantiomers 179, 288
entropies 159
enzymatic biochemical reaction 203
epitope mapping 202
ERETIC - Electronic Reference To Access In vivo Concentration 187
Ernst angle 10, 191, 273
ethyl anthranilate 175
ethylcrotonate 127
ethylene glycol sample 159
evolution period 15, 21, 26, 33, 39, 43, 51, 55, 59, 64, 155
excitation band width 107, 251
excitation profile 85
excitation pulse p1 6
excitation sculpting 85
EXORCYCLE 277
exponential decay 157
exponential shape 247
exponential window 13
EXSY 159, 203
external r.f. signal 187
extreme narrowing limit 155
Eyring equation 286

F

fan 234
$Fe(CO)_5$ 139
ferrocene 285
filling height 166

flip angle 235
FLIPSY 81
fluorescence 133
Fluorite mineral 133
food samples 215
formamide 123
forward linear prediction 228
frequency domain 247
frequency profile 247
frequency-swept adiabatic 180° ^{13}C pulses 23
friction 290
fructose 46
fructose subunit 51, 95

G

GARP decoupling 102, 228, 278, 282
gas torch 168
gated decoupling technique 71, 167, 280
Gaussian cascade shapes 251
Gaussian multiplication 72, 221, 228
Gaussian pulse 97, 202
Gaussian shape 247, 248, 250, 251
Gaussian weighting function 4
Gaussian windowing 180
G-BIRD(r) 172
$Gd(acac)_3$ 192
glassware 135
glucose moiety 51
glucose part 46
glucose unit 95
glycine 212
gradient coil 265
gradient dead time 265
gradient double quantum filter 57, 245
gradient DQ filter 241, 242
gradient echo 286
gradient pulses 15
gradient ratios 126
gradient-selected double quantum filter 11
gradient-selected HMBC 69
gradient-selected method 45, 93
gradient-selected pulse sequences 53
gradient-selected SELINCOR 101
gradient shape 271
gradient spin-echo experiment 270
gradient spin-echo method 97
gradient strengths 265
ground state vibrational energy 132
Gyromagnetic ratio 115, 116, 265

H

H_2BC 29
H_2O 129
half gauss pulse 251
hard pulse 75, 241
Hartmann–Hahn condition 211, 212, 214, 290
Helium refill 234
Hematite 143
Heteronuclear NMR 113
Heteronuclear Single Quantum Coherence 275
heteronuclear spin coupling 277
HETLOC 69
HF-filter units 134
HF-hydrogen bridge 55
higher order 282
higher-order effects 175
High-power proton decoupling 211
High-Resolution Magic-Angle Spinning 215, 290
HMBC [Heteronuclear Multiple Bond Correlation] 29, 109, 276
HMQC 23, 32, 139, 145, 274
HNCA 225, 291
HN HSQC 219, 290
HOESY (Heteronuclear Overhauser Effect SpectroscopY) 53, 131, 278
homonuclear decoupling 291
homonuclear spin–spin coupling 39
Host–guest chemistry 193
host–guest complex 193
HPLC-NMR 89
HR-MAS (High-Resolution Magic-Angle Spinning) 199, 215
HSCQ pulse 167
HSQC–BIRD 170
HSQC (Heteronuclear Single Quantum Coherence) 23, 45, 103, 135, 145, 199, 256, 274
HSQC-TOCSY 49
Human serum albumin 200
human ubiquitin 220, 227
hydrogen bonds 286
hyphenated techniques 89

I

IBURP pulse 110, 112
INADEQUATE Incredible Natural Abundance DoublE QUAntum Transfer Experiment 57, 61, 105, 279
Indirect Channel 241
INEPT 7, 103, 123, 139, 256
INEPT-DOSY 163
INEPT-INADEQUATE 61
INEPT step 219
INEPT transfer 26, 63, 222, 231, 275, 287
inhomogeneity of the magnet 157
initial concentrations 193
initial rate approximation 274

inorganic complexes 53
inorganic salts 292
in-phase magnetization 276
interferences 284
interleaved mode 200
intermolecular recognition 193
internal TMS 4
inverse gated experiment 125
inverse gated technique 71, 187
inverse probe 79, 83, 240
inversion recovery experiment 151
ionic liquids 53
Iron pentacarbonyl 285
irradiation power 79
IR spectroscopy 286
isotropic medium 167
isotropic scalar spin coupling constants 167
iterative computer fitting 197
iterative exponential fitting 153
IUPAC committee 114

J

J-HMBC 29, 65, 280
Job's plot 196

K

Karplus curves 65
Karplus equation 273, 274, 278
Kinetic Experiment 203, 289
kinetic parameters 203

L

lactose intolerance 207
lanthanide shift reagents 176
Laplace transformation 164
left-over transverse magnetization 200, 222
length of the spin lock 47
linearity of the field gradients 166
line broadening 289
line separation 161
line shape 77, 159
line width 161
lipids 215
liquid crystals 167
liquid nitrogen tank 123
liquid oxygen 127
lock channel 257
long-range C,H spin coupling constants 71
long-range correlations 29, 66
long-range COSY 11
long-range spin couplings 11, 276
low-abundance nuclei 241
low γ value 127
low gyromagnetic ratio 139
low pass filter 33, 126
low-temperature 161
low-temperature NMR measurements 260

M

Magic-angle spinning 211
magnitude calculation 266
magnitude mode 40
magnitude processing 278
maintenance 233
maintenance costs 233
mass relationship 190
Measurement of the Spin–Lattice Relaxation Time T_1 286
Measurement of the Spin–Spin Relaxation Time T_2 286
menthol 183
metabolomics 81, 93
metabolomics research 37
methanol 164, 257
methionine 221
MEXICO 160
micelles 167
Michaelis−Menten constant 204
Michaelis−Menten equation 289
Michaelis−Menten plot 204
mixing period 15, 21, 26, 33, 39, 43, 51, 55
mixing time 17, 22, 274
MLEV 278
MLEV16 spin lock 278
MLEV-17 sequence 52, 94
$Mn(acac)_2$ 192
molar relationship 190
Mosher esters 181
MTPA-Cl 183
multiexponential fitting 164
multinuclear probe 119
multiplet-selective 252, 293
multiplicity determination 23
multiplicity information 7

N

$Na_2[PtCl_6]$ 145
naphthalene 189
natural abundance 115, 116, 131, 135, 139, 145
N-(Diethylcarbamothioyl)-2,4-difluorobenzamide 54
negative gyromagnetic ratio 123, 135
negative NOE effects 100, 123
Nitratine 124
nitrogen gas flow 159
nitromethane 117

NMR sensitivity 131
N,N-azoisobutyronitrile 168
NOE build-up curves 100
NOE difference experiment 17
NOE spectroscopy 97
NOESY (Nuclear Overhauser Enhancement SpectroscopY) 17, 89, 159, 163, 219, 274
non-uniform data sampling NUS 219
NQS 211
nuclear Overhauser effect 41
nutation experiment 236

O

O-acetyl-mandelic acid 179
oblique mode 164
off-resonance irradiation 201
oligopeptides 283
on-resonance 201
organic set 1
organofluorine chemistry 53
organolithium compounds 53
orthogonal spin lock pulses 200
out-and-back 225
overlap of signals 175

P

Pake doublet 287
paramagnetic lanthanide complexes 179
paramagnetic lanthanide tags 167
paramagnetic relaxation 288
paramagnetic term 284
PENDANT 7
PEP 28, 225
PEP back transfer 224
PEP principle 64, 231
PEP scheme 222
perfluorodecalin 132
phase distortions 276
phase-sensitive 225
phase-sensitive COSY 11
phase-sensitive frequency 11
phenanthrene 189
phenylethylamine 179
phosphate buffer 200
phosphate-buffered D_2O solvent stock 194
phosphonates 183
Pirkle's reagent 179
plant materials 215
polarizability 147
polarization 214
polarization transfer 123, 163
polyacetylenes 167
poly-γ-benzyl-L-glutamate (PBLG) 167
polyisocyanides 167
polymer-bound monomers 215
polymer gels 215
polymerization 168
polymer signals 172
polymer sticks 168
Poor Man's Gradients 265
preacquisition delay 127, 156
precession frequency 214
preparation period 15, 21, 26, 32, 39, 43, 51, 59, 63
preservation of equivalent pathways 225
probe head coil 48
probe head ringing 127
product operator formalism 277
progressive saturation 151
proline residues 219
protein–ligand interaction 193, 199
proton–proton distances 17
proton relaxation 211
pseudo 2D 200
pseudo 2D data matrix 163
Pt-100 resistor 258
$Pt(NH_3)_2Cl_2$ 145
PULCON 187
pulsed field gradients 163, 265
pulse duration 241, 247
pulse imperfections 277
PUlse Length based CONcentration determination 187
pulse lengths 235
pulse shape 247
pulse train 200
PURGE 77
pyknometer 190
pyridine 176, 288

Q

quadrupolar couplings 211
quadrupolar nucleus 119, 127, 286
quadrupolar relaxation 284
quadrupolar splitting 168
quadrupole moment Q 116
quality factor 292
quantitative ^{13}C NMR 71
quantitative determinations 187
Quantitative NMR 187
Quantitative NMR and Relaxation Reagent 288
Quartz (SiO_2) 137

R

r−3 dependence 167
radiation damping 187, 236, 257, 262, 292
ramped spin lock 211

Rapid Injection NMR 203
rapid pulsing 290
rate constant 161
ratio of populations 161
REBURP shape 97, 98
receptivity 115, 116, 123
rectangular pulse 253
rectangular-shaped 180° inversion pulse 255
reduction in signal intensity 135
reference substance 114, 187
referencing 113
Referencing in Hetereonuclear NMR 114
relative ee-values 185
relaxation agent 191
relaxation effects 276
relaxation reagent 187
relaxation sink 282
relaxation time 273
relayed COSY 47
repetition time 273
reproducibility 160
Residual Dipolar Couplings (RDC) 167, 287
resolution in the indirect dimension 109
reverse INEPT 103
r.f. homogeneity 236
r.f. routings 235
RIDE 127
ring-down delay 271, 272
RIng Down Elimination 127
ROESY (Rotating frame Overhauser Enhancement SpectroscopY) 17, 22, 41, 274, 277
roof effect 273
rotating coordinate frame 274
rotating frame 41
rotational barrier 159
routine proton NMR spectrum 3
routing mode 235, 241

S

salicylaldehyde 288
saturation 187
saturation recovery experiments 151
saturation transfer 159, 202
scaling scheme 65
secans hyberbolicus 254
SEDUCE 92, 247
selective excitation 93, 97
selective irradiation 200
selective pulse on water 231
selective pulses 75, 89
selective square pulse 90
self-shielded gradient coils 268, 271
SELINCOR 101, 282
SELINCOR-COSY 101
SELINCOR-TOCSY 101
SELINQUATE 105, 283
SELNOESY 97, 282
SELTICS 211
SELTOCSY 93, 282
semi 3D techniques 29
semi-solids 215
sensitivity enhancement 225
sensitivity of an r.f. coil 187
separation of homonuclear spin couplings 37
SERF 37
service engineer 233
Seyfarth mixture 293
shaped pulses 247, 293
sideband pattern 212
sideband suppression 211
sinc shape 253
sinc-shaped excitation profile 247
sine-shaped intensity course 237
single-quantum coherence 26, 64, 293
single-quantum terms 59
sinusoidal window 25
slow exchange 159
small chemical shift differences 175
smoothed chirp pulse 254
smoothed square gradient pulse 271
SMQ10 smoothed-square shaped field gradients 228
SNOB 247
soft pulse 241
SOGGY-Excitation Sculpting 85
solid state 211
solute–solvent interactions 176
Solvent-optimized double gradient spectroscopy 87
Solvent Suppression 81, 89
Solvent Suppression by 1D-NOESY 281
Solvent Suppression using WET 282
spatially-selective composite pulse 91
spatial relationship 53
special ^{11}B probe 119
specific binding state 199
spill-over 95, 199
SPINAL 211
spin diffusion 155, 199, 274
spin echo 39
spin echo method 155
spin echo sequence 277
spin–lattice relaxation 191
spin–lattice relaxation time T_1 73, 151, 155
spin lock 41, 46, 211, 277, 282
spin-lock conditions 41
spin-lock duration 51
spin locking 135

spin-lock power 41
spin-lock pulse 103, 219, 278
spin-lock sequence 95, 231
spin simulation program 74
Spin–Spin Relaxation Time T_2 155
SpinWorks 159, 160
spoiling gradient 281
squared sinusoidal window 221
States-TPPI 19, 225
STD (Saturation Transfer Difference) 45, 199, 289
steady-state experiment 17
stimulated echo version 163
stock solution 194
stoichiometry 196
stopped flow 203
stretched polymer gels 167
strip FT 228
strychnine 3, 8, 13, 23, 24, 30, 62, 65, 66, 72, 97, 101, 102, 106, 125, 151, 168, 248
styrene 168
sucrose 46, 49, 57, 77, 81, 86, 93
superconducting magnets 270
susceptibility 292
symmetrization operations 39
symmetry 284

T

tangens hyperbolicus 254
teflon disk 266, 270
Temperature Calibration in NMR 257, 293
temperature controller 257
temperature-dependent effect 257
temperature gradient 166, 262
tetramethylsilane (TMS) 114, 287
theoretical line shape 161
thermal effects 241
three-spin effect 282
tilt 39
time domain 247
time shape 247
TMS 135
TMS frequency 289
TOCSY breakthrough 43
TOCSY (TOtal Correlation SpectroscopY) 45, 89, 93, 199, 219, 277
TOCSY transfer 95, 278
TOSS 211
total correlation 45
total coupling 167
TPPM (two pulse phase modulation) 211
transient experiment 17
transition metal complexes 183
transition-selective 252, 293
transmitter pulse 235
transverse or spin–spin relaxation time T_2 151
transverse relaxation time 285
Triethyleneglycol 164
trimethylsilyl chloride 168
trim pulse 26, 95, 222, 278
triple-resonance cryoprobe 221
TROSY principle 219
tryptophan 202
two-site exchange 159

U

ubiquitin 223, 228
UV- and fluorescence spectroscopy 289

V

van der Waals interactions 176
VEGA 247
volume integrals 274
volume percentage 190
volume restriction 281
volume selection 84

W

WALTZ16 10, 273
water distribution 270, 271
water suppression 17, 85, 275
water suppression by presaturation 77, 281
Water Suppression by SOGGY Excitation Sculpting 281
WET (Water suppression Enhanced through T_1 effects) 89
window functions 228
WURST shape 254

X

xsi.mf 114

Z

zero crossing 237
zero excitation 85
zero excitation points 281
zero filling 25
zero-quantum coherences 17, 21, 95
zero-quantum filtering 97
z-gradient 219
zinc porphyrins 179
zirconia rotor 216
zz-filter 172